4

FUNDAMENTALS
OF MACHINE DESIGN

P. ORLOV

A technical and methodic handbook for the designers of machines, useful as a textbook for mechanical engineering faculties. Gives a systematic exposition of the rules for rational machine design on the basis of unification and standardization, and for building industrial machines incorporating in their design provisions for further development, lengthening of service life, and improvement of reliability. Surveys ways of reducing weight and increasing strength and rigidity. Considers problems of thermal stress and the effect of thermal deformation on the operation of parts and sub-assemblies. Describes methods of improving efficiency, increasing sturdiness, making assembly easier, and improving operating conditions.

FUNDAMENTALS
OF MACHINE DESIGN

P. ORLOV

П. ОРЛОВ

ОСНОВЫ КОНСТРУИРОВАНИЯ

4
FUNDAMENTALS
OF MACHINE DESIGN

P. ORLOV

TRANSLATED FROM THE RUSSIAN
by A. TROITSKY

The Russian Alphabet and Transliteration

А	a	a	К	к	k	Х	х	kh
Б	б	b	Л	л	l	Ц	ц	ts
В	в	v	М	м	m	Ч	ч	ch
Г	г	g	Н	н	n	Ш	ш	sh
Д	д	d	О	о	o	Щ	щ	shch
Е	е	e	П	п	p	Ъ	ъ	"
Ё	ё	ё	Р	р	r	Ы	ы	y
Ж	ж	zh	С	с	s	Ь	ь	'
З	з	z	Т	т	t	Э	э	e
И	и	i	У	у	u	Ю	ю	yu
Й	й	y	Ф	ф	f	Я	я	ya

The Greek Alphabet

A	α	Alpha	I	ι	Iota	P	ρ	Rho
B	β	Beta	K	$\varkappa$	Kappa	Σ	σ	Sigma
Γ	γ	Gamma	Λ	λ	Lambda	T	τ	Tau
Δ	δ	Delta	M	μ	Mu	Υ	υ	Upsilon
E	ε	Epsilon	N	ν	Nu	Φ	φ	Phi
Z	ζ	Zeta	Ξ	ξ	Xi	X	χ	Chi
H	η	Eta	O	o	Omicron	Ψ	ψ	Psi
Θ	$\vartheta\theta$	Theta	Π	π	Pi	Ω	ω	Omega

На английском языке

Contents

Torque Transmission

The following two principal methods are used to transmit torque: by *positive connection* and by *friction*. With the first method torque is transmitted by stiff elements operating in shear, bending or compression, and with the second, by frictional forces produced between cylindrical, tapered or end-face surfaces of shaft and hub members.

Among the main types of connections with stiff elements are *keyed* (Fig. 1, *1* and *2*), *splined* (Fig. 1, *3* and *4*), *prismatic shaft-end* (Fig. 5), *shaped shaft-end* (Fig. 6), *pinned* (Fig. 1, *7* and *8*) and *flanged* (Fig. 1, *9-11*) joints.

Frictional connections include *press-fitted* (Fig. 1, *12*), *tapered* (Fig. 1, *13*), *Gripspring* (Fig. 1, *14* and *15*) and *clamped* (Fig. 1, *16*) joints.

Both methods are sometimes combined. The load-carrying capacity of connections with stiff elements can be increased by using friction produced by axial (Fig. 1, *3*) or radial-axial tightening (Fig. 1, *4*).

Stiff elements such as keys (Fig. 1, *17-19*) are introduced into frictional *joints* to prevent relative rotation of parts and lock them in a definite angular position.

1.1. Keyed Joints

Keys are employed in joints carrying low loads, mainly in parts manufactured on a small-lot production basis. The shortcomings of keyed joints are their small load-carrying capacity, the weakening of shaft members by keyways, stress concentration due to the unfavourable shape of the keyways, and poor suitability for industrial production.

The weakening is especially serious in hollow shafts with a hole-to-shaft diameter ratio $d/D > 0.6$. The use of power-drive keys on such shafts is almost completely excluded.

In large-lot and mass production, in critical joints transmitting large torques and operating under cyclic loads, keys have been replaced by the more perfect splines.

Distinction is made between *stressed* keyed joints (*taper* and *tangent* keys) and *unstressed* joints (*prismatic* and *Woodruff* keys).
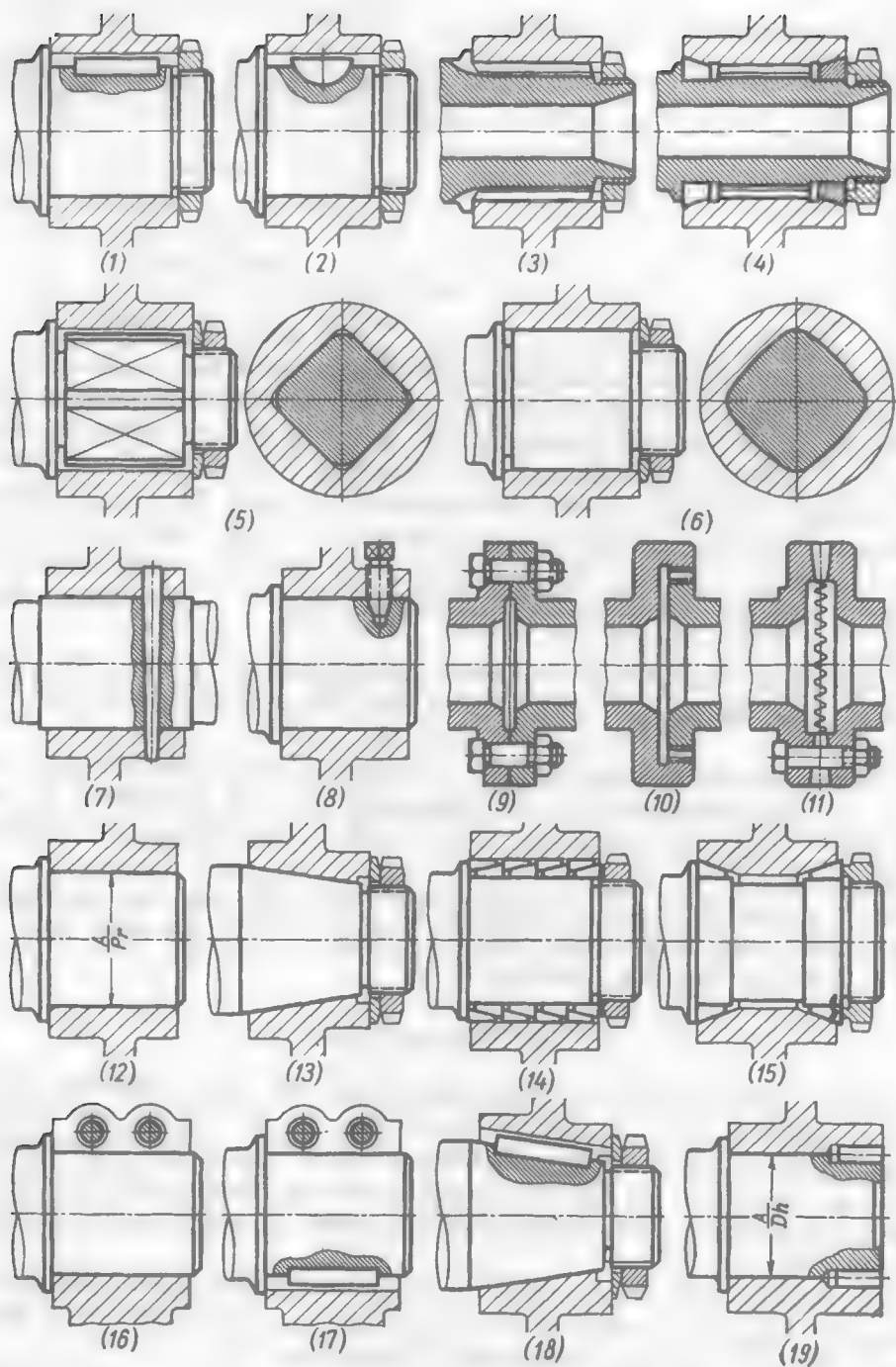
Fig. 1. Torque transmission methods

(a) Stressed Joints

Taper keys are made with flat (Fig. 2a) and rounded (Fig. 2b) end faces, and with gib heads (Fig. 2c).

The upper face of a key has a taper of $1 : 100$ ($\alpha = 35'$). The required interference between the shaft and the hub is obtained by
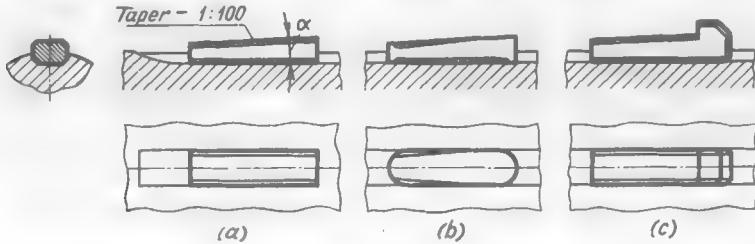

Fig. 2. Types of taper keys

driving in the key (Fig. 3a) or by tightening the hub against the key with a nut, the key being locked axially on the shaft (Fig. 3b).

Driven-in gib-head keys (Fig. 3c) are mainly used in shaft-end installations.
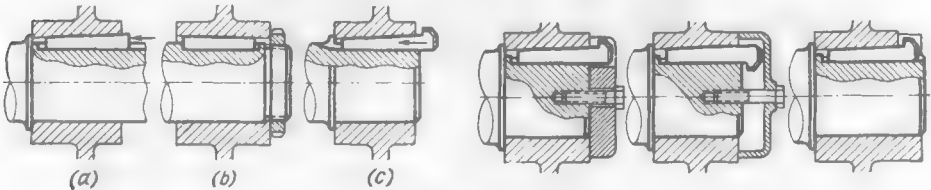
Fig. 3. Installation of taper keys   Fig. 4. Installation of driven-in gib-head keys

Figure 4 illustrates some methods of eliminating the gib-head projection in shaft-end joints, which is undesirable from the safety engineering viewpoint.

Flat taper keys (Fig. 5a) needing no keyway in the shaft are also broadly employed.

Saddle taper keys (Fig. 5b) are installed on a smooth shaft. Torque is transmitted by friction produced between the shaft and the key during its tightening.

Saddle keys with tongues which bite into the shaft during tightening (Fig. 5c) spoil the shaft surface and must never be used in detachable joints.

Tangent keys (Fig. 6) consist of fox wedges driven into the keyways formed by angular recesses in the shaft and hub. These keys are mounted only in pairs, the angle between the keys being $\alpha = 135\text{-}180°$ (Fig. 7).

Taper keys are now seldom used and only on large-diameter shafts and in joints which do not require accurate centring. The principal

Fig. 5. Taper keys
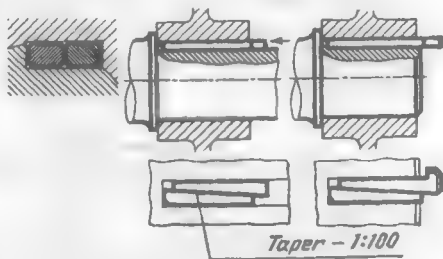
Fig. 6. Tangent keys

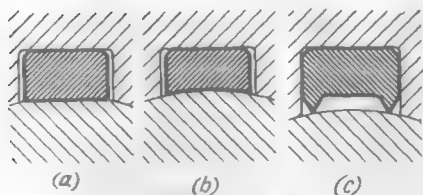shortcomings of taper keys are as follows: eccentricity of the hub because of its unilateral tightening, high stresses in the tightened hub, the hazard of overtightening, and difficult disassembly.
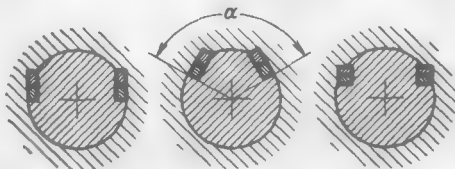
Fig. 7. Installation of tangent keys

(b) Unstressed Joints

Prismatic (Plain Parallel) Keys

Prismatic keys, which are most popular, are installed in the shaft keyway by an interference fit (*driving keys*) or by a push fit (*inserted* or *sunk keys*). A clearance s (Fig. 8a) is left between the upper face of the key and the bottom of the hub keyway.

The fit on the sides in the hub keyway may be slide (for centring joints), running (for moving joints) or push (for cyclically loaded joints).

Hubs are usually mounted on shafts by a centring fit, interference fits being preferred for hub-to-shaft joints subjected to cyclic loads.

The torque acting on the joint produces shearing stresses in the body of the key and crushing (bearing) stresses on its side faces (Fig. 8a). The bending moment M_{bend} which tends to wrench the key out of the keyseat in the shaft is of decisive importance for the strength and stability of the joint.

To improve the embedment strength it is advisable to use wringing fits for the key in the shaft and increase the depth of the keyseat (Fig. 8b). Keys of width $b > 10$ mm are fastened in the keyseat with fillister head (Fig. 8c) or hexagon socket screws.

Fig. 8. Installation of plain parallel keys

The fatigue strength of the shaft in the section weakened by the keyseat is increased by hammering over the key contour (Fig. 8d and e).

The working faces of the keyways in the hub and shaft members are machined to the 5th class of surface finish in standard joints and to the 6th class in critical joints; the bottoms of the keyways are machined to the 4th class of surface finish.

Keyways in hubs are made by slotting or by broaching with a single-spline broach, and in shafts, by milling with end (Fig. 9a) or side (Fig. 9b) milling cutters. The latter method is more efficient and ensures higher accuracy and better finish of the side sur-

Fig. 9. Machining of keyways in shafts

faces, but on the other hand, it increases the axial dimensions of the keyed joint, especially in joints with stop shoulders (Fig. 10), or reduces the key length, if the length of the joint is specified. Besides, the key in this case must be locked axially.

The end milling of keyways is the most popular machining process.

To avoid the fitting-in of the key ends the length l' of the keyseat is made 0.5-1 mm larger than the length of the key (Fig. 11a).

The keyseats are made to terminate at a distance $s = 2$-3 mm from the nearest shoulder for shafts less than 30 mm in diameter, and 4-5 mm for shafts of larger diameter. Stress concentration is increased if the keyseats cut into shoulders. To increase the strength at the shaft ends the value of s' is made 1-2 mm larger than the above figures.

As is usually the case in hub-type joints, thread diameter D_{thd} is 0.5-2 mm smaller than the diameter D of the shaft (Fig. 11b).
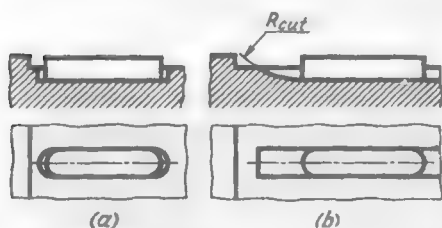
Fig. 10. Installation of keys in end-milled (a) and side-milled (b) keyways
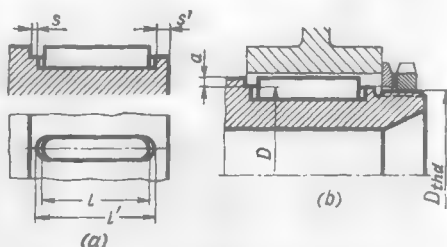
Fig. 11. Installation of keys in closed keyseats

It is reasoned that 2-4 mm is sufficient for the shaft shoulder height a since the hub thrusts against the shoulder over almost complete annular surface.

In shaft-end installations it is good practice to cut the keyway right up to the end face of the shaft (Fig. 12). This reduces the axial
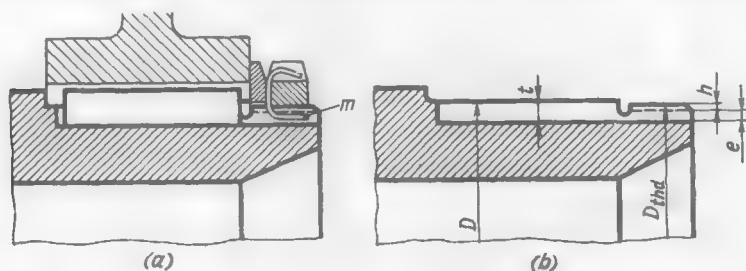
Fig. 12. Installation of keys in keyways cut right up to the shaft end face

dimensions of the joint and increases the effective length of the key, especially if the key end is made flat.

In tightened connections the key is locked axially with a washer and nut (Fig. 12a).

The cutting of the thread through by the keyway, which is inevitable in such connections, has no detrimental effect on the functioning of the thread. The slot in the thread is usually used for the tab m of a lock washer. The only thing required is that the distance e between the bottom of the keyway and the bottom of the thread (Fig. 12b) be sufficient to receive the tab.

From Fig. 12b we have

$$\frac{D}{2} - t = \frac{D_{thd}}{2} - h - e \qquad (1.1)$$

where D and D_{thd} = shaft and thread diameter, respectively

$\quad\quad\quad\quad t$ = keyway depth

$\quad\quad\quad\quad h$ = thread depth

$\quad\quad\quad\quad e$ = tab clearance

From Eq. (1.1) we get

$$D_{thd} = D - 2t + 2h + 2e \qquad (1.2)$$

For metric threads $h \approx 0.7S$ (where S is the thread pitch). With the usual thickness of the lock washer (0.5-1 mm) the minimum tab clearance e_{min} may be taken at 2 mm. Substituting these values into Eq. (1.2), we obtain

$$D_{thd} - (D - 2t + 1.4S) = 2e_{min} \qquad (1.3)$$

Besides, the following condition must be satisfied: $D_{thd} < D$. Let $D = 60$ mm, $t = 5.5$ mm and $S = 1.5$ mm.

The minimum thread diameter satisfying condition (1.3) is

$$D_{thd} = D - 2t + 1.4S + 2e_{min} = 60 - 11 + 1.4 \times 1.5 + 4 = 55 \text{ mm}$$

With the nearest larger value $D_{thd} = 58$ mm and according to Eq. (1.2)

$$e = \frac{1}{2}(D_{thd} - D + 2t - 1.4S) = \frac{1}{2}(58 - 60 + 11 - 2.1) = 3.5 \text{ mm}$$

In mid-shaft installations and on stepped shafts open keyways are seldom used since they require that the difference in diameter
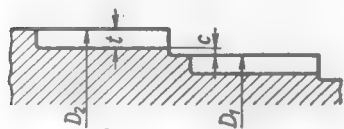
Fig. 13. Open keyways in stepped shafts
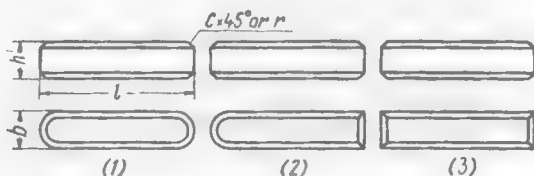
Fig. 14. Keys with rounded and flat ends

between the steps be considerably increased. The diameter D_2 of each subsequent step should be (Fig. 13)

$$D_2 = D_1 + 2t + 2c$$

where D_1 = diameter of the preceding step

$\quad\quad\quad t$ = keyway depth

$\quad\quad\quad c$ = margin for milling cutter overtravel ($c = 0.2$-0.5 mm)

For closed-end keyways the difference between the shaft step diameters is determined only by the assembly conditions, and may amount to several tenths of a millimetre when several parts are fitted on the shaft consecutively. Soviet standards specify three modifications of keys — with rounded ends (*1*), with one rounded and one flat end (*2*) and with flat ends (*3*) (Fig. 14).

The dimensions of plain parallel keys according with the USSR State Standard ГОСТ 8789-68 are illustrated in Table 1.

Table 1

Prismatic (Plain Parallel) Keys
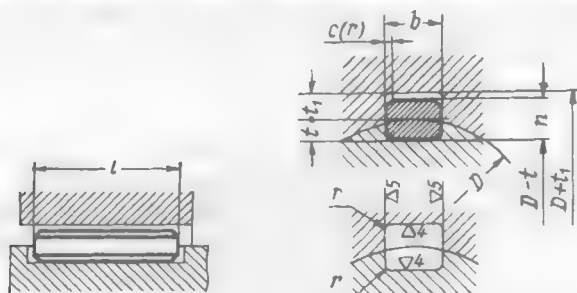
Dimensions in mm

Shaft diameter D	Key dimensions $b \times h$	Keyway depth		Key length l	Keyway corner radii	
		Shaft, t	Hub, t_1		r_{min}	r_{max}
6-8	2×2	1.2	1.0	6-20	0.08	0.16
8-10	3×3	1.8	1.4	6-36		
10-12	4×4	2.5	1.8	8-45		
12-17	5×5	3.0	2.3	10-56	0.16	0.25
17-22	6×6	3.5	2.8	14-70		
22-30	8×7	4.0	3.3	18-90		
30-38	10×8	5.0	3.3	22-110		
38-44	12×8	5.0	3.3	28-140		
44-50	14×9	5.5	3.8	36-160	0.25	0.40
50-58	16×10	6.0	4.3	45-180		
58-65	18×11	7.0	4.4	50-200		
65-75	20×12	7.5	4.9	56-220		
75-85	22×14	9.0	5.4	63-250		
85-95	25×14	9.0	5.4	70-280	0.40	0.60
95-100	28×16	10.0	6.4	80-320		
110-130	32×18	11.0	7.4	90-360		
130-150	36×20	12.0	8.4	100-400		
150-170	40×22	13.0	9.4	100-400	0.70	1.00
170-200	45×25	15.0	10.4	110-450		
200-230	50×28	17.0	11.4	125-500		
230-260	56×32	20.0	12.4	140-500		
260-290	63×32	20.0	12.4	160-500	1.20	1.60
290-330	70×36	22.0	14.4	180-500		
330-380	80×40	25.0	15.4	200-500		
380-440	90×45	28.0	17.4	220-500	2.00	2.50
440-500	100×50	31.0	19.5	250-500		

It is not necessary to strictly adhere to the ratios between the shaft diameter and key dimensions, given in Table 1. In many cases (small working torque, thin-walled hubs, hollow shafts) it is advisable to use keys of a smaller size, if they ensure sufficient load-carrying capacity of the joint.
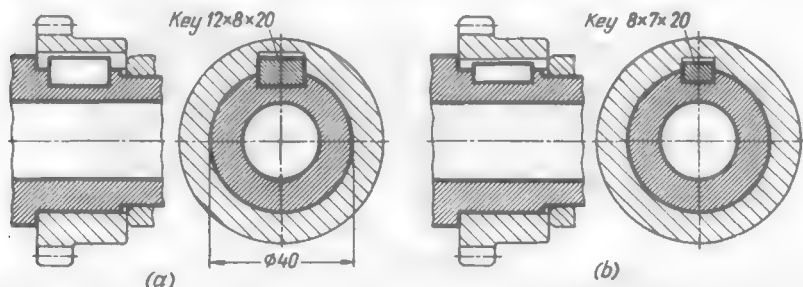

Fig. 15. Installation of keys in low-loaded joints

Figure 15 shows an auxiliary drive shaft transmitting a small torque. A key of normal size (Fig. 15a) weakens both the shaft and hub. In this case it is advisable to install a key of a smaller cross-section (Fig. 15b) and thus increase the strength of the joint.

The key length l in mm is established from the following series: 6, 8, 10, 12, 14, 16, 18, 20, 22, 25, 28, 32, 36, 40, 45, 50, 56, 63, 70, 80, 90, 100, 110, 125, 140, 160, 180, 200, 220, 250, 280, 320, 360, 400, 450, 500.

A key of type A is designated by its nominal dimensions $b \times \times h \times l$ and a State Standard No. For example, a key of modification *1* is designated as follows:

Key 16 × 10 × 80 ГОСТ 8789-68

The same for key modification 2:

Key 2-16 × 10 × 80 ГОСТ 8789-68

Keys of increased height are used when a stronger key embedment in the shaft is required, and also when the hub is made of a soft material (cast iron) to reduce the crushing stresses on the working faces of the keyway.

The dimensions of high prismatic keys are presented in Table 2.

Guide (Feather) Keys

Plain parallel keys fastened to a shaft as shown in Fig. 16, called *quide* or *feather keys*, are used where it is necessary to slide a keyed part (gear or pulley) along the shaft while torque is being transmitted.

In many cases it is more advantageous to fasten the key in the hub (Fig. 17) and make the keyway in the shaft (sliding keys).

Table 2

High Prismatic (Plain Parallel) Keys
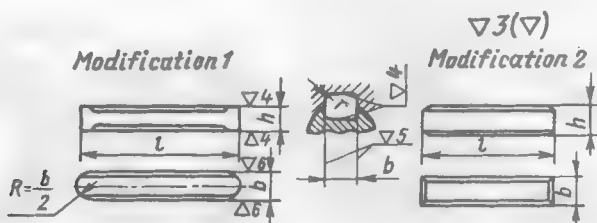
Dimensions in mm

Shaft diameter D	Key dimensions $b \times h$	Key length l	Keyway corner radii	
			r_{min}	r_{max}
30-38	10×9	22-110		
38-44	12×11	28-140		
44-50	14×12	36-160	0.25	0.40
50-58	16×14	45-180		
58-65	18×16	50-200		
65-75	20×18	56-220		
75-85	22×20	63-250		
85-95	25×22	70-280	0.40	0.60
95-110	28×25	80-320		
110-130	32×28	90-360		
130-150	36×32	100-400		
150-170	40×36	100-400		
170-200	45×40	110-450	0.70	1.00
200-230	50×45	125-500		
230-260	56×50	140-500		
260-290	63×60	160-500	1.20	1.60
290-330	70×65	180-500		
330-380	80×75	200-500		
380-440	90×85	220-500	2.00	2.50
440-500	100×95	250-500		

Such keys cannot always be fastened with screws (Fig. 17a and b) because of design. In such cases use is made of inserted keys (Fig. 17c and d). With light loads (if any), when the part sliding along the
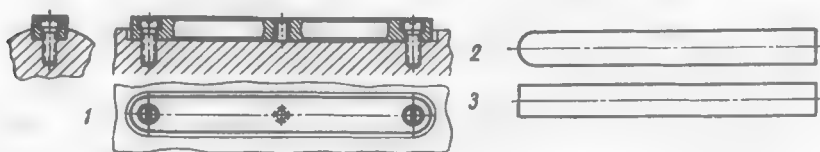

Fig. 16. Guide (feather) keys

shaft must only be locked in a definite angular position, insert guide pins secured in the hub are sufficient (Fig. 17e).

(a)   *(b)*   *(c)*   *(d)*   *(e)*
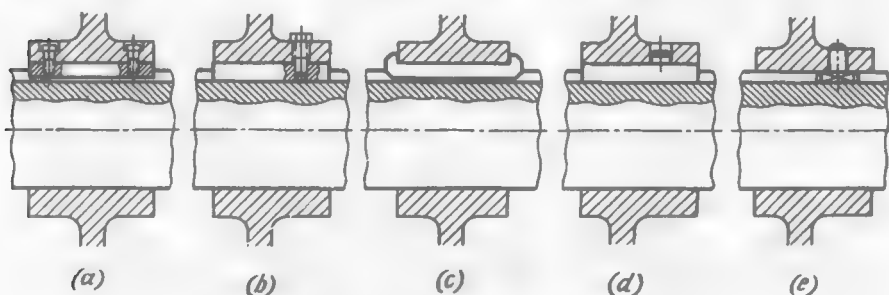
Fig. 17. Sliding keys

Woodruff (Semi-Circular) Keys

Woodruff keys (Fig. 18) are superior in some respects to prismatic keys. The keyslots in shafts are formed by special side milling cutters with higher productivity and accuracy than in the case of prismatic keys. The keys are manufactured from cold-drawn semi-circular sections, and in small-lot production, from round rolled stock then cut into segments. The keys can easily be removed by lightly tapping at their ends.

Such keys are more stable on the shaft because they cut deeper into it, but for all that, Woodruff keys appreciably weaken the shafts (especially hollow ones). This circumstance, in addition to the small key length causing higher crushing stresses on the working faces of the keys, limits their application to low-loaded joints.

With rare exceptions, Woodruff keys are installed only in solid shafts.

The dimensions of Woodruff keys, keyslots and keyways are given in Table 3.

Table 3

Woodruff Keys
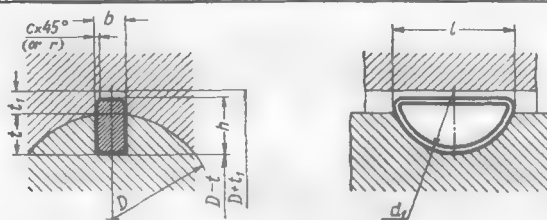
Dimensions in mm

Shaft diameter D		Key dimensions				Depth		Keyway corner radii	
for torque-trans-mitting keys	for locking keys	b	h	d_1	l	Key-slot t	Key-way t_1	r_{min}	r_{max}
From 3 to 4	From 6 to 8	1.0	1.4	4	3.8	1.0	0.6	—	0.05
More than 4 and up to 6	More than 8 and up to 10	1.5	2.6	7	6.8	2.0	0.8		
More than 6 and up to 8	More than 10 and up to 12	2.0	2.6	7		1.8	1.0	0.08	0.16
			3.7	10		2.9			
		2.5	3.7	10	9.7	2.9			
More than 8 and up to 10	More than 12 and up to 17	3.0	3.7	10		2.5	1.4		
			5.0	13	12.6	3.8			
			6.5	16	15.7	5.3			
More than 10 and up to 12	More than 17 and up to 22	4.0	5.0	13	12.6	3.5	1.8		
			6.5	16	15.7	5.0			
			7.5	19	18.6	6.0			
			9.0	22	21.6	7.5			
More than 12 and up to 17	More than 22 and up to 30	5.0	6.5	16	15.7	4.5	2.3		
			7.5	19	18.6	5.5			
			9.0	22	21.6	7.0			
			10.0	25	24.5	8.0			
More than 17 and up to 22	More than 30 and up to 38	6.0	(7.5)	(19)	18.6	(5.0)	2.8	0.16	0.25
			9.0	22	21.6	6.5			
			10.0	25	24.5	7.5			
			11.0	28	27.3	8.5			
			13.0	32	31.4	10.5			
More than 22 and up to 30	More than 38 and up to 44	8.0	(9.0)	(22)	21.6	(6.0)	3.3		
			11.0	28	27.3	8.0			
			13.0	32	31.4	10.0			
			15.0	38	37.1	12.0			
More than 30 and up to 38	More than 44 and up to 50	10.0	13.0	32	31.4	10.0	3.3	0.25	0.40
			15.0	38	37.1	12.0			
			16.0	45	43.1	13.0			
			17.0	55	50.8	14.0			
More than 38 and up to 44	More tnan 50 and up to 58	12.0	19.0	65	59.1	16.0			

Note. Bracketed dimensions should be avoided, if possible.

The side face fits for Woodruff keys are the same as for plain parallel keys.

The diameter d_1 of Woodruff keys is made to the B_5 class of accuracy. The keyslot diameter has a maximum plus deviation of $0.08d_1$ from the nominal key size.

The chamfers c (or radii r) over the contour of the key are made equal to 0.2-0.3 mm. The length l of the key is determined from the formula

$$l = 2h \sqrt{\frac{d}{h} - 1}$$

and for standard Woodruff keys is equal to $(0.92\text{-}0.98)\, d$.

A Woodruff key is designated by the dimensions $b \times h$ and a State Standard No. For example:

Woodruff key 6 × 10 USSR State Standard ГОСТ 8795-68

Fig. 18. Woodruff key

Woodruff key installation examples are illustrated in Fig. 19a-c (cylindrical shafts) and Fig. 19d, e (taper shafts).
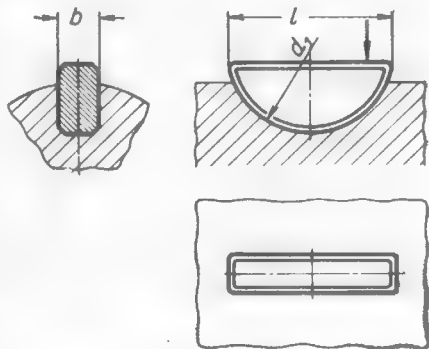

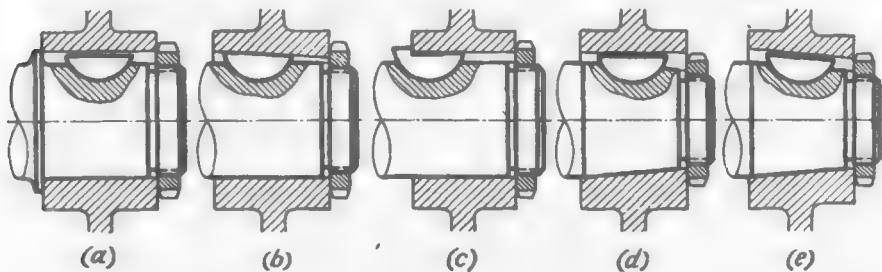*(a)*   *(b)*   *(c)*   *(d)*   *(e)*

Fig. 19. Installation of Woodruff keys

Woodruff keys can be used as tightening stops for hubs on cylindrical shafts (Fig. 19b, c), if the tightening force is not very great.

(c) Fits

Key fits according with the USSR State Standard ГОСТ 7227-58 are given in Table 4.

The tolerances (in microns) for key fits are given in Table 5.

The keyway depth t in the shaft and t_1 in the hub is made to the A_5 class of accuracy, and the length of the key and keyway in the shaft, to the B_7 and A_3 classes, respectively.

The standard does not cover key fits requiring the selection and fitting-in of the keys, and also special fits.

Table 4

Fits for Prismatic, Woodruff and Feather Keys

Fit in shaft keyway	Margin tolerance		Fit in hub keyway	Margin tolerance on hub keyway	Purpose
	on key	on shaft keyway			
Wringing	B_3		Slide	A_3	Piece and serial production
		KW	Running	KW_1	Mass production
Push	R_3		Running	A_3	Feather keys

Table 5

Tolerances on Keys and Keyways

Key width b, mm	Key			Shaft keyway		Hub keyway		
		R_3		KW		KW_1		
	B_3	upper limit	lower limit	upper limit	lower limit	upper limit	lower limit	A_3
1-3	−20	−7	−32	−10	−50	+55	+10	+20
3-6	−25	−11	−44	−10	−55	+65	+15	+25
6-10	−30	−15	−55	−15	−65	+75	+20	+30
10-18	−35	−20	−70	−20	−75	+85	+25	+35
18-30	−45	−25	−85	−25	−90	+100	+30	+45
30-50	−50	−32	−100	−32	−105	+120	+35	+50
50-80	−60	−40	−120	−40	−125	+140	+40	+60
80-120	−70	−50	−140	−50	−150	+160	+45	+70

(d) Allowable Stresses

Keys of ordinary purpose are manufactured from bright-rolled or cold-drawn sections of carbon steel grades 45, 50 and 60. Heavily loaded joints use keys made of alloy steel, for example steel grade 40X heat treated to 35-45 Rc. Heat-treated keys are ground on their working faces.

The dimensions b and h of keys are selected from Table 1 to suit the given shaft diameter. The average key length $l = (0.6$ to $1) D$ where D is the shaft diameter. Then, calculations are made to check the side faces of the key for crushing under the action of peripheral

force P_{per}

$$\sigma_{crush} = \frac{P_{per}}{kl_{work}} \approx 10^3 \frac{2T}{Dkl_{work}} \; (\text{kgf/mm}^2) \qquad (1.4)$$

where T = torque transmitted by the joint, kgf·m

D = shaft diameter, mm

l_{work} = length of the working surfaces of the key, mm

The height of the working surfaces of keys (see Table 1) is

$$k = h - t - c + 0.5D\left[1 - \sqrt{1 - \left(\frac{b}{D}\right)^2}\right] \approx 0.5h \; (\text{mm})$$

The allowable stresses depend on the material of the joint, the character of the load on it, and the type of fit. Approximate values of crushing (bearing) stresses σ_{crush} for *tightened* joints are given in Table 6.

Table 6

Hub material	Load		
	steady	cyclic	impact
	σ_{crush}, kgf/cm²		
Steel $Rc < 30$	1.5-2.0	1.0-1.5	0.5-1.0
Steel $Rc > 30$	3.0-4.0	2.0-3.0	1.0-2.0
Cast iron	1.0-1.2	0.8-1.0	0.5-0.8

In the case of *moving* joints (feather keys) the figures are reduced 2-3 times.

(e) Power Tightening

This type of tightening is extremely important for reliable operation of keyed joints.

The forces of friction between the hub end face and shaft shoulder take some part in transmitting torque, thus relieving the key. In the case of cyclic loads, the frictional forces effectively resist microscopic angular displacements of the hub with respect to the shaft, thus preventing wear and crushing of the side faces of the key and work hardening of the seating surfaces.

Let us determine the share of torque transmitted in keyed joints by the frictional forces due to tightening, accounting only for those produced on the shaft shoulder.

The torque transmitted by the frictional forces on the shoulder

$$T = \frac{P_{tight} f D_m}{2} \qquad (1.5)$$

where D_m = mean diameter of the shoulder (Fig. 20)

     f = coefficient of friction on the shoulder end face

The tightening force

$$P_{tight} = \sigma_{crush}\pi D_m h$$

where σ_{crush} = crushing stress on the shoulder end face

     h = shoulder height

Substituting P_{tight} into Eq. (1.5) we obtain

$$T = \frac{\sigma_{crush}\pi D_m^2 hf}{2} \qquad (1.6)$$

According to Eq. (1.4), the torque transmitted by the key

$$T' = \frac{\sigma'_{crush}l_{work}kD'_m}{2} \qquad (1.7)$$

where σ'_{crush} = crushing stress on the working surface of the key (shaded in the drawing)

     D'_m = mean peripheral force application diameter

k and l_{work} = working height and length of the key, respectively

In conformity with formulas (1.6) and (1.7),

$$\frac{T}{T'} = \frac{\sigma_{crush}}{\sigma'_{crush}} \cdot \frac{D_m^2 h}{D'_m l_{work} k} f\pi$$

Assuming $D_m \approx D'_m$, $h = 2k$, $l_{work} = 0.6\,D'_m$ and $f = 0.1$, we get

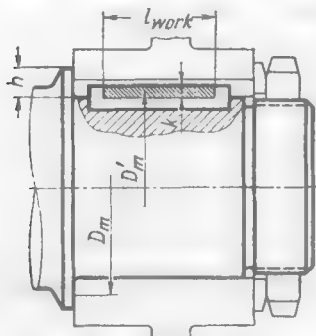$$\frac{T}{T'} = \frac{\sigma_{crush}}{\sigma'_{crush}}$$

Fig. 20. Design diagram

The stress σ_{crush} on the surface of the shoulder is determined by the bearing resistance of the shaft and hub materials. For heat-treated steel the allowable value of σ_{crush} is 20 kgf/mm². The design crushing stress on the key surface seldom exceeds 5 kgf/mm². Therefore,

$$\frac{T}{T'} = \frac{20}{5} = 4$$

Thus, the prevailing share of the torque is transmitted by friction. Power tightening drastically changes the operating conditions of the joint, making it essentially a friction joint where the key plays an auxiliary role, only securing the hub against rotation.

In tightened taper joints the key is practically fully relieved of peripheral forces.

The strongest tightening is provided by ring nuts (Fig. 21a). It is not sufficient to tighten the key with a pressure screw (Fig. 21b). Tightening against the key installed in an inclined position on the shaft (Fig. 21c) is likely to spoil the centring of the joint and increase the rupturing stresses in the hub.

On tapered shafts the key is installed parallel to the shaft axis (Fig. 21*d*) or parallel to the conical surface (Fig. 21*e*). The second method, which complicates the machining of the inclined keyways in the hub and shaft, is only used for long or steep tapers (1 : .10)
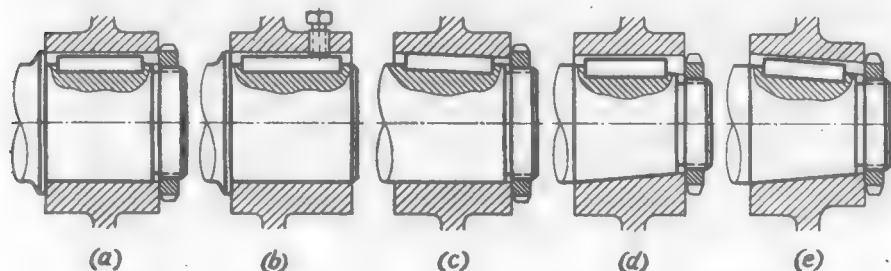

Fig. 21. Tightening of keyed joints

when the key installation parallel to the shaft axis would cause the key edges to emerge from the keyways in the shaft and hub. In such cases it is simpler to use keys of increased height.

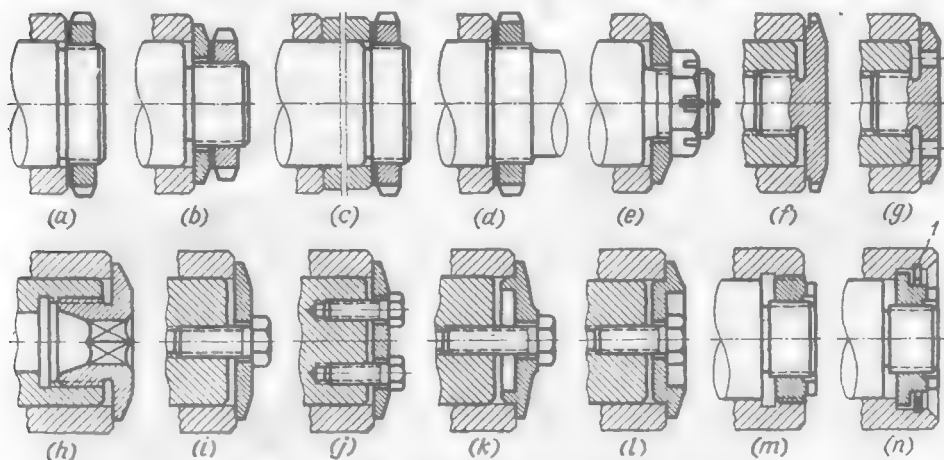Figure 22 illustrates design varieties of axial tightening.

Fig. 22. Design varieties of axial tightening

In shaft-end installations use is ordinarily made of annular nuts which tighten the installed part either directly (Fig. 22*a*), or through the intermediary of washers (Fig. 22*b*) or distance bushings (Fig. 22*c*). This method is also used to tighten parts in mid-shaft installations (Fig. 21*d*).

Tightening with hexagon nuts screwed on the shaft shank (Fig. 22*e*) increases the axial dimensions of the installation.

Internal nuts (Fig. 22*f-h*), whose tightening force is slightly less than that of annular nuts, are employed with hollow shafts. Even weaker is the tightening effected with a central bolt (Fig. 22*i*) or with several offset bolts (Fig. 22*j*).

Figure 22*k, l* presents tightening through the intermediary of centred washers. The design in Fig. 22*l* is preferable where the axial dimensions are to be reduced.

To facilitate disassembly, especially in the case of tight-fitted and taper joints, use is made of pulling means such as differential-thread nuts (Fig. 22*m*). In the design in Fig. 22*n* the nut, while being unscrewed, removes the hub by pressing against internal snap ring *1*.

(f) Design Rules

When determining the external diameter of a hub account should be taken of the fact that the keyway cuts into the hub to a distance of

$$\rho = \sqrt{\left(\frac{D}{2} + t_1\right)^2 + \frac{b^2}{4}}$$

The minimum ratios D_{hub}/D ensuring the proper hub strength at the section where the keyway is located are shown in Fig. 23. The diameter of cast hubs can be reduced, if the hub sections containing keyways are strengthened by local thickened portions (Fig. 24*a*) or ribs (Fig. 24*b*).
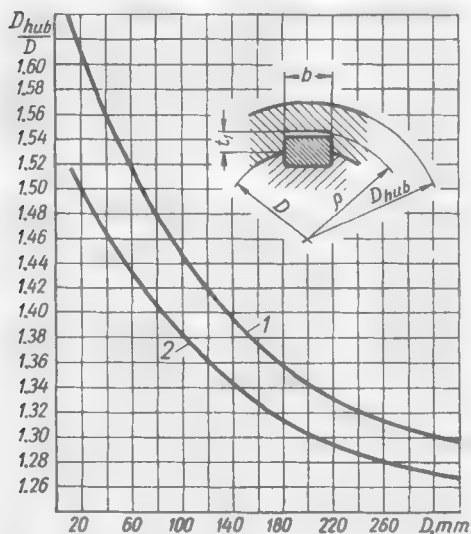

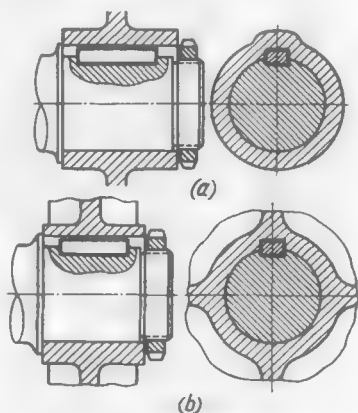Fig. 23. Minimum values of D_{hub}/D for cast-iron (*1*) and steel (*2*) hubs

Fig. 24. Local strengthening of hubs

Tight-fitted keys are not detachable. This fact should be taken into account when parts with a smooth hole (for example, rolling-

contact bearings) are to be mounted on stepped shafts. Assembly is impossible in the design shown in Fig. 25a, since the key projects
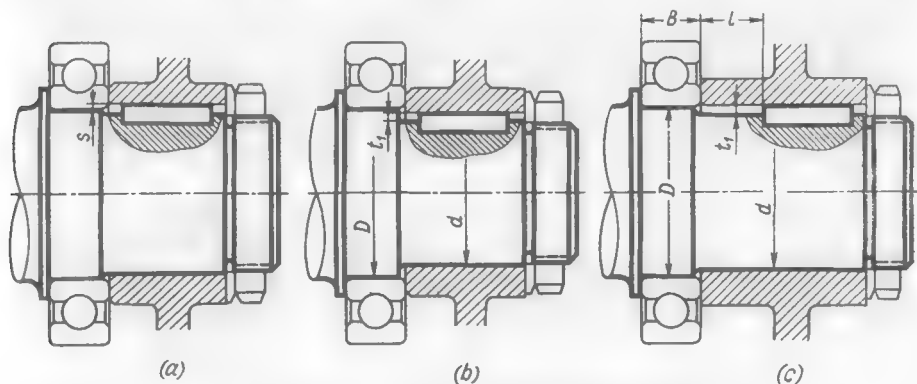

Fig. 25. Unfeasible (a) and feasible (b), (c) joints

(dimension s) and the bearing cannot be installed. For easy assembly the diameter D of the step (Fig. 25b) should be

$$D > d + 2t_1$$

where d is the diameter of the keyed joint and t_1, the key projection height.

The difference in diameter between the steps can be reduced, if the bearing-carrying shoulder is displaced from the key edge to a distance l slightly larger than the width B of the bearing (Fig. 25c).
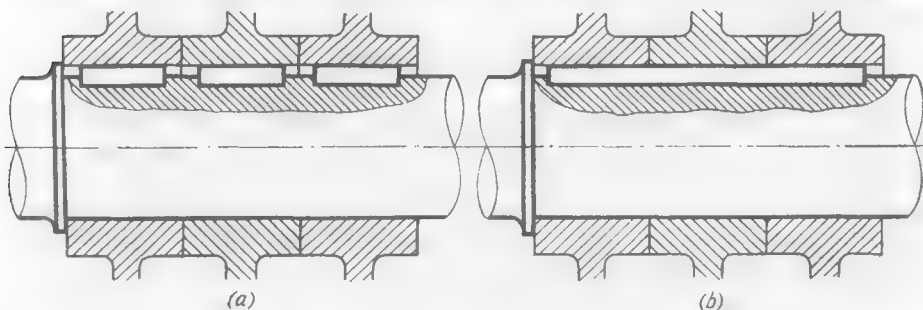

Fig. 26. Installation of parts on a smooth shaft

This allows the bearing to be passed over the key eccentrically and then aligned on the smooth portion of the shaft and installed on the shoulder. In this case the diameter D of the shoulder should be

$$D > d + t_1$$

Inserted (sunk) keys are preferable in such joints.

It is bad practice to mount several parts on smooth shafts using separate sunk keys (Fig. 26a). Inevitable errors in the angular position of the keyseats make it difficult and sometimes impossible to install the parts on the shaft in succession. The parts should preferably be mounted on a single key (Fig. 26b).

To facilitate the dismantling of tight-fitted keys, these are often provided with a threaded hole for a puller screw (Fig. 27a), or fitted in side-milled (sled-runner) keyways from which they can be knocked
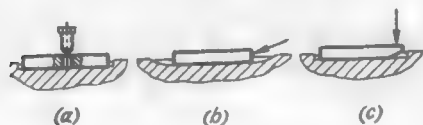

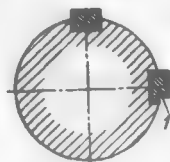Fig. 27. Extraction of driving keys

Fig. 28. Installation with two keys

out axially (Fig. 27b), or else are given a skew cut underneath which enables them to be knocked out radially (Fig. 27c).

Two or three angularly spaced keys (Fig. 28), sometimes used for transmitting large torques, are technologically inadvisable as it is difficult to maintain the same relative position of the keyways in the shaft and hub. As a rule, such keys require individual bench fitting in which one of them (key *1* in Fig. 28) is almost always given a stepped shape. It is far better to use only one key of increased cross-section or, if overall dimensions permit it, make the hub and the key longer.

(g) Special Designs

Figure 29 shows methods employed to strengthen the embedment of keys and prevent their being wrenched out of the keyway.

Increasing the key width (Fig. 29, *1*) makes it possible, while keeping the height of the working key faces unchanged, to enlarge the bearing surface *n*, improve the stability of the key, and reduce the radial dimensions of the joint.

With T-shaped keys (Fig. 29, *2*) stability is attained by making the key abut against flats on the shaft, in the design shown in Fig. 29, *3*, by making the key edges abut against walls *m* of the hole, and in the design in Fig. 29, *4*, by fitting the key into a wedge-shaped keyway.

In the designs shown in Fig. 29, *5* (trapezoidal keys), *6-8* (polyhedron keys), *9* (round keys) and *10, 11* (half-round keys) the peripheral force presses the key against the keyway walls with a force proportional to the transmitted torque.

Crested keys (Fig. 29, *12*) with an increased bearing surface are used when the hub is made of a soft material.
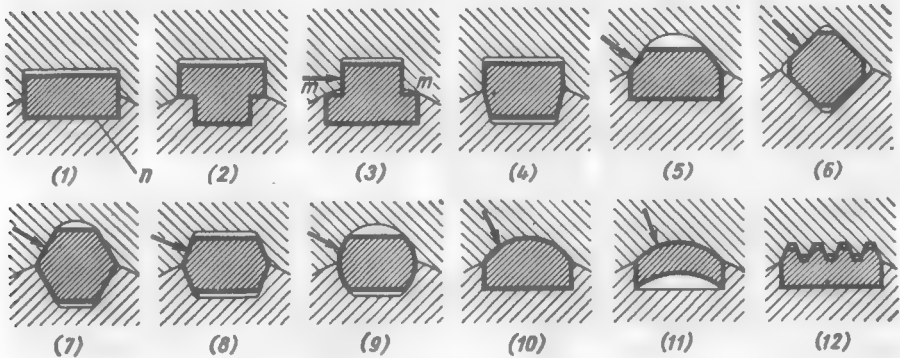

Fig. 29. Special keys

In heavily loaded joints the key is sometimes replaced by a tenon made integral with the shaft or the hub.

In the design in Fig. 30a the tenon is milled on the shaft and enters the keyway formed in the hub by a form broach.
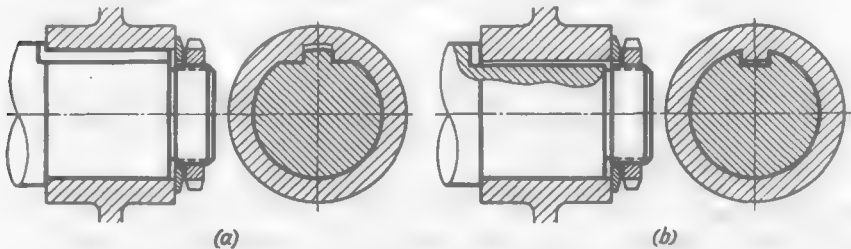

Fig. 30. Keys made integral with the shaft

In the design in Fig. 30b the tenon is formed in the hub by a form broach and enters the keyway milled in the shaft.

In essence, these designs are a transistory stage to splined joints, their strength being less than that of the latter. Inasmuch as either case requires the use of form broaches, splined joints are more preferable.

(h) Dimensioning of Keyed Joints on Drawings

The following three methods are in common use for dimensioning the depth of a shaft keyway: from the extreme shaft diameter point opposite to the keyway (Fig. 31a), from the edge of the cylindrical shaft surface nearest to the keyway (Fig. 31b) and from the extreme point of the diameter lying on the symmetry axis of the keyway (Fig. 31c).

Most correct is the third method as it directly follows from the methods of measuring the keyway depth on finished parts. The depth of keyways in critical shafts is measured with a micrometer depth gauge mounted in a V-block which is placed on the cylindrical surface of the shaft (Fig. 32a). The keyway depth
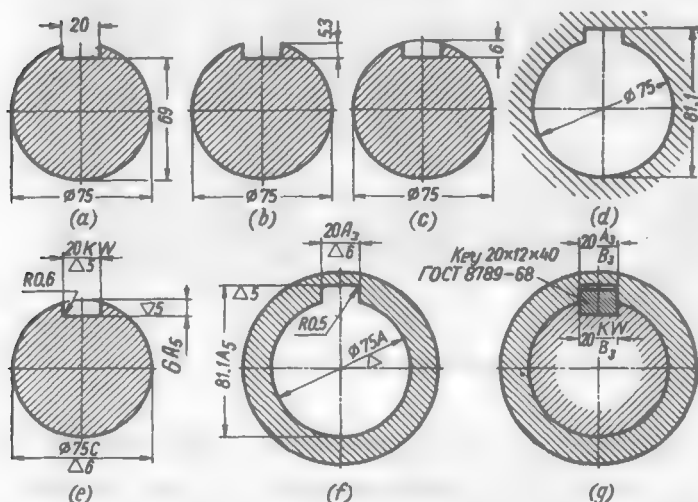

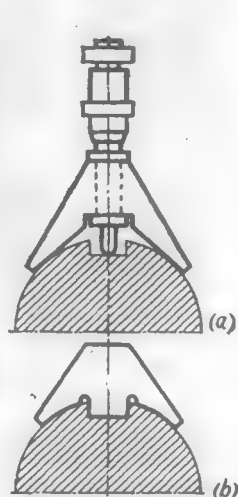Fig. 31. Dimensioning of keyed joints   Fig. 32. Measuring of keyway depth

is determined as the difference between the depth gauge readings taken in the position shown in the Figure and on any smooth portion of the shaft surface.

The keyway size is checked with a key-seat gauge applied to the cylindrical surface of the shaft (Fig. 32b).

Thus, in both cases, the keyway depth is determined with respect to the shaft diameter.

The depth of a hub keyway can best of all be determined by the dimension from the extreme hole diameter point opposite the keyway (see Fig. 31d), which can easily be checked with a vernier calliper or inside micrometer gauge.

Figure 31 illustrates examples of dimensioning on a keyed shaft (Fig. 31e), hub (Fig. 31f) and assembly (Fig. 31g) drawings.

1.2. Splined and Serrated Joints

These joints are markedly superior to keyed joints as to strength, accuracy and suitability for industrial production.

The higher strength of splined and serrated joints stems from the following:

the elements transmitting torque (projections on the shaft and in the hub) make one integral whole with the shaft and the walls of the hub;

the number of these elements is larger and the forces acting on them are correspondingly smaller;

stress concentration at the spline roots is less than in the keyways of a keyed joint.

Keys usually have to be fitted-in individually because of the inaccurate manufacture of the keyways. The manufacture of splined joints is a purely machining operation. It is more productive and less expensive despite the use of special tools.

The present-day methods of machining internal splines (broaching, grinding of the centring surfaces) and external splines (hobbing,
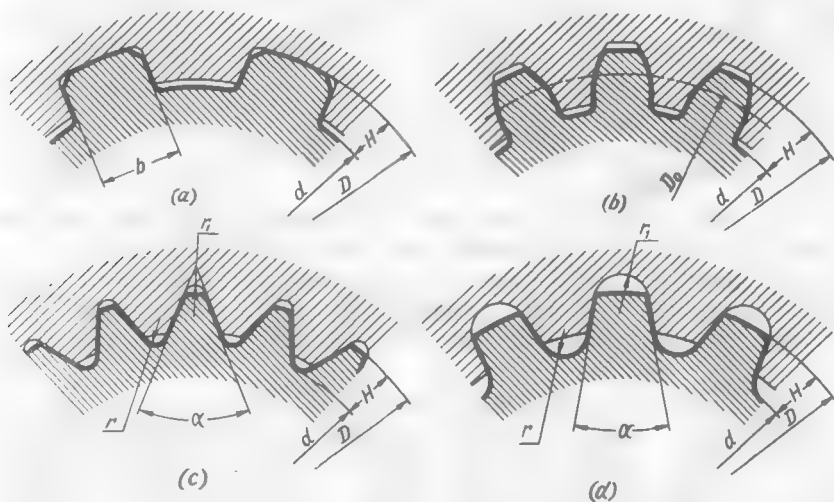

Fig. 33. Basic types of splines

shaping by the generating method, external broaching, grinding of the centring surfaces and working faces of splines) ensure high accuracy and interchangeability of splined parts.

Mechanical engineering employs straight-sided (parallel-side) (Fig. 33a), involute (Fig. 33b), triangular (Fig. 33c) and trapezoidal (Fig. 33d) splines.

(a) Straight-Sided Splines

Straight-sided splined joints are centred from the major or minor diameter or from the side faces of the splines.

Centring from the *major diameter* (*major-diameter fit*) is most accurate and simple (Fig. 34a). The major diameter of shaft splines is ground on a circular grinding machine. Conjugation of this diameter with broached spaces ensures reliable centring.

The re-entrant angles of the spaces are made to a radius $r = (0.1$ to $0.15)$ H where H is the total depth of splines ($H = \frac{D-d}{2}$).

The corners of splines are chamfered at an angle of 45° with a leg f somewhat larger than r.

The noncentring diameters are machined to the following classes of accuracy: d_1 — to class A_5; d — to class R_4. The clearance c left
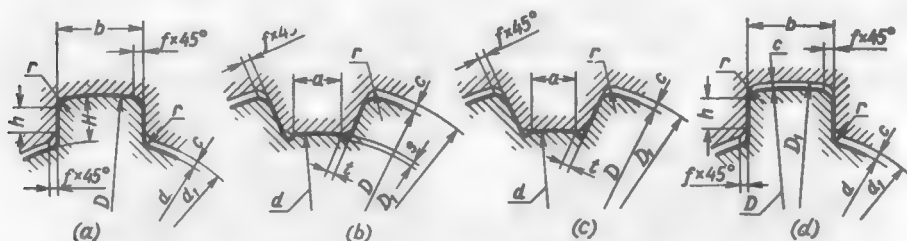

Fig. 34. Centring of splined joints

on the internal surface of the joint is determined by the difference between the margin tolerances according with these classes.

Centring from the *minor diameter* (*minor-diameter fit*, see Fig. 34b) is used when the hub member is heat treated to a hardness of $Rc >$ > 40. Warpage, which is inevitable in heat treatment, can be eli-
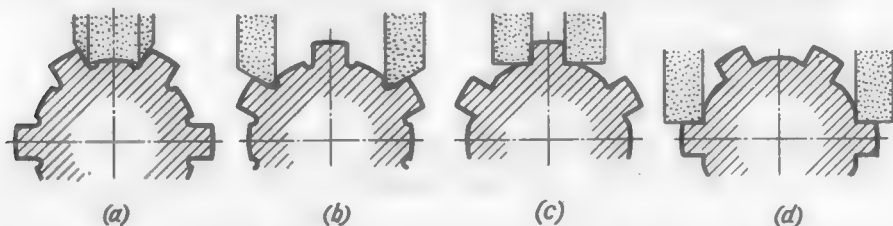

Fig. 35. Grinding schemes for tooth spaces and side faces of splines

minated and an accurate centring surface thus obtained only by grinding the minor diameter in the hub, and accurate surfaces on the shaft, only by grinding the spaces between the splines. The spaces are ground by form wheels with a longitudinal feed (Fig. 35a). Ordinarily the side faces of splines are ground at the same time.

When the grinding is done according to the schemes shown in Fig. 35a and b, undercuts are necessary in the re-entrant angles of the spaces to clear the grinding wheel edges. These undercuts are formed by tongues m on the teeth of a hob cutter (Fig. 36c). The dimensions of the undercuts are standardized.

The undercuts concentrate stresses at the spline roots. The more favourable form of transition is shown in Fig. 34c obtained when the grinding is done as shown in Fig. 35c and d.

The noncentring diameters are machined to the following classes of accuracy: D_1—to class R_5, D—to class R_4. The clearance c formed

on the external surface of the joint is determined by the difference between the margin tolerances according with these classes.

Centring from the *side faces of splines (side-bearing fit*, see Fig. 34d) is used:

(a) in joints requiring strict straightness and planeness of spline side surfaces (for example, in sliding guide joints);

(b) in joints where the shaft-mounted part is heated during operation, or subjected to tension under the action of centrifugal forces
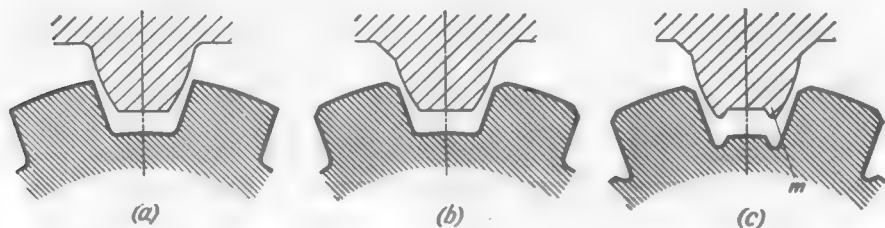

Fig. 36. Profiles of the cutting tooth of a hob cutter for machining splines
(a) with fillets at the root of splines; (b) with fillets and chamfers on the edges of splines; (c) with undercuts and chamfers

(high-speed rotors), which increases the size of the hub hole. This mode of centring enables the correct fit of the part on the shaft to be maintained.

The side faces of shaft splines are usually ground, and undercuts are provided at the spline roots (Fig. 34b, c).

Centring from the side faces may be resorted to only when the hub is made of a material with a hardness of $Rc < 40$, i.e., when broaching can be used as the final machining operation for the hub hole.

The diameters are machined to the following classes of accuracy: D_1—to class R_5, D and d—to class R_4, d_1—to class A_5. The magnitude of clearances c (Fig. 34d) formed on the external and internal surfaces of the joint is determined by the difference between the margin tolerances according with these classes.

Splined Joint Series

USSR State Standard ГОСТ 1139-58 establishes three series of splined joints—light, medium and heavy—differing in the dimensions and number of splines.

The parameters of the joints (z—number of splines, d—minor diameter, D—major diameter, b—width of splines) are given in Table 7.

Table 7

Light series		Medium series		Heavy series	
$z \times d \times D$	b	$z \times d \times D$	b	$z \times d \times D$	b
$6 \times 23 \times 26$	6.0	$6 \times 11 \times 14$	3.0	$10 \times 16 \times 20$	2.5
$6 \times 26 \times 30$	6.0	$6 \times 13 \times 16$	3.5	$10 \times 18 \times 23$	3.0
$6 \times 28 \times 32$	7.0	$6 \times 16 \times 20$	4.0	$10 \times 21 \times 26$	3.0
$8 \times 32 \times 36$	7.0	$6 \times 18 \times 22$	5.0	$10 \times 23 \times 29$	4.0
$8 \times 36 \times 40$	7.0	$6 \times 21 \times 25$	5.0	$10 \times 26 \times 32$	4.0
$8 \times 42 \times 46$	8.0	$6 \times 23 \times 28$	6.0	$10 \times 28 \times 35$	4.0
$8 \times 46 \times 50$	9.0	$6 \times 26 \times 32$	6.0	$10 \times 32 \times 40$	5.0
$8 \times 52 \times 58$	10.0	$6 \times 28 \times 34$	7.0	$10 \times 36 \times 45$	5.0
$8 \times 56 \times 62$	10.0	$8 \times 32 \times 38$	6.0	$10 \times 42 \times 52$	6.0
$8 \times 62 \times 68$	12.0	$8 \times 36 \times 42$	7.0	$10 \times 46 \times 56$	7.0
$10 \times 72 \times 78$	12.0	$8 \times 42 \times 48$	8.0	$16 \times 52 \times 60$	5.0
$10 \times 82 \times 88$	12.0	$8 \times 46 \times 54$	9.0	$16 \times 56 \times 65$	6.0
$10 \times 92 \times 98$	14.0	$8 \times 52 \times 60$	10.0	$16 \times 62 \times 72$	6.0
$10 \times 102 \times 108$	16.0	$8 \times 56 \times 65$	10.0	$16 \times 72 \times 82$	7.0
$10 \times 112 \times 120$	18.0	$8 \times 62 \times 72$	12.0	$20 \times 82 \times 92$	6.0
		$10 \times 72 \times 82$	12.0	$20 \times 92 \times 102$	7.0
		$10 \times 82 \times 92$	12.0	$20 \times 102 \times 115$	8.0
		$10 \times 92 \times 102$	14.0	$20 \times 112 \times 125$	9.0
		$10 \times 102 \times 112$	16.0		
		$10 \times 112 \times 125$	18.0		

The light series having the minimum total depth of splines is mainly intended for fixed joints which transmit small torques under steady impact-free loading conditions; the medium series, for fixed and sliding joints transmitting medium torques under steady or pulsating loading conditions; the heavy series having the maximum total depth and number of splines, for strenuous operating conditions.

Fits

According to the USSR State Standards, the centring-surface fits (major- and minor-diameter fits, side-bearing fits) are established from the standard basic-hole fits for smooth cylindrical surfaces.

Major-Diameter Fit. The tolerances for hubs are established to the accuracy classes A and A_3.

The fit on the centring diameter D depends on the operating conditions of the joint. In the case of permanent joints or joints which are rarely disassembled, use is made of force (F) or push (P) fits, for easily disassembled joints, of slide (S and S_{2a}) fits, and for sliding joints, of easy slide (Se), running (R), slack running (Rs) and loose running (Rl) fits.

In addition to the fit on the centring diameter, the character of the fit on the side faces of the splines is also specified: U for the hub space width, and S for the shaft tooth thickness. The tolerances are established in conformity with the following classes of accuracy: for the hub spaces—U_1, U_2, U_3 and U_4; for the shaft splines— S_1, S_2, S_{2a} and S_3.

The fits in use are as follows: push—S_1P; slide—S_1S and S_2S; running—S_1R and S_2R; slack running—S_2Rs.

Combinations of fits on D and b allowed by the assembly conditions are given in Table 8. The recommended combinations of fits are given in Table 9.

Table 8

Hub	A			A_3		
Tooth space	U_3			U_4		
Shaft	F	P S S_{2a}	$P,\ S$ $S_{2a},\ Se$ $R,\ Rs$	S S_{2a}	Rs Rl R	Rs_{2a}
Spline	S_1P S_2P	S_1P S_1S S_2S	S_1R S_2R	S_2R S_2Rs	S_2R S_2Rs	S_2Rs S_3Rs

Table 9

Hub	A		
Tooth space	U_3		
Shaft	P	R	$R,\ Rs$
Spline	S_1P	S_1R	S_2R

A splined joint with a major-diameter fit is designated on drawings by the symbol of the centring (major) diameter D and the basic parameters of the joint $(z \times d \times D)$.

In addition, the following is also indicated: for hubs—classes of accuracy for the centring diameter and space width; for shafts— fits on the centring diameter and spline side faces.

The most convenient is an expanded designation specifying the dimensions and surface finish of the elements in the joint. Additional detail drawings showing the tooth and space profiles to an enlarged scale are used for dimensioning small structural elements.

Soviet standards do not establish heavy drive spline fits. When necessary, heavy drive fits intended for smooth cylindrical surfaces are used.

Heavy drive fits can be obtained by means of standard cutting tools used for centring fits. For this purpose the hub member is heated to 80-150°C before broaching. After cooling the diameter of the hub hole becomes smaller and ensures adequate interference in the joint. The joint is assembled in a press either cold, or with heating the hub member (or sub-zero cooling the shaft member).

In heating the hub member before broaching, each 10°C increment ensures a diametral interference of ≈ 1 micron per each 10 mm of the diameter of the joint. For example, when a hub with a seating diameter of 80 mm is heated to 120°C an interference of ≈ 0.1 mm is obtained in the joint.

Minor-Diameter Fit. The tolerances on hub holes are established to the accuracy classes A and A_{2a}. The fits on the centring (minor) diameter are as follows: force (F), push (P), slide (S and S_{2a}), easy slide (Se), running (R), slack running (Rs and Rs_{2a}). The tolerances on hub spaces—U_1 and U_2, on shaft splines—S_1 and S_2.

The fits on the side faces of splines are as follows: push (S_1P), slide (S_1S and S_2S), running (S_1R and S_2R), and slack running (S_2Rs).

Combinations of fits on d and b, allowed by the assembly conditions, are given in Table 10.

Table 10

Hub	A			A, A_{2a}	A_{2a}		
Tooth space	U_1				U_3		
Shaft	F, P	P, S, S_{2a}	P, S S_{2a}, Se R, Rs		S_{2a}	Rs	Rs_{2a}
Spline	S_1P	S_1S	S_1R		S_2S	S_2R	S_2Rs

The recommended combinations are given in Table 11.

The designation of a splined joint includes the symbol of the centring surface d.

Table 11

Hub	A		
Tooth space	U_1		
Shaft	P	R	Rs
Spline	S_1P	S_1R	S_2R

Side-Bearing Fit. The tolerances on hub spaces are established to the accuracy classes U_3 and U_4; the tolerances on splines to classes S_1 and S_2. Fits on the side faces of splines are as follows: push (S_1P and S_2P) and running (S_1R and S_2R).

Any combinations of the margin tolerances on the hub spaces and shaft splines are permitted. The recommended combinations are U_3-S_1P and U_3-S_1R.

The symbol of the centring surface b is introduced into the designation.

Dimensioning of Splined Joints

Methods of dimensioning splined joints on drawings are illustrated in Table 12.

(b) Involute Splines

These splines (see Fig. 33b) have involute-profile teeth characterized by module m and pressure angle α_0. Centring is usually effected from the side faces (side-bearing type of fit). The fit may be with interference or clearance, or else it may be of a centring type. Centring from the major diameter of splines (major-diameter fit) is seldom used.

Involute splines have the following advantages over straight-sided ones:
(a) the strength of involute splines is higher: in bending, due to the thickened tooth profile at the root; in compression, due to the greater number of teeth on the periphery;
(b) involute splines are machined to a high accuracy with standard gear-cutting equipment by the generating method with the aid of hob cutters or (on short shafts) gear cutters;
(c) in contrast to straight-sided teeth which require individual hob cutters for the manufacture of each size, involute splines of the same module are formed by one and the same hob cutter (or gear cutter);
(d) the class of side-bearing fit (heavy drive, push, slide and running) can be varied within certain limits by displacing the cutting tool with respect to the shaft;

Table 12

Designation	Projection	Fit		
		major-diameter	minor-diameter	side-bearing
For parts	Hub, side view	$D8 \times 52 \times 60A \cdot U_3$	$d8 \times 52 \times 60A \cdot U_1$	$b8 \times 52 \times 60U_3$
	Plan view	$D8 \times 52 \times 60A \cdot U_3$	$d8 \times 52 \times 60A \cdot U_1$	$b8 \times 52 \times 60U_3$
For parts	Shaft, side view	$D8 \times 52 \times 60PS_1P$	$d8 \times 52 \times 60P \cdot S_1P$	$b8 \times 52 \times 60SP$
	Plan view	$D8 \times 52 \times 60P \cdot S_1P$	$d8 \times 52 \times 60PS_1P$	$b8 \times 52 \times 60 S_1P$
For parts, expanded	Hub	$10U_3 - 8$ spaces $\varnothing 52A_5$ $\varnothing 60A$	$10U_1 - 8$ spaces $\varnothing 52A$ $\varnothing 60R_5$	$10U_3 - 8$ spaces $\varnothing 52A_5$ $\varnothing 60R_5$
	Shaft	$10SP_1 - 8$ splines $\varnothing 52R_5$ $\varnothing 60W$	$\varnothing 52P$ $\varnothing 60R_4$	$10S_1P - 8$ splines $\varnothing 52R_5$ $\varnothing 60R_5$

Table 12 (cont.)

Designation	Projection	Fit		
		major-diameter	minor-diameter	side-bearing
For small elements	Hub			
	Shaft			
For assembled parts	Side view			
	Plan view			

(e) in the case of a side-bearing push fit the splines are appreciably relieved of bending, and the joint predominantly operates in shear at the root of the splines;

(f) involute splines can be subjected to correction (shifting the basic tooth profiles, changing the tooth form factor) to increase strength and obtain standard major diameters;

(g) involute splines on shafts may be subjected to finish machining (shaving for structurally improved or normalized steel, grinding for hardened and chemically heat-treated steel) and also to strain hardening with toothed rolls;

(h) in joints operating with cocking (*compensating connections*) the splines can be given a cambered form by shaving or grinding on a rocking table to ensure free cocking.

Since the shape of the hub hole does not permit the grinding of spaces, involute splines can be used if the hardness of the hub is not above 40 *Rc* when broaching is still possible. The exceptions are hubs subjected to nitriding when there is practically no warpage

Table 13

m	1		1.5		2		2.5		3.5		5		7		10	
D, mm	z	x	z	x	z	x	z	x	z	x	z	x	z	x	z	x
12	11	—	—	—	—	—	—	—	—	—	—	—	—	—	—	—
13	12	—	—	—	—	—	—	—	—	—	—	—	—	—	—	—
15	14	—	—	—	—	—	—	—	—	—	—	—	—	—	—	—
17	16	—	—	—	—	—	—	—	—	—	—	—	—	—	—	—
20	18	0.5	12	0.25	—	—	—	—	—	—	—	—	—	—	—	—
22	20	0.5	14	—0.25	—	—	—	—	—	—	—	—	—	—	—	—
26	24	—	16	—0.25	—	—	—	—	—	—	—	—	—	—	—	—
28	26	0.5	18	—0.25	12	1.0	—	—	—	—	—	—	—	—	—	—
30	28	0.5	18	0.75	14	—	—	—	—	—	—	—	—	—	—	—
32	30	0.5	20	0.25	14	1.0	—	—	—	—	—	—	—	—	—	—
35	34	—	22	0.25	16	0.5	12	1.25	—	—	—	—	—	—	—	—
38	36	0.5	24	0.25	18	—	14	0.25	—	—	—	—	—	—	—	—
40	38	0.5	26	—0.25	18	1.0	14	1.25	—	—	—	—	—	—	—	—
42	—	—	26	—0.75	20	—	16	—0.25	—	—	—	—	—	—	—	—
45	—	—	28	0.75	22	—0.5	16	1.25	—	—	—	—	—	—	—	—
50	—	—	32	0.25	24	—	18	1.25	—	—	—	—	—	—	—	—
55	—	—	36	—0.25	26	0.5	20	1.25	14	1.28	—	—	—	—	—	—
60	—	—	38	0.75	28	1.0	22	1.25	16	0.25	—	—	—	—	—	—
65	—	—	—	—	32	—0.5	24	1.25	18	—0.75	—	—	—	—	—	—
70	—	—	—	—	34	—	26	1.25	18	1.75	12	—	—	—	—	—
75	—	—	—	—	36	0.5	28	1.25	20	0.75	14	2.5	—	—	—	—

	C1	C2	C3	C4	C5	C6	C7	C8	C9	C10	C11	C12	C13	C14	C15	C16
80	—	—	—	—	2.5	14	0.25	22	1.25	30	1.0	38	—	—	—	—
85	—	—	—	—	—	16	−1.25	24	1.25	32	—	—	—	—	—	—
90	—	—	—	—	2.5	16	1.25	24	1.25	34	—	—	—	—	—	—
95	—	—	—	—	—	18	0.25	26	1.25	36	—	—	—	—	—	—
100	—	—	—	—	2.5	18	−0.75	28	1.25	38	—	—	—	—	—	—
110	—	—	2.5	14	2.5	20	0.75	30	1.25	42	—	—	—	—	—	—
120	—	—	0.5	16	2.5	22	−1.25	34	1.25	46	—	—	—	—	—	—
130	—	—	−1.5	18	2.5	24	0.25	36	1.25	50	—	—	—	—	—	—
140	—	—	3.5	18	2.5	26	1.75	38	—	—	—	—	—	—	—	—
150	—	14	1.5	20	2.5	28	−0.25	42	—	—	—	—	—	—	—	—
160	—	14	−0.5	22	2.5	30	1.25	44	—	—	—	—	—	—	—	—
170	—	16	−2.5	24	2.5	32	−0.75	48	—	—	—	—	—	—	—	—
180	—	16	2.5	24	2.5	34	0.75	50	—	—	—	—	—	—	—	—
190	—	18	0.5	26	2.5	36	—	—	—	—	—	—	—	—	—	—
200	—	18	−1.5	28	2.5	38	—	—	—	—	—	—	—	—	—	—
220	5.0	20	1.5	30	2.5	42	—	—	—	—	—	—	—	—	—	—
240	5.0	22	−2.5	34	2.5	46	—	—	—	—	—	—	—	—	—	—
260	5.0	24	0.5	36	—	50	—	—	—	—	—	—	—	—	—	—
280	5.0	26	3.5	38	—	—	—	—	—	—	—	—	—	—	—	—
300	5.0	28	−0.5	42	—	—	—	—	—	—	—	—	—	—	—	—
320	5.0	30	—	—	—	—	—	—	—	—	—	—	—	—	—	—
340	5.0	32	—	—	—	—	—	—	—	—	—	—	—	—	—	—
360	5.0	34	—	—	—	—	—	—	—	—	—	—	—	—	—	—
380	5.0	36	—	—	—	—	—	—	—	—	—	—	—	—	—	—
400	5.0	38	—	—	—	—	—	—	—	—	—	—	—	—	—	—

and broaching can therefore be the final operation in the machining process.

The USSR State Standard ГОСТ 6033-51 for involute splined joints (Table 13) stipulates the pressure angle (basic rack angle) $\alpha_0 = 30°$ and a number of modules m within the range from 1 to 10. To obtain standard major diameters a correction is introduced to some of the joints, the correction factor $x = 0.5\,[D - m\,(z + 1)]$ (where z is the number of splines and D, the major diameter) being either positive or negative.

The designation of an involute splined joint comprises the symbol *Inv.* and the parameters $D \times m \times z$ (major diameter, module, number of teeth).

The following is indicated when side-bearing fit is used: for the hub—accuracy class for spaces (S_3, S_{3a}, S_4), for the shaft—accuracy class for teeth, and fits (wringing S_3W and $S_{3a}W$, slide S_3S and $S_{3a}S$, running S_3R and $S_{3a}R$, loose running S_4Rl).

Example of designation:

for the hub

$$Inv.\ 60 \times 2.5 \times 22S_3$$

for the shaft

$$Inv.\ 60 \times 2.5 \times 22S_3W$$

for the assembled splined joint

$$Inv.\ 60 \times 2.5 \times 22\,\frac{S_3}{S_3W}$$

(c) Triangular Splines

Splines of triangular profile (see Fig. 33c) are principally employed in fine-spline (serrated) joints.
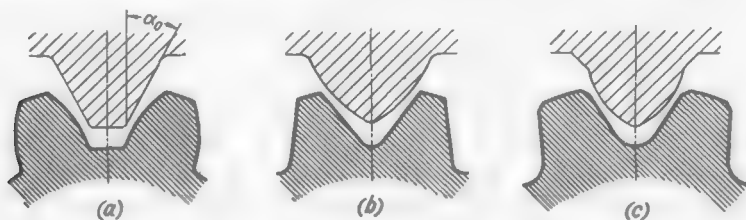
Fig. 37. Milling schemes for involute splines (a), triangular splines (b) and trapezoidal splines (c)

The apex angle α of a shaft spline is usually 60°. Centring is effected from the side faces (side-bearing type of fit).

Similarly to involute splines triangular splines can be used in joints with hubs made of not too hard a material.

Triangular splines with large-radius fillets at the root possess a greater bending strength than involute splines.

Triangular serrations can be formed on a shaft by rolling with a gain in strength and productivity.

A variety of triangular splines are trapezoidal splines (see Fig. 33d) characterized by a small apex angle α of the spline (40-60°) and large fillets at the root $[r = (0.5 \text{ to } 0.6) H]$.

Serrations are generally not standardized although local standards exist in the aircraft and automobile industries.

The methods of machining involute and triangular splines with the aid of hob cutters are shown in Fig. 37.

(d) Tapered Splined Joints

These joints ensure centring without clearances; the hub does not need any support (as in tightened cylindrical joints); tightening against a taper prevents strain hardening and crushing of the splines.

However, such joints are much more difficult to make than cylindrical ones.

When centring is effected from the major diameter (Fig. 38a) the shaft and the surfaces of spaces in the hub are tapered. Each space in the hub is broached individually with a single-spline broach set at an angle to the hub axis. In this case it is difficult to maintain accurate pitch of the splines. Angle φ of taper is equal to 3-5°.

When centring is effected from the minor diameter (Fig. 38b) the spaces in the hub are broached with an ordinary multi-spline broach; the internal surface of splines is ground to a taper. The spaces on the shaft are ground to a taper by means of form wheels fed longitudinally at an angle to the shaft axis.

Fig. 38. Tapered splined joints

In order to ensure sufficient spline depth over the length of the joint, angle φ' of the internal surface taper of the splines must not exceed 1-2° (taper $\approx 1 : 15$).

Joints of this type are tightened with a specified torque to prevent overtensioning and the development of excessive rupturing stresses in the hub and crushing stresses on the centring taper.
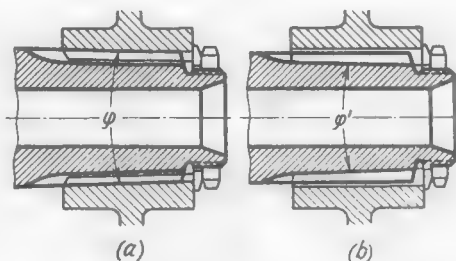
(e) Strength of Splines of Various Profiles

The comparative estimation of spline strength is based on the following assumptions:

(a) the depth of splines is small as compared with shaft diameter.

This assumption, which allows us to disregard the curvature of the pitch circle of a splined joint and consider the splines as being arranged in line, is fully justifiable since the ratios of the total

depth H of the splines to diameter D of the joint, used in practice, are very small (on the average $H/D = 0.05$);

(b) the share of the splines taking up the torque remains the same (it is assumed that the load is equally distributed among all the splines).

In the case of rectangular splines it is assumed that their thickness along the pitch circle is equal to the space width (symmetrical splines). This is the condition of equal strength of the splines on the shaft and in the hub, and also the condition necessary for arranging the maximum possible number of splines over the circumference of the joint and for obtaining minimum stresses in the splines.

In cylindrical joints the strength of splines in the hub is in this case somewhat larger than on the shaft because the splines in the hub widen towards the root.

Straight-Sided Splines

The crushing stress on the working surface of a spline (Fig. 39) is

$$\sigma_{crush} = \frac{P}{hL} = \frac{P}{(H-2r)L} \tag{1.8}$$

where H = total depth of the spline

h = effective depth of the spline, i.e., the total depth minus the fillet of radius r at the spline root and chamfer c at the outer edge of the spline (it is assumed that $r = c$)

L = length of the spline

The force acting on the spline

$$P = \frac{T}{Rz}$$
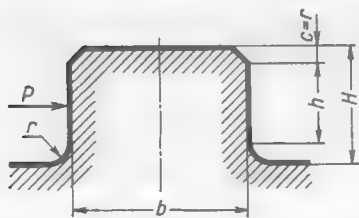
Fig. 39. Design diagram

where T = torque transmitted by the joint

R = mean radius of splines

z = number of splines equal, according to the initial assumption, to $\frac{\pi R}{b}$ (b is the spline thickness)

Hence,

$$P = \frac{Tb}{\pi R^2} \tag{1.9}$$

and

$$\sigma_{crush} = \frac{T}{\pi R^2 L} \cdot \frac{b}{H} \cdot \frac{1}{1-2\frac{r}{H}}$$

Let us call b/H the relative profile thickness and r/H the relative fillet radius, and introduce $b/H = u$ and $r/H = \rho_H$.

Assuming that

$$\frac{T}{\pi R^2 L} = 1 \tag{1.10}$$

we obtain a non-dimensional value—*corrected crushing stress*

$$\sigma_{0\,crush} = \frac{u}{1 - \rho_H} \tag{1.11}$$

The actual crushing stress is

$$\sigma_{crush} = \sigma_{0\,crush}\frac{T}{\pi R^2 L} \tag{1.12}$$

To determine the bending stresses we assume that force P is applied in the middle of the spline depth.

The bending stress in the critical cross-section at the spline root is

$$\sigma_{bend} = k_{eff}\frac{3P\,(H - 2r)}{b^2 L}$$

where k_{eff} is the coefficient of effective stress concentration.

Substituting the value of P from Eq. (1.9) into this expression we get

$$\sigma_{bend} = 3k_{eff}\frac{T}{\pi R^2 L}\cdot\frac{1 - 2\rho_H}{u}$$

The *corrected bending stress* $\left(\dfrac{T}{\pi R^2 L} = 1\right)$ is

$$\sigma_{0\,bend} = 3k_{eff}\frac{1 - 2\rho_H}{u} =$$

$$= \frac{3k_{eff}}{\sigma_{0\,crush}} \tag{1.13}$$

Fig. 40. Coefficient of effective stress concentration in bending of a prismatic bar

Stress concentration can be found from the diagram in Fig. 40a showing the coefficient of effective stress concentration k_{eff} as a function of $\rho_b = r/b$ for a prismatic bar made of strong steel, the diagram being plotted on the basis of averaged data provided by various authors.

The adopted designation $\rho_H = r/H$ is related to the value ρ_b by the relation $\rho_H = u\rho_b$. The diagram for k_{eff} reconstructed according to this relation is illustrated in Fig. 40b.

As can be seen from Eqs. (1.11) and (1.13) the crushing and bending stresses are determined only by the relative spline thickness u and relative fillet radius ρ_H. *The number of splines and their absolute*

dimensions are of no importance. Joints with a small number of large splines and those with many small splines (Fig. 41a) are equistrong if the profiles of the splines are geometrically similar.

Small splines are more advantageous. A reduction in the depth of splines with a given mean diameter of the joint decreases the radial dimensions of the joint and increases the minor diameter of the shaft and, hence, its strength.

The diagram in Fig. 42, plotted on the basis of Eqs. (1.11) and (1.13), shows the

(a)

(b)

(c)
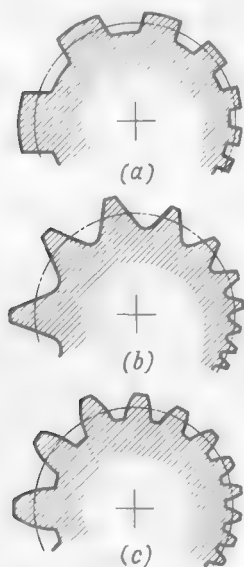
Fig. 41. Splined joints of equal strength
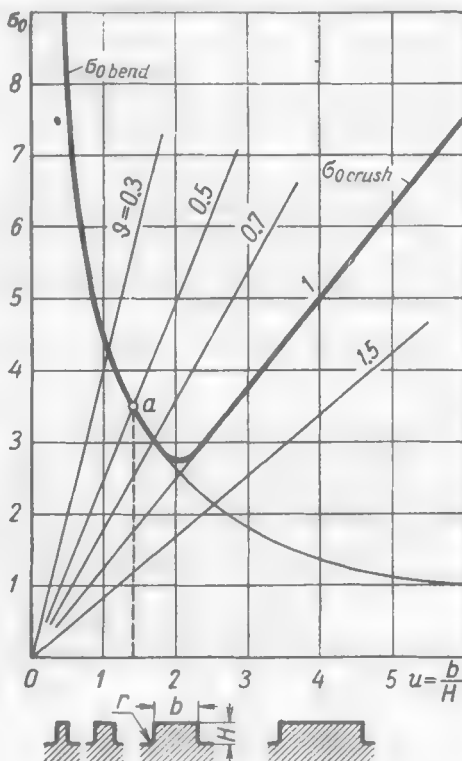
Fig. 42. Corrected crushing stresses $\sigma_{0\ crush}$ and bending stresses $\sigma_{0\ bend}$ as a function of u

values of the corrected crushing (right-hand branch) and bending (left-hand branch) stresses for various u when $\rho_H = 0.1$.

When $u < 2$ the bending stresses exceed the crushing ones and, therefore, determine the spline strength. When $u > 2$ the spline strength is entirely determined by the crushing stress.

Having connected the branches by a smooth transition portion at the point of their intersection, we obtain a regularity governing the change of the stresses in the splines, depending on their relative thickness. The minimum of the curve indicates optimum values u_{opt} (in our case $u_{opt} \approx 2$).

The relations in Fig. 42 hold true, if the allowable bending and crushing stresses are the same. If the allowable crushing stresses are smaller than the allowable bending stresses (sliding joints, hubs made of a softer material than the shaft), then, proceeding from the condition of equal strength, the crushing stresses must be reduced, which is attended by a reduction in the optimum values of u.

With the allowable crushing stresses $\sigma_{crush.al}$ differing from the allowable bending stresses $\sigma_{bend.al}$ the values of u_{opt} can be found if the crushing stress lines on the diagram in Fig. 42 are drawn at an angle whose tangent is changed by the amount $\vartheta = \dfrac{\sigma_{bend.al}}{\sigma_{crush.al}}$.

For example, if the allowable crushing stress is two times smaller than the allowable bending stress, the optimum value of u (point a) becomes $u_{opt} = 1.4$.

The optimum value of u can be determined analytically from the relation $\sigma_{0\ crush} = \vartheta\sigma_{0\ bend}$. Substituting in this equation the values
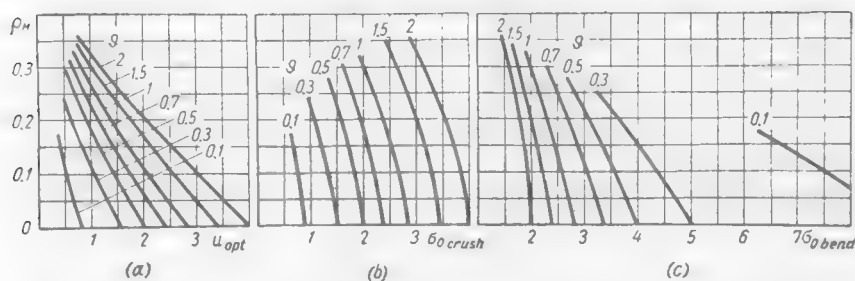
Fig. 43. Optimum values of u and corresponding values of $\sigma_{0\ crush}$ and $\sigma_{0\ bend}$ for various ρ_H and ϑ

of $\sigma_{0\ crush}$ and $\sigma_{0\ bend}$ from formulas (1.11) and (1.13) we obtain

$$u_{opt} = 1.74\,(1 - 2\rho_H)\,\sqrt{\vartheta k_{eff}} \qquad (1.14)$$

The values of u_{opt} calculated from formula (1.14) for various ϑ and ρ_H are presented in Fig. 43a and the corresponding values of crushing stresses $\sigma_{0\ crush}$ and bending stresses $\sigma_{0\ bend}$, in Fig. 43b and c.

The limiting value of ρ_H with $u > 1$ is 0.5 (the crushing area is zero and the crushing stress is ∞). When $u < 1$ the limiting value of ρ_H is $0.5u$ (the space between the splines is described by a circular arc of radius $r = \dfrac{b}{2}$).

Figure 43 shows that when ϑ is small ($\vartheta = 0.1$) the optimum values of u are reduced to 0.4-0.8 and the crushing stresses $\sigma_{0\ crush}$ to 0.6-0.8. At the same time there is a sharp increase in the bending stresses (with $\vartheta = 0.1$, $\sigma_{0\ bend} = 6$-8).

If the bending strength of the hub material is less than that of the shaft material it is better to make the thickness b_{hub} of the hub splines larger than the thickness b_{sh} of the shaft splines in the ratio

$$\frac{b_{hub}}{b_{sh}} = \sqrt{\frac{\sigma_{sh}}{\sigma_{hub}}}$$

where σ_{sh} and σ_{hub} are the bending strengths of the shaft and hub materials, respectively.

With the same spline pitch, the crushing stresses in asymmetrical and symmetrical splines are equal.

Figure 44a illustrates a generalized relation between the strength of straight-sided splines and u when $\vartheta = 1$ for $\rho_H = 0$-0.25.
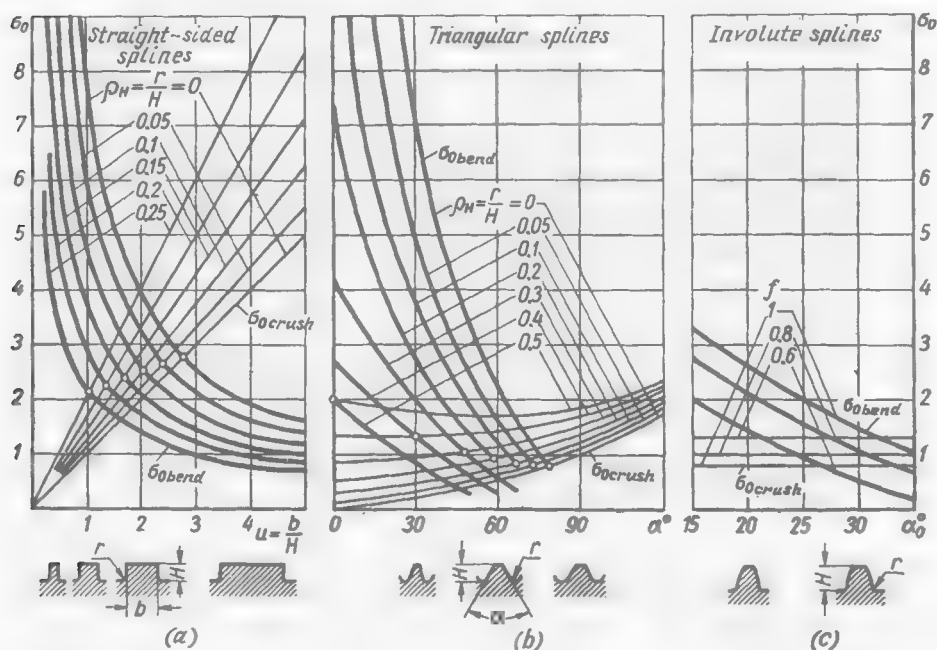
Fig. 44. Corrected stresses σ_0 for variously profiled splines

The optimum values of u (abscissas of the points where the curves meet) are within 1-2.8.

The minimum stresses σ_0 (bright dots) monotonically drop with a decrease in u, beginning at $\sigma_0 = 2.8$ when $u = 2.8$ and $\rho_H = 0$ and ending at $\sigma_0 = 2.1$ when $u = 1$ and $\rho_H = 0.25$.

In the case of joints whose strength is determined by the crushing stresses, the lower values of u are preferable.

Grooved Splines

A special class of straight-sided splines embraces what is called *grooved splines* having their spaces described by a circular arc (Fig. 45) whose radius, proceeding from the condition of the symmetry of the shaft and hub splines, is made equal to $b/2$ and the
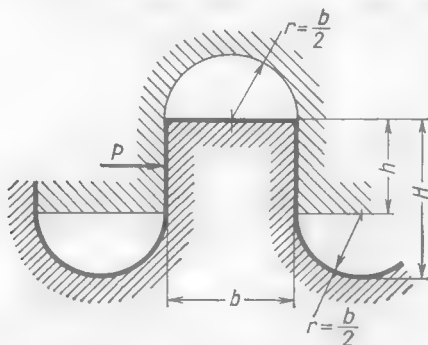
Fig. 45. Design diagram for a grooved spline

relative radius $\rho_H = r/H$, to $0.5u$. This form can be implemented when $u < 2$.

The crushing stress in grooved splines is

$$\sigma_{crush} = \frac{P}{hL} = \frac{P}{(H-r)L}$$

Substituting the value of P_{bend} from Eq. (1.9) and assuming as before that $\frac{T}{\pi R^2 L} = 1$ we obtain the corrected crushing stress

$$\sigma_{0\,crush} = \frac{u}{1-\rho_H} = \frac{u}{1-0.5u} \tag{1.15}$$

The bending stress is

$$\sigma_{bend} = k_{eff}\frac{3Ph}{b^2 L} = 3k_{eff}\frac{T}{\pi R^2 L}\cdot\frac{H-r}{b} = 3k_{eff}\frac{T}{\pi R^2 L}\cdot\frac{1-\rho_H}{u}$$

The corrected bending stress

$$\sigma_{0\,bend} = 3k_{eff}\frac{1-\rho_H}{u} = \frac{3k_{eff}}{\sigma_{0\,crush}} \tag{1.16}$$

With equal strength in bending and crushing

$$\sigma_{0\,crush} = \sigma_{0\,bend} = \frac{3k_{eff}}{\sigma_{0\,crush}}$$

and hence,

$$\sigma_{0\,crush} = \sqrt{3k_{eff}}$$

In this case the effective stress concentration coefficient k_{eff} is a function of $\rho_b = r/b = 0.5$ and, according to Fig. 40a, is equal to 1.2.

Therefore,

$$\sigma_{0\,crush} = \sqrt{3 \cdot 1.2} \approx 1.9 \qquad (1.17)$$

The corresponding optimum value of u may be found from equation (1.15) if we assume that $\sigma_{0\,crush} = 1.9$

$$u_{opt} = \frac{1.9}{1.95} \approx 1$$

It can be seen from Eq. (1.15) that grooved splines of optimum profile are 1.1-1.4 times stronger than straight-sided splines with a fillet at the root, for which, in conformity with Fig. 44, the minimum stresses σ_0 are equal to 2.1-2.8.

For the purpose of unifying cutting tools it is advisable to use the spline modules $m = t/\pi = D/z$ (t — pitch, z — number and D — major diameter of the splines). It is desirable that the series of splined joints be based on the modules $m = 1.25, 2, 5, 10$, for $D < 20$, 30-50, 60-100 and over 100 mm, respectively, with $u = 1$-2 and the number of splines $z = 10, 12, 14$, etc. Division into series will in this case be unnecessary.

Triangular Splines

The crushing stress on the working face of such a spline (Fig. 46) is

$$\sigma_{crush} = \frac{P}{hL} \qquad (1.18)$$

where P is the peripheral force acting on the spline and equal to $\frac{T}{Rz}$.

The number of splines

$$z = \frac{2\pi R}{S} = \frac{\pi R}{h \tan \alpha/2 + 2r \cos \alpha/2}$$

Hence,

$$P = \frac{T}{\pi R^2}(h \tan \alpha/2 + 2r \cos \alpha/2)$$

Substituting the value of P into Eq. (1.18) and assuming as before that $\frac{T}{\pi R^2 L} = 1$, we get the corrected crushing stress

$$\sigma_{0\,crush} = \tan \alpha/2 + 2\rho_h \cos \alpha/2 \qquad (1.19)$$

where

$$\rho_h = \frac{r}{h} = \frac{1}{\dfrac{1}{\rho_H} - 1 + \sin \alpha/2} \qquad (1.20)$$

The corrected bending stress (omitting the intermediate calculations) is

$$\sigma_{0\,bend} = k_{eff}\frac{3}{2}\cdot\frac{\tan\alpha/2 + 2\rho_h\cos\alpha/2}{\cos\alpha/2}$$

$$\times\frac{\dfrac{0.5}{\cos\alpha/2} - (\tan\alpha/2 + \rho_h\cos\alpha/2)\sin\alpha/2}{(\tan\alpha/2 + \rho_h\cos\alpha/2)^2} \tag{1.21}$$

The coefficient k_{eff} of effective stress concentration is the function of

$$\rho_b = \frac{r}{S'} = \frac{\rho_h}{2(\tan\alpha/2 + \rho_h\cos\alpha/2)} \tag{1.22}$$

As can be seen from formulas (1.19)-(1.21) the bending and crushing stresses are determined only by the apex angle α of the spline
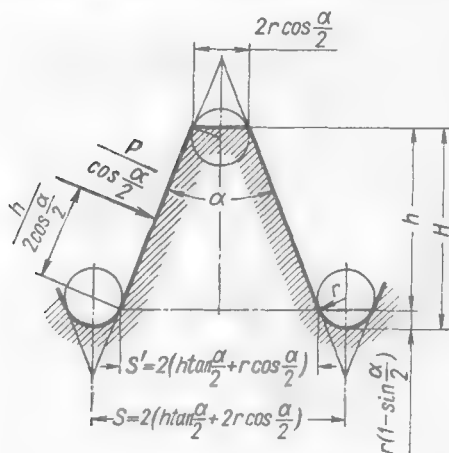
Fig. 46. Design diagram
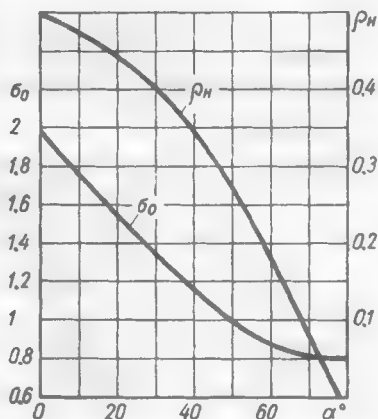
Fig. 47. Relation between ρ_H and α for triangular splines of optimum profile

profile and the relative fillet radius ρ_H. The number and dimension of the splines are immaterial. Joints with a small number of large splines and a large number of small ones (see Fig. 41b) have the same strength, if the spline profiles are geometrically similar.

Figure 44b shows a generalized strength diagram for triangular splines, plotted on the basis of Eqs. (1.19) and (1.21).

The relation between angle α and ρ_H for the splines of optimum profiles is illustrated in Fig. 47. The bending and crushing stresses are minimum ($\sigma_0 = 0.8\text{-}0.9$) when $\alpha = 60\text{-}70°$ ($\rho_H = 0.1\text{-}0.2$). With a drop in α the bending stresses increase. When $\alpha = 0$ and $\rho_H = 0.5$ triangular splines become straight-sided grooved splines (see Fig. 45) with a typical value of $\sigma_{0\,crush} \approx 2$.

When $\alpha = 75\text{-}85°$ ($\rho_H = 0.1\text{-}0.2$) and also when $\alpha > 90°$ the bending stresses are zero (unbending splines), but the crushing stresses increase.

The higher strength of triangular splines is due to the rational use of the circumference of the joint. The entire dedendum circle is practically employed as the base of the splines, this increasing their bending strength. Besides, the bending stresses are reduced because the working faces of the splines are inclined.

Triangular splines of optimum profile ($\sigma_0 \approx 0.9$) are 2.5-3 times stronger than straight-sided splines of optimum profile ($\sigma_0 = 2.1\text{-}2.8$)

Splines of trapezoidal profile (see Fig. 33*d*) are a particular case of triangular splines (small apex angles and large root radii). The stresses for them are determined from the diagrams (see Fig. 44 or 47) for the respective values of α and ρ_H.

Involute Splines

Since the depth of such splines is small as compared with the diameter of the joint, the calculation of the involute splines is based on the profile of the basic rack (Fig. 48).
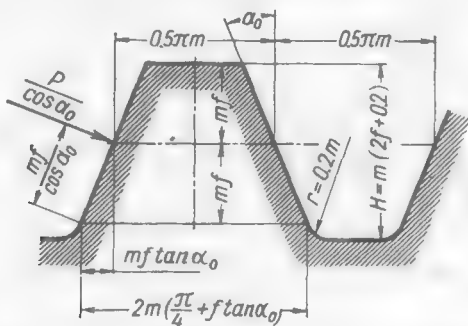
Fig. 48. Design diagram for an involute spline

With the designations adopted for involute engagement, the crushing stress on the working face of a spline is

$$\sigma_{crush} = \frac{P}{2mfL}$$

where m = module

f = tooth form factor

P = peripheral force on the spline $\left(P = \dfrac{T}{Rz}\right)$

L = length of splines

The number of splines

$$z = \frac{2R}{m}$$

Hence,

$$P = \frac{Tm}{2R^2} \tag{1.23}$$

and

$$\sigma_{crush} = \frac{T}{4R^2 fL}$$

The corrected crushing stress

$$\sigma_{0\ crush} = \frac{\pi}{4f} \tag{1.24}$$

Thus, the crushing stresses are determined only by the value of f and do not depend on the module and the pressure angle.

The corrected bending stress in the critical cross-section (omitting intermediate calculations) is

$$\alpha_{0\ bend} = k_{eff} \frac{0.75\pi}{f \cos \alpha_0} \cdot \frac{\frac{1}{\cos \alpha_0} - \left(\frac{\pi}{4f} + \tan \alpha_0\right) \sin \alpha_0}{\left(\frac{\pi}{4f} + \tan \alpha_0\right)^2} \tag{1.25}$$

where α_0 is the pressure angle.

The coefficient k_{eff} of effective stress concentration is in this case a function of

$$\rho_b = \frac{r}{2mf \left(\frac{\pi}{4f} + \tan \alpha_0\right)}$$

For a space with a standard fillet radius ($r = 0.2\ m$)

$$\rho_b = \frac{0.1}{f \left(\frac{\pi}{4f} + \tan \alpha_0\right)} \tag{1.26}$$

and

$$\rho_H = \frac{1}{10f+1}$$

It can be seen from formulas (1.24) and (1.25) that the bending and crushing stresses are determined only by the pressure angle α_0 and tooth form factor f and do not depend on the module. Joints with a small number of large splines and with a large number of small ones (see Fig. 41c) have the same strength if the profiles of the splines are similar.

Figure 44c illustrates the corrected crushing and bending stresses for involute splines as a function of α_0 for $f = 1$, 0.8, 0.6, calculated from Eqs. (1.24) and (1.25). The bending stresses diminish with an increase in the pressure angle. Splines with $\alpha_0 = 30°$ are about two times stronger than splines with $\alpha_0 = 20°$.

The reduction of the tooth form factor f to 0.8 only slightly (by about 20 per cent) increases the bending strength and reduces by as much the crushing strength. When f is reduced to 0.6, the bending strength is increased two or three times. In this case the crushing stresses increase 1.3 times as compared with those at $f = 1$. Splines with $\alpha_0 = 20°$ and $f = 0.6$ have the same bending strength as the splines with standard values of α_0 (30°) and f (1). They can be manufactured with the aid of ordinary tooth-cutting tools.
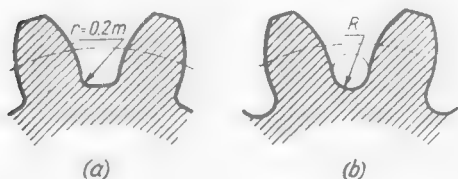
Fig. 49. Involute splines with standard tooth space (a) and rounded tooth space (b)

In terms of total strength involute splines are slightly inferior to triangular splines of optimum profile.

Involute splines with a rounded tooth space (Fig. 49b) may be regarded as a particular case of triangular splines. Their stresses are determined from the diagram in Fig. 44b for the respective values of $\alpha = 2\alpha_0$ and ρ_H.

The value of ρ_H for splines with a rounded tooth space is

$$\rho_H = \frac{1}{\dfrac{2 \cos \alpha_0}{\dfrac{\pi}{4f} - \tan \alpha_0} + 1 - \sin \alpha_0}$$

Calculations show that the bending strength of splines with a rounded tooth space is 10-30 per cent higher than that of splines with a standard tooth space profile. The crushing stresses are the same.

Conclusions. 1. The bending and crushing strengths of splined joints with symmetrical splines do not depend on the dimension and number of splines and are only determined by their profile.

2. As to strength, the greatest advantages are offered by triangular splines; involute splines are almost just as strong, while straight-sided splines are the least strong of the three.

3. The strength of straight-sided splines is determined by the spline thickness-to-depth ratio $u = b/H$, that of triangular splines by the apex angle α and fillet radius ρ_H, and of involute splines, by the pressure angle α_0 and tooth form factor f.

4. The spline parameters providing for their optimum strength are as follows: for straight-sided splines—$u = 1$-2; for triangular splines—$\alpha = 60$-$70°$ with $\rho_H = 0.1$-0.2; for involute splines— $\alpha_0 = 30°$ with $f = 1$, and $\alpha_0 = 20$-$25°$ with $f = 0.6$.

5. In all cases it is better to use small splines which help to reduce the radial dimensions of the joint and increase the strength of the shaft and hub.

6. To simplify manufacture, the unification of spline sizes within as wide a range as possible is advisable.

End-Face Splines

In joints where the axial dimensions are limited use is made of what is called *end-face splines* which take the form of teeth of triangular profile cut on the ends of the members being joined (Fig. 50) and clamped together by an axial force.

To attain full contact between the working surfaces of the mating splines, their generatrices must converge at the centre of the joint. The joint is self-centring. Additional centring (for example, from cylindrical surfaces) is not only superfluous but even harmful since it may spoil the tight clamping of the splines.

End-face splines are cut with a form milling cutter, or with a form gear cutter. The accurate surfaces of the members to be clamped (for example, the surface m in

Fig. 50. Joint with end-face splines

Fig. 50) are machined after assembly when the splines have been tightened. To prevent the spoiling of the accuracy attained previously, it is necessary to constructively ensure that the joint each time is assembled in the original position.

End-face splines differ from radial ones in the following:

(a) the length L_{e-f} of the splines (Fig. 51) is limited by the diametral dimensions of the joint $[L_{e-f} = R - R_0 = R (1 - R_0/R)]$. Usually, $L_{e-f} = (0.3 \text{ to } 0.5) R$;

(b) the peripheral force acting on end-face splines is increased as compared to the force acting on radial splines in the ratio

$$R/R_{mean} = \frac{2}{1 + R_0/R} \text{ (usually } R/R_{mean} = 1.2\text{-}1.4);$$

(c) when torque is transmitted, in the joint there develops an axial tension $P_{ax} = \frac{T}{R_{mean}} \tan \alpha/2$ where α is the spline apex angle in the middle spline section. To prevent the parting of the joint the tightening force must be $P_{tight} = nP_{ax}$ where n is the safety factor (usually $n = 1.5\text{-}2$).

A positive feature of end-face splines is the tightening of their working surfaces (*constrained bending*). Such splines operate practically in shear.

The crushing stresses on the working sides of the splines are the sum of stresses due to peripheral force P and tightening force P_{tight}

$$\sigma_{crush.\ e\text{-}f} = \frac{P}{zL_{e\text{-}f}h} + \frac{P_{tight}}{2zL_{e\text{-}f}h \tan \alpha/2}$$

where h is the effective depth of splines.
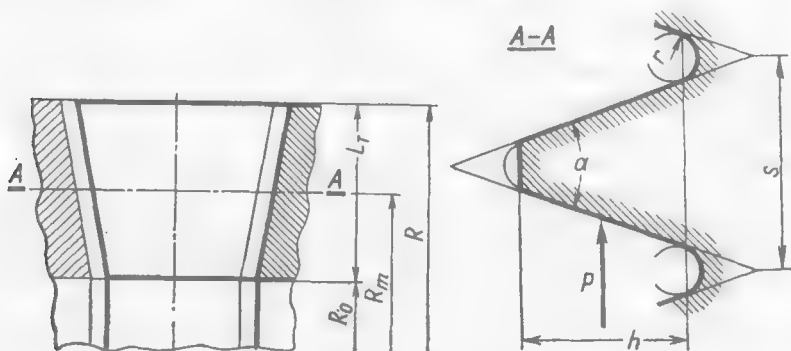
Fig. 51. Design diagram for end-face spline

Substituting in this expression the values

$$P = \frac{T}{R_{mean}}; \quad P_{tight} = \frac{nT \tan \alpha/2}{R_{mean}}$$

$$z = \frac{2\pi R_{mean}}{S}; \quad R_{mean} = \frac{R}{2}(1 + R_0/R)$$

we obtain

$$\sigma_{crush.\ e\text{-}f} = \frac{\cdot\ 4T}{2\pi R^2} \cdot \frac{(1 + 0.5n)\,S}{(1 + R_0/R)^2\, L_{e\text{-}f}h} \tag{1.27}$$

For radial triangular splines with the same external radius R the crushing stresses are

$$\sigma_{crush} = \frac{T}{RzLh} = \frac{TS}{2\pi R^2 Lh}$$

With the same spline profile in the middle cross-section (S and h are the same) the crushing stresses in end-face splines are higher than in radial ones in the ratio

$$\frac{\sigma_{crush.\ e\text{-}f}}{\sigma_{crush}} = \frac{4\,(1 + 0.5n)}{(1 + R_0/R)^2} \cdot \frac{L}{L_{e\text{-}f}}$$

Taking for average conditions $R_0/R = 0.5$, $n = 2$ and assuming that $L_{e\text{-}f} = L$, we obtain

$$\frac{\sigma_{crush.\ e\text{-}f}}{\sigma_{crush}} = \frac{4 \cdot 2}{1.5^2} \approx 3.5$$

Thus, with the major diameter, profile and length of splines being the same, the crushing stresses in the end-face splines are 3.5 times larger than in the radial ones, and the shearing stresses are larger in the ratio

$$\frac{4}{(1+R_0/R)^2} = \frac{4}{1.5^2} \approx 1.75$$

The crushing stresses can be decreased by reducing the apex angle α and the radius ρ_H of the tooth space. In practice, the value of α is taken at 40-60° and that of ρ_H, at 0.1-0.2.

To avoid overtensioning, the end-face splines should be tightened to a specified torque while keeping to the ratio

$$P_{tight} = n \frac{T}{R_{mean}} \tan \alpha/2$$

With the given α and R, the crushing stress, according to Eq. (1.27), is determined by factor φ (see Fig. 52) expressed as

$$\varphi = \frac{1}{(1+R_0/R)^2 L_{e-f}} = \frac{1}{(1+R_0/R)^2 (1-R_0/R)}$$

Fig. 52. Relation between φ and R_0/R

As can be seen, the crushing stresses are minimum ($\varphi = 0.85$-1) within the range $R_0/R = 0.2$-0.5, and sharply increase when $R_0/R > 0.7$.

In view of the inverse-cube relation between the stresses and R it is good practice to increase the diameter of the splined belt (flanged splined joints).
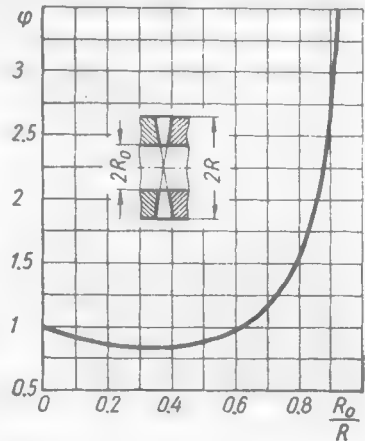
(f) Calculation of Splined Joints

Splined joints commonly fail as a result of the crushing of the spline working faces. Therefore splines are usually calculated for crushing only.

The crushing stress in kgf/mm² on the working faces of splines is

$$\sigma_{crush} = \frac{10^3 T}{RLkzh} \qquad . (1.28)$$

where T = torque acting on the joint, kgf·m
R = mean radius of splines, mm

L = effective length of splines, mm

z = number of splines

k = share of splines taking the load ($k = 0.6$-0.8)

h = effective depth of splines (total depth minus fillets and chamfers), mm

For joints with the same thickness of the shaft and hub splines on the pitch circle

$$\sigma_{crush} = \sigma_{0\ crush}\frac{T}{\pi R^2 Lk} \tag{1.29}$$

where $\sigma_{0\ crush}$ is the corrected crushing stress typical of each spline profile and determined from the diagram in Fig. 44.

The design stresses for fixed tightened splined joints with a steel shaft and hub are given in Table 14.

Table 14

Heat treatment of splines	Design stress σ_{crush}, kgf/mm²		
	steady load	cyclic load	impact load
Structural improvement (30-35 Rc)	3-4	2-3	1-2
Induction hardening, carburizing (55-60 Rc)	4-6	3-4	2-3
Nitriding (900-1000 VPH)	6-8	4-6	3-4

For sliding joints and joints with clearance on the side faces of splines these figures are reduced two-three times.

If the hub member is made of a soft material (grey iron, light alloys) the calculation is made on the basis of the crushing stresses permissible for the given material.

If the crushing stresses are to be reduced use is made of splines with a more advantageous profile, or the length and diameter of the joint are increased. In conformity with Eq. (1.12), the torque transmitted by the joint is

$$T = \frac{\sigma_{crush}}{\sigma_{0\ crush}}\pi R^2 L$$

i.e., with the spline profile being specified ($\sigma_{0\ crush}$ = const), the torque is proportional to the square of the diameter and if, as is usually the case, the length of the joint L is proportional to the diameter, the torque is proportional to the cube of the diameter.

When the hub members have a large major diameter (e.g., disks), the length of the splined joint is mainly determined by the condition of the longitudinal stability of the hub. Irrespective of the calculation results, the length of splines should not be less than (0.5 to 0.8)D, or, better still, (1 to 1.2)D (where D is the shaft diameter). There is no sense in increasing the length of the joint above (1.5

to 2) D because this will impair the accuracy of manufacture and reduce the actual area of contact between the splines.

Division of splines into two short belts with a recess in-between (Fig. 53), sometimes used in long joints, makes it difficult to broach the hub hole. Chips produced in the first belt (in the direction of broaching) fall out of the chip spaces of the broach and are pulled into the second belt, thus impairing the
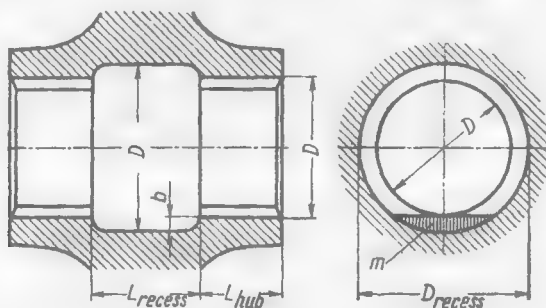
Fig. 53. Splined joint with a central recess

accuracy and surface finish of the splines. Such holes can be broached only in a horizontal broaching machine and only if the recess is large enough to accommodate the chips (allowing for the fact that the chips break up) in the segment m of the annular space between the circumference of the recess and the external diameter of the broach.

The required diameter D_{recess} of the recess may be found from the approximate formula

$$D_{recess} = D + 2\sqrt{sDKL_{hub}/L_{recess}}$$

where D = external diameter of splines, mm
s = mean allowance for broaching, mm
L_{hub} = length of the first splined belt in the hub (in the direction of broaching), mm
L_{recess} = length of recess, mm
K = break-up coefficient of chips ($K = 4\text{-}5$)

(g) Design Rules

The most stressed section in splined shafts is section A-A (Fig. 54a), the full torque transmitted by the joint and the bending stresses of the splines being active in this section. The degree of stress concentration depends on the form of transition from the splines to the shaft.

The stresses in this section can be effectively reduced if the minor spline diameter D_{min} (Fig. 54b) is made 15-20 per cent greater than the shaft diameter d.

The uniform load distribution over the length of splines largely depends on the form of the hub and shaft. No abrupt changes in cross-sections are allowed, and where such changes are required

by the design, account should be taken of the direction of the force flow. The design of the hub member shown in Fig. 54c is irrational. The load on the splines is mainly transmitted at the node of rigidity
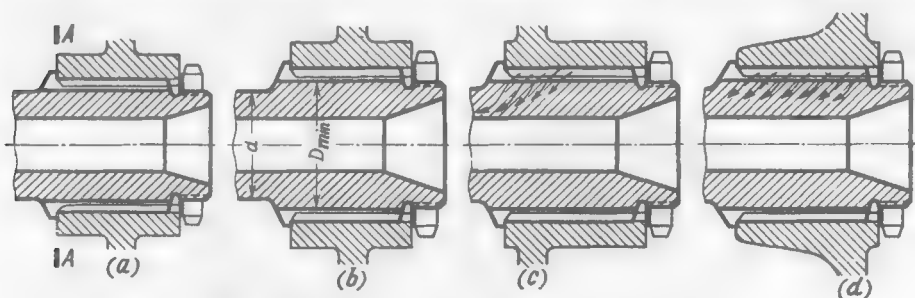
Fig. 54. Strengthening of splined joints

(where the hub passes into the disk). The rest of the splines are loaded weakly. The load on the splines is equalized if the disk is transferred to the front edge of the hub and the transition between the disk and the hub is made more smooth (Fig. 54d).
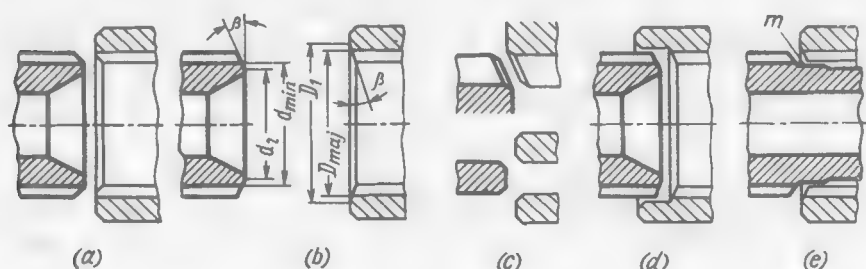
Fig. 55. Dressing of spline end faces

The entrance edges of the splines both on the shaft and in the hub must be chamfered to make assembly easier and to avoid the concentration of forces at the edges, and also to prevent an accidental denting of the splines during mounting, disassembly and shipment.

It is not sufficient to chamfer only the corners of the splines (Fig. 55a). It is better to bevel the splines to an angle $\beta = 15$-$30°$ (Fig. 55b) so as to make the external diameter D_1 of the hub chamfer slightly larger than the major diameter D_{maj} of the hub splines, and the internal diameter d_2 of the shaft chamfer smaller than the minor diameter d_{min} of the shaft splines.

It is good practice to make chamfers or fillets over the entire contour of spline end faces (Fig. 55c). In mass production this operation is done on special dressing machines.

The contour dressing of the spline end faces is obligatory for sliding gear splines (for example, in clutches).

The hub splines should preferably be sunk with respect to the hub end face (Fig. 55d). This measure prevents the denting of the splines,
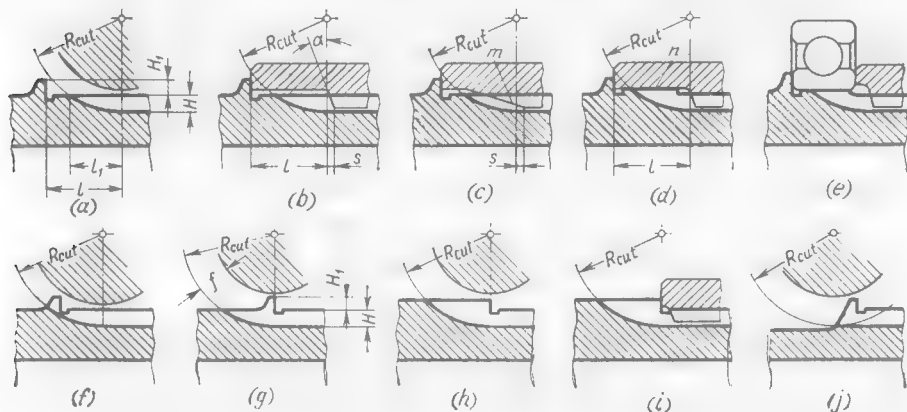
Fig. 56. Shapes of shaft splines

increases the strength of their exit portion and eases assembly, especially when heavy parts are assembled in a horizontal position.

If a splined shaft has an extension, assembly can be facilitated by providing a centring belt m (Fig. 55e) on the shaft portion nearest to the splines, the diameter of the belt being slightly less than the minor diameter of the shaft splines.

The tightening force is usually taken up by shoulders on shafts. If a rest against a solid annular surface is required, the shoulder is provided on the smooth portion of the shaft (Fig. 56a). Full-profile splines are terminated at a distance l from the shoulder so that the milling cutter does not cut into the shoulder.

Fig. 57. Setting of a hob cutter with respect to the blank

The tooth space bottom in section l_1 of the hob cutter overtravel is described by an ellipse whose minor axis is equal to D_{cut} and the major axis, to $D_{cut} \cos \varphi$ where D_{cut} is the external diameter of the cutter and φ is the skew angle, i.e., the plan angle of the cutter setting with respect to the shaft blank (Fig. 57), determined from the ratio $\tan \varphi = \dfrac{t}{\pi D_{0\ cut}}$ where $D_{0\ cut}$ is the mean diameter of the hob teeth and t, the pitch of the tooth helix.

According to the equation of an ellipse,

$$l_1 = \frac{H}{\cos \varphi} \sqrt{\frac{D_{cut}}{H} - 1}$$

where H is the depth of splines.

Since angle φ is small (usually $\varphi = 3\text{-}5°$) and $\cos \varphi$ is close to unity, it may be assumed that the section of the cutter overtravel is described by a circular arc with a diameter D_{cut}, and then the value of l_1 may be determined from the relationship

$$l_1 = H \sqrt{\frac{D_{cut}}{H} - 1} \qquad (1.30)$$

The minimum distance l_{min} when the shoulder is not undercut is

$$l_{min} = (H + H_1) \sqrt{\frac{R_{cut}}{H + H_1} - 1} \qquad (1.31)$$

where H_1 is the height of the shoulder.

The hob diameter can be found in appropriate standards or from the size range of the hob cutters available at the manufacturing plant. The value of D_{cut} may approximately be taken equal to the shaft diameter.

The hub splines should not protrude beyond the beginning of the shaft tooth space bottom climb, and a safety clearance $s = = 1\text{-}2$ mm (Fig. 56b) should be provided, which prevents the splines from touching the tooth space bottoms. For this purpose the spline ends are usually bevelled to an angle $\alpha = 15\text{-}20°$, beginning at the point corresponding to the extreme position of the hob cutter.

To increase strength, the hub splines in the cutter overtravel section are connected with the hub by sloping transition portions m (Fig. 56c).

The shaft portion l (Fig. 56b) is sometimes used to centre the hub by means of a centring collar n (Fig. 56d), or to fit on parts such as antifriction bearings (Fig. 56e).

In designs requiring no solid annular bearing surface the shoulders are cut either partially (Fig. 56f) or all the way through (Fig. 56g, h) so that the hub splines can be brought close to the shoulder (Fig. 56i) and the total length of the splined joint thereby reduced.

On splined shafts ground on the internal diameter or on the side faces of the splines the smooth surface of the shaft should be arranged below the tooth space bottoms (Fig. 56j) to allow through-pass machining. The strength of such splines is slightly less than in the designs shown in Fig. 56g and h. The shoulder can be cut through by a milling cutter having increased-height cutting teeth f (Fig. 56g). For better strength and durability of the teeth the height H_1 of the shoulder should not exceed $0.5H$ (Fig. 58a and b).

The height of shoulders in the case of involute splines is limited because the splines are thinned towards the tip (Fig. 58c). With

the basic rack angle $\alpha_0 = 30°$ the limiting height H_1 of the shoulder is approximately equal to $0.5m$ (where m is the module), or to 0.25
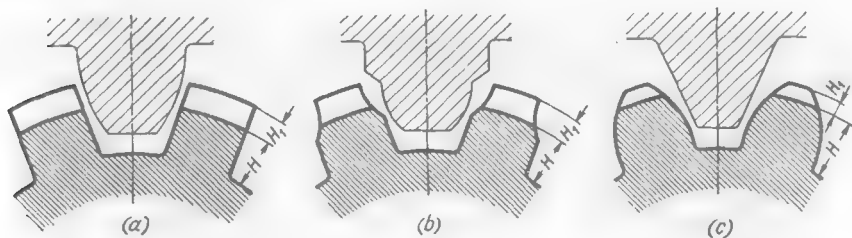
Fig. 58. Machining of splines with through-cut locating shoulders
(a) with fillets at the root of splines; (b) with fillets and chamfers on the edges of splines; (c) involute splines

of the spline depth; when $\alpha_0 = 20°$ the height H_1 of the shoulder is about $0.6\ m$, or about 0.3 of the spline depth.

Abutment against a cut-through shoulder cannot be used in the case of triangular splines.

A tight fit of the hub end face against the locating shoulder of the shaft is ensured either by a chamfer (Fig. 59a) or by a recess in the hub (Fig. 59b), or else by a groove in the shaft splines (Fig. 59c).

The numerical value of the radius of the tooth space bottom climb is usually not indicated on the drawings of splined shafts. The only designations are R_{cut} (Fig. 60a) and the length L of the section with fully profiled splines.

If the total spline length $L + l_1$ is to be strictly adhered to, the milling cutter radius is indicated or, more preferably, the coordinate l' of the point of emergence of the tooth space bottom specified.

The length of the portions to be ground (Fig. 60b) is indicated for splined shafts requiring grinding on the minor diameter or sides of the splines.

The length l_2 of the climb portion of the tooth space bottom must be sufficient to permit the over-travel of the grinding wheel, and may be determined from the relation

Fig. 59. Seating against spline shoulders

$$l_2 \geqslant H \sqrt{\frac{D_{wh}}{H} - 1}$$

where D_{wh} is the grinding wheel diameter, and H, the depth of the splines.

Apart from seating against a thrust shoulder, other methods are in common use. Seating against a pin press-fitted into the shaft

(Fig. 61a) does not allow power tightening and can be applied only to low-loaded joints. More practicable are designs where seating
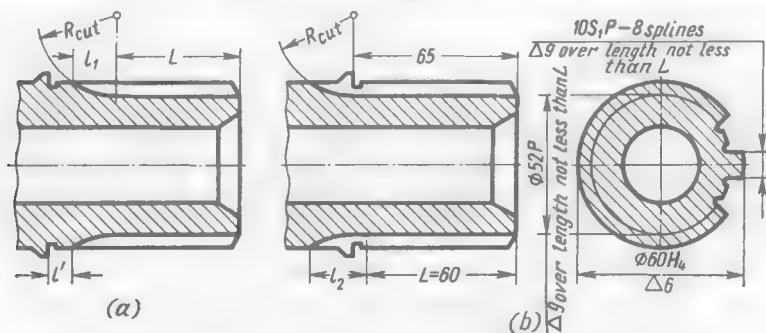
Fig. 60. Dimensioning

is done against a snap ring of a rectangular (Fig. 61b) or round (Fig. 61c) cross-section, fixed in a recess in the splines or in the cylindrical portion of the shaft.

In the design shown in Fig. 61d there is an annular groove in the section where the splines finish. The hub splines seat against the
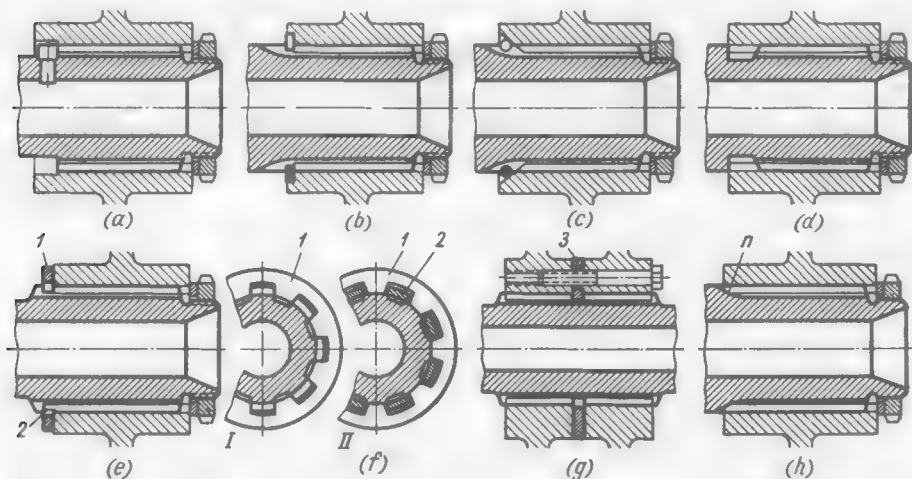
Fig. 61. Methods of seating in splined joints

wall of this groove. This method, however, drastically reduces the strength of the shaft splines.

In the design in Fig. 61e the thrust is taken up by a splined washer 1 introduced into an annular groove in the shaft splines. The washer is fitted on the shaft and turned in the groove so that its splines are

set against the shaft splines, and is held in this position by the extended ends *2* of the hub splines protruding beyond the hub end face (Fig. 61*e*, *II*).

Figure 61*f* illustrates an example when a splined washer *3* is used to secure two parts on a shaft. The hubs of the parts are clamped by bolts which simultaneously fix the washer in the groove in the required angular position (with its

(a)

(b)
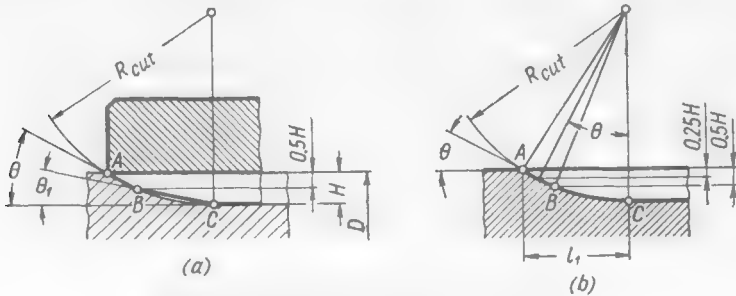
Fig. 62. Determining angles θ and θ₁

splines opposite to the shaft splines). This design does not ensure proper tightening of the joint.

Fixation will be reliable if the hub splines are made to seat against sections *n* where the shaft tooth space bottoms climb (Fig. 61*g*). To ensure seating over the entire circumference the cutter should be rotated through several revolutions, with the longitudinal feed being disengaged, at the final spline milling stage.

With this method the axial position of the hub on the shaft depends on the diameter of the milling cutter and the angle of chamfer on the bearing portion of the hub splines. The
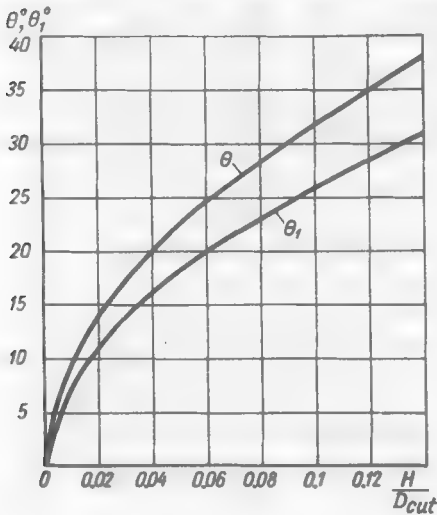
Fig. 63. Angles θ and θ₁ as a function of H/D_{cut}
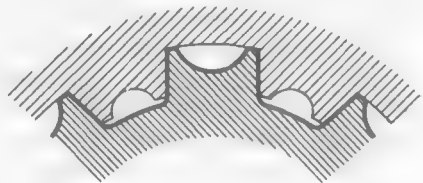
Fig. 64. Lightened splines

accuracy of axial fixation can be increased and tensile stresses in the hub reduced if the external diameter of the chamfer (Fig. 62*a*. point *A*) is taken

to be equal to the major diameter D of the splines, and the internal diameter (point B) is arranged at a distance of $0.5H$ from the diameter D, where H is the depth of splines.

Angle θ at which the chamfer is inclined is preferably made equal to the mean inclination angle of the tooth space profile in section A-B where tooth space bottoms of the shaft splines emerge (Fig. 62b). In this case the axial position of the hub will be determined by the coordinate l_1 of point A, calculated from Eq. (1.30).

Angle θ may be found from the relationship $\cos \theta = 1 - 1.5 \, H/D_{cut}$.

The inoperative section B-C of the hub splines (Fig. 62a) should be bevelled to an angle θ_1 determined from the relation $\cos \theta_1 = 1 - H/D_{cut}$.

The values of θ and θ_1 as a function of H/D_{cut} are given in Fig. 63.

In large-spline joints the splines are made lighter by means of longitudinal recesses made in inoperative surfaces (Fig. 64), for which purpose a special profile is imparted to the cutting teeth of hob cutters and broaches. The strength of the splines is not impaired by the recesses.

(h) Tightening of Splined Joints

Power tightening appreciably increases the operating ability of splined joints.

Axial tightening in shaft-end and mid-shaft installations is, as a rule, effected by means of ring nuts tightened either directly

(a) (b) (c) (d) (e) (f) (g) (h) (i)
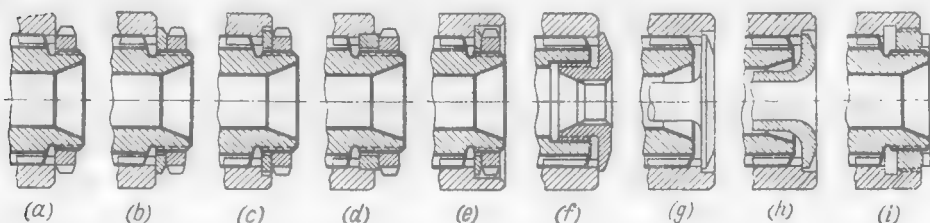
Fig. 65. Axial tightening of splined joints

against the end faces of the hub splines (Fig. 65a) or, which is better still, through the intermediary of washers (Fig. 65b-e).

Shaft-end joints are also tightened with internal nuts (Fig. 65f) or with through bolts (Fig. 65g-h).

Tightening by means of nuts with differential threads (Fig. 65i) makes it convenient to remove the hub, but complicates assembly.

Radial tightening in permanent joints is accomplished by press fitting a plug into the shaft (Fig. 66a), and in detachable joints by expanding the shaft by means of an internal taper 1 consisting of two halves which can be extracted from the shaft by unscrewing the tightening bolt (Fig. 66b). The hubs of parts made of light alloys are sometimes clamped by means of taper rings 2 and 3 (Fig. 66c).

In the design shown in Fig. 66*d* the hub of the shaft-fitted component is split by a deep recess into two parts connected to the body of the component by fillets. When the end faces of the hub are tightened radial forces arise, which are directed towards the shaft centre and compress the hub.
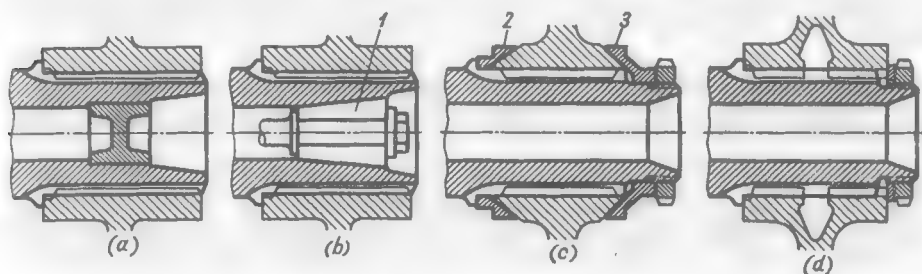
Fig. 66. Radial tightening of splined joints

(i) Special Types of Centring

Centring from specially provided surfaces is used (a) in joints with short splines which do not ensure the longitudinal stability of the shaft-fitted part; (b) in joints transmitting a pulsating torque or loaded by a periodically acting tilting moment; and (c) in joints with involute or triangular splines and hubs heat treated to a hardness of $Rc > 40$ where accurate centring from the side faces of the splines is impossible because the tooth spaces in the hub cannot be ground.

In such cases fits on splines are made free.

In the design shown in Fig. 67*a* the shaft carries an additional centring shoulder *f* where the splines finish.

If a higher centring accuracy is required and the transmitted torque is small, the length of the centring surface is increased and that of the splines, reduced (Fig. 67*b*).

When centring is effected from a cylindrical shoulder *h* on a smooth portion of a shaft (Fig. 67*c*) the shaft splines are weakened by the annular groove at the end of the splines. In the design shown in Fig. 67*d* the hub is centred by a collar on somewhat reduced minor diameter of the hub splines from cylindrical shoulder *i* on the shaft.

Centring is also done from split ring *1* (Fig. 67*e*) fitted into a groove at the end of the splines; from cylindrical shoulder *m* (Fig. 67*f*) on the shaft and ring *2* at the start of the splines; from two bushings (Fig. 67*g*) one of which, *3*, is split and the other, *4*, is solid.

Heavily loaded joints operating under cyclic loads are centred from tapered surfaces (Fig. 67*h-l*). The interference on the tapers produced by power tightening effectively brakes the microscopic angular displacements of the hub with respect to the shaft and thus prevents the wear, crushing and strain hardening of the working

surfaces. At the same time, the tapered surfaces take up frictionally most of the torque and the load on the splines is thus diminished.

Tightening against the tapered surfaces n (Fig. 67h) and q (Fig. 67i) of the shaft frequently causes the welding of the hub and shaft together. Better designs have intermediate bevel rings made of
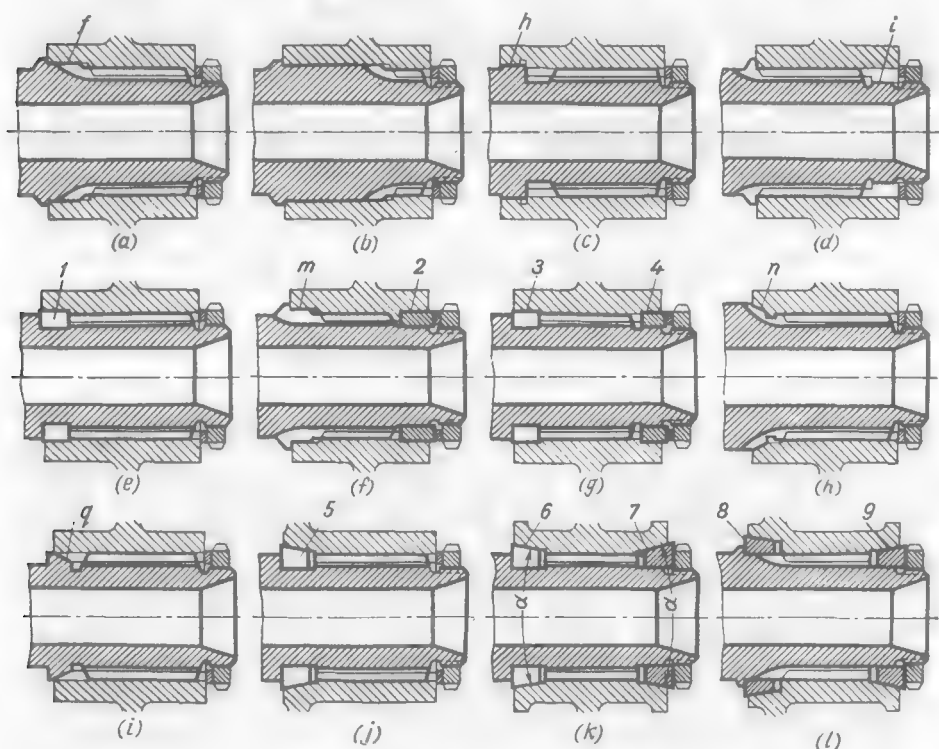
Fig. 67. Special types of centring of splined joints

hard forged bronze which, when used in combination with the steel surfaces of the shaft and hub, make up an unweldable couple.

Figure 67j presents a design with a split bevel ring 5 fitted into an annular groove at the spline end section. In the design shown in Fig. 67k two rings, one of which, 6, is split and the other, 7, solid, dampen the angular oscillations of the hub with respect to the shaft and ensure stability against the action of tilting moments. The shortcoming of such designs is that the shaft splines are weakened by the annular groove.

Solid rings 8, 9 (Fig. 67l) practically ensure a clearance-free centring just like the split rings. Deformed elastically under the tightening force, these rings tightly clamp the cylindrical surfaces of the shaft.

The angles α of tapers are within 30-60°. The smaller the angle α the tighter the clamping, but at the same time the greater are the radial forces which compress the shaft and tend to rupture the hub. The rings are arranged at the nodes of rigidity (Fig. 67*j*), or the hub is reinforced by annular ribs at places where the tapers are located (Fig. 67*k*, *l*).

In designs with centring from two tapered surfaces (Fig. 67*k*, *l*) the fit on the splines is made free to prevent double centring.

For heavily loaded joints additional methods are used to prevent strain hardening and welding together, e.g., the hardening, carburizing, nitriding, phosphating and sulphidizing of splines, metal coatings (copper plating, tin plating, cadmium plating, etc.) and also the lubrication of joints with separating greases with graphite, molybdenum disulphide, etc., as a base material.

(j) Connecting Coaxial Splined Shafts

Figure 68 illustrates methods for linking co-axial splined shafts. Fastening with a pin (Fig. 68*a*) does not ensure proper tightening.
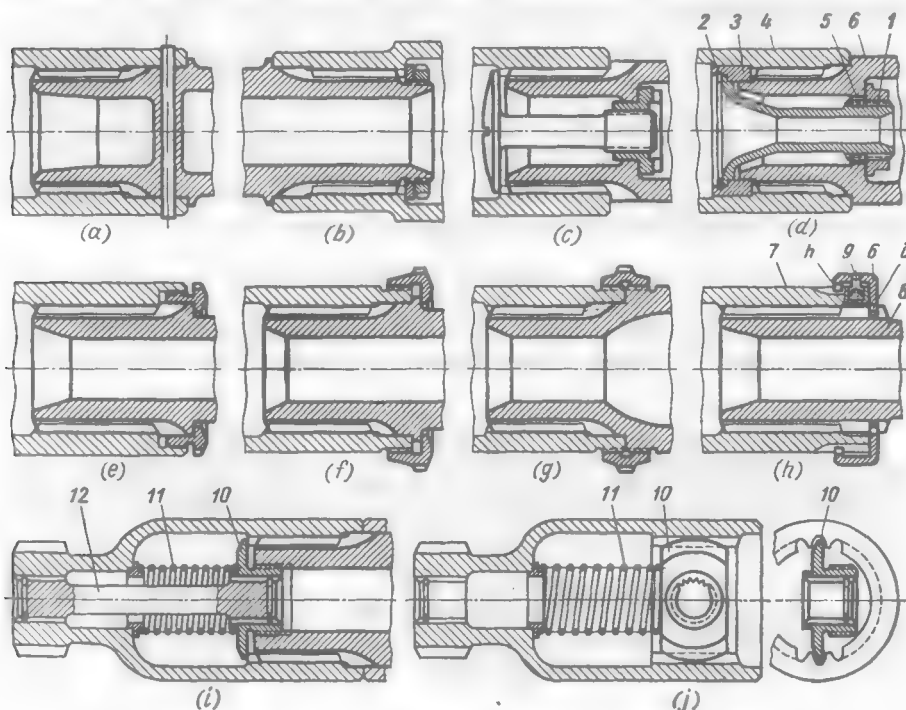
Fig. 68. Connecting of coaxial splined shafts

The fastening is unsuitable for industrial production and inconvenient in assembly and disassembly.

If a joint can be reached by a wrench through the internal cavity of the connected shafts, tightening is done with the aid of ring nuts (Fig. 68b) or through bolts (Fig. 68c).

In the design in Fig. 68d, for easier assembly a hollow bolt *1* is fixed axially with the aid of an internal snap ring *2* fitted into bushing *3* which is pressed into shaft *4*. During tightening the bolt is held in place by splines *5* of shaft *6*.

If approach is possible only from the outside, the joint is tightened by means of union nuts (Fig. 68e, f) or coupling nuts (Fig. 68g) with left- and right-hand threads.

Figure 68h shows an easily detachable fastening with a bayonet lock *6* with two crowns of the splines one of which, *h*, enters the annular groove in the splines of shaft *7* and the other, *i*, the groove in the splines of shaft *8*. The lock is placed on shafts *7* and *8* connected in advance (in this case the splines of the lock freely pass through the tooth spaces of the shafts), and then turned in the grooves so that the splines of the lock are set against the splines on the shafts, and thereafter locked in this position with spring-loaded pin *9*. This design does not ensure proper tightening of the joint.

The connection of a bottle-shaped shaft with the end of an engine crankshaft is illustrated in Fig. 68i and j. Tightening nut *10* is placed into the cavity of the bottle-shaped shaft through the splines (Fig. 68j), after which the nut is turned through 90° to the working position. The nut is locked in this position by spring *11* (Fig. 68i). Then, the shaft is fitted onto the end of the crankshaft; the nut is tightened by a wrench through the hole in the shaft and locked by stop *12* with two crowns of splines one of which enters the splines in the nut and the other, the splines of the bottle-shaped shaft.

(k) Withdrawal Means

In designs of splined joints assembled by push fits and, especially, where centring is effected from tapers the shaft-fitted parts should
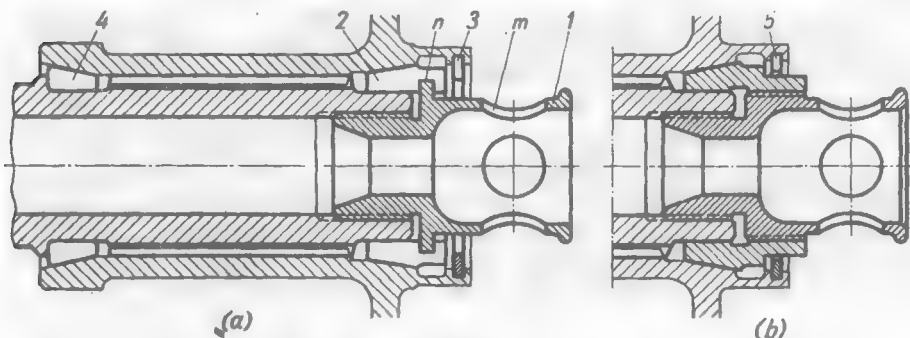
Fig. 69. Withdrawal devices

be provided with elements (flanges, projections, holes) permitting the use of demounting tools, or with special withdrawal means.

Figure 69a shows a withdrawal device used for the bushings of aircraft propellers.

Tubular nut *1* with crowbar holes *m* serving to help its tightening has its collar *n* fitted into the annular groove of taper half-rings *2*. When the nut is being unscrewed it shifts the half-rings which press against snap ring *3* and displace the bushing from the splines. After the bushing has been removed the rear half-rings *4* can easily be disassembled.

In the design with a solid front taper (Fig. 69b) the nut is screwed into the taper which has its thread pitch differing from that of the main nut thread. When the nut is being unscrewed it displaces the taper and the bushing through snap ring *5*.

In joints where the shaft-fitted part has to be fixed in a definite angular position with respect to the shaft certain means should be provided to prevent wrong assembly. Ordinarily a longitudinal groove is made in the top of one of the shaft splines (Fig. 70a), or the top of a spline is cut off over the entire length (Fig. 70b). Pins *1* and *2* are then press-fitted through the corresponding portion of the hub. The joint is assembled in the position when the pin is opposite the groove.

Fig. 70. Angular fixation of splined joints

In heavily loaded joints this method is used to allow repeated assembly which is frequently rendered difficult because of the nonuniform wear of the splines.

1.3. Prismatic and Shaped Shaft-End Joints

In prismatic shaft-end joints torque is transmitted by crushing stresses on flat shaft-end surfaces—flats (Fig. 71a, b) or faces (Fig. 71c-f).
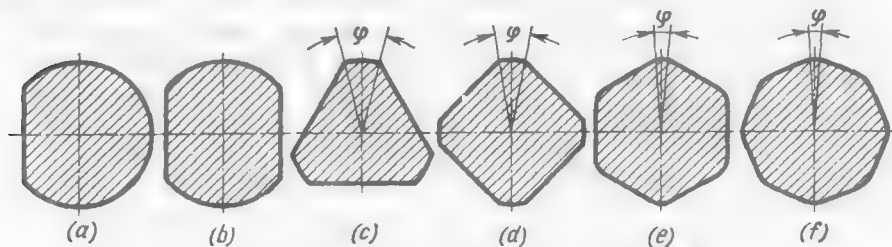
Fig. 71. Prismatic shaft ends

These joints have no projecting elements causing stress concentration. However, a sharp stress rise occurs in the sections where the load-bearing flat surfaces pass into the cylindrical portion of the shaft.

On shafts with flats the hub members are centred from the cylindrical shaft surface, and on polyhedral shafts, from the faces. The faces are ground to increase centring accuracy and make the load distribution more uniform.

The holes in the hub members are broached.

Prismatic shaft-end joints are as a rule tightened.

Tightening against the stepped portions m where the faces pass into the cylindrical part of the shaft (Fig. 72a) is used only in low-loaded joints because it is difficult to arrange the bearing surfaces in one plane.

When the hub is tightened against a shaft shoulder (Fig. 72b) the faces of the shaft-end polyhedron are made to terminate at
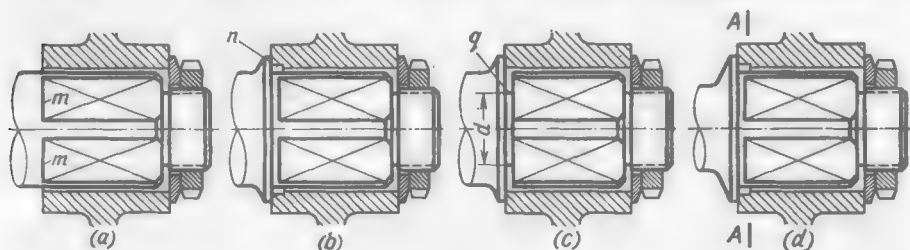
Fig. 72. Prismatic shaft-end joints

a distance of 1-3 mm from the shoulder, the remaining cylindrical collar being placed inside an annular recess n in the hub.

If the faces of the shaft-end polyhedron are to be ground, the shaft is provided with a groove q (Fig. 72c) 2-3 mm wide to allow for the overtravel of the grinding wheel edges, the internal diameter d of the groove being slightly less than the diameter of the circle inscribed in the shaft-end polygon. However, such grooves appreciably weaken the joint. For example, in the case of a tetrahedral shaft end the torsional resisting moment in the section along the groove is about three times less than that in a section across an unweakened shaft portion (it is assumed that the shaft diameter is equal to the external diameter of the polyhedron). Besides, considerable stress concentration occurs in the groove area.

In the design without any clearance groove, where the sections of the grinding wheel overtravel are inside an annular recess in the hub (Fig. 72d), the weakening of the shaft is slightly less but for all that the torsional stress in section A-A of the prismatic portion of the shaft is about two times larger than in the adjacent cylindrical portion.

In order to attain equal strength in torsion the diameter of the circle inscribed in the shaft-end polygon must be equal to the shaft diameter, which considerably increases the radial dimensions of

the joint, especially in shafts with a small number of faces (three or four).

The forces transmitting the torque are perpendicular to the faces and act on a short arm relative to the shaft centre. High crushing stresses therefore develop at the edges of the faces, which increase as the number of faces grows larger, i.e., as the shaft-end polygon approaches a circle.

Let us assume that the crushing stresses are distributed over the faces in conformity with a triangular law (Fig. 73).

The torque transmitted by the joint is

$$T = i \frac{\sigma_{max} S^2 L}{3} \qquad (1.32)$$

where i = number of faces

σ_{max} = maximum crushing stress

S = width of the effective area which depends on the number of faces and the angle φ of the cylindrical portions of the shaft

L = effective length of the joint

Fig. 73. Calculation of prismatic shaft-end joint

Let us assume that the total angle $i\varphi$ (see Fig. 71) of the cylindrical portions for each of the shafts being considered is the same and equal to 90°, i.e., $\varphi = 90°/i$. For shafts with flats the width of the face is assumed to be equal to that of a square shaft.

The radius R_1 of the circle inscribed into the polygon is

$$R_1 = \frac{S}{\tan\left(\dfrac{\alpha}{2} - \dfrac{\varphi}{2}\right)} = \frac{S}{\tan\left(\dfrac{360°}{2i} - \dfrac{90°}{2i}\right)} = \frac{S}{\tan\dfrac{135°}{i}}$$

The radius R_2 of the circumscribed circle is

$$R_2 = \frac{S}{\sin\dfrac{135°}{i}}$$

The mean radius is

$$R = \frac{R_1 + R_2}{2} = \frac{S}{2}\left(\frac{1}{\tan\dfrac{135°}{i}} + \frac{1}{\sin\dfrac{135°}{i}}\right)$$

and hence,

$$S = \frac{2R}{\dfrac{1}{\tan\dfrac{135°}{i}} + \dfrac{1}{\sin\dfrac{135°}{i}}}$$

Substituting this value of S into Eq. (1.32) we get

$$\sigma_{max} = \frac{3}{4} \cdot \frac{T}{iR^2L} \left(\frac{1}{\tan \dfrac{135°}{i}} + \frac{1}{\sin \dfrac{135°}{i}} \right)$$

The corrected stress $\left(\text{for } \dfrac{T}{\pi R^2 L} = 1 \right)$

$$\sigma_{0\,max} = \frac{3\pi}{4} \left(\frac{1}{\tan \dfrac{135°}{i}} + \frac{1}{\sin \dfrac{135°}{i}} \right) \tag{1.33}$$

The values of $\sigma_{0\,max}$, calculated from Eq. (1.33), are given in Table 15. For the sake of comparison the table also gives the corrected crushing stress for involute splines with pressure angle $\alpha_0 = 30°$ ($\sigma_0 = 0.8$), and the ratio σ_{0max}/σ_0.

Table 15

Parameters	$\delta_0=0.8$	$i=1$	$i=2$	$i=3$	$i=4$
$\sigma_{0\,max}$	—	25.8	12.9	4.5	6.45
$\sigma_{0\,max}/\sigma_0$	1	32	16	5.6	8
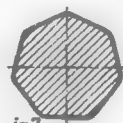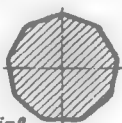
Parameters	$i=5$	$i=6$	$i=7$	$i=8$	$i=9$
$\sigma_{0\,max}$	8	9.8	11.5	13.4	14.9
σ_{0max}/σ_0	10	12.2	14.4	16.7	18.6

Table 15 shows that the crushing stresses in prismatic shaft ends are much higher than in involute splines. In the case of the most advantageous trihedral shaft ends these stresses exceed the stresses in splined shafts five to six times, and 8 to 32 times for shaft ends

of other shapes. For this reason prismatic shaft-end joints are used for low-load applications, for example, for transmitting torque from hand levers and handles.

Shaped shaft-end joints (Fig. 74) are close to prismatic ones as to their general design. The working surfaces of shaped shaft-end joints
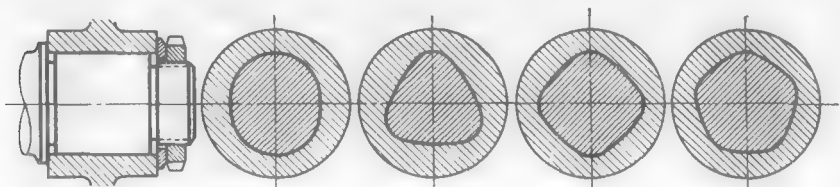
Fig. 74. Shaped shaft-end joints

are formed by cycloidal curves, which makes it possible to machine them with the aid of epi- or hypocycloid grinding mechanisms.

An advantage of shaped shaft-end joints is that the holes in the hubs heat treated to a high hardness can be machined to a high degree of accuracy.

The crushing stresses in shaped shaft-end joints with convex surfaces are higher than in prismatic shaft-end joints of the same general shaft-end shape because of the less favourable stress distribution (the arm of forces grows smaller as the shaft-end shape becomes more rounded). Therefore, with the crushing stresses being the same, the load-carrying capacity of shaped shaft-end joints is lower than that of prismatic ones, and is much lower as compared with splined joints.

Fig. 75. Cross-shaped joint

The force distribution in profiles with concave surfaces is better. *Cross-shaped joints* of this type (Fig. 75) are still used in rolling mill shafts. Being in essence large splines of a trapezoidal profile, they are identical to the latter in bending and crushing strength. But, as distinct from splined joints, they have a poorer resistance to torsion across the profile core.
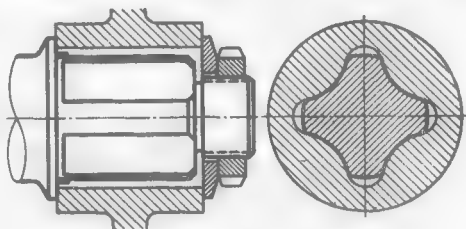
1.4. Pinned Joints

(a) Axial Pins

Axial pins (round keys) are used to transmit torque in permanent joints.

Pins are installed by a heavy drive fit into holes drilled and reamed simultaneously in the shaft and hub in the joint between

their seating surfaces (Fig. 76*a-e*). Taper pins are safeguarded against falling out by a washer and a nut (Fig. 76*b*). The hub is usually mounted on the shaft by an interference fit.
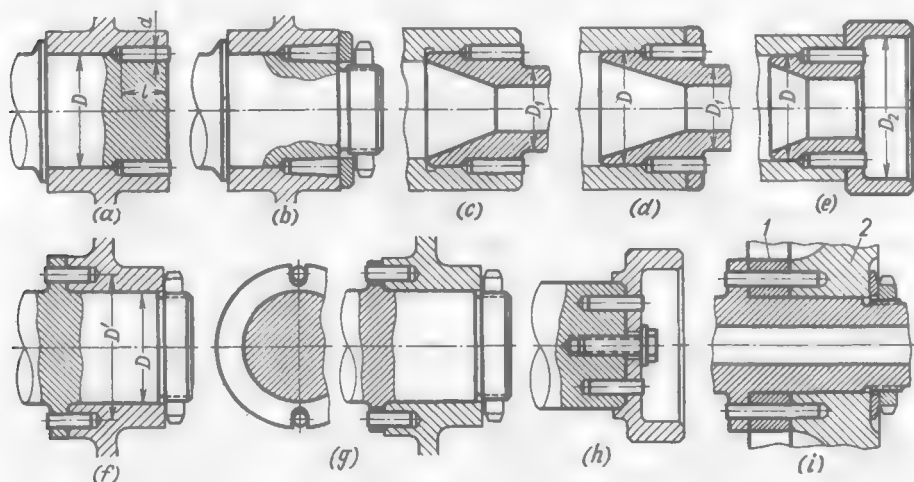
Fig. 76. Joints with axial pins

The torque transmitted by the joint (disregarding interference on the seating surfaces) is

$$T = 10^{-3} \frac{\tau z d l D}{2} \, (\text{kgf} \cdot \text{m}) \tag{1.34}$$

where d and l = diameter and length of pins, respectively, mm
 z = number of pins
 τ = allowable shearing stress, kgf/mm^2
 D = diameter of joint, mm

Thanks to the favourable shape of the recesses in the shaft and hub, stress concentration is comparatively low. Multiple-pin joints of this type are close in strength to splined joints and can even exceed them in this respect when heavy drive fits on the centring surfaces are used.

The shortcoming of this joint is that the holes for pins in the shaft and hub must be machined at one time. The materials of the hub and shaft must have about the same hardness, otherwise the deflection of the drill towards the softer metal is inevitable.

Joints with axial pins can be used to fasten hub members in shaft-end installations, if the shaft is not too long and a convenient approach of drills and reamers to the shaft end face is provided.

This method can also be utilized to secure parts in the internal hole of a shaft on condition that the part is not very long and the

external diameter D_1 of the part is smaller (Fig. 76c, d) or its internal diameter D_2 is larger (Fig. 76e) than the diameter D of the seating surface.

A positive feature of the designs shown in Fig. 76d and e is that the drill is well directed initially in the wall of the part.

In detachable joints the pins are press-fitted into the hub (Fig. 76f, g) or into the shaft end face (Fig. 76h). The free ends of the pins enter by slide or push fits the holes in the shaft or hub, respectively.

The fastening of parts differing in hardness is permissible. The joint is more suitable for industrial production than the first one (the holes in the shaft and hub can be jig-drilled separately), but is less strong.

Figure 76i illustrates the fastening of parts 1 and 2 to a shaft with round pins. The pins are installed by a heavy drive fit in part 1 with a long hole and enter by a centring fit the shoulder of the shaft and the second-shaft-fitted part 2.

The transmitted torque is

$$T = 10^{-3} \frac{\tau z \cdot 0.785 d^2 D_1'}{2} \text{ (kgf} \cdot \text{m)} \tag{1.35}$$

where D' is the diameter of the pin circle.

With z and d being the same, the torque is less than for the joints shown in Fig. 76f, g [Eq. (1.34)] by $1.27 \frac{l}{d} \cdot \frac{D}{D'}$ times (with the ordinary values $l/d \approx 4$ and with $D'/D \approx 1.3$, approximately by four times).

(b) Radial Pins

In weakly loaded joints (shafts of auxiliary drives) fastening is effected by means of cylindrical (Fig. 77a) or taper (Fig. 77b) radial pins which lock the hub member in a definite attitude with respect to the shaft.

The joint poorly suits industrial production (the holes in the hub and shaft must be jointly drilled and reamed), the holes appreciably weaken the shaft, and the joint is not tightened.

The transmitted torque is

$$T = 10^{-3} \frac{\tau \cdot 2 \cdot 0.785 d^2 D}{2} \text{ (kgf} \cdot \text{m)} \tag{1.36}$$

Comparing this equation with Eq. (1.35), it can be seen that the load-carrying capacity of this joint is $z/2$ times smaller than that of the joints with axial pins shown in Fig. 76f-h.

The pinned joint in Fig. 77c can be used if the materials of the shaft and hub have the same hardness.

If cutting tools cannot be radially approached to the hub member, inclined pins are used (Fig. 77*d*). This is practically a permanent joint.

Detachable joints transmitting small torques use threaded pins with cylindrical shanks entering a slot (Fig. 77*e*) or hole (Fig. 77*f*) in the shaft. A stronger fastening is provided by pins with tapered
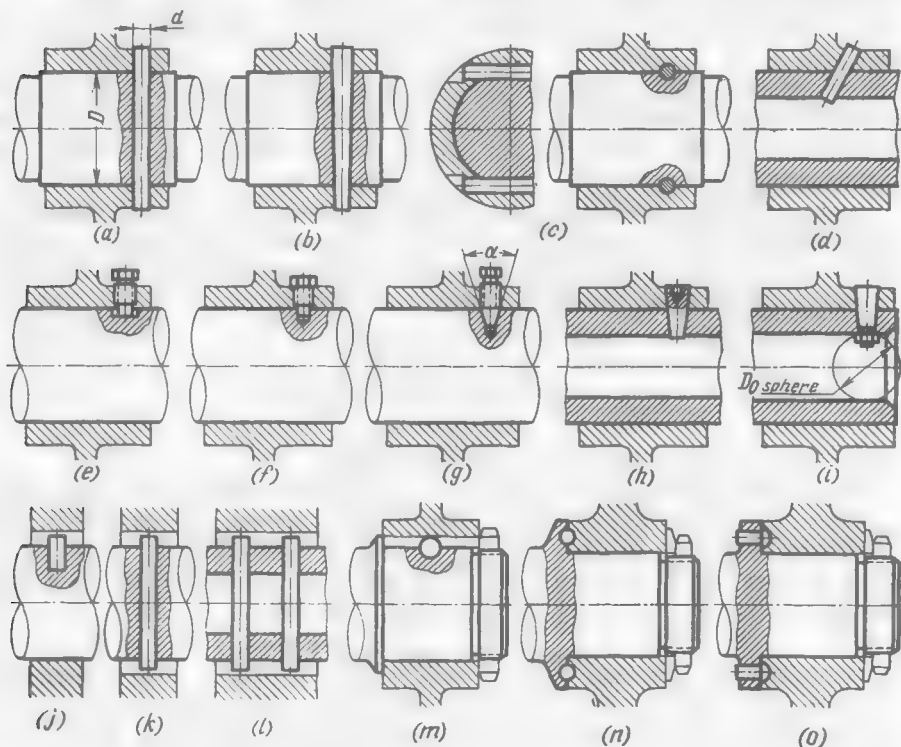
Fig. 77. Joints with radial pins

shanks (Fig. 77*g*). With a central angle of taper $\alpha < 40°$ the joint is self-locking. The joint formed by smooth taper pins with a threaded hole for a puller is still stronger (Fig. 77*h*).

Taper pins tightened by an internal nut (Fig. 77*i*) are suitable for shaft-end installations. The bearing surface of the nut must conform to a sphere with a diameter D_0 equal to the diameter of the hole in the shaft.

Such designs require that the holes for the pins in the hub and shaft be reamed jointly.

Radial pins press-fitted into the shaft and entering with their free ends slots in the hub are used in weakly loaded joints (Fig. 77*j-l*).

In joints for lightest loads the torque is sometimes transmitted by a ball fitted into a spherical recess in the shaft. The opposite side of the ball enters a semicircular slot in the hub (Fig. 77m).

Figure 77n illustrates a stronger joint formed with the aid of balls installed in-between the end faces of the hub and the bearing shoulder of the shaft. In this case the balls are intended to reduce stress concentration in the hub member (made of a light alloy). The semispherical recesses must be machined to a high degree of accuracy, otherwise the balls will operate untightened.

In a similar joint shown in Fig. 77o the torque is transmitted by the semispherical heads of pins press-fitted into the shoulder of the shaft.

1.5. Flanged Joints

These joints are mainly used to connect shafts (Fig. 78a) and also to fasten disk-type (Fig. 78b) and drum-type (Fig. 78c) parts to shafts.

Torque is transmitted by dowel bolts or by special elements operating in shear, and partly by the forces of friction produced on the abutting flange surfaces when tightening the clamping bolts.

The alignment of the connected parts is attained by means of a centring shoulder m (Fig. 78b) and strict squareness of the abutting flange surfaces with the axes of the parts.

The larger diameter of the torque-transmitting element circle reduces the peripheral force and makes it possible to increase the number of such elements.

An advantage of flanged joints is their practically clearance-free torque transmis-

Fig. 78. Flanged joints

sion achieved on account of the dowel bolts being interference-fitted. The forces of friction developing in the joint when the bolts are tightened prevent microscopic relative displacements of the contacting flange surfaces. For this reason flanged joints are hardly subject to strain hardening, welding and frictional corrosion frequently observed in hub-type joints.
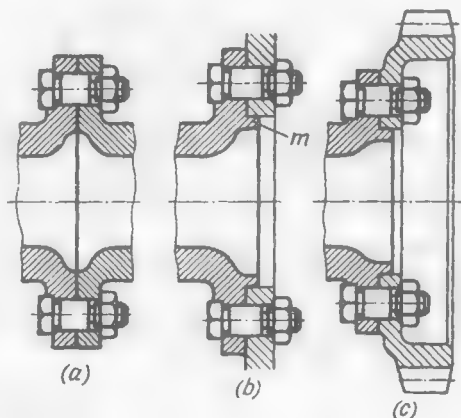
The torque transmitted by a flanged joint is determined by the resistance of the bolts to shear and the force of friction in the joint

$$T = T_{sh} + T_{fr} = \frac{D}{2} z_1 0.785 d_1^2 \tau + \frac{D}{2} (z_1 d_1^2 + z_2 d_2^2) 0.785 \sigma f \quad (1.37)$$

where D = diameter of the bolt circle
z_1 and d_1 = number and diameter of the dowel bolts
z_2 and d_2 = number and diameter of the clamping bolts
  τ and σ = allowable shear stresses, and tensile stresses developing when tightening the bolts
     f = coefficient of friction in the joint ($f = 0.1$-0.15)
   The ratio

$$\frac{T_{fr}}{T_{sh}} = \frac{(z_1 d_1^2 + z_2 d_2^2) \sigma f}{z_1 d_1^2 \tau}$$

gives the share of torque transmitted by friction.
   Let all the bolts be of the dowel type ($z_2 = 0$; $d_1 = d_2$), $f = 0.15$ and the shear stress equal to the tensile stress in the bolts ($\tau = \sigma$). Then

$$\frac{T_{fr}}{T_{sh}} 100\% = f 100\% = 15\%$$

When calculating flanged joints the force of friction is usually disregarded and attributed to the margin of safety. Assuming that
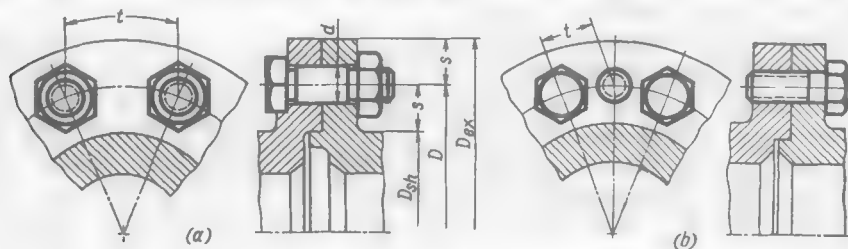
Fig. 79. Dimensions of flanged joints

all the bolts are of the dowel type, we find from Eq. (1.37) the diameter of the bolt circle

$$D = \frac{2.55T}{\tau z d^2} \quad (1.38)$$

where z and d are the number and diameter of the bolts in mm and T is the torque in kgf·mm.
   The maximum number of bolts a flange can accommodate is

$$z_{max} = \frac{\pi D}{t_{min}}$$

where t_{min} is the minimum bolt pitch determined by the free space required for tightening the nuts (Fig. 79a). When tightening hexa-

gon nuts with a socket wrench, $t_{min} \approx 2.5d$, and when an open-end wrench is used for the purpose $t_{min} \approx 3d$.

When radial dimensions are limited the number of the flange clamping bolts can be increased by making use of screwed bolts (Fig. 79b) with their heads arranged in a staggered order on both sides of the flanges. In this case the distance between the bolt axes can be reduced to $t_{min} \approx 1.8d$.

In a most general case, when tightening the nuts with open-end wrenches ($t_{min} \approx 3$), the limit on the number of bolts is given by

$$z_{lim} = \frac{\pi D}{3d} \approx \frac{D}{d} \qquad (1.39)$$

Substituting this expression into Eq. (1.38) we obtain the minimum flange diameter conditioned on the bolt arrangement

$$D_{min} = 1.6 \sqrt{\frac{T}{\tau d}} \qquad (1.40)$$

The minimum diameter is equal to the diameter D_{sh} of the shaft plus the double distance s from the surface of the shaft to the axes of the bolts. Assuming $s = 1.25d$, we get

$$D_{min} = D_{sh} + 2.5d \qquad (1.41)$$

Equating Eqs. (1.40) and (1.41) we obtain a formula for determining the bolt diameter d with which the flange diameter D will be minimal

$$1.6 \sqrt{\frac{T}{\tau}} = D_{sh} d^{0.5} + 2.5 d^{1.5} \qquad (1.42)$$

The diameter D_{sh} of the shaft depends on the load it carries. Equation (1.42) has been used to draw a nomographic chart (Fig. 80) for determining the minimum dimensions of flanged joints.

Let $T = 10^3$ kgf·m, $\tau = 10$ kgf/mm² and $D_{sh} = 100$ mm. Erect a perpendicular from the point $T = 10^3$ kgf·m on the X-axis and draw a horizontal line from the point of its intersection with the line $\tau = 10$ kgf/mm². The point where the horizontal line meets the ordinate $D_{sh} = 100$ mm gives $d = 14$ mm. The respective value of D_{min} is equal to 135 mm (thin lines). According to Eq. (1.39), the number of bolts is

$$z = \frac{D_{min}}{d} = \frac{135}{14} \approx 10$$

In designing flanges the most compact layout of bolts is not always the prime requirement. In a general case the designer knows only the torque and has to find the parameters of a flanged joint that will ensure the transmission of this torque. The problem has no unambiguous solution. The diameter of the flanges, the number and diameter of bolts—all these are independent variables; there is a vast number of these parameters which meet the strength requirements.
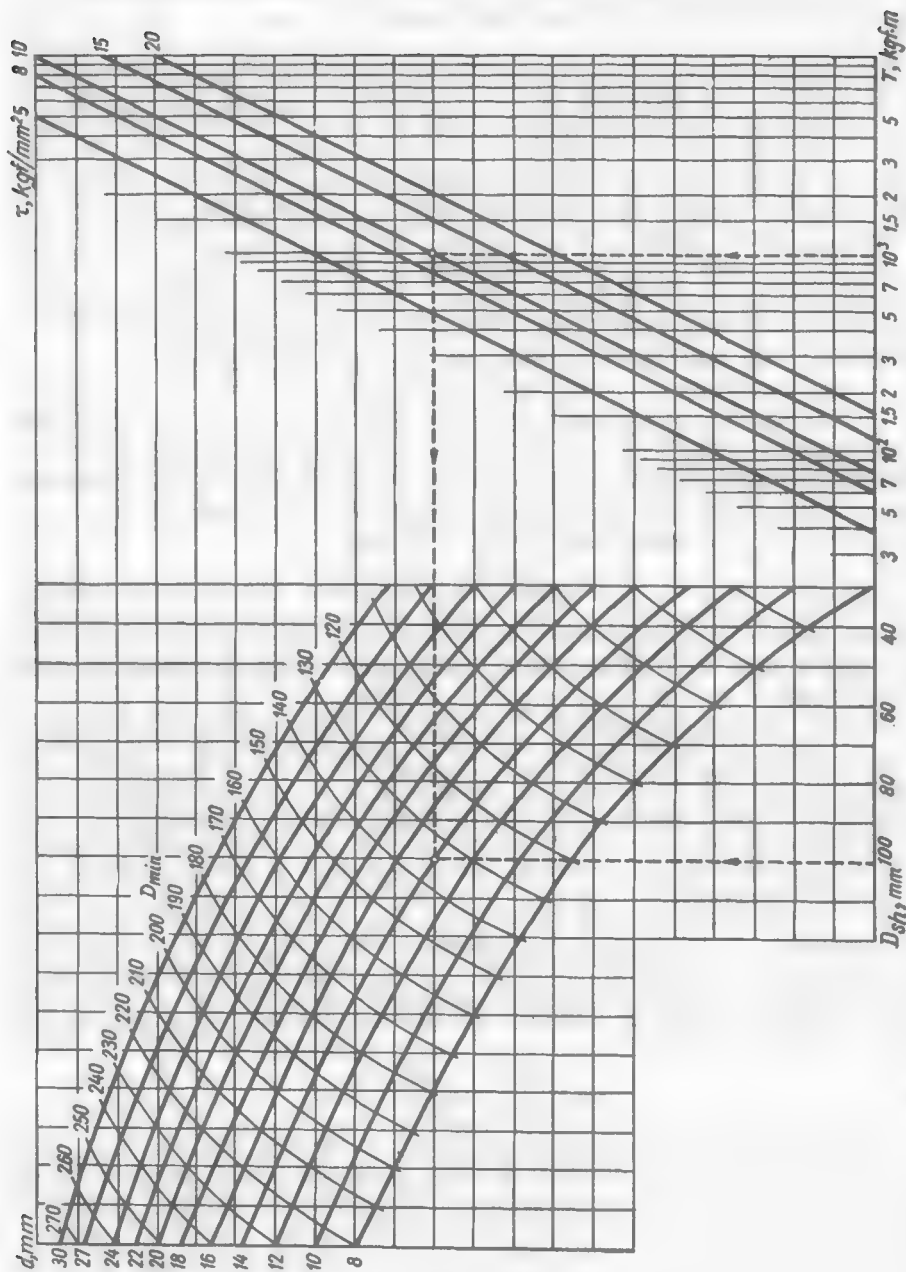
Fig. 80. Chart for determining the minimum dimensions of a flanged joint

Calculations are made in conformity with Eq. (1.38). The nomographic chart shown in Fig. 81 is used to facilitate the calculations.

Let $T = 10^3$ kgf·m, $\tau = 10$ kgf/mm². Erect a perpendicular from the point $T = 10^3$ kgf·m and draw through the point of its intersection with the line $\tau = 10$ kgf/mm² a horizontal line to intersect the lines in the top left-hand portion of the chart. The thick lines indicate the diameter of bolts and the thin ones, the limiting number of bolts z_{lim} for the given diameter in conformity with Eq. (1.39).

Figure 81 shows the plot for $d = 14$ mm. The point where the horizontal line meets the line $d = 14$ gives the limiting value $z_{lim} = 10$. Drawing from this point a vertical line to intersect the z lines (bottom left-hand portion of the chart) one can find on the Y-axis the values indicated in the table below.

z	10	8	6	5	4
D	130	165	220	260	330
$D_{sh.\,max}$	95	130	185	225	295
D_{ex}	165	200	255	295	365

The extreme values of the series should be avoided. Large values of z complicate the design and reduce the limiting diameter of the shaft (the third line in the table) which, according to Eq. (1.41), is $D_{sh.\,max} = D - 2.5d$. Small values of z increase the external diameter of the flange, which in average conditions may be assumed to be $D_{ex} = D + 2.5d$ (the fourth line). In our case $z = 8$ is the most suitable value.

The flange thickness in the section where the bolts are arranged may be determined from the rigidity of the flange and the crushing (bearing) strength of the bolts. The crushing stress is

$$\sigma_{crush} = \frac{2T}{zDdb} \tag{1.43}$$

where b is the flange thickness (Fig. 82).

The shear stress in the bolts

$$\tau = \frac{2T}{0.185d^2zD} \tag{1.44}$$

Dividing Eqs. (1.43) and (1.44) term by term we get

$$b = 0.785d\,\frac{\tau}{\sigma_{crush}}$$
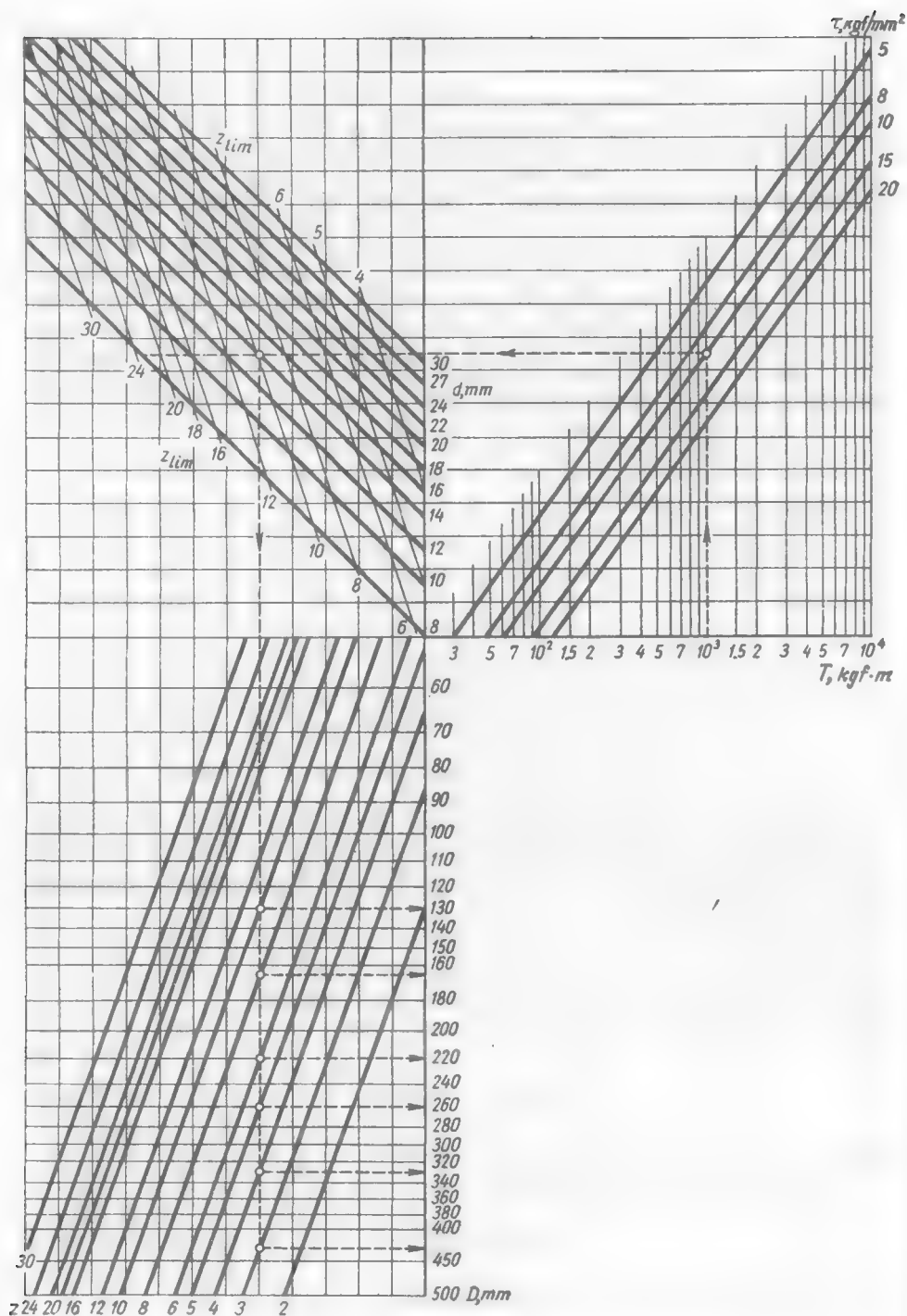
Fig. 81. Chart for calculating flanged joints

Assuming that $\tau = \sigma_{crush}$ and accounting for the reduction in the effective length of the bolts due to the thread and groove m where the bolt stem passes into the head, we usually take

$$b = (1 \text{ to } 1.2)\, d \qquad (1.45)$$

The flange thickness at the section of transition to the web portion is $b' \approx 0.8b$, and at the shaft transition, $b'' = (0.15$ to $0.2)\, d_{sh}$.

Typical shapes of small-diameter flanges are illustrated in Fig. 83a-d. Large-diameter flangers are made tapered (Fig. 83e). The shaft transition area is reinforced by a smooth fillet m and a rigidity belt n.

To increase their rigidity, especially in the presence of bending forces and moments, flanges are made cup-shaped (Fig. 83f), conical (Fig. 83g) or tulip-shaped (Fig. 83h).

Fig. 82. Dimensions of flanged joints

The abutting surfaces of flanges are machined to the 7th-8th class of surface finish, keeping the axes perpendicular within the limits
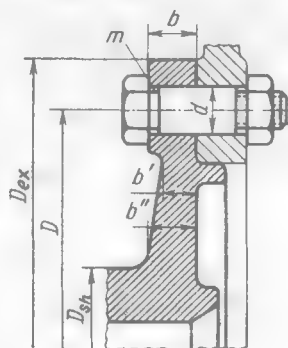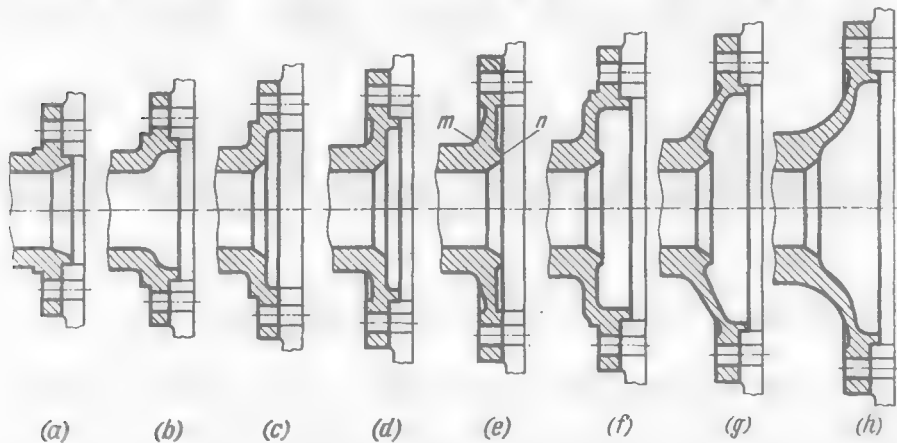
Fig. 83. Shapes of flanges

that suit the required directional accuracy (wobble, on the average, 0.01-0.03 mm per 100 mm of the radius).

The dowel bolt holes in the flanges are machined either jointly or separately in a jig, followed by their joint reaming to obtain tight or wringing fits. To make sure that the flanges will be assembled in the same position as they have been jointly machined, use

is made of set pins or one of the holes is spaced at an angle differing from that of the other holes.

Dowel bolts are made from carbon steel grades 45 and 50, or from alloy steel grade 40X, and heat treated to a hardness of 30-45 *Rc* (hardening with medium tempering).

The bolts are calculated for shear by the peripheral force and for tension by the force of preliminary tightening. The total stress in the critical cross-section (in the plane of shear), according to the third theory of strength, is

$$\sigma = \sqrt{\sigma_t^2 + 4\tau^2}$$

where σ_t and τ are the tensile and shear stresses, respectively.

Usually, $\sigma_t = 10$ kgf/mm² and $\tau = 5\text{-}10$ kgf/mm². The total stress is

$$\sigma = \sqrt{10^2 + 4(5 \text{ to } 10)^2} \approx 15\text{-}20 \text{ kgf/mm}^2$$

In addition to cylindrical dowel bolts (Fig. 84*a*, *b*), wide use is made of taper bolts (Fig. 84*c*). Taper bolts cannot properly tighten

(a)   (b)   (c)   (d)   (e)   (f)   (g)

(h)   (i)   (j)   (k)   (l)   (m)
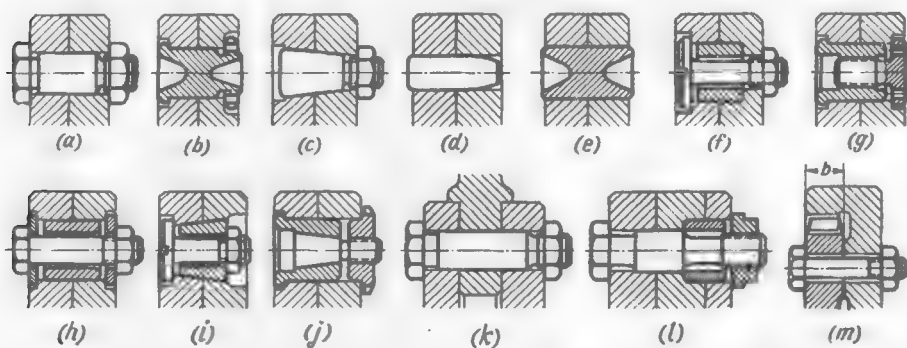
Fig. 84. Design varieties of torque-transmitting elements

the flanges and are therefore alternated with ordinary clamping bolts.

Torque is also transmitted by means of pins (Fig. 84*d*, *e*) placed in-between the clamping bolts. To save space the elements operating in shear are made as bushings installed concentrically with the clamping bolts (Fig. 84*f-j*). A strong joint is ensured by the design shown in Fig. 84*j*. Here, taper bolts, while being tightened, spread out the bushings and make them fit tightly against the walls of the flange holes in the plane of shear.

Figure 84*k* illustrates the transmission of torque in a multiple-flanged joint by dowel bolts, and Fig. 84*l*, by a combination method using dowel bolts and bushings.

Large torques are transmitted by making use of radial (usually involute) splines (Fig. 84m) or triangular end-face splines (Fig. 85a).
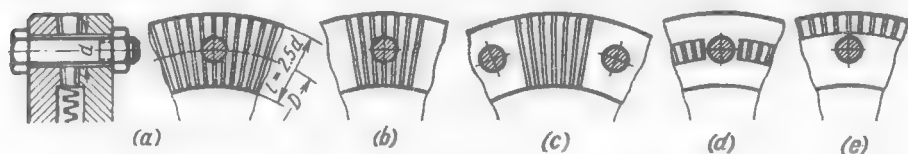
Fig. 85. Flanges with end-face splines

When making calculations for shear across the spline roots, the torque transmitted by the splines is

$$T' \approx \frac{\pi D^2}{2} l\tau$$

where D = mean diameter of the spline belt, mm
$\qquad l$ = width of spline belt, mm
$\qquad \tau$ = allowable shear stress, kgf/mm²

According to Eq. (1.40), the torque transmitted by a flanged joint with closely spaced dowel bolts is

$$T \approx 0.4D^2\tau d$$

The ratio between the torques transmitted by the splines and the bolts

$$\frac{T'}{T} \approx 4\frac{l}{d}$$

For radial splines (see Fig. 84m), when $l = b$, and with the usual flange thickness $b = d$

$$\frac{T'}{T} \approx 4$$

For end-face splines, when $l = 2.5d$ (Fig. 85a)

$$\frac{T'}{T} \approx 10$$

Thus, the load-carrying capacity of flanges with radial splines is about four times (and with end-face splines, ten times) higher than that of flanges with closely spaced dowel bolts.

In joints loaded with not very large forces the length of the end-face splines is usually reduced by making them as separate sectors at the clamping bolt positions (Fig. 85b) or between them (Fig. 85c), or by reducing the width of the spline belt (Fig. 85d, e).

The dimensions of the splined sections are found proceeding from the condition

$$T = F\tau R_m$$

where F = total area of splined sections
$\qquad R_m$ = mean radius of their arrangement
$\qquad \tau$ = allowable shear stress in the splines

In addition to the pretightening force, the clamping bolts of the flanges with end-face splines are loaded by an axial force produced during the transmission of torque due to the inclination of the working spline faces, this force being

$$P_{ax} = \frac{T}{R_m} \tan \alpha/2$$

where α is the apex angle of the spline profile in its middle cross-section.

With the usual value $\alpha = 60°$

$$P_{ax} = 0.577 \frac{T}{R_m}$$

1.6. Frictional Joints

(a) Taper Joints

Torque in taper joints is transmitted by friction developing on seating surfaces when tightening a hub on a shaft.

Strict control of the tightening force is required as too loose a tightening reduces the load-carrying capacity of the joint while too strong one may produce stresses dangerous for the strength of the external and internal members.

Similarly to press-fitted joints, taper joints are mainly used in shaft-end installations.

Taper joints can be assembled with the hub member in any angular position with respect to the shaft. When a definite angular position of the hub is required, locking elements, such as a light key, a set pin, etc., are introduced into the joint.

The axial position of a part fitted on a shaft varies due to manufacturing deviations in the diametral dimensions of the tapered surfaces of the shaft and the hole in the hub. When the hub is being tightened it moves along the shaft to a distance of up to several millimetres. Upon repeated tightening procedures the position of the part changes due to the crushing of the seating surfaces.

Press-fitted taper joints (Fig. 86a) are used for permanent and rarely disassembled connections, and *tightened taper joints* (Fig. 86b, c) for detachable connections.

The tapered surfaces of the shaft and hub are, as a rule, machined to the 2nd grade of accuracy and the 8th-10th class of surface finish. In critical detachable joints the tapers are lapped in and then checked by blacking-in until their contact occurs over an area of at least 80 per cent of their total surface area.

The lapping and repeated reassemblies can be facilitated by making the shaft taper protrude from the hub hole to a distance $s = 1.4$-2 mm (Fig. 86b, c). Otherwise an annular step hampering the motion of the hub along the shaft will form on the walls of the hole at the points q (Fig. 86d) during the lapping.

The overhanging portion of the shaft taper is overlapped by an annular pro jection m on the hub (Fig. 86c) or by a cup-shaped washer n (Fig. 86b) with a reserve s' for the axial displacement of the hub in tightening. Since the seating surfaces may be crushed in operation this reserve is made equal to $(1.5$ to $2)h$ where h is the design axial displacement of the hub in its initial tightening.

The shaft thread must also have some reserve s'. The opposite end of the taper should protrude beyond the hub to a distance of not less than s' so that the effective length of the joint is not reduced during reassemblies.

Thus, the length of the shaft taper must be $L = l + s + s'$ (l is the length of the working surface of the hub).

Intermediate hard-bronze bushings with an external (Fig. 86e) or internal (Fig. 86f) taper are introduced in joints subjected to
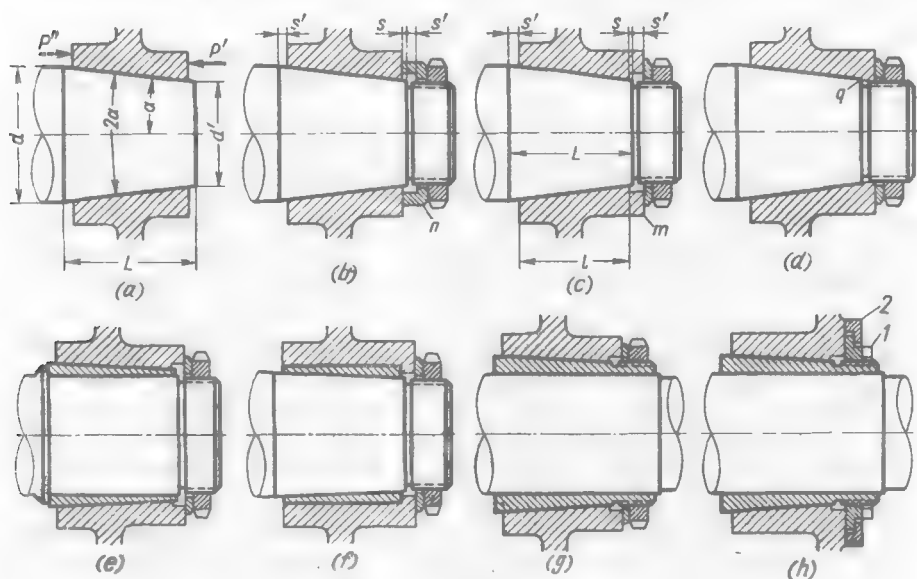
Fig. 86. Taper joints

cyclic loads to prevent the strain hardening and welding together of the seating surfaces.

In this case centring is effected from two surfaces, which places more stringent requirements upon the manufacturing accuracy of the bushings.

It is good practice to use galvanic or thermodiffusion coating of the contact surfaces with soft metals (Cu, Zn, Cd). Such coatings prevent the welding together of the surfaces and appreciably increase the load-carrying capacity of the joint.

When parts are mounted on long shafts and also when the axial position of parts on a shaft is to be adjustable within a broad range, use is made of clamping bushings (Fig. 86g and h).

A withdrawal device is provided in the design in Fig. 86*h*. When nut *1* is unscrewed its collar presses against washer *2* screwed to the hub and pulls the hub off the shaft.

Taper

Taper (conicity) is the ratio

$$C = \frac{d - d'}{L} = 2 \tan \alpha$$

where d and d' = major and minor diameters of the taper (Fig. 86*a*), mm
L = length of the taper, mm; usually $L = (1 \text{ to } 1.2)d$
α = half-angle of taper
Slope is the ratio

$$S = \frac{d - d'}{2L} = \tan \alpha$$

Hence,

$$S = 0.5C$$

The dependence of angle α on C and S is illustrated in Fig. 87. Taper has no effect on the magnitude of the transmitted torque, if the tightening of the joint is done to produce the design interference in it. As taper is reduced the required tightening force diminishes and the axial displacement of the hub member increases, and vice versa when taper is increased.

With the tightening force remaining constant, a reduction in taper increases the radial interference in the joint and the transmitted torque, but at the same time augments stresses in the shaft and hub.

The resistance of *press-fitted* taper joints to axial displacement is not the same in different directions. If the load is directed against the apex of the taper (solid arrow in Fig. 86*a*) the displacement is prevented by the force of friction on the seating surface and by the axial component of the reaction of the elastic compression of the shaft member and of the tension of the hub member.
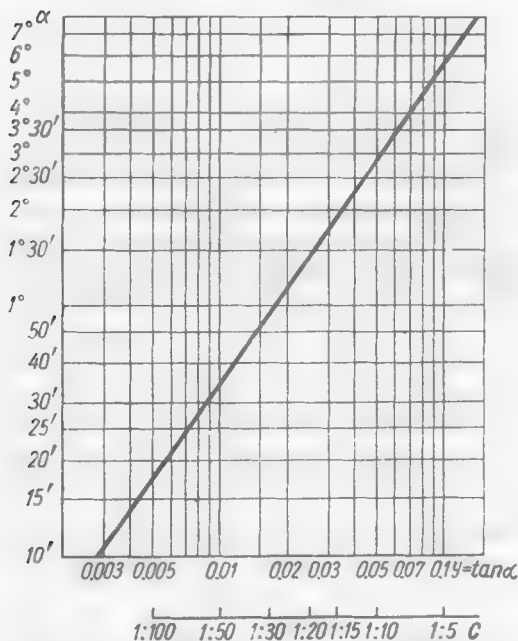
Fig. 87. Relation between α, C and S

The force of friction is

$$F = k\pi d_m l f$$

where $k =$ unit pressure on the seating surface
l and $d_m =$ length and diameter of the seating surface ($d_m \approx d$)
  $f =$ coefficient of friction

The axial force of reaction

$$P_{ax} = k\pi d_m l \tan \alpha$$

where α is the half-angle of taper.

The total displacing force

$$P' = F + P_{ax} = k\pi d_m l (f + \tan \alpha) \qquad (1.46)$$

The displacement in the opposite direction (dashed arrow) is prevented by the force of friction only, while the force of elastic reaction aids it.

In this case the displacing force is

$$P'' = F - P_{ax} = k\pi d_m l (f - \tan \alpha) \qquad (1.47)$$

The ratio P''/P'

$$\frac{P''}{P'} = \frac{f - \tan \alpha}{f + \tan \alpha} \qquad (1.48)$$

Figure 88 shows the dependence of forces P' and P'', calculated from Eqs. (1.46) and (1.47) on the angle α (the value $k\pi d_m l$ is assumed to be equal to unity), and also the ratios P''/P' determined from Eq. (1.48). The calculations are made for various values of f.

It can be seen from the drawing that force P' increases and force P'' decreases in direct proportion to C. A higher coefficient of friction increases these forces.

Fig. 88. Axial displacing forces P' and P'' and ratio P''/P' as a function of C and f

For a joint to operate reliably the ratio P''/P' must be as close to unity as possible. This condition is satisfied when $C < 1 : 50$

(with $f = 0.1$ the ratio $P''/P' > 0.8$). With an increase in C the ratio P''/P' diminishes (when $f = 0.1$ and $C > 1 : 20$ the ratio $P''/P' < 0.6$). With $C = 1 : 10$ and with minimum $f = 0.05$ the force P'' becomes zero (which means the breaking of the condition for self-braking: $C = 2\tan \alpha \leqslant 2f \leqslant 1 : 10$). With $C \leqslant 1 : 50$ the force P'' diminishes negligibly (with $C = 1 : 100$ the ratio P''/P' is about 10 per cent higher than with $C = 1 : 50$). At the same time a decrease in C causes a number of undesirable phenomena— a greater axial displacement during press-fitting and a higher sensitivity of the joint to overloads by the forces P'. The recommended tapers for press-fitted joints $C = 1 : 50$ to $1 : 30$ (shaded area in Fig. 88) with which the ratio $P''/P' \approx 0.8$–0.6 and has a satisfactory value of 0.5 even with $f = 0.05$.

The clamping bushings (see Fig. 86*e–h*) are made with tapers of up to $1 : 100$ to reduce the bushing thickness.

The capacity of *tightened joints* (see Fig. 86*b, c*) to carry loads from forces acting in the direction towards the apex of the taper is much larger and is determined by the resistance of the tightening nut to shear. There is no limit to the choice of the angle of taper in this case. A taper $C = 1 : 20$ to $1 : 10$ and sometimes up to $1 : 5$ is usually used to increase the axial load-carrying capacity in the direction away from the taper apex, reduce the axial displacement during tightening and make the lapping operation easier (when the hub has to be removed and fitted again several times).

Assembly of Taper Joints

The amount of interference in press-fitted taper joints is controlled by one of the following methods:

(a) by press-fitting with a *specified force*;

(b) by press-fitting with a *calibrated blow*;

(c) by press-fitting with a specified (design) axial displacement h (*axial interference*);

(d) by using a *thermal* assembly method (with heating the external member or cooling the interval member).

The method of press-fitting with a specified force is not accurate enough because this force depends on the coefficient of friction which may vary widely.

Experience shows that more stable results are obtained when the part is press-fitted with a calibrated blow when a weight is dropped from a definite height.

The weight and the dropping height are selected experimentally by using standard specimens and progressively increasing the force of blow until the required load-carrying capacity of the joint is obtained.

Press-fitting with a specified axial displacement is the most accurate method. The hub is tightly fitted onto the shaft taper by hand or by applying a slight (preferably calibrated) force and then pressed on by displacing it to the required distance h (Fig. 89a).

In the case of thermal assembly (with heating the hub or cooling the shaft) the part is mounted on the shaft with slight interference (if any). After the hub has cooled down (or the shaft has warmed up) in the joint there develops an interference whose magnitude is determined entirely by the heating (cooling) temperature.

Fig. 89. Tightening to specified axial displacement

The necessary heating temperature

$$t = 10^{-3} \frac{\Delta}{\alpha_2 d} + t_0 \tag{1.49}$$

the cooling temperature

$$-t = 10^{-3} \frac{\Delta}{\alpha_1 d} - t_0 \tag{1.50}$$

where Δ = necessary diametral interference, µm
α_2 and α_1 = coefficients of linear expansion of the materials of the hub and shaft, respectively
t_0 = temperature in the premises

As distinct from cylindrical press-fitted joints, in which the heating (cooling) temperature affects only the amount of the assembly clearance but does not tell on the final interference, this temperature in taper joints directly defines the amount of interference. In this case the temperature of assembly should be strictly controlled. This is difficult to achieve, especially during the cooling process (because the choice of the cooling media is restricted). Besides, the accuracy of the results is affected by the temperature changes difficult to account for which occur when heated (or cooled) parts are carried to the assembly site.

In tightened joints the interference is controlled by tightening the nut to a definite torque or (which is more accurate) by tightening it to the design displacement of the hub on the shaft.

The amount of axial interference h is controlled by the difference between the marks made on the shaft first after the hub has been tightly fitted on the shaft and then after it has been tightened, or by tightening the hub against a shoulder on the shaft (see Fig. 89b). The manufacturing deviations in the diametral dimensions of the tapers of the shaft and hub, causing appreciable variations in the axial position of the hub on the shaft, are compensated for by means of adjusting rings *1* mounted between the shoulder and the hub.

The thickness of the rings and the nominal distance from the shoulder to the hub end face should be selected with a margin of about 1.5h which will ensure interference during subsequent reassemblies and allow for possible repeated lapping of the joint.

Withdrawal means introduced into tightened taper joints will facilitate disassembly.

The system of *hydraulic withdrawal* (see *Fundamentals of Machine Design*, vol. 3, Fig. 13a) is the most convenient method (but, unfortunately, it cannot always be used in actual service conditions). When oil is delivered under a pressure of 1000-2000 kgf/cm² along a system of ducts to the seating surfaces the hub leaves the shaft on its own, sometimes with a sharp jerk which corresponds to the change-over from static friction to friction of motion.

Load-Carrying Capacity

The torque (in kgf·m) transmitted by a taper joint is

$$T = 10^{-3}\,\frac{\pi d_m^2 lkf}{2} = 5 \cdot 10^{-4} \pi d^2 lkf \tag{1.51}$$

where d_m = mean diameter of taper, mm (Fig. 90)

l = effective length of the joint, mm

k = pressure on the seating surface, kgf/mm²

f = coefficient of friction

The value $d_m = d\,(1 - l/d \tan \alpha)$ may be replaced without much error by the diameter d of the taper.

The maximum torque transmitted by the joint is determined by the allowable crushing stress σ_{crush} on the seating surfaces and also by the stresses developing in the shaft and hub during tightening (the limit is usually placed by the stresses in the hub).

Table 16 gives the values of σ_{crush} for the most popular materials.

Table 16

Hub material	σ_{crush}, kgf/mm²
Structurally improved steel	20-25
Grey cast iron	2-5
Aluminium alloys	1-2

Joints are calculated with a margin of safety $n = 2$-2.5 by increasing the design torque n times or, which is the same, by reducing n times the design coefficient of friction.

The axial force required to build up the pressure k

$$P_{ax} = k\pi d_m l \tan \alpha \tag{1.52}$$

Substituting the value of k from Eq. (1.51) into this expression, we get

$$P_{ax} = 10^3 \frac{T2 \tan \alpha}{d_m f} = 10^3 \frac{TC}{d_m f} \qquad (1.53)$$

The tightening force P_{tight} is equal to the sum of the force P_{ax} and the forces of friction arising when the hub is axially displaced on the shaft

$$P_{tight} = k \pi d_m l \, (f + \tan \alpha) =$$
$$= P_{ax} \left(\frac{f}{\tan \alpha} + 1 \right) = 10^3 \frac{TC}{d_m f} \left(\frac{f}{\tan \alpha} + 1 \right) \qquad (1.54)$$

Since $\tan \alpha = 0.5C$,

$$P_{tight} = 10^3 \frac{T}{d_m} \left(2 + \frac{C}{f} \right) \qquad (1.55)$$

The resistance to shear in the direction towards the taper apex (for press-fitted connection) is

$$P'' = k \pi d_m l \, (f - \tan \alpha) = 10^3 \frac{T}{d_m} \left(2 - \frac{C}{f} \right) \qquad (1.56)$$

The diametral interference Δ developing in the joint during tightening depends on the radial rigidity of the shaft and hub and, according to Lame's formula, is

$$\Delta = 10^3 k d \theta \ (\mu m) \qquad (1.57)$$

where k, according to Eq. (1.47), is

$$k = 10^3 \frac{2T}{\pi d_m l f} \qquad (1.58)$$

and θ is a coefficient expressed as

$$\theta = \frac{c_1 - \mu_1}{E_1} + \frac{c_2 + \mu_2}{E_2} \qquad (1.59)$$

Here E_1, E_2 and μ_1, μ_2 are the moduli of normal elasticity and Poisson's ratios for the shaft and hub materials, respectively; c_1 and c_2 are the coefficients expressed as

$$c_1 = \frac{1 + a_1^2}{1 - a_1^2} \qquad (1.60)$$

$$c_2 = \frac{1 + a_2^2}{a_2^2} \qquad (1.61)$$

where a_1 and a_2 are factors accounting for the wall thickness (ratio of the internal diameter d_{in} to the external diameter d_{ex}), for the shaft and hub, respectively ($a_1 = d_0/d_m$, $a_2 = d_m/D$, see Fig. 90).

Figure 91 shows the dependence of c on $a = d_{in}/d_{ex}$.

With the same material for the shaft and hub ($E_1 = E_2 = E$, $\mu_1 = \mu_2$)

$$\theta = \frac{c_1 + c_2}{E} \qquad (1.62)$$

The maximum compression stress in the shaft

$$\sigma_1 = \frac{2k}{1 - a_1^2} \qquad (1.63)$$

The maximum rupturing stress in the hub

$$\sigma_2 = \frac{2k}{1 - a_2^2} \qquad (1.64)$$
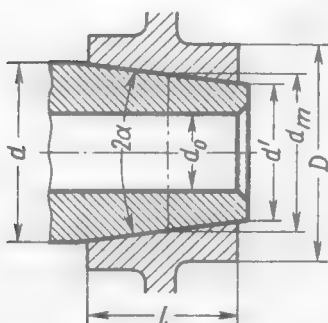
Fig. 90. Design diagram
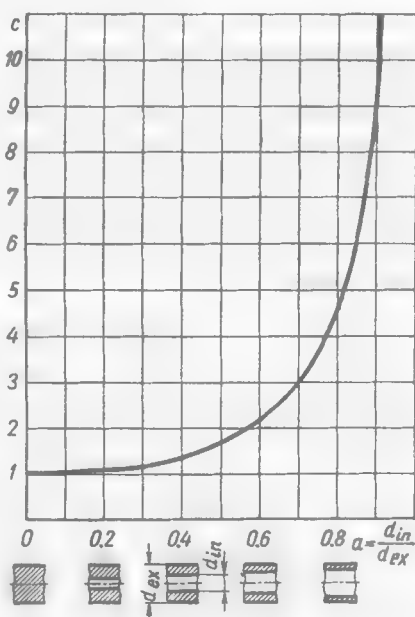
Fig. 91. Coefficient c as a function of a

Axial interference h required to obtain the design value of Δ

$$h = 10^{-3} \frac{\Delta'}{C} \text{ (mm)} \qquad (1.65)$$

where

$$\Delta' = \Delta + 2\varphi(R_{z1} + R_{z2})$$

Here, R_{z1} and R_{z2} are the heights of microirregularities on the surface of the shaft and hub, respectively (in microns) and φ is the crushing coefficient of the microirregularities.

Usually $\varphi = 0.5$. Then

$$\Delta' = \Delta + R_{z1} + R_{z2} \qquad (1.66)$$

The values of R_z depending on the surface finish are given in the Table below

Class of surface finish	∇6	∇7	∇8	∇9	∇10	∇11
R_z, μm	20	6.3	3.2	1.6	0.8	0.4

With the surface finish above Class 7 and usual interferences, the values of R_z are small as compared to Δ (< 10 per cent) and hence it may be assumed that $\Delta' = \Delta$. This assumption is more true for lapped-in tapers in which R_z diminishes as a result of the lapping.

Calculation example. The working torque $T = 100$ kgf·m. The diameter of the shaft (major diameter of the taper) $d = 60$ mm. Taper length $l = 70$ mm. The taper is 1 : 20. The shaft and hub are made of steel. The shaft is solid ($a_1 = 0$). The external hub diameter $D = 90$ mm ($a_2 = 0.66$). The seating surfaces are machined to the 8th class of surface finish ($R_z = 3.2$ μm). The coefficient of friction $f = 0.1$.

Determine the tightening force and the axial interference required to transmit the torque.

Assuming that the margin of safety $n = 2$, we get the design torque

$$T' = 200 \text{ kgf·m}$$

The required tightening force, according to Eq. (1.55), is

$$P_{tight} = 10^3 \frac{200}{60} \left(2 + \frac{0.05}{0.1}\right) = 8300 \text{ kgf}$$

The pressure on the seating surfaces, in conformity with Eq. (1.58), is

$$k = 10^3 \frac{2 \cdot 200}{\pi \cdot 3600 \cdot 70 \cdot 0.1} \approx 5 \text{ kgf/mm}^2$$

The maximum stress in the shaft, according to Eq. (1.63), is

$$\sigma_1 = 10 \text{ kgf/mm}^2$$

The stress in the hub, according to Eq. (1.64), is

$$\sigma_2 = \frac{10}{1 - 0.44} \approx 18 \text{ kgf/mm}^2$$

The required diametral interference, according to Eq. (1.57), is

$$\Delta = 10^3 \cdot 5 \cdot 60\theta = 3 \cdot 10^5 \theta$$

The value of θ may be found from Eq. (1.62), substituting into

$$E = 20 \cdot 10^3 \text{ kgf/mm}^2,$$
$$c_1 = 1,$$

and

$$c_2 = \frac{1 + a_2^2}{1 - a_2^2} = \frac{1 + 0.44}{1 - 0.44} \approx 2.5$$

Hence,

$$\theta = \frac{1 + 2.5}{20 \cdot 10^3} = 1.75 \cdot 10^{-4}$$

and the diametral interference

$$\Delta = 3 \cdot 10^5 \cdot 1.75 \cdot 10^{-4} = 53 \text{ μm}$$

Accounting for the crushing of microirregularities [Eq. (1.66)],

$$\Delta' = 53 + 6.4 = 59.4 \text{ μm}$$

The required axial interference by Eq. (1.65)

$$h = 10^{-3} \frac{59.4}{0.05} = 1.2 \text{ mm}$$

Let us now determine the heating (or cooling) temperature for a thermal assembly.

Within the range from 0 to 200° C the coefficient of linear expansion $\alpha = 13 \cdot 10^{-6}$. Assuming that the temperature in the premises is $t_0 = 20°C$ and substituting into Eq. (1.49) the numerical values of Δ and d from the previous example, we obtain

$$t = 10^{-3} \frac{59.4}{13 \cdot 10^{-6} \cdot 60} + 20 \approx 95°C$$

With account being taken of the hub cooling in carrying ($\Delta t = 30°C$),

$$t = 125°C$$

For the assembly with cooling (assuming that $\alpha = 8 \cdot 10^{-6}$ within the range from 0 to $-200°C$) we obtain from Eq. (1.50)

$$-t = 10^{-3} \frac{59.4}{8 \cdot 10^{-6} \cdot 60} - 20 \approx 105°C$$

Accounting for the shaft warming in carrying ($\Delta t = 30°C$)

$$t = -135°C$$

(b) Gripspring Joints

In these joints torque is transmitted by tapered rings or sleeves known as Gripsprings) which are installed in the annular space
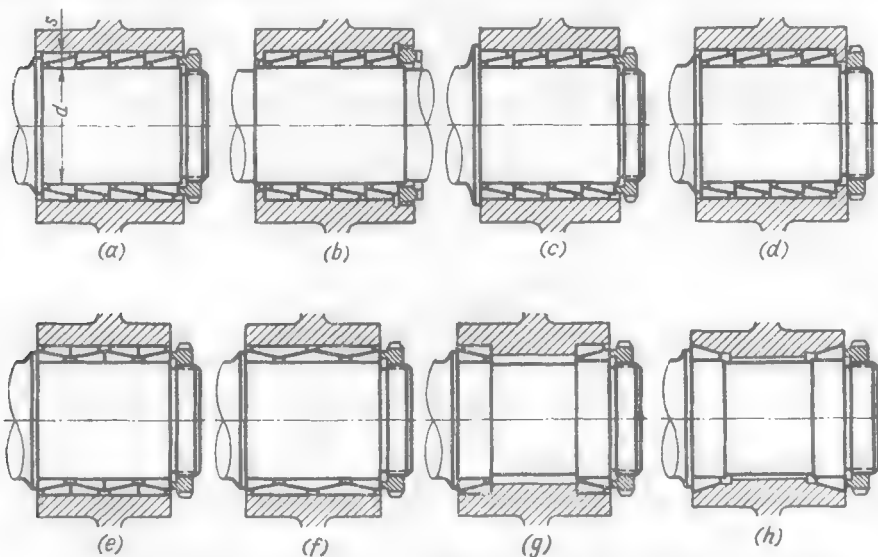
Fig. 92. Gripspring joints

between the shaft and hub and clamped by a nut on the shaft (Fig. 92a) or in the hub (Fig. 92b). As the tapered surfaces of the rings engage one another in tightening, the rings elastically deform:

the outer (enveloping) rings expand while the inner (enveloped) ones contract, thus producing interference on the surfaces of the shaft and hub.

In each pair of rings torque is transmitted through three frictional surfaces. The hub is centred on the shaft by three surfaces in each pair, which requires a highly accurate manufacture of the rings and strict axial alignment of their outer and inner surfaces.

The hub can be fitted in any angular position with respect to the shaft, and its axial position on the latter can be adjusted within some limits.

The joint can take up by friction rather large axial forces. If accurate axial location is required and also if the joint is acted upon by increased axial forces, use is made of bearing shoulders.

In the design in Fig. 92c the shoulder takes up uni-directional axial forces, the loads of the opposite direction being sustained by the forces of friction. In the design shown in Fig. 92d axial forces acting in one direction are taken up by a nut, those acting in the other direction being taken up by a shoulder on the shaft through a set of Gripsprings.

The Gripspring rings are installed either with their tapers facing one way (Fig. 92a-d) or alternately (Fig. 92e). Gripsprings with a double-sided taper (Fig. 92f) are rarely used (it is difficult to maintain the axial alignment of the working surfaces of the rings; it is necessary to mount additional side rings).

The magnitude of the transmitted torque can be adjusted by changing the clamping force. The maximum torque is determined by the allowable crushing stress on the contacting surfaces and the rupturing and compression stresses developing during tightening in the hub and shaft, respectively.

To avoid overstresses, the joint is tightened to a specified torque or the nut turned to the designed axial displacement.

In the course of time the clamping becomes loose due to the crushing (under cyclic loads) and attrition of the seating surfaces. The joint must therefore be periodically retightened. With a sufficient yielding of the hub and shaft (hollow shafts) the reduction of the interference is compensated for to a certain extent by the elastic restitution of the hub and shaft.

Gripsprings are installed on the shaft and in the hub by a centring fit (usually slide). During the first stage of clamping the mounting clearance is eliminated and the Gripsprings tightly pressed against the seating surfaces. With further tightening, on the seating surfaces there develops the interference necessary for transmitting the torque.

To reduce the force spent in the preliminary deformation of the Gripsprings within the clearance limits and diminish the radial dimensions of the joint, it is advisable to make the Gripsprings thinner, i.e., decrease the annular clearance s between the shaft

and hub (Fig. 92a). It is good practice to keep to an $s = (0.12$ to $0.08)$ d where d is the shaft diameter. The upper limit refers to joints of small diameter ($<$80 mm) and the lower limit, to joints of large diameter (80-200 mm). On the average $s = 0.1d$.

When Gripsprings are arranged in multiple rows and tightened on one side, the pair of them which is nearest to the nut and acted upon by the full tightening force develops the maximum pressure on the shaft and hub and transmits the principal share of the torque. The pressure drops in the next pairs since some of the tightening force is dampened by the axial components of the frictional forces
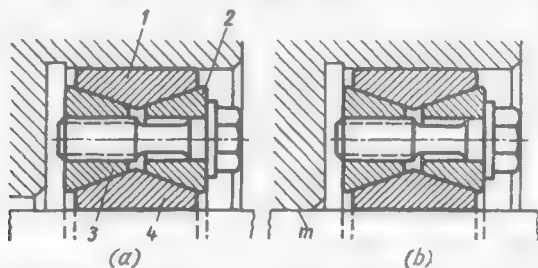
Fig. 93. Double-sided Gripsprings

on the surfaces of the Gripsprings. Accordingly, the share of the torque transmitted by these Gripsprings decreases. The tightening force on the Gripsprings farthest from the nut is so weak that it is not sufficient even to deform them and eliminate the initial mounting clearance. This impairs the centring and longitudinal stability of the joint.

The moments that bend the shaft-fitted part in the longitudinal plane redistribute the loads on the Gripsprings. The radial forces acting on their extreme pairs cause their misalignment and certain axial displacement attended by the compression of the entire set of the Gripsprings, and the part becomes skew.

A higher longitudinal stability of the part is ensured by installing the Gripsprings on both sides of the hub (Fig. 92g, h). The part here is rigidly fixed axially and the joint can take up large axial forces. However, the transmitted torque is less than in multiple-row designs.

In large-size units (Fig. 93a) on both sides of the hub there are installed outer 1 and inner 4 double-sided Gripsprings which are pressed outwards when intermediate rings 2 and 3 are tightened. The independent clamping of both sets of the Gripsprings increases the transmitted torque. Centring from four surfaces is the disadvantage of this joint.

An additional centring from cylindrical surface m (Fig. 93b) calls for very accurate axial alignment and precise diametral dimensions of all the centring surfaces.

Gripsprings are manufactured from spring steel grades 65ГС, 60C2A, 70C3A by either cutting tubular blanks to length, or forging individual annular pieces (for heavily loaded connections). Their heat treatment consists in hardening followed by medium tempering (45-55 Rc).

Strain hardening in joints subjected to cyclic loads can be prevented if one of the Gripsprings of each pair is made of forged silicon bronze or beryllium bronze (the critical joints). The latter are hardened at 800°C and tempered at 250-300°C.

The working surfaces of Gripsprings are machined to the 10th-11th class of surface finish according with the 1st grade of accuracy, strict concentricity of the outer and inner surfaces (allowable axial misalignment < 0.01-0.02 mm) being maintained. This is one of the primary conditions for the proper functioning of the joint.

The hardness of the working surfaces of shafts and hubs is not below 35-40 Rc (hardening with subsequent high tempering). It is better to subject shafts to induction surface hardening (50-55 Rc).

The working surfaces of the shafts are machined to the 9th-10th class of surface finish and those of the hubs, to the 8th-9th class.

Load-Carrying Capacity

The tightening force P_1 applied to the end face of the first Gripspring (Fig. 94) is equalized by the axial components of the pressure forces n acting on its tapered surface. Let us isolate on this surface an elementary area of length l and mean width $ds = \dfrac{D_m}{\partial \varphi^2}\, d\varphi$ where D_m is the mean diameter of the taper and $d\varphi$, the central angle. The resultant ΔN of the pressure forces n on this area is

$$\Delta N = nl \frac{D_m}{2}\, d\varphi$$

The axial component of force ΔN is

$$\Delta P = \Delta N \sin \alpha = nl \frac{D_m}{2} \sin \alpha\, d\varphi$$

Fig. 94. Design diagram

where α is the angle of taper.

The sum of the axial components over the entire circumference of the taper is equal to force P_1

$$nl \frac{D_m}{2} \sin \alpha \int\limits_{0}^{2\pi} d\varphi = P_1$$

hence,

$$n = \frac{P_1}{\pi D_m l \sin \alpha} \tag{1.67}$$

7*
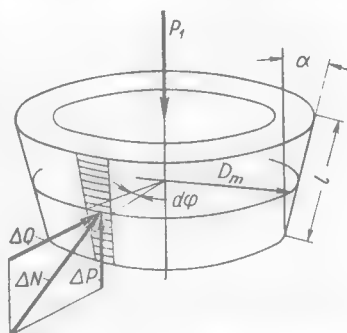
The sum of the normal forces acting on the entire tapered surface

$$N = n\pi D_m l = \frac{P_1}{\sin \alpha} \qquad (1.68)$$

The sum of the radial components over the entire tapered surface

$$Q_1 = n\pi D_m l \cos \alpha \frac{P_1}{\tan \alpha} \qquad (1.69)$$

The frictional forces F_1 on the external surface of the outer Gripspring and on the internal surface of the inner Gripspring (Fig. 95a)

$$F_1 = Q_1 f = \frac{P_1 f}{\tan \alpha} \qquad (1.70)$$

where f is the coefficient of friction.
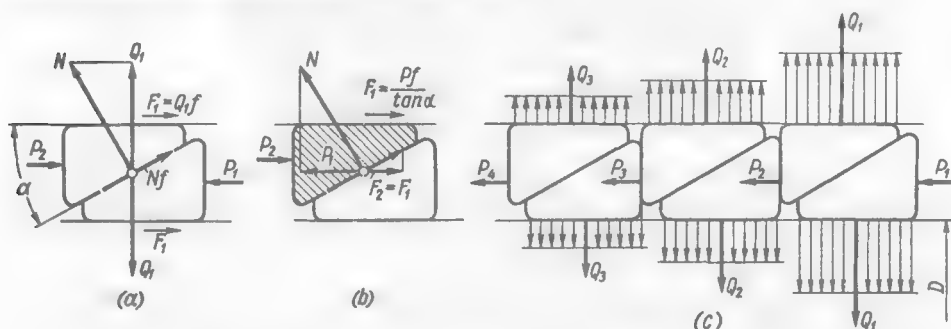
Fig. 95. Distribution of forces among Gripsprings

The frictional force on the tapered surface

$$F_1' = Nf = \frac{P_1 f}{\sin \alpha}$$

and its axial component

$$F_{ax} = Nf \cos \alpha = \frac{P_1 f}{\tan \alpha} = F_1 \qquad (1.71)$$

The axial force P_2 transmitted by the outer Gripspring of the first pair to the inner Gripspring of the second pair may be found proceeding from the condition of equilibrium of the axial forces acting on the outer Gripspring of the first pair (Fig. 95b).

$$P_2 = P_1 - 2F_1 = P_1 \left(1 - \frac{2f}{\tan \alpha}\right) \qquad (1.72)$$

When $\tan \frac{2f}{\tan \alpha} = 1$, force $P_2 = 0$. This means that the system becomes selfbraking. The axial force P_1 is dampened by the forces of friction in the first pair and no pressure is exerted on the second pair.

Thus, the *condition of self-braking* is

$$\frac{f}{\tan \alpha} \geqslant 0.5$$

or

$$\tan \alpha \leqslant 2f \qquad (1.73)$$

The frictional forces F_2 in the second pair of Gripsprings (Fig. 95c) are

$$F_2 = \frac{P_2 f}{\tan \alpha} = \frac{P_1 f}{\tan \alpha} \left(1 - \frac{2f}{\tan \alpha}\right) \qquad (1.74)$$

In the general form, for any pair of Gripsprings

$$P_z = P_1 \left(1 - \frac{2f}{\tan \alpha}\right)^{z-1} \qquad (1.75)$$

$$F_z = \frac{P_1 f}{\tan \alpha} \left(1 - \frac{2f}{\tan \alpha}\right)^{z-1} \qquad (1.76)$$

where z is the serial number of the pair.

Figure 96 shows the distribution of frictional forces F_z from one pair to another, calculated by Eq. (1.76) for the values of $f/\tan \alpha$ less than 0.5. The force F_1 in the first pair with $f/\tan \alpha = 0.4$ is taken as unity. The change in the forces is arbitrarily depicted by smooth curves (in actual fact they are distributed stepwise from pair to pair).

It can be seen from the plot that the greater the value of $f/\tan \alpha$ (high coefficient of friction, small angles α), the more sharply the forces F diminish from pair to pair.

For example, when $f/\tan \alpha = 0.4$ (which is close to the condition of self-braking) the frictional force in the second pair of Gripsprings is only $0.2 F_1$ and in the third pair, $0.04 F_1$. Obviously, one pair of Gripsprings is enough in our case. The pairs that follow only increase the axial dimensions and worsen the centring of the joint.

Fig. 96. Distribution of frictional forces among Gripsprings

When the values of $f/\tan \alpha$ are low the forces F are distributed more evenly. However, the magnitude of the frictional forces diminishes and, therefore, to transmit the given torque it is necessary to increase either the tightening force or the number of the Gripspring pairs.

The total force of friction on the seating surface, according to Eqs. (1.70), (1.74) and (1.76), is

$$\sum F = F_1 + F_2 + F_3 + \ldots + F_z = \frac{P_1 f}{\tan \alpha} \left[1 + \left(1 - \frac{2f}{\tan \alpha} \right) + \right.$$
$$\left. + \left(1 - \frac{2f}{\tan \alpha} \right)^2 + \ldots + \left(1 - \frac{2f}{\tan \alpha} \right)^{z-1} \right] \quad (1.77)$$

The expression in square brackets is a geometric progression with a common ratio of $1 - 2f/\tan \alpha$, the sum of whose members is

$$S = \frac{1 - (1 - 2f/\tan \alpha)^z}{2f/\tan \alpha} \quad (1.78)$$

Substituting this value into Eq. (1.77), we obtain

$$\sum F = \frac{P_1}{2} [1 - (1 - 2f/\tan \alpha)^z] = \frac{P_1}{2} \varphi \quad (1.79)$$
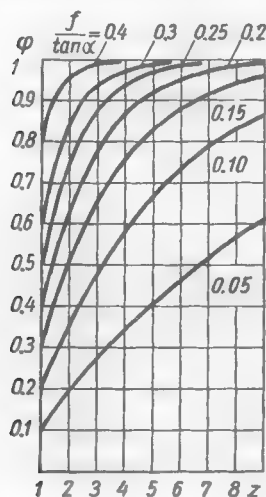
Fig. 97. Dependence of φ on $f/\tan \alpha$ and z
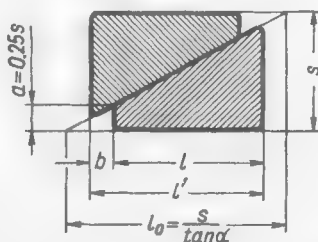
Fig. 98. Dimensions of Gripsprings

where φ is the *coefficient of the force distribution uniformity* expressed as

$$\varphi = f - (1 - 2f/\tan \alpha)^z \quad (1.80)$$

The dependence of φ on z for various values of $f/\tan \alpha$ is illustrated in Fig. 97.

The torque transmitted by the joint is

$$T = \frac{\sum Fd}{2} = \frac{P_1 d}{4} \varphi \quad (1.81)$$

where d is the shaft diameter.

The specific pressure is maximum in the section of the shaft under the first Gripspring and is expressed as

$$k_1 = \frac{Q_1}{\pi \, dl} = \frac{P_1}{\tan \alpha \pi \, dl} \quad (1.82)$$

where l is the width of the ring.

The value of l is determined by geometrical relationships (Fig. 98). The minimum thickness a of the Gripspring is taken at $0.25s$ (where s

is the annular clearance between the shaft and hub). The projection b of the Gripsprings with respect to each other is determined by their axial displacement in tightening. With some margin, $b = 0.15l$. It follows from the drawing that

$$l = l_0 - 2a/\tan \alpha + b = s/\tan \alpha - 0.5s/\tan \alpha + 0.15l$$

whence

$$l = 0.6s/\tan \alpha \tag{1.83}$$

The length of a pair of Gripsprings

$$l' = 1.15l \approx 0.7s/\tan \alpha \tag{1.84}$$

Substituting (1.83) into (1.82), we get

$$P_1 \approx 2k_1 \, ds \tag{1.85}$$

With an average value of $s = 0.1d$

$$P_1 = 0.2k_1 d^2 \tag{1.86}$$

According to Eqs. (1.81) and (1.86), the transmitted torque is

$$T = \frac{P_1 d}{4} \varphi = 0.05k_1 \, d^3\varphi = 5 \cdot 10^{-5}k_1 \, d^3\varphi \ (\text{kgf} \cdot \text{m}) \tag{1.87}$$

The displacement force taken up by the joint, according to Eqs. (1.79) and (1.86), is

$$S = \sum F = \frac{P_1}{2} \varphi = 0.1k_1 d^2\varphi \tag{1.88}$$

The value of k_1 should be less than the permissible crushing stress σ_{crush} for the given material (for heat-treated steel $\sigma_{crush} = 20\text{-}25$ kgf/mm², for cast-iron hubs, 2-5 kgf/mm²).

The limiting number z_{lim} of useful Gripspring pairs may be found if we disregard the Gripsprings carrying a small percentage of the torque, for example 15 per cent, i.e., if we assume that $\varphi = 0.85$. Then, according to Eq. (1.80),

$$z_{lim} = \frac{\log 0.15}{\log (1 - 2f/\tan \alpha)}$$

The diagram in Fig. 97 may also be used. Draw a horizontal line through the point $\varphi = 0.85$ on the diagram and read z_{lim} on the abscissas of the points where the horizontal line intersects the curves $f/\tan \alpha$. The values of z_{lim} approximated to the nearest whole numbers are illustrated in Fig. 99.

It can be seen from the plot that with the initial assumption ($\varphi = 0.85$) the limiting number of useful pairs for $f/\tan \alpha = 0.4$ is one. For smaller values of $f/\tan \varphi$ the number of the pairs increases.

The value of α should be selected so that with the maximum coefficient of friction possible in practice the Gripsprings do not

jam and freely disengage during disassembly. In stationary conditions when there is no load (for example, during assembly and
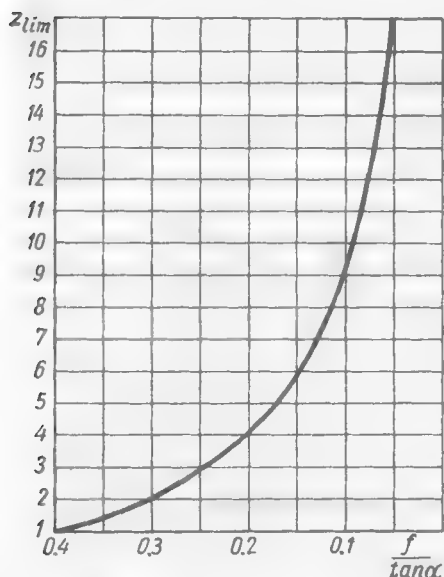
Fig. 99. Limiting number of useful Gripsprings
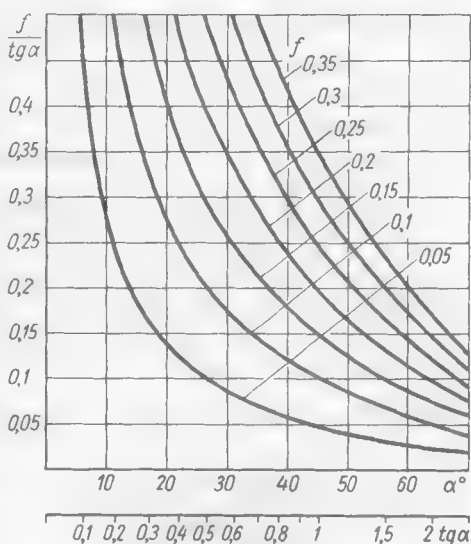
Fig. 100. Dependence of $f/\tan \alpha$ on α and f

disassembly) the coefficient of friction can reach 0.2-0.25. Thus, for the Gripsprings not to self-brake the following condition must be fulfilled:

$$\tan \alpha \geqslant 2f \geqslant 0.4\text{-}0.5,$$

i.e.,

$$\alpha \geqslant 22\text{-}27°$$

The transmitted torque should be calculated from the minimum coefficient of friction ($f = 0.08\text{-}0.1$). With $\alpha = 25°$ ($\tan \alpha = 0.466$) the design value of $f/\tan \alpha$ is

$$f/\tan \alpha = \frac{0.08 \text{ to } 0.1}{0.466} \approx 0.17 \text{ to } 0.21$$

On the average, $f/\tan \alpha$ may be taken at 0.2. In this case the limiting number of useful Gripspring pairs will be 3-4.

If the number of pairs is less, the values of φ may be found from the plot in Fig. 97 or from Eq. (1.80).

Figure 100 shows $f/\tan \alpha$ *versus* α for various values of f.

It is inadvisable to increase α in excess of 30-35° ($f/\tan \alpha < 0.15$) because this results in the reduction of φ (see Fig. 97) which has to be

compensated for by increasing the number of the Gripspring pairs. This worsens the centring. Besides, an increase in α reduces the ability of the joint to resist tilting moments.

With a given number *z* of the Gripsprings the uniformity factor (and hence, the transmitted torque) can be increased by the following methods:
(1) by diminishing progressively from pair to pair the radial assembly clearances between the Gripsprings and the seating surfaces of the shaft and hub as the distance from the tightening nut grows larger;
(2) by tightening up the Gripsprings on both sides (Fig. 101*a*);
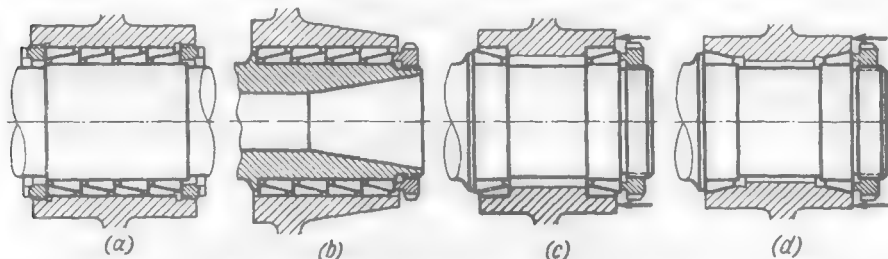
Fig. 101. Increasing the uniformity of load distribution among Gripsprings

(3) by reducing the stiffness of the shaft and hub in the section where the first Gripsprings are arranged and increasing it in the section with the last Gripsprings (Fig. 101*b* ;
(4) with the Gripsprings mounted on both sides of the hub (Fig. 101*c*, *d*), by applying an additional axial force shown by arrows in the drawing to the hub when tightening the nut;
(5) by using vibration tightening (reducing the coefficient of friction and hence, *f*/tan α).
The first method is unacceptable for operational considerations (the Gripsprings may be fitted in a wrong order during assembly). The methods as per (2), (3) and (4) are not always feasible for design considerations. The fifth method is universal but is sometimes difficult to implement (reassembly of the joint in repair shops).

It is difficult to maintain the design tightening force because friction in the threads and on the bearing surface of the nut is a variable. The method of tightening to the design axial displacement is more accurate. The displacement may be determined from the expression

$$h = 10^{-3}\, \frac{\Delta}{2 \tan \alpha}\ \text{(mm)}$$

where Δ is the diametral interference in μm, which may be found from the formula

$$\Delta = 10^3\, k D_m \theta\ \text{(μm)}$$

where k is the pressure on the seating surfaces in kgf/mm^2 and θ is the coefficient that depends on the radial rigidity of the shaft and

hub, and is expressed as

$$\theta = \frac{c_1 - \mu_1}{E_1} + \frac{c_2 + \mu_2}{E_2}$$

According to Eq. (1.82), for the first pair of Gripsprings

$$\Delta_1 = 10^3 \, k_1 D_m \theta = 10^3 \, \frac{P_1 D_m \theta}{\tan \alpha \pi \, dl}$$

With $s/d = 0.1$ the mean diameter $D_m = 1.1d$. In this case

$$\Delta_1 = 1.1 \cdot 10^3 \, \frac{P_1 \theta}{\tan \alpha \pi l}$$

The axial displacement in tightening the first pair of Gripsprings is

$$h_1 = \frac{1.1 P_1 \theta}{2 \pi l \tan^2 \alpha}$$

For the second pair of Gripsprings

$$h_2 = \frac{1.1 P_2 \theta}{2 \pi l \tan^2 \alpha} = \frac{1.1 P_1 \theta}{2 \pi l \tan^2 \alpha} \, (1 - 2f/\tan \alpha),$$

etc.

The sum of the axial displacements

$$\sum h = \frac{1.1 P_1 \theta}{2 \pi l \tan^2 \alpha} \cdot \frac{1 - (1 - 2f/\tan \alpha)^z}{2f/\tan \alpha} = \frac{1.1 P_1 \theta \varphi}{4 \pi l f \tan \alpha} \qquad (1.89)$$

Substituting the value $P_1 = \frac{4T}{d\varphi}$ into Eq. (1.89), we get

$$\sum h = 10^3 \, \frac{1.1 T \theta}{\pi dl f \tan \alpha} \, \text{(mm)} \qquad (1.90)$$

When taking up the initial assembly clearance between the Gripsprings and the seating surfaces of the shaft and hub the axial displacement is

$$h' = z \, \frac{\Delta_{hub} + \Delta_{sh}}{2 \tan \alpha}$$

where Δ_{hub} and Δ_{sh} are the diametral assembly clearances in the hub and on the shaft, respectively.

With slide fits according with the 2nd grade of accuracy the values of h' are negligible in comparison with Σh and may be disregarded.

In joints of this type the nut thread length must have an allowance of (1.5 to 2) $\sum h$ to permit the nut displacement during tightening.

The actual pressure force on the seating surfaces is slightly decreased by the opposing forces of elasticity produced in the Gripsprings during the first stage of their tightening when the radial assembly clearances are being taken up. But calculations show that with the usual values of $s/D = 0.1$ and with a slide fit of the Gripsprings the total opposing force does not exceed 3-5 per cent of the tightening force. The opposing force may therefore be neglected.

Calculation example. The shaft diameter $d = 100$ mm. The shaft and hub are made of steel. The Gripspring thickness $s = 0.1d = 10$ mm. The external hub diameter $d_{ex} = 160$ mm $\left(\dfrac{d_{Gr}}{d_{ex}} = \dfrac{120}{160} = 0.75\right)$. The design coefficient of friction $f = 0.1$. The allowable crushing stress $\sigma_{crush} = 10$ kgf/mm².

Determine the transmitted torque and the displacing force, if the number z of the Gripspring pairs is 1-6.

From Eq. (1.87) the torque is

$$T = 5 \cdot 10^{-5} \cdot 10 \cdot 10^6 \varphi = 500\varphi \quad (\text{kgf} \cdot \text{m})$$

The displacing force, according to Eq. (1.88), is

$$S = 0.1 \cdot 10 \cdot 10^4 \varphi = 10^4 \varphi \ (\text{kgf})$$

We assume that the angle α of taper is 27° ($\tan \alpha = 0.5$, $f/\tan \alpha = 0.2$). The values of φ at $f/\tan \alpha = 0.2$ for various z may be found from the plot in Fig. 97 or from Eq. (1.80).

From Eq. (1.83) the Gripspring width is

$$l = \frac{0.6 \cdot 10}{0.5} = 12 \ (\text{mm})$$

The length of the joint from Eq. (1.84)

$$L = \frac{z \cdot 0.7 \cdot 10}{0.5} = 14z$$

The necessary tightening force by Eq. (1.86)

$$P_{tight} = 0.2 \cdot 10 \cdot 10^4 = 20,000 \ (\text{kgf})$$

The axial displacement of the nut during tightening from Eq. (1.89)

$$\sum h = \frac{1.1 \cdot 2 \cdot 10^4 \theta \varphi}{4\pi \cdot 12 \cdot 0.1 \cdot 0.5} \approx 3 \cdot 10^3 \theta \varphi$$

The value θ for the shaft and hub made of steel

$$\theta = \frac{c_1 + c_2}{E}$$

Substituting

$$E = 20 \cdot 10^3 \ (\text{kgf/mm}^2),$$
$$c_1 = 1,$$

and

$$c_2 = \frac{1 + a_2^2}{1 - a_2^2} = \frac{1 + 0.75^2}{1 - 0.75^2} = 3.55,$$

we obtain

$$\theta = \frac{1 + 3.55}{20 \cdot 10^3} = 2.27 \cdot 10^{-4}$$

and

$$\sum h = 3 \cdot 10^3 \theta \varphi = 0.68\varphi$$

The calculation results are given in Table 17.

It is obvious that the torque and the displacing force appreciably increase when the number of the Gripspring pairs is increased to four, and only slightly with a further increase in the number of the Gripspring pairs.

Table 17

Parameters	z					
	1	2	3	4	5	6
φ	0.4	0.64	0.78	0.87	0.92	0.95
T, kgf·m	200	320	390	435	460	475
S, kgf	4000	6400	7800	8700	9200	9500
L, mm	14	28	42	56	70	84
$\sum h$, mm	0.28	0.43	0.53	0.59	0.62	0.65

The design values of T and S should be reduced by the safety margin value.

Let us compare the load-carrying capacity of a Gripspring joint and of a taper joint.

In conformity with Eq. (1.87) and (1.51), the ratio between the torques transmitted by the first and second joints is

$$\frac{T}{T'} = 0.1 \frac{k_1 d^3 \varphi}{\pi d^2 lkf}$$

With $k_1 = k$; $f = 0.1$; and $l = d$ (which is usual for taper joints)

$$\frac{T}{T'} = \frac{\varphi}{\pi}$$

For the limiting useful value $\varphi = 0.9$

$$T \approx 0.3 \ T'$$

Therefore, with the same pressure on the seating surfaces (under the first Gripspring in Gripspring joints and over the entire surface in taper joints), the load-carrying capacity of Gripspring joints is about three times less than that of taper joints.

If one takes account of the worse centring (centring from three surfaces instead of one as in taper joints, and shorter length of centring surfaces), larger radial dimensions and higher manufacturing costs of Gripspring joints, it is obvious that these joints are in all respects inferior to taper ones.

(c) Clamped Joints

This type of fastening is predominantly used to connect shafts to prismatic components (levers, webs of built-up crankshafts). It is difficult to accommodate clamping bolts in joints connecting cylindrical components to shafts.

The load-carrying capacity of clamped friction joints (Fig. 102a) depends on the force with which the clamping bolts are tightened. For this reason, in heavily loaded joints two (Fig. 102b) or more bolts are used.

Clamping bolts should preferably be installed on spherical supports and with a clearance in the hole to prevent their bending caused by the elastic deformation of the eyes.

The torque transmitted by such a joint may approximately be determined by regarding the clamp halves as levers of the second
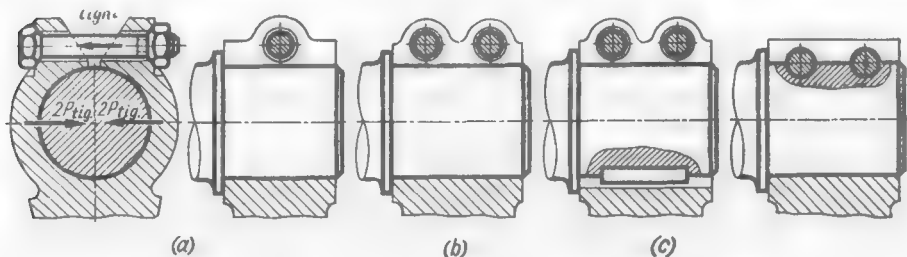
Fig. 102. Clamped joints

kind loaded by the tightening force P_{tight} (Fig. 102a)

The torque is

$$T = 2 \cdot 10^{-3} P_{tight} D f \quad (\text{kgf} \cdot \text{m}) \qquad (1.91)$$

where D is the shaft diameter in mm and f is the coefficient of friction on the seating surfaces.

The tightening force

$$P_{tight} = 0.785 i d^2 \sigma$$

where i = number of clamping bolts

d = bolt diameter, mm

σ = stress produced in the bolts by tightening, kgf/mm^2

Substituting the value of P_{tight} into Eq. (1.91), we get

$$T = 1.57 \cdot 10^{-3} i d^3 \sigma D f \quad (\text{kgf} \cdot \text{m}) \qquad (1.92)$$

The mean crushing stress on the surface of the joint is

$$\sigma_{crush} = \frac{2 P_{tight}}{\varphi \pi D L} = \frac{i d^2 \sigma}{\varphi D L} \quad (\text{kgf/mm}^2) \qquad (1.93)$$

where φ is the portion of the half-circle taking up the force $2 P_{tight}$, and L is the length of the joint in mm.

The torque T' transmitted by a press-fitted joint of the same diameter is

$$T' = 5 \cdot 10^{-4} \sigma_{crush} \pi D^2 L f \quad (\text{kgf} \cdot \text{m}) \qquad (1.94)$$

According to Eqs. (1.92) and (1.94), the ratio

$$T'/T = \frac{\sigma_{crush}}{\sigma} \cdot \frac{DL}{i d^2} \qquad (1.95)$$

Let us assume that the crushing stress on the seating surfaces in the press-fitted joint is the same as in the clamped joint. Substituting the value of σ_{crush} from Eq. (1.93) into Eq. (1.95), we obtain

$$T'/T = \frac{1}{\varphi} \qquad (1.96)$$

In conformity with experimental data $\varphi \approx 0.5$. Therefore,

$$T'/T \approx 2 \qquad (1.97)$$

Thus, with the initial assumptions being valid, the load-carrying capacity of a clamped joint is about two times less than that of a press-fitted joint.

Rigid elements such as keys (Fig. 102c) are introduced into clamped joints to increase their load-carrying capacity and also to ensure an accurate relative angular position of the joined parts. Another method of rigid coupling consists in placing the clamping bolts into semicircular recesses in the shaft (Fig. 102d). The bolts are of dowel type, and the recesses and the holes in the joint are machined jointly (by reaming or broaching).

1.7. Other Types of Joints

Figure 103 illustrates methods of transmitting torque with a a power tightening of a part against a shaft shoulder. In light joints the torque is transmitted by a pin press-fitted into the shaft and entering an end slot in the hub (Fig. 103a) or by teeth milled in the hub end face and entering slots cut in the shoulder (Fig. 103b).

A higher load-carrying capacity is characteristic of the joints with end-face teeth meshing with splines on the shaft (Fig. 103c and d). The shortcoming of these joints is that the tightening is effected against spaces m and n between the hub teeth which are difficult to position in one plane.

When two adjacent parts are mounted on a shaft, one of them (part 1 in Fig. 103e), which carries a heavy load, is installed on splines and the other (2), carrying a light load, is secured by means of end-face teeth entering the spaces between the splines. In a similar design, shown in Fig. 103f, the end-face teeth are introduced between the inner splines of the shaft-fitted part 3.

In the joint in Fig. 103g the part is tightened with its lathe-turned surface s against a shoulder having fine triangular or involute serrations cut on its periphery. The inner splines of the hub are machined by the generating method.

The joint with triangular end-face splines (Fig. 103h) is less suitable for industrial production (the shaft splines can only be formed by shaping at an angle by the indexing method).

The joints in Fig. 103g and h are frequently used to adjust the angular position of a part fitted onto a shaft. A fine adjustment can be achieved by means of an intermediate washer 4 (Fig. 103i) with two splined crowns slightly differing in the number of the splines (for example, by one spline). If the washer is turned one spline with respect to the shaft, and the hub, one spline with respect

to the washer in the opposite direction, the hub is turned through an angle

$$\varphi = 360° \frac{z_1 - z_2}{z_1 z_2}$$

where z_1 and z_2 are the numbers of splines on the washer crowns.

If, for example, $z_1 = 100$ and $z_2 = 99$, then

$$\varphi = \frac{360°}{9900} \approx 2'$$

In the joint shown in Fig. 103*j* the torque is transmitted by an end-face key introduced into slots cut in the shaft and hub. To avoid
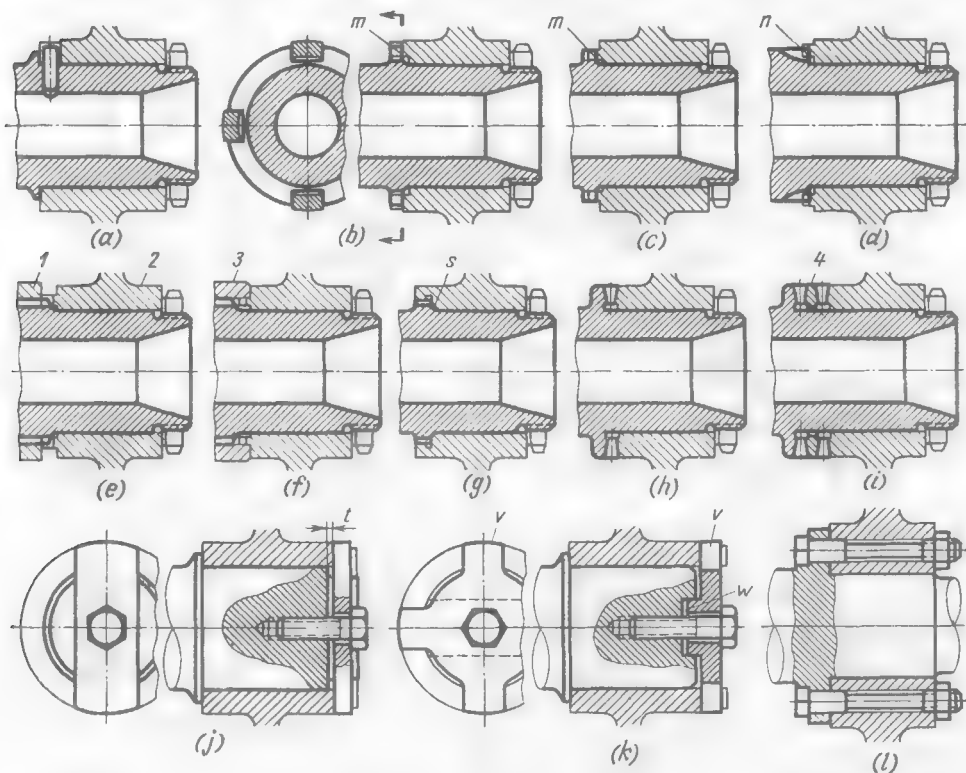
Fig. 103. Various joints

the overstressing of the key plate in tightening, the clearance t between the plate and the shaft is made not greater than 0.2-0.3 mm.

In the design in Fig. 103*k* the joint is tightened by a washer having radial teeth v entering slots in the hub and a longitudinal crest w which enters a slot in the shaft end. Figure 103*l* shows a design in which torque is transmitted with the aid of dowel bolts. This design is used for thick hubs (disk-type shaft-fitted parts).

Table 18
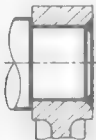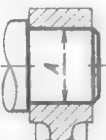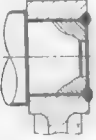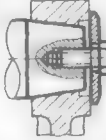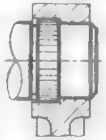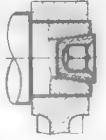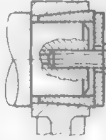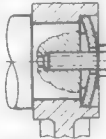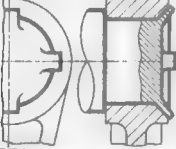
Design sketch	Description	Design sketch	Description
Welded Joints		*Frictional Joints*	
	Circular edge weld		Press-fitted joint
	Arc-spot edge weld		Taper joint
	Radial arc spot weld		Riffled joint
Joints Obtained by Plastic Deformation			Joint tightened by a taper plug
	Flaring		Joint tightened by a taper bushing
	Centre-punching of the shaft end to force the shaft metal into recesses made in the hub at the shaft-to-hub joint		Joint tightened by a plate spring
	Caulking the shaft end to force the shaft metal into slots made in the hub		Hydroplastic joint (quick-disconnect)
	Swaging the hub onto a flat on the shaft		

Table 18 (cont.)
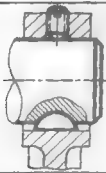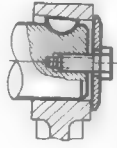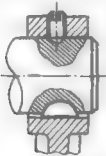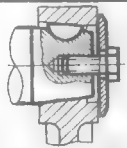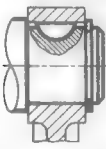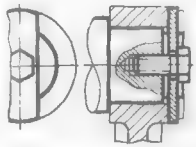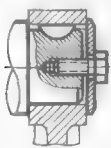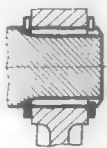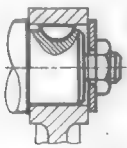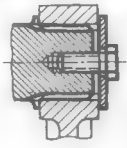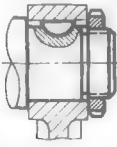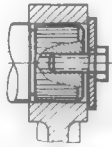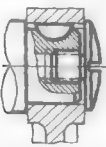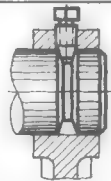
Design sketch	Description	Design sketch	Description
Keyed Joints			Hub tightened against an inclined key
	Woodruff key. Hub locked by a flat-point screw		Hub tightened against a taper
	Hub locked by a cone-point screw		End-face driving key
	Hub locked by an external snap ring	*Splined Joints*	
	Hub tightened by an axial screw		Straight-sided splines. Hub locked by external snap rings
	Hub tightened by a ring nut, on the shaft shank		Straight-sided splines. Hub locked by an axial screw
	Hub tightened by a ring nut		Triangular splines. Hub locked by an axial screw
	Hub tightened by an internal nut		Triangular splines. Hub locked by a cone-point screw

Table 18 (cont.)
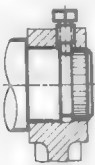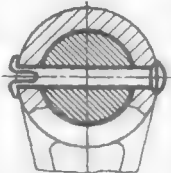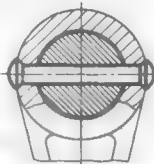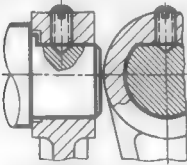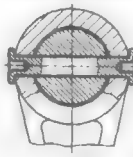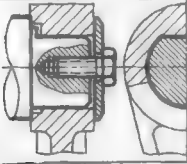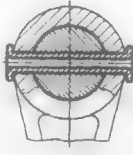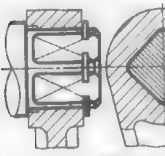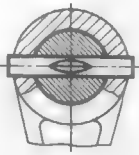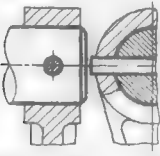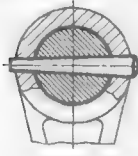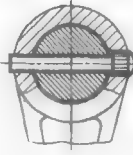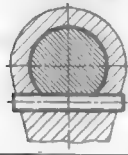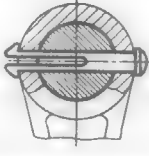
Design sketch	Description	Design sketch	Description
	Fine-splined (serrated) connection for fractional adjustment of the angular position of a lever		Slotted-end pin
Joints on Flats and Squares			
	Joint on a flat. Hub locked by a cone-point screw		Rivet pins (permanent joints)
	Joint on a flat. Hub tightened by an axial screw		
	Joint on a square. Hub locked by an external snap ring		Tubular pin
Pinned Joints			
	Cylindrical pin		Dented-centre pin
	Taper pin		Riffled pin
	Tangent pin		Spring pin

Table 18 (cont.)
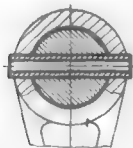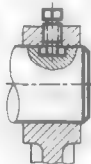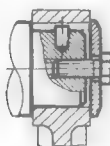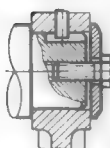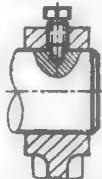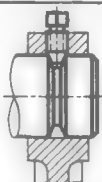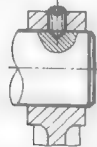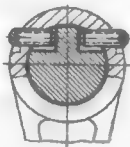
Design sketch	Description	Design sketch	Description
	Tubular spring pin		Round-shank screw
	Slot-and-pin joints		Slot-and-screw joint (design permits axial adjustment of the hub)
	Radial taper pin		Taper-shank screw
	Axial pins (permanent joints)		Frictional joint with a taper-shank screw (design permits setting of the lever into any angular position)
			Axial screws (permanent joints)
Screwed Joints			
	Cone-point pressing screw		Tangent screws (design permits angular adjustment of the lever within small limits)

Table 18 (cont.)
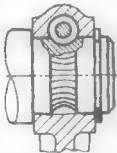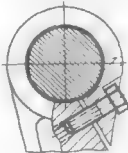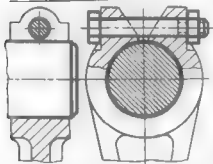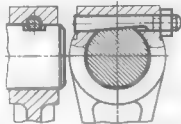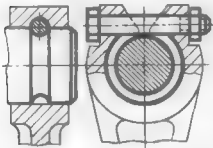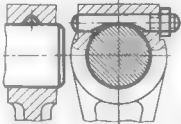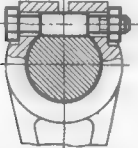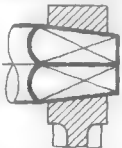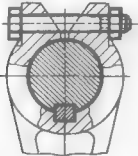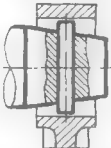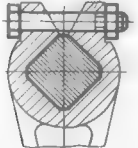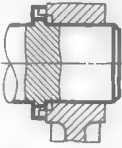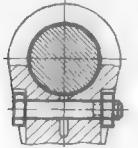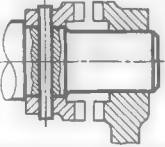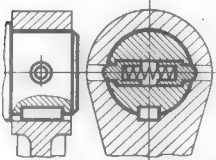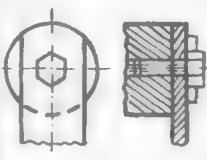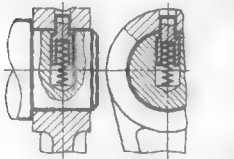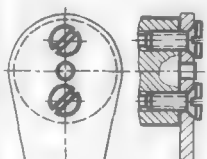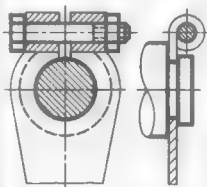
Design sketch	Description	Design sketch	Description
	Worm and crown of worm teeth (design permits angular adjustment of the lever within any limits)		Skew-slitted clamp (used in the case of restricted overall dimensions)
Clamped Joints		*Draw-Bolt Joints*	
	Frictional clamped joint		Frictional joint (bolt with a cylindrical recess)
	Frictional joint with the lever locked in a definite axial position		Positive joint (wedge bolt)
	Joint with a catch bolt	*Quick-Disconnect Joints*	
			Throw-on lever. Torque transmitted by a tapered square
	Joint with a key		Throw-on lever. Torque transmitted by a pin
	Joint on a square		Throw-on lever. Torque transmitted by end-face teeth
	Inverted clamp		End-face saw teeth. Used for starting handles

Table 18 (cont.)

Design sketch	Description	Design sketch	Description
	Lever locking by ball-point spring-loaded locks. Torque transmitted by a key		Cut-in lever
	Torque transmitted by a snap lock. Joint released by depressing the lock through a hole in the hub		Screwed-on lever
Connection of Flat (Thin Plate) Levers			Clamped connection
	Welded structure (butt welding)		
	Riveted structure		Throw-on lever

1.8. Fastening of Levers on Shafts

Table 18 shows design varieties of units for transmitting torque between shafts and parts such as levers, handles, wheels, etc.

Of all the designs illustrated in Table 18 the most simple and efficient one is the tapered shank joint with a screwed bolt, a joint which can be used for transmitting very large torques.

The joints with keys, flats, squares and, especially, clamped joints are inferior from the standpoint of manufacturing practice.

Designs with serrations, which can be readily obtained by rolling, are most expedient for joints intended to transmit large torques.

Simple welded constructions with arc spot welds are recommended for permanent joints while pinned joints are advisable for parts made of unweldable materials.

The angular position of a lever can be infinitely varied, if necessary, by using taper joints with a taper of from 1 : 30 to 1 : 50.

Plain (Sliding-Contact) Bearings

If designed and lubricated correctly, plain bearings can carry heavy loads at a high rotational speed. These bearings are light in weight, have small radial dimensions and do not require special equipment for manufacture.

Plain bearings can easily be designed as split structures. This facilitates assembly and makes these bearings almost the only possible type of support for the main journals and crankpins of multiple-throw shafts and also when it is impossible or difficult to use the solid antifriction (rolling-contact) bearings.

Plain bearings offer the advantage of noiseless operation and a ' a high damping ability under cyclic and impact loads.

The service life of plain bearings does not depend on their rotational speed (as distinct from antifriction bearings whose durability decreases in proportion to the increase in the rotational speed).

The coefficient of friction f of correctly designed plain bearings operating in conditions of liquid lubrication is 0.001-0.005. However, it increases up to 0.01-0.03 in unfavourable conditions (high oil viscosity, high peripheral speeds, small clearances). In bearings operating with semi-dry friction the coefficient f reaches 0.1-0.2.

The starting torque in plain bearings is rather high because the oil grows thicker at low temperatures. This shortcoming is especially pronounced in machines with sliding-contact main bearings and those operating in the open, which have to be started at subzero temperatures.

Heavily loaded bearings and bearings operating at high rotational speeds need an uninterrupted supply of oil under pressure to maintain proper liquid lubrication and withdraw the heat liberated in friction.

Periodic lubrication with oil or grease is sufficient for the bearings of low-speed shafts operating under light loads. In such cases use is often made of self-lubricating bearings which can operate for a long time without continuous oil supply.

Plain bearings operate reliably at temperatures not above 150°C. At higher temperatures the oil may become diluted and the oil film

ruptured. Besides, at high temperatures ordinary mineral oils rapidly oxidize and lose their lubricating properties.

Special lubricants (synthetic paraffine, polyphenylether ones) can be used at temperatures up to 300-350°C.

2.1. Clearances

Shafts are installed in bearings by the following fits: running (R), slack running (Rs), loose running (Rl) or thermal running (Rt).

Figure 104*a* illustrates the mean values of clearances Δ_m for various shaft diameters and fits, Fig. 104*b*, the dimensionless values of the mean clearance ratio ψ_m, and Fig. 104*c, d*, the clearance ratio fields obtained with the fits according with the 1st and 2nd grades of accuracy.

Within the range $d = 20$ to 250 mm the values of Δ_m and ψ_m can satisfactorily be approximated by the formulas

$$\Delta_m = m \sqrt{\bar{d}} \, (\mu m) \tag{2.1}$$

$$\varphi_m = 10^{-3} \frac{m}{\sqrt{\bar{d}}} \tag{2.2}$$

where d is the diameter in mm and m, the constants whose values are given in the table below.

Fits	Rt	Rl_3	Rl	R_3	Rs	R_{2a}	R	R_1
m	23	21.5	17	13	12	9	7.5	6

The optimum clearance for the given operating conditions and hence, the type and class of fit are determined by calculations.

2.2. Fluid, Semifluid and Semidry Friction

In plain bearings the following three basic types of friction are distinguished: *fluid, semifluid* and *semidry friction.*

With *fluid friction* the shaft and bearing surfaces are separated by a solid oil film and there is no direct friction between the metal surfaces.

The coefficient of fluid friction is small ($f \approx 0.001$), as are the losses due to friction and liberation of heat in the bearing. The metal surfaces do not wear in this case. For this reason fluid friction is most favourable for the operation of a bearing.

A continuous abundant supply of oil into the bearing is requisite for fluid friction. The pressures in the oil film, which are necessary to carry the loads acting on the bearing and prevent contact between
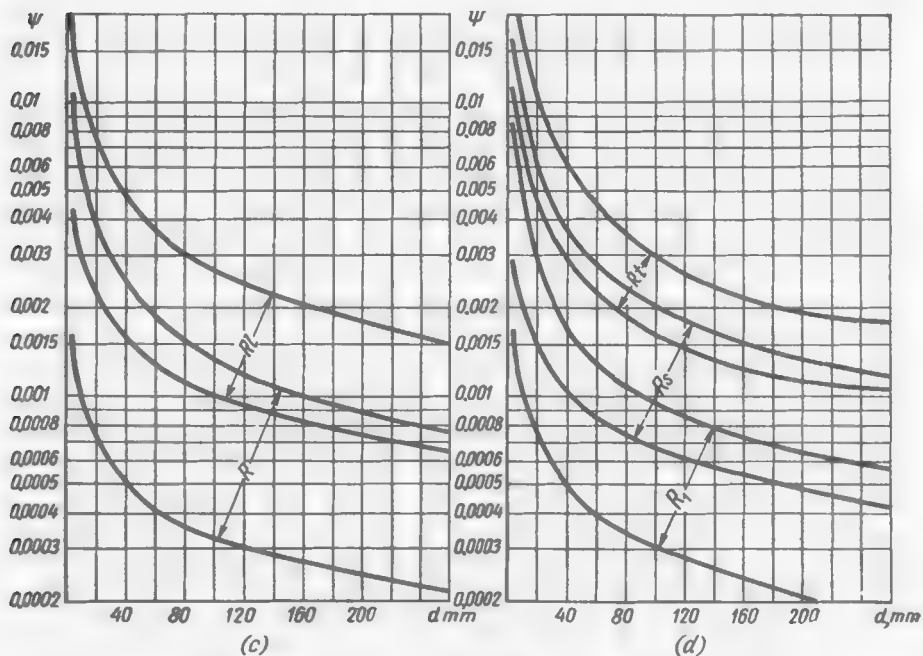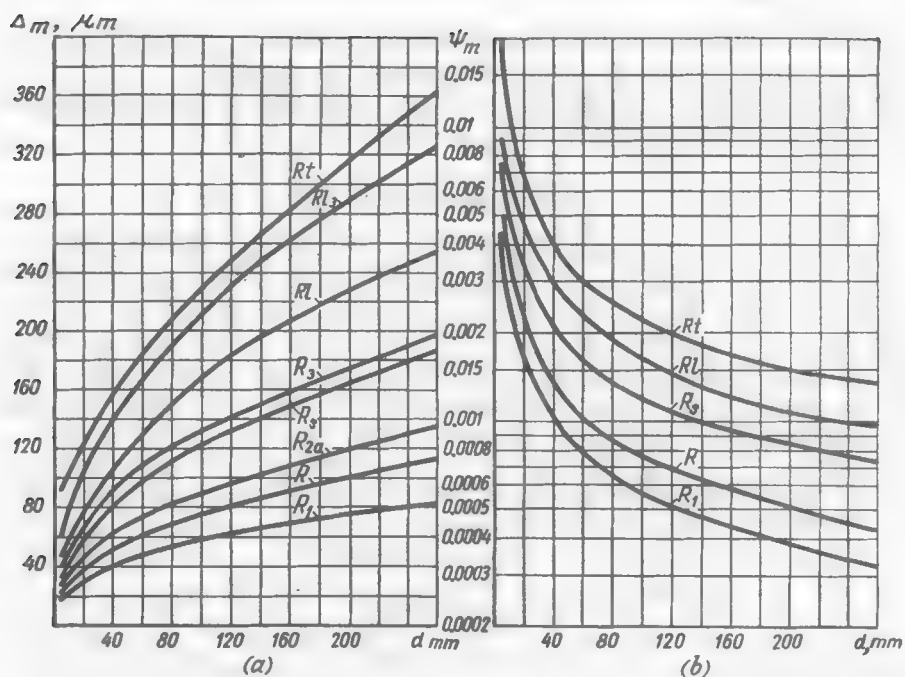
Fig. 104. Diametral clearances for various fits

the metal surfaces, are built up (when the shaft is positioned eccentrically in the bearing) as a result of the rotating shaft continuously forcing the oil into the converging portion of the clearance between the shaft and bearing. This self-sustained process of developing pressure in the oil film is known as *hydrodynamic lubrication.*

In the case of *semifluid friction* the continuity of the oil film is disrupted and the microirregularities on the shaft and bearing surfaces come into contact over more or less extended areas. Friction of this kind occurs when the oil supply is insufficient or if there is no hydrodynamic lubrication mechanism (for example, in thrust bearings with flat bearing surfaces).

Semifluid friction may as well occur in bearings with hydrodynamic lubrication, if the oil film is too thin to keep out of contact the microirregularities of the shaft and bearing surfaces.

The coefficient of semifluid friction is much higher than that of fluid friction, and more heat is liberated in the bearing. Therefore, the occurrence of semifluid friction, especially in bearings operating at high rotational speeds, may cause overheating and failure of the bearing.

Transition from fluid friction to semifluid friction is characterized by a sharp increase in the coefficient of friction, and is commonly known as *boundary* lubrication.

In the case of *semidry friction* the shaft and bearing surfaces are in full contact, or contact each other over very extended areas. There is no separating oil layer. The oil is present on the metal surfaces only in the form of an adsorbed film.

Thanks to the presence of the adsorbed oil, the coefficient of semidry friction is lower than that of dry friction, but much higher than that of semifluid friction and still higher than in the case of fluid friction.

Semidry friction sets in when the oil supply is insufficient and occurs, for example, in bearings with a periodic or deficient supply of oil. It can also be observed in fluid-friction bearings if the hydrodynamic mechanism lubrication is upset.

The occurrence of semidry friction in heavily loaded high-speed bearings may cause their overheating, the melting of the lining, and hence, their seizure and jamming.

2.3. Hydrodynamic Lubrication

A shaft installed in a bearing with a clearance Δ (Fig. 105a) and subjected to the action of a constant load P assumes an eccentric position. The clearance on both sides of the point where the shaft is closest to the bearing assumes the form of a wedge-shaped slit. The rotating shaft entrains oil. The first layer of the oil wetting the shaft is carried along due to its adsorption on the metal surface

of the shaft, and the next layers, by the force of internal friction of the oil. Thus, the shaft functions as a pump delivering the oil into the wedge-shaped slit.

As it enters the clearance converging in the direction of the shaft rotation, the oil, which is practically an incompressible liquid (at the usual pressure in the bearing) tends to flow in peripheral and axial (towards the end faces of the bearing) directions. This is impeded by the viscous forces. As a result, a pressure is built up in the oil layer, which progressively increases towards the point of the closest approach of the shaft to the bearing where the oil outflow is hampered by the small clearance (Fig. 105b).

Fig. 105. Formation of a carrying oil layer in a bearing

Some of the oil flows out through the end faces of the bearing, and in the direction opposite to the shaft rotation. The remaining

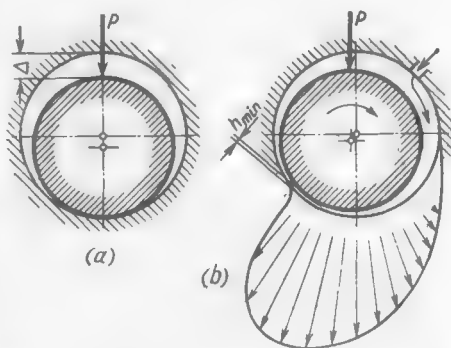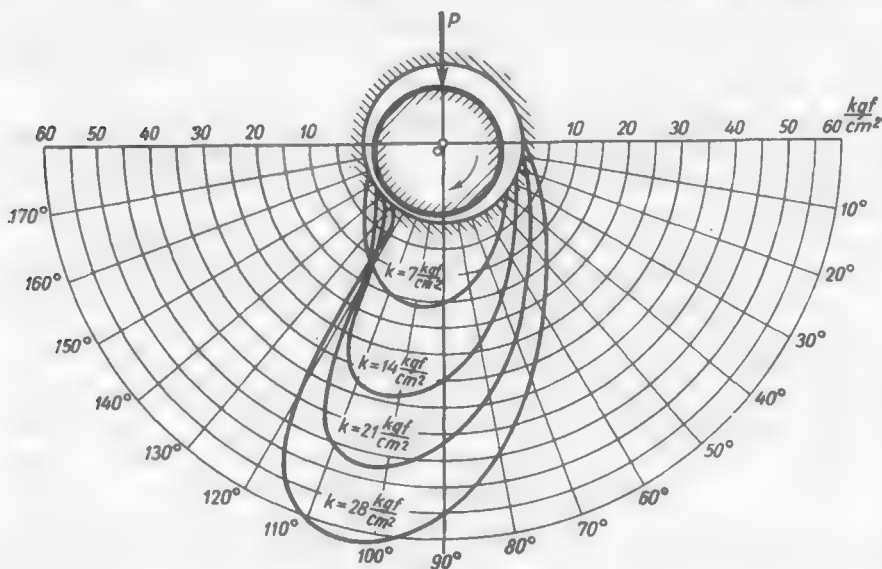Fig. 106. Pressure in the oil layer at different unit loads k (experimental data)

oil must pass through the narrowest portion of the clearance. The pressure forces developing in the oil layer raise the shaft and, at

the same time, shift it in the direction of rotation. The state of equilibrium is established when the clearance at the narrowest portion of the slit (h_{min}) is sufficient to let pass through the oil remaining after the end-face efflux.

The maximum pressure in the area of the closest approach of the shaft to the bearing exceeds about two or three times the mean unit
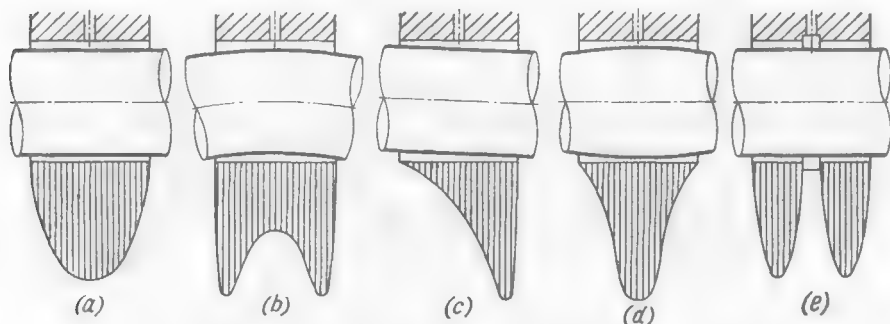

Fig. 107. Pressure in the oil layer along the bearing axis

pressure $k = P/dl$ (where d is the diameter and l is the length of the bearing) and can reach several tens and hundreds of kilogrammes per square centimetre (Fig. 106).

The pressure along the axis in a strictly cylindrical bearing changes following a parabolic curve (Fig. 107a) and drops sharply at the end faces of the bearing due to the outflow of oil through them.

The actual pressure distribution curve may appreciably differ from the theoretical one because of the elastic deformations (Fig. 107b), misalignments (Fig. 107c) and deviations from true cylindrical shape (for example, convex camber, Fig. 107d) of the shaft.

A sharp reduction in pressure occurs in the plane where annular grooves are arranged (Fig. 107e).

(a) Position of the Shaft in the Bearing

The position of the shaft under various operating conditions is schematically shown in Fig. 108a. During the starting period when the rotational speed is low and semidry friction prevails, the shaft shifts in the direction opposite to its rotation to an angle φ whose tangent is equal to the coefficient of semidry friction.

As the rotational speed increases semifluid friction sets in, the coefficient of friction diminishes and the shaft shifts in the direction of the rotation until the microirregularities on its surface come out of contact with those of the bearing.

In the region of fluid friction the position of the shaft centre is determined by the parameter $\frac{\eta\omega}{k}$ (where η is the dynamic viscosity of oil, ω, angular velocity and k, unit load). When this parameter increases the shaft centre moves towards the bearing centre,
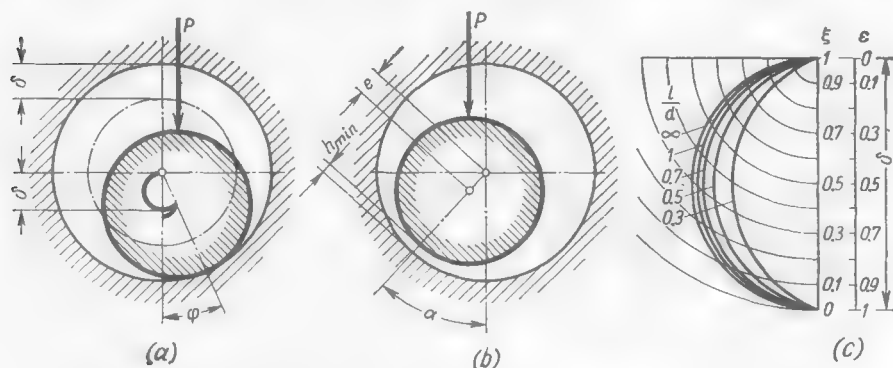

Fig. 108. Determining the position of the shaft in the bearing

following a path close to a semicircumference with a diameter equal to the radial clearance δ.

When $\frac{\eta\omega}{k}$ is infinitely large the centre of the shaft coincides with that of the bearing. In this case the oil film thickness $h_{min} = \delta$, the clearance is no longer wedge-shaped and the pressure in the oil layer becomes zero. This may happen when there is no external load.

Eccentricity ratio is the ratio of eccentricity e, i. e., the distance from the centre of the shaft to the centre of the bearing (Fig. 108b), to the radial clearance δ

$$\varepsilon = \frac{e}{\delta} = \frac{2e}{\Delta} \tag{2.3}$$

where $\Delta = 2\delta$ is the diametral clearance.

Relative minimum oil layer thickness is the ratio of the minimum oil layer thickness h_{min} at the point of the closest approach of the shaft and bearing to the radial clearance

$$\xi = \frac{h_{min}}{\delta} = \frac{2h_{min}}{\Delta} \tag{2.4}$$

Since $h_{min} = \delta - e$, then

$$\xi = \frac{\delta - e}{\delta} = 1 - \varepsilon \tag{2.5}$$

The paths described by the centre of the shaft moving in the bearing are shown in Fig. 108c. When $l/d = \infty$ the path is a true semicircumference (Gümbel semicircle). With finite values of l/d the path changes its form but generally remains close to a semicircumference.

(b) The Load-Carrying Capacity
of Fluid-Friction Bearings

With a decrease in $\frac{\eta\omega}{k}$ the shaft sinks in the bearing, the oil layer thickness h_{min} at the point of the closest approach of the shaft to the bearing diminishes, and the oil forced into this area by the pumping action of the shaft flows out with difficulty. All this tends to increase the pressure in the oil layer and the rigidity of the layer (the ratio of the acting force to the shaft displacement) theoretically to infinity.

An ideally smooth and absolutely rigid shaft separated by a layer of oil from a bearing just as smooth and rigid can on no account touch the bearing. The closest approach of the shaft and bearing, and therefore its carrying capacity, is only limited by the deviations of the shaft and bearing from the correct cylindrical form, caused by the machining inaccuracies and the elastic deformations of the shaft and bearing under the action of load, by the roughness of the shaft and bearing surfaces and also by the presence of metal dust and other hard particles in the oil.

The adverse effect of the surface roughness on the carrying capacity of the oil layer is explained first of all by its *drainage property*. The spaces s between the microirregularities (Fig. 109) form a network of channels along which the oil flows to the end faces of the bearing and in the circumferential direction. As long as the total cross-section of the channels is small (approximately proportional to s) as compared with the cross-section of the oil layer h, the efflux of oil through the channels is small too and does not tell on the carrying capacity of the oil layer. As the clearance grows smaller, the flow of oil through the channels increases, and the pressure in the oil layer no longer increases in proportion to the load. With a further growth of the load the projections of the microirregularities come into contact and semifluid friction arises in the bearing.

Fig. 109. Effect of surface roughness on the load-carrying capacity of the bearing

The drop of the pressure in the oil layer and of its carrying capacity is more pronounced with higher microirregularities, i.e., with greater roughness of the surfaces of the shaft and bearing. The minimum thickness of the oil layer must be greater than the average sum of the roughness heights of the shaft and bearing surfaces.
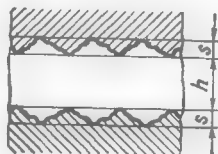
For the bearing to operate reliably, it is necessary that the critical clearance between the shaft and bearing, at which the microirregularities of the shaft and bearing come into contact, be reduced.

This can be attained by highly accurately machining the shaft and bearing surfaces, making their surfaces strictly cylindrical, eliminating misalignments and deformations in the system, and thorough cleaning of oil. Long operation must never impair the finish and correct cylindrical shape of the surfaces. This can be achieved by making the shaft and bearing highly resistant to wear.

The load-carrying capacity of the bearing is also limited by the temperature of the oil layer.

The viscosity of lubricants abruptly changes with temperature (Fig. 110). For example, the viscosity of industrial oil grade 45, which is equal to 350 cP at 20°C, drops down to 2-3 cP, i.e.., more than 100 times, at 150°C.

A rise in the bearing temperature may cause the dilution of the oil to such an extent as will preclude the formation of a stable oil layer of the required thickness.

When the temperature exceeds 150°C the volatile components in many oils begin to evaporate. This phenomenon is attended by the formation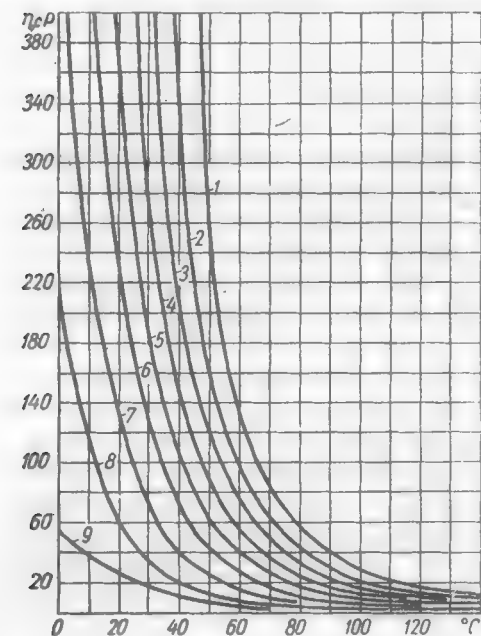 of vapour pockets and disruption of the oil layer continuity. Besides, the oxidation of the oil sharply increases. The oil loses its lubricating properties, gets tarred and gives off hard oxidation products (*carbonization of oil*).

Fig. 110. Viscosity *versus* temperature characteristics of lubricants

1 — aviation oil grade MC-24; *2* — aviation oil grade MC-20; *3* — automotive oil grade AK-15; *4* — aviation oil grade MC-14; *5* — industrial oil grade 45; *6* — industrial oil grade 30; *7* — industrial oil grade 20; *8* — industrial oil grade 12; *9* — spindle oil

The carrying capacity of bearings made of soft and plastic materials (babbitts) is limited by the softening of the material, which sets in at high temperatures. The material is destroyed under the action of high pressures in the oil layer long before semidry friction arises.

The working temperature of the bearing can effectively be reduced by intensifying heat withdrawal through supplying the oil under pressure (pressure-feed lubrication) and simultaneously increasing the bearing clearance and introducing drainage grooves in the unloaded area of the bearing.

(c) Operating Characteristic

The clearance h_{min} at the point of the closest approach of the shaft to the bearing must be sufficient to prevent the contact between the microirregularities on the shaft and bearing due to possible fluctuations in operating conditions (rise of the load, reduction of the rotational speed, drop of the oil viscosity due to overheating) and also because of the misalignment of the shaft in the bearing and elastic deformations of the shaft and bearing.

The eccentricity ratio ε and relative minimum oil layer thickness $\xi = 1 - \varepsilon$ are functions of the dimensionless Sommerfeld number

$$So = \frac{\eta\omega}{k\psi^2} \tag{2.6}$$

and of the ratio l/d of the length of the bearing to its diameter.

In Eq. (2.6):

η = dynamic viscosity of oil, kgf·s/m²

ω = angular velocity, s^{-1}

k = load per unit bearing surface, kgf/m²

ψ = clearance ratio ($\psi = \Delta/d$)

The theoretical relation (in good agreement with the experiment) between ξ and $\frac{\eta\omega}{k\psi^2}$ is shown in Fig. 111 for various values of l/d (the values of ξ are indicated on the left side of the plot and those of $\varepsilon = 1 - \xi$, on the right side).

If the value of So is known (from the known η, ω, k, ψ) the plot may be used to find ξ for a given l/d and determine the minimum oil layer thickness from the formula

$$h_{min} = \xi\frac{\Delta}{2} = 10^3 \frac{\psi d}{2} \text{ (μm)} \tag{2.7}$$

where d is the bearing diameter in mm.

The unit load exerted on the bearing ($k = P/ld$) is inversely proportional to the value of So and may be found from the formula

$$k = \frac{1}{So} \cdot \frac{\eta\omega}{\psi^2} \tag{2.8}$$

As can be seen from the plot, when $So < 1$, the relative minimum oil layer thickness ξ increases approximately in direct proportion to So. When $So > 1$ the increase is slower. With a further increase in So the value of ξ changes very slightly and tends to unity ($h_{min} = \delta$) when $So = \infty$.

The unit load on the bearing drops with an increase in So, and approaches zero when $So = \infty$.

For the given bearing, i.e., when ψ and *l/d* are constant, the minimum oil layer thickness and the load-carrying capacity are only determined by the factor $\frac{\eta\omega}{k}$.

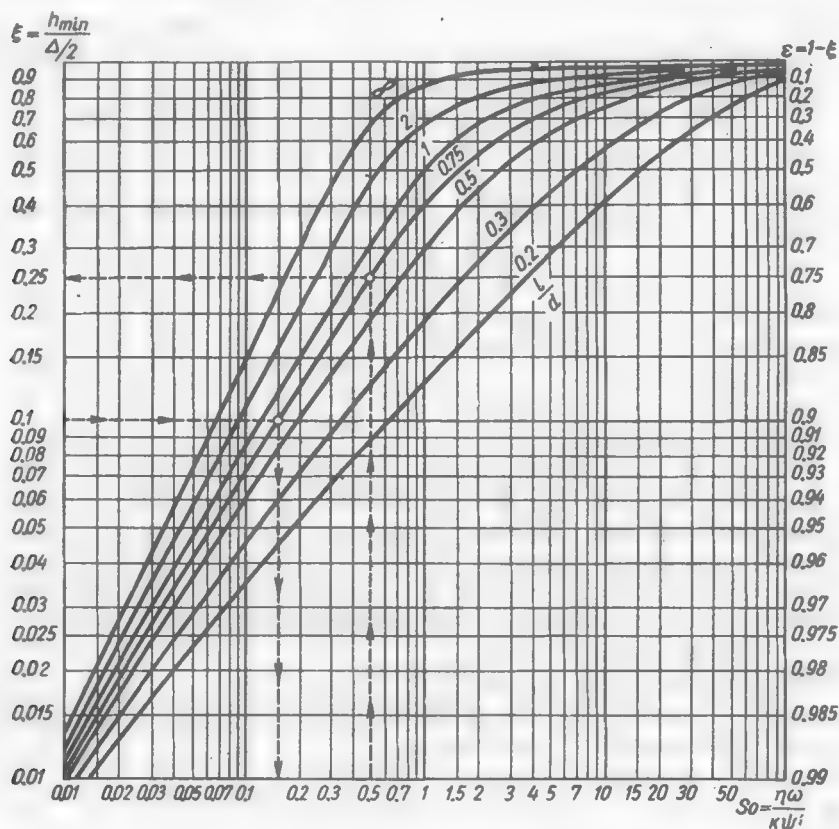Fig. 111. Relative minimum oil layer thickness ξ and eccentricity ratio ε depending on Sommerfeld's number

In practice it is more convenient to use *operating characteristic* expressed as

$$\lambda = \eta\frac{n}{k} \tag{2.9}$$

where η = viscosity, cP
      n = rotational speed, rpm
      k = unit pressure, kgf/cm²

Since

$$1 \text{ cP} = 9810 \text{ kgf·s/m}^2,$$
$$n = \frac{30\omega}{\pi} = 9.554\omega$$

and

$$1 \text{ kgf/cm}^2 = 10^{-4} \text{ kgf/m}^2,$$

then $\dfrac{\eta\omega}{k}$ and $\lambda = \dfrac{\eta n}{k}$ are interrelated by the following relations:

$$\lambda = \frac{\eta n}{k} = 9.37 \cdot 10^8 \, \frac{\eta\omega}{k} \tag{2.10}$$

and

$$\frac{\eta\omega}{k} = 1.065 \cdot 10^{-9} \lambda \tag{2.11}$$

The operating parameters of the bearing are determined by the numerical value of the factor $\dfrac{\eta n}{k}$ irrespective of the magnitudes of the terms it contains.

Thus, for example, high values of the operating characteristic can be obtained both by increasing oil viscosity η and the number of revolutions n and by reducing the unit load k.

This regularity agrees well with experiment.

(d) Critical Operating Characteristic.
Reliability Factor of the Bearing

The *critical operating characteristic* is the value of λ at which the minimum oil layer thickness is so much reduced that the microirregularities of the shaft and bearing come into direct contact. The oil layer thickness at which semifluid friction sets in is known as *critical* and designated as h_{cr}.

The value of h_{cr} for very smooth and rigid bearings and shafts is on the average equal to 5-10 μm.

If h_{cr} is known, Eq. (1.104) may be used to find the respective value ξ_{cr} and then determine from Fig. 111 the critical values So_{cr} and λ_{cr}.

The *reliability factor* of the bearing is the ratio of the working operating characteristic to the critical one

$$\varkappa = \frac{\lambda}{\lambda_{cr}} = \frac{So}{So_{cr}} \tag{2.12}$$

This value should be greater than unity. The greater the value of $\varkappa$ the less the hazard of the bearing operation entering the region of semifluid friction. If, for example, $\varkappa = 5$ the working viscosity of the oil can be reduced five times or the load on the bearing increased five times before the bearing begins to operate in conditions of semifluid friction.

Calculation example. Given: $d = 100$ mm, $l = 75$ mm, $P = 4000$ kgf, $\psi = 0.001$ (diametral clearance $\Delta = 100$ μm), $n = 1000$ rpm, $\eta = 25$ cP.
The unit load is

$$k = \frac{P}{ld} = \frac{4000}{10 \cdot 7.5} = 53.5 \text{ (kgf/cm}^2)$$

The operating characteristic

$$\lambda = \frac{\eta n}{k} = \frac{25 \cdot 1000}{53.5} = 470$$

Sommerfeld's number

$$So = 1.065 \cdot 10^{-9} \frac{\lambda}{\psi^2} = 1.065 \cdot 10^{-9} \cdot 470 \cdot 10^6 = 0.5$$

From the diagram in Fig. 111 (dashed line) we find for $l/d = 0.75$

$$\xi = 0.25$$

The minimum oil layer thickness

$$h_{min} = 10^3 \frac{\xi \psi d}{2} = 10^3 \frac{0.25 \cdot 0.001 \cdot 100}{2} = 12.5 \ (\mu m)$$

Let the critical oil layer thickness be $h_{cr} = 5$ microns. The critical value of ξ in conformity with Eq. (2.7) is

$$\xi_{cr} = \frac{2h_{min \ cr}}{\Delta} = \frac{2 \cdot 5}{100} = 0.1$$

Drawing a horizontal straight line on the diagram (Fig. 111) through this point until the line meets the curve $l/d = 0.75$, we find on the X-axis

$$So_{cr} = 0.15$$

The reliability factor from Eq. (2.12) is

$$\varkappa = \frac{So}{So_{cr}} = \frac{0.5}{0.15} = 3.3$$

(e) Optimum Clearance Ratio

The diagram in Fig. 111 is used to plot the graphs (Fig. 112) for determining h_{min} at various values of λ, depending on the clearance ratio ψ for $l/d = 1$ and 0.5 (d is taken at 100 mm). The thin lines show the values of the relative minimum oil layer thickness.

It can be seen from the graphs that the clearance h_{min} is the greatest with ξ constant for all λ ($\xi = 0.5$ when $l/d = 1$ and $\xi = 0.4$ when $l/d = 0.5$).

Figure 113 (curve 1) illustrates a generalized dependence of ξ on l/d at the greatest h_{min} determined by the same method.

If we proceeded only from the condition of obtaining the maximum values of h_{min}, curve 1 might be used as the basis for calculating the bearing. In actual fact, one has to take account of the stability of its operation. When the values of ξ are high the stiffness of the oil layer sharply drops and the position of the shaft in the bearing becomes unsteady. This is caused, firstly, by the reduction of the pressure in the oil layer due to its decreasing taper, and secondly, by the angle α between the direction of load P and the

resultant R of the forces of pressure of the oil layer growing larger
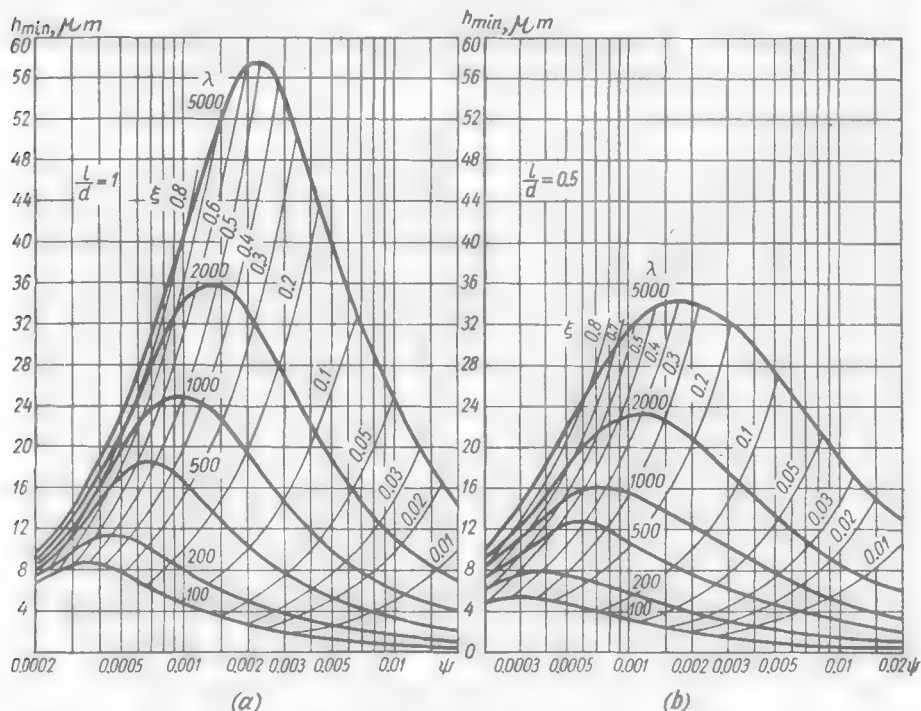as the shaft gradually shifts towards the centre of the bearing over

Fig. 112. Minimum oil layer thickness h_{min} depending on clearance ratio ψ for
various values of λ

the Gümbel semicircle (Fig. 114a). If for some reason or other the
load in this region (point A) increases, then to restore the equilib-
rium the centre of the shaft must move to a large distance to the
left and downwards over the Gümbel semicircle.

Thus, slight variations in the operating conditions in this region
cause considerable displacements of the shaft, which easily change
to cyclic vortex movements. When vortices develop, the laminar
flow of the oil becomes turbulent and friction and heat liberation
in the bearing are appreciably intensified. Cavitation processes
developing in the oil layer tend to destroy the material of the bea-
ring.

Two types of vortex are known: *cylindrical*, when the shaft axis moves pa-
rallel to the axis of the bearing, and *conical*, when the shaft axis moves conically.
The velocity of the vortex movements may be equal to $1/2$, $1/3$, $1/4$ or $2/3$ of the
shaft rotational speed, depending on the hydrodynamic parameters of the bear-
ings, their number and arrangement, and the rigidity of the system. The *cy-*

lindrical half-speed vortex (whose speed is equal to $^1/_2$ of the shaft speed) is the most important vortex and has been studied most.

If unbalanced masses are connected to the shaft, the cyclic movements of the shaft generate centrifugal forces proportional to the radius of the shaft centre motion. In the region of high ξ values the shaft displaced by external perturbations from the position of equilibrium (point B, Fig. 114b) moves along a spiral of an increasing radius until the shaft contacts the bearing.
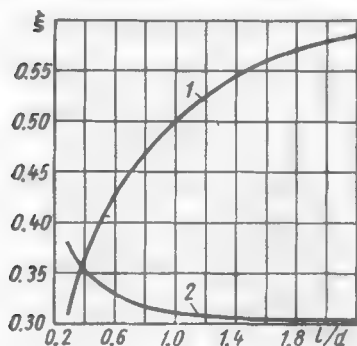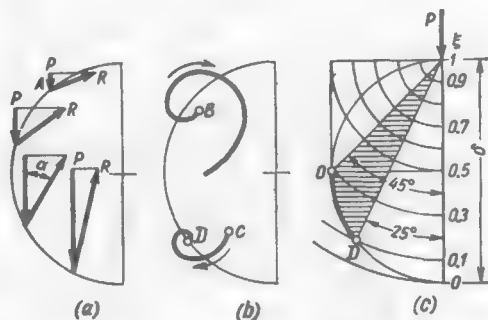

Fig. 113. Relative oil layer thickness   Fig. 114. Determining optimum clearance

In the region of small ξ values the shaft displaced from the position of equilibrium (point C) moves along a spiral of a diminishing radius, the vortex motion attenuates and the shaft rapidly regains its position of equilibrium D.

The point O where the Gümbel semicircle touches the line parallel to the direction of the load (Fig. 114c) is the boundary between the stable and unstable regions. At this point the line of the centres of the shaft and bearing is at an angle of 45° to the direction of the load and the relative minimum oil layer thickness $\xi = 1 - \varepsilon = 0.3$.

The limiting values of ξ (as far as vibration stability is concerned) for finite values of l/d (see Fig. 108c) are shown in Fig. 113 (curve 2). These are the optimum values because they correspond to the maximum values of h_{min} possible in the stable region.

As can be seen on the graph, the stable values ξ_{st} are close to 0.3 within a wide range of l/d (0.5 to 2). This value may be used as the basis for calculating the bearings, taking the higher values of ξ_{st} typical of the bearings with $l/d < 0.5$ as a margin of safety.

Drawing a horizontal line on the diagram in Fig. 111 through the point $\xi = 0.3$, and then determining the corresponding values of So on the X-axis and converting them by Eq. (2.10) into λ values, we obtain the optimum values of ψ as a function of λ (Fig. 115). Within the range $l/d = 0.5$-1.5 the curves are approximated by the formula

$$\psi_{\xi=0.3} = 4.6 \cdot 10^{-5} \sqrt{\overline{\lambda}} \sqrt{l/d} \tag{2.13}$$

When $\xi < 0.3$, the vibration stability increases, but at the same time the oil layer thickness h_{min} diminishes. In most cases, when $\xi < 0.1$ there is already some danger of the bearing entering the region of semifluid friction. When $\xi = 0.1$, the line of the shaft and bearing centres is at an angle of 25° to the direction of the load (point
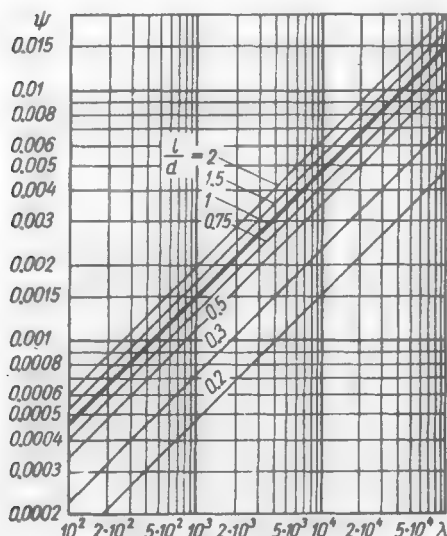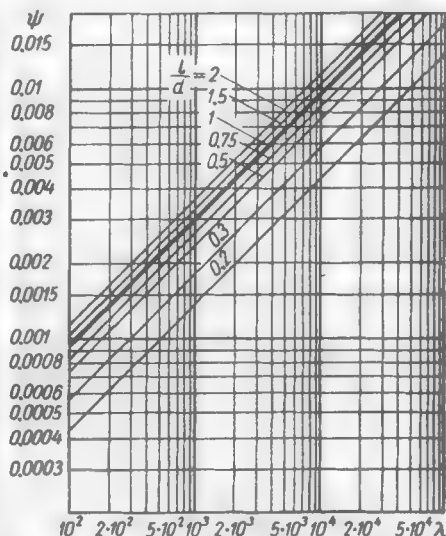

Fig. 115. Clearance ratios ψ with $\xi = 0.3$

Fig. 116. Clearances ratios ψ with $\xi = 0.1$

D in Fig. 114c). Thus, the allowable bearing operation region lies within the range of angles from 45 to 25° (shaded area on the drawing).

The values ψ_{max} corresponding to the limiting condition $\xi = 0.1$ are shown in Fig. 116. The curves are approximated by the formula

$$\psi_{max} = 9.2 \cdot 10^{-5} \sqrt{\lambda} \sqrt[3]{l/d} \qquad (2.14)$$

Vibration can be prevented not only by the proper choice of the bearing parameters, but also through increasing the rigidity of the shaft and bearings by all means possible and balancing carefully the shaft and the bodies rotating with it.

(f) Coefficient of Fluid Friction

The peripheral force F opposing the shaft rotation is equal to the sum of the forces of viscous oil shear in the clearance over the entire circumference of the shaft. According to Newton's law of viscous friction for the case of laminar flow, the force F is proportional to the shear surface (i.e., to πdl), oil viscosity η and shear velocity v, and inversely proportional to the thickness h of the oil layer.

With a *concentric* position of the shaft in the bearing the oil layer thickness $h = \Delta/2$. The shear velocity $v = \dfrac{\omega d}{2}$. Therefore,

$$F = \frac{\pi d l \eta \omega d}{\Delta} = \frac{\pi d l \eta \omega}{\psi}$$

The *coefficient of fluid friction* is

$$f = \frac{F}{p} = \frac{\pi d l}{p} \cdot \frac{\eta \omega}{\psi} = \pi \frac{\eta \omega}{k \psi} \tag{2.15}$$

This well-known formula derived by Petrov holds true when the shaft is almost concentric with the bearing ($So \gg 1$, $h \approx \Delta/2$).
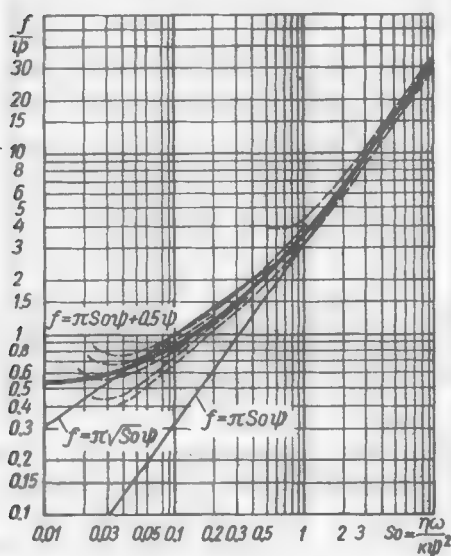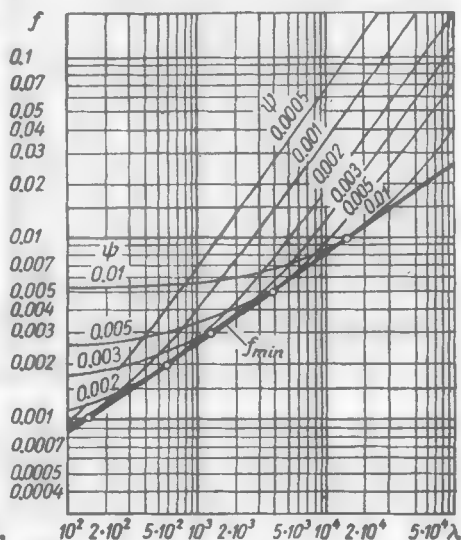

Fig. 117. Dependence of f/ψ on So Fig. 118. Dependence of f on λ

Substituting the value $So = \dfrac{\eta \omega}{k \psi^2}$ into Eq. (2.15) we obtain

$$f = \pi So \psi \tag{2.16}$$

With an *eccentric* position of the shaft ($So < 1$) the coefficient of friction may be determined from Vogelpohl's formula

$$f = \pi \sqrt{So} \, \psi \tag{2.17}$$

The coefficient of friction in the entire range of So values may be expressed by the formula

$$f = \pi So \psi + 0.5 \left(\frac{d}{l} \right)^{1.5} \psi \tag{2.18}$$

or in a more convenient form

$$f = 3.36 \cdot 10^{-9} \frac{\lambda}{\psi} + 0.5 \left(\frac{d}{l}\right)^{1.5} \psi \qquad (2.19)$$

where $\lambda = \frac{\eta n}{k}$ (η is the oil viscosity at the working temperature of the bearing, cP; n is the rotational speed of the shaft, rpm; k is the unit load on the bearing, kgf/cm²).

When l/d is close to unity it is sufficient to express f as

$$f = 3.36 \cdot 10^{-9} \frac{\lambda}{\psi} + 0.5\psi$$

Figure 117 illustrates the values of f/ψ calculated by Eq. (2.16), (2.17) and (2.18). The dashed lines show experimental data.

The values of f for various λ and ψ, calculated by Eq.(2.19), are presented in Fig. 118.

Differentiating Eq. (2.19) with respect to ψ and equating the derivative to zero, we may find the minimum coefficient of friction

$$f_{min} = 8.25 \cdot 10^{-5} \sqrt{\lambda} \qquad (2.20)$$

The values of f_{min} are shown in Fig. 117 by the thick line.

Fig. 119. Dependence of f on λ (with $\xi = 0.3$)

The clearance ratio at which the coefficient of friction is minimum

$$\psi_{f=min} = 8.25 \cdot 10^{-5} \sqrt{\lambda} \qquad (2.21)$$

i.e., *it is numerically equal to the minimum coefficient of friction* (bright dots in Fig. 118).

Substituting the values of ψ that correspond to the optimum $\xi = 0.3$ [Eq. (2.13)] into Eq. (2.19), we get

$$f_{\xi=0.3} = \sqrt{\lambda}\left(0.73 \cdot 10^{-4} \sqrt{d/l} + 2.3 \cdot 10^{-5} \sqrt{l/d}\right)$$

The lines expressing the dependence of f on λ for various l/d (Fig. 119) are plotted precisely from this equation.

The lower (thick) line shows f_{min} determined from Eq. (2.20). As can be seen, the values of $f_{\xi=0.3}$ within the range $l/d = 0.75$-1.5 are close to f_{min}. Therefore, the calculation conditioned on $\xi = 0.3$ ensures only small frictional losses.
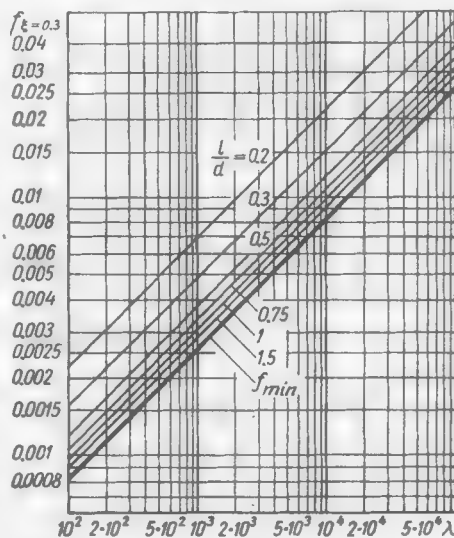
The lines $f_{\xi=0.3}$ are approximated within $l/d = 0.3\text{-}1.5$ by the formula

$$f_{\xi=0.3} = 10^{-4}\,\sqrt{\lambda}\,\sqrt[3]{d/l} \qquad (2.22)$$

Since the shaft position in the bearing is eccentric, the coefficient of friction is different for the shaft and for the bearing.

The coefficient of friction for the bearing is

$$f_b = f_{sh} - \psi\varepsilon$$

where f_{sh} = coefficient of friction for the shaft
$\quad\psi$ = clearance ratio
$\quad\varepsilon$ = eccentricity ratio $(\varepsilon = 1 - \xi)$

When, as is usually the case, $f_{sh} = 0.003$, $\psi = 0.001$ and $\varepsilon = 0.7$, the coefficient of friction for the bearing is

$$f_b = 0.003 - 0.7\cdot0.001 = 0.0023$$

i.e., it is 25 per cent lower than that for the shaft.

(g) Calculation Nomographic Charts

Figures 120 and 121 present nomographic charts, plotted on the basis of Fig. 111, which are convenient for calculating bearings. The chart in Fig. 120 can be used to determine the parameters of a bearing within the range $l/d = 0.8\text{-}1.2$. The one in Fig. 121 (for $l/d = 0.5$) can be used when $l/d = 0.3\text{-}0.7$.

The thick lines on the right side of the chart correspond to $\xi < 0.3$ and the thin ones, to $\xi > 0.3$.

Example. A bearing with $d = l = 100$ mm is loaded by force $P = 4000$ kgf. The rotational speed $n = 1000$ rpm. Oil viscosity $\eta = 20$ cP. The critical oil layer thickness $h_{cr} = 5\mu$m. Determine the optimum clearance ratio ψ.

The unit pressure is

$$k = \frac{P}{ld} = \frac{4000}{10\cdot10} = 40 \ \ (\text{kgf/cm}^2)$$

The operating characteristic is

$$\lambda = \frac{\eta n}{k} = \frac{20\cdot1000}{40} = 500$$

Erecting a perpendicular from the point corresponding to $\lambda = 500$ (on the right side of the chart in Fig. 120) to intersect curves ψ, and then drawing horizontal lines through the points of intersection thus obtained to intersect the vertical line corresponding to $d = 100$ mm on the left side of the chart, read on the grid of the inclined straight lines the corresponding values of $h_{\min}$. Then, using the given value of h_{cr} find by the reverse plotting the critical values of λ_{cr} and determine the reliability factor $\varkappa = \lambda/\lambda_{cr}$.

For example, when $\lambda = 500$ and $\psi = 0.001$ (point a) $h_{\min} = 16$ μm (point b). When $h_{cr} = 5$ μm (point c) the critical operating characteristic $\lambda_{cr} = 120$ (point d). Hence, the reliability factor $\varkappa = \dfrac{500}{120} = 4.2$.
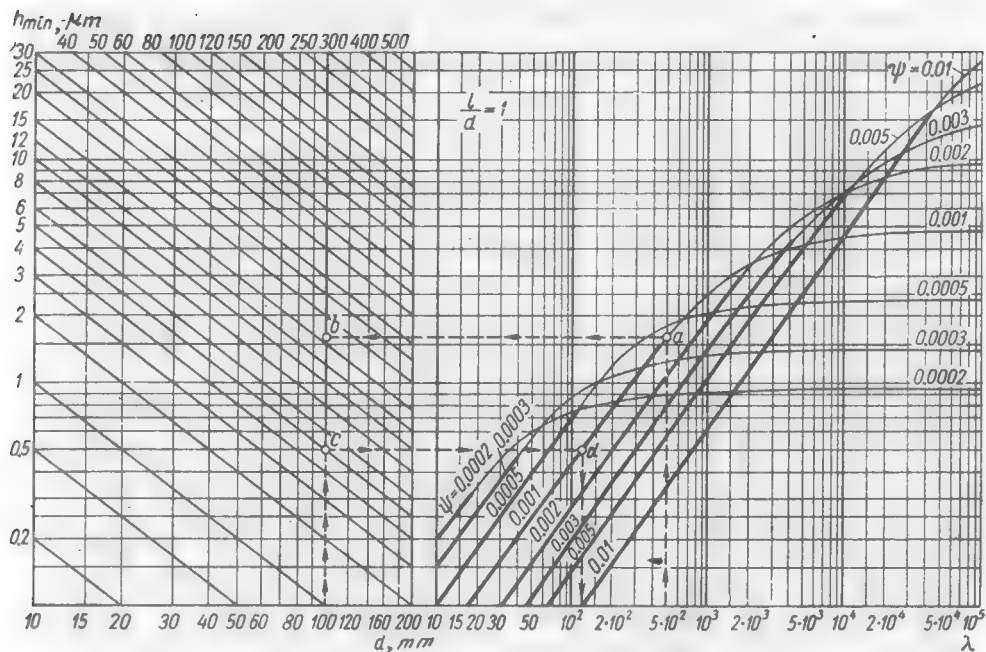
Fig. 120. Nomographic chart for calculating bearings ($l/d = 1$)
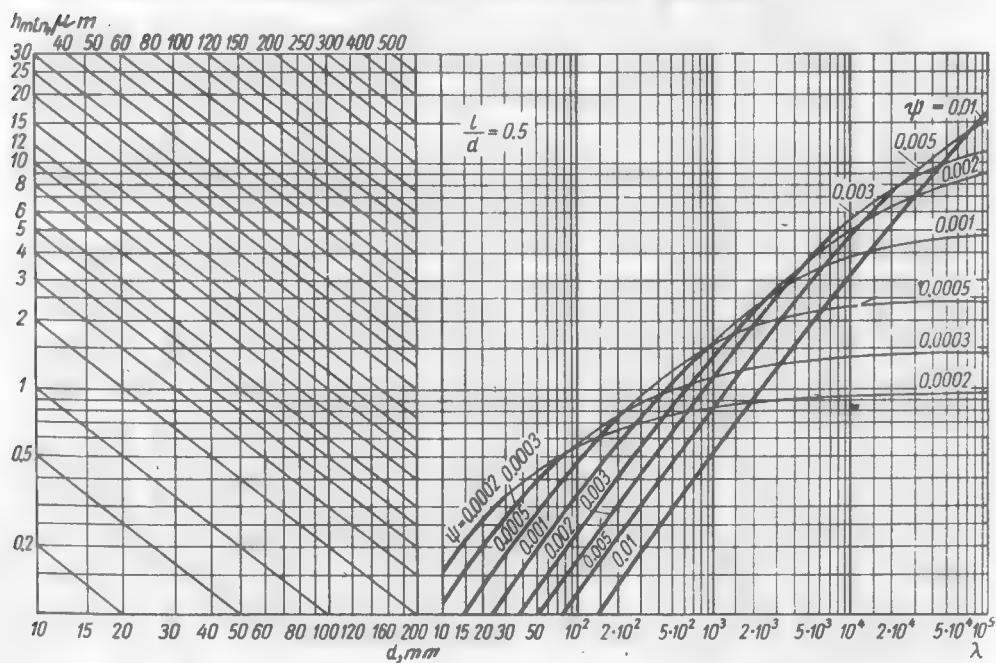

Fig. 121. Nomographic chart for calculating bearings ($l/d = 0.5$)

According to Eq. (2.7), the relative minimum oil layer thickness is

$$\xi = 10^{-3} \frac{2 \cdot 16}{0.001 \cdot 100} = 0.32$$

From Eq. (2.19) the coefficient of friction is

$$f = 3.36 \cdot 10^{-9} \frac{500}{0.001} + 0.5 \cdot 0.001 = 0.0022$$

When using this method to find the values of h_{min}, ξ, $\varkappa$ and f for various ψ, one gets a clear idea of the effect exerted by ψ on the operating parameters of a bearing (Fig. 122a).

The oil layer thickness is maximum ($h_{min} \approx 19\mu m$) when $\psi = 0.0008$, which corresponds to $\xi = 0.5$ (the values of ξ are plotted on the curve h_{min} by bright dots). With a decrease in ψ (the left-hand branch of the curve) the bearing enters the region of prohibited eccentricities ($\xi > 0.5$) and the coefficient of friction sharply increases. When ψ increases (right-hand branch) the values of h_{min} diminish and the reliability factor drops. The shaded area shows the allowable limits $\psi = 0.001-0.002$ ($\xi = 0.3-0.1$) within which h_{min} and $\varkappa$ remain at acceptable levels ($h_{min} = 16-10$ μm, $\varkappa = 4.2-2.5$). Within this interval the coefficient of friction has a comparatively flat minimum ($f \approx 0.002$).

The optimum clearance ratio which ensures the maximum values of h_{min} ($\approx 16\mu m$) and $\varkappa = 4.2$ with a stable position of the shaft in the bearing and low friction is $\psi = 0.001$ ($\xi = 0.3$).

The value of $\varkappa$ appreciably increases when the critical value h_{cr} is reduced. With $h_{cr} = 3$ μm the reliability factor (dashed curve) increases twofold ($\varkappa' = 8.4$ at $\psi = 0.001$ instead of $\varkappa = 4.2$ as is the case at $h_{cr} = 5$ μm).

The arrows on the graph indicate the ranges of ψ that correspond to standard fits. The mean values of ψ obtained with a slack running fit conform best of all to the recommended region $\psi = 0.001-0.002$. A thermal running fit (Rt) reduces both h_{min} and $\varkappa$. Running fits R and R_1 must not be employed because they make the bearing operate in the unstable region ($\xi > 0.5$).

Figure 122b presents a similar graph for a bearing of the same dimensions but with $\lambda = 1000$ (twofold increase of the oil viscosity or rotational speed, or twofold reduction of the load). An increase in λ favourably influences the parameters of the bearing. When $\xi = 0.3$ the oil layer thickness h_{min} rises to 23 microns and the reliability factor, to 6.2. The coefficient of friction slightly increases ($f \approx 0.003$). In this case the optimum value of ψ is equal to 0.0015, which corresponds to the mean values of ψ obtained with a loose running fit.

Figure 122c shows the graph for a bearing with the same l, P, η and n but with a diameter of 80 mm.

The unit load is

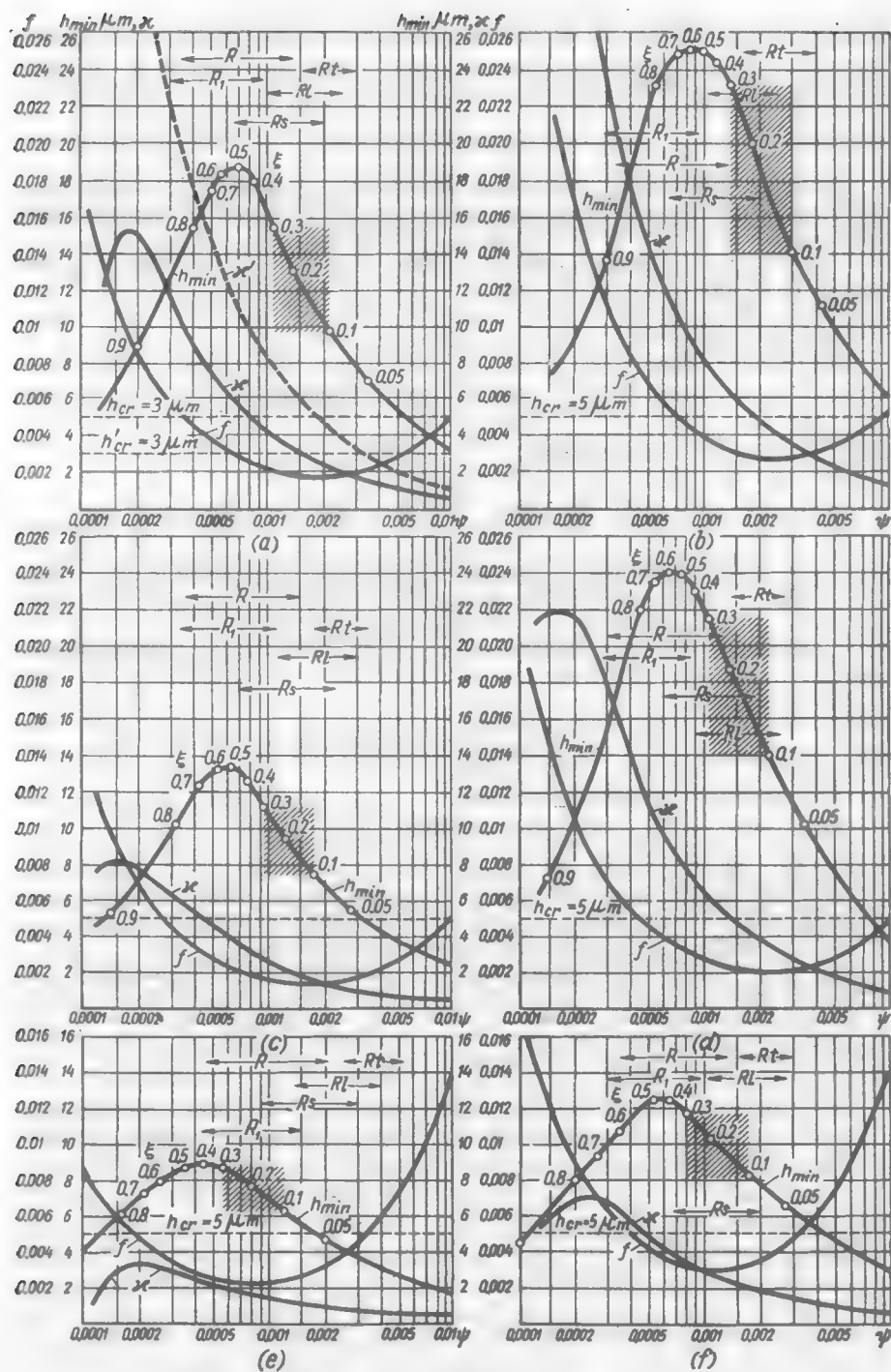$$k = \frac{P}{ld} = \frac{4000}{10 \cdot 8} = 50 \text{ (kgf/cm}^2)$$

Fig. 122. Operating parameters of bearings with various ψ

and the operating characteristic

$$\lambda = \frac{\eta n}{k} = \frac{20 \cdot 1000}{50} = 400$$

The graph shows that the bearing parameters are worse. The value of h_{min} with $\xi = 0.3$ drops to 11 microns and the reliability factor, to 2.5. The coefficient of friction decreases but little ($f = 0.0019$).

In this case the optimum clearance ratio $\psi = 0.0009$ (the nearest most suitable fit is a slack running one).

Figure 122d illustrates the graph for a bearing with the same l, P, η and n, but with $d = 120$ mm.

The unit load is

$$k = \frac{P}{ld} = \frac{4000}{10 \cdot 12} = 33.5 \ (\text{kgf/cm}^2)$$

and the operating characteristic

$$\lambda = \frac{\eta n}{k} = \frac{20 \cdot 1000}{33.5} = 600$$

The operating parameters of the bearing are appreciably improved. The value of h_{min} with $\xi = 0.3$ becomes equal to 21.5 μm, and the reliability factor, to 6.2. The coefficient of friction slightly increases ($f = 0.0026$). In this case the optimum clearance ratio $\psi = 0.0011$ (loose running fit).

Figure 122e shows the graph for a bearing with the same d, P η, and n, but with $l/d = 0.5$ ($l = 50$ mm).

The unit load is

$$k = \frac{P}{ld} = \frac{4000}{5 \cdot 10} = 80 \ (\text{kgf/cm}^2)$$

and the operating characteristic

$$\lambda = \frac{\eta n}{k} = \frac{20 \cdot 1000}{80} = 250$$

The oil layer thickness h_{min} with $\xi = 0.3$ is 8.5 μm, the reliability factor is 2, the coefficient of friction, 0.0022 and the optimum clearance ratio $\psi = 0.0006$ (the nearest most suitable fit is a running one).

The parameters of a bearing with $l/d = 0.5$ can be improved by increasing the operating characteristic through using oil of a higher viscosity or reducing k (increasing the diameter). When $\lambda = 500$ (Fig. 122f), h_{min} (at $\xi = 0.3$) rises to 12 and the reliability factor, to 3.5. The optimum clearance ratio $\psi = 0.0008$ (the nearest most suitable fit is a slack running one).

The plotting of the ψ-h_{min} diagrams gives a most full insight into the operation of a bearing but it is a rather laborious process. It is much simpler to determine the clearance ratio proceeding from the condition $\xi = 0.3$ on the basis of Fig. 115 or Eq. (2.13) and select the nearest standard fit from Fig. 104c, d so that the value of ξ remains within 0.1-0.15 with the extreme values of ψ and equals, on the average, to about 0.3. To account for wear during operation, it is advisable to use slightly increased initial average values ($\xi = 0.35$-0.4) so that in the course of running-in and wear the bearing is made to operate in the region of the optimum value of ξ equal to 0.3.

When the value of ψ is selected proceeding from this condition the bearing will operate unfailingly and maintain its working ability for a long time.

In conformity with the diagrams (see Fig. 122), the minimum values of the coefficient of friction correspond to $\xi = 0.3$-0.1. For this reason, the value of ψ may also be selected so as to have the minimum coefficient of friction, i.e., it may be determined from Eq. (2.21).

However, this method tends to decrease somewhat the values of ξ.

(h) Bearing Diameter

Solving Eq. (2.13) (for $\xi = 0.3$) for λ, we obtain

$$\lambda = \frac{\eta n}{k} = \frac{4.75 \cdot 10^8 \psi^2}{l/d} \qquad (2.23)$$

where k is the unit load in kgf/cm²

$$k = \frac{P \cdot 10^2}{ld}$$

Substituting this value of k and the value of ψ from Eq. (2.2) into Eq. (2.23), we find

$$P = \frac{2}{m^2} 10^{-5} d^3 (l/d)^2 \eta n \quad (2.24)$$

It follows from this equation that, all other things being equal (the same η, n, m and l/d), the load-carrying capacity of the bearing is proportional to the *cube of its diameter*. Therefore, increasing the diameter is an extremely effective means for augmenting the carrying capacity of the bearing.

Increasing the diameter not only increases the carrying capacity but also reduces, with the given h_{cr}, the critical operating characteristic λ_{cr} and hence, increases the reliability of the bearing operation.

Fig. 123. Critical operating characteristic λ_{cr} as a function of diameter d and clearance ratio ψ (for $l/d = 1$ and $h_{cr} = 5$ μm)

Figure 123 presents the dependence of λ_{cr} on the bearing diameter and clearance ratio ψ (it is assumed that $l/d = 1$, $h_{cr} = 5$ μm), determined from the graph in Fig. 120. It can be seen that λ_{cr} sharply
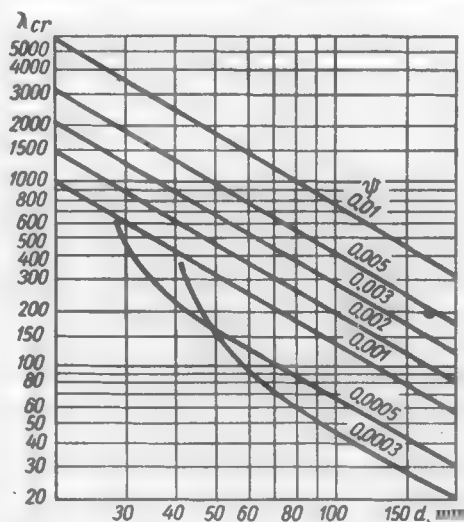
drops with an increase in the diameter and a decrease in the clearance ratio. Clearances with $\psi < 0.001$ are not recommended since in this case the bearing enters the region of $\xi > 0.3$.

An increase in d also makes the shaft more rigid, lessens its elastic deformations (which determine in a large measure the critical thickness of the oil layer) and improves the vibration stability of the bearing.

Figure 123 shows that the values of λ_{cr} are very high for bearings of small diameter ($d = 20$-30 mm). Therefore, such bearings can only operate reliably with high values of the operating characteristic (high rotational speeds, light unit loads). Just as in the case of large-diameter bearings, it is good practice to use moderate clearance ratios (but not below $\psi = 0.001$).

Equation (2.24) may be used to find the diameter of a bearing with the given P, η and n, such as will satisfy the condition $\xi = 0.3$

$$d = 37 \sqrt[3]{\frac{Pm^2}{(l/d)^2 \, \eta n}} \qquad (2.25)$$

(the values of m are given on page 119).
For $l/d = 1$ and the most widespread slack running fit ($m = 12$)

$$d = 190 \sqrt[3]{\frac{P}{\eta n}}$$

(i) Ratio l/d

In conformity with Eq. (2.24), the load-carrying capacity of a bearing is proportional to the squared ratio l/d.

The carrying capacity of bearings with a small l/d ratio is reduced because of the easy outflow of oil from the end faces (side leakage). With the same values of λ, the minimum thickness of the oil layer in such bearings is smaller than in bearings with a high l/d ratio. Higher values of λ and smaller clearances are required to form an oil layer of sufficient thickness.

However, bearings with low l/d ratios are less sensitive to misalignment, and the critical thickness of the oil layer in them is much less than in bearings with high l/d ratios. This to a considerable extent compensates for the reduced carrying capacity of bearings with low l/d ratios.

Conversely, bearings with high l/d ratios are extremely sensitive to misalignment and therefore the critical thickness of the oil layer in such bearings is always larger.

Accounting for the positive and negative effect of l/d on the carrying capacity, it is better in practice to adhere to moderate values of $l/d = 0.8$-1.2 (Fig. 124a).

The ratio l/d has sometimes to be reduced to 0.3 because of limited axial dimensions (Fig. 124b). When their other parameters are properly selected (sufficiently small clearances, high values of λ), such bearings function quite efficiently.

Low l/d ratios are also used for large-diameter bearings ($d > 100$ mm) distinguished by their high load-carrying capacity.

As a rule, bearings with $l/d > 1.5$ are made self-aligning. This makes it possible for high l/d ratios to be used to the best advantage.

(j) Operational Phases of the Plain Bearing

These phases clearly manifest themselves on a diagram showing the change in the coefficient of friction f depending on the operating characteristic λ.

Fig. 124. Bearings with various l/d values

Such diagrams, obtained experimentally, make it possible to determine the critical operating conditions of the bearing and the critical minimum oil film thickness h_{cr}.
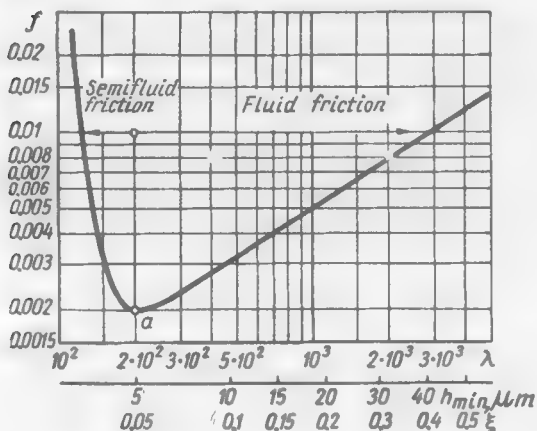
Figure 125 illustrates a plot in λ-f coordinates for a bearing with a diameter $d = 100$ mm, $l/d = 1$ and clearance ratio $\psi = 0.002$ ($\Delta = 200$ μm).

The left branch of the curve refers to the region of semifluid friction where contact takes place between the metal surfaces of the shaft and bearing.

The extreme point on the curve (outside the confines of the diagram) corresponds to the coefficient of semidry friction.

Fig. 125. Coefficient of friction *versus* λ

The coefficient of friction in the region of semifluid friction diminishes with an increase in λ, i.e., with an increase in the rotational
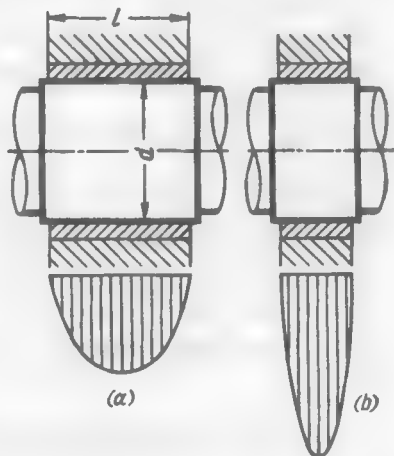
speed for a bearing with specified unit load and oil viscosity. This means that as the rotational speed increases the shaft departs from the bearing surface, and the number of the contacting microirregularities diminishes.

At point a ($\lambda = 2 \cdot 10^2$) the metal surfaces separate, the oil film "floats" the shaft and the bearing begins to operate in the fluid-friction region.

Beyond point a, the coefficient of friction is determined by hydrodynamic factors.

According to Eq. (2.18), the coefficient of friction continually grows higher with an increase in λ.

The minimum of the curve (*boundary friction*) indicates the critical value of the operating characteristic. From the graph in Fig. 111 one may find ξ and then, from the graph in Fig. 125, $h_{\min} = \frac{\xi \Delta}{2}$ (second scale on the X-axis) and h_{cr} (in Fig. 125 $h_{cr} = 5$ μm).

(k) Fluid-Friction Bearing as a Self-Adjusting System

Plain bearings operate stably within a wide range of operating conditions because they easily adapt themselves to various conditions of operation, thanks to the property of lubricants to change their viscosity with temperature.

Large clearances have an unfavourable effect on the carrying capacity, but reduce friction and increase the amount of oil pumped through the bearing. The working temperature of bearings with a large clearance is lower. The resultant higher viscosity of oil compensates for their small carrying capacity.

This explains why plain bearings can operate even when they are excessively worn.

In view of the increased heat generation, bearings with a small clearance operate at a high temperature, but the reduced viscosity of oil is compensated for by the high load-carrying capacity inherent in such bearings.

The bearing exhibits this ability of self-adjustment also when the operating conditions vary.

If, for example, the unit load increases, the operating characteristic drops down, as does the minimum thickness of the oil layer. The bearing approximates to the conditions of semifluid friction. But the drop of λ simultaneously decreases the coefficient of friction (see Fig. 125) and heat generation. This increases oil viscosity and, for this reason, the former operating characteristic is completely or partly regained and the bearing operates in a state of stable equilibrium.

If the bearing temperature increases (for example, due to a short-time reduction in oil supply) the working viscosity of the oil drops

down, the thickness of the oil layer decreases and seizure may occur. The reduction of the oil viscosity decreases the coefficient of friction and the generation of heat. As a result, a new state of equilibrium sets in, although possibly with a lower λ as compared with its initial magnitude.

With the transition to the region of high λ (rise of the rotational speed, drop of the load) the operation of the bearing may become unsteady because of the reduction of the shaft eccentricity. However, the vortex motion of the shaft sharply increases the frictional losses, the temperature of the bearing rises, the oil viscosity drops down and the shaft is returned to the stable region of operation.

The self-dampening of vibrations ceases only in the region of small eccentricities ($\varepsilon < 0.5$).

Thus, the factor η in the expression $\frac{\eta n}{k}$ acts as a governor which tends to restore the initial operating conditions when they are changed.

The principal condition is that equilibrium must be restored within the entire range of possible variations in the operating conditions without trespassing dangerous values of h_{min}. For this purpose the bearing must be designed with a sufficient reliability factor and operated in the region of sufficiently high eccentricities.

As distinct from the fluid-friction region, the region of semifluid friction is unstable. If the bearing begins to operate in this region, any factor tending to reduce λ (drop in the oil viscosity, increase in the load) increases the coefficient of friction (see Fig. 125) and, as a result, the temperature of the bearing, and then again, the coefficient of friction. The process is terminated in the establishment of semidry friction, unless some favourable factor manifests itself (for example, the smoothing down of microirregularities in plastic bearing materials under the action of high temperatures, which is attended by a drop in h_{cr}).

An increase in the rotational speed has a favourable effect in the region of semifluid friction. When n (and, therefore, λ) increases, the coefficient of friction is sharply reduced and the bearing begins to operate in the region of fluid friction. This explains the comparatively safe transition of plain bearings through the region of semifluid friction during starting periods.

2.4. Calculation of Fluid-Friction Bearings

Bearings operating in conditions of fluid friction can easily be calculated, if the temperature of the oil layer and the working viscosity of the oil are known.

A *check* calculation (with known geometrical parameters of the bearing, load and rotational speed) means determining the minimum thickness of the oil layer, the coefficient of friction and the reliability factor of the bearing. The temperature-viscosity curve (see Fig. 110) is used to find the oil viscosity at the given temperature and Sommerfeld's number So, and the graph in Fig. 111, to determine the relative minimum oil layer thickness ξ. The minimum oil

layer thickness in microns is

$$h_{min} = \xi \frac{\psi d}{2} 10^3$$

The value of ξ_{cr} may be calculated from the formula

$$\xi_{cr} = \frac{2h_{cr}}{\Delta} = 10^{-3} \frac{2h_{cr}}{\psi d}$$

after which the same diagram is used to find the corresponding value of So_{cr} and the reliability factor as the ratio So/So_{cr}. The coefficient of friction is calculated by Eq. (2.19).

The charts in Figs. 120 and 121 are more convenient: they directly show the values of h_{min} depending on λ and ψ.

The critical operating characteristic λ_{cr} is determined from the same charts on the basis of h_{cr}. The reliability factor $\varkappa = \lambda/\lambda_{cr}$.

The value of h_{cr} depends on the surface finish, length and diameter of the bearing, the rigidity of the shaft-bearing system and the ability of the bearing material to wear-in.

With the usual surface finish according with the 9th-10th class the value of h_{cr} may be found from the following approximate relation:

$$h_{cr} = a \sqrt{\overline{l/d}} \sqrt{\overline{d}} \ (\mu m) \tag{2.26}$$

where d is the shaft diameter in mm and a, a coefficient equal to 0.7 for babbitt-lined bearings, 1 for bearings with a lead bronze lining, and 1.5 for bearings made of bronze and aluminium alloys.

In the case of multi-bearing shafts (crankshafts, for example) the values of h_{cr} determined from Eq. (2.26) should be increased 1.2-1.5 times.

Design calculations operate with specified load and rotational speed. The shaft diameter is also frequently specified by the design conditions. The ratio l/d is usually equal to 0.8-1 (except for some special cases).

In most cases the problem is to find the clearance ratio ψ that will ensure the most reliable operation of the bearing.

The operating characteristic can also be varied by changing the viscosity of oil (selecting the proper lubricant grade).

The simplest calculation consists in determining the value of ψ on condition that $\xi = 0.3$. With the selected shaft diameter and ratio l/d and with the given grade of lubricant the operating characteristic $\lambda = \frac{\eta n}{k}$ is determined, and after that the optimum clearance ratio ψ is found from the graph in Fig. 115 or from Eq. (2.13).

Then, the nearest standard fit is selected so that the maximum value of ξ (with account being taken of wear during operation) is ≈ 0.4 and at any rate kept within 0.1-0.5 with the extreme values of ψ which are determined by the margin tolerances.
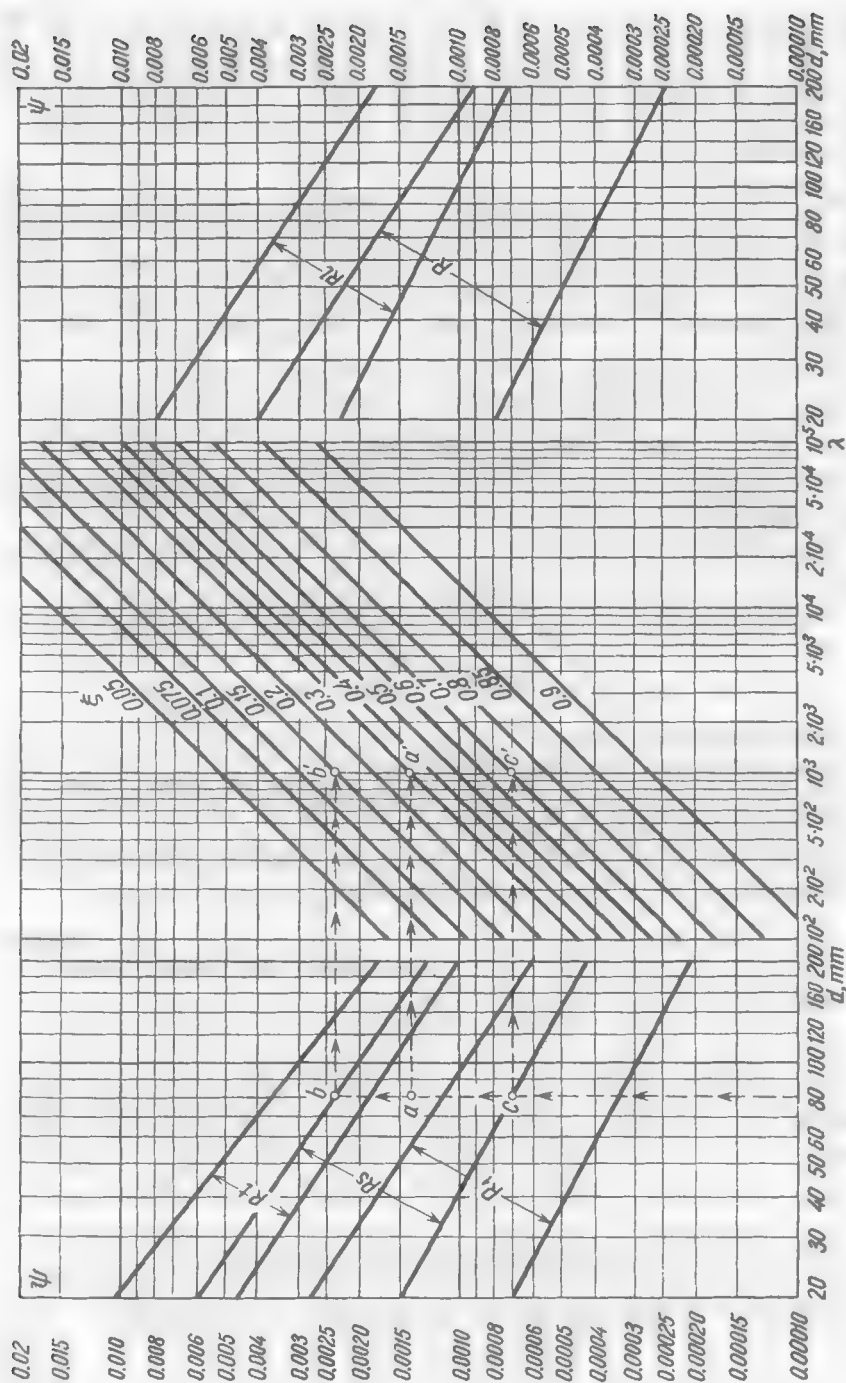
Fig. 126. Nomographic chart for selecting fits

10*

The nomographic chart shown in Fig. 126 is plotted to make the selection of the proper clearance easier. This chart shows the relation between clearance ratios obtained with standard fits and the values of ξ (the chart is plotted for $l/d = 1$ and is suitable for $l/d = 0.8$-1.2).

Let, for example, $d = 80$ mm and the operating characteristic $\lambda = 1000$. Erecting a perpendicular from the point corresponding to $d = 80$ mm (on the left or right side of the chart) to intersect the lines corresponding to the extreme values of ψ obtained with various fits, and then drawing horizontal lines through the points of intersection thus obtained to intersect the vertical line $\lambda = 1000$ in the middle of the chart, we read the corresponding values of ξ on the inclined lines.

In our case the nearest suitable fit is a slack running one (Rs) for which the values of ξ are equal to 0.3, 0.15 and 0.7 (points a', b', c') for the mean value $\psi = 0.0014$ (point a), extreme upper value $\psi = 0.0023$ (point b) and extreme lower value $\psi = 0.0007$ (point c), respectively.

Loose running fits Rl ($\xi = 0.18$, 0.09, 0.45) may also be adopted. A thermal running fit (Rt) gives too low values of ξ (0.1, 0.075, 0.2), with which semifluid friction may set in.

Running fits R ($\xi = 0.65$, 0.27, 0.85) and R_1 ($\xi = 0.75$, 0.45, 0.87) are impermissible because they make the bearing operate in the unstable region.

The mean and extreme values of h_{min} are found from the formula

$$h_{min} = 10^3 \frac{\xi \psi d}{2}$$

where ξ is the relative minimum oil layer thickness and ψ, the clearance ratio with mean and extreme values of clearances.

The value of λ_{cr} may be found from the nomographic charts (Fig. 120 or 121) on the basis of the adopted h_{cr}. The reliability factor $\varkappa = \lambda/\lambda_{cr}$. The coefficient of friction is calculated by Eq. (2.19).

The results of calculations for the mean and extreme clearance values of the previous example $(Rs$ fit, $h_{cr} = 5$ μm) are given in Table 19.

Table 19

Clearance	ψ	δ, μm	ξ	h_{min}	λ_{cr}	$\varkappa$	f
Mean	0.0014	56	0.3	16.5	200	5	0.003
Maximum	0.0023	92	0.15	14.7	320	3.1	0.0027
Minimum	0.0007	28	0.7	19.6	120	8.4	0.05

(a) Thermal Calculation of Bearings

The amount of heat (in kcal/s) generated in a bearing

$$R = \frac{Pvf}{A} = \frac{Pvf}{427} \tag{2.27}$$

where P = load on the bearing, kgf

v = peripheral speed, m/s

f = coefficient of friction

A = mechanical equivalent of heat $(A = 427 \text{ kgf} \cdot \text{m/cal})$

In fluid-friction bearings with a pressure-feed lubrication the heat dissipated from the bearing to the surrounding medium is disregarded, assuming that under steady thermal conditions all the heat is withdrawn by the circulating oil.

The amount of heat (cal/s) carried away from the bearing by the oil

$$R' = 10^{-3}Q\gamma c\,(t_{out} - t_{in}) = 10^{-3}Q\gamma c\Delta t \tag{2.28}$$

where Q = amount of oil flowing out of the bearing, cm³/s

γ = specific weight of oil, gf/cm³

c = heat capacity of oil, cal/kgf·°C

t_{in} and t_{out} = oil temperature at the inlet and outlet of the bearing, respectively

$\Delta t = t_{out} - t_{in}$ = oil temperature rise in the bearing

In a state of thermal equilibrium $R = R'$, i.e., according to Eqs. (2.27) and (2.28),

$$\frac{Pvf}{427} = 10^{-3}Q\gamma c\Delta t \tag{2.29}$$

hence,

$$\Delta t = 10^3\,\frac{Pvf}{427Q\gamma c} = 2.34\,\frac{Pvf}{Q\gamma c} \tag{2.30}$$

The temperature of oil at the outlet from the bearing

$$t_{out} = t_{in} + \Delta t \tag{2.31}$$

Mean temperature of oil in the bearing

$$t_m = \frac{t_{out} + t_{in}}{2} = t_{in} + \frac{\Delta t}{2} \tag{2.32}$$

Substituting into Eq. (2.30) $P = kld$ and

$$v = \frac{\pi dn}{30 \cdot 2 \cdot 100} = 5.22 \cdot 10^{-4}\,dn$$

where d and l are the diameter and length of the bearing in cm, $k = P/ld$, the unit load in kgf/cm² and n, the rotational speed in rpm, we obtain

$$\Delta t = 1.22 \cdot 10^{-3}\,\frac{kld^2nf}{Q\gamma c} \tag{2.33}$$

The specific weight of mineral lubricants at 20-100°C varies within $\gamma = 0.85$-0.95 and the heat capacity, within 0.45-0.55. Substituting the mean values $\gamma = 0.9$ and $c = 0.5$ into Eq. (2.33), we get

$$\Delta t = 2.7 \cdot 10^{-3}\,\frac{kld^2nf}{Q} \tag{2.34}$$

The amount of oil Q (in cm³/s) flowing out of the bearing, according to Vogelpohl, is

$$Q = 3.3 \cdot 10^{-3} (2.8 - l/d) \, \psi l d^2 n \sqrt[3]{1+p} \qquad (2.35)$$

where d and l = diameter and length of the bearing, cm
    ψ = clearance ratio
    n = rotational speed, rpm
    p = oil-feed pressure, kgf/cm²

Substituting this expression for Q into Eq. (2.33), we obtain

$$\Delta t = \frac{0.82}{(2.8 - l/d) \sqrt[3]{1+p}} \cdot \frac{kf}{\psi} \qquad (2.36)$$

For a bearing designed to operate with the optimum $\xi = 0.3$, in conformity with Eqs. (2.22) and (2.13),

Fig. 127. Factor a for various values of p and l/d

$$f = 10^{-4} \sqrt{\lambda} \sqrt[3]{d/l}$$

$$\psi = 4.6 \cdot 10^{-5} \sqrt{\lambda} \sqrt{l/d}$$

Substituting these values into Eq. (2.36), we find that

$$\Delta t \approx \frac{1.8k \, (d/l)^{0.8}}{(2.8 - l/d) \sqrt[3]{1+p}} \qquad (2.37)$$

Presenting k in the form $k = \frac{P}{d^2(l/d)}$, we get

$$\Delta t = \frac{1.8P}{d^2 (l/d)^{1.8} (2.8 - l/d) \sqrt[3]{1+p}}$$

$$= a \frac{P}{d^2} \qquad (2.38)$$

It follows from this expression that with a given load the temperature rise in a bearing is inversely proportional to the square of the diameter and directly proportional to the factor a (Fig. 127)

$$a = \frac{1.8}{(l/d)^{1.8} (2.8 - l/d) \sqrt[3]{1+p}}$$

For the design calculation of a bearing with the optimum $\xi = 0.3$ one must know P and n, and specify the values of d and l/d, the pressure p and the temperature t_{in} and grade of oil.

Equation (2.36) is used to determine the oil temperature rise Δt in the bearing, and Eq. (2.32), the mean temperature of the oil

layer, after which the temperature-viscosity curve is employed to find the working oil viscosity η, and then the operating characteristic λ is calculated.

Calculations are continued by the methods described above, determining ψ by Eq. (2.13) or from the graph in Fig. 115 and selecting the nearest standard fit. Then, the minimum thickness of the oil layer is calculated by Eq. (2.7), the chart in Fig. 120 or 121 is used to find λ_{cr} and thereafter the reliability factor $\varkappa = \lambda/\lambda_{cr}$ is determined.

In this case the operation of the bearing can be improved by increasing not only its diameter, but also the oil-feed pressure.

The outflow of oil from the bearing can appreciably be increased (and thus the working temperature of the oil layer reduced) by means of longitudinal recesses in the unloaded area of the bearing [Eq. (2.35) holds true for bearings without recesses and with an oil supply through a hole made in the unloaded area].

Assume that $P = 4000$ kgf, $n = 2000$ rpm, $d = 80$ mm and $l/d = 1$. The oil temperature $t_{in} = 60°C$ and the oil-feed pressure $p = 4$ kgf/cm². The lubricant used is oil grade AK-15.

The specific load is

$$k = \frac{4000}{8 \cdot 8} = 62 \ (\text{kgf/cm}^2)$$

The temperature rise in the bearing by Eq. (2.37)

$$\Delta t = \frac{1.8 \cdot 62}{1.8 \sqrt[3]{5}} = 36 \ (°C)$$

The mean temperature of oil by Eq. (2.32)

$$t_m = 60 + 18 = 78 \ (°C)$$

According to Fig. 110, the viscosity of oil at this temperature is $\eta = 35$ cP. The operating characteristic is

$$\lambda = \frac{\eta n}{k} = \frac{35 \cdot 2000}{62} = 1130$$

The optimum clearance ratio by Eq. (2.13)

$$\psi = 4.6 \cdot 10^{-5} \sqrt{1130} = 0.0015$$

In conformity with the graph in Fig. 126 the nearest suitable fit is a slack running one· (*Rs*).

The minimum thickness of the oil layer

$$h_{\text{min}} = \frac{\xi \psi d 10^3}{2} = \frac{0.3 \cdot 0.0015 \cdot 80 \cdot 10^3}{2} = 18 \ (\mu\text{m})$$

From Fig. 120 (for $h_{cr} = 5$ μm) the critical operating characteristic is $\lambda_{cr} = 160$.

The reliability factor is

$$\varkappa = \frac{\lambda}{\lambda_{cr}} = \frac{1130}{160} = 7$$

Coefficient of friction by Eq. (2.19)

$$f = 3.36 \cdot 10^{-9} \frac{1130}{0.0015} + 0.00075 = 0.0033$$

The power consumed in overcoming friction

$$N = Pvf = \frac{P\pi n}{30} 10^{-3} \frac{df}{2} = 4000 \frac{\pi 2000}{30} 10^{-3} \cdot 40 \cdot 0.0033 =$$

$$= 116 \text{ kgf} \cdot \text{m/s} = 1.12 \text{ (kW)}$$

When checking the already designed bearings (the parameters of which are not necessarily selected proceeding from the condition $\xi = 0.3$) for heating, the mean temperature t_m of the oil layer is determined by the method of successive approximations. At first a tentative value of t_m is specified, the viscosity of oil is determined, $\lambda = \frac{\eta n}{k}$ is found and, finally, the coefficient of friction is calculated by Eq. (2.19). Then, the oil efflux is found by Eq. (2.35), the value of Δt, by Eq. (2.36) and the value of t_m, by Eq. (2.32).

If the calculated value of t_m differs from the preliminary value, recalculation is made until these values coincide. Further calculation is conducted as described above.

(b) Types of Loading

The formulas in the previous sections are based on the assumption that the load maintains the same magnitude and direction, and
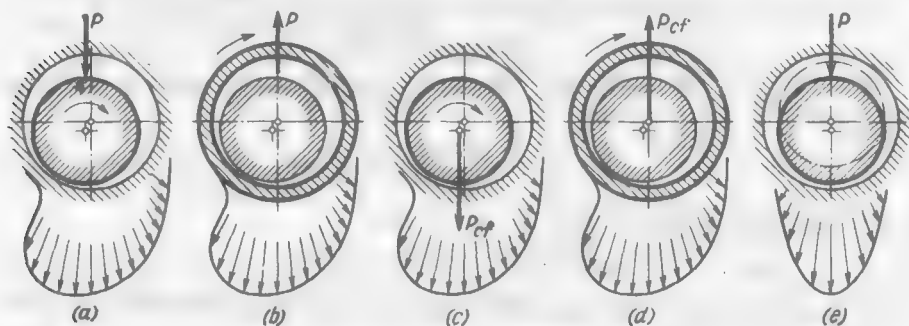
Fig. 128. Types of loading

that the rotational speed remains constant. These formulas are used when:

(a) the shaft, loaded by a constant force, rotates and the bearing is stationary; the pressure zone does not change its position with respect to the bearing (Fig. 128a);

(b) the shaft is stationary and the bearing, loaded by a constant force, rotates; the pressure zone moves with respect to the shaft with an angular velocity equal to that of the bearing rotation, but does not change its position with respect to the bearing (Fig. 128b);

(c) the shaft, loaded by a constant centrifugal force, rotates and the bearing is stationary; the pressure zone moves with respect to the bearing with an angular velocity equal to that of the shaft rotation, but does not change its position with respect to the shaft (Fig. 128c);

(d) the shaft is stationary and the bearing, loaded by a constant centrifugal force, rotates; the pressure zone moves with respect to the shaft with an angular velocity equal to that of the bearing rotation, but does not change its position with respect to the bearing (Fig. 128d).

If the shaft, bearing and load vector rotate each with its own velocity, the calculation is made proceeding from the corrected velocity

$$\omega_{corr} = \omega_{sh} + \omega_b - 2\omega_l$$

where ω_{sh}, ω_b and ω_l are the angular velocities of the shaft, bearing and load vector, respectively.

The calculation grows more complicated when the load varies in direction and magnitude (unstable loading conditions).Such bearings can approximately be calculated on the basis of the mean load and the mean rotational velocity of the load vector per cycle.

Electronic computers make possible accurate calculations by the *iteration method*.

The initial material for calculation is a polar load cycle diagram. The initial point of the cycle is specified by a certain probable position of the shaft in the bearing. The magnitude and direction of the hydrodynamic force is determined from the known magnitude and direction of the load and the corrected rotational velocity.

Comparing the obtained values with the magnitude and direction of the external force, it is possible to determine the direction of the instantaneous velocity vector of the shaft centre movement. Repeating the calculations for a series of consecutive shaft positions through small intervals (for example, 5°) the approximate path of the shaft centre movement can be obtained, this then serving as the initial material for the next series of calculations.

If the number of calculations is large enough, the results begin to repeat themselves and the consecutively determined paths, coincide.

If the path of the shaft centre movement is known, the minimum oil layer thickness h_{min} can be found, compared with the critical oil layer thickness h_{cr}, and the reliability factor $\varkappa$ determined.

If the obtained values of h_{min} and $\varkappa$ are insufficient, one has to specify other values of d, d/l, ψ and η, being guided by the regularities governing the effect of these parameters on the carrying capacity, and repeat the calculation until a satisfactory result is obtained.

A special case (Fig. 128e) is the application of a pulsating or alternating load to a shaft (or a bearing) either rotating at a low speed, or oscillating or remaining stationary. In this case the carrying force of the oil layer develops as a result of the oil being periodically expel-

led from the area of the maximum approach of the shaft to the bearing. The magnitude of this force is proportional to the oil viscosity and the cube of the bearing diameter, and inversely proportional to the square of the clearance ratio.

The shift of the shaft in the bearing during time $\Delta\tau$ depends on the impulse $P\Delta\tau$. If the regularity governing the change of the load with time is known, it is possible to select such geometrical parameters of the bearing and oil viscosity as would ensure the existence at the end of each load rise cycle of a sufficiently thick oil layer at the point of the closest approach of the shaft to the bearing, and thus sustain fluid friction despite the weak pumping effect of the shaft or its total absence (with the stationary shaft).

The increase of the load-carrying capacity of the bearing as a result of the periodic approach of the shaft to the bearing under the action of the alternating load is also observed with an unstable load, although this is not accounted for by the calculation.

(c) Approximate Criteria of Load-Carrying Capacity

The design of bearings is frequently based on the *permissible unit load* $k = P/ld$ (kgf/cm^2). This criterion can only be applied to soft, low-strength bearing materials (babbitts, plastics), and then only with reservations.

The actual load-carrying capacity of a bearing depends on its design, rigidity, the method of placing the antifriction coating, geometrical parameters (clearance, ratio l/d), the nature of load, speed of the shaft rotation, amount of oil supplied, and other factors.

Let us consider babbitt-lined bearings. The fatigue limit of babbitt in compression, as determined on test specimens, is about 200 kgf/cm^2 at 20°C and about 100 kgf/cm^2 at 100°C. Bearing in mind that the maximum pressure in the oil layer exceeds the mean unit pressure by about three times, it would seem correct, proceeding from these data, to consider $k = 0.3 \cdot 200 = 60$ kgf/cm^2 to be the permissible load at 20°C, and $k = 0.3 \cdot 100 = 30$ kgf/cm^2, at 100°C.

The actual load-carrying capacity of bearings can appreciably be improved by reducing the lining thickness, increasing the rigidity of the shells and beds, and correctly selecting the clearance and l/d ratio. Rationally designed bearings with a thin-layer babbitt lining can safely bear unit pressures of 100-150 kgf/cm^2 under a cyclic load.

The load-carrying capacity of plastics bearings is determined not so much by their compressive strength as by their *resistance to creep*, which is the development of residual deformations under stresses much below the ultimate compressive stress, thermal stability and linear expansion coefficient, but, primarily, by their design. Their carrying capacity depends very widely on these factors ($k = 5$-50 kgf/cm^2).

When calculating bearings of stronger materials (bronze, aluminium alloy, silver), the decisive factors are the hydrodynamics of the bearing, its geometry (d, l/d, ψ) and operating conditions (λ), the rational choice of which makes it possible to increase the unit loads to 150-300 kgf/cm^2 and, sometimes, even to 500-600 kgf/cm^2.

(d) Design, Production and Operational Factors

The overheating of a bearing, its excessive wear, cracking and melting of its lining, galling of the bearing material on the shaft, and other phenomena of its unsatisfactory operation are almost always caused by the transition (total or local) beyond the critical oil layer thickness and the establishment of semifluid or semidry friction in the bearing, but are seldom the result of insufficiently high design values of h_{min} and λ.

In most cases the defects are due to errors in the bearing design, manufacture and operation. The most frequent causes of bearing failure are:

incorrect oil supply;

insufficient oil supply during starting periods;

retarded oil outflow from the bearing;

wrong design of the bearing unit, unfavourable distribution of forces on the bearings, excessive edge loads;

low rigidity of the shaft and bearing;

wrong choice of the shaft and bearing materials;

insufficient hardness of the shaft surface, wrong relationship between the hardness of shaft and bearing;

wrong macro- and microgeometry of the load-carrying surfaces;

poor quality of oil, oxidation of oil during operation;

unsatisfactory filtering of mechanical impurities and hard oxidation products from oil.

In the case of multi-bearing shafts one of the most frequent causes of bearing failure is the misalignment of the supports or shaft journals, and poor rigidity of the housing carrying the supports.

The bearings will operate effectively if such defects are eliminated.

It must not be concluded from the basic equations of the hydrodynamic theory of lubrication that increasing the rotational speed of the shaft and oil viscosity improves the load-carrying capacity and reliability of the bearing because these equations include the *working* viscosity of oil which becomes established as a result of the balance between the generation and withdrawal of heat.

Increasing the rotational speed, which formally augments the operating characteristic, practically often reduces it, since the increased rotational speed intensifies the generation of heat and lowers the working viscosity of oil. High rotational speeds are dangerous; the design parameters of high-speed bearings must be selected with special care to diminish heat generation.

Likewise, it is not always rational to improve the operating characteristic by using oil of increased viscosity. High viscosity of lubricants increases friction and heat generation and hampers the efflux of oil from the bearing. This increases the temperature of the oil layer and worsens the working viscosity of oil. As a result, the load-

carrying capacity of a bearing using a highly viscous oil may be smaller than with a less viscous oil. Besides, too viscous an oil makes starting difficult.

The use of oil with a high viscosity is justified only when the bearing operates at a temperature increased by outside heating, for example in bearings of hot machines (internal-combustion engines) whose bodies are acted upon by the heat generated by the working processes. In this case the use of oil with an increased viscosity is frequently the only possible method to ensure reliable operation of the bearings.

The load-carrying capacity of the bearing sharply increases with a reduction in the critical oil layer thickness (better surface finish of the shaft and bearing, higher surface hardness of the shaft to reduce wear, higher rigidity of the shaft-and-bearing system, the use of self-aligning bearings, good cleaning of oil from mechanical impurities).

The most effective method for improving the carrying capacity is to increase the bearing diameter since, all other things being equal, the carrying capacity is proportional to the cube of the diameter [Eq. (2.24)].

2.5. Introduction of Oil into Bearings

As a rule, oil is introduced into bearings through holes drilled in the housing (Fig. 129a) or in the shaft (Fig. 129b). Oil supply through
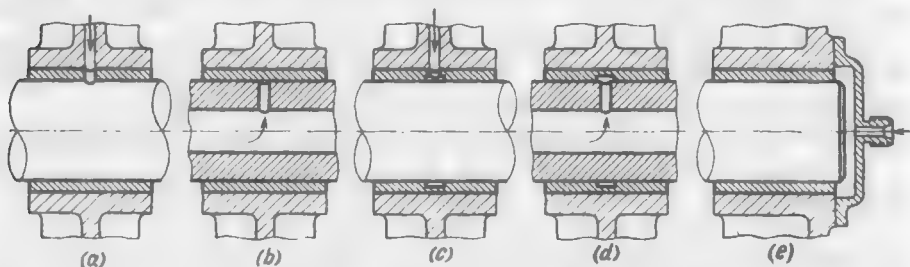
Fig. 129. Methods of introducing oil into bearings

annular grooves (Fig. 129c, d) is used when it is required to increase the flow of the oil through the bearing, and also when the bearing is acted upon by an alternating load. It should be borne in mind that annular grooves sharply reduce the carrying capacity and, in fact, convert the bearing into two short bearings. The end-face supply (Fig. 129e) does not decrease the carrying capacity of the bearing but in this case the flow of the oil through the bearing is about two times less than in the case of central annular grooves.

As a rule, oil should be introduced into the unloaded zone of the bearing.

(a) Load of Constant Direction

When the load is of constant direction it is good practice to arrange oil-feed holes in the region limited by an angle of 45-60° on both sides of the acting load (Fig. 130a).

The introduction of oil into the loaded zone is an obvious error (Fig. 130b). The high pressure in this zone, reaching several tens
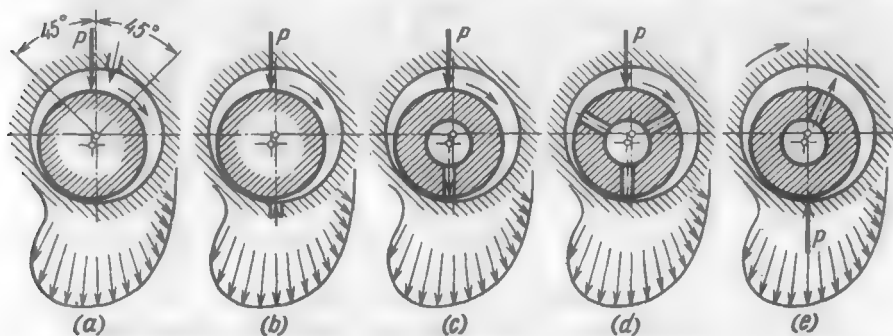
Fig. 130. Introducing oil into bearings under load of constant direction

and hundreds of kgf/cm², does not admit the oil (usually supplied under a pressure of 2-6 kgf/cm²) into the clearance but squeezes it out of the bearing and into the oil duct.

This circumstance is used in some designs to feed the oil to hard-to-reach surfaces (for example, in crankgears the lubricant for the piston pins is taken from the big-end bearings through the holes made in the high-pressure zone).

When oil is fed through a radial hole in the shaft (Fig. 130c) the oil-feed hole traverses the loaded zone each time the shaft makes a revolution, the oil is fed periodically and pulsations develop in the oil duct.

If the design requires that the oil be fed through the shaft, the latter should be provided with at least three oil-feed holes (Fig. 130d) or the oil supplied either via an annular groove or from the end face (see Fig. 129c-e).

If the *shaft* is stationary and the *housing*, loaded by a force of constant direction, rotates, the zone of increased pressure retains its position with respect to the shaft. In this case it is expedient to feed the oil through a hole drilled in the shaft in its portion opposite to the loaded zone (Fig. 130e). With other oil-supply methods (through the housing, annular grooves, from the end face) the remarks made on the occasion of the stationary housing should be taken into account.

- The edges of oil-feed holes reaching the friction surface must be smoothly rounded.

(b) Load of Variable Direction

A most simple case of the bearing load of variable direction is that of a bearing loaded by the centrifugal force of masses connected to a rotating shaft. As the shaft rotates the zone of increased pressure in the oil layer moves over the circumference of the bearing.
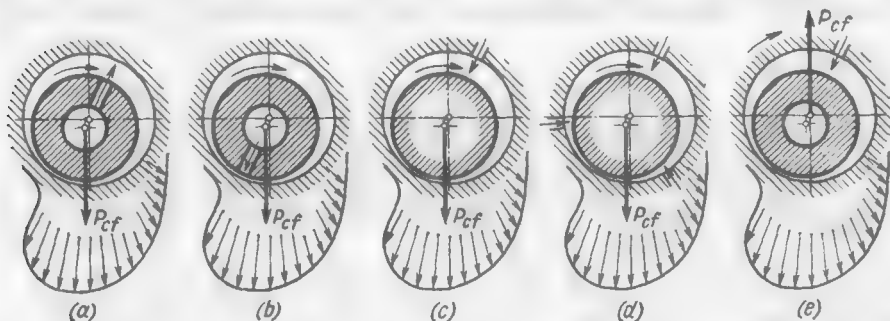
Fig. 131. Introducing oil into bearings under centrifugal load

In this case it is advisable to feed oil through a hole drilled in the shaft portion approximately opposite to the action of the centrifugal force (Fig. 131a). The oil feed in the direction of the load (Fig. 131b) is impermissible.

The supply of oil through the bearing (Fig. 131c) is undesirable because with any position of the oil-feed hole it will be overlapped by the high-pressure zone each time the shaft makes a revolution. Three holes (Fig. 131d) are needed to ensure continuous oil delivery into the clearance. Oil can also be fed through annular grooves and from the end face.

If the *shaft* is stationary and the *bearing* rotates together with the masses connected to it, oil should preferably be fed through a hole in the bearing, the hole being arranged in the direction of the load (Fig. 131e).

If the design does not permit this, the oil is supplied through several radial holes in the shaft.

If the load varies in both magnitude and direction and the rotation of the load vector does not coincide with the rotation of the shaft, the oil-feed holes should be made in the zone where the shaft approaches the bearing most rarely and for the shortest time during the load change cycle.

This zone can be found with the aid of *wear diagrams* (Fig. 132) which show the approximate distribution of wear over the surfaces of the shaft and bearing, and also the position of the sections where the shaft and the bearing mutually approach most frequently during the load change cycle.

Wear diagrams are plotted on the basis of polar diagrams of the load acting on the shaft and bearing during complete load change cycle (which need not necessarily coincide with one revolution of the shaft).
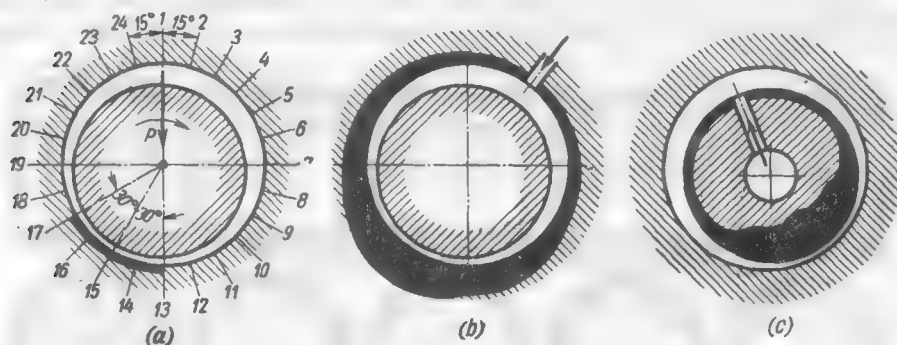
Fig. 132. Wear diagrams

The circumference of the bearing is broken into equal divisions, for example, through each 15° (see Fig. 132a), which are numbered and entered into a table. Since the accurate position of the shaft in the bearing at each given moment is unknown, it is assumed, for the sake of simplicity, that the action of the force applied to the shaft (or the bearing) extends over a region with a central angle of 60° (or 90°), which is displaced through 30° from the direction of the load in the direction of rotation.

If, for example, a force $P = 300$ kgf acts, in conformity with the polar diagram, at point 1, this figure is written down in the table under all the divisions lying within this region, i.e., for points 13-17.

After filling the table, the resulting figures are written down under each division and then marked to a convenient scale on the circumference of the shaft and bearing in the form of radius vectors the ends of which are connected by a smooth curve.

The wear diagram of a *bearing* (view b) is employed to select the position of the oil-feed hole in the bearing, and the wear diagram of a *shaft* (view c) —to choose the position of the hole in the shaft.

The oil-feed holes are made at places where the wear curves have their minimum.

The method of iteration (see p. 153) is used to determine more accurately the rational arrangement of the oil-feed holes.

(c) Oil Grooves

The loaded zone of the fluid-friction bearing must be free from grooves and recesses which impair the smoothness of the bearing surface and deteriorate the load-carrying capacity of the bearing. Annular grooves connect the high-pressure zone of the bearing with

its low-pressure zones, and longitudinal grooves facilitate the out-flow of oil from the loaded zone.

Oil distributing grooves arranged in the unloaded zone directly near the oil-feed hole are extremely useful.

Semiannular grooves (Fig. 133a) serve to distribute the oil over the circumference of the bearing. Longitudinal grooves (Fig. 133b)
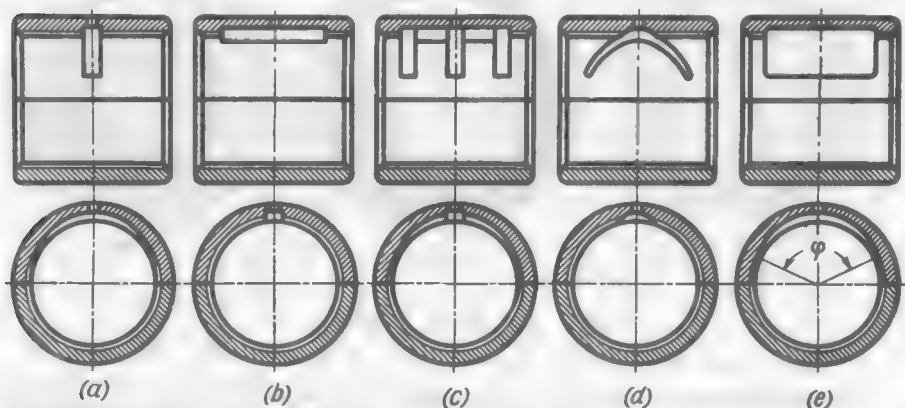
Fig. 133. Oil distributing grooves

are used in long bearings to feed oil along the bearing axis. At the same time they slightly increase the efflux of oil from the end faces of the bearing (side leakage). Combination (Fig. 133c) and spiral (Fig. 133d) grooves distribute oil in peripheral and axial directions.

Fig. 134. Oil grooves in bearings (a) and in shafts (b)

The grooves are made very wide (Fig. 133e) in bearings that carry a load of constant direction at high rotational speeds. Sometimes these are through grooves intended to increase the flow of oil through from the bearing and thus intensify heat withdrawal.

At the same time such recesses reduce friction and generation of heat in the bearing (approximately in the ratio $\varphi°/360°$, where φ is the central angle of the recess).

The edges of oil distributing and cooling grooves must be smoothly rounded (Fig. 134a, b).

It is not very difficult to machine oil grooves in open shells. The problem becomes more complicated when grooves, especially spiral ones, are to be made

in solid bushings. In such cases, use is commonly made of simple semiannular and longitudinal grooves. No grooves are usually cut in bushings of small diameter (less than 20 mm).

In bearings carrying a load of variable direction and having an oil-feed hole in the shaft, the oil distributing grooves are sometimes made in the shaft in the form of longitudinal, helical and cross-type recesses. This must be done very carefully because such grooves tend to reduce the fatigue strength of the shaft. Acute re-entrant angles must be avoided, the recesses must have smooth outlines or be replaced by shallow flats (Fig. 134*b*, on the right) which weaken the shaft less.

(d) Through-Flow Circulation of Oil

In fluid-friction bearings with forced lubrication a provision should be made for a free side leakage.

Figure 135*a* shows a shaft installed in an end bearing equipped with a cap. Oil is fed through hole *1* in the housing. It flows out freely from the left-hand end face of the bearing, while a blind space is formed on the right side. A stagnation zone is formed in section *s*, and the oil here is overheated.

In correct designs the used oil is drained along duct *2* in the housing (Fig. 135*b*) or through the central hole in the shaft (Fig. 135*c*).

In the design shown in Fig. 133*d* oil is fed through the shaft end into the internal space of the shaft, and therefrom, to the bearing via radial holes. Since the circulating oil pressure at places where the radial holes are cut is about the same as at the right-hand end face of the bearing, there is no oil circulation in section *s*.

The error can be corrected by dispensing with the radial holes (Fig. 135*e*) in order to provide for a through-flow circulation of the oil through the bearing.

It is bad practice to feed oil through adjacent holes (Fig. 135*f*) between which a stagnation zone *s* forms. A correct outflow is ensured when the oil is delivered through holes arranged approximately on the axis of symmetry of the bearing (Fig. 135*g*). If an intensified feed is required, the oil is introduced through holes (shown by dashed lines) arranged in a staggered order.

Figure 135*h* shows an erroneous oil-feed system in a unit where the shaft is installed in two adjacent bearings. The oil is fed to the bearings from the central hole of the shaft through radial holes. Stagnation zones form in sections *s*.

A drain hole *3* provided in the space between the bearings (Fig. 135*i*), or oil supply into space *4* between them (Fig. 135*j*), ensures correct circulation of the oil.

In a bearing with a shoulder intended to take up unilateral axial force *P* (Fig. 135*k*) the efflux of oil on the side of the shoulder is

shut off by the thrust shoulder of the shaft. A stagnation zone forms
in section s, and too little oil is fed to the thrust shoulder. In the
design shown in Fig. 135l, the error is aggravated by the fact that
the diameter of the shoulder on the bearing exceeds that of the shaft
shoulder. In the course of wear the latter cuts into the bearing shoul-
der and hampers still more the oil outflow. Fillets between the end
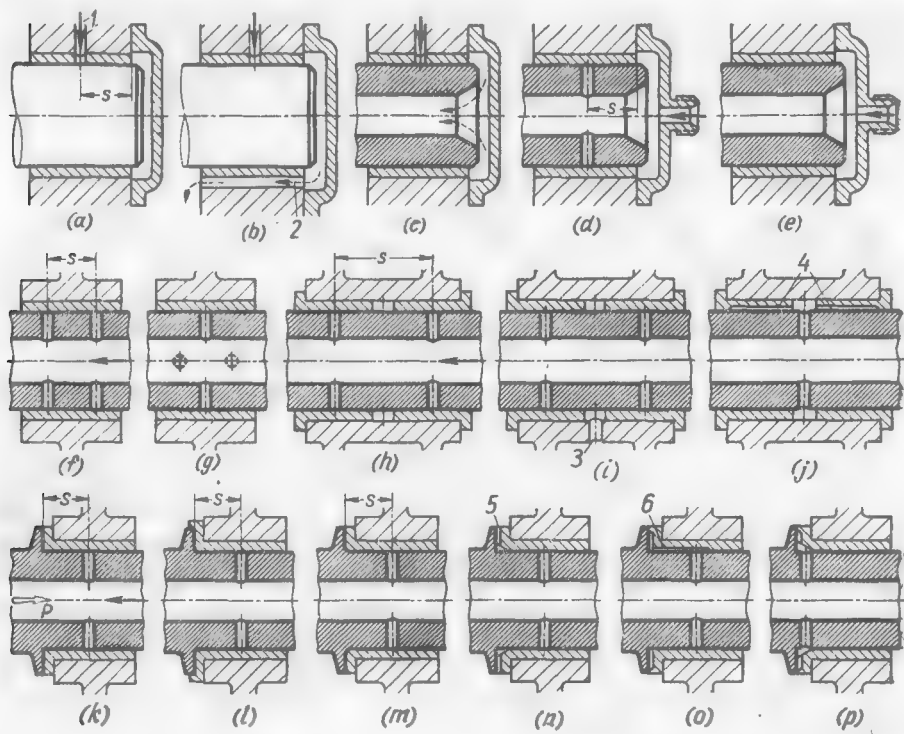
Fig. 135. Circulation of oil

and cylindrical surfaces (Fig. 135m) should be avoided. Due to ma-
nufacturing inaccuracies the fillet of the shaft may encroach upon
the fillet of the bearing and shut off the access of oil to the thrust
surfaces.

Proper oil circulation will be ensured, if radial grooves 5 for the
oil outflow are made in the thrust surface of the bearing (Fig. 135n).
In the design in Fig. 135o the grooves communicate with the oil-
feed holes by longitudinal slots 6 cut in the unloaded zone of the
bearing. The radial grooves are made blind to prevent rapid oil
ejection. In the design shown in Fig. 135p oil is fed into the annular
space formed by a chamfer on the bearing flange and then supplied
to the end and cylindrical frictional surfaces.

(e) Lubrication During Starting Periods

The maximum wear and most frequent damage to the working surfaces of bearings occur during starting when the bearings operate in conditions of semidry or semifluid friction.

In starting periods the oil is usually thick and reluctant to flow along the oil ducts. Besides, when a machine is started, the oil is not at once supplied to lubricating points due to the delay in filling the oil ducts. The supply of oil to the lubricating points can be accelerated, if the volume of the spaces in the oil line (holes in shafts, for example) is reduced by means of displacers in the form of light-alloy cores or plugged thin-walled tubes *1* (Fig. 136). The oil enters via a narrow annular space between the displacer and the shaft walls.

Fig. 136. Feed of oil during starting periods

Bearings installed in oil-containing spaces have oil collectors *2* which feed the bearings during starting periods with the foamed oil accumulated therein.

In critical machines the bearings are lubricated during starting by a self-contained system using an electrically-driven pump.

2.6. Elimination of Edge Loads

The operating ability of bearings depends on the uniformity of the load distribution along the bearing axis and the position of the load-carrying surface with respect to the acting forces.

Figure 137*a* illustrates a wrong position of the bearing of an idle gear. The force acting on the gear is applied to the bearing eccentrically. High unit loads develop at the bearing edges (especially at the edge closest to the plane of action of this force). Besides, the shaft is not rigid, and the design as a whole is inoperable.

In the design with an elongated bearing (Fig. 137*b*) the load is primarily taken up by the bearing portion disposed in the plane of action of the force, while the rest of the bearing hardly operates at all.

It is better to place the bearing centrally with respect to the plane of action of the force. In the design shown in Fig. 137*c* the bearing is too short; the small load-carrying surface and low ratio *l/d* reduce its operating ability.

In the design in Fig. 137*d* the load-carrying capacity is increased by making the gear support longer, but in this case the separation

of the bearing into two bushings with a low ratio l/d is irrational. A solid bearing (Fig. 137e) with the maximum diameter permitted by the gear design exhibits the greatest load-carrying capacity with minimum axial dimensions.
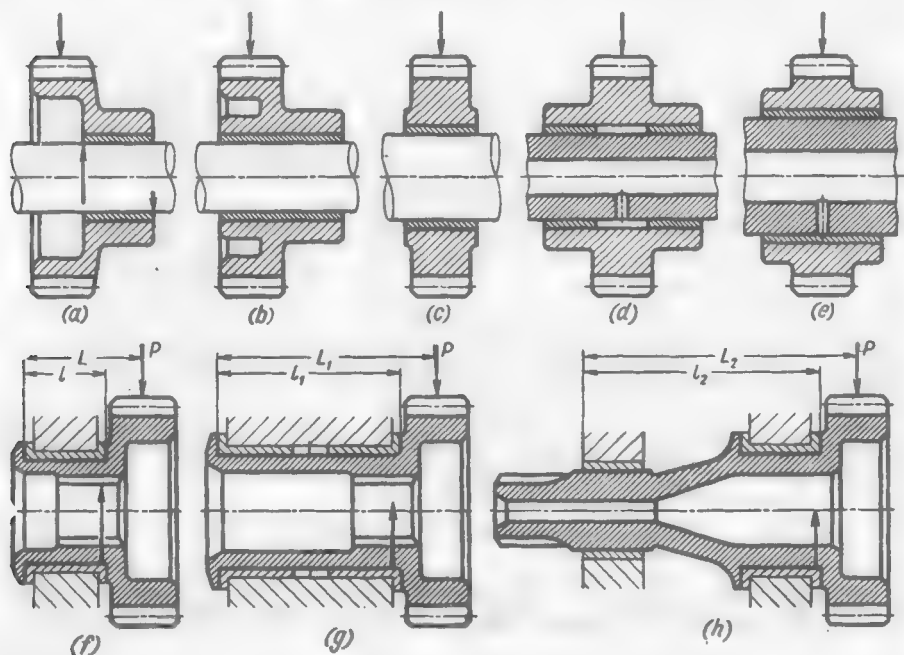
Fig. 137. Diminishing edge loads

It is a mistake to mount a cantilevered gear in a bearing in a housing as shown in Fig. 137f: the bearing is too short and the edge pressures, high.

The force acting on the edge nearest to the gear is approximately equal to PL/l.

The accuracy of the radial fixation of the gear is low.

The load causes the gear axis to shift through an angle α whose tangent is Δ/l, where Δ is the diametral clearance in the bearing. The gear misalignment increases still more as the edges wear down.

In the design shown in Fig. 137g the error is corrected by increasing the gear support length and using two bearings. In this case the force on the edge nearest to the gear is less ($\approx P \dfrac{L_1}{l_1}$); the tangent of the axis angle is $\tan \alpha = \Delta/l_1$. The shortcoming of the design is the uneven load on the bearings; the bearing farthest from the gear is loaded less than the one closest to it.

In the rational design shown in Fig. 137h the unit load on the bearings is about the same. The edge pressures are reduced by placing the bearings farther apart. The tangent of the axis angle is $\dfrac{\Delta + \Delta_1}{2l_2}$ where Δ is the clearance in the front bearing and Δ_1, that in the rear bearing.

With the dimensions shown on the drawing, the edge forces in the designs (f), (g), (h) are in the ratio 1 : 0.75 : 0.7, and the tangents of the axis angle, 1 : 0.45 : 0.25, respectively.

2.7. Bearings Operating in Conditions of Semifluid and Semidry Friction

It is not always possible and economically justifiable for design considerations to provide for circulatory lubrication and thus ensure fluid friction.

Periodic lubrication is sufficient for the bearings of auxiliary drives acted upon by small loads and operating at moderate rotational speeds. Fluid friction is out of the question in bearings which carry high loads at low rotational speeds, or in the case of oscillatory motion (bushings of levers, leaf spring bearings, etc.).

With their material, design parameters and lubrication being selected correctly, semifluid-friction bearings operate reliably enough.

Bearings operating in conditions of semifluid friction in oil-containing spaces are most often lubricated with foamed oil through holes in the bearing housing (Fig. 138a). The oil is collected in troughs connected by a hole to the oil gap of the bearing (Fig. 138b).
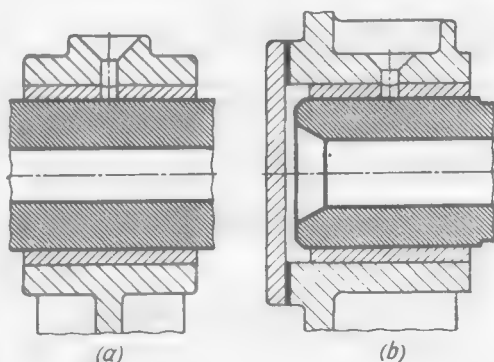
Fig. 138. Feeding oil to semifluid friction bearings

External bearings are periodically supplied with oil or grease through lubricators. Sometimes it is sufficient to place grease in a space near the bearing (*packing*). Self-lubricating porous bearings are used in places difficult of access, and plastics bearings (mainly polyamide bearings), for small loads.

The coefficient of friction in bearings with a periodic supply of oil varies, depending on the lubricating and operating conditions, from values corresponding to fluid friction to those corresponding to semidry friction.

Approximate values of coefficients f of semidry friction for some bearing materials (liquid-oil lubrication) are given below.

Tin babbitts	0.01-0.02
Lead babbitts	0.015-0.025
Lead bronze	0.02-0.03

Aluminium alloys	0.03-0.04
Bronze grade Бp.АЖ	0.04-0.05
Antifriction cast iron	0.05-0.08

The calculation of semifluid-friction bearings is complicated because of the uncertain coefficient of friction and heat withdrawal conditions. To improve the load-carrying capacity and reliability of bearings operating in conditions of semifluid friction, it is recommended to do the following:

(a) reduce unit pressure k by increasing the diameter (but not the length) of the bearing. Never employ the ratio $l/d > 1.2$;

(b) ensure an abundant supply of oil of increased viscosity and oiliness and high adsorbability on metal surfaces. It is good practice to introduce antiseize additions;

(c) use babbitt-lined bearings for small loads and relatively high peripheral speeds, bearings lined with lead bronze for increased loads, and bronze bearings for high loads and low rotational speeds.
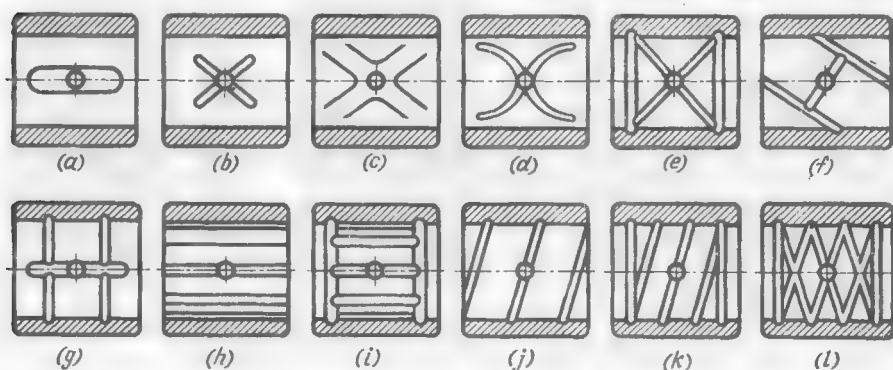
Fig. 139. Oil grooves in semifluid friction bearings

The hardness of shafts must not be below $50 Rc$. The shaft surface should be machined to the maximum economically justifiable finish. It is advisable to subject the shaft surface to sulphidizing or siliciding.

The clearances in the bearings with a semifluid friction are made smaller than in fluid-friction bearings ($\psi = 0.0005\text{-}0.001$). If an abundant supply of oil is provided, the clearance is increased to the usual values of $\psi = 0.001\text{-}0.002$.

Floating bushings are practicable in many cases.

Oil grooves may be cut both in unloaded and loaded zones.

Since in these bearings there is no positively formed oil film with typical high and low pressure zones, the grooves only negligibly weaken the load-carrying capacity of the bearings (to the extent of reducing the bearing surface area)

and play at the same time the useful role of accumulating reservoirs which feed oil to the bearing when the general oil supply is interrupted.

Typical shapes of oil grooves are illustrated in Fig. 139.

Through grooves (Fig. 139*f, h, j*) are used to intensify heat withdrawal (with abundant lubrication). The grooves are made blind (Fig. 139*a-d, g*) in bearings with a limited supply of oil. In bearings lubricated with grease *annular grooves* (Fig. 139*e, i, k, l*) are provided near the end faces, which serve to retain grease.

Bearings with closely spaced longitudinal grooves (Fig. 139*h, i*) are used in the case of oscillatory motion of low amplitude.

2.8. Antifriction Properties of Materials

The following properties of shaft and bearing materials are essential for proper functioning of a bearing in conditions of fluid and semifluid friction.

Mechanical strength. The maximum loads that can be carried by a bearing are determined by the compression strength of the bearing metal at the working temperature. The load on a bearing made of the softest bearing metal (babbitt) depends in a large measure on its fatigue limit at an increased temperature. An excessive load on the bearing, especially when its shell or housing are not rigid enough, causes fatigue cracks resulting in the spalling of the lining.

Wettability with oil. The lubricant forms on some materials strong adsorbed films which are retained on the surface of the metal and thus prevent dry friction even with an insufficient supply of oil. Best of all oil wets babbitts, somewhat worse, bronze and still worse, brass. Teflon is hardly wetted at all. Adsorption can be increased, if activating additions (oleic and palmitic acids) are introduced into the oil.

Coefficient of semidry friction. The magnitude of the coefficient of semidry friction largely determines heat generation in semidry and semifluid friction and, therefore, the operating ability in conditions of scanty lubrication. The lowest coefficient of friction is observed in the case of steel sliding upon tin babbitt; it is much higher when steel slides upon lead bronze and aluminium alloys. Colloidal graphite, molybdenum disulphide and sulphur added to oil will reduce the coefficient of semidry friction.

Heat conductivity. The higher is the heat conductivity of a material, the better is the heat generated in the oil layer withdrawn. For this reason, bearings made of materials with a low heat conductivity (plastics, for example) have, as a rule, a lower load-carrying capacity than those made of metals exhibiting good heat conductivity.

Heat conductivity is extremely important in the case of a short-time local temperature rise brought about by the development of the foci of semifluid or semidry friction. Heat-conductive materials withdraw heat faster and prevent in many a case the breakdown of the bearing.

Wear-in properties. The wear-in process consists in the smoothing down of microirregularities and protruding portions on the bearing surface, which stem from manufacturing and assembly inaccuracies.

In bearings made of soft materials (babbitt, and partly lead bronze) the principal role is played by the plastic deformation of the material under the action of increased pressures and temperatures arising on the protruding portions. Wear-in in such bearings not only smoothes down micro- and macroirregularities (waviness and other errors in correct cylindrical form) but also causes the material to sag at the points of local increase in pressure (for example, edge pressures due to elastic deformations of the shaft).

Practically no plastic deformation takes place in bearings made of hard materials (bronze, cast iron). Wear-in here boils down to the shearing off and crumbling out of the microcrests. In such bearings macroirregularities cannot be eliminated by wear-in.

Antiseize properties. Metals similar in their atomic-crystal lattice and physical and chemical properties tend to weld together in conditions of semidry friction. The process begins with a transfer of the particles of one metal onto the other (galling). The stuck-on particles entrain other particles into the process until the surface grows so uneven that the bearing becomes *seized*. This phenomenon is mostly observed when a shaft which has not been subjected to heat treatment slides upon bronze. After overheating and seizure, the shaft surface is sometimes entirely covered by a layer of bronze.

Multiple-phase copper-tin, copper-aluminium and tin-antimony bearing alloys with a plastic matrix and hard structural components effectively resist seizure. The antiseize properties of steel improve when nonmetal components (nitrides, sulphides and silicides) are incorporated into the structure.

Antiseize additions (silicone fluids, triphenylphosphate) introduced into the oil have a favourable effect.

Wear resistance. The harder the surface of the shaft material, the higher its wear resistance. The Brinell hardness scale characterizes wear resistance most accurately.

Sulphidizing and siliciding (saturation of the surface layer of a shaft with sulphur and silicon) sharply increase wear resistance. Despite the fact that the surface hardness is not improved in this case (as is the case with other types of thermochemical treatment), the wear resistance of sulphidized and silicized shafts increases by 10-20 times. At the same time the tendency to galling and seizure is diminished.

There is no direct relationship between hardness and wear resistance in bearing materials. High-tin babbitts, plastics and rubber exhibit high stability against attrition despite their softness.

Corrosion resistance. Bearing materials must effectively resist the action of acids appearing in the oil after a long period of operation at high temperatures. Pb, Zn and Cd are most vulnerable to corrosion.

Corrosion can effectively be prevented by the diffusion saturation of the surface layer of bearing materials with indium.

Chemical neutrality. Bearing materials must be chemically neutral with respect to oil. Most of the antifriction metals satisfy this condition, except for Pb and Cu which catalytically accelerate the oxidation of oil at increased temperatures.

When these metals are present in the bearing alloy anti-oxidizing additions (metal-organic compounds of S, P and N) should be introduced into the oil.

Machinability. The finish of friction surfaces depends to a certain extent on the machinability of the materials. Some bearing materials (for example, hard bronze, thermoplastics) are difficult to machine to high finish with cutting tools. Babbitts, plastic bronzes and aluminium alloys can be machined easily.

As a rule, the harder the surface of steel shafts, the better their machinability.

2.9. Bearing Materials

There exist plastic ($Bhn < 50$), soft (Bhn 50-100) and hard ($Bhn > 100$) bearing alloys.

The plastic materials include babbitts, lead bronzes, plastic aluminium alloys and silver; soft alloys are soft bronzes (tin, tin-lead, tin-lead-zinc bronzes) and aluminium alloys; hard alloys are hard bronzes (aluminium-iron bronzes) and cast irons.

Highly loaded high-speed bearings intended to operate in the region of fluid friction use almost exclusively the plastic alloys in the form of thin layers deposited on steel (more rarely bronze) bushings and shells.

The soft and hard alloys are used to make bearings operating in conditions of mixed and semifluid friction and at moderate speeds.

(a) Babbitts

Babbitts are alloys of soft metals (Sn, Pb, Cd, Sb, Zn) incorporating hard structural components in a plastic matrix.

Babbitts are distinguished by their low coefficient of semidry friction and good plasticity, wear-in properties and wear resistance.

Plasticity ensures uniform load distribution over the bearing surface, and it is not so dangerous if fine hard particles (metal dust, hard products of oil oxidation) get into the bearings. These particles are pressed into the babbitt and become quite harmless.

The disadvantage of babbitts is their low fatigue resistance, especially at high temperatures.

Babbitts can work in pair with normalized and structurally improved steel shafts (25-35 Rc). However, to increase the reliability and service life of the bearings it is expedient to subject the shafts to hardening with low tempering (50-55 Rc).

The highest antifriction properties are displayed by *high-tin babbitts* which are tin-antimony alloys with a small addition of copper (introduced to prevent liquation). The structure of babbitt is formed by hard crystals of SnSb imbedded into a plastic eutectic.

The main high-tin babbitt grades (Soviet nomenclature) are Б89 and Б83 (the figures indicate the tin content in per cent).

They have a heat conductivity of 25-35 cal/m·h·°C and linear expansion coefficient of (22-24) 10^{-6}. Their modulus of normal elasticity $E = 5000$-6000 kgf/mm^2, specific weight, 7.3 gf/cm^3, Brinell hardness at 20°C, 20-30, and the yield point in compression, 4-6 kgf/mm^2. At 100-120°C the hardness and yield point drop by about 50 per cent.

The melting point of tin babbitts: initial 240-250°C, and final—400-420°C. Babbitt is poured at 450-480°C onto shells preheated to 250°C.
Centrifugal lining of shells with babbitt gives the best results. Chill and pressure die casting are also used.

The thickness of the babbitt lining in bearings of ordinary design is 1-3 mm. The cyclic strength of the babbitt lining increases with a reduction in the thickness of the lining layer and with an increase in the rigidity of the shell-bed system. Of late, lining is made up to 0.25-0.4 mm thick. Still better results are obtained when a babbitt layer 10-20 μm thick is electrolytically deposited onto a backing of porous bronze.

The drop of the babbitt lining strength at high temperatures can be prevented by an intensive oil cooling of the bearings. All this makes it possible to increase the unit loads on babbitt-lined bearings to 100-150 kgf/cm².

Scarce tin can be saved by making use of *low-tin babbitts* which are more or less effective substitutes for high-tin babbitts.

Lead-tin babbitt grades Б16, Б6, БН, БТ (Soviet nomenclature) contain 60-75 per cent Pb, 5-20 per cent Sn and 10-20 per cent Sb, with small additions of Cu, Cd, Ni and Fe. Some 0.5-1 per cent As is introduced as an inoculant.

The antifriction properties of lead babbitts in conditions of semifluid friction are lower than those of high-tin babbitts.

The heat conductivity of such babbitts is 10-20 cal/m·h·°C, specific weight, 9.5-10 gf/cm³. Their hardness and mechanical properties are about the same as those of tin babbitts. The resistance to corrosion is much lower.

In conditions of purely fluid friction there is almost no difference between lead and tin babbitts.

Tinless babbitt grades БК1 and БК2 (Soviet nomenclature) consist almost entirely of lead with additions of approximately 1 per cent Ca and Na. The antifriction properties and corrosion resistance of lead babbitts can be improved by small additions of Sr, Ba, Zi and Te.

The composition and properties of tin and lead babbitts are given in Table 20.

Cadmium babbitts contain 90-97% Cd with small additions of Cu, Ni, Ag and other metals forming hard structural components in the plastic cadmium matrix. The Brinell hardness of cadmium babbitts is 30-40, the linear expansion coefficient, about $30 \cdot 10^{-6}$, and heat conductivity, 70-80 cal/m·h·°C.

Their antifriction properties are high. The disadvantage of cadmium babbitts is their low resistance to corrosion.

Aluminium-tin alloys with up to 20% Sn are used in bimetal thin-walled shells. Most widespread are the A020 grade alloys (20% Sn, 1% Cu, balance Al) and an alloy containing 6% Sn, 1% Cu, 0.5-1% Ni, 1-1.5% Si (balance Al). The hardness of aluminium alloys is 35-45 BH, heat conductivity, 150-200 cal/m·h·°C, linear expansion coefficient, $(20 \text{ to } 22) 10^{-6}$, and specific weight, 2.7 gf/cm³.

Aluminium alloys possess high cyclic strength and can bear unit loads of up to 500 kgf/cm². They are liable to galling on the shaft. An intensive flow of oil through the bearing is required, as well as the use of shafts with increased hardness ($Rc > 40$).

Uncritical bearings are made of inexpensive *zinc-aluminium* alloys of grades ЦАМ 10-5 (10% Al, 5% Cu, balance Zn) and ЦАМ 9-1.5 (9% Al, 1.5% Cu). Their hardness is 60-80 BH, linear expansion coefficient, $(30-32) 10^{-6}$, and specific weight, 6.2 gf/cm³. The antifric-

Table 20

Babbitts

| Grade | Composition, % | | | | | | Bhn | Specific weight, gf/cm³ | Strength, kgf/mm² | | Relative elongation, % |
	Sn	Sb	Cu	Pb	Ca	other elements			tensile	compressive	
Tin babbitts											
Б89	88-90	7-8	2.5-3.5	<0.3	—	—	24	7.3	8	11	10
Б83	82-84	10-12	5.5-6.5	<0.3	—	—	30		9	11.5	6
Lead-tin babbitts											
Б16	15-17	15-17	1.5-2	64-68	—	—	30	9.5	8	12	0.2
Б6	5-6	14-16	2.5-3	72-75	1.8-2	0.5-1 As	32		7	10	0.2
БН	9-11	13-15	1.5-2	70-75	1.2-1.7	{ 0.5-1 As, 0.8-1 Ni	30		7	13	1.7
БТ	9-11	14-16	0.7-1	72-75	—	0.1-0.2 Te	20		6	13	1.8
Lead babbitts											
БК1	—	—	—	99-98.5	0.9-1.2	0.6-0.9 Na	30				
Б52	1.5-2.5	—	0.15	96-98	0.3-0.5	0.6-0.9 Na	—	10.5	8-10	12-15	2.5-3
БКА	—	—	—	98-99	0.9-1.2	0.6-0.9 Na	30				
						0.1-0.2 Al	—				

tion properties of zinc-aluminium alloys are moderate. Shafts with $Rc > 50$ must be used. The best qualities are displayed by nonstandard high-aluminium zinc alloys (30-40% Al, 5-10% Cu); their hardness is 50-60 *BH*.

(b) Lead Bronzes

Lead bronzes are alloys of Cu (40-70 per cent) and Pb (60-30 per cent) with additions of small quantities of Sn, Zn, Ni and Ag. The lead bronze grades commonly used in the Soviet Union are Бp.C-30 (30% Pb, balance Cu) and Бp.OC 5-25 (5% Sn, 25% Pb, balance Cu). Use is also made of high-lead nickel bronze grade Бp.CH 60-2.5 (60% Pb, 2.5% Ni).

Lead is practically insoluble in copper and is present in alloys in the form of round inclusions more or less uniformly distributed in the copper matrix.

Lead bronzes are stronger and harder than babbitts (40-70 *BH*). As distinct from babbitts, the hardness and strength of bronzes remain practically constant at temperatures of up to 200°C. Their heat conductivity is 100-110 cal/m·h·°C.

The disadvantage of lead bronzes is their low resistance to corrosion (due to the presence of free lead). Besides, lead accelerates the oxidation of oil during operation.

The wear-in and antifriction properties of lead bronzes are worse than those of babbitts. The friction surfaces of bearings lined with lead bronze must be machined to a very high finish, misalignments must be eliminated, the rigidity of the shaft-bearing system increased, the flow of oil intensified, the oil carefully filtered and the surface hardness of the shaft improved ($Rc > 50$). The clearances in bearings lined with lead bronze are made, on the average, 30-50 per cent greater than in babbitt-lined bearings. The oil used should have a low acid number (< 1 mg KOH/g) and contain anti-oxidation additions.

The working surfaces of bearings lined with lead bronze are fine bored with diamond or cemented-carbide cutters at low feeds and high cutting speeds (600-800 m/min).

Lead bronze is poured in a layer 0.5-0.8 mm thick onto shells of low-carbon steel in graphite moulds at 1050°C.

To avoid liquation and obtain a uniform and finely dispersed distribution of lead in the alloy the shells are intensively cooled with water pulverized by compressed air immediately after lining.

Improved compositions of lead bronze have been developed with 30 per cent Pb and additions of Ni (up to 5 per cent), Sn (up to 25 per cent) and small quantities of S and Ca. The addition of Ni improves corrosion resistance, and S and Ca are introduced to prevent the liquation of lead.

Alongside high-lead bronzes, bearings may also be lined with plastic bronzes (60-80 *BH*) containing 5-7 per cent lead 5 per cent phosphorus and 5 per cent zinc.

(c) Silver

Bearings with their friction surface made of silver (with an addition of small quantities of Sn and Pb) are used for heavily loaded shafts of machines produced in small lots.

Silver coatings are plastic and soft (25-35 *BH* in an annealed state) and possess good antifriction properties and high endurance.

The heat conductivity of silver coatings is high (300-350 cal/m·h·°C). Their linear expansion coefficient is $18 \cdot 10^{-6}$. The modulus of elasticity $E = 8200$ kgf/mm^2. The melting point is 960°C.

Silver is either poured onto the surface of shells in a layer 0.1-0.3 mm thick or deposited electrolytically on porous bronze or copper-nickel backing in a layer 20-50 μm thick.

In some cases the bond with the shell can be improved, if silver is poured onto a finely cellular steel backing. The portions of the steel matrix protruding onto the surface increase the load-carrying capacity of the bearing.

To improve wear-in, the surface of the silver lining is covered by a layer of lead or lead-antimony alloy 10-30 microns thick, on which a layer of indium several microns thick is placed to prevent corrosion.

The shafts used must have an increased hardness ($Rc > 50$).

(d) Multi-Layer Coatings

In the case of a multi-layer lining a thin layer of tin babbitt is placed on a backing made of an antifriction alloy 0.2-0.5 mm thick. This method utilizes to the full the valuable properties of tin babbitt, sharply reduces the consumption of tin and increases at the same time the cyclic strength of the lining and its resistance to impact loads.

Lead bronzes, aluminium alloys and bronzes are commonly used as the backings. The best results are obtained with porous backings from sintered Cu-Al and Cu-Ni (60% Cu, 40% Ni) alloys which ensure a strong bond between the babbitt lining and the shell.

Two babbitting methods are in use. The first method consists in pouring a layer of babbitt 0.3-0.4 mm thick. After the finish machining of the shells the thickness of the babbitt layer is about 0.15-0.2 mm.

The second method is more preferable. By this method babbitt is electrolytically deposited to a depth of 15-20 μm. In this case, the finish machining can be dispensed with. This method requires

the use of a porous backing which, being impregnated with babbitt, forms an antifriction sublayer and allows] the bearing to operate properly when the surface layer of babbitt becomes worn locally or completely.

Sometimes lead babbitt is used for the surface layer. Corrosion is prevented by a layer of indium several microns thick electrolytically deposited onto the babbitt lining. This layer is then subjected to diffusion by heating to 150°C and holding for two or three hours.

A promising method is the coating of friction surfaces with micron-thick metal-polymer films composed of glycerol-phthalate varnish or epoxide resin with an addition of 2-3 per cent colloidal iron (organosol of iron).

The films reduce the coefficient of friction, improve wear- in and increase the wear resistance of bearings.

The positive effect of metal-polymer films obviously accrues from the property of high-dispersion colloidal particles of iron to orient the oil molecules and thus increase the stability of the boundary layers of the oil. At the same time, one can observe a definite mechanical effect—the filling of the pits of microirregularities—which reduces oil leakage through the microirregularities and thus increases the carrying capacity of the hydrodynamic oil layer.

(e) Bronzes

Bronzes are used to make bearings which are to operate mainly in the region of semifluid friction at small peripheral speeds (bearings of auxiliary drives). Their high hardness allows them to endure high unit loads.

Tin, tin-lead and tin-zinc-lead bronzes are most popular (Table 21).

Good antifriction properties are displayed by tin bronzes of the Бp.OФ variety. Tin bronzes with a tin content of more than 0.5 per cent are cast (preferably in chills) and those with a tin content of less than 0.5 per cent are die-forged. The hardness of the latter can be reduced to 50-60 *BH* by soft annealing.

Tin-lead bronzes of the Бp.OC variety are close to tin bronzes. The addition of lead improves the machinability and plasticity and reduces the hardness of the bronze. Bronze grade Бp.OC 5-25 ranks among semiplastic types of bronze.

The most wide use is made of tin-zinc-lead bronzes in which the content of scarce tin is reduced to 2-6 per cent. These bronzes are more plastic than tin bronzes (elongation 6-15 per cent) and their hardness is 50-70 *BH*.

Tin-zinc-lead bronze grade Бp.OЦC 4-4-2.5 is used in the form of cold-rolled strips to make thin-walled bushings.

Aluminium-iron bronzes of the Бp.AЖ variety have an increased hardness (70-100 *BH*) and are used for making bushings intended to operate at high loads and low speeds in conditions of semifluid and semidry friction (for example, guide bushings of intake valves in internal-combustion engines).

Table 21

Antifriction Bronzes

Grade	Composition, % (balance Cu)						Ultimate strength, kgf/mm²	Relative elongation, %	BH
	Sn	Zn	Pb	Al	Fe	other elements			
Tin bronzes									
Бр. ОФ 6.5-0.15	6-7	—	—	—	—	(0.1-0.15) P	25-35	2	70-80
Бр. ОФ 10-1	9-11	—	—	—	—	(0.8-0.2) P	20-30	3	80-100
Tin-lead bronzes									
Бр. ОС 10-10	9-11	—	9-11	—	—	—	20	3	70
Бр. ОС 8-12	7-9	—	11-13	—	—	—	18	3	65
Бр. ОС 5-25	4-6	—	24-26	—	—	—	12	4	45
Tin-zinc-lead bronzes									
Бр. ОЦС 3-12-5	2-4	11-13	4-6	—	—	—	18	6-8	60
Бр. ОЦС 4-4-2.5	3-5	3-5	1.5-3.5	—	—	—	35	15-20	60
Бр. ОЦС 4-4-17	3-5	3-5	16-18	—	—	—	20	8-10	50
Бр. ОЦС 5-5-5	4-6	4-6	4-6	—	—	—	20-25	6-10	60
Бр. ОЦС 6-6-3	5-7	5-7	2.5-3.5	—	—	—	15-20	8-12	70
Aluminium-iron bronzes									
Бр. АЖС 7-1.5-1.5	—	—	1-2	6-8	1.2	—	30	15	70
Бр. АЖ 9-4	—	—	—	8-10	3.5-5.5	—	50	10	100
Бр. АЖН 10-4-4	—	—	—	9-11	3.5-5.5	(3.5-5.5) Ni	60	5	170
Бр. АЖН 11-6-6	—	—	—	10-12	5-7	(5-7) Ni	60	2	220

Bearings operating at high temperatures with semidry or dry friction (guide bushings of exhaust valves) are made of heat-resistant aluminium-iron-nickel alloys of the Бр.АЖН type.

The heat conductivity of antifriction bronzes is 50-100 cal/m·h·°C, linear expansion coefficient, $(16$ to $18) \cdot 10^{-6}$, and modulus of elasticity $E = 8000$-$10,000$ kgf/mm^2.

Shafts operating in bronze bearings of medium hardness must be rated at $Rc > 50$, and those operating in bronze bearings of high hardness, at $Rc > 55$.

(f) Antifriction Cast Irons

Antifriction cast irons can be used as inexpensive substitutes for bronzes. Common types of the cast iron are: gray iron grade АСЧ with laminated graphite, high-strength iron grade АВЧ with globular graphite, malleable cast iron grade АКЧ with flaky graphite and copper-bearing cast iron grade ЧМ (see Table 22).

The disadvantages of antifriction cast irons are their brittleness and high hardness (160-250 BH) that make their self-wear-in impossible. Cast-iron bearings are sensitive to misalignment causing high edge pressures.

Cast-iron bearings are used with shafts having very high surface hardness ($Rc > 55$). Soft antifriction cast irons (grades АСЧ-3, АВЧ-2, and АКЧ-2) can operate under small loads in pair with normalized or structurally improved steel (Rc 25-35).

(g) Light Alloys

Out of all light alloys aluminium alloys are the ones most frequently used as antifriction materials.

Uncritical bearings are manufactured from cast Al-Si alloys (grades АЛ2, АЛ4, АЛ5), Al-Mg alloys (grade АЛ8), Al-Cu alloys (grades АЛ10В, АЛ18В) preferably by casting into metal moulds (65-70 BH). It is more economical to make bearings by closed-die forging using deformable alloys grades АК2, АК4, АК4-1 (80-90 BH).

Wide use is made of untreated (40-60 BH) alloys grades АМ8 (8% Cu), АМК2 (8% Cu, 2% Si), АЖ6 (6% Fe), АН 2,5 (2.5% N), АСС6-5 (6% Sb, 5% Pb). The plastic alloys grades АМК2 and АН2,5 (35-45 BH) are used in bimetal strip shells.

The highest antifriction properties are exhibited by tin-aluminium alloys (up to 20 per cent Sn). One of the best alloys of this type, combining good plasticity and high strength, is composed of 6% Sn, 1.5% Ni, 0.5-1% Sb, 0.5% Si, 0.5-1% Mn, balance Al.

The hardness of antifriction aluminium alloys is 40-80 BH, heat conductivity, 100-200 cal/m·h·°C, linear expansion coefficient, $(21$ to $24)$ 10^{-6} and modulus of elasticity E, approximately 7000 kgf/mm^2.

Table 22

Antifriction Cast Irons

Grade	Composition, %								BH
	C	Si	Mn	Cr	Ni	Cu	P	S	
АСЧ-1	3.2-3.6	1.6-2.4	0.6-0.9	0.2-0.35	0.2-0.4	⩽0.7	0.15-0.2	⩽0.12	180-230
АСЧ-2	3.2-3.8	1.4-2.2	0.4-0.7	0.2-0.4	0.2-0.4	0.3-0.5	0.15-0.4	0.1	190-230
АСЧ-3	3.2-3.8	1.7-2.6	0.4-0.7	—	0.3	0.3-0.5	0.15-0.4	0.1	160-190
АВЧ-1	2.8-3.5	1.8-2.5	0.5-1.2	—	—	0.3-0.7	0.2	0.03	210-260
АВЧ-2	2.8-3.5	2.2-2.7	0.5-0.8	—	—	—	0.2	0.03	170-200
АКЧ-1	2.6	0.8	0.3	0.6	—	—	0.15	0.1	200-220
АКЧ-2	3.0	1.3	0.6	—	—	—	—	—	170-200
ЧМ-1.3	2.3-3.0	0.5-1.1	0.6-1.2	0.15	—	2.0	0.2	0.1	190-260
ЧМ-1.8	2.8-3.6	1.3-1.9	0.6-1.2	0.2-0.4	—	1.5-2	0.3	0.1	210-260

The ultimate strength of cast alloys is 12-18 kgf/mm² and of die-forged alloys, 20-30 kgf/mm². Aluminium alloys are corrosion resistant and do not oxidize oil.

Their disadvantage is their poor wear-in properties and tendency to galling on the shaft. Oil must be supplied under pressure and the shafts must have an increased hardness ($Rc > 50$).

The modulus of elasticity of aluminium alloys is rather low. For this reason a higher bearing rigidity (thicker walls, rigid shoulders, stiffer beds) is required to ensure normal operation.

The design of bearings made of aluminium alloys must take account of their high coefficient of linear expansion. Heating increases the clearance in the bearing. Therefore, the "cold" clearance is reduced to the minimum in agreement with the conditions of reliable bearing' operation during starting periods. Besides, heating increases the interference on the seating surface of the bearing. Aluminium-alloy bearings are mainly used in housings made of the same alloys.

Bushings manufactured from aluminium alloys and installed in housings made of materials with a low coefficient of linear expansion (steel, cast iron) may develop residual compressive deformations with a rise in temperature. In such cases use is made of minimum interferences and the bushings are always locked. It is good practice to increase the diameter of the lock pins so that the bearing material is not crushed.

The bushings are provided with an expansion or contraction joint in the unloaded zone to compensate for the change in the linear dimensions of the bushings consequent upon heating. Such bushings are installed in the housing with interference which maintains more or less the same magnitude during temperature fluctuations. Bushings with such a joint must be secured against rotation.

Magnesium alloys, as antifriction material, are close to aluminium alloys, but differ from the latter by their lower modulus of elasticity ($E = 4200$ kgf/mm²) and higher linear expansion coefficient [$\alpha = (26$ to $28)$ 10^{-6}].

Cast magnesium alloys grades MЛ3 and MЛ4, and deformable alloys grades MA1 and MA2 may be used to make bearings.

The hardness of magnesium alloys is 30-40 BH. Their heat conductivity is 60-70 cal/m·h·°C.

In designing bearings of magnesium alloys the same rules as for aluminium alloys must be observed.

Comparative Characteristics of Bearings Alloys

The comparative characteristics of plastic bearing alloys are given in Table 23.

The wear-in and antiseize properties, resistance to corrosion, effect on oil oxidation and cyclic strength (the last column in the table) are estimated by a five-mark system (mark 5 is the highest).

Properties of Bearing Materials

| Material | BH at | | Maximum allowable temperature, °C | Minimum allowable hardness of shaft, Rc | Wear-in properties | Anti-seize properties | Corrosion resistance | Effect on oil oxidation | Fatigue limit |
	20° C	150° C							
Tin babbitts	20-30	6-12	150	25	5	5	5	5	1
Lead babbitts	15-20	6-12	150	25	5	5	3	1	1
Multi-layer coatings (upper layer is babbitt)	20-30	6-12	250	25	5	5	5	5	4
Cadmium babbitts	30-40	15	250	30	4	5	1	4	2
Lead bronzes	40-70	40-60	300	45	2	3	2	2	4
Silver	25-30	25-30	400	45	3	4	5	5	5
Tin bronzes	60-80	60-70	400	45	1	1	4	4	5
Plastic aluminium alloys	35-40	32-46	300	45	2	2	5	5	4

(h) Metal Ceramics

Bearings operating in conditions of semidry friction with scanty lubrication or without oil at all are made of selflubricating metal ceramic bronze-graphite and iron-graphite compositions obtained by pressing and sintering metal and graphite powders.

Metal ceramic materials are distinguished by their microporosity (volume of pores 20-40 per cent) and the ability to imbibe large quantities of oil.

Before use the bearings made from such materials are impregnated with turbine oil at 100-120°C. This store of oil is sufficient for several months of operation without lubrication. Impregnation must periodically be repeated (after dissolving the used oil).

Such bearings are provided with pockets filled with oil to prolong their service life.

The highest quality is observed in iron-graphite compositions (*voisites*) which are a mixture of 97-98 per cent of iron obtained by electrolytic sedimentation with 2-3 per cent of graphite and small additions of powdered Cu and Pb. Up to 7% Ni is introduced to increase plasticity and impact strength.

Iron-graphite compositions are more stable against oxidation than bronze-graphite ones.

Powdered iron and graphite are pressed in moulds under a pressure of 1500-2000 kgf/cm² and sintered at 1050-1100°C for 2-3 hours. The final dimensions are imparted to bearings by sizing under a pressure of 500-800 kgf/cm² (the dimensional accuracy is within hundredths fractions of a millimetre). Iron-graphite compositions have poor machinability.

During sintering, graphite combines with iron and forms ferro-cementite mixtures with inclusions of free graphite. The metal acquires the structure of gray iron which, depending on the composition of the charge and sintering conditions, may have a ferritic, perlitic or cementite matrix (a perlitic matrix is preferable).

The grades of Soviet-made iron-graphite compositions (the first figure indicates the content of graphite in the charge and the second, the per-cent volume of the pores) are:

>   ЖГ-3-30 — for light loads
>   ЖГ-7-25 — for medium loads
>   ЖГ-3-20 — for heavy loads

Iron-graphite bearings effectively operate at small peripheral speeds and under moderate loads. They can endure instantaneous loads of up to 300 kgf/cm².

The working temperature of bearings must not exceed 50-60°C for otherwise the pores will rapidly be clogged by the oil oxidation products and the self-lubricating property of the bearings will be lost. Shafts of increased hardness ($Rc > 50$) should be used.

The load-carrying capacity of porous bearings operating in hydrodynamic conditions (abundant lubrication, high rotational speed) is lower than that of solid bearings. The oil in the loaded zone leaves the clearance for the pores and flows along the walls of the bushing partly to the end faces, where it emerges outside, and partly into the unloaded zone from which it again returns into the clearance. In this way a continuous circulation of oil takes place in the walls of the bushing, the intensity of which (and hence, the degree of the reduction of the carrying capacity) depends on the permeability of the bearing material (dimensions and relative volume of the pores), the geometrical parameters of the bushing (length and thickness), oil viscosity (temperature of the bearing), pressure in the loaded zone and other factors.

(i) Nonmetal Materials

Such materials for bearings include plastics, hard natural wood, compregnated wood, rubber and graphite.

All these materials are used with shafts of increased hardness ($Rc > 50$). With this condition being satisfied, nonmetal bearings exhibit high wear resistance.

Nonmetal bearing materials are distinguished by their low heat conductivity. Almost all of them operate better with water than with oil.

The use of water lubrication is justified when the machine handles water (water pumps) or operates in water (propulsion screws, underwater power tools, etc.).

In individual cases water lubrication is also used in general-purpose machines. The shafts here are made of hardened stainless steel (grades 3X13, 4X13). The metal housings of the bearings must be protected against corrosion.

Plastics

Plastics bearings are predominantly used with semifluid friction (low rotational speeds, oscillatory motion) and also when it is impossible to lubricate the bearings regularly. These bearings can operate with single and periodic lubrication, and without lubrication at all at low loads and peripheral speeds. Bearings made of plastics which do not swell can function with water lubrication, and those manufactured from chemically stable plastics, with lubrication by chemically active liquids.

The allowable unit load depends on the hardness and strength of the plastic, temperature, peripheral speed, type and quantity of the lubricant fed in, and varies within 10-100 kgf/cm^2.

Plastics bearings are usually manufactured from phenoplasts (textolite), polycarbonates (diflon), polyamides (polycaprolactam, nylon), fluoroplasts (teflon). The properties of these plastics are given in Table 24. Plastics as bearing materials have the following features:

low hardness (without fillers, 5-20 BH);
low modulus of elasticity (without fillers, $E = 10^2$-10^3 kgf/mm^2);
low heat conductivity (0.2-0.3 cal/m$\cdot$h$\cdot$°C);
high linear expansion coefficient (50 to 100) $\times 10^{-6}$;
low thermal stability (80-150°C after Martens).

Phenoplasts and polyamides swell in water (the absorption of water after prolonged contact with it is up to 15 per cent by weight). Fluoroplasts exhibit a tendency to creep (the development of residual deformations under long-term action of comparatively small stresses).

The wear resistance and antifriction properties of plastics are rather high.

Plastics, especially thermoplasts, are difficult to machine. Polyamide and polycarbonate bearings are manufactured by plunger moulding, and fluoroplastic bearings are formed by hot mould pressing. Reactoplasts (phenoplasts) can be machined with cemented-carbide tools at low feeds and high cutting speeds.

In view of their low heat conductivity, high coefficient of linear expansion and easy deformation, plastics bearings are seldom made in the form of thick-walled bushings. Plastics are mainly used as thin coatings (0.1-0.5 mm thick) on metal surfaces, and also to impregnate the surface layer of porous antifriction metals (sintered bronze).

When plastics are used in thin layers, their negative features hardly affect the operation of the bearing.

Antifriction

Material	Specific weight, kgf/dm³	Hardness, BH	Strength, kgf/mm²		Modulus of elasticity E, kgf/mm²
			tensile	compressive	
Textolite	1.3-1.4	25-40	6-10	⊥ 25 ∥ 12	250-1000
Polycarb nate	1.2-1.3	20-25	8-8	8-10	200-250
Polycaprolactam	1.1-1.2	8-12	5-8	8-12	100-150
Nylon	1.1-1.2	10-20	7-12	10-15	150-200
Teflon	2.1-2.4	3-5	3-4	3-4	40-50

Note. ⊥ — across the layers, ∥ — parallel to the layers.

Solid plastic bushings are predominantly used with small diameters (less than 30 mm), low loads and rotational speeds. To account for possible volume changes in the plastics, the bearing clearances are made, on the average, 2-3 times larger than for metal bearings ($\psi = 0.003$-0.006). With large diameters, the volume changes in the bushings are compensated for by splitting them and making a straight, spiral or herringbone joint. In such bearings the clearance ratio can be increased to 0.001-0.002.

The strength of plastics is improved by introducing fibrous or fabric fillers, and their heat conductivity, by introducing metal powders (Pb, lead bronze).

Textolite (laminated fabric) bearings are made of a multi-layer chiffon cloth impregnated with bakelite and pressed under a pressure of 1000 kgf/cm² at 150-180°C.

These bearings operate better if the ends of the cloth layers are perpendicular to the frictional surface. In large-size bearings, textolite is installed in blocks in metal cases with the layers arranged endwise.

The maximum unit load with abundant oil or water lubrication is 100 kgf/cm². The limiting long-term temperature is 60-80°C.

Capron (Soviet name for polycaprolactam) and *nylon* are mainly used to make bearings with a diameter of less than 50 mm, operating either with scanty lubrication or dry.

Their strength is increased by introducing fillers (fabric, fibreglass, graphite fibres).

Like all thermoplastics, polyamides are difficult to machine. Capron and nylon bearings are manufactured by plunger moulding in metal moulds to a dimensional accuracy within several hundredths of a millimetre and a surface finish of up to 12th class.

To increase their strength, heat and wear resistance, and reduce water absorption, capron bearings are heat treated, immersed in mineral oil at 150-180°C for 3-4 hours, boiled in water for the same time and then slowly cooled.

Table 24

Plastics

Relative elongation, %	Linear expansion coefficient, $\alpha \cdot 10^6$	Thermal stability after Martens, °C	Water absorption for 24 hours, %	Coefficient of friction on steel (without lubricant)
0.2-0.6	20-40	120-130	1.5-2	0.2-0.3
30-80	60-80	140-160	0.1-0.2	0.15-0.25
150-200	60-150	50-60	2-3	0.1-0.15
50-100	60-120	60-70	1.5-2	0.1-0.15
150-200	100-200	80-120	0	0.08-0.1

Teflon in its pure form is hardly suitable for the manufacture of bearings due to its softness, high linear expansion coefficient, cold creep and complete incapability of being wetted with oil. Teflon is applied only in thin layers and always with an addition of lead (up to 20 per cent by weight). It is difficult to coat metal surfaces with teflon. The best coating method is the vacuum impregnation of the porous antifriction layer of sintered bronze alloys by a teflon-lead composition dispersed in a liquid. Colloidal graphite and molybdenum disulphide are introduced into the composition to improve antifriction properties.

Such bearings are by no means inferior in their antifriction properties to bearings with a tin-babbitt lining, and in fatigue limit exceed them. They can operate within the range from —50 to +250°C. Bearings operating at high peripheral speeds require circulatory lubrication.

Use is also made of thin-layer (0.1-0.2 mm thick) polyamide, polyurethane and epoxy coatings applied by hard facing, hot spraying, bonding (epoxies) and sedimentation in a pseudodiluted layer in an electrostatic field.

Wood Materials

Bearings can be made of oil-soaked hard wood (lignum vitae, boxwood), or of birch, maple and oak as substitutes.

Still better properties are displayed by compregnated wood which is either multi-layer birch veneer (laminated wood) or birch wood chips (lignostone) impregnated with phenolformaldehyde resins and pressed under a pressure of 300-500 kgf/cm² at 150-180°C.

Compregnated wood materials operate better in water; they are used to make bearings for hydraulic machines, and also low-speed heavily loaded and large-sized bearings of rolling mills.

Laminated-wood bearing shells are made up of blocks with their layers perpendicular to the frictional surface. The shells are fastened in metal housings (Fig. 140).
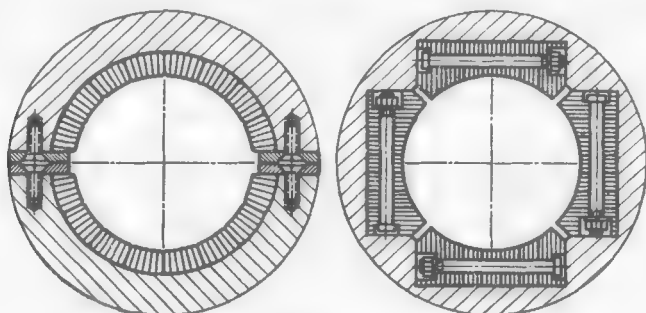
Fig. 140. Laminated-wood bearings

The permissible load for such bearings is, on the average, 20-30 kgf/cm², the permissible short-term load coming up to 150 kgf/cm². The limiting temperature is 60-70°C.

Rubber

Rubber bearings are metal bushings lined with natural or synthetic rubber [chloro- and fluoroprene, silicone and polysulphide rubber (Thiokol)]. The best synthetic rubber is fluoroprene.
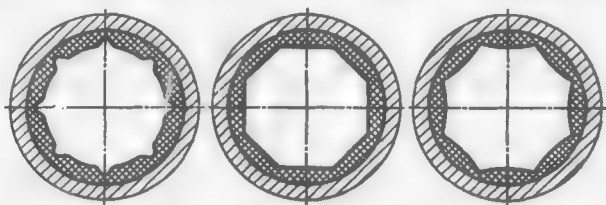
Fig. 141. Rubber bearings

The hardness and elasticity of rubber can be varied within broad limits by changing its composition and manufacturing process.

Rubber bearings can operate only in water. They are used in hydraulic machines, in underwater power tools and in tail installations of propeller shafts (deadwood bearings). The metal housings of the bearings are made of stainless steel or are protected against corrosion by polymer films.

Through grooves (Fig. 141) are provided on the working surface of the bearings to remove dirt.

The coefficient of friction of steel on wet rubber is $f = 0.05\text{-}0.1$. With sufficient water flow through the bearing and high peripheral speeds (10-20 m/s) purely fluid friction ($f = 0.002\text{-}0.003$) can be obtained despite the low viscosity of water.

Bearings made of soft rubber are used to ensure the self-alignment of the shaft and dampen its oscillations. The load-carrying capacity of such bearings is low ($k = 1\text{-}2$ kgf/cm^2).

Bearings manufactured from hard rubber can endure loads up to 30-50 kgf/cm^2.

Carbon Graphite

Carbon graphite (a mixture of graphite, coal, carbon black and coke with a coal tar pitch binder, pressed and sintered) is used to make bearings which operate dry, at high temperatures, and under the action of chemically aggressive media.

The physical and mechanical properties of carbon graphite are as follows: specific weight 2.2 gf/cm^3, melting point, 3500°C, tensile strength, 2 kgf/mm^2, modulus of normal elasticity, 800 kgf/mm^2, linear expansion coefficient, $(0.5 \text{ to } 1) \times 10^{-6}$, and heat conductivity, 5-7 cal/m·h·°C.

Carbon graphite possesses good antifriction properties (coefficient of dry friction 0.05-0.08), heat resistance, and chemical stability, and low linear expansion coefficient $[\alpha = (2 \text{ to } 3) \times 10^{-6}]$. Carbon graphite can easily be machined by cutting, but it is brittle.

Metal powders (Cu, Cd, babbitt) are introduced into carbon graphite to increase its strength, heat conductivity and wear resistance. Its brittleness is diminished by impregnation with phenolformaldehyde and siloxane resins, and teflon (*graphitoplasts*).

The best overall properties are displayed by *antegmites* (Table 25).

Table 25

Grade	Specific weight, gf/cm^3	Compressive strength, kgf/mm^2	Impact strength, kgf·m/cm^2	Thermal stability, °C	Heat conductivity, cal/m·h·°C	Linear expansion coefficient $\alpha \cdot 10^6$
ATM-1	1.8	1000	0.03	170	30	8.5
ATM-10	1.7	550	0.015	400	80	2.5
ATM-1Г	1.7	450	0.015	600	100	2.2

Shafts operating in carbon graphite bearings must have a hardness of $Rc > 50$.

Carbon graphite is widely used to seal high-temperature units (sealing rings of turbines, disks of end seals).

2.10. Microgeometry of Bearing Surfaces

In heavily loaded bearings it is advisable, irrespectively of the hardness of the bearing material, to impart to the journals an increased surface hardness by means of induction hardening (55-58 *Rc*), case hardening, sulphocyaniding (58-60 *Rc*), diffusion chrome plating (800-1000 *VPH*) and nitriding (1000-1200 *VPH*). These methods increase wear resistance and cyclic strength, and reduce stress concentration at transition sections and at places where oil holes are positioned.

Shaft journals should be ground so that the peripheral speed of the abrasive wheel has the same direction as that of the working rotation of the shaft; the journals should preferably be polished in the reverse direction.

The journals are finish machined by polishing, superfinishing, burnishing and diamond smoothing. The smoothing is done on engine lathes with a rounded diamond tool (curvature radius $R_{sph} = 1.5$-3 mm) at a feed $s = 0.03$-0.05 mm/rev, cutting speed $v = 20$-50 m/min and tool pressure of 20-40 kgf.
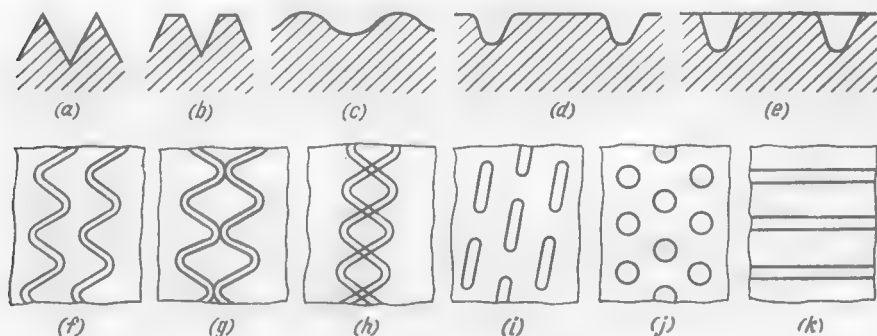
Fig. 142. Microscopic profiles of shaft and bearing surfaces

Almost all bearing materials (except for antifriction cast irons) cannot be ground. Bearings are finish machined by fine boring, reaming, burnish broaching and diamond smoothing. These methods ensure the 8th-10th class of surface finish ($R_z = 3.2$-0.8 μm).

Thin-layer galvanic and plastic coatings are not subjected to machining.

With the haphazard arrangement of microirregularities resulting from ordinary machining methods the optimum roughness height is that corresponding to the 8th-10th class of surface finish. Greater roughness (surface finish below the 8th class) reduces the carrying capacity due to the higher oil leakage through the valleys between the microirregularities. Finer roughness (surface finish above the 11th class) reduces the oil retaining capacity of the surface and increases the tendency to galling and seizure. However, the most important factor is the shape and arrangement of microirregularities and not their height.

Profiles with sharp crests and valleys (Fig. 142*a*, machine cutting) are unfavourable, somewhat better profiles are those with blunted crests (Fig. 142*b*, superfinishing, burnishing), and still better, wavy surfaces with smooth irregularities (Fig. 142*c*, diamond smoothing).

The optimum profiles are the ones with a well developed smooth carrying surface intersected by oil retaining microgrooves (Fig. 142*d*) or recesses (Fig. 142*e*) which supply oil during the periods of slack oil feed (starting) and adequately

distribute oil over the surface, thus preventing galling and seizure. The size of the microrecesses must be such as will make them of sufficient oil retaining capacity. The total area of the oil-accumulating pockets is made equal to 20-30 per cent of the entire bearing surface, their depth reaching 5-10 microns. Thus, the nominal roughness of the bearing surface, determined on the basis of R_z values, increases as compared with the usually recommended values (formally to that corresponding to the 7th-6th class of surface finish) despite the fact that the carrying capacity of the surface grows higher.

The oil retaining relief in Fig. 142d is produced by the vibration burnishing of the bearing surfaces (previously machined to the 11th-12th class of surface finish) by means of a rounded diamond tool (R_z =1.5-2 mm) to which, in addition to the longitudinal feed motion ($s = 0.8$-1.2 mm/rev), are imparted longitudinal oscillations with an amplitude of 1-1.5 mm. This forms on the surface a network of helical sinusoidal grooves which can either take an equidistant position (Fig. 142f), or come into contact (Fig. 142g) or intersect (Fig. 142h), depending on the amount of feed and the amplitude of the oscillations. The tool is fixed in a spring-loaded holder. The width and depth of the grooves are adjusted by changing the tightening force of the spring.

This method enables one to produce a controlled microrelief with its parameters being optimum for the specified conditions of operation.

The closed cellular recesses shown in Fig. 142e are advantageous in that they do not interconnect the high and low pressure zones of the bearing and do not decrease therefore its hydrodynamic carrying capacity. Such recesses are made with a tool oscillating radially that forms stitch-like spiral grooves in the surface (Fig. 142i). Another method consists in making dents in the bearing surface (Fig. 142j) by means of knurls with rounded projections.

Without any detriment to the load-carrying capacity of the bearing, closed cells can be made several tenths of a millimetre deep.

Longitudinal grooves (Fig. 142k), obtained by form broaching, increase the side leakage of oil and serve to cool the bearing as well as distribute the oil.

The oil retaining capacity of electrolytic coatings can be increased by means of porous deposition (by changing periodically the direction of current).

Oil retaining reliefs on shafts can be formed by a metered shot blasting, or by etching with reagents which act selectively on the soft structural components.

2.11. Split Bearings

Bearings of this type are made in the form of steel (more rarely bronze) shells lined witn antifriction alloys. The shells are installed into the housing by push, wringing or heavy drive fits.

The centring of the shells is achieved by the joint machining of their beds in the housings. The housings halves are locked in position by means of set pins or dowel bolts.

Thick- and thin-walled shells are in general use.

(a) Thick-Walled Shells

The wall thickness of the shells of this type is selected depending on the bearing diameter, the material of the shells and housing and the rigidity of the beds. In ordinary conditions (steel shells, cast-iron housings) the external diameter of the shells may be found from the approximate relation $D = 1.2d$ (where d is the shaft diameter), rounding off the obtained values to the nearest standard size.

The method of bonding antifriction metal to a dovetail (Fig. 143a) is now used only for materials which poorly stick to steel (lead babbitts of the БК-1 variety). As a rule, the metal is poured over a cylindrical surface (Fig. 143b) which is rough machined (to the 2nd-4th class of surface finish) to facilitate cohesion.

Careful degreasing and etching of the shell surface are extremely important for a good cohesion between the lining and the shell.
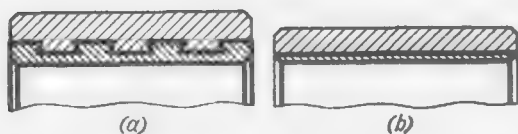
Fig. 143.Methods of lining with antifric-
tion metal
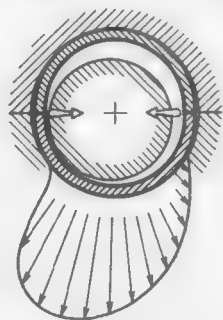
Fig. 144. Deflection of
shell joints under load

Today, there is a tendency to reduce the lining thickness. This increases the fatigue limit of the lining and, besides, reduces the amount of the lining material, which is extremely important in the case of scarce and costly metals (tin, silver). Nowadays, the lining
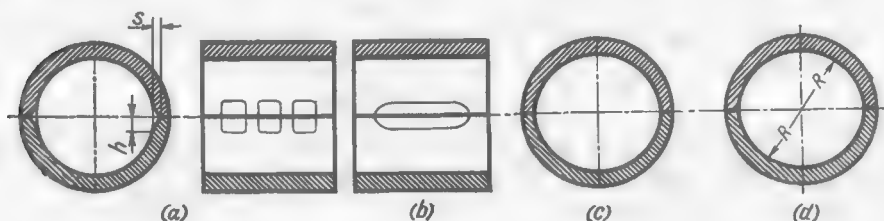
Fig. 145. Eliminating excessive friction at shell joints

thickness is reduced to several tenths of a millimetre, and to several hundredths of a millimetre when the coating is electrolytically deposited on porous bronze.

During operation the joints between the shells slightly deflect inwards (Fig. 144, bright arrows) under the action of the assembly interference and the pressure forces in the oil layer. This produces high friction in the sections close to the joint. This defect, often observed in thin-walled and non-rigid shells, can be prevented by means of tapered recesses (Fig. 145a) with an average height $h = 4$-6 mm and depth $s = 0.2$-0.5 mm made on the internal surface

of the shells near the joints. The simplest shape of the recesses is illustrated in Fig. 145*b*.

With the same purpose in view the shells are sometimes bored to an ellipse (Fig. 145*c*) or imparted a "lemon"-shaped form (Fig. 145*d*).
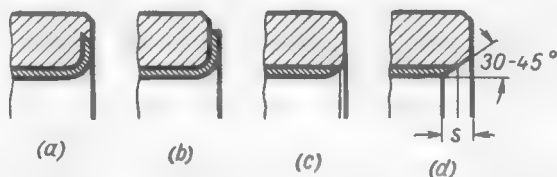
Fig. 146. Fillets and chamfers at the end faces of bearings

The difference in the bore diameter between the joint plane and the plane square with it is made equal to $(0.001$ to $0.0015)d$ (where d is the nominal bore diameter of the shell).

Fillets or chamfers are provided at the end faces of the working surfaces of the bearings to diminish edge pressures.

The fillets are difficult to make (especially when the lining protrudes onto the end face of the shell, Fig. 146*a*, *b*). Most frequently
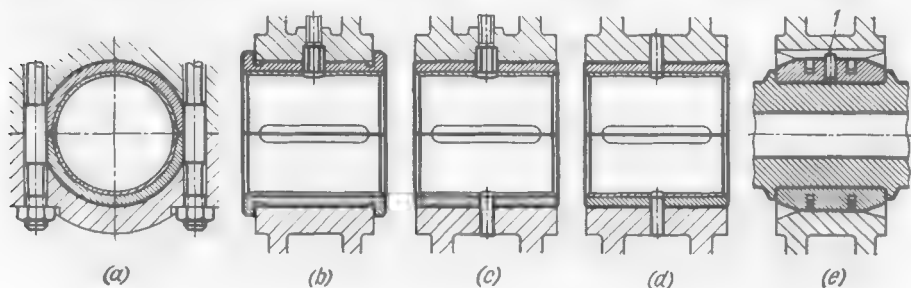
Fig. 147. Securing of shells

chamfers are made at an angle $\alpha = 30\text{-}45°$ to the bearing axis (Fig. 146*d*). Small axial loads (for example, in locking bearings) are taken up by thrust against the shell body.

Chamfers should not be too long, for otherwise they appreciably shorten the bearing surface. The chamfer leg (parallel to the bearing axis) is 0.5-1 mm for bearings of diameter up to 100 mm.

The methods of locking shells in split housings are shown in Fig. 147.

The locking by cylindrical collars on the bolts clamping both halves of the housing (Fig. 147*a*) is unsuitable for industrial production and is seldom used because the bolt holes have to be machined

simultaneously in the shells and housing when they are assembled together.

In bearings carrying axial loads the shells are secured in the longitudinal direction by shoulders and in the peripheral direction by pins or oil-feed nipples (Fig. 147b).

Smooth shells are locked in both directions by means of oil-feed nipples (Fig. 147c), and by pins in bearings where oil is supplied
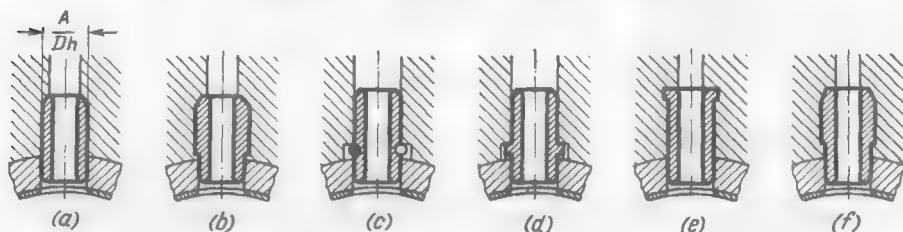
Fig. 148. Installation of oil-feed nipples

through the shaft (Fig. 147d). The holes for the pins in the shells are made slightly elongated (in peripheral direction) to ensure free self-alignment of the shells when they are being tightened.

When multi-support shafts are installed into solid housings the locking is sometimes done with the aid of circlips introduced into grooves cut jointly in both shells (Fig. 147e). The shells are assembled on the shaft and introduced into the recesses in the housing. The shells are retained in plane by pin 1 press-fitted into one of the shells and entering a longitudinal slot in the housing bore. Such bearings cannot carry axial loads.

The oil-feed nipples are press-fitted in the housing (Fig. 148a) and secured against falling out, which may cause a breakdown of the bearing.

The safety methods shown in Fig. 148b-d do not allow an assembled nipple to fall out (when the shells are installed in place). To prevent their fall-out during disassembly, the nipples are locked in the housing by expanding them into annular grooves in the housing (Fig. 148e), and in soft-metal housings, by caulking the housing metal onto steps on the nipples (Fig. 148f).

(b) Thin-Walled Shells

These shells, made from low-carbon strip steel with a thin layer of babbitt (0.3-0.5 mm), lead bronze or plastic aluminium alloys (0.8-1.5 mm), are widely used in machines of serial production. Shells of this design are manufactured on the mass production basis and are completely interchangeable.

The thickness of such shells may be found from the following approximate formula:

$$b = 0.35 \sqrt{\overline{d}} \qquad (2.39)$$

The obtained values are then rounded off to the nearest standard size.

The abutting portions of thin-walled shells are especially liable to deflection inside the bearing. Longitudinal recesses, such as shown in Fig. 145b, are provided in the sections near the joints to prevent semidry friction
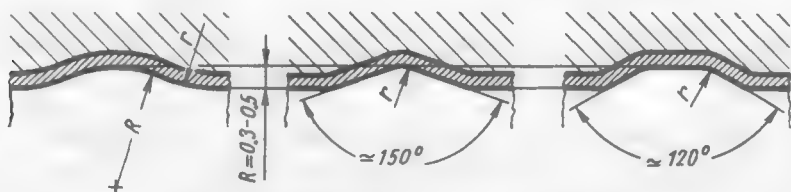
Fig. 149. Shapes of die-forged grooves

In bearings coated with plastic antifriction metals, oil grooves, chamfers and recesses are die-forged. The holes for locking pins and oil-feed nipples are punched.

The recommended shapes of die-forged grooves are shown in Fig. 149.

Thin-walled shells are press-fitted into their beds. Excessive interference may overstress and distort the shell walls (bend the joint edges into the bearing).

The magnitude of the fitting interference is determined by the circumferential length of the shell. To ensure a diametral interference δ the length l of the shell as measured along its mean diameter should be (without tolerances)

$$l = \frac{\pi}{2}(d_0 - b + \delta)$$

where d_0 is the diameter of the seating bore of the bed and b, the shell thickness.

Since the value of $\frac{\pi\delta}{2}$ is very small (with a heavy drive fit according with the 2nd grade of accuracy for a diameter of 100 mm, $\delta = 60\text{-}85$ μm; $\frac{\pi\delta}{2} = 0.1\text{-}0.13$ mm) and it is difficult to maintain the necessary dimension l when blanking, the blank is made with a length allowance of 0.5-0.8 mm and is then tightly clamped in a fixture having a hole diameter d_0 and the protruding shell ends are ground to the $\frac{\pi\delta}{4}$ size (Fig. 150a).

When the shell is fitted into its bed, one of its ends is installed flush with the parting plane (Fig. 150b) and the amount of protrusion of the opposite end, which must be equal to $\frac{\pi\delta}{2}$ when the shell fits tightly to the bed, is checked.

The diametral clearance in the bearing depends on the size of the shaft and the seating bore in the bed, and the thickness of the
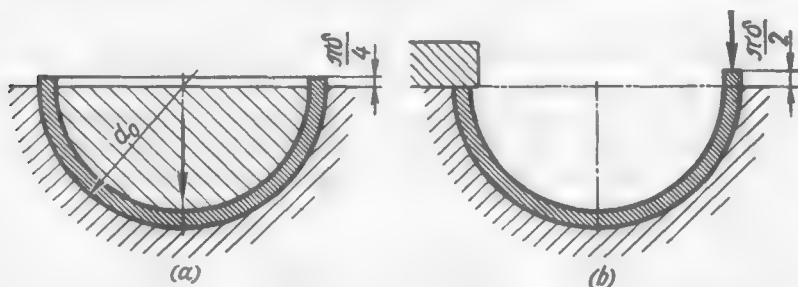
Fig. 150. Installation of thin-walled shells

shells. Let us assume that the beds are stiff and do not deform during tightening, and the shell thickness practically does not change during tightening. Then, the minimum clearance is

$$\Delta_{min} = d_0 - 2b - d^{-C_1} \qquad (2.40)$$

and the maximum clearance

$$\Delta_{max} = d_0^{+A} - 2b^{-B} - d^{-C_2} \qquad (2.41)$$

where d_0 = diameter of the bore in the bed
b = shell thickness
d = shaft diameter
A = plus tolerance on the bed bore diameter
C_1 and C_2 = minus tolerances on the shaft diameter
B = minus tolerance on the shell thickness

Let $d_0 = 80$ mm, $b = 2.5$ mm ($d = 75$ mm). When machining to the 2nd grade of accuracy, $A = 30$ μm; $C_1 = -65$ μm; $C_2 = -105$ μm (slack running fit), $B = 40$ μm.

The minimum and maximum clearances according to Eqs. (2.40) and (2.41) are

$$\Delta_{min} = 80 - 5 - 75^{-65} = 65 \text{ (μm)}$$
$$\Delta_{max} = 80^{30} - 2 \cdot 2.5^{-40} - 75^{-105} = 215 \text{ (μm)}$$

With thick-walled shells machined after installation in the bed we would have

$$\Delta_{min} = 65 \text{μm}, \ \Delta_{max} = 30 + 105 = 135 \text{μm}$$

Thus, variations in the shell thickness appreciably affect the magnitude of the diametral clearance. This makes it necessary to maintain the shell thickness within narrow limits (10-30 μm).

If the shells and the seating bores in the housing are made to a high degree of accuracy, the line boring of the bearings may be dispensed with even in multi-bearing installations.

Shells can be replaced without additional machining operations and adjustment because they are centred in the accurately machined bed bores which are not subjected to wear.

Thin-walled shells are locked in beds by means of pins (Fig. 151*a*) or oil-feed nipples (Fig. 151*b*). The holes in the shells are made elongated (in the peripheral direction) to ensure free self-alignment of the shells when they are being tightened.

The locking is often effected by means of locking lips stamped at the abutting surfaces (Fig. 151*c-e*) and fitting into inclined nesting
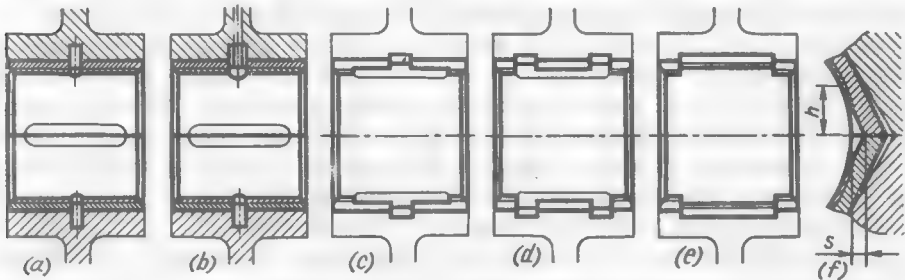
Fig. 151. Locking of thin-walled shells

slots in the beds. The depth *s* of the lip (Fig. 151*f*) is equal to 1.5-2 mm and their height is $h = 4$-6 mm.

The locking lips increase the contact surface and effectively prevent the deflection of the abutting surfaces of the shells into the bearing. If the lips are long enough (Fig. 151*e*) they can be used instead of the recesses which are sometimes used to eliminate semidry friction at the joint surfaces.

2.12. Bushings

Solid bearings are made in the form of bushings, which for small diameters (< 50 mm on the average) are manufactured entirely from antifriction materials (bronze, light alloys, antifriction cast iron), and for large diameters, from steel lined with a plastic antifriction material (babbitt, lead bronze).

The bushing thickness is selected from the approximate relation $b \approx 0.1d$ where *d* is the shaft diameter (the external diameter of the bushings $D \approx 1.2d$) and the obtained values are rounded off to the nearest standard size.

Bushings are installed in housings by force, heavy drive and shrink fits.

In the case of large-interference fits the bushings, especially thin-walled ones, shrink and their internal diameter diminishes. Such bushings, after being pressed in, are usually reamed.

If the design of the unit does not allow the bushing to be reamed, the diameter of the bushing bore is increased as compared with the nominal size by the amount of the bushing shrinkage determined by calculation or experimentally. ·

Press fits are not always a guarantee against rotation.

The working temperature of the bushing can considerably exceed that of the housing, for example, when the rotational speed of the machine is sharply increased and the heat generated in the bushing by friction has no time to pass into the housing. A large difference in the temperatures is observed during the starting periods when the bushing is rapidly heated while the housing still remains cold. If the bushing is made of a material with a higher coefficient of linear expansion than that of the housing material, the bushing prestressed by the forcing-in may develop residual deformations. Upon subsequent cooling the fit of the bushing weakens.

In hot engines (internal-combustion engines) the fit of the bushing may weaken with the heating of the housing.

In practice the following rules are observed.

Large-interference fits are used if the linear expansion coefficient of the bushing is less than that of the housing, and if the housing is heated during operation.

If the linear expansion coefficient of the bushing is greater than that of the housing, and the housing is cold, moderate interferences are used.

In all cases the bushings should be safeguarded against rotation and axial shift.

Locking methods are illustrated in Table 26. The most simple and sound designs *9-12* are used with solid housings. Designs *16* and *17* are preferred for tight locking.

(a) Bushings Made of Sheet Materials

Thin-walled bushings made from bent strips are widely used in machines of serial production.

Bushings of small diameter (<50 mm on the average) are manufactured from cold-rolled bronze or brass strips or from other anti-friction metals that can be bent in a cold state. Large-diameter bushings are formed from bimetal strips (a steel strip with a thin layer of antifriction material).

The thickness of the bushings may be determined from Eq. (2.39).

With the bushing joint closed, the diameter of the bushing is selected so that it fits tightly into the seating bore.

After installation, bushings made of bronze and brass strip are expanded by burnish broaching or rolling out and then finish machined by a broach with rounded sizing teeth. In this case the bushing surface obtains a high finish and the joint is practically completely closed.

Table 26

Locking Methods for Bushings

Design sketch and description

Installation in split housings

1. Axial locking with shoulders and angular locking with a pin

2. Locking with an oil-feed nipple

Installation in solid housings

3. Locking with an axial screw

4. Flanged fastening. The design requires a cast bushing

5. Locking with a flange and an axial pin. The design can be used with an axial load of constant direction

6. Ditto, with a small-diameter flange

Table 26 (cont.

Design sketch and description
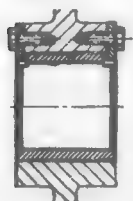
7. Locking with screwed-on plates. Not less than two bolts in each plate

8. Locking with a screwed-on plate and a shoulder

9. Locking with a radial screw

10. Locking with a radial pin

11. Locking with an inclined pin

12. Ditto, the pin is locked in the housing by a shoulder in the pin hole

Table 26 (cont.)

Design sketch and description

Tight installation

13. Centre punching of housing material

14. Swaging the housing material onto the serrated shoulder of the bushing
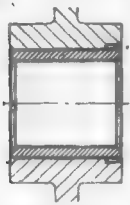
15. Locking with a serrated flange of the bushing. The design is applicable to steel bushings installed in soft-metal housings

16. Flaring the ends of the bushing into bevelled recesses in the housing
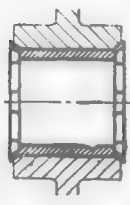
17. Centre punching the end face of the bushing into local recesses in the housing
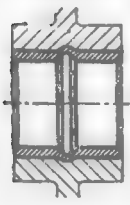
18. Expanding the bushing into an annular groove in the housing

Bushings are locked in the housing bore by expanding (Fig. 152a) or caulking their ends (Fig.152b) or by rolling into an annular groove in the housing (Fig. 152c). This method is mainly used to fix bushings in hard-metal housings (steel, cast iron).

Bushings made from bimetal strip are installed in the bent state onto a mandrel with a diameter slightly less than that of the shaft
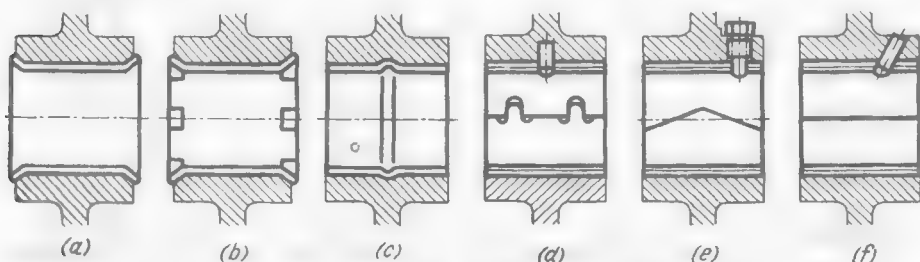
Fig. 152. Locking of thin-walled bushings

and ground on the outside diameter so as to obtain a heavy drive fit. The bushings are then inserted into the bores in the housing, locked by pins (Fig. 152d-f) and reamed. For such bushings preference is given to a lock joint (Fig. 152d) although simpler joints—herring-bone (Fig. 152e) and straight (Fig. 152f)—are frequently used in practice.

2.13. Adjusting the Clearance in Bearings

Even if bearings are correctly designed to operate with fluid fric-tion, they get worn in the course of time mainly due to the semifluid friction conditions obtaining during the starting periods.
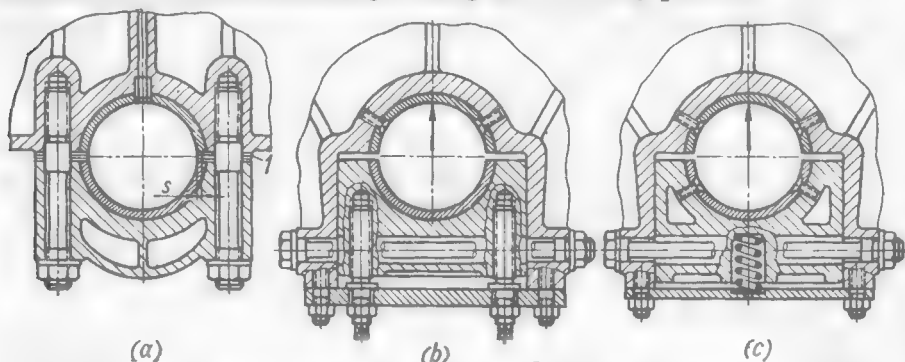
Fig. 153. Adjusting the clearance in split bearings

Bearings subjected to rapid wear (varying operating conditions with frequent starts and stops), and also those of shafts requiring accurate centring, are provided with means for adjusting the clearance.

In split bearings with thick-walled shells the clearance is adjusted by means of shims *1* (Fig. 153*a*) made of sheet brass about 0.05 mm thick and installed in the joint of the bearing. The shim ends are fitted with a clearance $s = 0.3$-0.5 mm with respect to the bearing surface to avoid contact with the shaft.

When boring shells with shims (Fig. 154) the abutting surfaces are finish machined and interspaced by pads with a thickness equal to the original (assembly) thickness *t* of the set of shims (usually $t = 0.4$-0.5 mm) after which the bore and the external surface of the assembled shells are machined to obtain true cylindrical surfaces.

During operation the bearings are periodically tightened up. The caps are taken off, one or several shims are removed and the bearing tightened anew.

In this case the cylindrical shape of the bearing hole is somewhat distorted. The hole acquires a slightly oval shape; the distortions in the bore shape resulting from wear remain uncorrected.

It is difficult to maintain the correct clearance when retightening the bearing. The usual rule, according to which the shaft after tightening must be free to rotate by hand, by no means guarantees a correct clearance.

Fig. 154. Boring of bearings with shims

Sometimes the clearance in the bearing is taken up by tightening the bearing cap with screws (Fig. 153*b*).

Figure 153*c* shows a design with a semiautomatic clearance adjustment. The bearing cap is tightened by transverse bolts. When the clearance has to be reduced the bolts are slightly released and the spring presses the cap against the shaft, after which the transverse bolts are tightened again.

The design in Fig. 153*b*, and especially that in Fig. 153*c*, where the cap is not locked accurately enough, is used with a load of constant direction; the load must be directed towards the fixed shell of the bearing.

When fine clearance adjustment is required together with accurate shaft centring (spindles of grinding machines) use is made of bushings with a tapered frictional surface (Fig. 155*a*). The clearance is adjusted by displacing the bushing axially by means of nut *1*.

It is better to make the frictional surface cylindrical, and the external seating surface of the bushing tapered (Fig. 155*b*). When the bushing is tightened in its mating taper the clearance in the bearing diminishes due to the elastic deformation of the bushing.

The adjustment range can be widened if split bushings are used or the elasticity of the bushing increased by means of radial slots (Fig. 155*c*).

In the design shown in Fig. 155d the external surface of the bushing rests in a taper recess on three tapered projections. When the bushing is tightened the
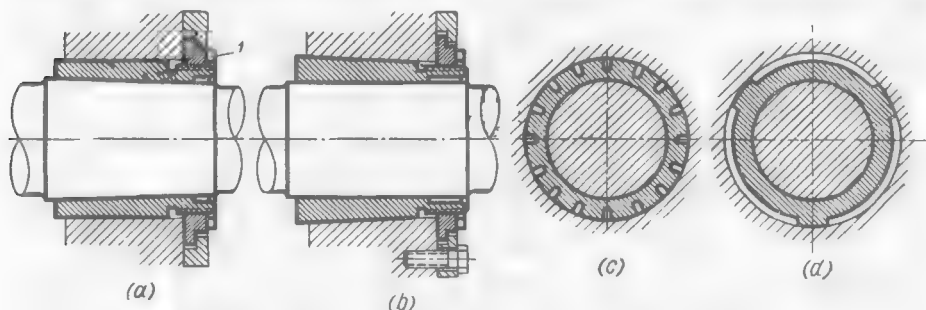
Fig. 155. Adjusting the clearance in solid bearings

clearance diminishes at these sections and oil wedges form on either side of each section. This centres the shaft and assists the bearing to operate without vibration.

2.14. Self-Aligning Bearings

Such bearings with spherical supports are used when $l/d > 1.5$, when the shafts and housings are not rigid enough, in supports distant from one another, and in supports mounted in different housings when it is difficult to ensure their strict alignment.
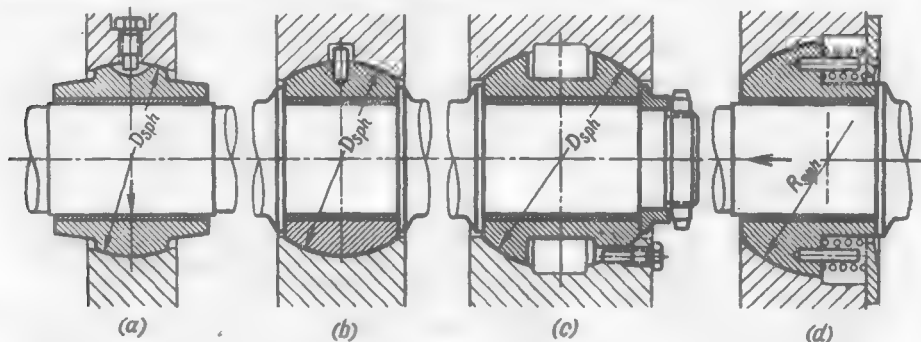
Fig. 156. Self-aligning bearings

Figure 156 illustrates various designs of spherical self-aligning bearings.

The design with a short spherical support (Fig. 156a) is used with small axial loads or when such loads are absent.

In the design shown in Fig. 156b the entire external surface of the bearing is made spherical and, in addition to radial loads, the bearing can carry very high axial loads in both directions.

When axial loads are high, the diameter of the sphere and the length of the bearing are increased and, as a result, the supporting surfaces are arranged closer to the edges of the bearing (Fig. 156c), their mean inclination angle to the bearing axis increases as does the ability of the bearing to carry axial loads.

Bearings with a semispherical supporting surface (Fig. 156d) locked in the housing recess by springs are used for larger unidirectional axial loads and negligible radial loads.

Self-aligning bearings are retained in place by stops mounted in the housing (Fig. 156a) or in the bearing (Fig. 156b). The retaining means must have a clearance allowing the bearing to self-align within the required limits.

The supporting spherical surfaces of the bearing and housing are manufactured from materials forming an antifriction pair. Bearings intended to be fitted into a steel housing are made of bronze, or their spherical surface is lined with lead bronze. If a bearing is to be installed into a cast-iron housing or a housing made of a light alloy, it is manufactured from steel and the Rockwell hardness of the spherical surface must be in excess of 50.

The supply of oil (preferably under pressure) to the spherical surfaces is obligatory. It is good practice to form on the surface of the sphere a fine network of closed oil channels which ensure (when the oil is delivered under pressure) a definite hydrostatic effect that makes the self-alignment of the sphere easier.

It is not difficult to install spherical bearings into housings split in the meridional or equatorial plane.

Installation into solid housings is a more complicated procedure.

Short spherical bearings are installed through diametrally opposite slots cut in the bearing seat in the housing (Fig. 157a), the length l of the slots being
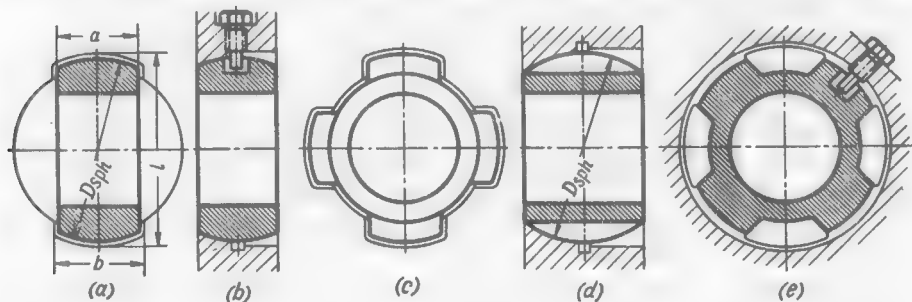
Fig. 157. Installation of spheres into solid housings

somewhat larger than the diameter D of the sphere and their width b slightly exceeding that of the bearing. The bearing is introduced into the slots being turned through 90° with respect to its working position until it rests against the wall of the spherical seat. After this the bearing is turned to the working posi-

tion and, as a result, it becomes locked in the axial direction by the walls of the seat (Fig. 157b). The bearing is secured against rotation by a stop.

If the bearing is very long, the spherical supporting surfaces are made in the form of projections, and corresponding slots (Fig. 157c) are cut in the housing. The bearing is inserted into the seat in the working position (Fig. 157d), turned in the plane perpendicular to its axis through an angle equal to half the angle between the projections, and is locked in this position by a stop (Fig. 157e).

Figure 158a shows a self-aligning bearing in which the bending oscillations of the shaft are damped by means of elastomer rings installed on the sides of the bushing.

In the design b shown in Fig. 158 self-alignment is ensured by mounting the bearing on four cylindrical dowels inserted into longitudinal slots in the housing. The bearing must be locked in the axial
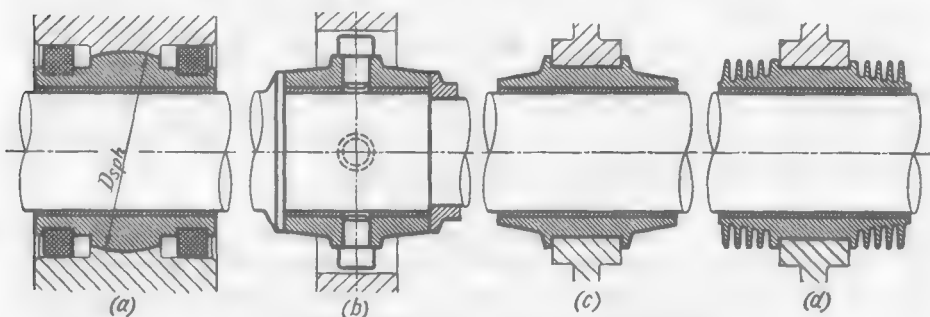
Fig. 158. Self-aligning and elastic bearings

direction (for example, by stops on the shaft, as shown on the drawing). This bearing cannot carry axial loads.

Figure 158c, d shows designs that provide for partial self-alignment on account of elastic deformation.

In the design in Fig. 158c the bearing is mounted in its seat in the housing on a short cylindrical portion and its ends are thinned. The elastic deformations of the seating surface and the thin ends of the bearing enable it to adapt itself to shaft misalignments. The shortcoming of the design is that the bearing ends in the case of bending are elongated in the bending direction and become oval. The clearance between the shaft and bearing along the minor axis of the oval diminishes.

In the design shown in Fig. 158d the radial stiffness of the bearing ends is increased by means of annular ribs. At the same time the bearing ends can deform and thus follow the bending deformations of the shaft. The ribs also help to cool the bearing.

A certain latitude in the self-alignment of a shaft is allowed when the bearings are bored to a "corset"-like shape. The friction surface is imparted the form of a hyperboloid of rotation. The bore diameter at the ends faces is made several hundredths of a millimetre larger than in the middle.

2.15. Bearings with Floating Bushings

Floating bushings are installed with a clearance with respect to the shaft and housing. The forces of friction cause these bushings to rotate with a peripheral speed approximately equal to half that of the shaft.

The advantages of bearings with floating bushings are:

reduced generation of heat (the work of friction is proportional to the square of the peripheral speed; for this reason when a floating bushing rotates with a speed equal to half that of the shaft the total heat generation is about two times less than in a rigid bearing, and in the case of two concentric floating bushings, about three times less);

uniform wear over the circumference, ensuring the cylindrical shape of the bushings;

higher reliability of operation (when one side is seized the bushing continues to operate with its other side);

increased vibration resistance;

greater (due to the presence of two oil buffers) damping of the radial displacements of the shaft under the action of impact and variable loads.

The shortcoming of these bearings is poorer shaft centring due to the increased total clearance in the bearing.

Floating bushings can rationally be used in high-speed bearings where it is necessary to diminish the generation of heat and prevent vibration, in bearings operating under high impact loads, and in bearings with semifluid and semidry friction (for example, swinging motion supports) where the nature of motion makes it impossible to form a stable oil film.

In the latter case the stability of floating bushings against seizure and their property of uniform wear over the circumference prove extremely useful.

Floating bushings are commonly made solid. Sometimes the conditions of assembly require split designs (this complicates manufacture). Floating bushings are made of bronze and antifriction cast iron, and large-diameter bushings, of steel with a double-sided lining of babbitt or lead bronze. The housing and shaft are manufactured from steel with $Rc > 50$; if the housing is made of a soft material, a steel bushing is press-fitted into it.

When oil is supplied on one side of a floating bushing, radial holes are made in it to feed oil to its other side. The oil should preferably be introduced from inside, since in this case the access of oil to the external frictional surface is facilitated by centrifugal forces.

The thickness of bushings is, on the average, made $0.1d$ (where d is the shaft diameter).

Radial clearances in floating bushings are 20-30 per cent smaller than in rigid bearings. The clearance on the external frictional surface must be larger than on the internal one, since this clearance (especially with bronze bushings) diminishes in operation due to heating.

Floating bushings are locked in the axial direction as follows: in solid housings—by means of webs (Fig. 159a), flanges (Fig. 159b)
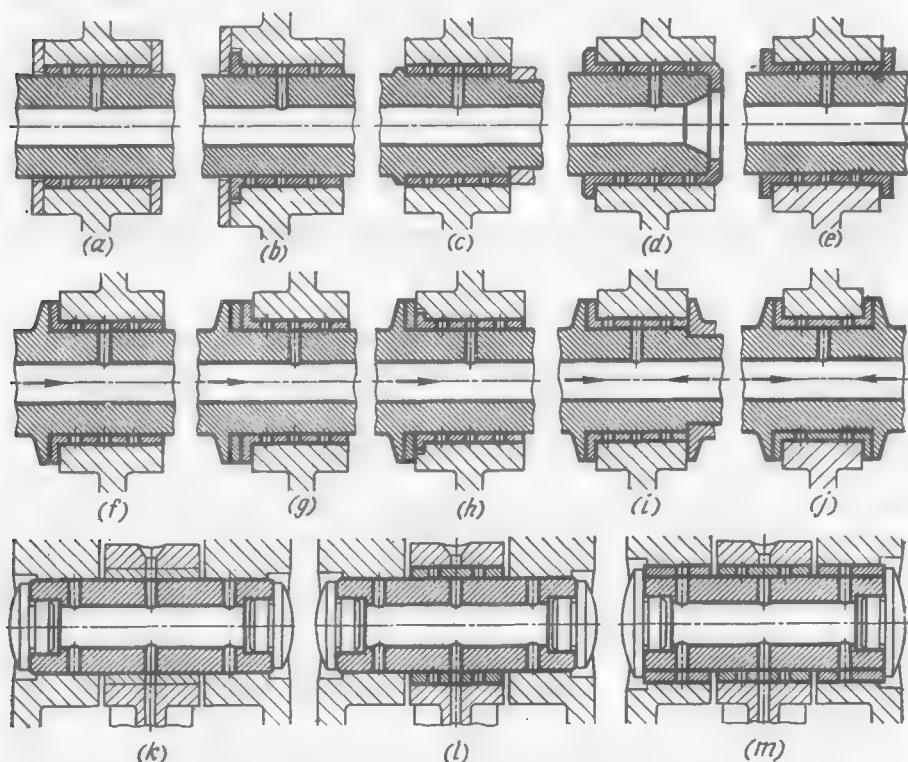
Fig. 159. Bearings with floating elements

and shoulders on the shaft (Fig. 159c); at the ends—by the shaft end face (Fig. 159d); and in split housings—by means of flanges (Fig. 159e).

In the presence of well developed end surfaces (Fig. 159f-j) bearings with floating bushings can carry very high axial loads.

Figure 159k-m shows a connecting-rod-to-piston connection with a floating piston pin.

Figure 159k—the piston pin floats in the piston bosses and in the bushing of the connecting rod end (the unit contains three clearances and two consecutively operating oil buffers).

Figure 159*l*—the bushing of the connecting rod end floats (four clearances, three oil buffers).

Figure 159*m*—the pin is fitted into the piston on floating bushings (six clearances, four oil buffers).

2.16. High-Speed and Vibration-Proof Bearings

In bearings operating at high rotational speeds (turbine shafts, 6000-10,000 rpm; internal grinding machine spindles, 10,000-30,000 rpm; gyroscope shafts, 20,000-50,000 rpm; and centrifuge shafts, up to 150,000 rpm) the operating characteristic $\lambda = 30,000$-50,000, and the Sommerfeld number $So = 10$-50. Due to the low shaft eccentricity these bearings operate unstably, and the coefficient of friction is very high ($f = 0.05$-0.1).

The following two basic problems come to the fore when designing high-speed bearings: (1) prevention of the shaft vibrations and the resulting cavitation processes and (2) prevention of the bearing overheating from the abundant heat generation.

The problems of designing high-speed bearings are in many respects opposite to the problems involved in designing heavily loaded comparatively low-speed bearings ($\lambda = 500$-1000, $So < 1$) where the load-carrying capacity of the bearing and the minimum oil layer thickness h_{min} have usually to be increased.

When designing high-speed bearings the principal task is to reduce the excessive value of h_{min} until the values of $\xi < 0.3$, which are necessary for vibrationless operation, are obtained.

In the case of bearings loaded by a force of *constant* direction vibrationless operation can be attained by rationally selecting the operational and design parameters with a view to reducing So and h_{min}. It is good practice to use oil of low viscosity, decrease the bearing diameter (higher k), increase the clearance ratio ψ and use small values of l/d.

Let the operating characteristic λ be equal to 50,000. Using the graph in Fig. 115 we find that when $l/d = 1$, vibrationless operation ($\xi = 0.3$) can be ensured by a clearance ratio $\psi = 0.011$. This is an excessively high magnitude (for $d = 100$ mm, the diametral clearance $\Delta = 1.1$ mm). Bearings with such a clearance cannot operate properly during starting and racing. According to Fig. 119, the coefficient of friction $f = 0.22$.

Let us reduce l/d to 0.3. Bearing in mind that with the same diameter the unit pressure k increases and the value of λ diminishes 3.33 times ($\lambda = 15,000$), and disregarding the fact that the vibrationless value of ξ is slightly increase, in bearings with $l/d = 0.3$ (see Fig. 113), we obtain, in conformity with Fig. 115, $\psi = 0.0028$ (for $d = 100$ mm, $\Delta = 0.28$ mm). The oil layer thickness $h_{min} = 0.5 \times 10^3 \times 0.0028 \times 100 \times 0.3 = 42$ microns. The coefficient of friction $f = 0.018$.

When the diameter of the shaft is reduced to 50 mm and $l/d = 0.3$ the parameters of the bearing assume their normal values ($\lambda = 7500$, $\psi = 0.002$, $\Delta = 0.1$ mm, $h_{min} = 15$ μm, $f = 0.013$).

The design methods intended to make bearings vibration-proof are illustrated in Table 27.

Table 27

High-Speed and Vibration Proof Bearings
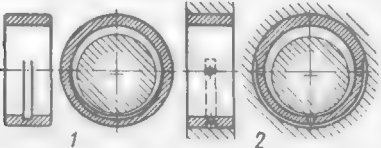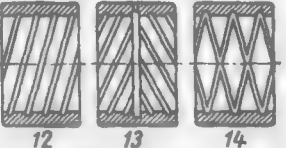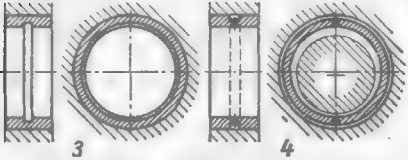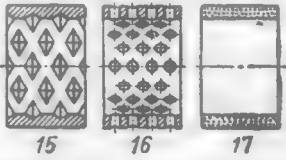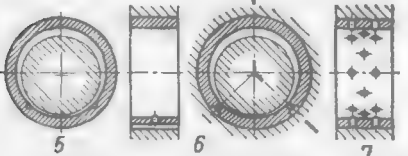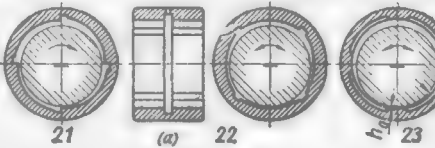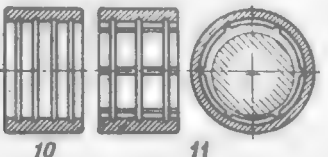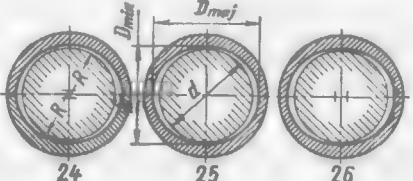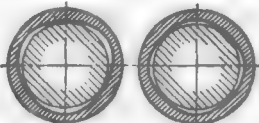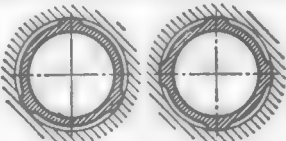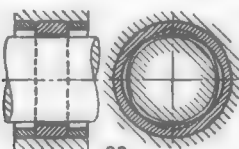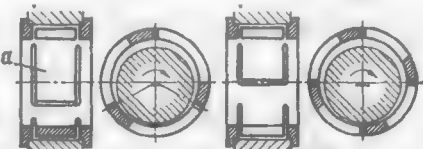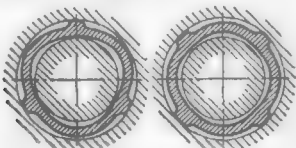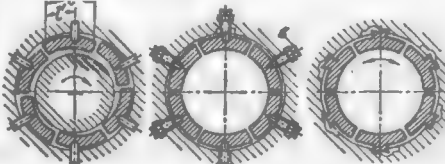
Sketch	Sketch

Bearings with semiannular grooves

Bearings with annular grooves

Bearings with recesses in loaded zone (*5, 6*); floating bearings (*7*)

Bearings with recesses in unloaded zone

Bearings with annular and wafer-type grooves

Bearings with helical, herringbone and criss-cross grooves

Bearings with rhombic recesses and through holes (*15, 16*); porous bearings (*17*)

Multiple-wedge bearings

Four-wedge bearings (*21, 22*); stepped bearings (*23*)

Bearings with "lemon"-shaped, elliptic and oval holes

Table 27 (cont.)

Sketch	Sketch
27 *28* Bearings with many-faced bores	*32* *33* Bearings with elastic bushings
 29 Bearings made of rings with opposed elliptic bores	 *34* *35* Lobed bearings
 30 *31* Multiple-wedge bearings with elastically deformable bushings	 *36* *37* *38* Segmental bearings

The carrying capacity (and hence, the clearance ratio) can be reduced by providing the active or back side of the bearing with semiannular (*1, 2*) or annular (*3, 4*) grooves connecting the high and low pressure zones, and longitudinal grooves in the loaded zone (*5, 6*) which facilitate the efflux of oil from this zone and limit the bearing surface arc.

The temperature of the bearing can be reduced by means of floating bushings (*7*), and, in the case of stationary bushings, by intensifying oil circulation through increasing the feed pressure or providing through longitudinal recesses (*8a*) or recesses terminating at the end faces (*8b*) in the unloaded zone. Very long recesses intensify the outflow of oil and at the same time lessen friction (approximately in proportion to the ratio between the arc of the recess and the circumference of the bearing).

The recesses *9* with an angle of 270° prevent the rise of the shaft beyond 45° (boundary point on Gümbel's semicircle), and ensure proper operation of the bearing in the stable region.

When the load is applied in *different* directions large clearances are impermissible. In this case vibrationless operation is ensured by making the bearing surface in the form of individual carrying areas separated by recesses and arranged with a small radial clearance with respect to the shaft.

Bearings with annular *(10)* and wafer-shaped *(11)* carrying surfaces are the simplest designs of this type. More practicable designs are those with helical *(12)*, herringbone *(13)* and rhombic *(14)* areas. Bearings with knurled rhombic recesses *(15)* and with staggered through holes *(16)*, and porous bearings *(17)* form a special class of bearings.

The most popular are *multiple-wedge bearings* operating on the principle of hydrodynamic limitation of the shaft displacements. The carrying surfaces of such bearings are designed as inclined areas *(19)* with a clearance (at the points of the closest approach of the shaft to the bearing) smaller than in cylindrical bearings *(18)*. Pressure is developed simultaneously on all the areas, but it is larger on the areas opposite to the direction of the load *(20)*. The total load-carrying capacity of the bearing is equal to the difference in pressure between the loaded and unloaded side of the bearing. If the load changes its direction, high pressures hampering the shift of the shaft and damping its oscillations arise on the areas opposite to the load. The displacements of the shaft diminish with higher rotational speeds and smaller local clearance ratios.

The oil-feed grooves between the wedge-shaped surfaces are made through, or stop short of the bearing end faces. The supply of oil along the central annular groove *(22a)* is the best method. In the case of through recesses the oil can be fed from the bearing end face.

In bearings with a stepped carrying surface *(23)* the carrying force is produced due to the oil being forced into the recesses h and its flow throttled in the narrow clearances h_0 between the shaft and bearing. The depth of the recesses h is several hundredths of a millimetre. The design is reversible.

Double-wedge bearings with "lemon"-shaped *(24)*, elliptic *(25)* and oval *(26)* holes are seldom used and only with a load of constant direction, because these bearings tend to oscillate the shaft in the direction of the major axis of the bore.

When the load changes its direction, at least three wedges are required. Bushings with a trihedral hole *(27)* are used in solid bearings. Bearings with a tetrahedral bore *(28)* may be used both in solid and split bearings. Design *(29)* composed of three bushings, the middle one having an elliptic bore in one direction and the extreme ones, in the opposite direction, allows the arrangement of the ellipses to be adjusted by turning the middle bushing.

Designs *27-29* are reversible.

Double-wedge elliptic bearings can be machined with the aid of an ordinary borer, the blank being inclined with respect to the spindle axis at an angle α determined from the ratio

$$\cos \alpha = \frac{1 + \psi_{min}}{1 + \psi_{max}}$$

where $\psi_{min} = \dfrac{D_{min} - d}{d}$ and $\psi_{max} = \dfrac{D_{maj} - d}{d}$ are the respective minimum and maximum clearance ratios, and d is the shaft diameter (see sketch *25*).

With the usual values of $\psi_{max}/\psi_{min} = 2$ and $\psi_{min} = 0.001$

$$\cos \alpha = \frac{1.001}{1.002} = 0.995 \qquad (\alpha = 6°)$$

Repeating this process with the blank being turned through 90° around its axis we obtain a four-wedge-shaped bore.

Many-faced bores are produced by tracer boring or broaching, and in solid bearings by means of a metered plastic deformation of the bushing followed by its machining on the external surface to a cylindrical shape.

The method of elastic deformation is also used. The bushings are provided with three or four crests machined to a taper and fitted with interference into the tapered bore in the housing. The interference deforms the bushing which assumes a trihedral (*30*) or tetrahedral (*31*) shape which can be controlled by moving the bushing in the housing.

Another method is based on the elastic deformation of the bushing walls under the pressure in the oil layer. Bushings with projections (*32, 33*) are tightly fitted into the bore in the housing. The unsupported portions of the bushing are deflected outwards under the action of hydrodynamic forces. The load is principally carried by the supported portions. The shape of the bearing surfaces is determined in these designs by the pliability of the bushing walls and the magnitude of the hydrodynamic forces.

A further development of this principle is illustraed by *lobed* bearings (*34-35*) in which the carrying surfaces are the areas *a* (lobes) cut in the body of the bushing. The hydrodynamic forces deflect the lobes outwards, thus forming oil wedges.

The bushings are installed in housings with a radial clearance that makes it possible for the lobes to deflect. A floating design is just as practicable.

The carrying surfaces in *segmental bearings* (*36-38*) are segmental shells hinge-mounted in the housing. The hinges allow the segments to automatically adapt themselves to load variations. When the load is increased the front edge (in the direction of the shaft motion) departs to the periphery while the rear edge approaches the shaft; for this reason the clearance diminishes at this point and the carrying capacity of the segment increases.

Like all multiple-wedge bearings, segmental bearings are proof against vibration only if the clearance ratio (in the sections where the hinges are arranged) is small.

The hydrodynamic characteristics of the bearing are determined by the arrangement of the hinges and remain unchanged despite variations in the operating conditions. The carrying capacity is maximum and the coefficient of friction minimum, if the hinge is mounted at a distance $l' = 0.58\ l$ (where l is the circumferential length of the segment) from the front edge (in the direction of the shaft motion) of the segment (*36*).

In reversible bearings the hinges are installed in the centre of the segments (*37*), which impairs their performance, or preferably in the recesses of the housing (*38*) so that these segments are shifted under the action of frictional forces to the most advantageous position when the direction of rotation is reversed. The amount of clearances (and the position of the shaft in the bearing) can be adjusted by means of screws *b*.

Despite their good antivibration properties, segmental bearings are seldom used. They are much more difficult to make than multiple-wedge bearings with stationary carrying surfaces. Because of the formation of vortices in the spaces between the segments the total heat generation is much greater than in bearings with smooth transitions between the carrying surfaces.

2.17. Feeding Oil into Shafts

Figure 160*a-f* shows some methods of introducing oil from the end face of the shaft.

When the oil feed is effected without pressure the oil is introduced along a pipe into the internal space of the shaft which is provided with a flange to distribute the oil among lubricating holes (Fig. 160*a*).

The simplest pressure-feed method is to introduce oil into the end of the shaft through a cover mounted on the housing (Fig. 160*b*).

Figure 160*c* shows the method used to supply oil through an end seal. The spring compressing seal disk *1* must be strong enough to prevent the sealing surface being pressed back by the oil pressure.

In the design shown in Fig. 160*d* oil is introduced into the shank of the shaft through an idle bushing locked against rotation by segment *2*, and in the design in Fig. 160*e*, through floating nipple *3* held in place by splines in the housing.

In the most compact design (Fig. 160*f*) oil is fed through a bushing installed in the shaft bore and secured against rotation by splined washer *4*.

In mid-shaft installations oil is as a rule introduced along an annular groove in the bearing (Fig. 160*g*) whence it reaches the shaft bore through radial holes.

Oil can also be fed through idle bushings locked on the shaft (Fig. 160h). In the design shown in Fig. 160i the bushing is secured on the housing by a flange with radial slots to receive elevator bolts 5. The design provides for the axial locking of the bushing with a certain freedom of its self-alignment on the shaft.
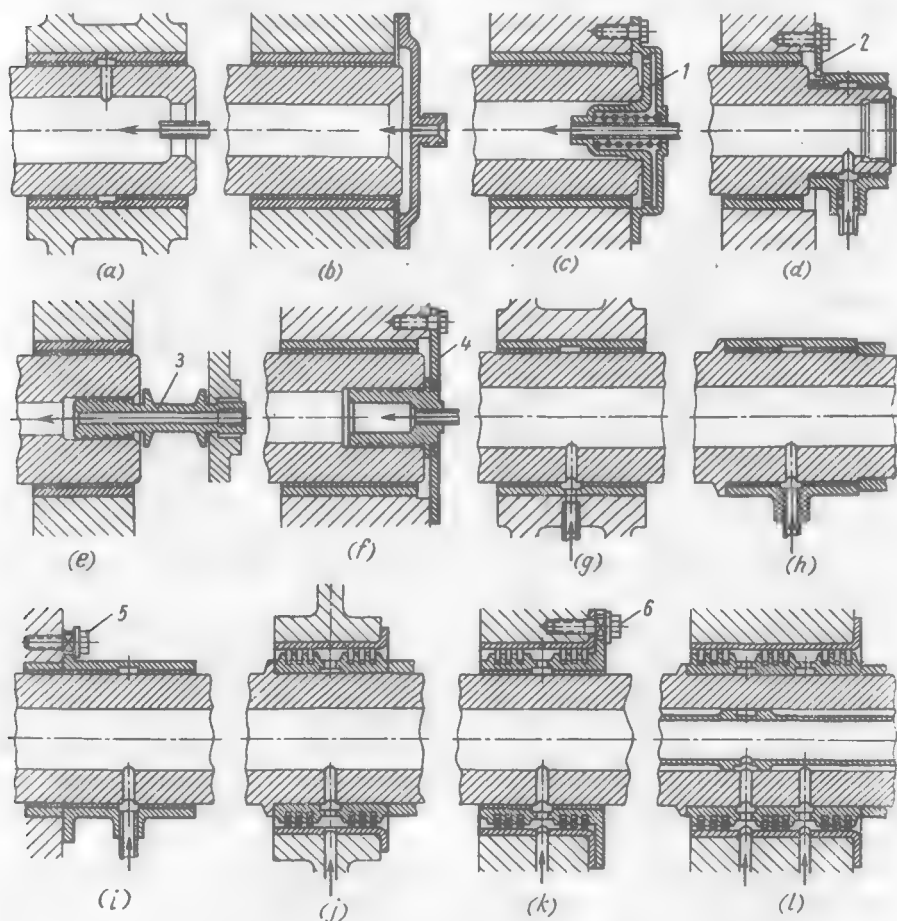
Fig. 160. Feeding oil into shafts

When a high-pressure oil feed is required, the oil is introduced through a shaft-mounted seal with snap rings (Fig. 160j). The ring housing is tightened on the shaft between a shoulder and a distance bushing.

If it is impossible to tighten the housing (when the shaft is smooth) the housing is made floating and locked in the longitudinal and peripheral directions by elevator bolts 6 fitting into radial slots

in the housing flange (Fig. 160*k*). The internal surface of the housing is lined with babbitt for sealing.

Figure 160*l* shows the case of sealing with snap rings to feed oil separately into two concentric spaces of the shaft (for example, to drive hydraulic servo-mechanisms mounted on the shaft).

(a) Oil Channelling in Crankshafts

Ordinarily, oil is introduced into crankshafts through the main bearings from which it flows along radial holes into the internal cavities of the main journals, and then along holes in the webs into the crankpin cavities to lubricate the big-end bearings. Some oil is withdrawn from the annular grooves of the bearings through the central holes in the connecting rods to lubricate the piston pins.

The oil is fed from the main bearing via inclined pipes into the annular groove of the big-end bearing and then into the hole in the connecting rod (Fig. 161*a*). This design tends to increase the rate of oil feed to the lubricating points during starting. The lubricating system can easily be cleaned by scratch brushing.

The design in Fig. 161*b* utilizes the shaft rotation for centrifuging the oil. The oil flows from the main bearing via an inclined pipe into the internal crankpin cavity closed by plugs where it is centrifuged. Oil is fed into the big-end bearing along a radial pipe lowered into the crankpin cavity. Oil residues remain in the upper part of the cavity. The disadvantage of the design is that the shaft webs are weakened by the threads for the plugs.

In the design shown in Fig. 161*c* the cavities in the main journals and crankpins are closed by tapered plugs. The plugs are provided with cylindrical projections to facilitate the lapping of the plugs to their seats. Oil is delivered along inclined holes drilled through the upper faces of the webs, then it enters the crankpins and is fed to the big-end bearings through radial holes. When the holes are arranged below the crankpin axis a definite centrifuging effect is obtained.

The oil contained in the internal cavities of the main journals and crankpins provides the feed during starting periods.

In the design in Fig. 161*d* light-alloy plugs are push fitted into the cylindrical holes in the journals and locked in place by bolts. The plugs have threaded holes to make disassembly easier. Oil is fed through straight holes in the shaft webs, which can be drilled easier than skewed holes.

The specific feature of this design is that the oil is fed to the crankpin from two sides, from both adjacent main bearings.

In the design shown in Fig. 161*e* thin-walled steel displacers are installed in the internal cavities of the main journals and crankpins to accelerate the oil feed during starting periods, the displacers
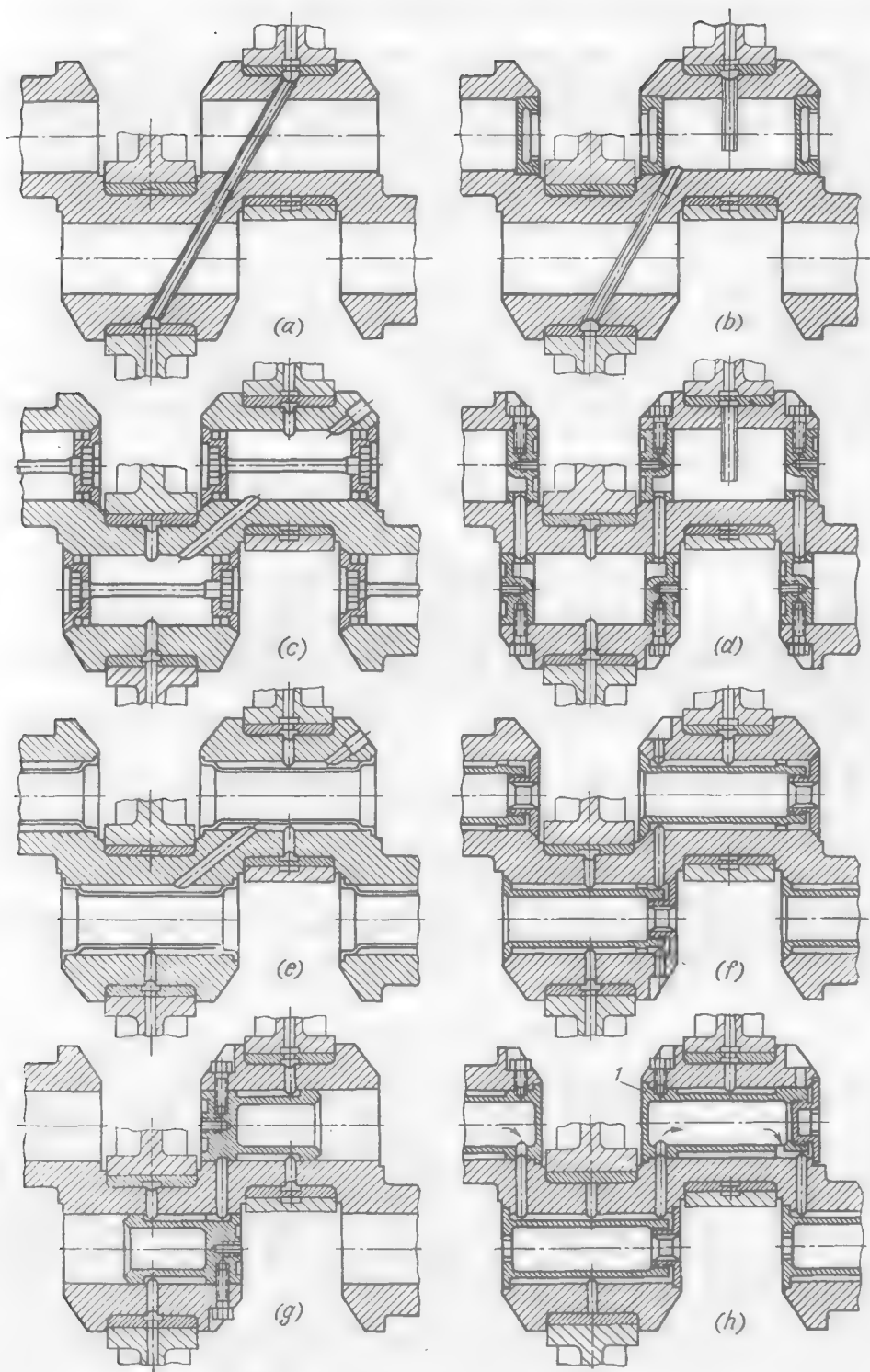
Fig. 161. Oil ducts in crankshafts

being fixed in place by rolling in. This is a solid construction and
the lubricating system of the shaft can be flushed only by pumping.

In the design in Fig. 161*f* the displacers are detachable. The designs
shown in Fig. 161*e* and *f* are for cranks arranged at an angle to one
another. When the crankpins are arranged in one line (crankpins of
the middle shaft bearings) it is difficult to install the displacers.

In the design in Fig. 161*g* use is made of short easily detachable
displacers.

Figure 161*h* illustrates *centrifuging lubrication scheme*. Oil intro-
duced through the front or rear main bearing passes through the shaft
where it is successively centrifuged in all the cranks. The main
bearings receive oil through radial holes in the shaft. The crankpins
are equipped with sleeves *1* which accumulate residues. The sleeves
are periodically removed for cleaning.

In a combined system oil is fed to every other main bearing.
Centrifuged oil is admitted into the intermediate main bearings
and the crankpins.

2.18. Thrust Bearings

By their function these bearings are classified as:

end supports used to secure shafts in the axial direction and car-
rying small loads at moderate rotational speeds;

thrust bearings intended to take up large axial forces at increased
rotational speeds.

End supports take the form of flanges on bushings, or of washers
resting against the ends of a radial bearing. They usually operate
with semifluid friction.

Thrust bearings are made as fluid-friction supports with hydro-
dynamic or hydrostatic lubrication.

The term *footstep bearing* is generally applied to thrust bearings
installed on vertical shafts.

(a) End Supports

Varieties of end supports are presented in Fig. 162.

In simplest designs the bearing surface is a flange on the bearing
bushing, against which a shaft shoulder (Fig. 162*a*), or a disk
(Fig. 162*b*) fitted on the shaft, rests.

Large-diameter flanges complicate the manufacture of the bearings.

If the bearing housing is made of a hard metal (steel, cast iron)
it is often sufficient to rest the shaft against the machined end faces
of the housing (Fig. 162*c*). When housings are made of soft alloys,
or of metals with poor antifriction properties, bronze washers or
bimetal washers (steel disks lined with an antifriction metal) are
installed on the bearing end faces (Fig. 162*d*).

The washers are (0.05 to 0.1) D thick, where D is the external diameter of the washer (the lower limits are for washers up to 50 mm in diameter and the upper ones, for washers larger than 50 mm in diameter).

Thick washers are locked by pins which are press-fitted into the housing and enter holes (Fig. 162*d*) or slots (Fig. 162*e*) in the washer.
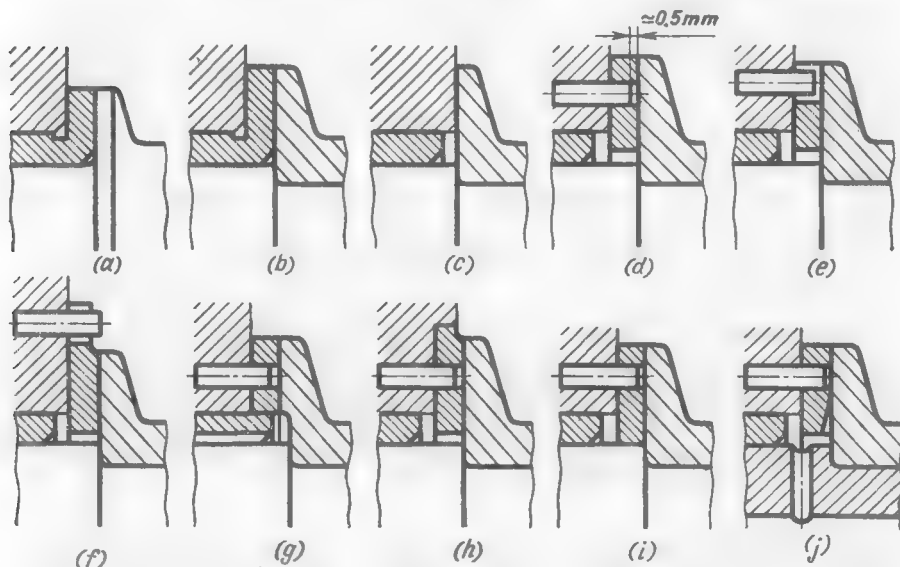
Fig. 162. End supports

The ends of the pins are made sunk at least 0.5 mm deep with respect to the frictional surface to account for the possibility of its wear. The edges of the hole protruding onto the frictional surface must be rounded.

In the design shown in Fig. 162*f* the pin is brought beyond the bearing surface and for this reason the height of its free end is unlimited. However, this method requires a considerable increase in the washer diameter.

Two diametrally opposite pins, and three pins spaced at 120° in the designs in Fig. 162*e* and *f*, are required to secure the washer in the plane perpendicular to the shaft axis.

If the washers are centred from the bearing bushing (Fig. 162*g*) or from a recess in the housing (Fig. 162*h*) one lock pin is enough.

The centring of the washer from the shaft (Fig. 162*i*) should be avoided since the frictional torque turns the washer with respect to the lock pin and causes local wear of the shaft.

The frictional surfaces of thrust flanges and washers operating under low loads are usually lubricated with the oil flowing out from the end faces of the bearing. The flow of oil through the bearings can be increased by means of longitudinal grooves (Fig. 162g) or by feeding the oil directly underneath the thrust washer (Fig. 162j).
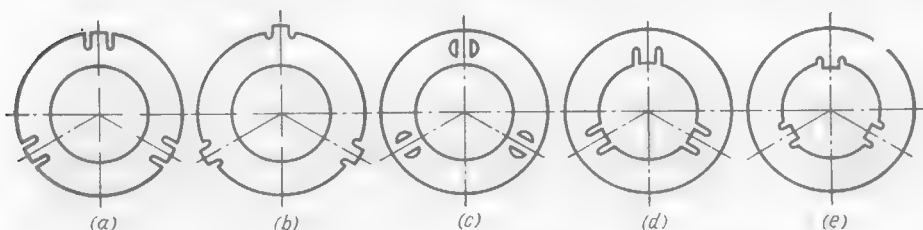
Fig. 163. Locking of thin washers

Thin-walled (1.5-2 mm thick) washers are locked by means of tongues on their external (Fig. 163a, b), middle (Fig. 163c) or internal (Fig. 163d, e) circumference, which enter slots in the housing (Fig. 164a-g). At least three slots are needed to centre the washers. One slot is enough when the centring is effected from the bushing of the bearing (Fig. 164h).
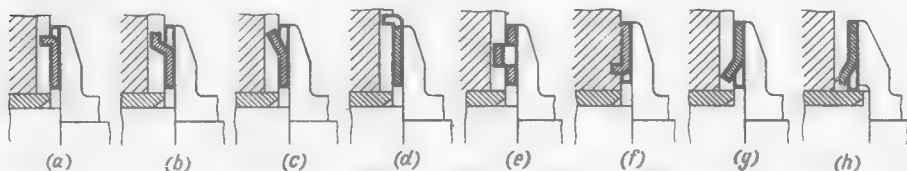
Fig. 164. Locking of thin washers

Frictional surfaces (usually surfaces of a soft material) are provided with oil distributing grooves which are made either through (Fig. 165a) or blind (Fig. 165b). Skew (Fig. 165c) and helical (Fig. 165d) grooves inclined in the direction of rotation intensify the flow of oil, and grooves inclined oppositely diminish it.

The grooves have a depth $s = 0.5\text{-}1$ mm for thick and $s = 0.3\text{-}0.5$ mm for thin washers (Fig. 165f) and are bevelled at an angle $\alpha = 5\text{-}15°$ in the direction of rotation (Fig. 165f, g). In reversible units the bevels are made on both sides of the groove (Fig. 165e, h-j).

It is an erroneous idea that these bevels form a hydrodynamic oil wedge. In actual fact, the carrying oil film develops only when the inclination angles do not exceed 10', which is possible only in washers of a larger diameter.

The load-carrying capacity of end supports is

$$P = 10^{-2}k \, [0.785 \, (D^2 - d^2) - A]$$

where D and $d =$ external and internal diameters of the washer, mm

$A =$ total area of oil distributing grooves, mm^2

$k =$ allowable unit load ($k = 1\text{-}3$ kgf/cm^2)

Unloaded end supports frequently develop undefinable random loads due to inaccuracies in their manufacture and assembly (wobble of the carrying sur-
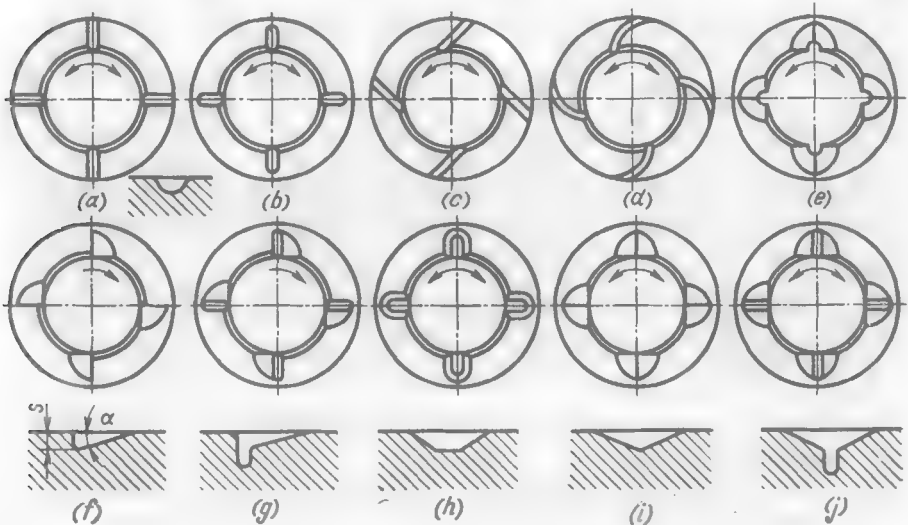
Fig. 165. Oil distributing grooves

faces of the shaft and bearing, misalignment of the shaft, etc.) which cause wear on the bearing surfaces.

The spur gear in Fig. 166a rests against the narrow annular shoulder of the bearing bushing. Although the design axial forces are absent (except for the
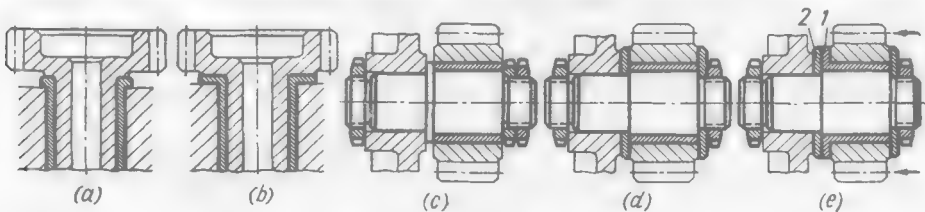
Fig. 166. Designs of end supports

negligible weight of the gear) the shoulder rapidly wears down. In the correct design (Fig. 166b) the bushing has a large-diameter flange.

In the unit where the gear is mounted on a horizontal shaft (c) the error due to the insufficient bearing surfaces is aggravated by the fact that one of these surfaces is formed by the end face of the annular nut and it is practically impossible to make this end face strictly square with the bearing axis.

In the correct design (Fig. 166d) the gear is secured by making it rest against large-diameter washers.

If the gear is loaded with axial forces (helical gear in Fig. 166e) it is necessary to use an antifriction couple (bronze flange 1 resting against steel washer 2).

When the shaft is locked on both sides (locking bearings), an axial clearance must be provided to compensate for the thermal
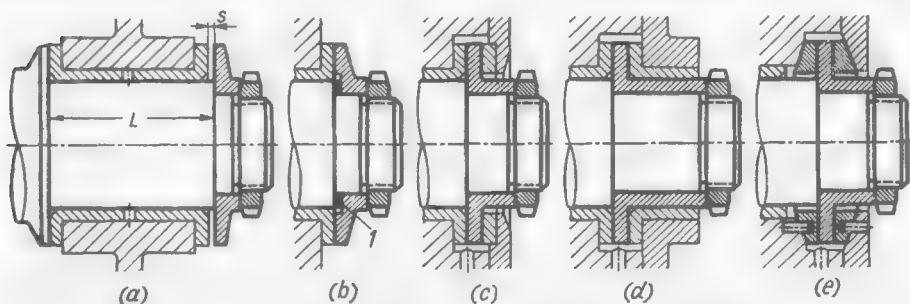
Fig. 167. Locking bearings

deformations and variations in the axial dimensions of the shaft and bearing.

In units operating at moderate temperatures the clearance s, on the average, is made equal to (0.003 to 0.005) L, where L is the bearing length (Fig. 167a).

If the bearings operate at increased temperatures and, especially, if they are installed in housings made of light alloys, this clearance must be supplemented with the *temperature clearance* s_t which accounts for the change in the axial dimensions of the system upon heating

$$s_t = L\left[\alpha_h\left(t_h - t_0\right) - \alpha_{sh}\left(t_{sh} - t_0\right)\right]$$

where L = bearing length, mm
α_h and α_{sh} = linear expansion coefficients of the housing and shaft materials, respectively
t_h and t_{sh} = working temperatures of the housing and shaft
t_0 = assembly temperature (shop temperature)

Given : $L = 100$ mm, $\alpha_h = 24 \cdot 10^{-6}$ (aluminium alloy), $\alpha_{sh} = 11 \cdot 10^{-6}$ (steel), $t_h = t_{sh} = 90°C$, $t_0 = 20°C$. Then, $s_t = 100\,(24 - 11)\,10^{-6}\,(80 - 20) \approx$ ≈ 0.1 mm.

Assuming the cold clearance to be $s = 0.003L = 0.3$ mm, we can find the total clearance $s + s_t = 0.3 + 0.1 = 0.4$ mm.

If the axial clearance needs adjustment, the thrust disk is mounted with the aid of sized washers *1* (Fig. 167*b*).

Especially accurate locking can be obtained by means of double-action thrust washers (Fig. 167*c, d*). In this case the axial clearance can be reduced to several hundredths of a millimetre.

Spherical thrust washers (Fig. 167*e*) are preferred in heavily loaded bearings.

(b) Bearings with Floating Washers

Floating washers are used with high rotational speeds when there is a hazard of the bearing being overheated. In the simplest single-
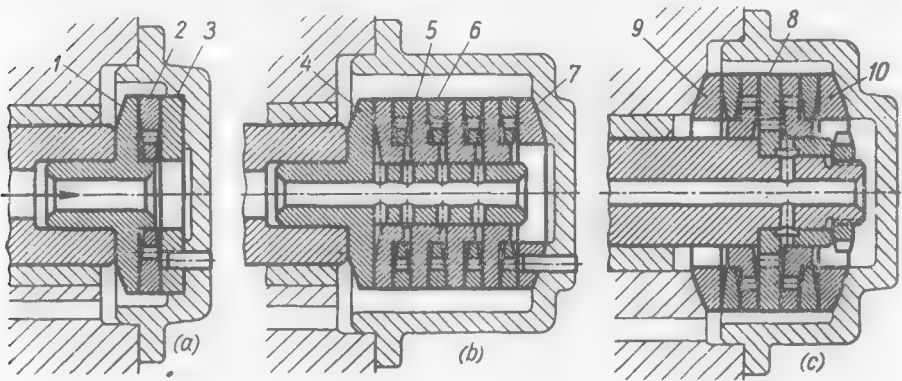
Fig. 168. Bearings with floating washers

action bearing (Fig. 168*a*) bronze floating washer *2* is installed between disk *1* of the shaft and stationary steel disk *3*. Oil is fed through the hole in the shaft and flows to the frictional surfaces along wedge-shaped recesses in the washer.

When the rotational speed is very high, heat generation can be reduced with the aid of several floating washers mounted in series.

In the single-action multiple-disk bearing (Fig.168*b*) bronze floating washers *5* are centred by their hubs on nipple *4* press-fitted into the shaft. Steel floating washers *6* with wedge-shaped recesses, which are centred on the external surfaces of the hubs, are installed between the bronze washers. The set of washers rests on one side against the disk of the nipple and on the other, against bronze washer *7* having a spherical supporting surface.

In the double-action bearing (Fig. 168*c*) the load is taken up by sets of alternating bronze and steel washers arranged on both sides of thrust disk *8* of the shaft. The system is confined between bronze self-aligning washers *9* and *10*. The total heat generation in bearings

with floating disks is less than in bearings with a stationary support-
ing surface — twice in bearings with one floating disk, three times
in bearings with two disks, etc. Multiple-disk bearings can operate
at very high rotational speeds ($\approx 20,000$ rpm).

(c) Collar Thrust Bearings

A collar thrust bearing is composed of a number of disks made
integral either with the shaft (Fig. 169a) or, which is more often,
with a shaft-fitted bushing (Fig. 169b). The disks enter annular
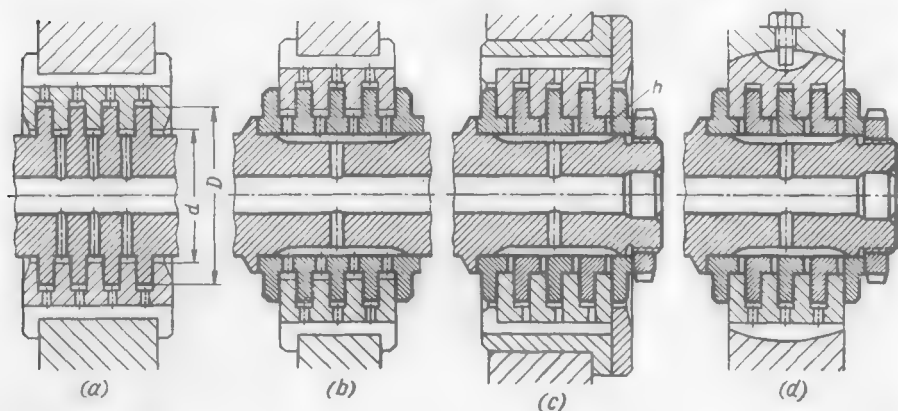
Fig. 169. Collar thrust bearings

grooves in the housing made of an antifriction material. In large
bearings the frictional surfaces of the housing are lined with babbitt
or lead bronze. A clearance of several hundredths of a millimetre
is left between each disk and the active surfaces.

The load-carrying capacity of the bearing (assuming that the load is uniform-
ly distributed among the disks) is

$$P = 10^{-2}kz\,(D^2 - d^2)$$

where D and d = external and internal diameters of frictional surfaces, mm
        k = allowable unit load, kgf/cm²
        z = number of frictional surfaces

Oil is usually fed to each frictional surface through radial holes
in the shaft (Fig. 169a) or bushing (Fig. 169b). A provision must be
made for the drainage of the used oil from each working space.

The designs in Fig. 169a and b are intended for radial assembly
(housing split in the meridional plane). In the case of axial assembly
the disks of the shaft and the collars of the housing are stacked
(Fig. 169c). Oil is supplied through end-face grooves h milled in the

disks. The housings are either rigidly fitted into the beds (Fig. 169a-c) or, which is preferable, installed on self-aligning supports (Fig. 169d).

The principal condition for the proper operation of the bearing (simultaneous contact between all the disks and the supporting surfaces) presupposes a very high machining accuracy. The active surfaces of the shaft and housing are machined by crested cutters and are lapped in during assembly. In the designs with stacked disks the axial dimensions of the latter are kept within close tolerances.

(d) Bearings with Spherical Thrust Surfaces

A special kind of thrust bearings are such as take up the load through their thrust against a sphere with its centre in line with the shaft axis. Since the contact area is very small the speed of relative motion at the point of contact is insignificant.

The load-carrying capacity of such bearings is determined, according to Hertz, by the amount of the contact stress which depends on the shape of the contacting surfaces. The highest stresses arise
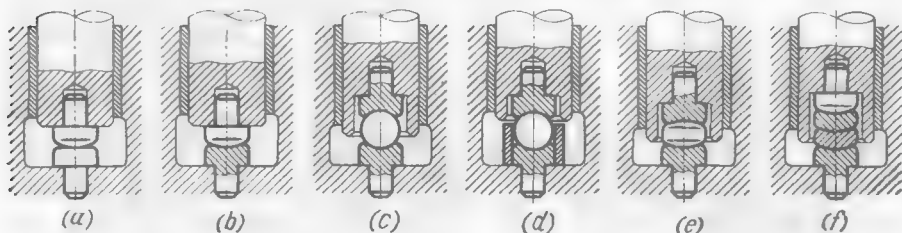
Fig. 170. Bearings with spherical thrust surfaces

when two spheres are in contact, smaller stresses are observed if a flat surface contacts a sphere, and very low stresses are in the case of contact of a sphere with a spherical concave surface with a radius equal to (1.01 to 1.02) R, where R is the sphere radius. In all cases the stresses diminish with an increase in the diameter of the spheres.

The thrust bodies are manufactured from ball-bearing steel and heat treated to a hardness of 62-65 Rc.

The allowable load on the spheres is taken at 0.01-0.02 of the crippling load in compression. For a sphere with a diameter of 10 mm, for example, the crippling load in compression between two surfaces is equal to $5 \cdot 10^4$ kgf and the allowable load is $(0.01 \text{ to } 0.02) \times \times 5 \cdot 10^4 = 500$ to 1000 kgf.

Some designs of spherical supports are displayed in Fig. 170. In the design in Fig. 170a the spherical tip pressed into the shaft rests against a flat heel mounted in the housing. The design with a spherical heel (Fig. 170b) is distinguished by a higher load-carrying

capacity. The design with a complete sphere (Fig. 170c) is superior
due to the fact that the sphere rotates during operation because of
the misalignment of the supporting surfaces observed practically
always, and wears sufficiently uniformly on its entire surface.
In the design shown in Fig. 170d the sphere is additionally held
in position by a bushing centred from the lower heel.

In the design with a floating block and spherical supporting sur-
faces of large radius (Fig. 170e) the speed of relative motion across
the contact areas diminishes about twice. Supports intended to take
up large axial forces at increased rotational speeds are made as a set
of self-aligning floating meniscus washers (Fig. 170f).

Bearings with spherical supports are used with a unilateral load
preferably in units with vertical shafts where it is easier to ensure
the self-alignment of frictional spherical bodies.

(e) Hydraulic Footstep Bearings

In hydraulic footstep bearings the axial load is taken up by an
oil cushion in an enclosed space fed with oil by a pump. The shaft
is kept in a permanent ver-
tical position by means of
oil distributing devices.
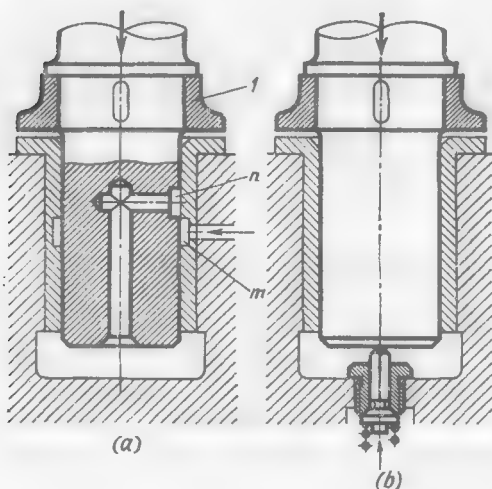
In the simplest design
(Fig. 171a) the oil is deliv-
ered into the annular
groove m of the footstep
bearing and is then fed
through the flat recess n
and the radial hole in the
shaft into the enclosed ca-
vity under the shaft end
face. The position shown
on the drawing (the edge
of the flat touches the edge
of the annular groove) cor-
responds to the state of
equilibrium. The oil-feed
groove is shut off and the
oil is not supplied under

Fig. 171. Hydraulic footstep bearings

the shaft end face. As the shaft sinks the radial hole communica-
tes with the annular groove, and the oil flows under the shaft
end face and returns it to the initial position. In this way the shaft
continuously oscillates with a small amplitude near the equilibrium
position.

The flat which opens at once large flow cross-sections helps reduce
the oscillation amplitude.

Thrust washer *1* installed with a small clearance with respect to the flange of the footstep bearing is intended to hold the shaft during idle periods.

In the design shown in Fig. 171*b* the infeed to the oil cushion is effected with the aid of a needle valve controlled by the shaft. The equilibrium position will be attained when the end of the shaft slightly touches the tang of the closed valve. As the shaft sinks it opens the valve and the oil enters the cavity thereby returning the shaft to the original position.

The load-carrying capacity of hydraulic footstep bearings depends on the oil-feed pressure and the cross-sectional area of the shaft. With pressures of 30-40 kgf/cm² the load-carrying capacity of such bearings can be compared with that of mechanical footstep bearings of the same radial dimensions.

Example. Shaft diameter $d = 50$ mm, feed pressure $p = 30$ kgf/cm². The carrying capacity $P = 0.785 d^2 \cdot p = 0.785 \cdot 5^2 \cdot 30 = 600$ kgf.

Friction (on the oil cushion) is insignificant.

If the oil cushion is fed from a pump with an independent drive no friction occurs on washer *1* during the starting and racing periods.

The shortcomings of hydraulic footstep bearings are: high oil pressure, relatively large power consumption in forming the oil cushion and poor axial fixing of the shaft.

Hydraulic footstep bearings are used for shafts of a small diameter (up to 50 mm on the average) loaded with forces of up to 1000 kgf. For greater loads it is more expedient to use hydrostatic bearings (see below) which are more advantageous from the power consumption viewpoint.

(f) Hydrodynamic Thrust Bearings

Bearings with Inclined Carrying Surfaces

The diagram of a bearing with an inclined carrying surface is illustrated in Fig. 172. Surface *1* moves with a speed *v* relative to stationary surface *2*

Fig. 172. Design diagram for a bearing with an oil wedge

having length *L* and width *B* and inclined at an angle α. The oil entrained by the moving surface enters the converging clearance and tends to flow to the sides and the inlet edge of surface *2*.

The forces of oil viscosity hamper the flow and increase the pressure in the oil layer (top diagram). The oil left after the side leakage passes through the narrowest section of the clearance and draws surface *1* away from the inclined surface, thereby producing a continuously renewed oil layer with a minimum thickness h_0. The pressure developing in the oil layer allows the system to withstand loads perpendicular to the direction of motion. The resultant R of the pressure forces of the oil layer is at a distance $l = (0.55 \text{ to } 0.65) L$ from the front edge of the inclined surface.

Smooth rounding of the front edge (in the direction of motion) of the carrying surface is the prime requirement for the oil wedge formation.

The minimum thickness h_0 of the oil layer is directly proportional to the oil viscosity η and the speed of motion v, and inversely proportional to the load P, and depends on the ratio L/B and the inclination angle α. If h_0 exceeds the critical value h_{cr}, at which contact between the metal surfaces is possible, purely fluid friction occurs in the bearing.

The theory shows that the carrying capacity is determined by the dimensionless factor (Gümbel's number)

$$G\ddot{u} = \frac{Ph_0^2}{\eta v L B^2} = \frac{kh_0^2}{\eta v B} \tag{2.42}$$

where P = axial load, kgf
        η = oil viscosity, kgf·s/m²
        v = speed of motion, m/s
L and B = length and width of the inclined surface, m
       h_0 = minimum thickness of the oil layer, m
       $k = \dfrac{P}{LB}$ is the unit load, kgf/m²

In conformity with Eq. (2.42), the load-carrying capacity of the bearings is

$$P = G\ddot{u} \frac{\eta v L B^2}{h_0^2} \tag{2.43}$$

Figure 173 shows the dependence of $G\ddot{u}$ on h_0/t for various L/B values, where t is the maximum height of the slope. The value of $G\ddot{u}$ (and hence, the load-carrying capacity of the bearing) is maximum ($G\ddot{u} = 0.07$) when $h_0/t = 0.8$ and $L/B = 1$. In this case the coefficient of friction is close to the minimum.

Slight deviations from the optimum values do not affect to any appreciable degree the value of $G\ddot{u}$. When $h_0/t = 0.6$-1.2. (shaded area on the diagram) and $L/B = 1$-1.4 the value of $G\ddot{u}$ varies within. 0.067-0.07. These values of h_0/t and L/B should be adhered to in designing.

The same diagram displays the curve l/L (l is the distance between the resultant of the pressure forces and the front edge of the inclined surface). With the optimum $h_0/t = 0.8$, the ratio $l/L = 0.58$.
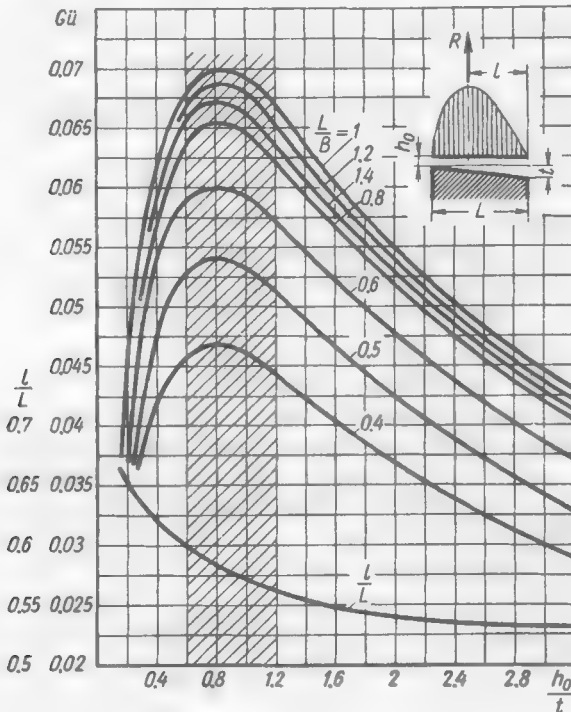
Fig. 173. Dependence of $G\ddot{u}$ on h_0/t for various L/B values

In bearings of this type ($t = $ const) the ratio h_0/t and also $G\ddot{u}$ change due to the change in h_0 occurring when the operating conditions vary. A reduction in h_0 (increase in the load, drop in oil viscosity) is dangerous. For this reason it is advisable to use somewhat higher values $h_0/t = 1\text{-}1.2$ for the nominal conditions of operation so that a reserve of the carrying capacity is built up. This will ensure the bearing operating under optimum conditions when the load is increased.

The coefficient of friction is

$$f = 3 \sqrt{\frac{\eta v}{kB}} = 3 \frac{h_0}{B} \sqrt{\frac{1}{G\ddot{u}}} \tag{2.44}$$

The work of friction per second

$$N = Pfv = 3Pv \sqrt{\frac{\eta v}{kB}} \tag{2.45}$$

Generation of heat per second

$$R = \frac{N}{427} \approx 0.007 Pv \sqrt{\frac{\eta v}{kB}} \tag{2.46}$$

The efflux of oil per second from under the inclined surface

$$Q = 0.7 \cdot 10^3 B v h_0 \tag{2.47}$$

The heat balance equation (assuming that all the heat is absorbed by the oil) is

$$R = Q \gamma c (t - t_0) \tag{2.48}$$

where γ = specific weight of oil, kgf/l
c = heat capacity of oil, cal/kgf·°C
t_0 and t = temperature of oil at the inlet and outlet of the bearing
The mean temperature of the oil layer is

$$t_m = \frac{t + t_0}{2} \tag{2.49}$$

In disk-type thrust bearings the inclined surfaces are made in the form of segments separated by oil-feed grooves (Fig. 174). Six to eight segments are usually used.

The width of the segment is

$$B = \frac{D - d}{2} \tag{2.50}$$

where D and d are the external and internal diameters of the disk.

The speed over the mean circumference is

$$v = \frac{\omega d_m}{2} = \frac{\pi n d_m}{60}$$

where ω is the angular velocity of the shaft and n is the rotational speed of the shaft in rpm.

The length of the segment over the mean circumference is

Fig. 174. Design diagram for a disk-type thrust bearing

$$L = \frac{\pi d_m \beta}{z} = \frac{\pi (D + d) \beta}{2z} \tag{2.51}$$

where z is the number of segments and β is the utilization factor of the circumference, which is expressed as

$$\beta = \frac{\pi d_m - zm}{\pi d_m} = 1 - \frac{zm}{\pi d_m} \tag{2.52}$$

where m is the width of the oil-feed grooves over the mean circumference (with account being taken of the fillets at the edges of the grooves). Usually, $\beta = 0.8$-0.85.
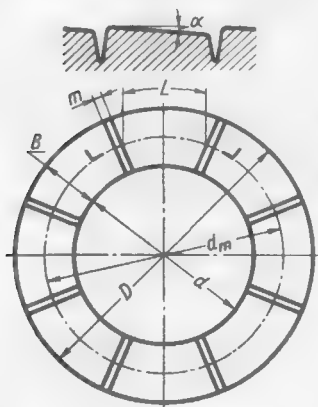
It follows from Eqs. (2.50) and (2.51) that

$$\frac{D/d+1}{D/d-1} = \frac{z}{\pi\beta} \cdot \frac{L}{B} \tag{2.53}$$

This expression is used to plot the graph (Fig. 175) showing the dependence of D/d on z with various ratios L/B (assuming that $\beta = 0.85$). The range of L/B and D/d values in most common use is shaded.

According to Eq. (2.43), the total load-carrying capacity of the bearing is

$$P = \frac{z\eta v L B^2}{h_0^2} G\ddot{u} = \frac{\eta n\beta A^2}{60 h_0^2} G\ddot{u} \tag{2.54}$$

or

$$P = 0.017 \frac{\eta n A^2 \beta}{h_0^2} G\ddot{u} \tag{2.55}$$

where η = oil viscosity, cP
A = carrying area of the bearing, cm²
h_0 = minimum clearance, μm
n = rotational speed of the shaft, rpm

The values of $G\ddot{u}$ are found from the graph (see Fig. 173), depending on the adopted h_0/t and L/B. With the optimum values ($h_0/t = 0.8$-1, $L/B = 1$) $G\ddot{u} = 0.07$ and Eq. (2.55) takes the form

Fig. 175. Dependence of D/d on z for various L/B values

$$P = 1.2 \cdot 10^{-3} \frac{\eta n A^2 \beta}{h_0^2} \tag{2.56}$$

where the designations are the same as in Eq. (2.55).

As can be seen from Eqs. (2.55) and (2.56), the load-carrying capacity of the bearing sharply increases with the greater bearing area A and smaller minimum clearance h_0.

The inclination angle α of the bearing surface may be found from the formula

$$\tan \alpha = \frac{t}{L} \tag{2.57}$$

With the optimum $t = 1.25 h_0$

$$\tan \alpha = \frac{1.25 h_0}{L} \qquad (2.58)$$

With the ratios h_0/L within the range 0.00025-0.0005, which is usual for disk-type bearings,

$$\tan \alpha = 0.0003\text{-}0.001 \ (\alpha = 1\text{-}4')$$

Load P, rotational speed n and oil viscosity η are usually specified in design calculations, and the dimensions of the bearing are to be found.

The minimum value of h_0 (in μm) ensuring fluid friction is determined from the empirical formula

$$h_0 = a \sqrt{d_m} \qquad (2.59)$$

In the case of highly accurate manufacture and assembly the coefficient $a = 0.7\text{-}1$, but for bearings of ordinary accuracy $a = 1\text{-}1.5$.

Having specified an approximate value of d_m, this formula is used to find h_0, and preliminarily assuming that $\beta = 0.85$, the bearing area A is determined from Eq. (2.55).

Selecting d to suit the design, the ratio D/d is calculated from the formula

$$A = \frac{\pi}{4} \beta d^2 \left[\left(\frac{D}{d} \right)^2 - 1 \right] \qquad (2.60)$$

and the graph in Fig. 175 is used to find the nearest whole number of segments z (preferably even) that will ensure the acceptable values of $L/B = 1\text{-}1.4$.

Then, the value of β is corrected and the calculations are repeated, if necessary.

The external diameter is

$$D = (D/d) \, d$$

The mean diameter

$$d_m = \frac{D+d}{2}$$

If the value of d_m appreciably differs from the one adopted when determining h_0 by Eq. (2.55), the results are recalculated.

The unit load on the bearing surfaces is

$$k = \frac{P}{zBL}$$

In ready designs the load is, on the average, 20-50 kgf/cm², and can be as high as 100 kgf/cm² with careful manufacture and assembly.

According to Eq. (2.44), the coefficient of friction is

$$f = 6.7 \cdot 10^{-5} \sqrt{\frac{\eta n d_m}{kB}} = 3 \cdot 10^{-4} \frac{h_0}{B} \sqrt{\frac{1}{G\ddot{u}}} \qquad (2.61)$$

where η is in cP, k in kgf/cm^2, B and d_m in cm and n in rpm.

From Eq. (2.57) the inclination angle α is given by

$$\tan \alpha = \frac{t}{L} = \frac{h_0}{L(h_0/t)} \qquad (2.62)$$

During check calculation (the dimensions and operating conditions of the bearing are given) the value of h_0 is determined and compared with the allowable value given by Eq. (2.59).

Heat calculations are made using the method of successive approximations. A trial value of the mean oil layer temperature is first specified, then the working oil viscosity (for the given grade of oil) is found and, finally, the heat generation per second is calculated from Eq. (2.46).

The total efflux of oil per second is

$$Q' = zQ \qquad (2.63)$$

where z is the number of the segments and Q is the efflux of oil from under one segment, determined by Eq. (2.47).

The heat balance equation (2.48) is used to find the mean temperature t_m of the oil layer. If the obtained value of t_m differs from the preliminary value, calculations are repeated until these values coincide.

The basic varieties of bearings with inclined supporting surfaces are presented in Fig. 176a-e. The diagrams illustrate the maximum values of $G\ddot{u}$.

The manufacture of the segments is simplified if they are made with flat areas (Fig. 176b) serving as the base for machining the inclined surfaces. The hydrodynamically optimum width of such areas is $0.2L$. The other geometrical relationships, the load-carrying capacity and the sequence of calculating the segments with flat areas are the same as for inclined segments.

Segments of reversible bearings are made with two symmetrical bevels inclined oppositely (Fig. 176c). Their carrying capacity is about two times less than that of the segments with a unilateral bevel. The coefficient of friction is higher than in single-wedge bearings $\left(f = 5.2 \sqrt{\frac{\eta v}{kB}} \right)$.

With the same h_0/t, reversible bearings of a sinusoidal shape (Fig. 176d) possess a somewhat larger load-carrying capacity than bearings with double-sided bevels, but it is much more difficult to machine them. In the design shown in Fig. 176e waviness is

formed by elastically deforming the carrying disk *1* by means of wedges *2*. The design allows the value of t_0 to be adjusted as required.
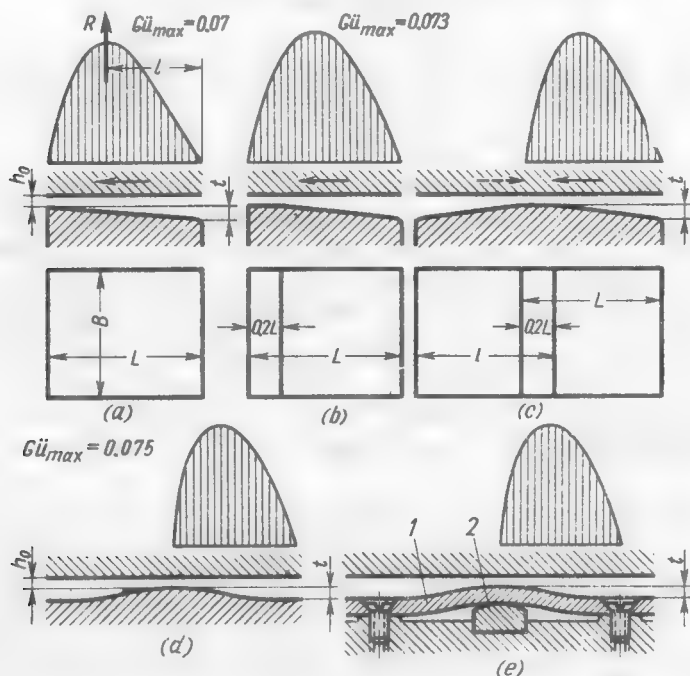
Fig. 176. Design diagrams for bearings with inclined supporting surfaces
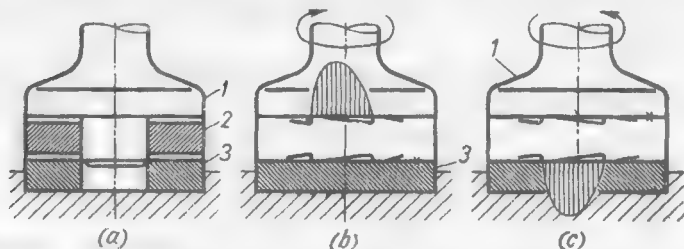
Fig. 177. Reversible bearing with an intermediate floating washer

It is more advisable to use reversible bearings with an intermediate floating washer *2* (Fig. 177a) installed between thrust disk *1* of the shaft and stationary bearing surface *3*. Mirror-inverted bevels are provided on the upper and lower surfaces of the washer. When the thrust disk rotates clockwise (Fig. 177b) oil wedges form on the upper side of the washer. Semifluid friction which retains the washer in place relative to the bearing surface *3* sets in on the opposite side where the hydrodynamic effect is absent.

If the shaft rotates in the reverse direction (Fig. 177c) the washer rotates together with thrust disk *1* of the shaft over the oil wedges formed on surface *3*.

The carrying surfaces of bearings of small and medium size are made in the form of disks of antifriction bronze with milled inclined areas and oil distributing grooves. In serial production the active surfaces are manufactured by cold closed-die coining which ensures high accuracy and good finish of the surfaces.

The carrying surfaces of bearings with a constant direction of rotation are made with single-sided bevels (Fig. 178a) and those of reversible bearings, with double-sided bevels (Fig. 178b).
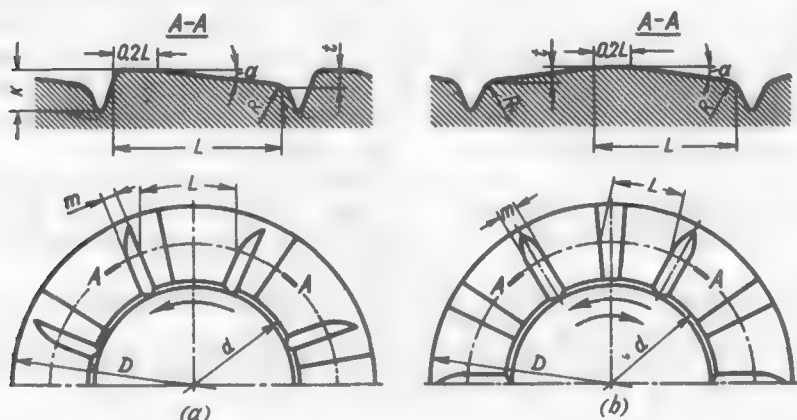
Fig. 178. Disks with inclined carrying surfaces

The depth k of oil-feed grooves is 1-1.5 mm, their width being $m = 2$-5 mm. The edges of the grooves are rounded by smooth fillets and the internal circumference of the disks is chamfered at an angle of 45° with a leg length at least equal to m.
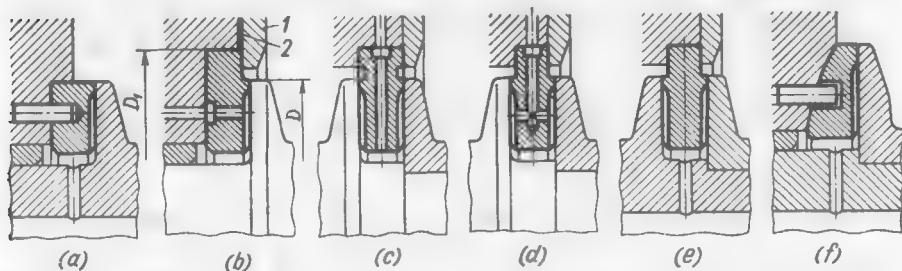
Fig. 179. Installation of disks in housings

The disks of bearings carrying a load of constant direction are centred in the housing from their external diameter and are locked against rotation by pins (Fig. 179a). If there is an axial clearance

in the system, it is advisable to fasten the disk by tightening it with washer *1* (Fig. 179*b*) mounted on an elastic gasket *2*. In this case the centring diameter *D'* must be larger than the diameter *D* of the active surface.

Oil is fed to the active surfaces either through the shaft (Fig. 179*a*) or through the housing (Fig. 179*b*).

The disks of double-action bearings are usually locked by tighteing. To provide for the exit of oil, use is made of annular grooves (Fig. 179*c*), or the active surfaces are arranged above the fastening ones (Fig. 179*d*).

Oil is fed from the housing either through radial holes in the disk (Fig. 179*c, d*) or through the shaft (Fig. 179*e*).

Fig. 180. Self-aligning double-action segmental bearing

Misalignment is eliminated if the supporting washers are installed on spherical elements (Fig. 179*f*).

In large bearings the segments are stacked (Fig. 180), and their active surfaces are lined with babbitt or lead bronze.

Single- and Double-Wedge Thrust Bearings

The simplest method to form single-wedge bearings consists in making the surface of a disk (Fig. 181*a*) or a washer (Fig. 181*b*)·
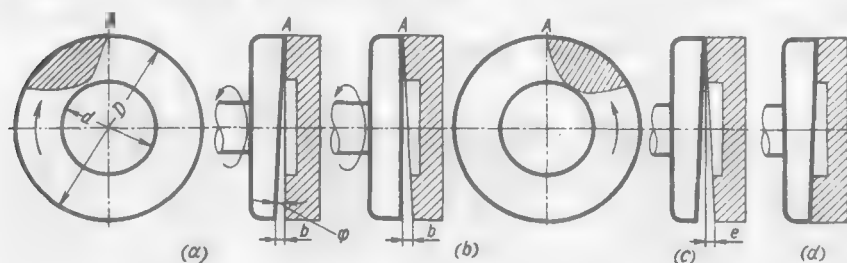
Fig. 181. Single-wedge bearings with skew surfaces

skew relative to the plane of rotation. The wedge-shaped clearance formed between the surfaces expands in the peripheral direction on both sides from point *A*, where the surfaces are closest together, and in the radial direction proportionally to the approach to the centre. If the wedge angle over the circumference is sufficiently small, a hydrodynamic pressure propagating through an angle of

about 60° from point A towards the side opposite to the shaft rotation (shaded area) develops in the portion of the clearance converging in the direction of rotation. The pressure is maximum at point A and drops in the peripheral and radial directions as the clearance grows larger.

With a skew disk the pressure zone moves together with the shaft with respect to the washer, and it is stationary if the washer is skew.

Oil is usually introduced through central holes in the shaft or in the washer.

The inclination of the surfaces is determined on the condition of the equality of the wedge angle over the circumference to the hydrodynamic angle α (tan $\alpha = 0.0003-0.001$).

The wobble b of the disk (or washer) is

$$b = \frac{\pi D}{2} \tan \alpha$$

The skew angle φ of the washer

$$\tan \varphi = \frac{b}{D} = \frac{\pi}{2} \tan \alpha \qquad (2.64)$$

If, for example, tan $\alpha = 0.0006$ and $d = 100$ mm, then

$$\tan \varphi = 1.57 \cdot 0.0006 \approx 0.001$$

and

$$b = 0.001 \cdot 100 = 0.1 \text{ (mm)}$$

The surface opposite to the inclined surface must be strictly square with the axis of rotation. If both surfaces are inclined (Fig. 181c), the shaft will oscillate in the axial direction with an amplitude e and a frequency equal to the rotational speed.

If the inclination angles of the surfaces of the disk and washer are close in absolute magnitude the clearance wedge becomes zero (when the inclinations coincide) once every revolution (Fig. 181d) and semifluid friction periodically sets in in the bearing.

The disadvantage of single-wedge bearings is that the resultant of the pressure forces of the oil layer is applied eccentrically (average eccentricity is equal to $0.8D/2$). The shaft is subjected to the action of a bending moment $M_{bend} \approx 0.4P$ (where P is the axial force) in a plane which either remains stationary, if the disk is skew, or rotates with respect to the shaft, if the washer is skew.

The force is applied centrally, if double-wedge bearings are used. Two wedges can easily be formed, if the surfaces of the disk or the washer are imparted a slightly concave (Fig. 182a, d), or convex (Fig. 182b, c) cylindrical form. The pressure zones in this case are arranged symmetrically in the quadrants adjoining points A of the closest approach on the side opposite to the direction of the shaft

rotation. In these bearings the value of b must be twice less than in single-wedge bearings. Flat surfaces must be strictly perpendicular to the axis of rotation.
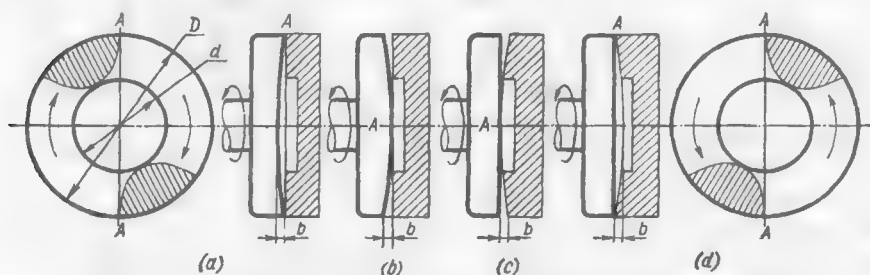
Fig. 182. Double-wedge bearings with cylindrical surfaces

Bearings of this type are utilized to take up small loads when the use of more complicated multiple-wedge supports is economically not justified.
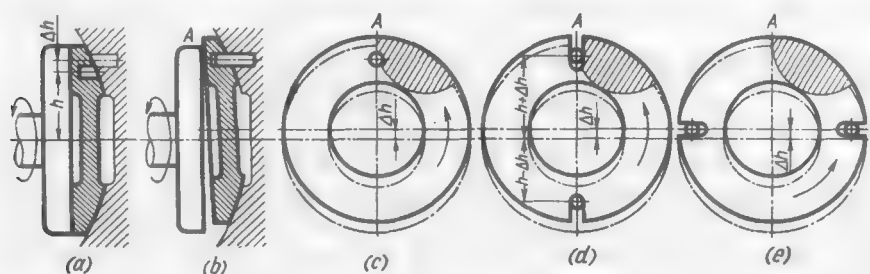
Fig. 183. Formation of an oil wedge in bearings with a spherical support

Thrust washers installed on a spherical member can also form oil wedges. The oil wedge is produced as the washer inclines during its deviations on the spherical bed.

The simplest method to produce inclination consists in a metered displacement of the lock pin axis on the bed with respect to the axis of the recess for the lock pin in the washer.

If the lock pin axis is placed above the axis of the recess at a distance Δh (Fig. 183a), the washer mounted on the pin rises slightly from its seat, forming a clearance diverging as a wedge from point A of the closest approach of the washer and disk (Fig. 183b). A pressure zone (Fig. 183c) is formed in the quadrant adjoining point A where the disk climbs.

If the lock pin is below the centre of the recess, the washer during installation sinks on the bed and a wedge-shaped clearance is formed on the lower side of the washer.

When two pins entering slots in the washer are used for locking, inclination is attained by shifting the pins to a distance Δh either with respect to the centre of the bed (Fig. 183d) or with respect to the horizontal axis of the bed (Fig. 183e).

Let us find the value of Δh that will ensure the formation of the hydrodynamic wedge.

Let the distance between the recess centre (point A, Fig. 184) and the washer axis be

$$h = R_{sph} \sin \beta = \psi D \sin \beta \qquad (2.65)$$

where β = nominal angle establishing the pin position

R_{sph} = radius of the sphere

$\psi = R_{sph}/D$ is the ratio of the sphere radius to the diameter D of the washer ($\psi = 0.8\text{-}1$)

Fig. 184. Determining the value of Δh

With the usual arrangement of the pin on the mean circumference of the wash-er

$$h = \frac{d_m}{2} = \frac{D+d}{4}$$

and

$$\sin \beta = \frac{h}{R_{sph}} = \frac{D+d}{4R_{sph}} \approx \frac{D+d}{4\psi D} = \frac{1+d/D}{4\psi}$$

Let the pin centre (point A') be displaced to a distance Δh, i.e., it is at a distance of $H = h + \Delta h$ from the axis of the bed. As the washer is placed on the pin (matching of points A and A') it becomes inclined at an angle φ determined from the expression

$$\sin (\beta + \varphi) = \frac{H}{R_{sph}} \approx \frac{h + \Delta h}{\psi D}$$

Substituting into this expression the value of h from Eq. (2.65), we obtain

$$\Delta h = H - h = \psi D [\sin (\beta + \varphi) - \sin \beta] \qquad (2.66)$$

To form a hydrodynamic wedge the following condition must be satisfied:

$$\tan \varphi = \frac{\pi}{2} \tan \alpha$$

where α is the hydrodynamic angle ($\tan \alpha = 0.0003\text{-}0.001$).

Example. Let $D = 100$ mm, $d/D = 0.5$, $\psi = 1$ and $\tan \alpha = 0.0006$ ($\alpha = 2'20''$). Then

$$\sin \beta = \frac{1 + d/D}{4\psi} = 0.375 \ (\beta = 22°)$$

$$\tan \varphi = 1.57 \cdot 0.0006 \approx 0.001 \ (\varphi = 3'30'')$$

From Eq. (2.66) we get

$$\Delta h = \psi D [\sin (\beta + \varphi) - \sin \beta] = 100 \ (\sin 22°3'30'' - \sin 22°) =$$
$$= 100 \ (0.376 - 0.375) = 100 \cdot 0.001 = 0.1 \ \text{(mm)}$$

Thus, the displacement necessary to form a hydrodynamic wedge is insignificant and with usual manufacturing accuracy lies within the manufacturing tolerances. In ready designs we can almost always observe displacements of this kind, and therefore hydrodynamic lubrication is ensured to a larger or lesser degree. This mainly
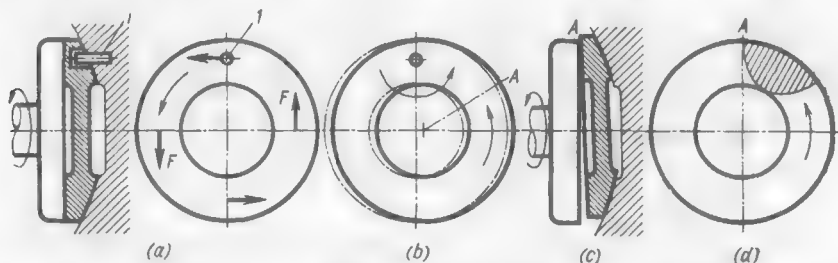
Fig. 185. Formation of an oil wedge under the action of frictional forces

explains the increased carrying capacity of washers on spherical seats. By controlling the displacement it is possible to attain stable hydrodynamic lubrication with optimum parameters.

When spherical washers are locked by one pin the hydrodynamic wedge is also formed as a result of the frictional forces displacing the washer.

The washer locked by pin *1* (Fig. 185*a*) is turned by the frictional forces *F* around the pin contrary to the direction of rotation (Fig. 185*b*) and becomes misaligned as it moves over the spherical surface, its edge being raised in the section *A* (Fig. 185*c*), and a pressure zone develops in the adjacent quadrant on the disk run-on side (Fig. 185*d*).

The wedge angle depends on the relation between the moment of the frictional forces and the axial load tending to return the washer to the central position.
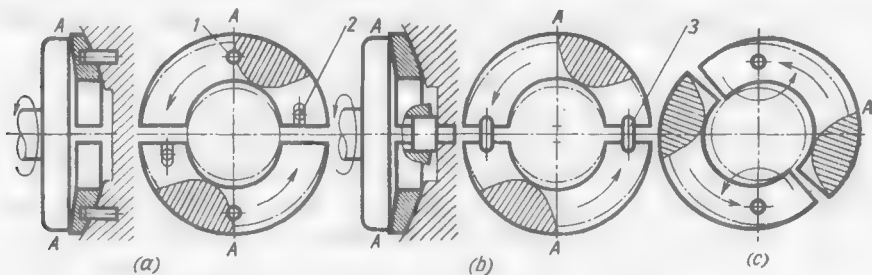
Fig. 186. Double-wedge bearings on spherical supports

The disadvantage of spherical washers is the eccentric application of the resultant of the pressure forces in the oil layer. In the case

of double-wedge bearings the washers are cut in the equatorial plane (Fig. 186a), their inclination being obtained by displacing lock pins *1* (pins *2* retain the half-wash-ers in place), or by drawing the half-washers apart by means of pins *3* installed in the cut (Fig. 186b) or by making use of the displacement of the half-washers by the frictional forces (Fig. 186c).

Fig. 187. Bearing with a spherical washer

The design of a thrust bearing with a spherical washer is exemplified in Fig. 187.

The ratio d/D is usually taken at 0.5. The sphere radius $R_{sph} = 0.8$-1. Larger values of R_{sph} impair self-alignment, and smaller values appreciably increase the axial dimensions of the bearing.

Oil must always be fed to the surface of the sphere. The active surface of the washer is provided with oil distributing grooves with single bevels in the case of rotation of constant direction, and with double bevels for reversible bearings.

Bearings with Stepped Carrying Surfaces

In these bearings (Fig. 188a) the fluid film is formed as a result of the oil being forced into the clearance h between the thrust disk
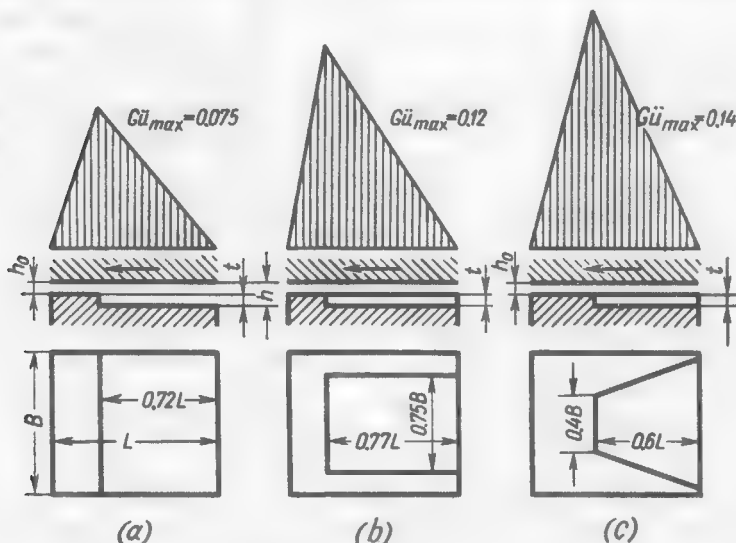
Fig. 188. Bearings with stepped carrying surfaces

and stationary segments, and the oil flow throttled in the narrow slit h_0 between the step and the disk.

With the optimum ratios (recess length $\lambda \approx 0.7L$, $h_0/t = 0.8\text{-}1$) the load-carrying capacity of stepped bearings is about the same as that of the wedge-type bearings.

A higher carrying capacity is observed in stepped bearings with locking edges (Fig. 188*b*, *c*) that restrict the efflux of oil in radial directions.

The dependence of $Gü$ on h_0/t for various L/B (with optimum values of λ for each value of L/B) is shown in Fig. 189. For the sake of comparison the plot also displays the $Gü$ curve for a wedge-type bearing with the optimum ratio $L/B = 1$ (dashed line).

It can be seen on the plot that the load-carrying capacity of stepped bearings with locking edges is much higher than that of the wedge-type bearings. The carrying capacity grows higher even with the L/B ratio increasing in excess of 1 whereas in the case of wedge-type bearings the carrying capacity reaches its maximum at $L/B = 1$ (see Fig. 173).

Fig. 189. Dependence of $Gü$ on h_0/t (stepped bearings)

However, the loading maxima of stepped bearings, especially with high L/B ratios, lie within very narrow h_0/t limits. It follows therefore that such bearings are extremely sensitive to variations in operating conditions.

Bearing in mind this feature, the value of L/B is selected within 1-1.5 (lower values for high rotational speeds and upper values for low speeds). In this case the optimum values are $h_0/t = 0.6\text{-}1$, $\lambda = 0.76\text{-}0.8$, and $Gü = 0.12\text{-}0.14$, i.e., it exceeds by 1.7-2 times the Gümbel number for a wedge-type bearing with optimum parameters.

As for the rest, stepped bearings are calculated in the same manner as wedge-type bearings.

Reversible stepped bearings are made with symmetrical recesses (Fig. 190a) or with an intermediate floating washer (see Fig. 177).
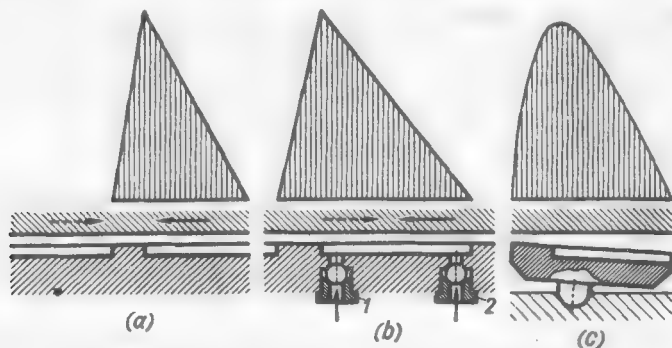
Fig. 190. Reversible stepped bearings

In the design in Fig. 190b reversibility is assured by means of nonreturn valves 1 and 2 in the oil-feed holes. In the case of rotation in the direction indicated
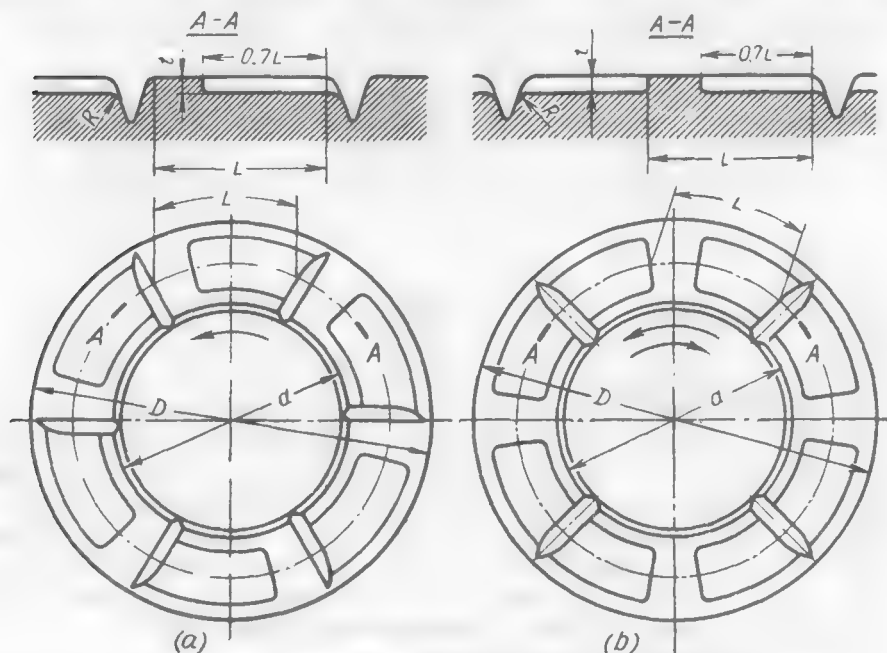
Fig. 191. Disks with stepped supporting surfaces

by the solid arrow, valve 1 is shut off by the pressure of oil in the recess, while valve 2 is opened by the pressure built up by the pump. If the direction of rotation

is reversed (dashed arrow), valve *2* is shut off and valve *1* is open. This produces a carrying oil layer in the recess with any direction of rotation.

Bearings of this type can operate during the starting period as hydrostatic bearings, and as hydrodynamic ones in steady-state operating conditions.

It is expedient to use self-aligning stepped segments (Fig. 190c).

Figure 191a, b illustrates the design of disks with stepped bearing surfaces for unidirectional and bidirectional rotation, respectively.

Bearings with Self-Aligning Segments

In bearings of this type the segments are mounted on hinges resting on a stationary surface (Fig. 192).

With any segment inclination angle α the resultant of the pressure forces of the oil layer passes through the hinge axis. For this
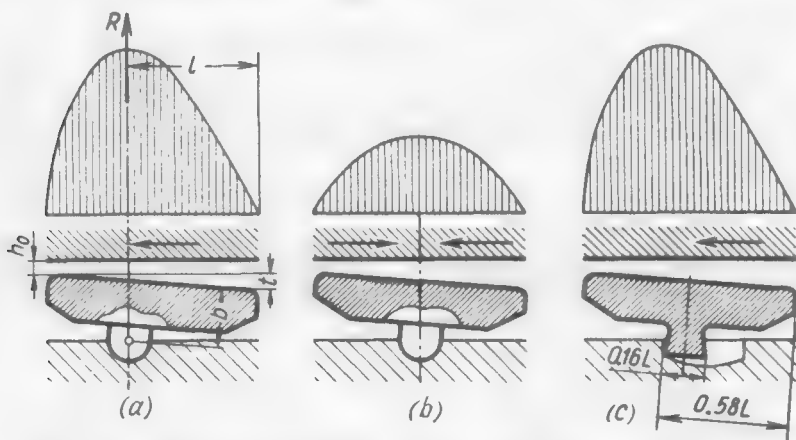
Fig. 192. Design diagrams for bearings with self-aligning segments

reason, the position of the hinge (coordinate l in Fig. 192a) specifies quite definitely the value of h_0/t which remains constant with any variations in the operating conditions. In conformity with the plot (see Fig. 173) the coordinate $l = 0.58L$ corresponds to the optimum $h_0/t = 0.8$. If the hinge is arranged at this point the optimum characteristics will remain whatever the variations in the operating conditions. This is the principal distinction and advantage of bearings with self-aligning segments as compared to bearings with stationary segments, whose characteristics change with the variations in the operating conditions.

According to the plot (see Fig. 173), the allowable size l at which $G\bar{u} = 0.07$-0.067 (shaded area on the plot) is very limited: $l = (0.56$ to $0.6)$ L. When this size changes the performance of the bearing sharply deteriorates. For

example, when $l = 0.53$ $(h_0/t = 3)$, Gümbel's number diminishes (for a bearing with $L/B = 1$) to 0.045, i.e., the load-carrying capacity of the bearing drops $\frac{0.07}{0.045} = 1.55$ times as compared with the maximum value.

The distance b from the centre of the hinge to the sliding plane of the segment (Fig. 192a) does not affect in any appreciable manner the self-alignment, and can vary within very wide limits.

Bearings with self-aligning segments are calculated by Eqs. (2.43)-(2.56), i.e., in the same manner as in the case of stationary segments.

Hinges in reversible bearings are installed in the centre of the segments (Fig. 192b). The load-carrying capacity of such bearings is much less than that of the bearings with the optimum hinge arrangement.

The design with shifting segments (Fig. 192c) having two knife-type supports, the distance between which is 0.16L, is more practicable. The supporting foot of the segment is installed in a recess with a concave bottom. When the direction of rotation is reversed the forces of friction cause the segment to shift along the recess until the knives press against its end-face walls. If the shaft rotates in the direction shown in Fig. 192c the left-hand support is in operation, and the rocking centre of the segment is at the optimum distance of $0.5L + 0.08L = 0.58L$ from the front edge of the segment. The right-hand support, being in the recess, does not hamper the ability of the segment to align itself. If the direction of rotation is reversed, the right-hand support is in operation, and the segment rocking centre is again in its optimum position.

The segments of bearings carrying small loads are made of anti-friction bronze. In highly loaded bearings the active surfaces of the segments are lined with babbitt or lead bronze.
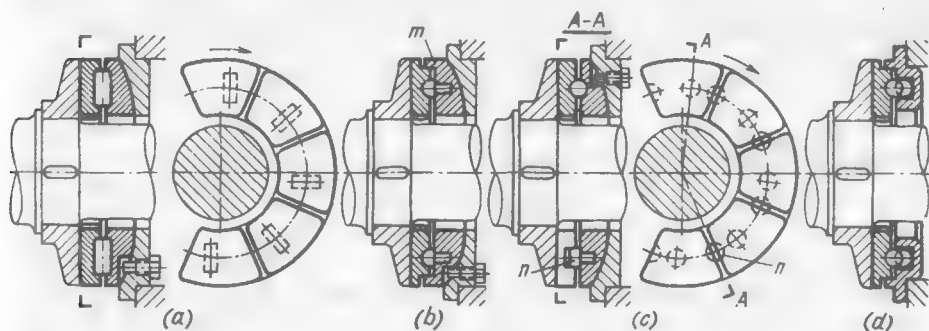
Fig. 193. Bearings with self-aligning segments

The segments are installed on a washer (as a rule, with a spherical supporting surface) with the aid of cylindrical (Fig. 193a) or spherical (Fig. 193b) hinges.

Spherical hinges are more preferable because they ensure the self-alignment of the segments not only in the peripheral but also in the radial direction, and thus compensate for manufacturing errors.

Cylindrical hinges lock the segments in the peripheral and radial directions, and also retain them in the plane of rotation. When the hinges are spherical the segments are held against rotation by means of flanges *m* on the thrust washer or by pins *n* (Fig. 193*c*) in the spaces between the segments, which enter semicircular seats in the end faces of the segments.

Segments can also be made self-aligning by means of cylindrical or spherical stops installed between the segments (Fig. 194).

The position of the rocking centre *A* of the segments depends on the bevel angles β at the ends of the segments.

When the angles β (Fig. 194*a*) are the same, the rocking centre lies on the axis of symmetry of the segment and slightly deviates from this position when the segment aligns itself within the working values of angles α.
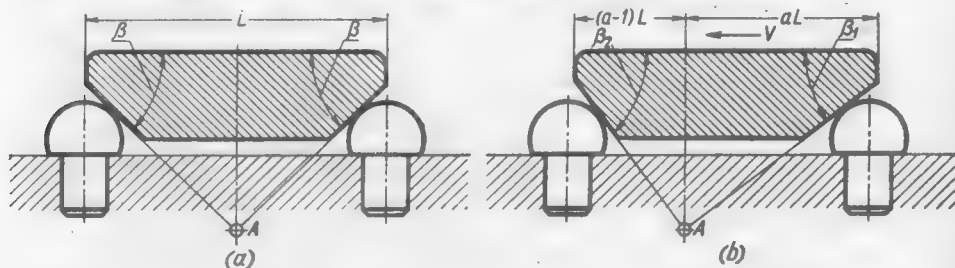
Fig. 194. Installation of segments on intermediate stops

In order to displace the rocking centre to a distance *aL* from the front edge (in the direction of motion, Fig. 194*b*) the angle β_1 of the front bevel must be made smaller than the angle β_2 of the rear bevel in conformity with the ratio

$$\frac{\tan \beta_1}{\tan \beta_2} = \frac{1-a}{a}$$

With the optimum $a = 0.58$

$$\frac{\tan \beta_1}{\tan \beta_2} = 0.74$$

In all the designs described above the load can uniformly be distributed among the segments only if these segments and their supports are manufactured to a high degree of accuracy which assures the arrangement of the sliding surfaces in one plane.

Systems with *automatic equalization of the load* among the segments are more perfect.

In the design shown in Fig. 195*a* segments *1* rest on balls fitted into a closed annular slot in thrust washer *2*. An increase of the load

on one of the segments makes it sink into the space between the balls and raises at the same time the other, less loaded segments.

In the design in Fig. 195b the equalizing mechanism consists of a number of floating blocks 3 (having a segmental form in plan) placed into an annular slot in the thrust washer. This mechanism acts as the previous one. One of the blocks must be secured against motion in the peripheral direction.

Figure 195c illustrates a self-equalizing mechanism used to adjust segments with their bevelled edges on intermediate spherical supports. As distinct from the diagrams displayed in Fig. 194, the
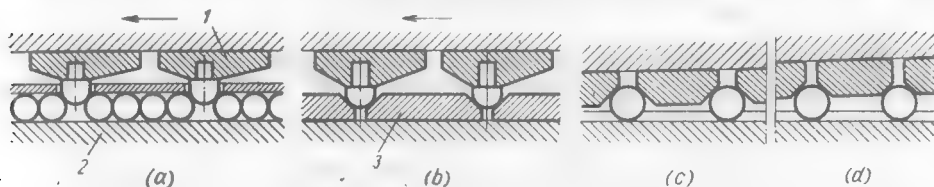
Fig. 195. Equalizing devices

spherical members are freely mounted in the annular slot in the thrust washer, which ensures automatic equalization of the load. One of the segments must be locked against motion in the peripheral direction.

Equalizing devices also provide for the self-alignment of the bearing as a whole and thus dispense with spherical thrust washers.

Let us illustrate this fact by an example of the equalizing mechanism shown in Fig. 195c. Assume that the thrust disk of the shaft is misaligned. In the narrowest portion of the clearance the segments sink into the spaces between the balls and draw them apart. This brings the balls closer together and raises the segments in the opposite, wide section of the clearance (Fig. 195d). Since the segments can align themselves, their sliding surfaces are arranged in a single inclined plane. At the same time the load is uniformly distributed among the segments.

A self-aligning bearing with a ball-type equalizing mechanism designed as shown in Fig. 195a is presented in Fig. 193d.

Calculation example. Given: $P = 5000$ kgf, $n = 1000$ rpm, $\eta = 50$ cP. Determine the dimensions of a hydrodynamic bearing with self-aligning segments.

Specifying a preliminary value $d_m = 170$ mm and assuming that $a = 1.5$ in Eq. (2.59), we get

$$h_0 = 1.5 \sqrt{170} \approx 20 \ (\mu m)$$

The bearing area A can be found from Eq. (2.56) for $G\ddot{u} = 0.07$. Assuming tentatively that $\beta = 0.85$, we find that

$$A = 29 \cdot 20 \sqrt{\frac{5000}{60 \cdot 1000 \cdot 0.85}} = 200 \ (cm^2)$$

From Eq. (2.60) the ratio D/d is

$$\frac{D}{d} = \sqrt{\frac{4A}{\pi\beta d^2} + 1} = \sqrt{\frac{4 \cdot 200}{0.85 \cdot 12^2} + 1} = 1.75$$

In Fig. 175 this value, when $z = 6$, corresponds to $L/B = 1.5$, and when $z = 8$, $L/B = 1.15$. Let us take $z = 8$. For design considerations we assume that $d = 12$ cm.

The external diameter is

$$D = 1.75 \cdot 12 = 21 \quad \text{(cm)}$$

The mean diameter

$$d_m = \frac{21 + 12}{2} = 16.5 \quad \text{(cm)}$$

It is not necessary to recalculate the value of h_0 since the difference between the preliminary value of d_m (17 cm) and the obtained value is negligible.

The width of the segment is

$$B = \frac{D - d}{2} = \frac{21 - 12}{2} = 4.5 \quad \text{(cm)}$$

The length of the segment over the mean circumference

$$L = 1.15 \cdot 4.5 = 5.2 \quad \text{(cm)}$$

Assuming that the distance between the segments is 6 mm and the radius R of the fillets at the outlet and inlet of the segment, 2 mm, we obtain the total space between the segments $m = 6 + 4 = 10$ mm.

From Eq. (2.52) we find

$$\beta = 1 - \frac{8}{\pi 16.5} = 0.845$$

i.e., it is likewise unnecessary to recalculate β.

The active length of the segment is

$$L' = 5.2 - 2R = 5.2 - 0.4 = 4.8 \quad \text{(cm)}$$

The actual ratio $L'/B = 4.8/4.5 = 1.07$ is close to the optimum one and for this reason the choice of $G\ddot{u} = 0.07$ is fully justified.

The unit load on the segments is

$$k = \frac{P}{zL'B} = \frac{5000}{8 \cdot 4.8 \cdot 4.5} = 29 \quad \text{(kgf/cm}^2)$$

We place the hinge at the optimum distance $l = 0.58L'$ from the front edge

$$l = 0.58 \cdot 4.8 = 2.9 \quad \text{(cm)}$$

According to Eq. (2.58), for the optimum $t = 1.25h_0$

$$\tan \alpha = 1.25 \frac{h_0}{L'} = 1.25 \cdot 10^{-4} \frac{20}{4.8} = 0.00052$$

$$\alpha = 1'50''$$

The speed over the mean circumference of the bearing

$$v = \frac{\pi n \cdot 0.165}{30 \cdot 2} = 8.65 \quad \text{(m/s)}$$

Coefficient of friction may be determined from Eq. (2.44)

$$f = 3 \cdot 10^{-3} \sqrt{\frac{50 \cdot 8.65}{29 \cdot 4.5}} = 0.0054$$

Power consumption in friction may be found from Eq. (2.45)

$$N = 5000 \cdot 8.65 \cdot 0.0054 = 235 \ (\text{kgf} \cdot \text{m/s}) = 2.3 \ (\text{kW})$$

Generation of heat per second

$$R = \frac{N}{427} = \frac{235}{427} = 0.55 \ (\text{cal/s})$$

The efflux of oil per second for all segments

$$Q = 0.7 z \cdot 10^{-5} B v h_0 = 0.7 \cdot 8 \cdot 10^{-5} \cdot 4.5 \cdot 8.65 \cdot 20 = 0.043 \ (\text{l/s})$$

The increase of oil temperature in the bearing is determined from Eq. (2.48), assuming that $\gamma = 0.9$ kgf/l and $c = 0.5$ cal/kgf·°C

$$t - t_0 = \frac{0.55}{0.043 \cdot 0.9 \cdot 0.5} = 28 \ (\text{°C})$$

Let the oil temperature at the inlet be $t_0 = 30$°C.
Then, the mean temperature of the oil in the bearing will be

$$t_m = 30 + \frac{28}{2} = 44 \ (\text{°C})$$

The grade of oil is selected so that its viscosity is 50 cP at 44°C.

(g) Hydrostatic Thrust Bearings

The carrying force in these bearings is produced by feeding oil from a pump underneath a thrust disk (Fig. 196). Oil enters pocket *2* with a retaining edge *3* via throttle valve *1*. The pressure in the pocket depends on the relationship between the cross-section of the throttle and the variable section *h* of the slit. When the load is increased the slit diminishes and the pressure in the pocket grows up to the pump pressure. This corresponds to the maximum carrying capacity.

In the case of an impact load the sharp increase in the hydraulic resistance of the throttle (hydraulic clogging) may cause the pressure in the pocket to rise appreciably above the pressure produced by the pump.

Fig. 196. Design diagram of a hydrostatic bearing

Nonreturn valves installed in the throttles are intended to increase the ability to sustain dynamic loads.

Hydrostatic bearings are superior to the hydrodynamic ones in the following respects:

absence of semifluid friction during starting and racing;
much larger thickness of the oil layer and hence, a lower coeffi-
cient of friction;
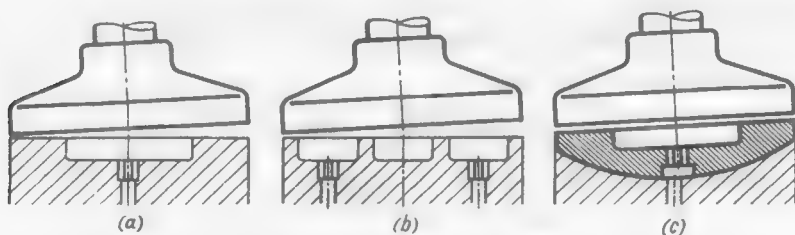
Fig. 197. Effect of misalignments on load-carrying capacity

less power consumption in friction (with account being taken
of the power consumption of the pump drive).

Among the shortcomings are high sensitivity to the variations
in the operating conditions and the need for an additional pumping
unit, thorough filtration of
oil and separation of air
bubbles.
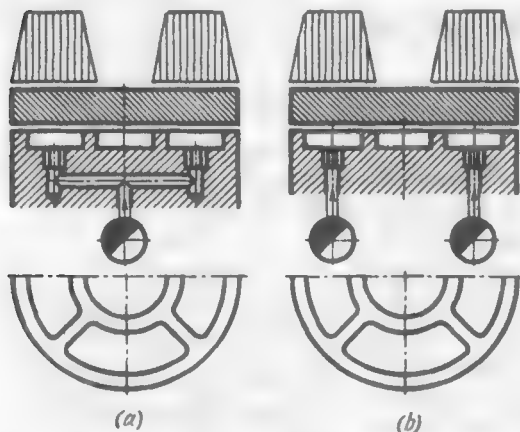
Fig. 198. Hydrostatic bearings with pockets

The insufficient rigidity
of hydrostatic bearings re-
sulting from their very
thick oil layer can consi-
derably be improved with
the aid of special oil dis-
tributing devices.

Hydrostatic bearings are
extremely sensitive to mis-
alignments. When the disk gets
inclined (Fig. 197a) the flow of
oil through the wide section of
the slit increases and the pres-
sure in the pocket is reduced,
the more so as the throttle
begins in this case to limit the
feed of oil. At the point of the closest approach of the disk to the thrust
washer metal contact may occur even with moderate misalignments.

The drop in the carrying capacity is prevented by dividing the bearing into
individual pockets (Fig. 197b) supplied either by one pump through individual
throttles (Fig. 198a) or, which is more preferable, by individual pumps
(Fig. 198b). In this case the pressure in the pockets in the sections where the
disk approaches closer to the bearing surface is maintained and even slightly
increased. This prevents metal contact and makes the bearing operate in con-
ditions of fluid friction although with a reduced carrying capacity (due to the
drop of the pressure in the other pockets).

The rigidity of bearings with pockets supplied with oil by individual pumps is appreciably higher than that of bearings with an annular pocket.
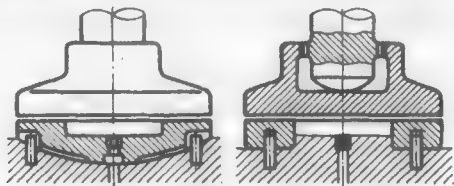
Fig. 199. Self-aligning hydrostatic bearings

It is advisable to make bearings self-aligning (see Fig. 197c). In this case the bearing surface remains parallel to the disk with all misalignments.

Some designs of self-aligning bearings are illustrated in Fig. 199.

Load-Carrying Capacity. Losses Due to Friction

Figure 200 shows a pressure diagram of a hydrostatic bearing. The pressure p_p in the pocket is constant, and in the slit it falls almost linearly to zero at the periphery of the bearing (Fig. 200a).

With a sufficient degree of accuracy the pressure diagram may be replaced by a rectangle (Fig. 200b) of height p_p and the base equal to the diameter d_{ac} of the active bearing surface A_{acc} determined from the relation
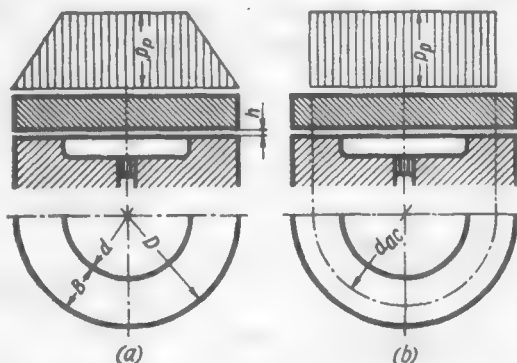
Fig. 200. Calculation of hydrostatic bearings

$$A_{ac} = A_p + \frac{A_{sl}}{2} \quad (2.67)$$

where A_p is the area of the pocket ($A_p = 0.785d^2$) and A_{sl} is the area of the slit:

$$A_{sl} = 0.785D^2 \left[1 - (d/D)^2\right] \quad (2.68)$$

Substituting the values of A_p and A_{sl} into Eq. (2.67), we obtain

$$A_{ac} = 0.39D^2 \left[1 + (d/D)^2\right] \quad (2.69)$$

The active diameter is

$$d_{ac} = 0.7D \sqrt{1 + (d/D)^2} \quad (2.70)$$

The load-carrying capacity of hydrostatic bearings is maximum and the losses due to friction are close to the minimum when $d/D = 0.5$ (acceptable limits $d/D = 0.4$-0.6).

Assuming that $d/D = 0.5$, we obtain from Eqs. (2.70) and (2.68)

$$d_{ac} = 0.8D \qquad (2.71)$$
$$A_{ac} = 0.5D^2 \qquad (2.72)$$
$$A_{sl} = 0.59D^2 \qquad (2.73)$$

The load-carrying capacity of the bearing is

$$P = p_p A_{ac} = 0.785 p_p d_{ac}^2 \qquad (2.74)$$

and when $d/D = 0.5$, is

$$P = 0.5 p_p D^2 \qquad (2.75)$$

According to the Reynolds equation, the outflow of oil through clearance h is

$$Q = \frac{p_p h^3}{12\eta} \cdot \frac{B}{S} \qquad (2.76)$$

where B = width of the slit ($B = \dfrac{D-d}{2}$)

S = length of the slit over external circumference ($S = \pi D$)

η = dynamic viscosity of oil

Inasmuch as

$$p_p = P/A_{ac}$$

then

$$Q = \frac{P h^3}{12 A_{ac} \eta} \cdot \frac{B}{S} \qquad (2.77)$$

whence

$$P = \frac{12 A_{ac} \eta Q}{h^3} \cdot \frac{S}{B} \qquad (2.78)$$

The ratio

$$S/B = \frac{2\pi}{1 - d/D} \qquad (2.79)$$

when $d/D = 0.5$

$$S/B = 4\pi \qquad (2.80)$$

In this case

$$P = \frac{150 A_{ac} \eta Q}{h^3} \qquad (2.81)$$

The power consumption of the pump drive (in kgf·m/s) is

$$N_{pump} = \frac{Q p_{pump}}{\eta_{pump}} \qquad (2.82)$$

where Q = flow of oil through the bearings, m^3/s

p_{pump} = pressure built up by the pump, kgf/m^2

η_{pump} = pump efficiency with account being taken of the losses due to oil overflow through the reducing valve ($\eta_{pump} = 0.6\text{-}0.8$)

Substituting the value of Q from Eq. (2.77) into Eq. (2.82), we get

$$N_{pump} = \frac{Ph^3}{A_{ac}12\eta} \cdot \frac{B}{S} \cdot \frac{p_{pump}}{\eta_{pump}} \qquad (2.83)$$

The power consumption in the slit friction (friction in the pocket is disregarded) is

$$N_{fr} = Fv \qquad (2.84)$$

where v is the speed of motion over the mean circumference of the slit

$$v = \frac{\omega d_m}{2} = \frac{\pi n (D+d)}{120}$$

and F is the peripheral force over the mean circumference, which, according to Newton's law, is

$$F = \frac{\eta v A_{sl}}{h} \qquad (2.85)$$

The coefficient of friction is

$$f = \frac{F}{P} = \frac{\eta v A_{sl}}{Ph} = \frac{\eta v}{kh}[1-(d/D)^2] \qquad (2.86)$$

where k is the mean unit load on the bearing

$$k = \frac{P}{0.785D^2} \qquad (2.87)$$

When $d/D = 0.5$

$$f = 0.75\frac{\eta v}{kh} \qquad (2.88)$$

According to Eqs. (2.84) and (2.85), the power consumption in friction is

$$N_{fr} = \frac{\eta v^2 A_{sl}}{h} \qquad (2.89)$$

The total power consumption

$$N = N_{pump} + N_{fr} = \frac{P}{A_{ac}} \cdot \frac{h^3}{12\eta} \cdot \frac{B}{S} \cdot \frac{p_{pump}}{\eta_{pump}} + \frac{\eta v^2 A_{sl}}{h} \qquad (2.90)$$

With the specified geometrical parameters of the bearing and constant P, v and p_{pump}

$$N = \text{const}\,\frac{h^3}{\eta} + \text{const}\,\frac{\eta}{h}$$

i.e., the power consumption of the pump drive is directly proportional to h^3 and inversely proportional to η; the power consumption

in friction is directly proportional to η and inversely proportional to h.

Differentiating Eq. (2.90) with respect to η and equating the derivative to zero, we obtain the optimum η at which $N = \min$

$$\eta_{opt} = 0.29 \frac{h^2}{v} \sqrt{-\frac{P}{A_{ac}A_{sl}} \cdot \frac{p_{pump}}{\eta_{pump}} \cdot \frac{B}{S}} \tag{2.91}$$

In conformity with Eqs. (2.68) and (2.69),

$$A_{ac}A_{sl} = 0.29 D^4 \left[1 - \left(\frac{d}{D}\right)^4\right] \tag{2.92}$$

Substituting this value into Eq. (2.91), we get

$$\eta_{opt} = 0.29 \frac{h}{vD^2} \sqrt{\frac{P}{1 - \left(\frac{d}{D}\right)^4} \cdot \frac{p_{pump}}{\eta_{pump}} \cdot \frac{B}{S}} \tag{2.93}$$

when $d/D = 0.5$, $S/B = 4\pi$ and $\eta_{pump} = 0.8$

$$\eta_{opt} \approx 0.1 \frac{h^2}{vD^2} \sqrt{Pp_{pump}} \tag{2.94}$$

In practice, it is better to determine the optimum parameters from the clearance.

Differentiating Eq. (2.90) with respect to h and equating the derivative to zero, we obtain the optimum h at which $N = \min$

$$h_{opt} = \sqrt[4]{4\eta^2 v^2 \frac{A_{ac}A_{sl}}{P} \cdot \frac{\eta_{pump}}{p_{pump}} \cdot \frac{S}{B}} \tag{2.95}$$

Substituting $A_{ac}A_{sl}$ from Eq. (2.92), we get

$$h_{opt} = D \sqrt[4]{\frac{\eta^2 v^2 [1 - (d/D)^4]}{P} \cdot \frac{\eta_{pump}}{p_{pump}} \cdot \frac{S}{B}} \tag{2.96}$$

When $d/D = 0.5$ and $\eta_{pump} = 0.8$

$$h_{opt} = 1.83 D \sqrt[4]{\frac{\eta^2 v^2}{Pp_{pump}}} \tag{2.97}$$

The value of h_{opt} must be greater than the minimum permissible value of h_0. This condition is easily satisfied in hydrostatic bearings.

The ratio of the power consumption of the pump drive to the power consumption in friction, in conformity with Eqs. (2.83), (2.89) and (2.92), is

$$\frac{N_{pump}}{N_{fr}} = 0.03 \frac{h^4}{D^4} \cdot \frac{p_{pump}}{\eta^2 v^2} \tag{2.98}$$

For the optimum value h_{opt}

$$\frac{N_{pump}}{N_{fr}} = 0.335$$

When h decreases as compared with the optimum value the ratio N_{pump}/N_{fr} sharply drops, but increases with an increase in h.

Rigidity

Differentiating Eq. (2.78) with respect to h we may find the rigidity of the bearing

$$\lambda = \frac{dP}{dh} = \frac{36Q\eta A_{oc}}{h^4} \cdot \frac{S}{B} \tag{2.99}$$

Substituting the value of Q from Eq. (2.77) into Eq. (2.99), we get

$$\lambda = \frac{3P}{h} \tag{2.100}$$

It can be seen from this formula that rigidity drops with a decrease in P and an increase in h. To make the rigidity constant the following condition must be satisfied:

$$\frac{P}{h} = \text{const}$$

or since

$$P = p_p A_{ac} = p_p \text{ const}$$

then

$$\frac{p_p}{h} = \text{const}$$

i.e., the pressure in the pocket must be proportional to the clearance. This condition can nearly be obtained if a throttle is installed at the inlet to the pocket.

Throttles may take the form of capillaries or diaphragm orifices. Use is usually made of capillaries since their orifices are larger than those in a diaphragm (manufacture is easier and there is almost no hazard of clogging) and their throughput can readily be controlled (by changing the length of the capillary). Besides, as distinct from bearings with diaphragm throttles, the characteristics of bearings with capillary throttles do not depend on oil viscosity (i.e., on the temperature of the bearing).

The role of controlled throttles is played by threaded holes with a rod screwed into them. The throughput of these holes can be changed by screwing the rod in or out as required.

When the loads are high, h is small and the throughput of the slit is comparable with that of the throttle, the latter does not affect the rigidity of the bearing which still remains rather high. At low loads, when h increases, as does the efflux of oil through the slit, the throttle restricts the feed of oil into the pocket thus delaying the rise of h and increasing thereby the rigidity of the bearing. In this case the pressure p_p in the pocket becomes less than the pressure p_{pump}.

When the resistance of the throttle is properly selected it is possible to make the rigidity nearly constant within the working range of the load variations.

The hydraulic resistance of a capillary is

$$R_{cap} = \frac{\Delta p}{Q_{cap}} = \frac{p_{pump} - p_p}{Q_{cap}} \qquad (2.101)$$

where Δp is the difference in pressure between the inlet and outlet of the capillary

$$\Delta p = p_{pump} - p_p \qquad (2.102)$$

Q_{cap} is the flow of oil through the capillary. In conformity with the Poiseuille equation

$$Q_{cap} = \frac{\pi d_{cap}^4 \Delta p}{128 \eta l_{cap}} \qquad (2.103)$$

where d_{cap} and l_{cap} are the diameter and length of the capillary (see Fig. 196).

Substituting this expression into Eq. (2.101), we obtain

$$R_{cap} = \frac{41 \eta l_{cap}}{d_{cap}^4} \qquad (2.104)$$

The hydraulic resistance of the slit is

$$R = \frac{p_p}{Q} \qquad (2.105)$$

Substituting the value of Q from Eq. (2.76), we get

$$R = \frac{12 \eta}{h^3} \cdot \frac{S}{B} \qquad (2.106)$$

The efflux of oil through the capillary is always equal to its outflow through the slit

$$Q_{cap} = Q$$

Substituting the value of Q_{cap} from Eq. (2.101) and that of Q from Eq. (2.105), we obtain

$$\frac{p_p}{p_{pump}} = \frac{1}{R_{cap}/R + 1} \qquad (2.107)$$

According to Eqs. (2.104) and (2.106), the ratio

$$\frac{R_{cap}}{R} = 3.4 \frac{l_{cap} h^3}{d_{cap}^4} \cdot \frac{B}{S} \qquad (2.108)$$

Substituting this value into Eq. (2.107), we get

$$\frac{p_p}{p_{pump}} = \frac{1}{3.4 \dfrac{l_{cap} h^3}{d_{cap}^4} \cdot \dfrac{B}{S} + 1} \qquad (2.109)$$

When $S/B = 4\pi$ [Eq. (2.80)]

$$\frac{p_p}{p_{pump}} = \frac{1}{0.27 \dfrac{l_{cap}h^3}{d_{cap}^4} + 1} \tag{2.110}$$

Since $P = p_p A_{ac}$ the rigidity of the bearing will be

$$\lambda = \frac{dP}{dh} = A_{ac}\frac{dp_p}{dh} = A_{ac}p_{pump}\frac{d}{dh} \cdot \frac{p_p}{p_{pump}} \tag{2.111}$$

Differentiating Eq. (2.110) with respect to h and substituting the derivative into Eq. (2.111), we obtain

$$\lambda = \frac{A_{ac}p_{pump}0.27 \dfrac{l_{cap}}{d_{cap}^4} h^2}{\left(0.27 \dfrac{l_{cap}h^3}{d_{cap}^4} + 1\right)^2} = 0.27 A_{ac}p_{pump}\frac{l_{cap}h^2}{d_{cap}^4}\left(\frac{p_p}{p_{pump}}\right)^2 \tag{2.112}$$

The graph in Fig. 201, showing the change in p_p/p_{pump} depending on the clearance h for various capillary diameters d_{cap} ($l_{cap}/d_{cap} = 10$) is plotted on the basis of Eq. (2.110). In conformity with Eq. (2.111), the tangent of angles α, at which the curves p_p/p_{pump} are inclined to the X-axis, is proportional to the rigidity of the bearing.

As can be seen from the graph the rigidities are maximum and practically constant (tan $\alpha = $ const) within the range $p_p/p_{pump} = 0.4$-0.65 (shaded area). Bearings are designed precisely on the basis of these values of p_p/p_{pump}. For each given design value of h, determined from the condition of minimum frictional losses by Eq. (2.96), the diameter of the capillary should be selected so that the operating values of p_p/p_{pump} are within 0.4-0.65. If an increase in the load (decrease in h) during operation is possible, it is advisable to adhere to the lower values ($p_p/p_{pump} = 0.4$) to maintain sufficient rigidity under nominal operating conditions. If periodical low-load operation is possible (increased h) the higher design values ($p_p/p_{pump} = 0.65$-0.7) are preferred. On the average, $p_p/p_{pump} = 0.5$.

A sufficiently high rigidity is also maintained within a wider range of the p_p/p_{pump} values (0.2-0.8). However, the values $0.9 < p_p/p_{pump} < 0.1$, when the rigidity tends to zero and the operation of the bearing becomes unstable, should be avoided.

Equation (2.112) is used to plot the graph (Fig. 202) which shows the dependence of the rigidity factor $\lambda/A_{ac}p_{pump}$ on the ratio p_p/p_{pump} for various h. With all values of h the rigidity has a gently sloping maximum at $p_p/p_{pump} = 0.5$-0.6. The recommended region of the design p_p/p_{pump} values is shaded on the graph.

The nature of the factor $\lambda/A_{ac}p_{pump}$ and the curves on the graph show that the rigidity of the bearing rises with an increase in A_{ac}

and in the oil-feed pressure p_{pump}, and with a reduction in the clearance h. Since the efficiency of the bearing changes little when the
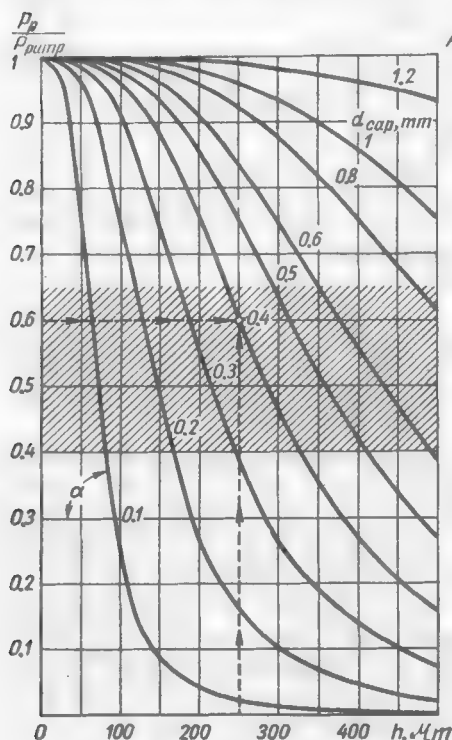
Fig. 201. Dependence of p_p/p_{pump} on h and d_{cap}
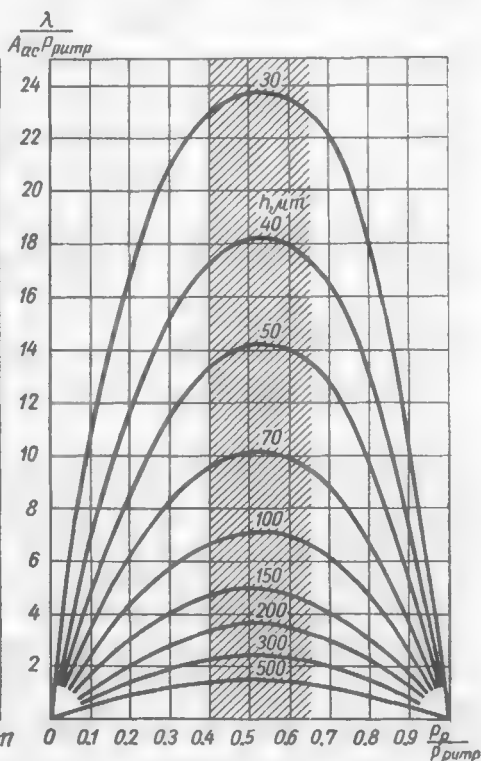
Fig. 202. Dependence of rigidity on p_p/p_{pump} and h

clearance is reduced to approximately 60 per cent of the optimum value, it will be expedient to take $h = (0.6$ to $0.7)\, h_{opt}$ in calculations to increase the rigidity of the bearing.

The rigidity of hydrostatic bearings can be improved by introducing slide-valve or diaphragm-type pressure regulators which automatically build up in the pocket a pressure proportional to the working load. The best designs of this type ensure a permanent position of the thrust disk within a wide range of load variations, i.e., the bearing is practically imparted an infinitely high rigidity.

What is called *enclosed supports* possess very high rigidity. In such supports the thrust disk is arranged between two bearing surfaces one of which takes up the working load and the other additionally loads the bearing when the working load lessens and thus maintains the total load at a constant level.

Example. Let us compare the characteristics of hydrodynamic and hydrostatic bearings, using the same initial data as in the previous calculation of the hydrodynamic bearing: diameter $D = 21$ cm, load $P = 5000$ kgf, rotational speed $n = 1000$ rpm and oil viscosity $\eta = 50$ cP.

For the optimum $d/D = 0.5$, A_{ac} may be found from Eq. (2.72)

$$A_{ac} = 0.5 \cdot 21^2 = 220 \ (\text{cm}^2)$$

According to Eq. (2.74), the required pressure in the pocket is

$$p_p = \frac{5000}{220} = 23 \ (\text{kgf/cm}^2)$$

Assuming that $p_p/p_{pump} = 0.6$, we find the oil-feed pressure

$$p_{pump} = \frac{p_p}{0.6} = \frac{23}{0.6} = 38.5 \ (\text{kgf/cm}^2)$$

The mean diameter of the bearing

$$d_m = \frac{D + 0.5D}{2} = \frac{21 + 10.5}{2} = 15.75 \ (\text{cm})$$

The mean speed

$$v = \frac{\pi n}{30} \cdot \frac{d_m}{2} = \frac{\pi \cdot 1000 \cdot 15.75}{60} = 8.25 \ (\text{m/s})$$

The optimum clearance is calculated from Eq. (2.97). Substituting

$$\eta = 50 \ (\text{cP}) \approx 5 \cdot 10^{-3} \ (\text{kgf} \cdot \text{s/m}^2)$$
$$p_{pump} = 38.5 \cdot 10^4 \ (\text{kgf/m}^2)$$
$$D = 21 \cdot 10^{-2} \ (\text{m})$$

we obtain

$$h_{opt} = 10^6 \cdot 1.83 \cdot 21 \cdot 10^{-2} \ \sqrt[4]{\frac{5^2 \cdot 10^{-6} \cdot 8.25^2}{5000 \cdot 38.5 \cdot 10^4}} = 370 \ (\mu\text{m})$$

With a view to increasing the bearing rigidity we assume that

$$h = 0.7 h_{opt} = 250 \ (\mu\text{m})$$

In order to obtain the selected $p_p/p_{pump} = 0.6$ with this clearance a capillary with a hole $d_{cap} = 0.4$ mm (Fig. 201) is needed. The graph shows that the rigidity of the bearing hardly changes when the load is increased 1.25 times or decreased 1.5 times as compared to the nominal value.

The ratio B/S when $d/D = 0.5$, according to Eq. (2.80), is $\frac{1}{4\pi} = 0.08$. The pump efficiency η_{pump} is taken at 0.8. From Eq. (2.83) the power consumption of the pump drive is

$$N_{pump} = \frac{5000}{220 \cdot 10^{-4}} \cdot \frac{250^3 \cdot 0.08}{10^{18} \cdot 12 \cdot 5 \cdot 10^{-3}} \frac{38.5 \cdot 10^4}{0.8} = 2.3 \ (\text{kgf} \cdot \text{m/s})$$

By Eq. (2.82), the pump capacity is

$$Q = \frac{2.3 \cdot 0.8}{38.5 \cdot 10^4} = 4.8 \cdot 10^{-6} \ (\text{m}^3/\text{s}) \approx 0.3 \ (l/\text{min})$$

By Eq. (2.73), the area of the slit

$$A_{sl} = 0.59 \cdot 21^2 = 260 \ (\text{cm}^2)$$

By Eq. (2.89), the power consumption in friction is

$$N_{fr} = \frac{5 \cdot 10^{-3} \cdot 8.25^2 \cdot 260 \cdot 10^{-4}}{250 \cdot 10^{-6}} = 35 \ (\text{kgf} \cdot \text{m/s})$$

The total power consumption

$$N = N_{pump} + N_{fr} = 2.3 + 35 = 37.3 \ (\text{kgf} \cdot \text{m/s}) = 0.36 \ (\text{kW})$$

The unit pressure from Eq. (2.87)

$$k = \frac{P}{0.785 D^2} = \frac{5000}{345} = 14.5 \ (\text{kgf/cm}^2)$$

The coefficient of friction from Eq. (2.88)

$$f = 0.75 \ \frac{5 \cdot 10^{-3} \cdot 8.25}{14.5 \cdot 10^4 \cdot 250 \cdot 10^{-6}} = 0.00085$$

Let us now compare the parameters of hydrodynamic and hydrostatic bearings:

Parameters	Hydrodynamic bearing	Hydrostatic bearing
h, μm	20	250
f	0.0054	0.00085
N, kW	2.3	0.36

Thus, the thickness of the oil layer in the hydrostatic bearing with the selected parameters (very close to the optimum ones) is 12.5 times greater, and the coefficient of friction and the losses due to friction 6.5 times lower than in the hydrodynamic bearing.

Figure 203 shows the curves of N_{pump}, N_{fr}, N and f as dependent on the magnitude of clearance h. As can be seen from the graph, rather large deviations of h from $h_{opt} = 370$ microns affect but little the value of N.

The design values $h = (0.6 \text{ to } 0.7) \ h_{opt}$ may be accepted without any noticeable detriment to the efficiency of the bearing. This increases the rigidity of the bearing by about 1.5 times.

In installations where easy rotation is the prime concern and the load is constant, it is good practice to take $h > h_{opt}$. When $h = 1.5$, $h_{opt} = 550$ microns and the coefficient of friction drops to $f = 0.0004$ almost without detriment to the efficiency ($N = 0.4 \text{ kW}$).

Fig. 203. Effect of clearance h on power consumption and coefficient of friction

With still higher values of $h = (700-1000$ μm) it is possible to obtain $f = 0.0003-0.0002$, but then with the increase of N to 0.7-1.4 kW.

Antifriction (Rolling-Contact) Bearings

Rolling-contact bearings are superior to plain bearings in the following respects:

more accurate centring of the shaft;

low coefficient of friction;

weak dependence of the coefficient of friction on operating conditions; low resisting moments during starting periods;

small axial dimensions;

ability to operate with a small oil feed;

ability to operate within a wide temperature range—from temperatures close to absolute zero to $+500\text{-}600°C$ (when the bearings
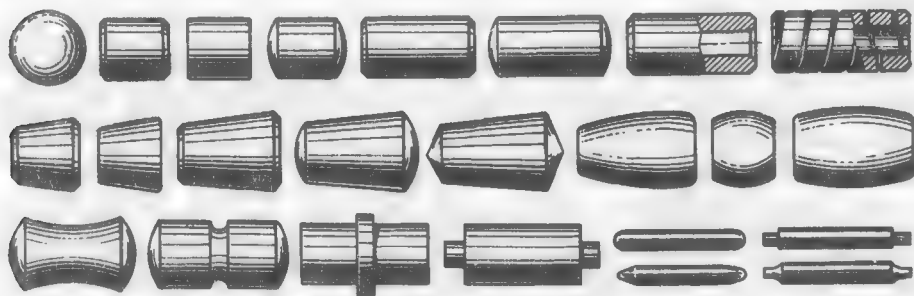
Fig. 204. Forms of rolling elements

are manufactured from special alloys and operated with special lubricants);

ability to operate in high vacuum.

Their disadvantages are as follows:

large radial dimensions and weight, high cost;

uneven operation, incapability of dampening load variations;

noise in operation due to the form inaccuracies;

complicated installation and assembly;

high sensitivity to installation inaccuracies;

incapability of being split in the meridional plane;

metallic contact between rolling elements and races.

The service life (durability) of rolling-contact bearings is determined by the number of load cycles that the bearing material can withstand at a given load and, therefore, depends on the speed of rotation. The durability sharply decreases with increased loads (the durability of plain bearings with fluid friction depends on neither the speed of rotation nor the load).

Typical forms of rolling elements are illustrated in Fig. 204.

3.1. Types of Bearings

(a) Radial Bearings

Basic types of radial rolling-contact bearings are presented in Table 28.

Single-row radial ball bearings (sketches *1* and *2*) are intended to carry mainly radial loads, but at the same time they can also carry heavy axial loads.

In bearings of this type the balls roll on raceways profiled as circular arcs with the radius equal to approximately 1.03 of the ball radius. The balls are inserted into pressed-steel or massive cages that prevent friction and ensure a uniform spacing of the balls.

The bearings shown in sketch *1* are assembled by displacing the inner race with respect to the outer one and inserting the balls into the crescent-shaped clearance thus formed. The design in sketch *2* provides for filling slots to admit the balls, thus making it possible to insert more balls. Bearings of this type have increased radial load-carrying capacity. They are not recommended for axial loads acting in the direction of the slots.

The axial rigidity of ball bearings is not very high. The axial shift of the inner race relative to the outer one under a heavy load amounts to several tenths of a millimetre. The rigidity of twin installations can be increased by preloading the bearings.

Due to the point contact, single-row ball bearings have the lowest coefficient of friction among all bearings and are prevalent in high-speeds applications.
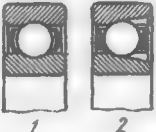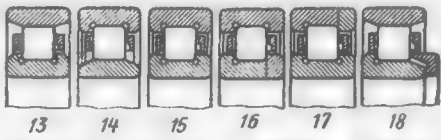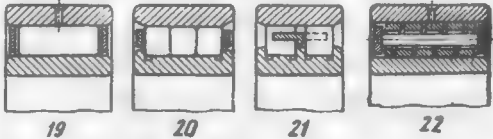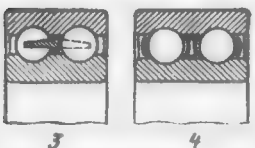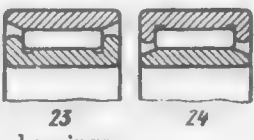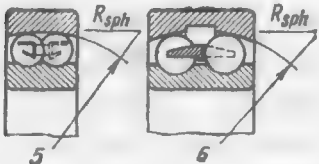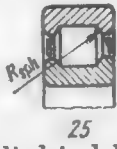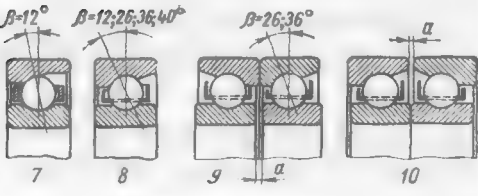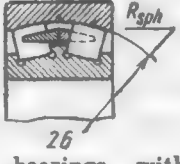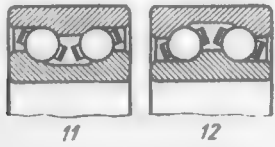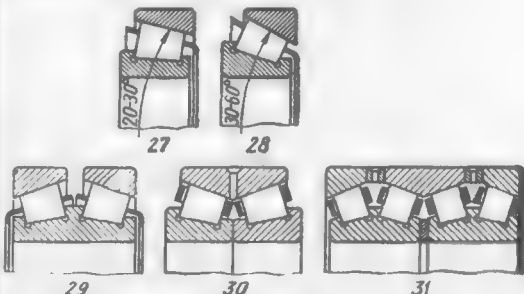
Double-row radial ball bearings (sketches *3*, and *4*) are distinguished by their increased load-carrying capacity, but they are more sensitive to misalignment.

Double-row spherical ball bearings (sketches *5* and *6*) with self-aligning ability are used in installations with possible elastic deformations of the shaft or with possible displacement of the axis of one bearing with respect to the axis of the other.

The presence of two rows of balls compensates for the reduction in the radial load-carrying capacity resulting from the shape of the outer raceway which is unfavourable for contact strength. The shape

Radial Rolling-Contact Bearings

Sketch	Sketch

Single-row radial ball bearings

Double-row radial ball bearings

Double-row spherical ball bearings

Radial thrust ball bearings

Radial roller bearings

Needle bearings

Spherocylindrical bearings

Spherical bearings with barrel-shaped rollers

Tapered-roller bearings

of the raceways of spherical bearings does not permit high axial loads. The axial rigidity of these bearings is low.

Radial thrust ball bearings (sketches 7 and 8) are intended to carry radial and axial loads simultaneously.

The shape of the outer raceway makes it possible to increase the number of the balls and improve the load-carrying capacity of the bearing. Split radial thrust bearings (sketch 7) allow the outer race to be easily removed. In solid bearings (sketch 8) the outer race is locked on the balls by a small flange on the raceway. The latter design is more convenient for mounting the assembled bearing.

Bearings intended for carrying small axial loads are made with a contact angle $\beta = 12°$, whereas bearings for heavy axial loads are made with $\beta = 26\text{-}40°$.

Radial thrust bearings are installed singly only when the axial load is of constant direction (for example, on vertical shafts). Generally they are installed as duplex bearings locked by tightening the races (outer or inner).

Duplex radial thrust bearings (sketches 9 and 10) are manufactured with a preset clearance a which is taken up during tightening.

Preloaded duplex radial thrust bearings permit practically clearance-free centring and axial locking of the shaft.

Solid double-action radial thrust bearings (sketches 11 and 12) which are used in some cases do not have this advantage.

Radial roller bearings (sketches 13-15) are used to carry heavy radial loads in the absence of axial loads. The increased load-carrying capacity of roller bearings (1.5-2 times higher than that of ball bearings of the same size) is due to the line contact between the rollers and the raceways and the larger number of the rollers (which can be easily inserted into the races).

One of the races, usually the inner one (sketch 13), and sometimes the outer one (sketch 14), is provided with lips which guide the rollers on the raceways. The other race is made smooth.

Bearings of this type allow a certain freedom of axial movement of one race with respect to the other, and they are frequently used as floating supports.

Both races must be locked in the axial direction.

Bearings with lips on both races (sketch 15) can carry small axial loads, and are commonly used to lock shafts.

Bearings with detachable lips (sketches 16 and 17) are also in use. Bearings according with sketch 18 are not used nowadays because of their large axial dimensions.

Roller bearings with long rollers (sketch 19) are distinguished by their high load-carrying capacity and small radial dimensions. The rollers, rolling on the raceways, are guided not as precisely as in the case of bearings with short rollers. For this reason short

rollers are sometimes inserted in multiple rows in a common cage (sketch *20*), or use is made of double-row roller bearings (sketch *21*).

Bearings with helically wound cylindrical rollers (sketch *22*) have somewhat higher elasticity in the radial direction. Their load-carrying capacity is much less than that of bearings with massive rollers.

When intended to be mounted on crankshafts, bearings of this type are manufactured with their inner races split in the meridional plane and dovetailed. These bearings are not very popular.

Needle bearings with long rollers of small diameter (sketches *23* and *24*) are used in the case of constricted radial dimensions and heavy radial loads at low rotational speeds.

Spherocylindrical bearings (sketch *25*) with spherical ends of the rollers can take up both radial loads and rather heavy axial loads. The rolling of the roller end does not satisfy the condition of pure rolling.

Self-aligning double-row roller bearings with barrel-shaped rollers (sketch *26*) favourably differ from spherical ball bearings by their higher radial and axial load-carrying capacity. The contact of the rolling elements in such bearings is not pure rolling in a strict sense.

Tapered roller bearings (sketches *27* and *28*) are used for carrying heavy radial and axial loads.

In standard bearings the angle of taper of the outer raceway is $\alpha = 20\text{-}30°$. Their axial rigidity is not very high. An axial force P_{ax}, if applied to these bearings, results in heavy loads on the rollers $(N = P_{ax}/\sin \alpha/2)$, thus limiting their rotational speed. These bearings are sensitive to overtightening. In bearings intended to carry heavy axial loads the angle α is increased to $60°$. A single tapered roller bearing is used only as a thrust bearing (primarily on vertical shafts). Usually, such bearings are installed in pairs. Locking is effected by installing the bearings oppositely and by tightening the paired races (outer or inner) to ensure clearance-free centring and axial locking of the shaft.

Duplex (sketches *29* and *30*) and multiple-row (sketch *31*) large-size tapered roller bearings available today are intended to carry especially heavy loads.
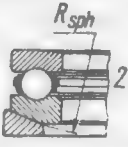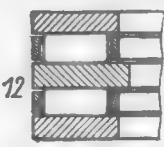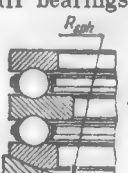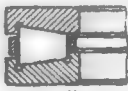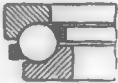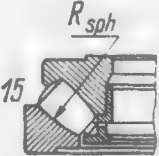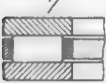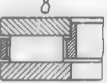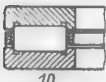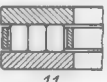
(b) Thrust Bearings

The basic varieties of rolling-contact thrust bearings are illustrated in Table 29.

Single-row thrust ball bearings (sketch *1*) are intended to carry unidirectional axial loads. Thrust ball bearings cannot take up radial loads. They are used only in combination with radial (plain or rolling-contact) bearings.

Table 29

Thrust Bearings

Sketch and type	Sketch and type
Single-row thrust ball bearings	Double-row thrust bearings with cylindrical rollers
Double-row thrust ball bearings	Thrust bearings with tapered rollers
Thrust-radial ball bearings	Spherotapered thrust bearings
Single-row thrust bearings with cylindrical rollers	

One of the races of such a bearing is tightly fitted onto the shaft (by diameter d_1) and the other is installed in the housing. To prevent friction between the shaft and the free race, the inner diameter d of the latter is made several tenths of a millimetre larger than that of the shaft-fitted race.

Self-alignment is provided by installing a spherical supporting surface of one of the bearing races on a washer with a spherical supporting surface (sketch *2*).

Double-row ball bearings (sketches *3* and *4*) serve to take up bidirectional axial loads.

The rotational speed of the thrust ball bearings is limited. Large centrifugal forces tend to displace the balls from the raceways (especially if the axial load is pulsating or alternating) and thus impair the proper operation of the bearing.

Thrust-radial ball bearings (sketches *5* and *6*) can carry both axial loads and rather heavy radial loads.

Thrust bearings with cylindrical rollers (sketches *7-12*) consist of two flat races with cylindrical rollers inserted between them.

The rollers are centred in the bearings by cages (sketch *7*) which in turn are centred on the shaft or by one of the bearing races (sketch *8*). Rollers can also be centred by lips on one (sketch *9*) or two (sketch *10*) races.

In bearings of this type rolling contact occurs only at one point along the length of the rollers, their other sections slipping on the surface of the raceways. In some cases, to diminish this slipping several short rollers are installed in one row (sketch *11*). In the case of bidirectional axial forces use is made of double-row roller bearings (sketch *12*). The rotational speed of thrust roller bearings is very limited. They are used in low-speed heavily loaded supports.

Thrust bearings with tapered rollers are designed as tapers whose vertices intersect at one point on the axis of the bearing (sketches *13* and *14*) to ensure correct rolling.

Spherotapered bearings (sketch *15*) are self-aligning and capable of carrying heavy radial and axial loads. The outer raceway has the form of a sphere whose centre is outside of the bearing. The profiles of the rollers are formed by circular arcs with a radius equal to that of the sphere.

The contact of the rolling bodies in such bearings is not pure rolling in a strict sense.

(c) Bearings with Split Races

Heavy axial and radial-axial loads are usually carried by bearings with their outer (Fig. 205a), or, more rarely, inner (Fig. 205b) races split in the equatorial plane. The split makes it possible to increase the number of balls and deepen the raceways.

With a purely radial load three points of contact are formed in the bearings of this type—two on the split race and one on the solid race. That is why such bearings are intentionally called "three-contact" bearings. Correct rolling of the balls simultaneously on three surfaces is of course impossible. Being braked by the two-point contact with the split race, the balls slip on the solid race. For this reason three-contact bearings are used to carry axial loads, or radial loads and simultaneously axial ones. The axial load presses the balls to one side (Fig. 205c) and they depart from the surface of the raceway on its other side and move without friction with respect to it.

The contact angle β depends on the ratio between the radial and axial loads. For purely axial load β = 20-30° in ready designs.

Split races are usually clamped by nuts, and mutually centred from the seating surface.
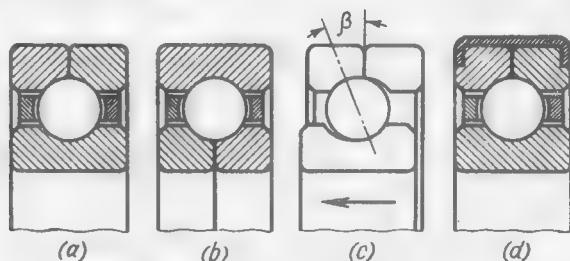
Fig. 205. Bearings with split races

The bearings, intended to carry purely axial loads are installed in housings with a radial clearance. In this case, use is made of bearings with half-races tightly connected by means of a sleeve whose ends are rolled onto the end faces of the races (Fig. 205*d*).

(d) Bearings with Built-in Seals

Radial ball bearings with built-in seals are available in several types.

One-sided (Fig. 206*a*, *b*) and double-sided (Fig. 206*c-f*) shields protect the bearings against the ingress of dirt. Internal shields are used to protect the bearings against excessive lubricant.
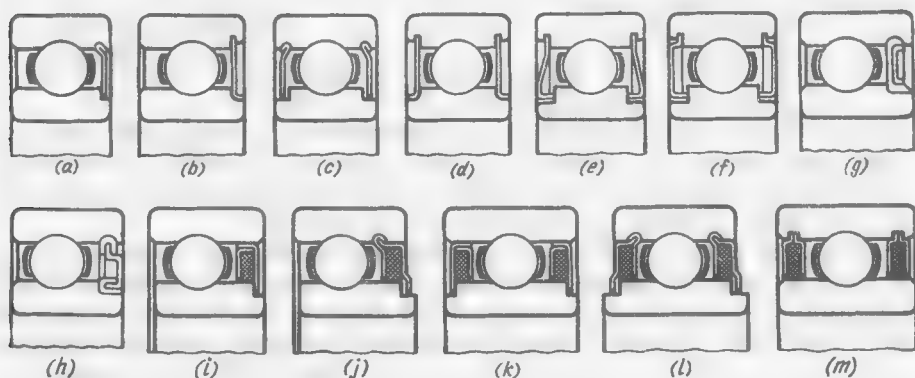
Fig. 206. Bearings with built-in seals

End bearings are sealed by means of shields with pressed-on elastomers (Fig. 206*g*, *h*), or by felt glands (Fig. 206*i*, *j*).

Table 30

Structural Proportions of the Rolling-Contact Bearing Elements
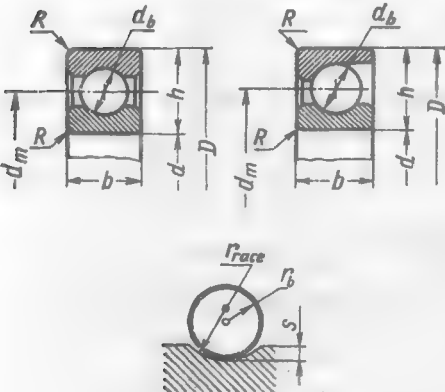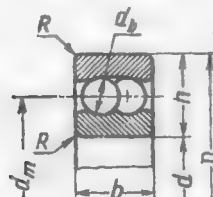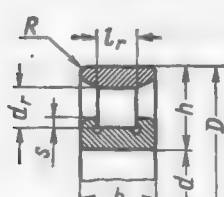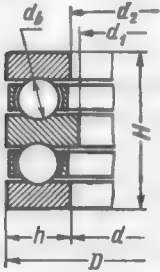
Type of bearings	Dimensions			
	Series	D/d	d_b/d_m	b/h
Radial and radial thrust ball bearings	Light	1.8-2	≈ 0.18	0.85-0.9
	Medium	2.15-2.3	≈ 0.23	0.85-1
	Heavy	2.5-2.8	≈ 0.28	0.75-0.9

$$d_b = (0.55 \text{ to } 0.63)\, h$$
where $h = 0.5\,(D - d)$
Fillet radius (or chamfer leg)
$$R = 0.1h$$
Raceway radius
$$r_{race} \approx 1.03 r_b$$
Raceway depth
$$s \approx 0.1h \approx 0.15 d_b$$

Double-row self-aligning ball bearings

$$d_b = (0.45 \text{ to } 0.5)\, h$$
$$b = (0.85 \text{ to } 1)\, h$$

Roller bearings

$$d_r = l_r \approx 0.5h$$
Light and medium series
$$b = (0.85 \text{ to } 1)\, h$$
$$s = (0.1 \text{ to } 0.12)\, h$$
Light wide series
$$b = (1 \text{ to } 1.25)\, h$$
$$s = (0.2 \text{ to } 0.25)\, d_r$$

Table 30 (cont.)

Type of bearings	Dimensions
Double-row self-aligning roller bearings 	$d_r = 0.5\,h$ $b = (1.15 \text{ to } 1.25)\,h$
Tapered roller bearings 	$d_r = (0.5 \text{ to } 0.53)\,h$ $l_r = (1.2 \text{ to } 1.25)\,h$ Inner race width b and overall width T of the bearing are: for light series $b = (0.9 \text{ to } 1)\,h,\ \ T = (1 \text{ to } 1.25)\,h$ for medium series $b = (0.7 \text{ to } 0.9)\,h\ \ T = (0.85 \text{ to } 1)\,h,$
Tapered roller bearings of wide series 	$d_r = (0.5 \text{ to } 0.53)\,h,$ $l_r = (1.7 \text{ to } 1.9)\,h$ Light series $b = h,\ \ T = (1.2 \text{ to } 1.6)\,h$ Medium series $b = (0.9 \text{ to } 1.25)\,h$ $T = (1.4 \text{ to } 2)\,h$
Single-row thrust ball bearings 	$d_b = (0.7 \text{ to } 0.8)\,h$ Inner diameter of non-centrable race $d_1 = d + (0.2\text{-}0.5)\text{ mm}$ Bearing height $H = (1.35 \text{ to } 1.6)\,h$ Raceway radius $r_{race} \approx 1.08 r_b$ Raceway depth $s = 0.1 d_b$

Table 30 (cont.)

Type of bearings	Dimensions
Double-row thrust ball bearings 	$d_b = (0.7 \text{ to } 0.8)\, h$ Inner diameter of non-centrable race $d_1 = d + (0.2\text{-}0.5) \text{ mm}$ Inner diameter of thrust race $d_2 = (0.83 \text{ to } 0.85)\, d$ $H = (2.5 \text{ to } 3)\, h$

Bearings with a one-time lubrication have their internal cavity filled at the manufacturing plant with a measured amount of grease and sealed with shields of the type shown in Fig. 206*g* and *h*, or with two-sided felt glands (Fig. 206*k-m*).

(e) Structural Proportions

Table 30 illustrates the averaged dimensional proportions of the structural elements of rolling contact bearings, statistically calculated on the basis of standard bearing dimensions.

3.2. Materials

Rolling-contact bearings are made of high carbon (1-1.2% C) chromium steel grade ШХ (Table 31). The numerals denoting the grade of steel indicate the mean content of Cr in tenths per cent.

Table 31

Ball Bearing Grades of Steel

Grade	Composition, %			
	C	Cr	Mn	Si
ШХ6	1.05-1.15	0.4-0.7	0.2-0.4	0.15-0.35
ШХ9	1-1.1	0.9-1.2	0.2-0.4	0.15-0.35
ШХ15	0.95-1.1	1.3-1.65	0.2-0.4	0.15-0.35
ШХ15СГ	0.95-1.1	1.3-1.65	0.9-1.2	0.4-0.65

The rolling elements are made of steel grades ШХ6, ШХ9 and ШХ15 and the races, of steel grades ШХ15, ШХ9 and ШХ15СГ.

The blanks are subjected to spheroidizing annealing to granulate cementite.

Hardening is done from a temperature of 820 ± 10°C with subsequent tempering at 150-160°C (62-66 *Rc*).

The hardened blanks are treated with cold (at —30°C) to decrease the amount of the residual austenite.

The races of large bearings with case-hardened working surfaces are made of steel grade 20X2H4A. The depth of the case-hardened layer is 5-6 mm (the duration of the case-hardening process is 120-150 hours and the temperature, 850-900°C). Case-hardened blanks are then annealed for grain-refining, hardened from 750-800°C and tempered at 150-160°C.

Bearings intended for use in aggressive media are made of stainless martensitic steel grade X18 (1% C, 18% Cr, < 0.7% Mn and Si). The steel is hardened in oil from 1000-1070°C and tempered at 150-160°C; its hardness is 60-62 *Rc*.

3.3. Manufacturing Accuracy Grades

In accordance with their manufacturing accuracy rolling-contact bearings are subdivided into the following classes (Soviet nomenclature):

Standard . . . . H   Mid-extra-high . . . . AB
Improved . . . . П   Extra-high . . . . A
Mid-high . . . . BП   Mid-super-high . . . . CA
High . . . . B   Super-high C

The classes of accuracy are distinguished by the manufacturing tolerances for the basic bearing elements (seating diameters, coaxiality of active surfaces, dimensions and forms of rolling bodies, profiles of raceways), and also by the standards determining the smoothness of run.

In bearings of intermediate classes (BП, AB, CA) the first letter of the designation denotes the accuracy class of the inner race, and the second letter, that of the outer race.

The bearings of the H, П and B classes are used in general machine building. Precision bearings (classes A, CA, C) are used in special cases (precision instruments, high-speed bearing units).

3.4. Coefficient of Friction.
Allowable Peripheral Speeds

The main causes of losses in rolling-contact bearings are:

hysteresis losses due to the cyclic elastic compressive deformation of the material of the rolling bodies and raceways at the points of contact;

slipping of the rolling bodies on the raceways, caused by the shearing deformation of the bearing material at the points of contact;

sliding of the rolling bodies on the raceways when rolling is disturbed by the displacement and misalignment of the bearing races under load;

friction of the rolling bodies against the cage, and friction of the cage against the races (in bearings with the centred cage);

squeezing out and viscous shear of oil at the points of contact;

turbulence and splashing of lubricating oil contacting the bearing.

Additional losses in roller bearings are caused by friction of the rollers against the guiding lips; in bearings with the contact angle other than zero (thrust and radial thrust ball bearings), by rotation of the balls induced by gyroscopic moments, and in cageless bearings (needle bearings), by friction of the rolling bodies against one another. In some types of bearings (thrust bearings with cylindrical rollers, spherotapered bearings) pure rolling is impossible and the motion of the rollers is attended by slipping on the raceways.

The frictional losses depend on the bearing manufacturing accuracy. The errors in the raceways profile, in the rolling bodies shape and in their various dimensions, and misalignment of the locating and active surfaces spoil the smoothness of run and result in cyclic loads which sharply increase friction.

The coefficient of friction in the rolling-contact bearings is determined by the ratio of the peripheral friction force F_{fr} on the shaft diameter d to the load P carried by the bearing

$$f = \frac{F_{fr}}{P} = 10^3 \frac{2M_{fr}}{Pd} \qquad (3.1)$$

where M_{fr} is the frictional moment in kgf·m and d is the shaft diameter in mm.

Table 32 gives the mean values of f for standard bearings (at a bearing working temperature of 50-80°C and with machine oil lubrication).

The coefficient of friction depends on the bearing dimensions, rotational speed, working temperature, properties of lubricant, method of lubrication, bearing manufacturing accuracy, method of installation, load application conditions and assembly accuracy. In unfavourable conditions (excessive oil feed, high oil viscosity, wear of rolling-contact surfaces, wrong assembly causing misalignment and pinching of the rolling bodies) the coefficient of friction may considerably exceed the values given in the table.

The permissible rotational speed is determined by the magnitude of the arbitrary peripheral speed v_{per} at the centre line of the rolling bodies or (which is practically the same) at the mean bearing diameter $(d_m = \frac{D+d}{2})$

$$v_{per} = \frac{\omega d_m}{2} = 10^{-3} \frac{\pi n}{30} \cdot \frac{d_m}{2} \approx 5 \cdot 10^{-5} n d_m \text{ (m/s)} \qquad (3.2)$$

where n is the rotational speed in rpm, and d_m is the mean bearing diameter in mm.

Alongside the peripheral speed, for estimating the rotational speed of bearing use is also made of the factor nd_m which, according to Eq. (3.2), is

$$nd_m = 2 \cdot 10^4 v \tag{3.3}$$

The mean values of v_{per} and nd_m for various types of bearings are given in Table 32.

Table 32

Coefficients of Friction and Permissible Rotational Speeds

Bearing type	Coefficient of friction f		Permissible peripheral speed v_{per}, m/s	$nd_m \cdot 10^{-6}$
	radial load	axial load		
Radial ball bearings	0.001-0.002	0.002-0.003	10-30	0.2-0.6
Spherical ball bearings	0.002-0.004	—	10-20	0.2-0.4
Radial thrust ball bearings	0.002-0.003	0.0025-0.004	10-20	0.2-0.4
Roller bearings	0.002-0.003	—	10-20	0.2-0.4
Spherical roller bearings	0.003-0.005	—	10-20	0.2-0.4
Tapered roller bearings	0.004-0.008	0.01-0.02	5-15	0.1-0.3
Needle bearings	0.005-0.01	—	5-10	0.1-0.2
Thrust ball bearings	—	0.004-0.006	5-10	0.1-0.2
Thrust bearings with tapered rollers	—	0.01-0.02	5-10	0.1-0.2
Thrust bearings with cylindrical rollers	—	0.02-0.03	3-5	0.05-0.1

3.5. Load-Carrying Capacity and Durability

The durability and load-carrying capacity of rolling-contact bearings of standard accuracy are calculated on the basis of an empirical formula

$$(nh)^{0.3} = \frac{C}{Q} \tag{3.4}$$

where h = durability, h

n = rotational speed, rpm

Q = corrected load on the bearing, kgf

C = coefficient of operating capacity of the bearing (given in catalogues)

The corrected load Q is calculated from the formula

$$Q = (R + mA)k_h k_\sigma k_t$$

where R = radial load, kgf

A = axial load, kgf

m = coefficient of correcting axial load to radial one

k_h = coefficient accounting for which race rotates (outer or inner)

k_σ = coefficient of loading conditions

k_t = coefficient of the temperature conditions of the bearing

The values of the coefficients m and k_σ are given in Table 33.

The coefficient k_h for bearings with the revolving inner race is $k_h = 1$, and for bearings with the revolving outer race, $k_h = 1.1$ for spherical bearings and $k_h = 1.35$ for all other bearings. The coefficient k_t is given below:

Working temperature of bearings, °C	100	125	150	175	200	225	250
k_t	1	1.05	1.1	1.15	1.25	1.35	1.4

Calculations usually consist in selecting a proper bearing, i.e., in determining the required operating capacity coefficient C on the basis of the given corrected load Q, rotational speed n and durability h.

The required operating capacity coefficient from Eq. (3.4) is

$$C = Q\,(nh)^{0.3} \tag{3.5}$$

If C, Q and n are known, check calculations are made to determine the bearing durability

$$h = \frac{1}{n}\left(\frac{C}{Q}\right)^{3.33}$$

The durability, expressed by the ultimate number of revolutions (number of cycles) during the operational period of the bearing, is

$$N\ (rev) = 60\ hn$$

The graph of $(nh)^{0.3}$ *versus* n for various values of h (Fig. 207) is plotted to simplify the calculations.

When choosing a bearing for the known n and specified durability h, the value of $(nh)^{0.3}$ is first found on the Y-axis of the graph and the required operating capacity coefficient is then determined by Eq. (3.5).

Example. Given: $Q = 500$ kgf; $n = 2500$ rpm; $h = 40,000$ h. We find from the graph (dashed lines) that $(nh)^{0.3} = 130$. Hence, $C = 130 \cdot 500 = 65,000$.

The graph can also be used to verify easily the bearing calculations. If $(nh)^{0.3} = C/Q$ is known, a horizontal line is drawn to intersect

Table 33

Coefficient m for Correcting Axial Load

Bearing type	Series	Bearing diameter	m at R/A			
			> 2	2	1	0
Single-row ball bearings	—	For all dimensions	1.5	1.7	1.9	2
Spherical ball bearings	Light	<17	2.5	2.9	3.1	3.4
		20-40	3.5	4.0	4.3	4.7
		>45	4.5	5.1	5.6	6.0
	Medium	<30	3.0	3.45	3.75	4.0
		>35	4.0	4.6	5.0	5.6
	Wide	For all dimensions	2.5	2.9	3.1	3.4
Double-row spherical roller bearings	Light	Ditto	4.5	5.1	5.6	6.0
	Medium	Ditto	3.5	4.0	4.3	4.7
Radial thrust ball bearings	—	Ditto	0.6	0.7	0.75	0.8
Tapered roller bearings	Light	Ditto	1.5	1.7	1.9	2.0
	Medium	Ditto	1.8	2.0	2.25	2.4
	With large angle of taper	Ditto	0.7	0.8	0.88	0.95

Loading Conditions Coefficient k_σ

Nature of load	k_σ	Nature of load	k_σ
Steady	1	Pulsating, short-time overloads up to 200%	1.8-2.5
With light jerks, short-time overloads	1-1.2	Impact, short-time overloads up to 300%	2.5-3
Pulsating, short-time overloads up to 150%	1.3-1.8		

the perpendicular erected from the point corresponding to the given n value and the bearing durability h is found at the point of intersection on the rigid of h curves.

Example. Given: $Q = 2000$ kgf, $C = 180,000$ ($C/Q = 90$); $n = 1500$ rpm· In conformity with the graph (dashed lines) the durability $h = 20,000$ h.

The bearing durability must conform to that of the machine in which the bearing is to be used. The machine durability varies within a very wide range depending on its purpose, the stress level of
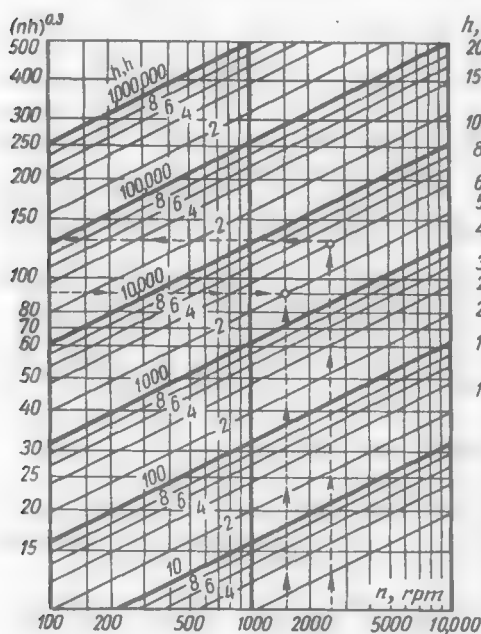
Fig. 207. Graph of function $(nh)^{0.3}$
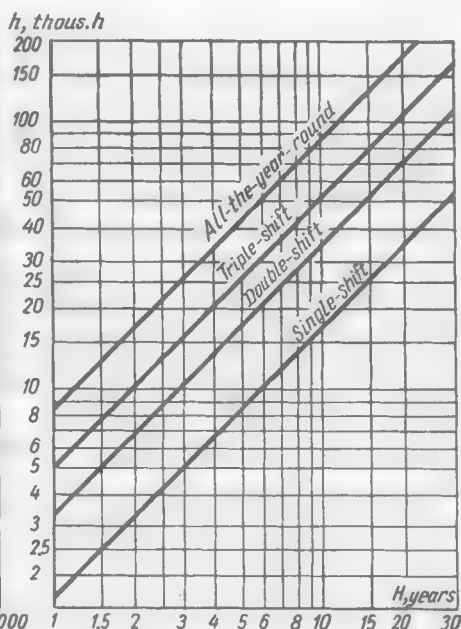
Fig. 208. Design durability depending on service life and operating conditions

its operative components, conditions of operation, and its obsolescence period which is principally determined by the duration of its service life H expressed as

$$H = \frac{h}{\eta_{use}} \qquad (3.6)$$

where h is the durability and η_{use}, the use factor of the machine (the share of the actual operation of the machine during its service period).

For general-purpose machines operating on a calendar basis

$$\eta_{use} = \eta_{shift} \cdot \eta_{off\text{-}d} \cdot \eta_{acc.br}$$

where η_{shift} = shift factor (for single-, double- and triple-shift operation $\eta_{shift} \approx 0.3$, 0.6 and 0.9, respectively)

$\eta_{off\text{-}d}$ = off-day factor (on the average $\eta_{off\text{-}d}$ = 0.8)

$\eta_{acc.br}$ = accidental breakdown factor

Assuming that $\eta_{acc.br}$ = 0.8, we get

$$\eta_{use} = 0.64\eta_{shift}$$

Substituting this value into Eq. (3.6), we obtain a formula for determining the durability depending on the service life

$$h = 0.64\eta_{shift}H$$

This formula is used to plot the *h versus H* graph (Fig. 208) for single, double- and triple-shift operation, and also for all-the-year-round twenty-four hour operation (in the latter case $h = 0.95H$ where the coefficient 0.95 accounts for accidental breakdowns).

The graph can be used to find the design durability of general-purpose machines depending on their operating conditions and service life.

For the most common case of double-shift operation with a service life of 10-15 years the design durability h = 35-50 thousand hours. With the same service life h = 50-100 thousand hours for intensively used machines (triple-shift and all-the-year-round operation).

3.6. Selection of Bearing Series

Rolling-contact bearings of almost all types are manufactured in several modifications (series) differing in dimensions, load-carrying capacity and speed.

Figure 209*a, b* shows the operating capacity coefficients and maximum permissible rotational speeds for bearings of various standard sizes and series, depending on shaft diameter *d*.

The operating capacity coefficients increase and the rotational speed drops for heavier series and larger bearing diameters.

For example, in the case of roller bearings the operating capacity coefficients for medium series are approximately 1.7 times higher than those for light series; the coefficients for heavy series are quite the same number of times higher than those for medium series and about three times higher than those for light series.

The durability of bearings, because of its exponential dependence on the operating capacity coefficient, increases much more abruptly for heavier series.

In conformity with Eq. (3.5) the durability is

$$h = \frac{1}{n}\left(\frac{C}{O}\right)^{3.33} \tag{3.7}$$
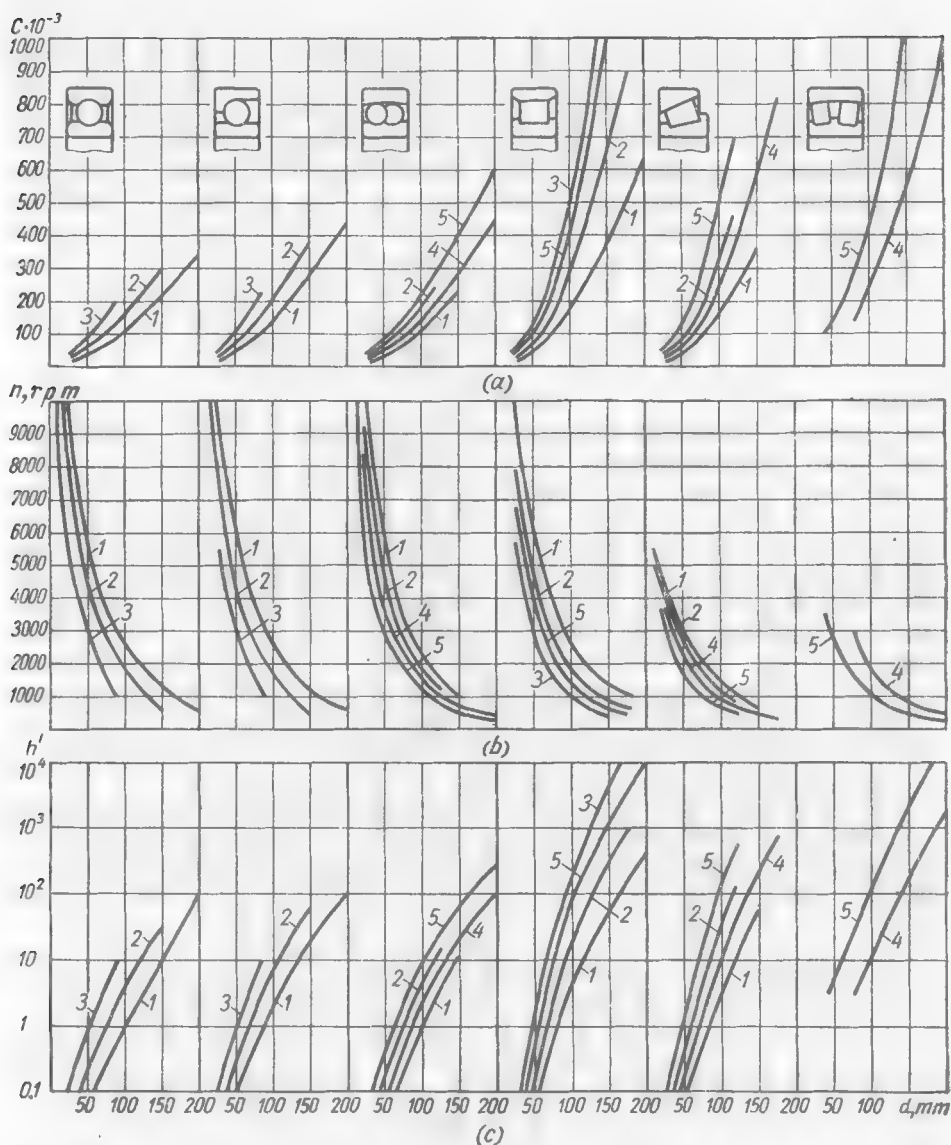
Fig. 209. Operating capacity coefficient C, limiting number of revolutions n and relative durability h' of bearings

1 — light series; *2* — medium series; *3* — heavy series; *4* — light wide series; *5* — medium wide series

i.e., when $n =$ const and $Q =$ const the durability is proportional to $C^{3.33}$. Therefore, all other things being equal, the durability of roller bearings of medium series is $1.7^{3.33} \approx 6$ times higher than that of light ones; the durability of bearings of heavy series is the same number of times higher than that of bearings of medium series, and about 36 times higher than that of bearings of light series.

Figure 209c shows the relative durability h' calculated by Eq. (3.7) on the assumption that the loads and rotational speeds are the same. The durability of a radial ball bearing of light series with $d = 100$ mm is taken as unity.

Bearings	Series		
	light	medium	heavy
Ball bearings	1	4	15
Roller bearings	4	25	150

As can be seen, the durability of bearings of heavy series exceeds by about one order of magnitude that of light-series bearings, and the durability of roller bearings is by one or two orders of magnitude higher than that of ball bearings.

Figure 209c can be used to estimate the relative durability of bearings, comparable in functional purpose and speed. The table above gives the figures of relative durability of radial ball and roller bearings with $d = 100$ mm, obtained on the assumption that the loads and rotational speeds are the same (the durability of the light-series ball bearing is taken as unity).

As can be seen, the durability of roller bearings exceeds that of light-series ball bearings by four times, that of ball bearings of medium series, by six times, and that of ball bearings of heavy series, by ten times. The durability of heavy-series roller bearings is 150 times higher than that of light-series ball bearings.

When selecting the proper series, along with the carrying capacity, account should also be taken of the dimensions, weight and rotational speed of the bearing. Fig. 210 presents the basic characteristics of bearings of various types and series with the same shaft diameter ($d = 80$ mm). The drawing shows the appreciable advantage of light-series bearings as far as overall dimensions, weight and speed are concerned. Their carrying capacity is of course lower than that of bearings of medium and, especially, heavy series.

Bearings of light and medium series are more popular, even if their operating capacity coefficient has to be increased, when necessary, by enlarging the diameter of the shaft, which is just as effective for improving the carrying capacity and durability as using a heavier bearing series. This method reflects the present-day tendency to use
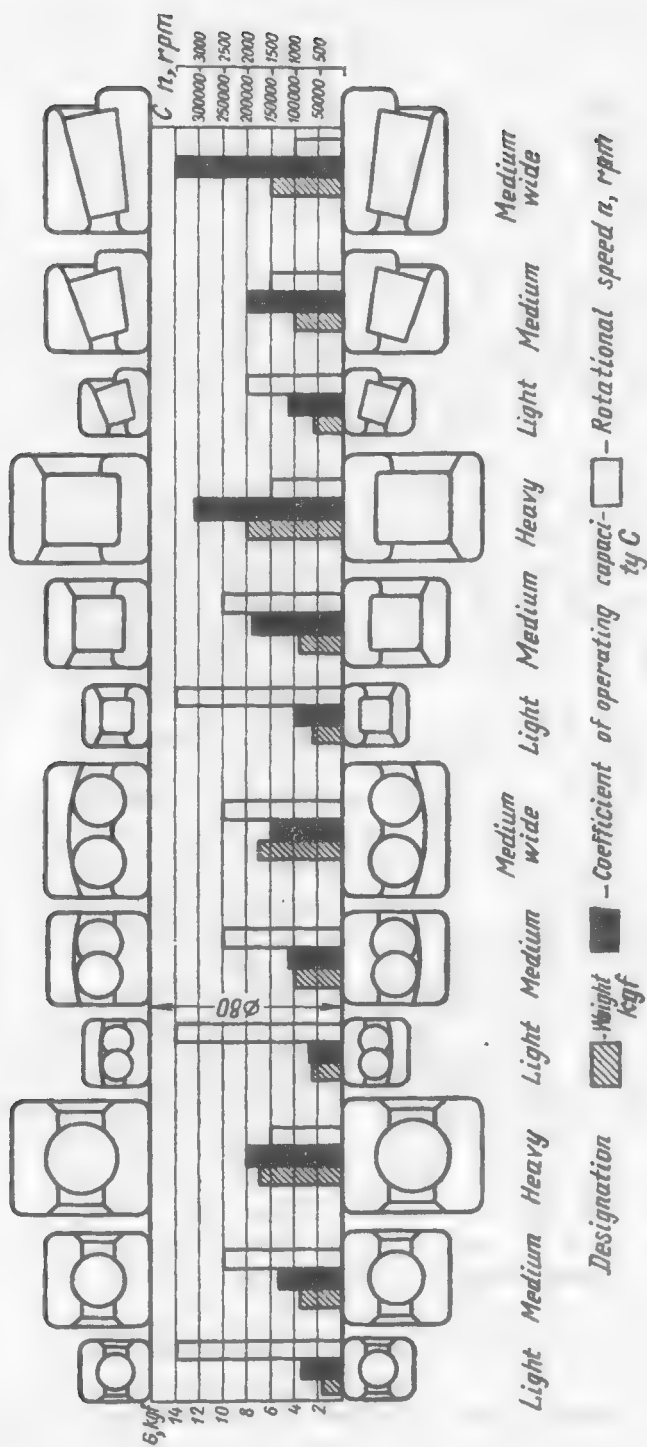
Fig. 210. Comparative characteristics of bearings

hollow shafts of increased diameter in power units to improve the strength and rigidity and reduce weight of the structure.

Bearings of heavy series are used in low-speed units subjected to especially heavy loads (shafts of rolling mills). It is also expedient to use them as the end supports of large shafts, where the diameter of the journals can be made, without any detriment to strength, much smaller than that of the active shaft portion, and thus reduce the overall dimensions of the bearing unit.

The calculation of bearings on the basis of the above formulas and information from respective catalogues yields only averaged and, moreover, slightly reduced durability figures. According to statistical data, the durability of 50 per cent of all bearings is 3-4 times higher than their rated durability and that of 10 per cent of all bearings exceeds the rated value by 10-20 times. Besides, the durability of bearings of higher accuracy is much higher than that of bearings of standard accuracy. The durability and load-carrying capacity of bearings depend in a large measure on the design of the unit they are used in, their correct installation, the rigidity of the shaft and housing, the amount of interference on the locating surfaces, and, especially, on the lubricating conditions. The durability of rationally preloaded bearings in properly designed units often exceeds many times the design service life.On the other hand, a high value of the operating capacity coefficient does not guarantee reliability. Such bearings may possibly fail rapidly because of poor installation (overtightening, misalignment of axes, insufficient or excessive lubrication).

3.7. Fastening of Bearings on Shafts

Bearings are usually fastened on shafts by tightening their inner races with a nut. This type of fastening ensures accurate axial location of the bearing, prevents the inner race from rotating on the shaft and makes it possible to install the bearing on the shaft with a small interference without running the risk of crushing and breaking the seating surface of the shaft.

The strongest tightening is effected by pressing the race against a shaft shoulder (Fig. 211*a*), a spacing ring (Fig. 211*b*), or against any shaft-fitted part, pressed in its turn against the shoulder.

Also in'wide use is the tightening of the bearing on the shaft through the intermediary of a shaft-fitted part (Fig. 211*c*) or between distance bushings (Fig. 211*d*) clamped with a nut.

Power tightening against a snap ring (Fig. 211*e*) is impossible because the ring may be shorn off or forced out of its groove.

Round snap rings reinforced with enveloping taper rings (Fig. 211*f*) can sustain increased tightening forces.

These methods are used both for shaft-end and mid-shaft installations.

In shaft-end installations power tightening is also effected by means of internal nuts (Fig. 211*g*) or washers pressed against the end face of the shaft either by a single central bolt (Fig.211*h*) or by several bolts (Fig. 211*i*).

All other fastening methods do not ensure power tightening and, as a rule, require fits with a greater interference and a higher shaft hardness to prevent the crushing of the seating surface.
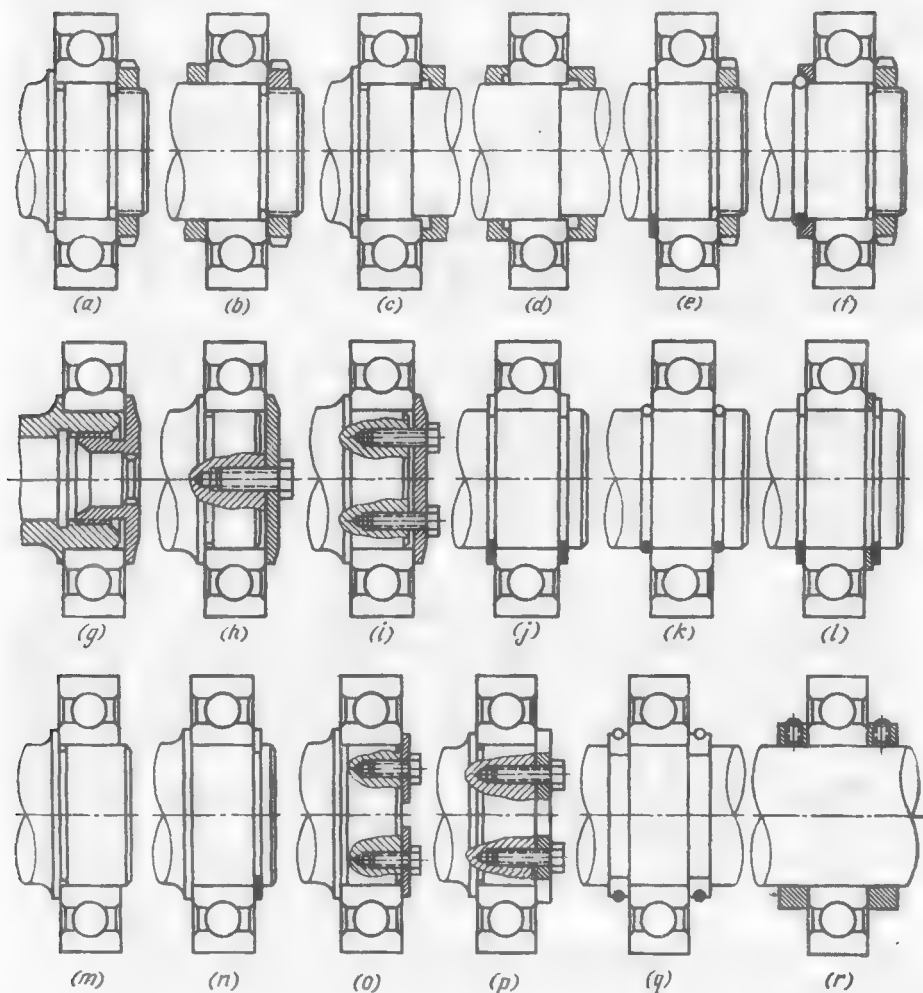
Fig. 211. Fastening of bearings on shafts

Lightly loaded bearing units are fixed with snap rings (Fig. 211*j*, *k*). In order to ensure clearance-free locking with snap rings (especially when they are made of round wire), it is necessary either to keep a strict distance between the grooves for the rings or use sized spacer washers (Fig. 211*l*). In lightly loaded bearing units it is sometimes sufficient to fit the bearings on the shaft with an interference

and make them rest against a shoulder (Fig. 211*m*). This method is not proof against the displacement of the bearing on the shaft as the interference grows weaker. In such cases it would be more correct to safeguard the bearing against shifting by means of a snap ring (Fig. 211*n*).

An end bearing is locked by washers fixed by bolts, arranged on the periphery of the shaft end (Fig. 211*o*), and also by a plate (Fig. 211*p*). This method fails to ensure proper tightening because the fastening elements must abut upon the shaft end to prevent misalignment.

Today, bearings are almost never locked with half-rings clamped by snap rings (Fig. 211*q*), or with adjusting rings with pressure screws (Fig. 211*r*). The latter method is still used sometimes to mount bearings on a smooth shaft where their axial position has to be adjusted.

Installation of Bearings with a Tapered Bore

These bearings are made with a tapered bore (taper 1 : 12, central coning angle $\alpha \approx 5°$) and mounted on smooth shafts by means of spilt fastening sleeves with tapered external and cylindrical internal surfaces (Fig. 212*a*). The bearing is tightened on the sleeve by
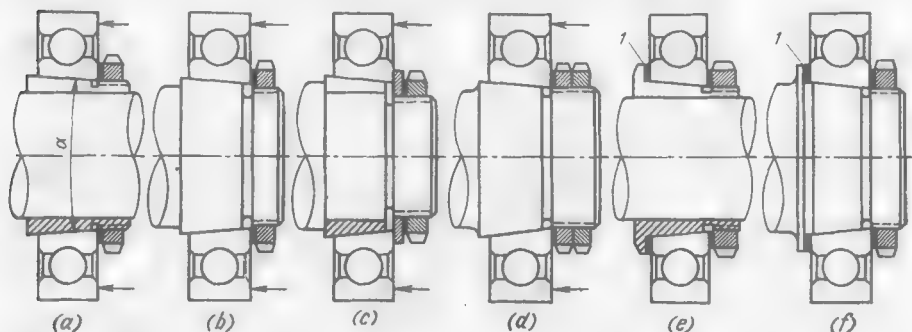
Fig. 212. Installation of bearings with a tapered bore

a nut which produces interference between the internal surface of the bearing and the fastening sleeve on one side and between the sleeve and the shaft on the other, which is necessary to lock the bearing.

Bearings of this type have the following disadvantages:

poor centring of the shaft due to the additional seating surfaces;

possible overtightening of the bearing which results in reducing the clearance between the rolling bodies and the races; excessive overtightening may cause jamming;

change in the position of the bearing on the shaft during tightening, due to the elastic deformation of the race, and during retightening, due to the crushing of the thrust surfaces;

incapability of withstanding heavy axial loads directed towards the major diameter of the taper which cause the pinching of the rolling bodies.

Installation on a fastening sleeve is still used as a method of securing bearings on smooth shafts so that the axial position of the bearing on the shaft can be adjusted.

In some cases bearings with tapered bores are used to adjust the clearance between the rolling bodies and races and take up the clearance between the balls or rollers increased due to wear, and also as a means of producing radial preload.

Figure 212b shows the case of fastening a tapered bearing directly on a shaft having a tapered seating surface and Fig. 212c, on a stepped cylindrical shaft with an intermediate tapered bushing.

The arrows on the drawings indicate the directions of axial forces with which there is a possibility of the bearings being jammed.

Overtightening of bearings during assembly can be prevented by tightening them with a torque or limit wrench, the nut being subsequently secured with a locknut (Fig.212d) or by tightening the bearing against sized washers *1* (Fig. 212e,f) which limit the displacement of the tightening nut.

The sized washers enable the bearing to carry axial forces of either direction. The washer thickness must be kept to very close tolerances, because too thick a washer loosens the fit of the bearing on the shaft, while an insufficiently thick one may cause the overtightening of the bearing. When the bearing is reassembled, new washers must be installed. It is unpracticable to use sized washers in mass production.

3.8. Installation of Bearings in Housings

The methods of installing bearings in solid housings (axial assembly) are illustrated in Fig. 213.

In heavily loaded supports the outer race of the bearing is tightened by nuts against a shoulder (Fig. 213a) or distance bushing (Fig. 213b) rigidly fixed in the housing. The tightening against snap rings (Fig. 213c) is weaker. In the design in Fig. 213d the snap ring is reinforced by a cup-shaped washer.

In shaft-end installations the bearings are locked by means of caps. A fit with a clearance *s* or with an interference (Fig. 213f, g) can be obtained depending on the depth *l* of the bearing seat and the thickness of the sealing gasket *1* (Fig. 213e).

Blind caps are usually not centred; caps with seals (Fig. 213h) are centred from the seating surface.
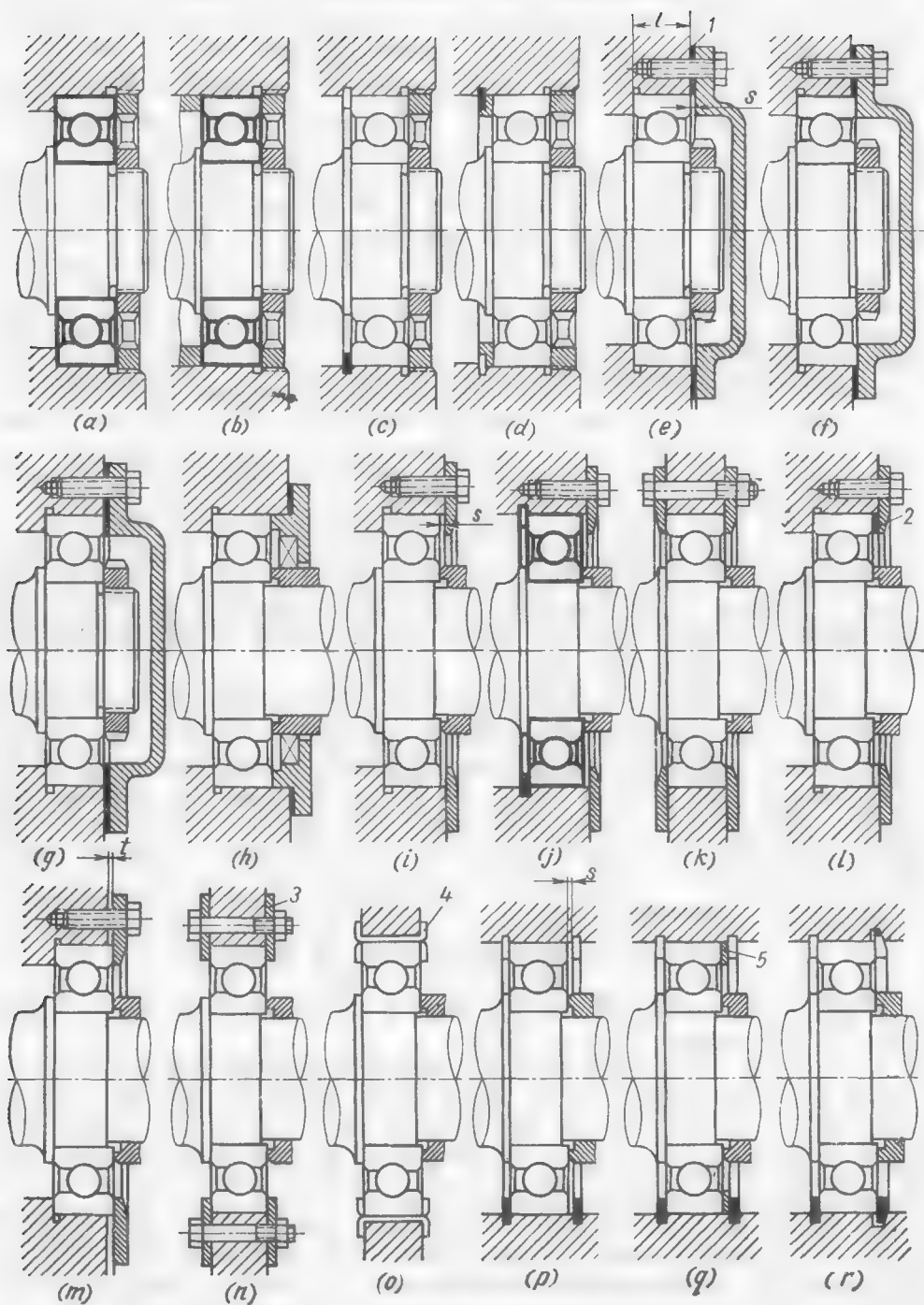
Fig. 213. Installation of bearings in housings

Bearings installed in internal walls, partitions, diaphragms, etc., are held in position by disks (Fig. 213*i-k*) usually with a small axial clearance ($s = 0.1$-0.2 mm). When a clearance-free fit is necessary, use is made of sized washers 2 (Fig. 213*l*). Tightening is effected by providing a clearance $t = 0.05$-0.1 mm between the disk and housing (Fig. 213*m*).

Washers 3 (Fig. 213*n*) are frequently used instead of the disks. If the washers are tightly fitted against the end surfaces of the
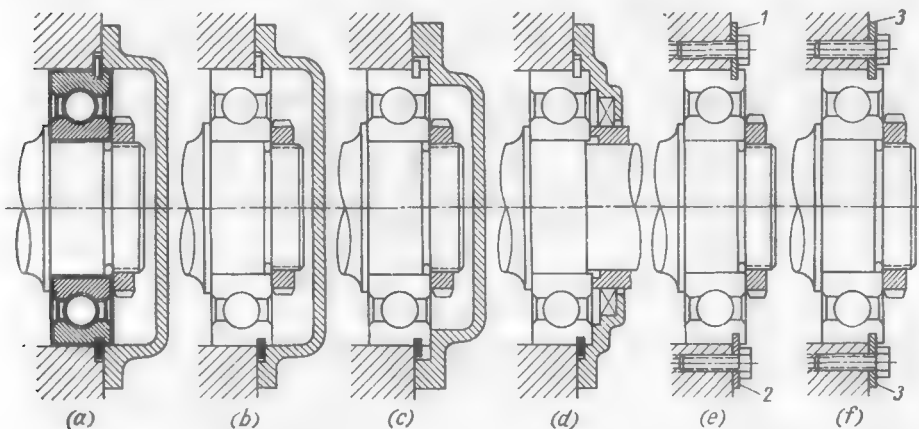
Fig. 214. Fastening of bearings by means of snap rings

housing (i.e., with a clearance with respect to the bearing) there is no hazard of the washers and the bearing being misaligned despite the tightening at several points.

In lightly loaded supports which carry axial forces the locking of the bearing is effected with the aid of strips 4 (Fig. 213*o*) with bent ends, which are installed in axial grooves in the bearing seating bore.

Snap rings are widely used for locking the bearings. To facilitate assembly, the rings are usually inserted with a clearance $s = 0.1$-0.2 mm (Fig. 213*p*). For clearance-free locking, sized washers 5 (Fig. 213*q*) or tapered snap rings (Fig. 213*r*) are used.

Bearing locking by means of snap rings inserted into grooves in the outer race of the bearing is especially convenient for shaft-end installations (radial ball bearings with such grooves are mass produced).

As a rule, the ring is clamped between the housing and the cap (or disk). The recess for the ring is made in the housing (Fig. 214*a*) or, which is still better, in the cap (Fig. 214*b*). This method does not ensure a clearance-free fit (a clearance still remains between the

snap ring and the walls of the groove in the bearings race). The axial forces acting on the bearing are taken up by the snap ring whose carrying capacity is limited.

Clearance-free locking is effected by tightening the cap against the end face of the outer race (Fig.214c). The bearing can be tightened in some measure by strictly keeping to the required axial dimensions, or by introducing elastic gaskets. The axial load in one direction is taken up by the cap and in the other, by the snap ring. Duplex installations with opposed bearings secured by this method can carry heavy axial loads in both directions.

Caps with seals are usually centred from the outer bearing race (Fig. 214d).

Bearings with grooves in their outer race can also be locked by means of half-rings *1*, *2* (Fig. 214e) or washers *3* introduced into the groove (Fig. 214f).

The structural proportions of bearings with grooves are as follows (Fig. 215):

snap ring height
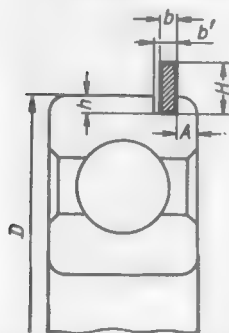
$$H = (0.05 \text{ to } 0.1) D$$

snap ring thickness

$$b \approx 0.3H$$

distance from the groove to the race end face

$$A = (0.03 \text{ to } 0.06) D$$

groove depth

$$h \approx 0.3H$$

groove width

$$b' = b + (0.1 \text{ to } 0.15)$$

Fig. 215. Dimensions of grooves in outer bearing races

where *b* is the snap ring thickness, mm.

In these formulas the lower limits refer to medium and large bearings ($d > 60$ mm) and the upper ones, to small bearings ($d < 60$ mm).

In split housings (radial assembly) bearings are installed in annular grooves (Fig. 216a) cut jointly in both halves of the assembled housing. Fastening methods that allow through-pass machining are preferable. Such methods comprise the use of rings (Fig. 216b), disks (Fig. 216c, d), snap rings (Fig. 216e) and flanged sleeves (Fig. 216f) inserted into the grooves in the housing.

In shaft-end installations the bearings are fastened with caps just as this is done in solid housings.

If there are some special requirements of the bearing unit as to its weight, size and installation accuracy, useis made of special bearings with fastening elements incorporated into the race design (Fig. 217a-c).

Figure 217d, e presents special bearings intended for installation in housings split in the meridional plane.

The bearing with temperature-independent centring (Fig. 217*f*) intended for installation in a light-alloy housing has two centring surfaces on the outer race and on the flange made integral with the race. Cold centring is effected
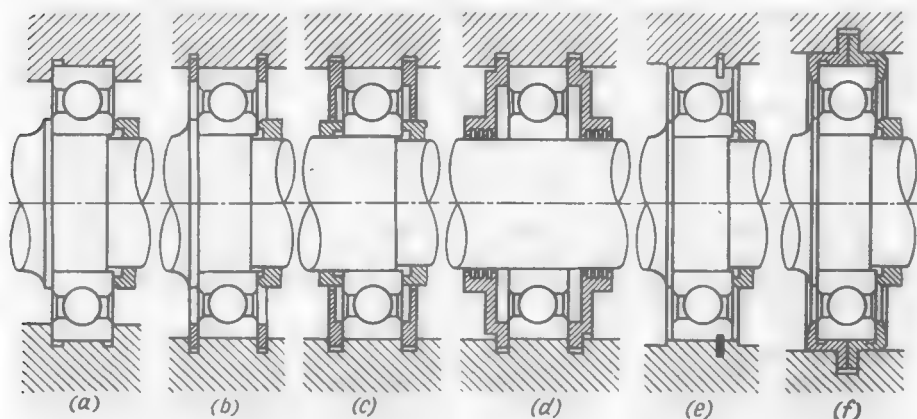
Fig. 216. Installation of bearings in split housings

from the race. The second centring surface fits the housing with a clearance *s* equal to the difference in temperature deformations between the housing and
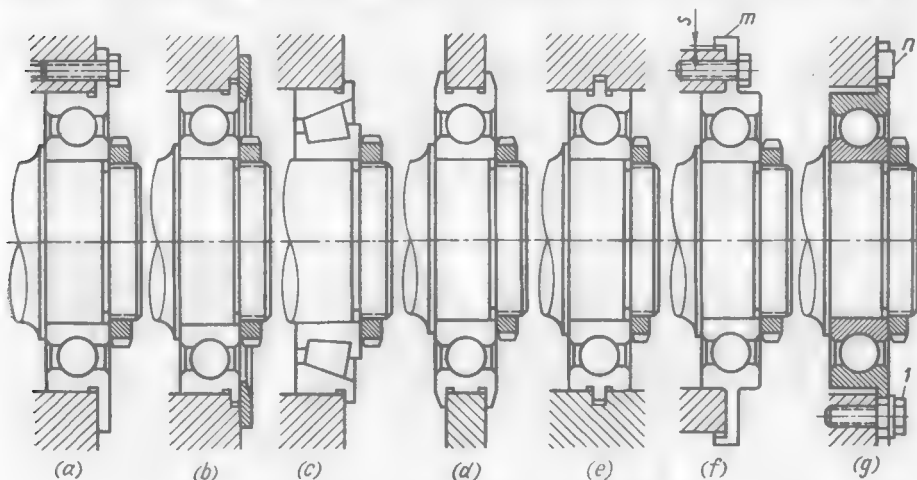
Fig. 217. Special types of fastening

bearing. When the housing is heated the clearance is eliminated and the bearing is centred on the shoulder *m*.

The temperature-independent installation as per Fig. 217*g* uses a radial-ray centring from projections *n* of the housing, which enter corresponding slots in the flange of the outer race. The bearing is attached to the housing by elevator bolts *i* ensuring free movement in the course of thermal deformations.

Installation of Bearings on Adapter Sleeves

In light-alloy housings rolling-contact bearings are generally mounted on adapter sleeves to prevent the crushing and breaking of the seating surfaces and the galling of the soft housing metal on the external surface of the bearing when its outer race moves (especially in the case of floating-race installation).

When bearings are installed directly in the housing, an oversize bore can make the costly housing casting a reject, and this during the final machining stages.

For this reason the installation of bearings on adapter sleeves is also used in cast-iron housings, except when the bearing seats are bored in a preset operation, on jig boring or unit-built machines where there is practically no possibility for the seats being made oversize.
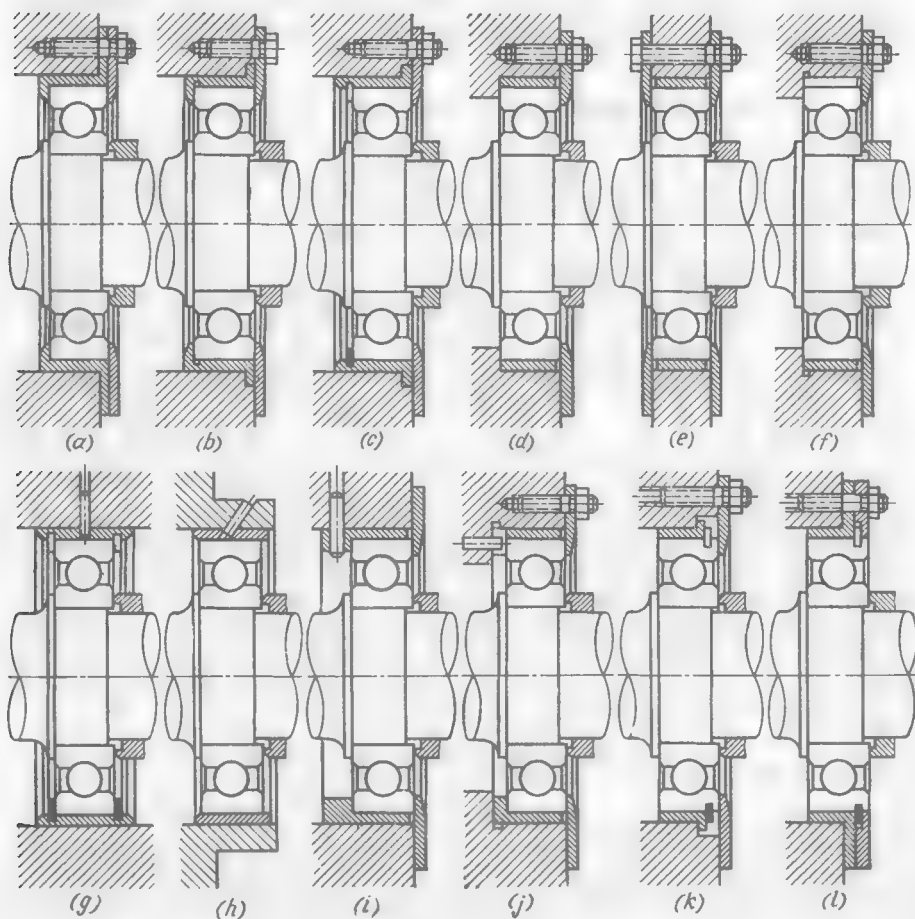
Fig. 218. Installation of bearings sleeves

The sleeves are usually made of normalized carbon steel. The thickness of the sleeve walls is, on the average, $s = 2 + 0.015D$ (where D is the external bearing diameter in mm); the sleeves are installed in housings by push, tight and wringing fits. The coaxiality of the external and internal surfaces of the sleeves is ensured by establishing close tolerances on their wall thickness. Heavy drive fits require the finish boring of the sleeves after pressing in.

Adapter sleeves with flanges for fastening to the housing (Fig. 218a) are die-forged. The designs with a reduced flange height (Fig. 218b, c) are advisable.

In the designs shown in Fig. 218d and e the sleeves are made from thin-walled pipe. This results in minimal waste when machining.

Sleeves made from bent sized strip (Fig. 218f) are most suitable for industrial production. The sleeves are bent so as to ensure their interference fit in the housing bores, leaving a small clearance remaining between the ends of the bent strip.

As distinct from solid sleeves whose hole size is reduced when they are being interference-fitted into the housing, strip sleeves maintain their internal diameter which depends only on the housing bore diameter and strip thickness.

The adapter sleeves are locked axially and secured from rotation with bolts (Fig. 218a), by tightening (Fig. 218b, c), and with radial and inclined pins (Fig. 218g-i). Axial pins (Fig. 218j) secure the sleeves only from rotation.

Figure 218k, l illustrates the methods of installing bearings with snap rings on their outer race in adapter sleeves.

3.9. Design Elements of Bearing Fastenings

Figure 219 shows methods of locating the bearing end faces against shaft shoulders.

The shoulders with an undercut groove for the grinding wheel overtravel (Fig. 219a, b) are made on lightly loaded shafts. The fatigue strength of shafts carrying cyclic loads is increased, if the cylindrical surface of the shaft is connected to the shoulder by a fillet (Fig. 219c). To make the race end face tightly fit the shoulder, the fillet radius must not exceed $0.8R$, where R is the fillet radius (or the chamfer leg) of the bearing race (usually equal to $0.1\frac{D-d}{2}$, where D and d are the external and internal bearing diameters, respectively).

In transitions with large-radius and elliptic fillets and in tapered transitions intermediate thrust washers (Fig. 219d-f) are used.

To reduce the amount of precise machining and provide for the grinding wheel overtravel, the seating surfaces must be several tenths of a millimetre above the adjacent shaft surfaces which do not require precise machining.

The seating surface (Fig. 219g) usually extends only to the bearing fillet ($l \approx b - R$, where R is the fillet radius). The bushing is chamfered at an angle of 45° to overlap the step m and facilitate the mounting of the bushing on the shaft. The undercut on the bushing
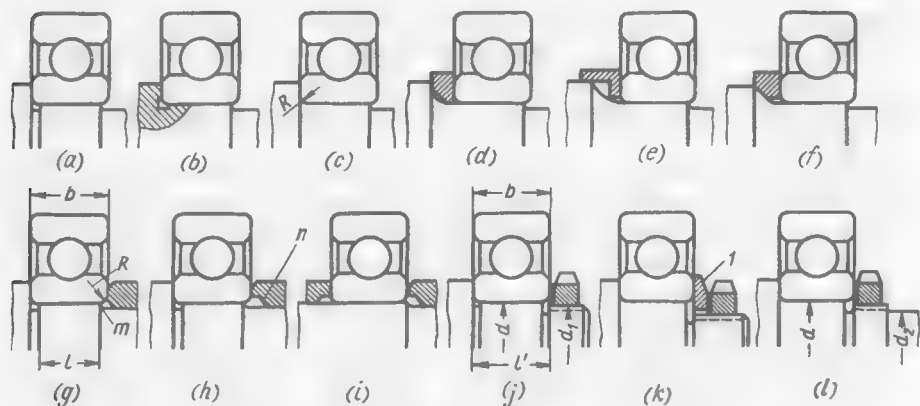
Fig. 219. Fastening of bearings on shafts

(Fig. 219h) provides for more reliable tightening and does not impose strict limitations on the seating surface length.

The chamfer n on the undercut facilitates assembly.

In mid-shaft installations, where the bearing is held between two bushings (or the hubs of shaft-fitted parts), the seating surface extends to the end face of the bearing (Fig. 219i), or even made to extend beyond its limits to allow for manufacturing variations in the axial dimensions. In the latter case the use of the undercuts is obligatory.

In shaft-end installations with a lock nut the active threads are usually made to terminate at a distance $l' = b$ from the shoulder (Fig. 219j) in order to arrange the undercut groove under the bearing fillet.

The thread diameter d_1 should be as close as possible to the diameter d of the seating surface so as to make unnecessary the use of washer 1 (Fig. 219k).

It is especially important to follow this rule in mid-shaft installations (Fig. 219l) thus reducing the difference between the shaft diameters d and d_2. With the same purpose in mind a fine thread is always used in bearing tightening units.

The height of thrust shoulders and other elements locking the bearings in the axial direction depends on the bearing dismantling conditions.

Rolling-contact bearings are mounted and dismantled by applying a force only to the secured race (the inner race for bearings inter-

ference-fitted on the shaft and the outer race for those interference-fitted in the housing). No force must be applied to the other race since in this case the effort is transmitted through the rolling bodies and raceways which can be damaged.
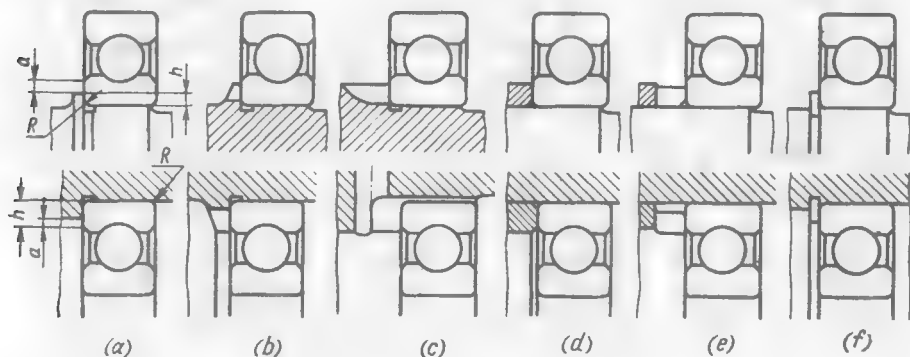
Fig. 220. Height of thrust shoulders

The thrust shoulder height h must be less than the race thickness by an amount a (Fig. 220a) sufficient to rest a remover bushing or puller directly against the bearing race.

The ultimate height of the shoulders is standardized. This height can approximately be determined from the relation

$$h = 0.1 \frac{D-d}{2} + (2 \text{ to } 3) \text{ mm}$$

The shoulder height can be increased, if two or three sufficiently deep cuts are made in them enabling the puller to grip the race securely with both claws (Fig. 220b, c).

The height of distance bushings (Fig. 220d) is not limited, if they can be removed prior to dismantling the bearing or utilized as remover bushings. If a bearing has to be removed with its distance bushing remaining in place, the bushing height should be limited or the bushing should be provided with slots for the puller claws (Fig. 220e).

The height of the bearing locking snap rings (Fig. 220f) is not limited, if the rings can be removed before dismantling the bearing. If the dismantling is done with the rings remaining in place, then the height to which the rings project above the seating surface must be limited. The height of standard snap rings, determined proceeding from the condition of their strength, almost always allows easy removal of the bearings.

Distance bushings used for tightening the bearings in duplex installations must be centred to avoid misalignment.

The method of centring from the entire bushing surface on the shaft and in the housing, displayed in Fig. 221a, is unsuitable for
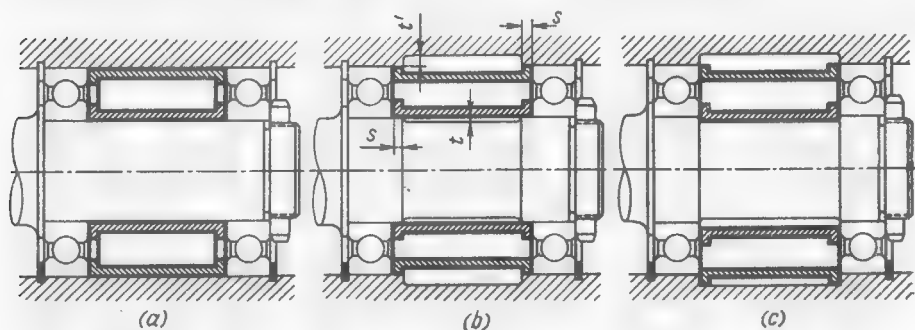
Fig. 221. Installation of distance bushings

industrial production since in this case the shaft and housing must be accurately machined all over the portions occupied by the distance bushings.

It is good practice to arrange the surfaces which do not require accurate machining to lie a distance t below the seating surfaces and extend the latter to a distance $s = 4$-5 mm (Fig. 221b) sufficient for centring.

The value of t for machined surfaces is taken equal to several tenths of a millimetre, whereas for rough cast surfaces of housings the size t' is specified within 4-5 mm.

Distance bushings are, as a rule, centred by S_{2a} and S_3 fits.

If bearings are push-fitted on the shaft, the basic-shaft system must be used to centre internal distance bushings on the seating portions of the shaft.

In uncritical bearing units the internal bushing diameter is made 0.1-0.2 mm larger than the diameter of the shaft seating surfaces, the basic-hole system being used when boring the bushing.

It is a gross error to install distance bushings without any centring or with poor centring (small s). The chamfers on the centring surfaces of the bushings and also inaccuracies in the length of the seating portions of the shaft and housing may result in the disturbed centring and radial displacement of the bushings (Fig. 221c).

(a) Installation of Radial Bearings

Radial bearings are predominantly used in duplex and less frequently, multiple-row installations.

Loaded parts must never be mounted on one bearing (Fig. 222a, b) as the angular clearance of ball bearings, coming to 1-2° even with small loads, causes the misalignment of the part. If the bearing is

subjected to the action of a bending moment (Fig. 222b), the operating conditions of the balls are markedly worsened. The balls roll on the sides of the raceways and the bending moment M_{bend} produced by the couple of forces acting on the opposite balls (Fig. 222c)
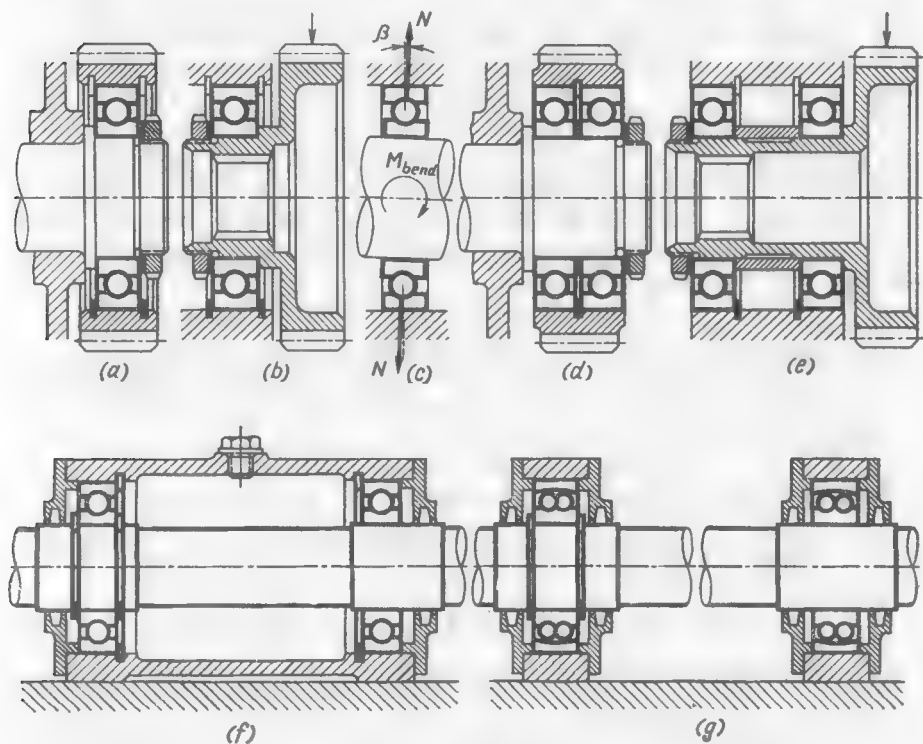
Fig. 222. Installation of ball bearings

causes, due to the small contact angle β, the development of very high loads N normal to the contact surface. Bearings operating in such conditions rapidly fail.

In correct designs (Fig. 222d, e) the bearings carry only radial loads.

It is generally recommended that bearings be installed in one and the same housing (Fig. 222f) or in housing parts rigidly connected and locked with respect to one another.

If, for design considerations, bearings have to be mounted in different housings, self-aligning bearings (Fig. 222g) should be used.

For the bearings to operate properly in twin and multiple-support installations it is necessary that only one bearing (the locking one) be secured both on the shaft and in the housing. The other bearings

must be fastened either on the shaft or in the housing and be free to
move axially with respect to the housing in the first case or with
respect to the shaft in the second.

When both bearings are to be secured both on the shaft and in the
housing (Fig. 223a) the axial distances between the locking elements
(in our case the distance l between the snap rings retaining the left-
and right-hand bearings) must be kept to close tolerances. Otherwise
the bearings are liable to be overtightened already during the initial
installation. During operation the unit is heated by friction (and in
hot machines, also by the heat generated in the working process of
the machine). If the housing is manufactured from a material with
a coefficient of linear expansion higher than that of the shaft mate-
rial, then while heating the housing elongates more than the shaft.
Even if bearings are correctly installed in the cold machine, they
will be pinched when heated.

Example. Let the distance between bearings be $l = 150$ mm. The housing
material is an aluminium alloy ($\alpha_h = 22 \cdot 10^{-6}$). The linear expansion coeffi-
cient of the shaft material (steel) is $\alpha_{sh} = 10 \cdot 10^{-6}$. The working temperature of
the unit is 100°C.

The housing elongation upon heating is

$$\Delta l_h = \alpha_h t l = 22 \cdot 10^{-6} \cdot 100 \cdot 150 = 0.33 \ (\text{mm})$$

and the shaft elongation in the same section

$$\Delta l_{sh} = \alpha_{sh} t l = 10 \cdot 10^{-6} \cdot 100 \cdot 150 = 0.15 \ (\text{mm})$$

Upon heating, the bearing will be overtightened by an amount

$$\Delta l_h - \Delta l_{sh} = 0.33 - 0.15 = 0\ 18 \ (\text{mm})$$

In the correct installation (Fig. 223b) the right-hand bearing is
rigidly secured on the shaft and in the housing, whereas the left-
hand one is floating. Its inner race is secured only on the shaft, and
the outer race can move in the housing. Such an installation scheme
allows less accurate axial dimensions of the unit and does away with
the effect of thermal deformations on its functioning.

The fit of the floating races in the housing is made sufficiently
free (easy slide, slide and, at the utmost, push) so that no load
is applied to the rolling bodies when the races shift.

The design with the floating bearing having its outer race fixed
in the housing and the inner race sliding on the shaft (Fig. 223c) is
seldom used because in this case the surface over which the bearing
slides is sharply reduced (on the average by 2-2.5 times) and the ha-
zard of crushing and breaking the seating portion of the shaft occurs.
In this case the seating portion of the shaft must have increased hard-
ness.

When ball and roller bearings are mounted together (Fig. 223d) the ball
bearing locks the shaft. The opposite end of the shaft is free since the rollers can
shift over the raceway of the outer bearing race.
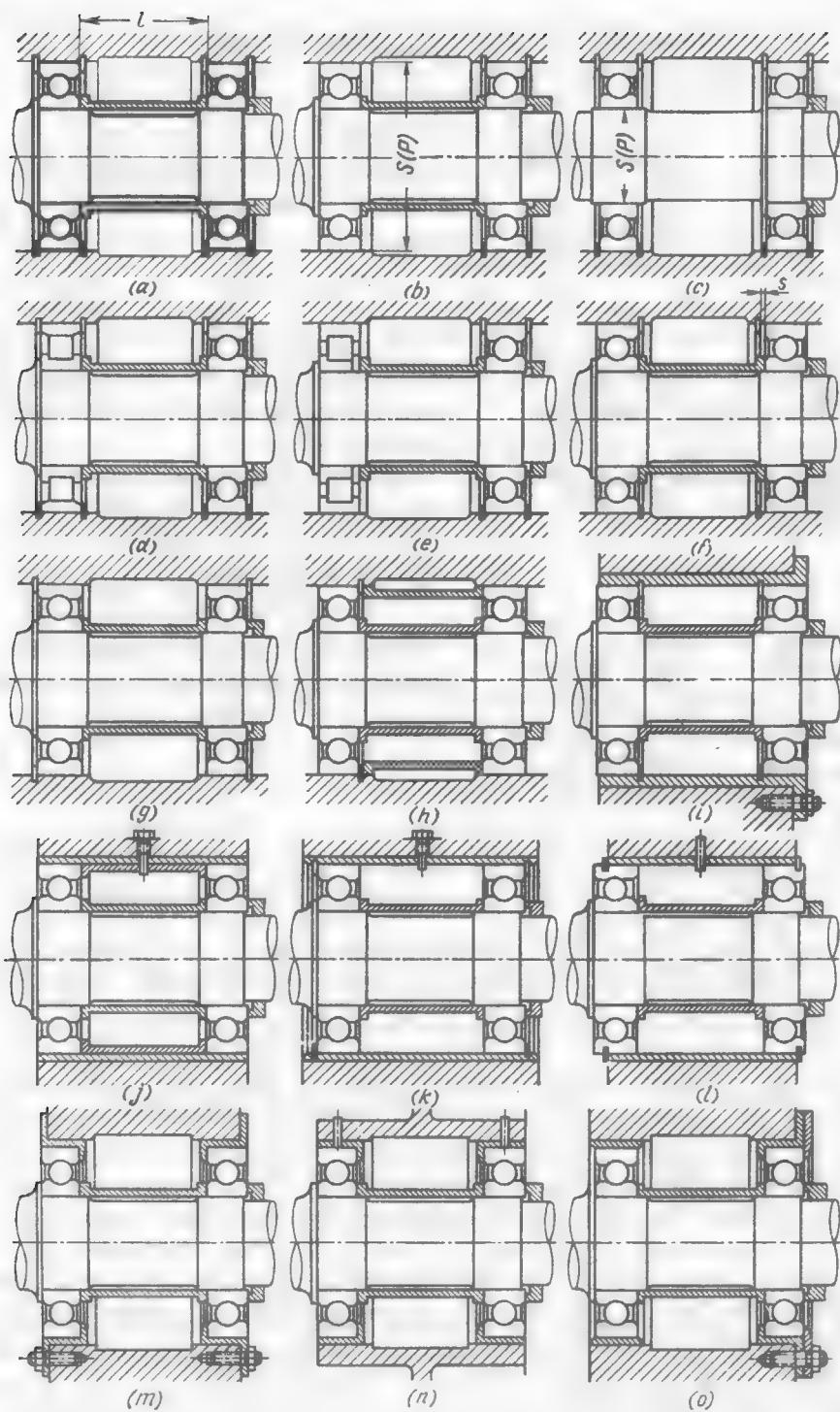
Fig. 223. Twin-mounted ball bearings

Table 34

Errors in Twin Bearing Installations
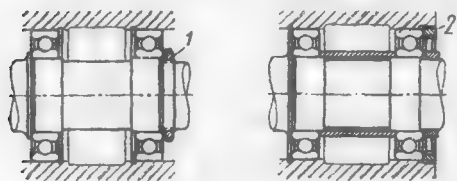
	Inevitable overtightening of the bearings when tightening nuts *1* and *2*. Place distance bushings between the clamped races
	Poor design is shown in view *a*. Insufficient length of distance bushing *3* may cause overtightening of the bearings and snap rings. Such an installation scheme is only permissible when a clearance *s* between the outer bearing races and snap ring (view *b*) is guaranteed
	Shaft is not secured against axial displacement in the directions shown by the arrows
	Shaft is not secured against axial displacement in both directions
	Left-hand bearing is not secured against axial displacement
	(a) left-hand bearing is not secured against displacement in the direction indicated by the arrow; (b) correct design
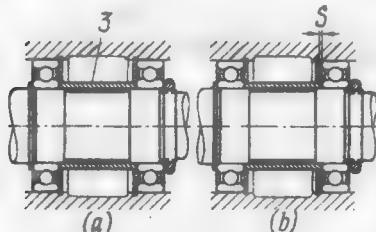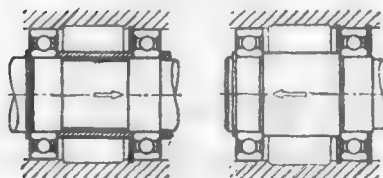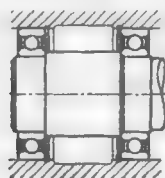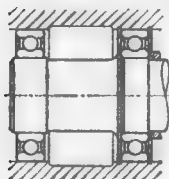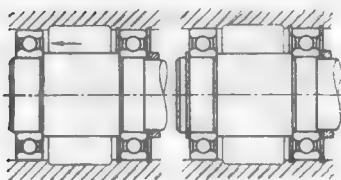
Table 34 (cont.)
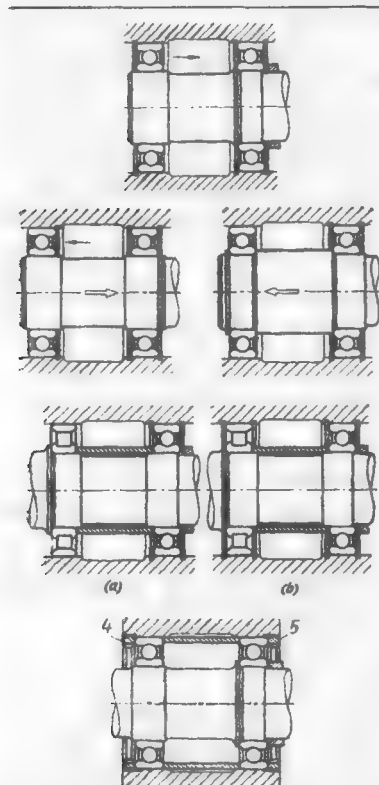
	Left-hand bearing is not secured against displacement in the direction indicated by the arrow
	Shaft is not secured against displacement in the directions indicated by the arrows. Left-hand bearing is not secured against leftward displacement
	(*a*) outer race of the roller bearing is not secured against axial displacement; (*b*) correct installation
	Shaft can move together with the bearings in the axial direction, depending on the position of nuts 4 and 5. Such an installation scheme is only permissible as a method of adjusting the axial position of the shaft

This method may be used when the distance between the bearings is comparatively small. With larger displacements, when the rollers are apt to shift beyond the raceway, use is made of bearings with rollers held in place by lips on both bearing races (Fig. 223*e*). The outer race of the bearing floats in the housing.

These rules need not be stringently observed, if the distance between the bearings is small, if the shaft and the housing are made of materials with about the same coefficient of linear expansion, and if the working temperatures of the shaft and housing are about the same.

Frequently the inner bearing races are tightened on the shaft and the outer ones are locked in both directions by means of snap rings between the outer races (Fig. 223*f*). Such systems operate quite reliably, if there are no relative thermal deformations. Manufacturing errors are accounted for by a guaranteed clearance $s = 0.2$-0.3 mm between the locking elements and the outer bearing races.

When bearings are locked by external snap rings (Fig. 223*g*) the expansion of the housing causes an increase in the axial clearance in the system, and there is no hazard of pinching the bearings. From the

standpoint of assembly conditions this system is preferable to the one in Fig. 223f (the shaft can be installed into the housing with the bearings assembled).

These systems are used if there is no need to lock the shaft without any clearance.

In the system that does not depend on temperature (Fig. 223h) the bearings are locked in the housing with the aid of an intermediate steel bushing secured in the housing by a snap ring. Since the coefficients of linear expansion of the materials of the bushings and shaft are the same, the changes in the linear dimensions of the housing, caused by the temperature variations, do not affect the installation accuracy (if the temperature of the bushing does not appreciably differ from that of the shaft).

The property of independence from temperature is also inherent in units where the bearings are mounted in intermediate steel sleeves (Fig. 223i-l).

Individual installation of bearings in sleeves (Fig. 223m, n) depends on temperature. In such cases one of the bearings must be made floating (Fig. 223o).

Table 34 shows the most frequent errors met with in twin radial bearing installations.

(b) Radial Thrust (Angular-Contact) Bearings

Radial thrust ball bearings are almost always used in a twin opposed installation with obligatory axial tightening.
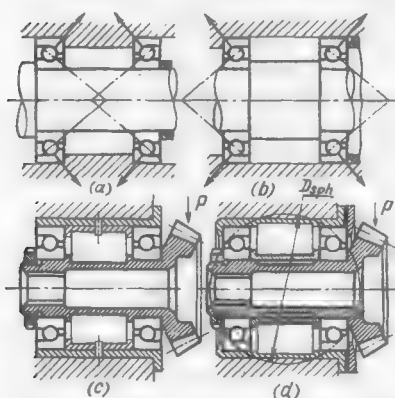
Fig. 224. Installation of radial thrust bearings

The operation of the unit depends on the method of tightening and the arrangement of the bearings. When the axes of rolling of the balls intersect between the bearings (X device) the tightening is done on the inner races (Fig. 224a), which ensures a higher rigidity of the unit in comparison with that obtained with the tightening effected on the outer races (Fig. 224b) when the axes of rolling of the balls intersect outside of the bearings (O device).

This is clearly shown in Fig. 224d illustrating a most ill-chosen arrangement according with the O device, in which the rolling-contact surfaces of the outer races almost exactly fit into a sphere with its centre on the axis of symmetry of the unit. The stability of the shaft against the wrenching effect of the transverse force P is rather low; the shaft turns out to be installed, as it were, on a spherical support. The arrangement according with the X device (Fig. 224c) makes the shaft quite stable.

Depending on the installation device, the bearings react different-ly to the thermal deformations of the system. If during operation the housing is heated more than the shaft, or the former is made of a material with a higher linear expansion coefficient, the X device provides for an additional axial interference, whereas the O device tends to diminish the interference.

If the temperature of the shaft exceeds that of the housing the interference decreases in the X device and increases in the O one.

Gyroscopic Moments

Since in radial thrust bearings the axis of rotation of the balls is inclined at an angle β with respect to that of the bearing, the balls
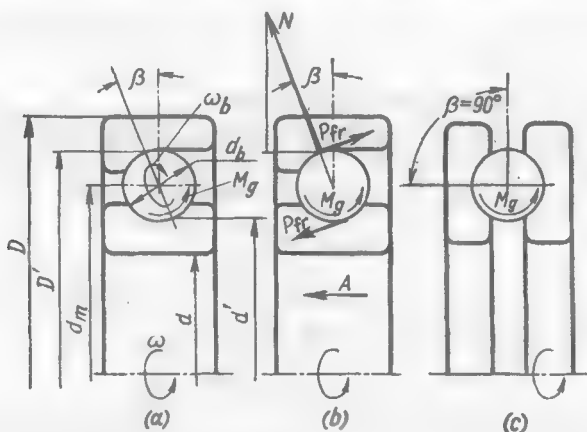
Fig. 225. Diagrams of action of gyroscopic moments

are acted upon by gyroscopic moments which tend to turn the balls around their axes tangential to the direction of their peripheral velocity (Fig. 225a).

The gyroscopic moment is

$$M_g = I \omega_0 \omega_b \sin \beta \qquad (3.8)$$

where ω_0 = angular velocity of the ball centre revolution about the bearing axis

ω_b = angular velocity of the ball rotation around its own axis

I = moment of inertia of the ball, expressed as

$$I = \frac{\pi}{60} d_b^5 \frac{\gamma}{g} \qquad (3.9)$$

where d_b = ball diameter

γ = specific weight of the ball material (for ball bearing steel $\gamma = 0.008$ kgf/cm³)

g = gravitational constant ($g = 981$ cm/s²)

The angular velocity of the ball centre is

$$\omega_0 = \frac{\omega}{1 + D'/d'} \tag{3.10}$$

where ω = angular velocity of the shaft $\left(\omega = \frac{\pi n}{30} \right)$

D' and d' = diameters of contact circumferences on the outer and inner races, respectively, expressed as

$$D' = d_m + d_b \cos\beta = d_m \left(1 + \frac{d_b}{d_m} \cos\beta \right) \tag{3.11}$$

and

$$d' = d_m - d_b \cos\beta = d_m \left(1 - \frac{d_b}{d_m} \cos\beta \right) \tag{3.12}$$

where d_m is the bearing mean diameter.

For light-series bearings the ratio d_b/d_m is 0.18-0.22, for medium-series ones, 0.22-0.25, and for those of heavy series, 0.27-0.3.

The angular velocity of the ball rotation around its own axis is

$$\omega_b = \omega_0 \frac{D'}{d_b} \tag{3.13}$$

Substituting the value of I from Eq. (3.9) and that of ω_b from Eq. (3.13) into Eq. (3.8), we obtain

$$M_g = \frac{\pi}{60} \cdot \frac{\gamma}{g} = d_b^4 \omega_0^2 D' \sin\beta \tag{3.14}$$

As can be seen from this equation, the gyroscopic moment is proportional to the square of the rotational velocity and the fourth power of the ball diameter, and increases by following a sinusoidal law with an increase in the contact angle β, reaching its maximum in thrust bearings where $\beta = 90°$ (Fig. 225c).

The gyroscopic moment may conveniently be expressed in terms of the centrifugal force of the ball

$$P_{cf} = \frac{\pi d_b^3}{6} \cdot \frac{\gamma}{g} \; \omega_0^2 \frac{d_m}{2} \tag{3.15}$$

Substituting the value of P_{cf} into Eq. (3.14), we get

$$M_g = 0.2 P_{cf} \frac{d_b}{d_m} D' \sin\beta \tag{3.16}$$

Substituting the value of D' from (3.11) and denoting d_b/d_m as a, we find that

$$M_g = 0.2 \, P_{cf} d_b \, (1 + a \cos\beta) \sin\beta \tag{3.17}$$

The spinning (skewing) of the balls, caused by M_g, is opposed by the moment of friction (Fig. 225b)

$$M_{fr} = P_{fr}d_b = Nfd_b$$

where f is the coefficient of sliding friction (due to vibrations inevitable in operation this coefficient has very low value of $f = 0.01$-0.02) and N is the reactive force on the contact surfaces, which (with even load distribution among all the balls) is

$$N = \frac{A}{z \sin \beta}$$

where A is the axial load on the bearing and z, the number of balls. Hence,

$$M_{fr} = \frac{Afd_b}{z \sin \beta} \tag{3.18}$$

The balls will not spin if

$$M_{fr} > M_g$$

Substituting M_{fr} from Eq. (3.18) and M_g from Eq. (3.16) into this relation, we may find the minimum axial load with which there will be no spinning

$$A_{min} = 0.2 \frac{P_{cf}D'z \sin^2 \beta}{d_m f}$$

or, since $D' = d_m (1 + a \cos \beta)$,

$$A_{min} = \frac{0.2zP_{cf}}{f} (1 + a \cos \beta) \sin^2 \beta \tag{3.19}$$

Example. Calculate the bearing No. 46316 of medium series ($d = 8$ cm, $D = 17$ cm, $d_m = 12.5$ cm, $d_b = 2.8$ cm, $\beta = 26°$, number of balls $z = 12$).

Assume that $n = 3000$ rpm ($\omega = 314$ s^{-1}) and the coefficient of friction $f = 0.02$.

The diameters of contact circumferences, by Eqs. (3.11) and (3.12), are

$$D' = 12.5 + 2.8 \cdot 0.9 \approx 15 \quad \text{(cm)}$$
$$d' = 12.5 - 2.8 \cdot 0.9 \approx 10 \quad \text{(cm)}$$

The angular velocity of the ball centres, by Eq. (3.10), is

$$\omega_0 = \frac{314}{1 + \dfrac{15}{10}} = 125.5 \; (\text{s}^{-1})$$

The centrifugal force of the ball, by Eq. (3.15), is

$$P_{cf} = \frac{\pi \cdot 2.8^3}{6} \cdot \frac{0.008}{981} \cdot 125.5^2 \cdot \frac{12.5}{2} = 9.5 \; (\text{kgf})$$

The minimum axial force preventing the spinning of the balls, by Eq. (3.19), is

$$A_{min} = \frac{0.2 \cdot 9.5 \cdot 12}{0.02} \left(1 + \frac{2.8}{12.5} \cdot 0.9 \right) 0.438^2 = 260 \; (\text{kgf})$$

In bearings loaded by a sufficiently high axial force no ball spinning is usually observed (except for the balls whose diameter, within the manufacturing tolerance limits, is smaller than that of the other balls).

Ball spinning in unloaded bearings (end bearings in twin installations) is observed when the tightening is not strong enough and also when the preload is weakened as a result of the axial displacement of the shaft under the action of the working load.

In bearings loaded by a radial force alone ball spinning may occur in the unloaded zone of the bearing. To prevent this phenomenon the bearings must be tightened with a sufficiently large axial force.

In radial ball bearings gyroscopic moments develop when the contact lines get inclined as a result of the application of axial forces and also when the bearing is misaligned. Since contact angles β are small the gyroscopic moments are small too.

In tapered roller bearings gyroscopic moments, which at large angles β grow considerably, are taken up by the rolling-contact surfaces and only increase the edge loads.

Preloading

Axial preloading is of prime importance for the proper operation of radial thrust bearings.

With a correct preload the balls tightly fit the raceways, wear on the rolling-contact surfaces diminishes, the carrying capacity and durability of the bearing increase, and the ball spinning caused by gyroscopic moments vanishes, thus reducing the coefficient of friction.

An excessive preload is just as dangerous as too small a preload, because it tends to pinch the balls, overload the contact surfaces and increase heat generation.

The following preloading methods are in use:

(1) tightening the bearings to a specified amount of the axial displacement of the outer races with respect to the inner ones;

(2) tightening the bearings to a definite rotational resisting moment;

(3) applying to the bearings a constant axial force (spring preloading).

By the first method distance bushings of unequal length are placed between the inner and outer races of twin bearings. With the X device (Fig. 226a) the inner races are tightened by nut 1 against the end face of the inner distance bushing. The amount of preload in this case is determined by the difference a between the lengths of the bushings.

With the O device (Fig. 226b) the outer races are tightened by nut 2 against the end face of the outer distance bushing.

It is also possible to tighten the outer races with an end-face washer *3* (Fig. 226*c*) by taking up clearance *a* whose amount is controlled by means of sized washers *4*. If the bearings are close to each other
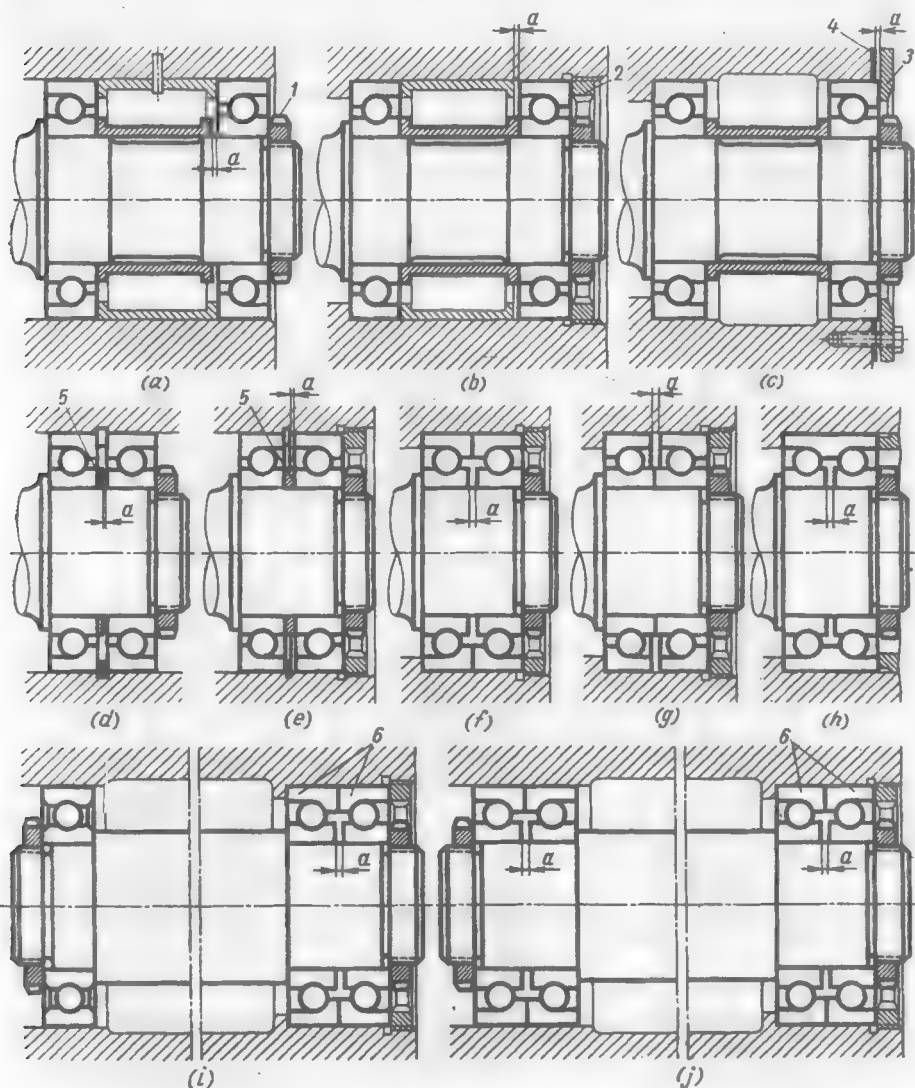
Fig. 226. Installation of preloaded radial thrust bearings

(Fig. 226*d*, *e*) preloading is effected by interspacing the races to be tightened with sized washers *5* whose thickness differs from that of the locking element (snap ring) by an amount *a*.

Soviet factories manufacture twin radial thrust bearings with a preset clearance a which is taken up during tightening (Fig. 226f-h).

The required amount of preload depends on the shape of the contact surfaces, contact angle, the distance between the bearings, nature of load, rotational speed, temperature of the unit, coefficient of friction, magnitude of the working load (radial and axial), and other factors. It is extremely difficult to take all these factors into account during calculations.

Soviet factories producing preloaded bearings follow standards valid only for bearings of a given type-size installed at a specified distance from each other. In all other cases the preload is selected experimentally.

Approximate figures are as follows: $a = 0.05$-0.07 mm for small- and medium-size bearings installed at a relatively small distance from each other, and $a = 0.07$-0.12 for large bearings. In the case of heavy loads, low rotational speeds and large contact angles use is made of higher values of a whereas for high rotational speeds and small contact angles one should use lower values of a.
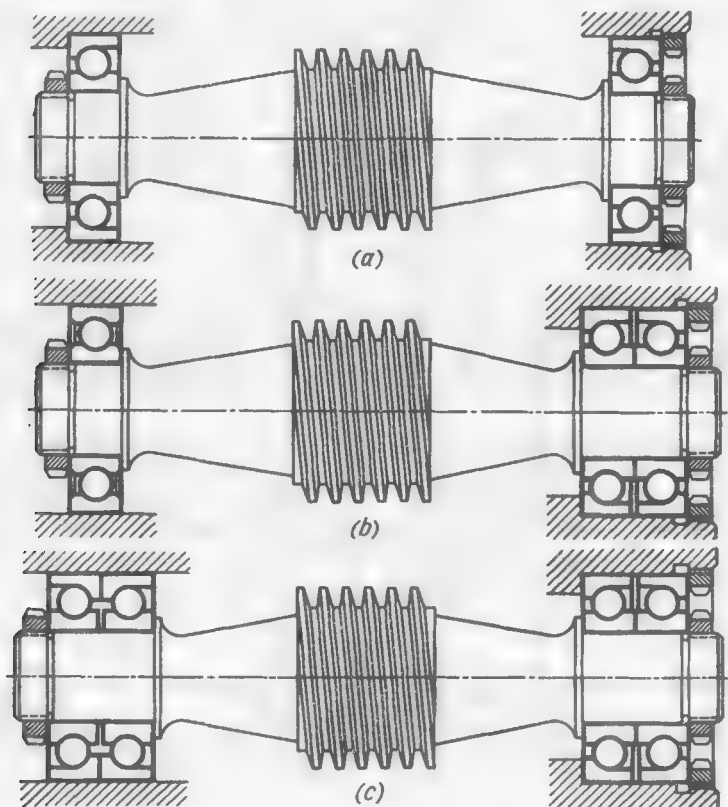
Fig. 227. Installation of a worm shaft on radial thrust bearings

It is recommended to avoid the joint preloading of bearings spaced at large distances apart, when in the system there occur temperature deformations which are difficult to account for. In such cases

it is advisable to make the locking support as a preloaded twin-bearing unit *6* and use for the second (floating) support a radial bearing (Fig. 226*i*) or a preloaded twin-bearing unit (Fig. 226*j*).

Figure 227 shows examples of (*a*) wrong and (*b, c*) correct worm shaft installation.

Bearings in supports where the preload rapidly vanishes (heavily loaded supports, bearings with small contact angles β) should periodically be retightened.

Adjustment by means of sized washers *1* (Fig. 228*a*) is not convenient. More often use is made of smooth adjustment by tightening
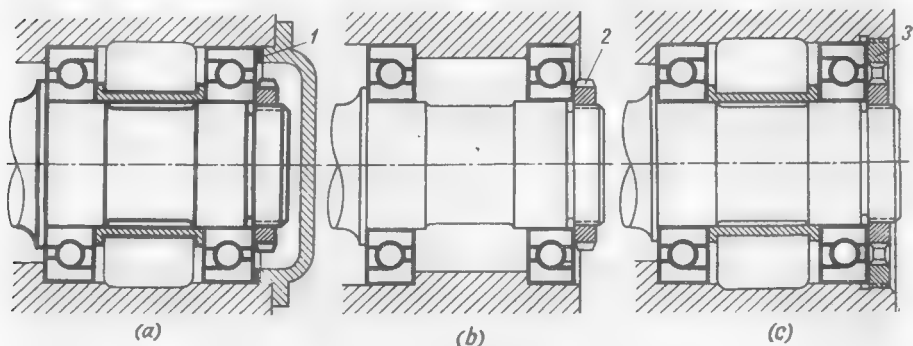
Fig. 228. Preload adjustment diagrams

either the inner races with nut *2* (Fig. 228*b*) or the outer ones with nut *3* (Fig. 228*c*). The other races (the outer one in Fig. 228*b* and the inner one in Fig. 228*c*) are in this case installed firmly.

The preload is adjusted by tightening the nuts until clearance-free but sufficiently easy rotation is obtained.

Usually, use is made of the following rather rough methods.

The nut is tightened until the shaft (or the part mounted on it) can no longer be rotated by hand, and then it is unscrewed through a definite angle (usually a quarter of a turn) and locked in this position.

By another method, one tightens the nut as far as it will go and then slowly slackens it, constantly trying to turn by hand the part being checked. The nut is locked as soon as the part begins to turn.

If the part cannot be turned by hand because of some mechanisms being connected to it, the nut is tightened to a rated torque experimentally established earlier. In this case account should be taken of the changing friction in the thread and on the seating surface of the race being tightened. Increased friction is liable to absorb most of the tightening force.

Spring Preloading

With this method the system incorporates spiral or disk springs ensuring a practically constant preload almost irrespective of wear on the rolling-contact surfaces, variations in linear dimensions, and thermal deformations.

Spring preloading is used:

(1) in supports spaced at large distances apart;

(2) in precision applications where free plays spoiling the accuracy of operations performed by the machine must be eliminated;
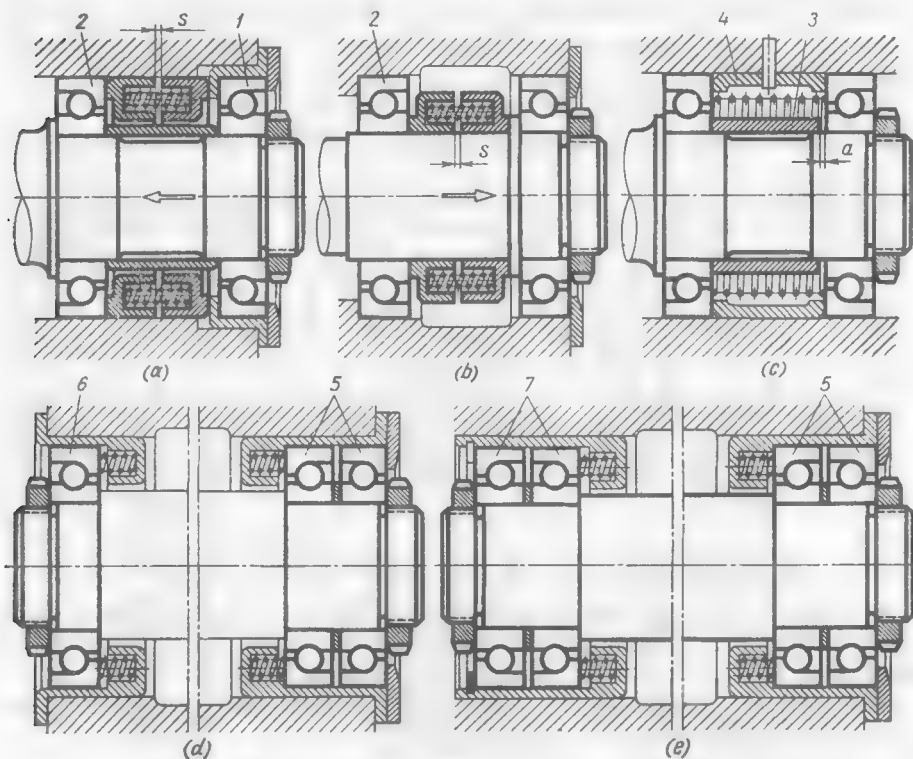
Fig. 229. Spring preloading diagrams

(3) in high-speed applications where free plays cause the displacement of the centre of gravity of the rotating parts from the geometrical axis of rotation, resulting in increased centrifugal loads;

(4) in applications subject to dynamic loads, where free plays result in the crushing and rapid wear of the rolling-contact surfaces.

In the spring preloaded device shown in Fig. 229a bearing *1* is firmly fixed both on the shaft and in the housing; the outer race of bearing *2* floats in the housing. The floating race is loaded with springs which constantly preload both bearings.

The design in Fig. 229b differs from the previous one in that the inner race of bearing *2* floats on the shaft.

The shortcoming of both designs is that the shaft is rigidly locked only in one direction (light arrows). In the opposite direction the shaft

is locked only by springs and can move within the limits of clearance *s* in the tightening device, when the axial load exceeds the force exerted by the springs.

These designs are applicable in the following instances:

when the working axial load is unidirectional and there are no loads of the opposite direction, or these are small in comparison with the tightening force of the springs;

when the axial displacement of the shaft within the limits of clearance *s*, caused by increased axial forces acting in opposition to the working load, is permissible.

Practically clearance-free locking is provided in the design shown in Fig. 229*c*, where the bearings are installed with a preload produced by tightening the bearings against internal distance bushing *3* which is somewhat shorter than the external distance bushing *4*. The preload is produced by a spiral spring acting on the outer races of the bearings.

Since the bearings are firmly fixed in the housing the design is applied in the case of small distances between the bearings when thermal deformations are not very large.

When the distances between the shaft supports are large, the locking support is made in the form of a twin radial thrust bearing unit *5* with spring preloading (Fig. 229*d*). The other support is made floating and comprises a single spring-preloaded radial thrust bearing *6* or preloaded twin radial thrust bearing unit *7* (Fig. 229*e*).

It is difficult to calculate spring preloading. The preload calculation by Eq. (3.19), conditioned on the prevention of the ball spinning under the effect of gyroscopic moments, yields too low preload values, even if the factor of safety is taken at 1.5-2. This is explained by the fact that the force exerted by the springs must be high enough to overcome friction on the seating surfaces of the movable races. For this reason the preload is determined experimentally. In the spring-preloaded systems provision should be made for adjusting the spring force.

(c) Tapered Roller Bearings

These bearings are used in twin installations with the inner bearing races being tightened according to the *X* device (Fig. 230*a*), and less frequently, with the outer

Fig. 230. Installation of tapered roller bearings

bearing races being tightened according to the *O* device (Fig. 230*b*).

With the proper preload these bearings can carry high radial and axial loads at moderate rotational speeds. Since there are no clearances between rolling-contact bodies and raceways, tapered roller

bearings effectively endure impact loads and may therefore be used in heavily loaded units (hubs of automobile wheels, axle boxes of railway carriages, rolls of rolling mills). The supports with prevailing
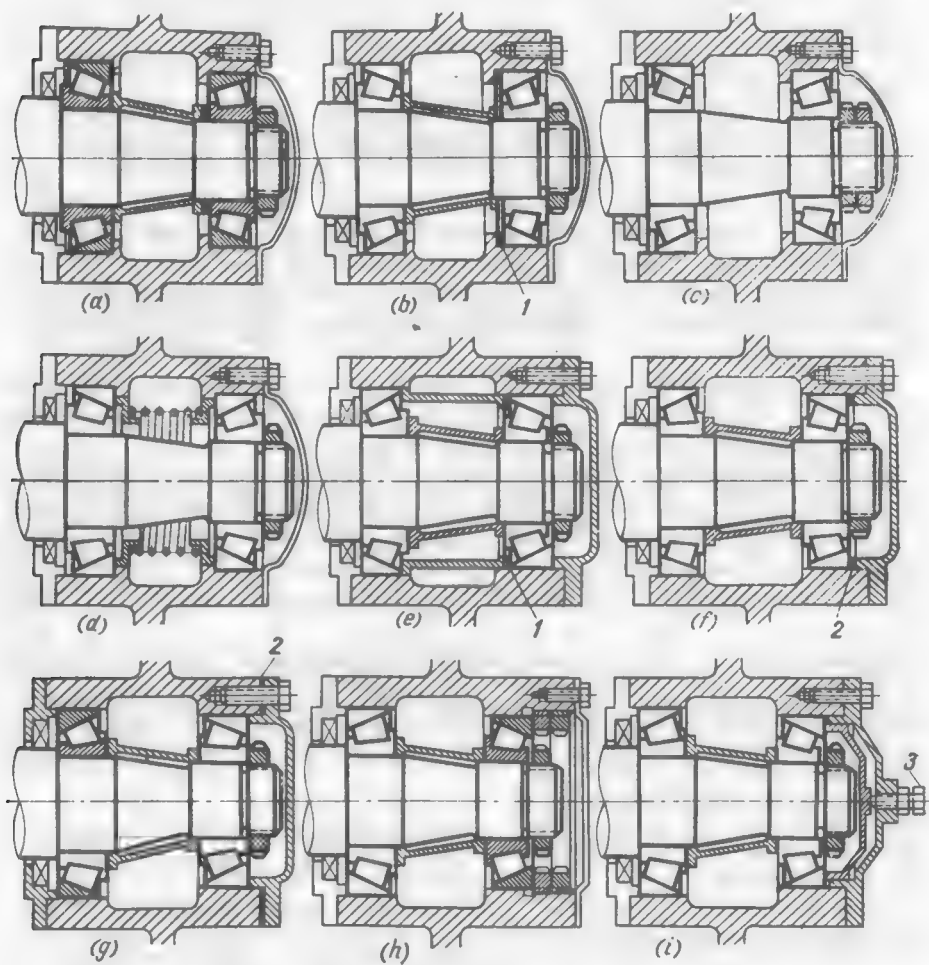
Fig. 231. Preload adjustment in tapered roller bearings

radial loads use bearings with a central angle of taper of 15-25°, whereas for increased axial loads use is made of bearings with the angle equal to 30-60°.

The methods for adjusting the preload of tapered roller bearings are presented in Fig. 231a-d (the X device) and e-i (the O device).

The preload adjustment by means of sized washers 1 installed behind the races (Fig. 231a, b, e), which requires that the front bear-

ing be removed, is only used in units needing no frequent readjustment (light operating conditions, bearings with a large angle of taper).

In the designs with washers 2 installed in front of the races (Fig. 213f) or under the bearing cap (Fig. 231g) the removal of the cap is sufficient for one to do the adjustment.

In units where periodic retightening is required the inner (Fig. 231c) or outer (Fig. 231h) races are tightened by means of ring nuts.

The tightening force is usually checked by the easiness of rotation. When continuous adjustment is required, the nuts are secured by
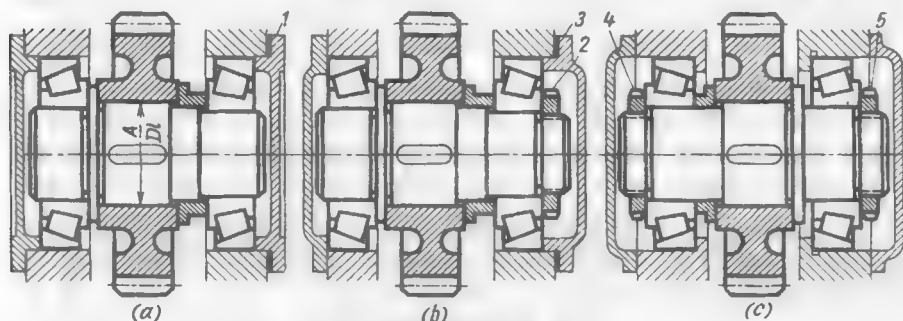
Fig. 232. Tightening systems

locknuts. Locking by means of highly reliable tab washers provides for sufficiently fine adjustment.

The design with a central adjusting (locked) bolt 3 (Fig. 231i) allows adjustment without dismantling the unit.

Figure 231d illustrates a spring-preloading system according with the scheme shown in Fig. 229c, that allows the unit to operate for a long time without retightening.

The bearing preload must never be used to fasten parts installed on the shaft by centring or transition fits (Fig. 232). In the wrong design shown in Fig. 232a the gear is tightened on the shaft by cap 1 through the intermediary of the right-hand bearing. The bearings will be pinched if their preload is determined on condition of the power tightening of the gear. The moderate tightening necessary to preload the bearings is not sufficient for fixing the gear.

In the correct design shown in Fig. 232b the gear is power tightened by nut 2; the bearings are preloaded by cap 3.

In the design with the bearings installed according to the X device (Fig. 232c) the gear is tightened by nut 4 and the bearing preloading is effected by means of nut 5.

When designing units with tapered roller bearings it should be borne in mind that the roller cages project distances m and n beyond the outer race (Fig. 233a).

The value of m is usually immaterial; the value of n must be taken into account when installing parts such as oil slingers 1, ring nuts 2 (Fig. 233b) and twin bearings (Fig. 233c) close to the bearing.

The cage projection sizes are specified in catalogues.
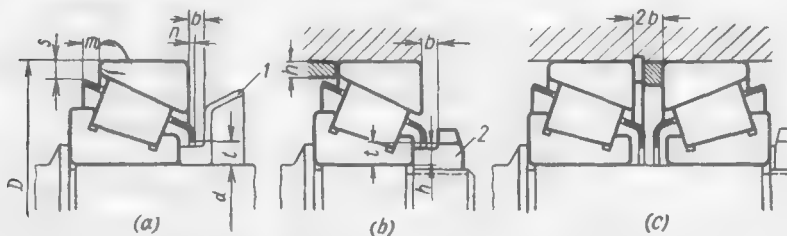
Fig. 233. Cage projection in tapered roller bearings

As a rule, the part adjacent to the bearing must be located at a distance $b = 4$-5 mm (in large bearings $b = 5$-8 mm)! from the end face of the outer race.

The height h of the cylindrical surfaces of the adjacent part (Fig. 233b) must not exceed $0.1 (D - d)$ in order to prevent their contact with the edges of the cage (sizes s, t).

3.10. Needle Bearings

The basic types of needle bearings are shown in Fig. 234.

In the designs shown in Fig. 234a, b the needles can only be assembled by using a viscous grease; in this case there is a hazard of some
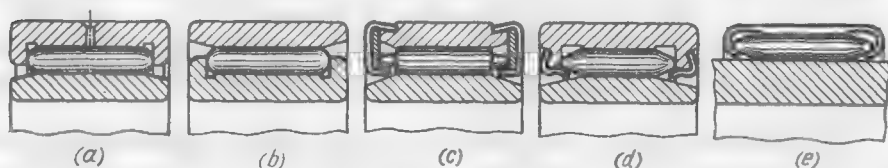
Fig. 234. Needle bearings

of the needles falling out. Needles that have operated with oil dissolving the grease scatter during disassembly.

It is better to use integrated designs where the needles do not fall out (Fig. 234c, d) because they are locked in the bearings by bent soft-steel rings rolled on the ends of the races.

In the bearing shown in Fig. 234e, intended to be installed without races in lightly loaded supports, the needles are inserted into a die-forged race with bent edges.

The races are made of low-carbon cold-rolled steel and their active surface is cyanided to a depth of about 0.1 mm.

It is known from experience that there is no pure rolling in needle bearings. The needles in the loaded zone, where they are tightly fitted against the shaft, rotate around their own axes with a peripheral velocity

$$n = n_{sh} \frac{d}{\delta} \qquad (3.20)$$

where n_{sh} = rotational speed of the shaft
d = shaft diameter
δ = needle diameter

Needles rotate at a very high speed. With the usual $d/\delta = 10$ and the shaft speed, for example, $n_{sh} = 1000$ rpm the needles rotate at a speed $n = 10,000$ rpm.

The speed $n = 20,000\text{-}30,000$ rpm is considered to be the maximum permissible speed of rotation of the needles around their own axes.

As they enter the unloaded zone, the needles continue to rotate by inertia but their speed decreases due to friction. When the needles return to the loaded zone the speed of their rotation increases again.
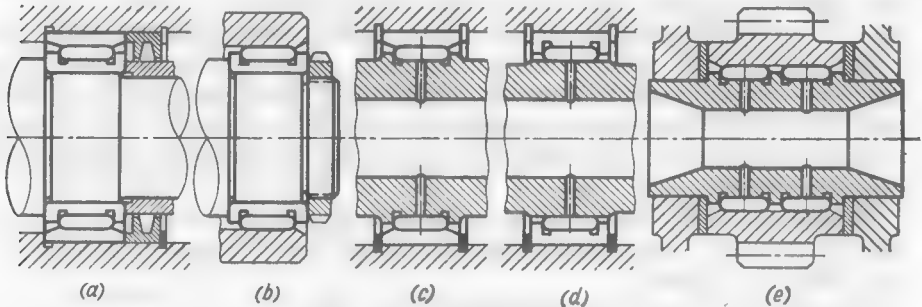
Fig. 235. Installation of needle bearings

The slipping of the needles in the unloaded zone and also their friction against one another result in high coefficients of friction ($f = 0.01\text{-}0.02$) and limit the rotational speed of the bearings to 1000-2000 rpm.

It is advisable to use needle bearings in low-speed heavily loaded supports, and also in supports with oscillatory rotation (connecting road small ends, shafts of rocker arms and levers).

Needle bearings cannot carry any axial load. When using such bearings, the shaft-fitted parts must be fixed axially in some way or other, and the outer and inner races must be locked in the housing and on the shaft, respectively (Fig. 235a).

The bearing races are installed in housings and on shafts by tight and force fits. Heavy drive fits are liable to overstress the thin races of the bearings.

To reduce radial dimensions needle bearings are often installed with the inner (Fig. 235b) or outer (Fig. 235c, d) races alone. In this case the needles run on raceways made directly in the part being supported. Not infrequently both raceways are provided in such parts (Fig. 235e). The radial dimensions of the raceless needle bearings do not exceed those of sliding-contact bearings.
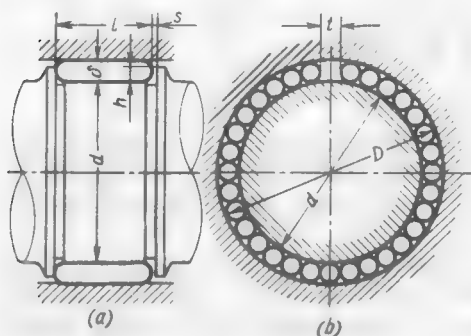
Fig. 236. Structural proportions of needle bearings

Needle bearings can operate with grease or oil lubrication. Lubrication with foamed oil is difficult because the annular side slits in the bearings are narrow. The best method to lubricate the raceless units it is to feed oil through radial holes in the shaft, the holes being arranged along the axes of symmetry of the bearings (Fig. 235c, d).

The raceways in the supported parts are made to the 1st grade of accuracy. The hardness of the active surfaces $R_c > 58$, and their surface finish corresponds to the 11th-12th class. Deep raceways must be provided with grooves for the overtravel of the grinding wheel.

In the case of the raceless installation, needles are grouped by their diameter (the deviations of the needle diameters in a set must not exceed 2 μm).

The recommended needle length (Fig. 236a) is

$$l = (5 \text{ to } 10) \delta \tag{3.21}$$

where δ is the diameter of the needles.

The lower limit refers to small-diameter bearings and the upper one, to large-diameter ones.

Depending on the diameter of the inner raceway, the needle length is

$$l = (0.25 \text{ to } 0.5)d \tag{3.22}$$

where d is the diameter of the inner raceway.

The lower limit refers to large-diameter bearings and the upper one, to small-diameter ones.

Equating the right-hand sides of Eqs. (3.21) and (3.22), we get a formula for finding the needle diameter.

$$\delta = (0.05 \text{ to } 0.1)d \tag{3.23}$$

where the lower limit refers to large-diameter bearings and the upper one, to small-diameter ones.

If the design requires a bearing length greater than that calculated from Eqs. (3.21) and (3.22), the needles are installed in two rows (see Fig. 235e).

The end play s between the needles and the guide lips must be

$$s = (0.1 \text{ to } 0.015)d$$

The lip height is taken at

$$h = (0.7 \text{ to } 0.8)\,\delta$$

The diametral clearance in the bearing, i.e., the clearance $\Delta = D - (d + 2\delta)$ is selected so as to have a needle fit between slack running and thermal running ones. The mean diametral clearance in μm, according to Eq. (2.1) with $m = 10\text{-}20$, is

$$\Delta = (10 \text{ to } 20)\sqrt{d}$$

where d is in mm.

The higher the rotational speed the greater the clearance must be made.

The side clearance between the needles is determined on condition that after the needles are packed tightly around the shaft there remains a clearance $t = q\delta$ between the first and the last needles (Fig. 236b), where δ is the needle diameter and q, a coefficient equal to 0.4-0.8. When $q < 0.4$ the bearing develops high friction and when $q > 0.8$ the needles may become skewed and pinched.

The number of needles is

$$z = \frac{\pi d_m - q\delta}{\delta} = \frac{\pi (D + d)}{2\delta} - q$$

Substituting $D = d + 2\delta$, we obtain

$$z = \frac{\pi (d + \delta)}{\delta} - q \tag{3.24}$$

whence

$$d = \delta \left(\frac{z + q}{\pi} - 1 \right) \tag{3.25}$$

When designing a bearing, the internal diameter d is usually specified. The needle diameter may be found from Eq. (3.23). The number of needles is tentatively determined by Eq. (3.24), assuming that $q = 0$,

$$z' = \frac{\pi (d + \delta)}{2} \tag{3.26}$$

and the obtained value is rounded off to the nearest smaller integral number z. As can be seen from Eqs. (3.26) and (3.24), the difference $z' - z$ is equal to q.

If the condition $q = 0.4\text{-}0.8$ is not satisfied, recalculation is made using new values of d and δ.

Example. Let $d = 20$ mm and $\delta = 2$ mm. According to Eq. (3.26),

$$z' = \frac{\pi(d+\delta)}{2} = \frac{\pi(20+2)}{2} = 34.5$$

Let us assume that $z = 34$. Then

$$q = z' - z = 34.5 - 34 = 0.5$$

which is permissible.

The standard needle dimensions are given in Table 35.

Table 35

δ, mm	Length l, mm									
2.0	8	10	12	14	16	(18)	(20)	(22)	(24)	—
2.5	8	10	12	14	16	(18)	(20)	(22)	(24)	—
3.0	—	10	12	14	16	18	(20)	(22)	(24)	27
3.5	30	35	—	—	—	—	—	—	—	—
4.0	40	—	—	—	—	—	—	—	—	—
5.0	50	—	—	—	—	—	—	—	—	—

Note. Dimensions in brackets are not recommended.

3.11. Thrust Ball Bearings

These bearings are used in heavily loaded supports at low rotational speeds.

The speed of the thrust bearings is limited by the displacement of the balls from the axis of symmetry of the raceways under the action of centrifugal forces developing at high rotational speeds (Fig. 237a).

Fig. 237. Diagram of action of centrifugal forces and gyroscopic moments in thrust ball bearings

Centrifugal forces may also shift the cage (Fig. 237b). In both cases the deviation of the contact lines OC from the normal disturbs correct rolling and results in a sharp increase of friction in the bearing.

Gyroscopic moments cause the balls to spin around the axis tangential to the direction of the peripheral velocity of the ball centres. The magnitude of the gyroscopic moment can be determined from Eq. (3.17), if we take $\beta = 90°$ and $D' = d_m$

$$M_g = 0.2 P_{cf} d_b \tag{3.27}$$

According to Eq. (3.19), the minimum load A, at which no spinning occurs, is

$$A_{min} = 0.2 \frac{P_{cf}z}{f} \qquad (3.28)$$

Example. Calculate the bearing No. 8220 of medium series ($d = 10$ cm, $D = 15$ cm, $d_m = 12.5$ cm, $d_b = 2$ cm, $z = 18$). Assume that $n = 1000$ rpm $\left(\omega = \frac{\pi n}{30} = 105 \text{ s}^{-1} \right)$ and the coefficient of friction $f = 0.02$.

The rotational speed of the ball centres, by Eq. (3.10), is

$$\omega_0 = \frac{105}{2} = 52.5 \text{ (s}^{-1})$$

The centrifugal force of the ball, by Eq. (3.15), is

$$P_{cf} = \frac{\pi \cdot 2^3}{6} \cdot \frac{0.008}{981} 52.5^2 \cdot 6.25 = 0.6 \text{ (kgf)}$$

The gyroscopic moment, by Eq. (3.17), is

$$M_g = 0.2 \cdot 0.6 \cdot 2 = 0.24 \text{ (kgf·cm)}$$

The minimum axial load preventing the ball spinning, by Eq. (3.19), is

$$A_{min} = 0.2 \frac{0.6 \cdot 18}{0.02} = 114 \text{ (kgf)}$$

Where single-row thrust bearings carry vertical shafts, free ring *1*, i.e., the ring fitted on the shaft with clearance, should not be centred in the housing (Fig. 238a) since the practically inevitable misalign-
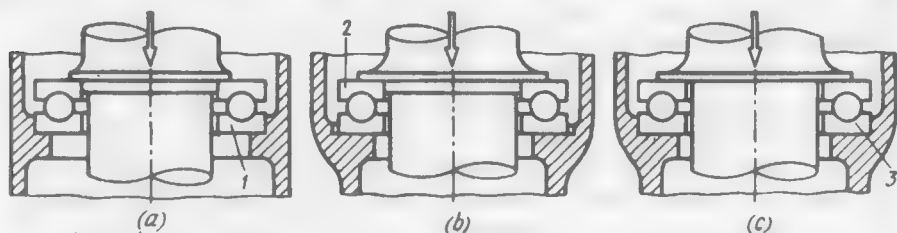
Fig. 238. Installation of thrust bearings on vertical shafts

ment of the centring surfaces on the shaft and in the housing may cause the balls to shift from the raceway axis of symmetry and thus disturb the proper functioning of the bearing. It is advisable to centre one of the races on the shaft (race *2* in Fig. 238b) or in the housing (race *3* in Fig. 238c) and allow the other to move freely in the transverse direction. Under the action of the applied load (and under the weight of the shaft at standstill) the free race centres itself with respect to the balls.

To prevent the bending of bearing races under load the diameter of the thrust surfaces of the shaft and the housing should be increased at least to the mean circumference of the balls (the design in Fig. 238a is poor, and those in Fig. 238b and c are correct).

Heavily loaded supports should be equipped with self-aligning thrust bearings with spherical supporting surfaces. The self-alignment of supports eliminates the effect of inevitable distortions, wobble of supporting shoulders, etc., ensures more even distribution of the load among the balls, and increases the bearing durability.

When thrust bearings are installed in combination with spherical self-aligning radial bearings, the former must not have flat surfaces (Fig. 239a) which hamper self-alignment. It is necessary to use thrust bearings with spherical supporting surfaces or fix flat bearings on spherical washers (Fig. 239b). The centre of the sphere of the supporting surface washer should coincide with that of the radial bearing.
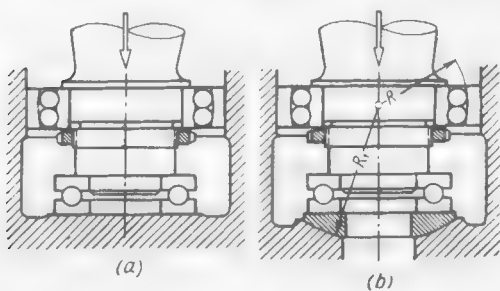
Fig. 239. Self-aligning thrust bearings

Where single-row thrust bearings are installed on horizontal shafts the shaft must be fixed axially in the direction opposite to the action of the working load. The shaft is commonly fixed by means of a thrust bearing, and all the radial supports of the shaft are made floating. In the housing the bearing is installed in an enclosed recess one side of which (side a in Fig. 240) is carrying and the opposite side (b) is locking. The shaft is provided with locking stop 2 located opposite to thrust shoulder 1. The contact between revolving and stationary components is prevented by the axial clearances — clearance s in the housing and clearance t on the shaft — several tenths of a millimetre wide. Thus, an axial clearance s + t forms in the joint.
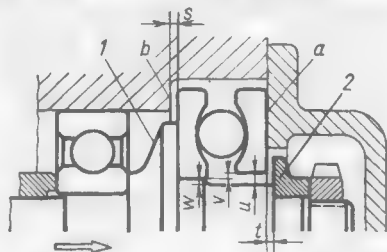
Fig. 240. Installation of a thrust bearing on a horizontal shaft

The rotating race is mounted on the shaft by an interference fit on the locating section. The stationary race is separated from the shaft by a radial clearance $u = v + w$, where v is half the difference between the bore diameters of the rotating and stationary races (in standard bearings $v = 0.2$-0.5 mm) and w is half the difference between

the diameters of the locating and nonlocating sections of the shaft. All in all, the clearance u amounts to 0.3-0.5 mm.

In contrast to the vertical supports, the floating installation of the stationary races should be avoided in horizontal supports. In the case of stoppages, and pulsations and occasional changes in the direction of the load, the shaft moves away from the bearing to a distance $s + t$ (axial clearance) and the unfastened race shifts within the limits of the radial clearance u and hangs on the shaft (Fig. 241a). The subsequent application of axial load fails to return the race to its concentric position because the radial component of
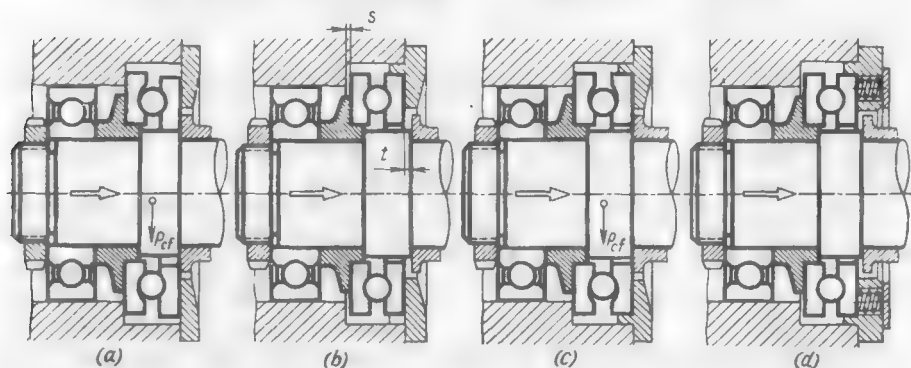
Fig. 241. Installation of thrust bearings on horizontal shafts

the pressure forces is negligible due to the sloping profile of the raceway sections next to the contact ones. The balls and the cage are set up eccentrically with respect to the rotating race. The eccentricity increases under the action of the centrifugal force P_{cf} resulting from the shifting of the centre of gravity of the set of balls and the cage with respect to the axis of rotation.

The proper rolling of the balls is disturbed, the contact lines deviate from the normal and friction increases.

The shortcoming of the design can only partly be remedied by centring the stationary race (Fig. 214b). When the shaft moves away from the bearing the races are drawn apart within the limits of the axial clearance t; the weight of the balls and the centrifugal force cause the balls together with the cage to occupy an eccentric position (Fig. 241c) and the same phenomena as in the previous case happen to take place in the bearing. To lessen these effects the clearance t should be reduced to the minimum (0.1-0.2 mm).

The best method is to compress the bearing races with springs which maintain a constant bearing preload with all possible movements of the shaft (Fig. 241d).

The springs are installed on the side of the stationary race (Fig. 242a), or in intermediate locating disks in double-action
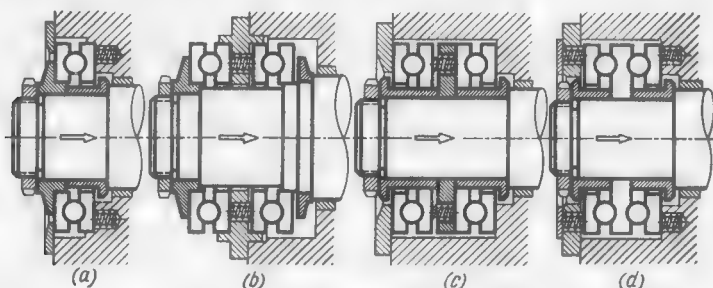
Fig. 242. Installation of spring-preloaded thrust bearings

installations with single-row bearings (Fig. 242b, c), or on both sides of the double-row bearings (Fig. 242d).

A sufficiently strong spring preloading prevents the ball displacement caused by centrifugal force, and their spinning under the action of gyroscopic moments, reduces friction and allows the bearing rotational speeds to be increased. The preload adds to the working load on the balls, but their orderly rolling in the final analysis augments the load-carrying capacity of the bearing.
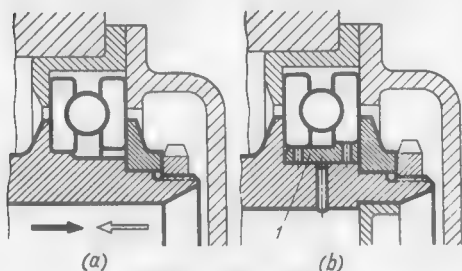
Fig. 243. The use of a single-row thrust bearing for carrying axial loads in both directions

If the springs are strong enough, the centring of the stationary race can be dispensed with (see Fig. 242c, d).

Attempts are being made to utilize single-row ball bearings for carrying axial loads in both directions. In ordinary installations this cannot be implemented since the left-hand race of the bearing normally designed for one-way loads (black arrow in Fig. 243a) will rotate on the locating portion when the load is reversed (bright arrow). The centring and easy rotation of the bearing races are ensured by their mounting on a floating bushing *1* (Fig. 243b) made of an anti-friction material and by lubricating the frictional surfaces.

High-speed units use other types of thrust bearings. Single-action supports employ thrust-radial, tapered roller and spherotapered bearings. Double-action supports widely use duplex preloaded thrust-radial bearings (Fig. 244a) and also ball bearings with deep grooves, relieved of radial forces through mounting in the housing with a radial clearance *s* (Fig. 244b, c). Such supports are

compact, can carry high axial loads, and hold the shaft in the axial direction practically without any clearance. They can be assembled easier than thrust ball bearings.

Figure 244*d* shows a unit that takes up radial and axial loads.
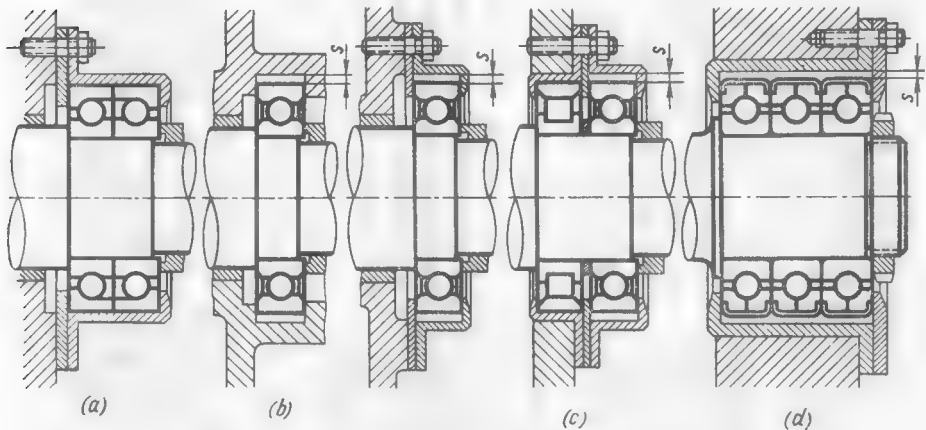
Fig. 244. Double-action thrust bearings

Multiple-row bearings with split outer races (three-contact bearings) relieved of radial forces (Fig. 244*e*) are used in supports, intended to carry especially high loads at increased rotational speeds.

3.12. Typical Bearing Units

Some examples of typical bearing units are illustrated in Table 36.
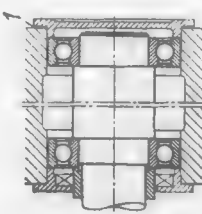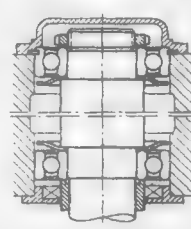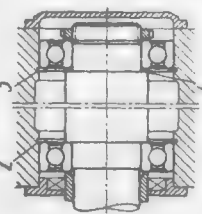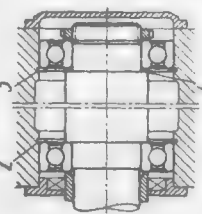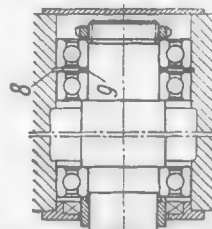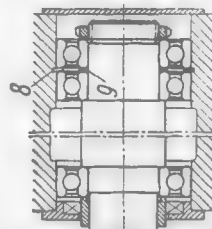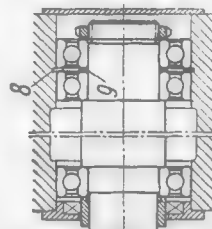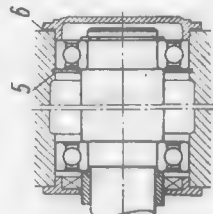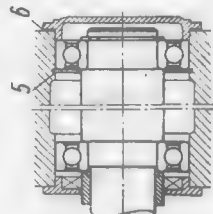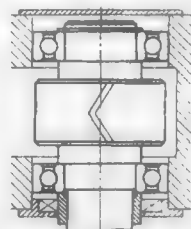
3.13. Fits

Rolling-contact bearings are installed on the shaft according to the *basic-hole system* and in the housing, to the *basic-shaft system*.

When assigning the bearing fit, account should be taken of the following:

(1) type of the bearing;

(2) speed of the unit;

(3) magnitude and nature of the load on the bearing (constant or variable in magnitude and direction, steady or impact);

(4) rigidity of the shaft and housing;

(5) nature of thermal deformations in the system (increase or reduction of the tightness of fit at working temperatures);

(6) method of fastening the bearing (with or without tightening);

(7) convenience of assembly and disassembly.

As a rule, the heavier the operating conditions, i.e., the greater the load, the wider range of its variation, and the higher the rate of

Table 36

Set-up sketch and description	Set-up sketch and description
Ball bearing set-up with the shaft locked by caps on two sides. The bearings may be installed with axial clearance or interference (adjusted by shim *1*). The design is suitable for small distances between supports and cast-iron or steel housings	Ball bearing set-up with oil slingers. The rest of the design is the same as in the previous design
Ball bearing set-up with the shaft locked by snap rings *2*, *3*. The bearings may be installed with clearance or interference (adjusted by washer *4*). The design is applicable under the same conditions as above	Ball bearing set-up locked by twin bearings tightened against snap ring *8*. The twin bearings may be installed with a preload (adjusted by washer *9*)
Ball bearing set-up with the right-hand bearing locked by snap ring *5* and the cap. The other bearing floats in the housing. The design is suitable for large distances between bearings and any housing material. The locked bearing may be installed with an axial clearance or tightly (adjusted by shim *6*)	Floating ball bearing set-up. The shaft is held axially in position by the teeth of the herringbone gear. The shaft of the mating herringbone gear is locked axially

Ball bearing set-up in a split housing (radial assembly) with the right-hand bearing locked by a recess in the housing. The left-hand bearing is floating	Ball bearing set-up in a split housing with the right-hand bearing locked by the cap and an oil seal disk. The left-hand bearing floats in the housing	Spherical double-row ball bearing set-up. The right-hand bearing is locked by the caps and the left-hand one floats in the housing. The design is used where bearings are installed in different housings and where elastic deformations of the shaft are likely to occur
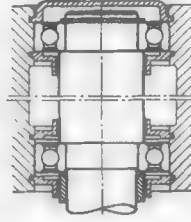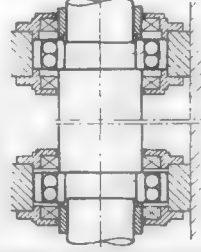
Ball bearing set-up with the right-hand bearing locked by snap rings and the cap. The other bearing floats on the shaft	Ball bearing set-up with the right-hand bearing locked by intermediate sleeve 7 and the cap. The other bearing floats in the housing	Ball bearing set-up in a light-alloy housing with the use of intermediate sleeves	Ball bearing set-up with the right-hand bearing locked by snap ring 8 installed in the outer race. The other bearing floats in the housing

Table 36 (cont.)

Set-up sketch and description	Set-up sketch and description
Roller bearing set-up locked by the caps on both sides. The design is suitable for small distances between supports and cast-iron or steel housings. Clearance *s* is provided to prevent overtightening of the bearings. The set-up can carry only light axial loads	Tapered roller bearing set-up with the outer races tightened through the intermediary of shim *14* (the *O* device). The design is suitable for small distances between supports and cast-iron or steel housings. The set-up can carry considerable bidirectional radial and axial loads
Roller bearing set-up with the right-hand bearing locked by snap ring *10* and the cap. The locking bearing is provided with lips on the outer and inner races. The rollers of the other bearing can freely move axially on the outer race. The design is suitable for small distances between supports	Tapered roller bearing set-up with the tightened inner races (the X device). The design ensures a more rigid shaft location than in the previous case. The tightening must be done to a specified torque
Roller bearing set-up with detachable lips on the inner races. The right-hand bearing is locked by a snap ring and the cap; the outer race of the left-hand bearing floats in the housing. The design provides for a larger range of axial displacements than the previous one	Combined set-up of duplex tapered bearings, serving as a locking unit, and a floating roller bearing. The tightening of the tapered bearings is adjusted by washer *15*. The design is suitable for large distances between supports, high axial loads and precise axial location of the shaft
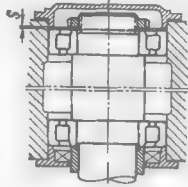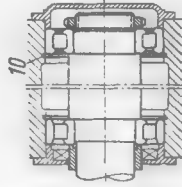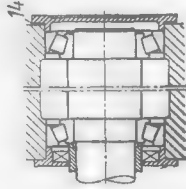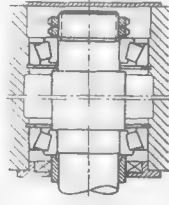
Duplex tapered roller bearing set-up.
The right-hand support is locking and the left-hand one is floating.
The set-up can carry high radial and axial loads

16
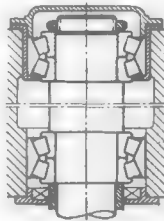
Combined set-up of radial ball bearings and a thrust ball bearing (for unidirectional axial load).
The clearance in the thrust bearing is adjusted by shim 16.
The radial bearings are floating

17
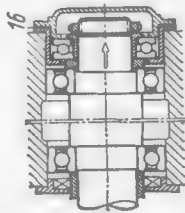
Combined set-up of radial ball bearings and a double-action thrust ball bearing (the design is suitable for high bidirectional axial loads).
The clearance in the thrust bearing is adjusted by shim 17.
The radial bearings are floating
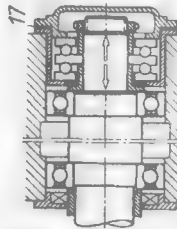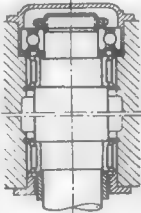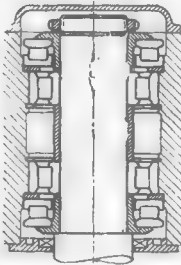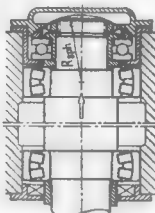
Roller bearing set-up.
Axial (bidirectional) loads are taken up by the ball bearing which is relieved of radial loads

11

Radial thrust ball bearing set-up with the outer races tightened by the cap with adjusting shim 11.
The design is suitable for small distances between supports and cast-iron or steel housings

12

Radial thrust bearing set-up with the inner races tightened against adjusting washer 12.
By its characteristics the design is similar to the previous one

Three radial thrust bearings set-up (for an increased unidirectional axial load).
The right-hand twin-bearing support carries the axial load; the left-hand bearing locks the set-up.
The design is suitable for small distances between supports

13

Combined locking twin radial thrust bearing set-up with a floating ball bearing on the opposite side.
The tightening of the radial thrust bearings is adjusted by washer 13.
The design is suitable for large distances between supports

Table 36 (cont)

Set-up sketch and description	Set-up sketch and description
Needle bearing set-up. The shaft is locked and axial loads are taken up by the radial ball bearing which is relieved of radial loads	Set-up of wide-series roller bearings. Axial loads are taken up by the thrust roller bearings. The design is intended to carry high radial and axial loads at low rotational speeds
Self-aligning roller bearing set-up. Axial load is taken up by the thrust ball bearing installed on a spherical washer. The centre of the sphere coincides with that of the nearest self-aligning bearing	

its change and the degree of its impact nature, the tighter should be the fit.

Interference fits prevent the slipping of the races on their seating surfaces, and the crushing, breaking and frictional corrosion of the surfaces.

The races slip as a result of the reduction of friction between them and their seating surfaces, caused by vibrations, the crushing of the seating surface micro-irregularities under the effect of load and the expansion of housings upon their heating.

But heavy interferences complicate the installation and dismantling of bearings, increase stresses in the races, and may cause the pinching of the antifriction bodies and overheating of the bearings.

It is good practice to tighten the heavily loaded races axially, which prevents the overstressing of the bearings and facilitates their installation and dismantling, dispensing with the considerable forces otherwise required to place and remove the bearings.

Therefore, in all cases where the design permits, the heavily loaded races should be installed by centring or transition fits and then tightened, interference fits being used only when the power tightening of the races is impossible for design considerations.

The operating capacity of heavily loaded bearing units can also be improved by increasing the hardness of the seating surfaces.

Shafts should be heat treated to $Rc > 35\text{-}40$. Heavily loaded shafts are carburized or induction surface hardened to 55-58 Rc with subsequent roll-burnishing.

It is advisable to coat the shaft surfaces with copper, bronze or brass to prevent frictional corrosion.

In soft-alloy housings bearings should be installed in heat-treated steel sleeves.

The finish and machining accuracy of the seating surfaces are of great importance. The crushing of the microirregularities left after inadequate finish machining results in a rapid weakening of the original interferences and increases the clearances.

The seating surfaces for bearings of the H, П and B classes are machined to the 9th-10th class of surface finish on the shafts and to the 8th-9th class in the housings. For bearings of a higher accuracy the surface finish is one or two classes higher.

The out-of-roundness (ovality, conicity) for the bearings of the H, П and B classes is not more than 0.5, and for those of higher accuracy, not more than 0.25 of the manufacturing tolerance for a given grade of accuracy.

The misalignment of the seating surfaces in twin and multiple-support installations is not more than 0.01-0.02 mm.

The end faces of thrust shoulders and distance bushings are machined to a finish not worse than that of the 8th class. The wobble of thrust surfaces is not more than 0.01 mm at the extreme points.

21*

(a) Circulating and Local Loading

The following two basic types of loading are distinguished: *local*, when the load is applied to a limited section of the race surface, and *circulating*, when the load application point periodically moves along the race circumference.

The basic loading patterns are illustrated in Table 37.

If the load vector moves randomly getting periodically ahead of or behind the revolving race, the loading pattern is determined by plotting polar loading diagrams per load change cycle.

Circulating load tends to turn the race on the seating surface and causes cyclic pressure on these surfaces. For this reason the races carrying circulating loads must be tightly fitted or tightened axially. Locally loaded races can be installed more freely.

(b) Effect of Thermal Deformations

As a result of heat generation due to friction the bearings in cold machines are heated, as a rule, more than the housing and shaft as a result of which the clearance between the inner race and the shaft increases during operation whereas that between the outer race and the housing decreases. Therefore, it is appropriate in this case to specify tighter fits on the shaft and slacker ones in the housing.

Example. The external diameter of a bearing is 100 mm and the internal one, 50 mm. The working temperature of the bearing is 100°C, and that of the shaft and housing, 20°C. The linear expansion coefficient α of the ball bearing steel is $14 \cdot 10^{-6}$. The bearing is installed on the shaft by a tight fit with a diametral interference of 25 μm and in the housing, by a slide fit with zero clearance.

Upon heating, the internal diameter of the bearing increases by $\Delta = (100 - 20)\, 50 \cdot 14 \cdot 10^{-6} = 0.056$ mm.

Thus, the initial assembly interference on the shaft disappears and a clearance of $56 - 25 = 31$ μm forms between the shaft and the inner race.

The external diameter of the bearing increases by $\Delta' = (100 - 20)\, 100 \times 14 \times 10^{-6} = 0.112$ mm.

Therefore, an interference of 112 μm develops between the outer race and the housing.
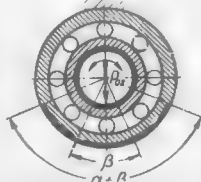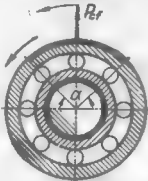
The change of the fit in the housing must be taken into account by assigning a looser fit. Axial tightening both on the shaft and in the housing is advisable.

In hot machines the radial dimensions of the shaft and housing upon heating change in the same direction as those of the bearing, except when the housing is heated to high temperatures and, especially, when the housing is made of a light alloy with a high linear expansion coefficient. Here, one has to reckon with the possible considerable increase in the clearance between the outer race and the housing.

Example. A bearing with an external diameter of 100 mm is installed in a housing made of an aluminium alloy with a linear expansion coefficient $\alpha = 24 \cdot 10^{-6}$. The working temperature of the bearing and housing is 100°C. The

Table 37

Basic Loading Patterns

Conditions of load application	Sketch	Nature of race loading	
		outer	inner
Outer race stationary, inner race rotating			
Shaft is loaded with force P of constant direction		Local loading (over effective bearing load angle α)	Circulating
Shaft is loaded with centrifugal force P_{cf}		Circulating	Local
Shaft is loaded with a force P_{os} oscillating with an angular amplitude β		Circulating loading with amplitude $\alpha + \beta$	Circulating
Inner race stationary, outer race rotating			
Outer race is loaded with force P of constant direction		Circulating	Local
Outer race is loaded with centrifugal force P_{cf}		Local	Circulating
Race is loaded with an oscillatory force P_{os}		Circulating	Circulating with amplitude $\alpha + \beta$

bearing is installed in the housing by a force fit with a diametral interference of 20 μm.

Upon heating, the diameter of the seating bore in the housing increases by $\Delta = 100 \cdot 100 \cdot 24 \cdot 10^{-6} = 0.24$ mm, and the external diameter of the bearing, by $\Delta' = 100 \cdot 100 \cdot 14 \cdot 10^{-6} = 0.14$ mm.

The difference in increment between the diameters is $0.24 - 0.14 = 0.1$ mm. Thus, the initial interference disappears and a clearance of $100 - 20 = 80$ μm forms between the bearing and the housing.

To maintain the bearing centring in the housing a tighter initial fit in the housing or axial tightening should be used in this case.

In accurate applications, where the correct centring is to be maintained in all operating conditions, use is made of temperature-independent centring methods of which the radial-ray method is most effective.

(c) Classes of Fits

Figure 245 shows mean values of diametral clearances and interferences for the bearing fits according with the USSR State Standards.
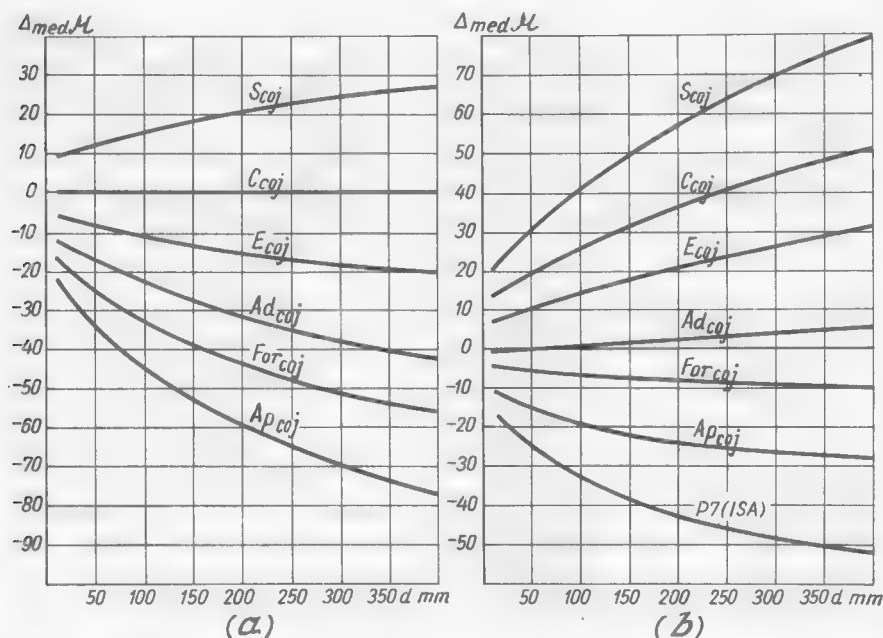
Fig. 245. Mean values of clearances and interferences for bearings fitted on the shaft (a) and in the housing bore (b)

The uses of fits (for the bearings of the H, Π and B classes) given below may be used as a guide.

Bearing Fits on Shafts (Basic-Hole System)

Running fit (R). Light loads. High rotational speeds. Floating races.

Easy slide fit (Se). Light loads. High rotational speeds. Locally loaded races. Floating races.

Slide fit (S). Light loads. Light pulsating loads. High rotational speeds. Locally loaded races. Floating races. Moderately and heavily loaded bearings with the inner races tightened by nuts.

Push fit (P). Medium loads, light alternating and impact loads. High and medium rotational speeds. Locally loaded races. Floating races. Oscillatory motion. Heavily loaded bearings with the inner races tightened by nuts.

Wringing fit (W). Medium loads, pulsating, alternating and impact. Circulatively loaded races. Medium rotational speeds. Heavily loaded bearings under impact load with the inner races tightened by nuts.

Tight fit (T). Heavy loads, pulsating, alternating and impact. Circulatively loaded races. Roller bearings and large ball bearings.

Force fit (F). High alternating and impact loads. Circulatively loaded races. Low and medium rotational speeds. Large roller bearings.

Bearings Fits in Housings (Basic-Shaft System)

Easy slide fit (Se). Light loads. High rotational speeds. Locally loaded races. Floating races.

Slide fit (S). Light loads. Medium and high rotational speeds. Locally loaded races. Floating races. Moderately loaded bearings with loaded races tightened by nuts. Bearings installed in split (in the meridional plane) housings.

Push fit (P). Medium loads; light alternating and impact loads. Medium rotational speeds. Locally loaded races. Floating races. Oscillatory motion. Heavily loaded bearings with tightened outer races. Bearings installed in split (in the meridional plane) housings.

Wringing fit (W). Medium loads, pulsating, alternating and impact. Circulatively loaded races. Medium rotational speeds. Heavily loaded bearings under impact load with tightened outer races.

Tight fit (T). Medium loads, alternating and impact. Circulatively loaded races. Medium and low rotational speeds. Heavily loaded bearings under impact load with tightened outer races.

Force fit (F). Heavy loads, alternating and impact. Circulatively loaded races. Medium and low rotational speeds. Roller and large ball bearings. Bearings installed in thermoexpansible housings.

Light drive fit P7 (ISA). Bearings installed in thin-walled or thermoexpansible housings.

Fits to the 1st grade of accuracy are used for the bearings of the A and C classes.

Fits on the shaft are: Se_1, S_1, P_1, W_1, T_1 and F_1.

Fits in the housing are: S_1, P_1, T_1 and F_1.

(d) Selection of Fits with Account of Assembly and Disassembly Conditions

To facilitate the installation and dismantling of bearings do the following:

(1) install the bearings with interference on one race only (preferably the inner one), the other race being fitted freely;

(2) avoid identical interferences when several bearings are instal-
led successively on the same shaft or in the same housing (axial
assembly); the fit on the first (by the order of assembly) seating por-
tion of the shaft should be more free to ease the fitting of the second
bearing on its seating portion.

Figure 246a shows a poor arrangement of fits for mounting bearings
by interference fits (a force fit on the shaft and a wringing fit in the
housing). When being mounted on the shaft, bearing *1* in the course
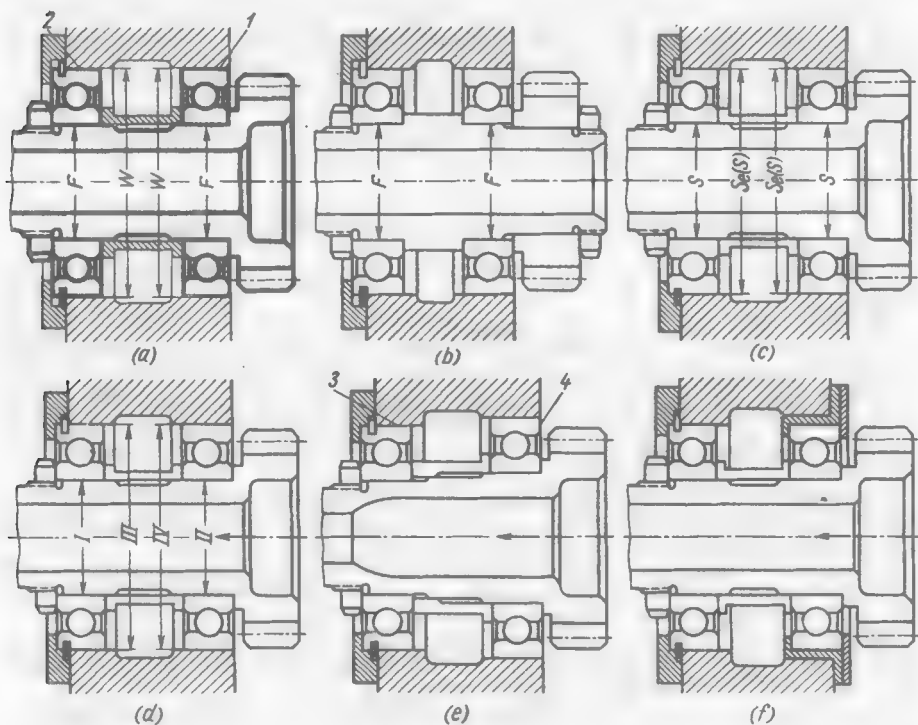
Fig. 246. Fits of twin bearings

of assembly must first pass with interference over the other bearing
seating portion before it reaches its own position. When the shaft,
on which the bearings have been fitted in advance, is assembled, bear-
ing *2* has to pass into the housing with interference through the first
bearing seat. The fitting force is transmitted to the outer races of
the bearings through the balls and may cause their damage.

Fits with the same interference for both bearings may be applied
when the bearings can be mounted from both ends of the shaft
(Fig. 246b).

It is easy to mount bearings successively on the shaft by clearance fits (R, Se), or by centring fits (S, see Fig. 246c). However, clearance fits are not always applicable because of the bearing operating conditions.

A more popular method is to specify different fits for both bearings. In this case more free fits are specified for the sections through and or over which the bearing has to be drawn during assembly (Table 38).

Table 38

Possible Combinations of Fits (Fig. 246d)

Fits on the shaft		Fits in the housing	
I	II	III	IV
Se	S, P, W, T, F	S	P, W, T, F
S	P, W, T, F	P	W, T, F
P	W, T, F	W	T, F
W	T, F	T	F
T	F		

The greater the difference between the fits, the easier the assembly. Thus, the most advantageous combination of fits for the shaft is Se-F. The least advantageous combinations are obtained with the first fits in the corresponding lines in columns II and IV.

When installing bearings together with the shaft in the housing, it is also advantageous to choose fits which differ most from one another, for example, slide (S) and force (F) fits in the first line of the table.

The best assembly method it is to use bearings of different diameters (Fig. 246e). With this method no limitations are imposed on the choice of fits. Preferred, however, is the case when bearing 3, being the first to be installed in the housing, is put in by a more free fit than the second bearing (4). As good as the above (as far as the conditions of installation in the housing are concerned) is the method of enclosing one of the bearings in a permanent bushing (Fig. 246f).

3.14. Assembly of Rolling-Contact Bearings

Bearing units should be designed so as to ensure the most convenient and effective installation and removal of the unit, and dispense with adjusting operations.

As a rule, the bearings which are to be interference-fitted should be mounted first (on the shaft or in the housing); the assembly of the

unit as a whole should be done on the locating sections having clearances.

The interference-fitting of bearings both on the shaft and in the housing complicates the assembly.

Clearance or centring fits should be supplemented with the axial tightening of the races.

Let us consider the basic assembly methods for the simplest case of an end bearing locked on the shaft and in the housing by snap rings.

Axial Assembly

Method 1. *Installing a shaft with a prefitted bearing in a housing* (Fig. 247a).

The bearing is first fitted onto the shaft and locked by the shaft shoulder and snap ring *1*.

The shaft together with the bearing is then introduced into the housing (Fig. 247b) until the bearing rests against snap ring *2* previously installed in
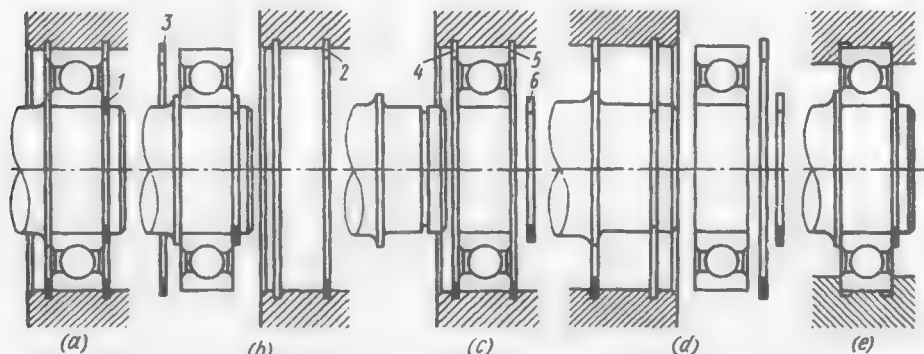
Fig. 247. Mounting of an end bearing

the housing and after that the unit is fixed by snap ring *3* mounted in advance behind the bearing.

The method is most sound if the bearing is interference-fitted on the shaft and installed in the housing by a centring fit. It may also be applied when the bearing is installed by a centring fit both on the shaft and in the housing.

The method is of no practical use if the bearing is interference-fitted in the housing. In this case the pressing-in force affects the antifriction bodies. The pressing-in process is complicated by the necessity to operate with two parts — the shaft and the housing — which may have very large overall dimensions.

Method 2. *Installing a shaft in a bearing prefitted in a housing* (Fig. 247c).

The bearing is first installed and locked in the housing by snap rings *4* and *5*. The shaft is then introduced into the bearing bore and locked by snap ring *6*.

The method is most sound when the bearing is installed in the housing by an interference fit, and on the shaft, by a centring fit. The method may also be applied when the bearing is clearance-fitted both on the shaft and in the housing.

The method is of no practical use if the bearing is interference-fitted on the shaft.

Method 3. *Installing a bearing simultaneously on a shaft and in a housing* (Fig. 247d).

The shaft, supported by the other bearing (not shown on the drawing), is inserted into the housing until the locating sections on the shaft and in the housing are matched. The bearing is then inserted into the annular space between the shaft and housing. The assembly is accomplished after locking snap rings are fitted in place.

The method is applicable if the bearing is clearance-fitted both on the shaft and in the housing; it is limitedly applied if one of the fits (on the shaft or in the housing) is free, and cannot be applied at all if the bearing is interference-fitted both on the shaft and in the housing.

Radial Assembly

A shaft with a premounted and prelocked bearing (Fig. 247e) is placed into the lower half of a split housing and covered by its upper half. The bearing is usually locked in the housing by shoulders.

Any types and combinations of fits on the shaft and in the housing can be used. Usually, bearings are installed in the housing by clearance, centring or small-interference fits. It is difficult to use large-interference fits because the parting planes have to be accurately aligned with the bearing centre and because the bearing may possibly be overstressed when the parting plane is erroneously displaced with respect to the bearing centre.

(a) Assembly of Twin Installations

Let us consider the case of installing a pinion shaft with bearings tightened on it through the intermediary of a distance bushing
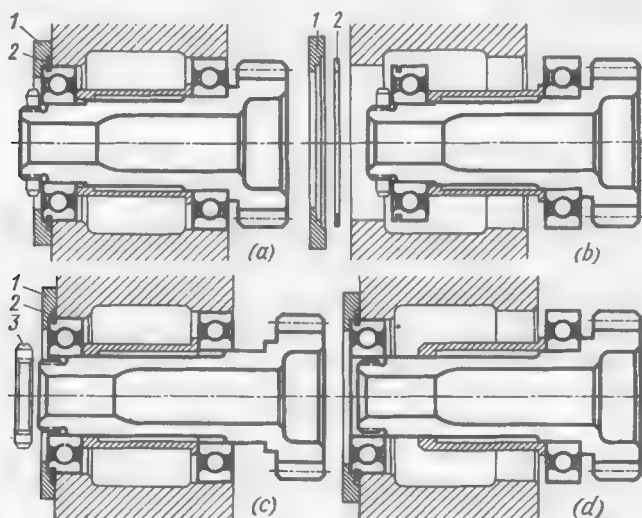
Fig. 248. Mounting of bearings in twin installations

(Fig. 248a). The shaft is held in the housing by cap *1* and snap ring *2* placed in its groove in the outer race of the smaller bearing.

Method 1. *Installing a shaft with prefitted bearings into a housing* (Fig. 248b).
The shaft together with the bearings is introduced into the housing and locked by snap ring *2* and cap *1*. During assembly it is important that the first bearing (by the order of assembly) enter its seating hole before the other bearing engages its own. Otherwise, the shaft may be misaligned and assembly will be impossible.

This method permits any type of the bearings fit on the shaft, while in the housing the bearings are better to be installed by clearance, centring or small-interference fits.

Method 2. *Installing a shaft into bearings prefitted in a housing* (Fig. 248c).
The bearings with a distance bushing in between are installed into the housing. The left-hand bearing is secured in the housing by snap ring *2* and cap *1*, after which the shaft is inserted into the bores of the bearings. The assembly is accomplished after the shaft is tightened by nut *3*.

The first seating section of the shaft (by the order of assembly) should enter its bearing bore before the other seating section engages the bore of the other bearing.

The bearing fit in the housing may be of any class (the right-hand floating bearing should of course be installed by a fit not tighter than a push fit), whereas on the shaft the bearings should be fitted by a clearance or centring fit. This assembly method is more complicated than method 1. The assembly is further complicated by the necessity to preliminarily install the distance bushing before the bearings are inserted into the housing.

Method 3 (combined). Firstly the rear bearing (by the order of assembly) and the distance bushing are installed on the shaft (Fig. 248d), and the locking bearing is installed in the housing.

The shaft is introduced into the housing so that its shank enters the bore of the locking bearing, and the rear bearing enters its seat in the housing. The assembly is completed after the shaft nut is tightened.

The rear bearing can be installed on the shaft and the locking bearing, in the housing by any fit. The locking bearing is mounted on the shaft by a clearance or centring fit. The rear bearing is usually installed in the housing by clearance, centring or push fits.

The assembly method largely depends on the fastening scheme of the bearings, the design and arrangement of the elements that lock the bearings on the shaft and in the housing (Fig. 249). The system shown in Fig. 249a allows the bearings to be fastened only by method 1, that in Fig. 249b, by method 2, the one in Fig. 249c, by method 3, and those in Fig. 249d, e, by methods 2 and 3. The design shown in Fig. 249f allows the use of any of the three methods.

Thus, a close relationship exists between the bearing fastening system and the system of the bearing fits on the shaft and in the housing.

The assembly conditions and the choice of the most convenient and efficient assembly method determine the system of fastening the bearings and their allowable fits on the shaft and in the housing, which may be other than those required for reliable operation of the unit.

The system of bearing fastening, determined on the basis of the best operating conditions, and the corresponding optimum fits may not necessarily be the most convenient and effective ones.

In practice, the variant chosen is frequently the one which fulfils the most important conditions for the proper operation of the unit and does not excessively complicate the assembly.
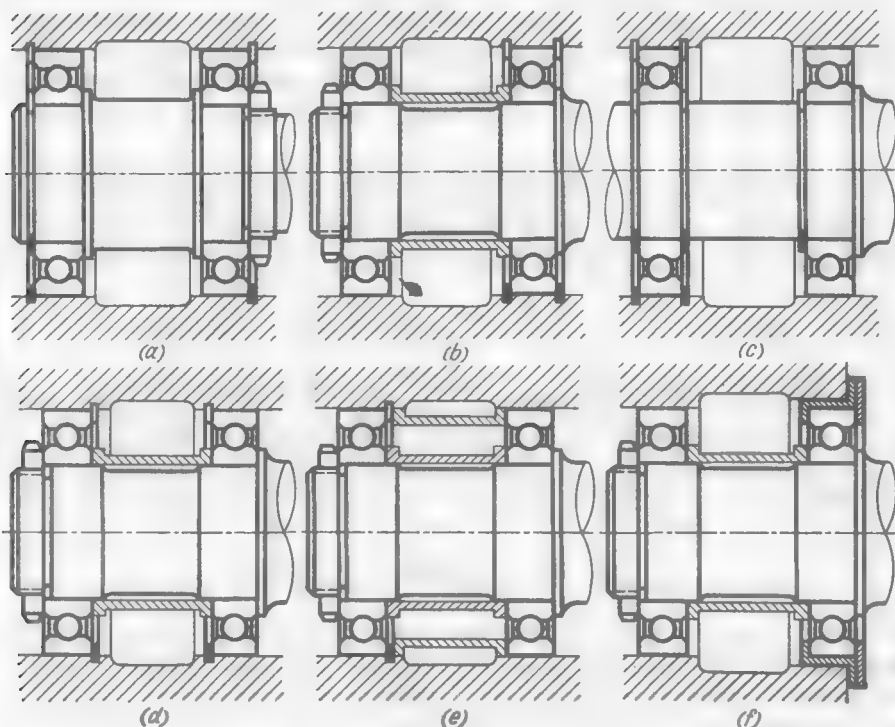
Fig. 249. Systems of fastening twin bearings

The assembly is made easier, if bearings are *tightened axially* on the shaft and in the housing. Power tightening is tantamount in its effect to interference fits and allows the use of more free fits without any detriment to the operating ability of the unit and with more convenient assembly.

(b) Self-Aligning Bearings

These bearings are used when:

(1) the manufacturing process cannot ensure strict coaxiality of supports (the supports located in different housings or in different parts of housings, which are not secured accurately enough one relative to the other);

(2) the housing components are not rigid enough and get deformed under the action of the working forces (thin-walled housings such as, for example, those made of sheet materials);

(3) the shaft gets deformed under load due to its insufficient rigidity or large transverse forces acting on it (long shafts with poorly balanced rotors).

As often as not the use of tight bearings in such cases results in the pinching of the rolling elements and unilateral loading of the bearings many times in excess of the working loads, and causes a rapid wear and failure of the bearings. These phenomena are especially pronounced in bearings which, due to the shape of their rolling elements and
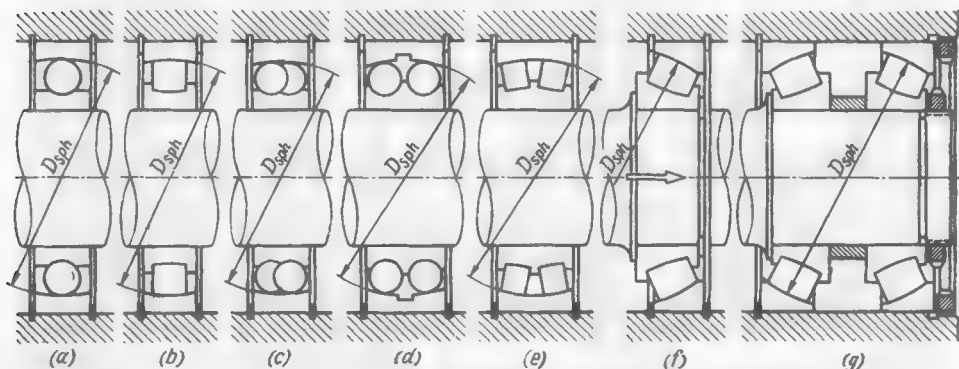
Fig. 250. Self-aligning bearings

raceways, cannot yield to skewing (roller bearings with cylindrical and tapered rollers). Ball bearings endure misalignments somewhat better because of their angular clearance.

It is expedient to use self-aligning bearings when there are no obvious signs of misalignment and distortion. Production inaccuracies, assembly errors and unforeseen thermal deformations of the system produce local loads in the bearings, which can easily be eliminated if the bearings are mounted freely.

Self-alignment is an effective means to increase the reliability and durability of heavily loaded and high-speed rolling-contact bearings.

Single-row ball bearings with a spherical active surface of the outer race (Fig. 250a) are seldom used today since the bearings of this type have a reduced load-carrying capacity, are liable to the pinching of their balls when an axial load is applied to them, and inaccurately lock the shaft in the axial direction.

For the same reasons single-row roller bearings with barrel-shaped rollers (Fig. 250b) are also seldom used.

The most popular type of self-aligning bearing is a double-row ball bearing with a staggered arrangement of the balls (Fig. 250c).

As to the form of the raceway, these bearings are little adapted for taking up axial loads. Their axial carrying capacity can be increased

by spacing the balls farther apart, when the contact surfaces are trans-
ferred to the portions of the sphere positioned at a larger angle to the
transverse plane of symmetry (Fig. 250d).

Self-aligning roller bearings are made in the form of double-row
bearings with barrel-shaped rollers (Fig. 250e).

Spherotapered self-aligning bearings are used singly (Fig. 250f)
as thrust bearings, and in twin-bearing units (Fig. 250g) as radial
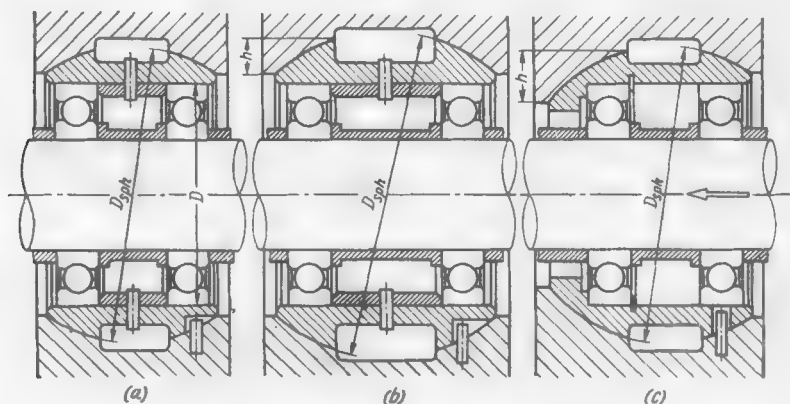
Fig. 251. Installation of bearings in spherical supports

shrust bearings. For the twin units to operate properly it is neces-
tary to maintain the distance between the bearings to close tolerances
so that the centres of the spherical rolling-contact surfaces are
matched.

Self-alignment can also be implemented by enclosing standard
bearings in spherical housings (Fig. 251). This method is, as a rule,
used only in the case of multiple-support installations (with two and
more bearings).

In bearings mounted on spheres the rolling elements operate in
conditions of pure rolling, whereas in self-aligning bearings there oc-
curs, in the case of misalignments, a periodic (or, at high speeds,
a high-frequency) displacement of the rolling elements over the
spherical surface attended by intensive wear.

The ratio D_{sph}/D of the sphere diameter to the external diameter
of the bearings in twin units is made equal to 1.25-1.3 (Fig. 251a).
This ratio ensures a favourable orientation of the carrying surfaces
on the sphere with respect to the axial and radial loads. When the
axial load is high, the ratio D_{sph}/D is enlarged to 1.4-1.5 to increase
the height h of the carrying portion of the sphere (Fig. 251b).

For a higher unidirectional axial load the sphere is made asymmet-
ric (Fig. 251c) to extend its carrying surface h.

Proper self-alignment is ensured if enough oil is supplied (preferably under pressure) to the spherical supporting surfaces. Solid grease is used in places difficult of access.

(c) Elastic Installation of Bearings

This method extends the use of rolling-contact bearings and makes it possible to change the conditions of their loading.

When bearings are installed in a rigid housing (Fig. 252a) the distribution of axial and radial loads on these bearings is indefinite and depends on the accuracy of assembly and the direction of the shaft bending deformations. If the left-hand side of the shaft is deformed and the right-hand one, held by the other support (not shown on the drawing), is deformed to a lesser degree, the left-hand bearing is overloaded as compared with the right-hand one.

When bearings are installed in an elastic cantilevered bushing (Fig. 252b) the loads are distributed quite definitely. The radial load is carried by the right-hand bearing installed at the rigidity node and the axial load, by the left-hand bearing which is relieved of radial forces, thanks to the compliance of the bushing.

In the design shown in Fig. 252c radial loads are taken up by the roller bearing; the ball bearings carry axial loads in both directions.

In the design of increased elasticity (Fig. 252d) the housing itself is elastic and, besides, the inner race of the bearing is mounted on an elastic bushing which in turn is cantilever-mounted on the shaft.

These systems are equivalent to the method of loading one of the bearings with axial forces only by installing it in the housing with a radial clearance s (Fig. 252e). This method is frequently used in mechanical engineering.

When triple ball bearings are installed in an elastic housing and on an elastic bushing (Fig. 252f), the radial forces progressively diminish from the rigidity node towards the cantilever free end, and the axial forces acting on the bearings increase in the same direction. Likewise, the forces taken up by the bearings are uniformly distributed.

A twin installation of ball bearings in an elastic housing and on an elastic cantilevered bushing (Fig. 252g) ensures uniform distribution of the radial forces among the two bearings. The system as a whole is pliable in the radial direction and can align itself.

Figure 252h shows triple ball bearings with uniform distribution of forces among the bearings. The system also provides for the shaft to have a certain degree of freedom to align itself.

The designs with a symmetrical arrangement of the bearings (with respect to the rigidity node) installed in an elastic housing (Fig. 252i) or in an elastic housing and on an elastic bushing (Fig. 252j) are

self-aligning and can be used instead of spherical bearing install-ations. These designs also ensure an elastic taking up of the loads by the bearings.
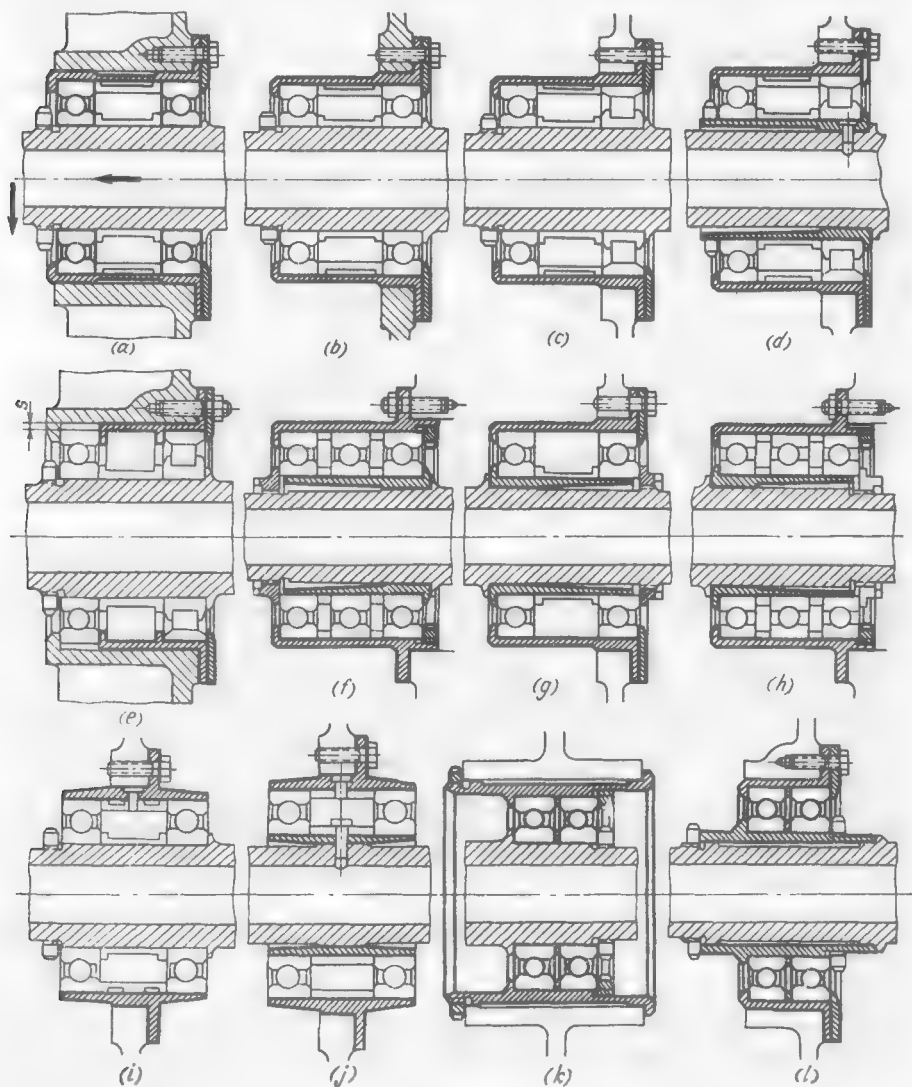
Fig. 252. Elastic installation of bearings

Figure 252 _k_, _l_ shows an elastic installation of twin bearings in-tended to dampen impact loads.

(d) Multiple-Bearing Installations

Multiple-bearing installations are used to increase the load-carrying capcity of shaft supports and reduce the load on individual bearings, which is especially important for high-speed and heavy-load applications.

The main problem with the multiple-bearing units is to ensure uniform load distribution among the bearings. In the case of bearings which carry radial loads the problem is solved by accurately machining the seating surfaces of the outer and inner races, by enclosing the bearings in uniformly rigid housings, or by making use of elastic housings.

It is more difficult to attain uniform axial load distribution. With inaccurate manufacture and assembly, the axial load is taken up by one bearing only, while the other ones do not participate in the work or participate but slightly.

But this problem also has been solved by preloading the bearings and improving the accuracy of their manufacture, and multiple-bearing installations are extensively used today.

Figure 253a, b shows one of the early methods used to ensure the uniform axial loading of bearings mounted in succession.

Each bearing is enclosed in its own housing arranged concentrically in the housing of the adjacent bearing. The length of distance rings 1 (Fig. 253a) is selected so that the end faces of the housings in the free state project with respect to the end faces of the adjacent housings by amounts c and c′ equal to the axial deformations of the bearings when loaded with a strictly identical force on a test stand. Then the unit is compressed under a press until the end faces of all the housings coincide. In this position the bearing housings are secured by taper pins 2 (Fig. 253b), the bearings being preloaded with forces determined by the values of c and c′. Only the last bearing (installed in the external housing) is not preloaded.

When the bearings are being loaded by an axial force opposite to their preload (bright arrow), the load is distributed among them according to their preloads (equally, if the preloads are the same). The extreme, untightened bearing mainly carries radial loads and locks the shaft in the direction opposite to the load.

This system requires individual adjustment and assembly of the unit and is therefore unsuitable for mass production. Today it is ousted by more perfect designs.

In the design shown in Fig. 253c the bearings, fitted into a common housing, are separated on the shaft and in the housing by distance rings and clamped by nut 3. The length of the last distance ring 4 (viewed from the tightening side) in the housing is selected so that a design clearance s remains between the ring and the outer race of the adjacent bearing.

When nut 3 is being tightened, the entire set of the outer races of the front bearings is displaced to a distance s and thus these bearings become preloaded. Bearing 4 remains unpreloaded.

The system can carry an increased axial load in the direction opposite to the preload (shown by the arrow). The load in the opposite direction is carried only by the extreme, unpreloaded bearing, the other bearings, while being relieved of the preload, carry practically no load in this direction.

If the unit has to bear an increased axial load in the direction opposite to the one indicated by the arrow, it is necessary either to change
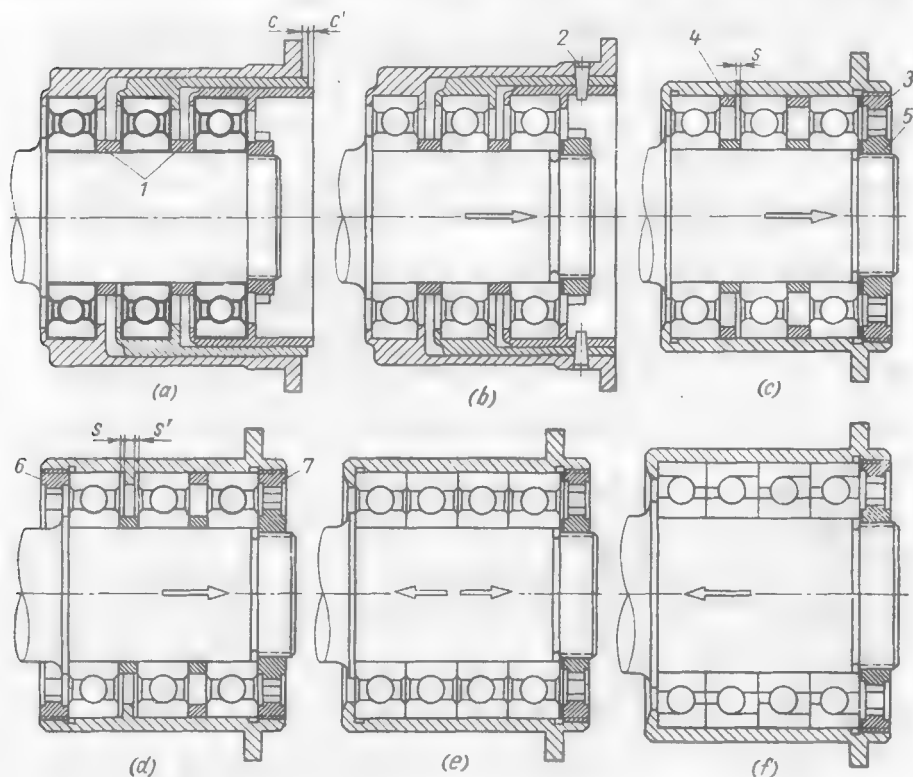
Fig. 253. Multiple-bearing installations

the direction of the preload, i.e., transfer nut *3* to the left, or tighten the inner races of the bearings with nut *5*, leaving a clearance between the last distance ring on the shaft and the inner race of the adjacent bearing.

To obtain a uniform preload, before their assembly the bearings are grouped by the magnitude of their elastic axial deformation under a definite test load, and only those having the same elastic deflection are used in one unit.

In the design shown in Fig. 253*d* all the bearings are preloaded by nuts *6* and *7* until clearances *s* and *s'* are taken up. The system

can carry high axial loads in the direction indicated by the arrow.

A uniform axial load distribution among the bearings of multiple-support systems can be achieved without preload by using high-accuracy bearings (Fig. 253e).

In this case the principal condition is the precise coincidence of the end faces of the outer and inner races. The initial axial rigidity of the bearings must be the same for all of them.

The system can carry increased axial loads in both directions.

Multiple radial thrust bearing installations (Fig. 253f) are designed for large unidirectional axial loads. The axial load is carried by three bearings, the fourth, closing bearing locks the shaft in the direction opposite to the action of the main load. The uniform loading of the bearings is ensured by keeping their dimensions to close tolerances and making them of the same axial rigidity.

(e) Combined Installation of Rolling- and Sliding-Contact Bearings

As a rule, it is bad practice to combine rolling- and sliding-contact bearings in one installation. The radial clearances in sliding-contact bearings are appreciably larger than those in rolling-contact ones. This tends to overload and misalign the rolling-contact bearings and underload the sliding-contact bearings.

If such combinations have still to be used for the lack of space, it will be advisable to remove the plain bearing as far as possible from the rolling-contact one, reduce the diameter of the plain bearing and use a self-aligning rolling-contact bearing (Fig. 254).

Figure 255 illustrates combination examples of rolling- and sliding-contact bearings in a concentric shaft unit.
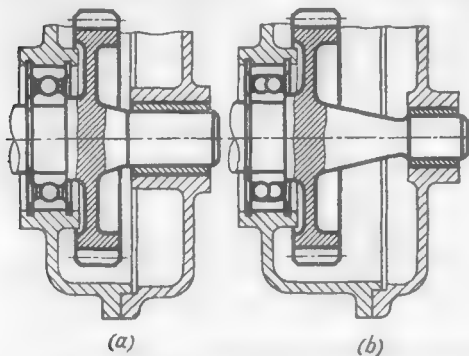
Fig. 254. Combined installation of rolling- and sliding-contact bearings
(a) unpracticable; (b) practicable

In the design in Fig. 255a the left-hand shaft rests in two rolling-contact bearings; the shank of the right-hand shaft is installed in a plain bearing arranged in the plane of the rolling-contact bearing of the left-hand shaft.

In the design shown in Fig. 255b the shank is lengthened and rests in the plain bearing placed between the rolling-contact bearings of the left-hand shaft.

In the design in Fig. 255c the shank of the left-hand shaft is introduced into the plain bearing positioned in the plane of the rolling-contact bearing of the right-hand shaft. The other support for the
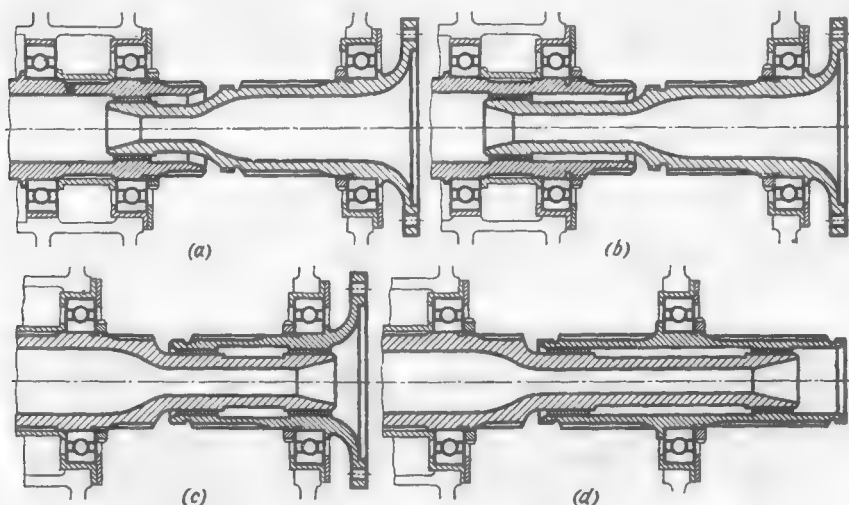
Fig. 255. Combined installation of rolling- and sliding-contact bearings in concentric shafts

right-hand shaft is the plain bearing on the shank of the left-hand shaft.

When the plain supports on the shank are installed sufficiently far apart (Fig. 255d) the left-hand shaft can be installed in one rolling-contact bearing only.

(f) Concentric Installation of Rolling-Contact Bearings

When the bearings are arranged concentrically, it is expedient to do the following:

(1) arrange the bearings as far as possible in one plane;

(2) avoid cantilevered installation of the bearings;

(3) ensure the maximum coaxiality of the mating seating surfaces.

In the design shown in Fig. 256a the right-hand shaft is installed in the housing on two ball bearings, and the left-hand shaft, on one ball bearing. The shank of the left-hand shaft is supported in the ball bearing positioned in the elongated end of the right-hand shaft.

The design error is that the additional support of the left-hand shaft is cantilever-mounted. The inevitable misalignment of the seating surfaces of the shank and the cantilever due to manufacturing and assembly inaccuracies causes shank runout which rapidly wears

the main bearing of the shaft and impairs the operation of the gear mounted on it.

In the design shown in Fig. 256b the auxiliary support of the left-hand shaft is placed in between the bearings of the right-hand shaft, and this reduces the runout to the minimum. The left-hand shaft will be more stable if the distance between its supports is increased.

The additional load transmitted by the shank to the supports of the right-hand shaft is reduced.

The axial dimensions can be reduced if each of the two shafts is mounted on one main and one auxiliary bearing.

The design in Fig. 256c contains an error: the auxiliary support of the shank on the left-hand shaft, which at the same time must
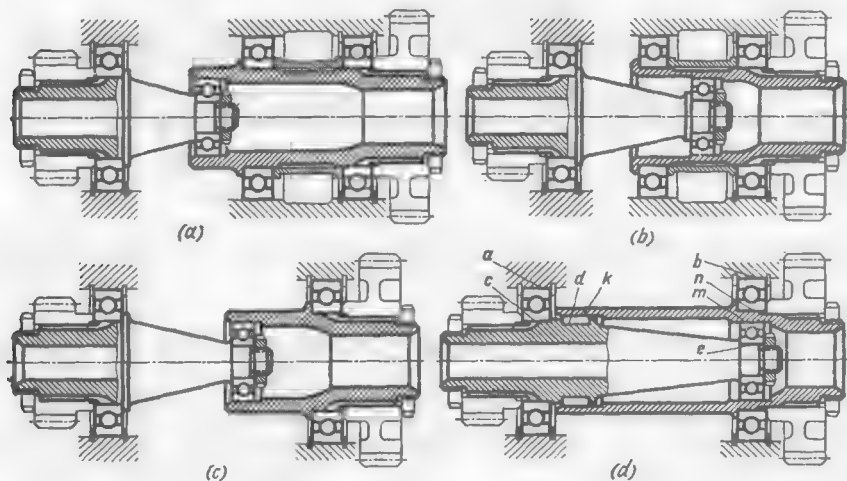
Fig. 256. Concentric installation of rolling-contact bearings

serve as the auxiliary support for the right-hand shaft, is far from the main supports. The support rigidity is fictitious. The load is carried only by the main bearings operating in the most unfavourable conditions, i.e., out of alignment.

In the design shown in Fig. 256d the auxiliary support of the left-hand shaft is positioned directly under the main support of the right-hand shaft, and the auxiliary support of the right-hand shaft (a needle bearing), in close proximity to the main support of the left-hand shaft. The position of the shafts becomes stable. The axial dimensions of the installation can appreciably be decreased.

In all cases of the concentric bearing installation the design should provide for the maximum attainable alignment of the seating surfaces. For example, in the design in Fig. 256d it is necessary to make

coaxial the surfaces *a* and *b* in the housings, *c*, *d* and *e* on the left-hand shaft, and *n*, *m* and *k* on the right-hand shaft.

The direction of rotation of the shafts should also be considered. When the shafts rotate in opposite directions the actual rotational speed of the auxiliary bearings is equal to the sum of the speeds of the shafts, and to the difference in speed between the shafts when they rotate in the same direction.

(g) Installation of Bearings on Output and Input Shafts

Bearings installed on output and input shafts intensively draw oil from the housing cavity, which causes its ejection from the seals. This clearly manifests itself in tapered bearings with rollers diverging towards the seal (Fig. 257a) which, acting in the same manner as the vanes of a centrifugal pump, force the oil into the space between the bearing and the seal. The reverse installation of the bearings (Fig. 257b) is more expedient in this respect.

To prevent the overheating of the bearing, the oil must be drained from the space between the bearing and the seal through ducts or holes of sufficiently large cross-section (*m*, Fig. 258a-c).

In twin installations (Fig. 258d) the oil must also

Fig. 257. Pumping effect of a bearing

be removed from the space between the bearings (hole *n*), and in the case of multiple-step seals (Fig. 258e), from the spaces between the seals (hole *q*).

It is good practice to insert light seals in the form of slingers *1* (Fig. 258a-e), traps *2* (Fig. 258f) and labyrinths *3* (Fig. 258g) in front of the bearings on the housing side.

The oil slinger design in the form of stamped sheet-steel impeller *4* with spiral vanes (Fig. 258h) is a rational one. When the unit is stopped, the oil slinger lets oil freely pass to the bearing, thus building up a store of oil for the starting period. After starting the slinger acts as an axial pump and protects the bearing against excess oil.

Fig. 258. Drainage of oil in shaft-end installations of bearings

(h) Installation of Bearings
on Incomplete Cylindrical Surfaces

As far as possible, bearings should not be fitted on cylindrical surfaces interrupted by recesses, grooves, etc.

When the balls run on the unsupported race sections, the race deforms and the carrying capacity in this section is sharply reduced.

If for design purposes such recesses are required, they should be made as short as possible. In the case of bearings loaded with a uni-directional force recesses with an arc $\alpha = 20\text{-}30°$ can be made on the unloaded side (Fig. 259a). For heavy-series bearings the length of the recess can be larger.

In exceptional cases rolling-contact bearings are arranged on se-
parate symmetrical supporting portions, for example, on the bosses
of the housing (Fig. 259b).
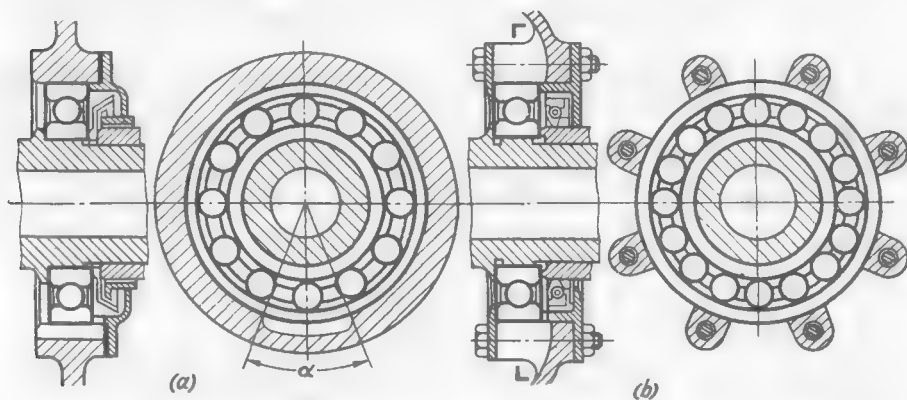
Fig. 259. Installation of bearings on incomplete cylindrical surfaces

Bearings are frequently installed on splined shafts (Fig. 260a, b).
Under moderate loads such units operate satisfactorily, if the number
of the splines is large enough.
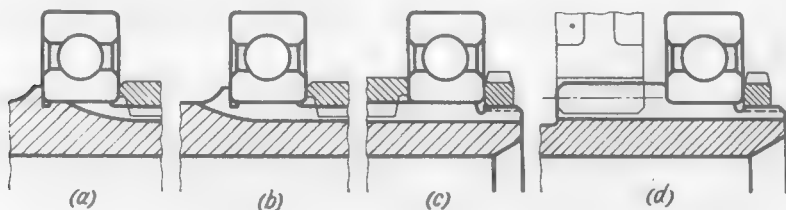
Fig. 260. Installation of bearings on splined shafts and gear teeth

The diameter of the bearing-seating surface on the splines must be
somewhat larger than the major spline diameter. The seating surface
is machined to the accuracy usual for bearing units. Interference fits
should be avoided in this case. The inner race of the bearing must
always be tightened axially through the intermediary of shaft-
fitted parts or by means of a nut.

The thread for the tightening nut is also frequently cut on the
splines (Fig. 260c).

Figure 260d shows a bearing installed on a reduced gear tooth
diameter.

(i) Raceless Installation of Bearings

To reduce the radial dimensions and weight of a structure, one of the races of a standard bearing is removed, the corresponding raceways being cut directly in the parts to be supported (Fig. 261*a-c*).
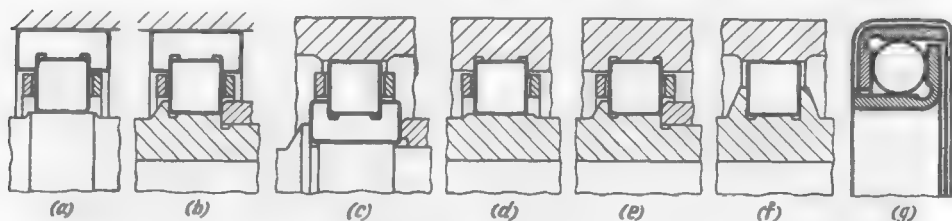
Fig. 261. Raceless installation of bearings

This method is most frequently used for bearings with cylindrical rollers, for cylindrical raceways on parts can be machined rather easily.

In some cases both raceways are made on the parts, using only the set of rollers and the cage from a standard bearing (Fig. 261*d, e*).

Frequently, cages are also dispensed with (Fig. 261*f*). Bearings of this type operate quite satisfactorily but with an increased heat generation resulting from the mutual friction of the rollers.

The surfaces of raceways must be hardened to 62-65 *Rc* and machined to the 1st grade of accuracy and surface finish not worse than that corresponding to the 12th class. Standard radial and end clearances must be maintained as for rolling-contact bearings.

The parts with raceways are usually manufactured from structural steel, and the required surface hardness is obtained by carburizing, induction hardening or nitriding.

In the case of carburized and cyanided parts use is made of low-carbon alloy steel grades 20X, 18XΓТ, 12XH3A, and 20X2HA; alloy steels with 0.8-1% C are used for induction hardened parts, and steel grade 38XMЮA, for nitrided parts.

The raceless installation of ball bearings is seldom used because it is difficult to make profiled raceways. Such designs are utilized
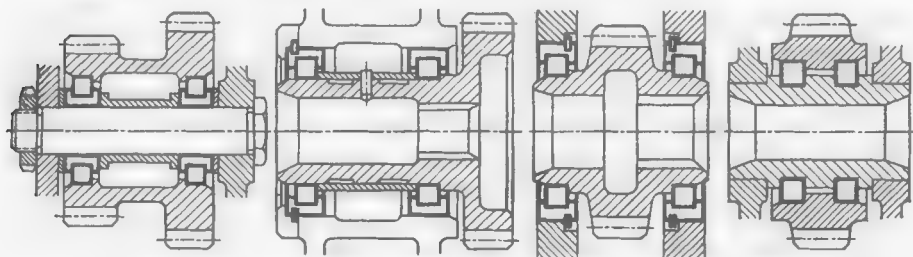
Fig. 262. Raceless and cageless installation of bearings

for uncritical bearings, the raceways being made of a simplified form. In the ball bearing of an auxiliary drive (Fig. 261g) the races are die-forged of sheet steel, ground and cyanided.

Figure 262 illustrates examples of the raceless and cageless installation of roller bearings in gear drive units.

The range of standard cylindrical rollers is as follows: $d = l = 5$, 6.5, 7.5, 9, 10, 11, 12, 13, 14, 15, 17, 18, 20, 22, 23, 24, 25, 26, 28, 30, 32, 34, 36, 38, 40.

The tolerances on the roller diameters are from -4 to $+16$ μm. In the case of cageless installation it is necessary to group rollers with the deviations in dimensions in a set not exceeding the values given in the table below.

Roller diameter, mm	Maximum deviation, μm	
	in diameter	in length
< 18	1	6
18-30	2	8
> 30	3	10

(j) Adjusting the Axial Position of Shafts

The adjustment is usually done by means of a nut and changeable sized washers mounted behind the outer *1* (Fig. 263a) or inner *2* (Fig. 263b) races of the bearing.
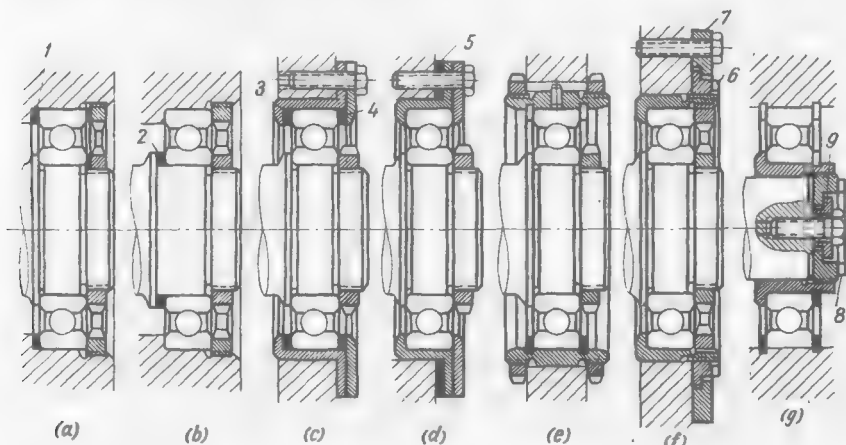
Fig. 263. Adjusting the axial position of shafts

When the race in the housing is tightened by a disk (Fig. 263c), two sized washers *3* and *4* are required.

In the design shown in Fig. 263*d* the shaft position is adjusted by installing changeable washer *5* behind the flange of the intermediate housing.

The shortcoming of these designs is that the unit has to be disassembled each time it needs adjustment. These methods are used when the adjustment is done only once (when the machine is being assembled) or infrequently.

In the design in Fig. 263*e* the shaft position is adjusted, without disassembling the unit, by means of two nuts placed on the intermediate housing of the bearing. The shortcoming of the design is the need to manipulate both nuts, which is not always possible for design considerations.

In a more convenient design (Fig. 263*f*) adjustment is done by turning nut *6* mounted on the intermediate housing of the bearing and locked in the axial direction by ring *7*.

In the design shown in Fig. 263*g* the adjusting unit composed of nut *8* and ring *9* is transferred to the end face of the shaft and acts on the inner race of the bearing.

In the designs in Fig. 263*f, g* there is an inevitable axial clearance in the adjusting device, this clearance being made up of the clearance in the thread and that between the shoulder on the nut and the limiting rings *8* and *9*. These methods do not provide locking without clearance.

3.15. High-Speed Bearings

According to their rotational speed rolling-contact bearings are classified into the groups given in the table below.

Speed	$nd \cdot 10^{-6}$, mm	v_{per}, m/s
Normal	0.1-0.5	5-25
Increased	0.5-1	25-50
High	1-2	50-100
Superhigh	> 2	> 100

The first group includes standard bearings for which the mean value of nd equals 0.3, the maximum value being 0.5-0.6 (for small-diameter ball and roller bearings of light series).

Higher rotational speeds can be attained if the bearing design and lubrication methods are significantly changed.

Superhigh-speed bearings ($nd > 2$) are now in the stage of experiment and met with in mechanical engineering only in unique designs.

High-speed shafts are, as a rule, supported by radial and radial thrust ball bearings which have the minimum coefficient of friction due to the point contact of their balls. Roller bearings with light rollers are used for high radial loads.

(a) Design of Supports with High-Speed Bearings

The generation of heat in a bearing increases in proportion to the load on it, and its durability diminishes approximately in proportion to the cube of the load. For this reason, when designing supports the principal attention must be given to reducing the working loads and eliminating internal and parasitic loads.

The working loads can be reduced by:

(1) decreasing the weight of the rotor and of the rotating parts linked with it;

(2) thoroughly balancing statically and dynamically the rotors;

(3) eliminating the simultaneous action of radial and axial loads (by loading some bearings only with radial forces, and others, with axial forces);

(4) installing several bearings in parallel, ensuring a uniform load distribution among them.

In gear transmissions it is expedient to relieve high-speed shafts of radial loads by means of a multiple-limb drive (i.e., drive through several gears arranged symmetrically around the driven shaft).

Parasitic loads can be eliminated by:

(1) completely relieving the bearings of the thermal forces resulting from the thermal deformations of the system;

(2) improving the manufacturing accuracy of the rolling elements, keeping to close tolerances the cylindricity of the seating surfaces, and eliminating their misalignment, nonparallelism and distortion causing additional loads on the bearings;

(3) improving the rigidity of shafts and housings with a view to preventing elastic deformations and the resulting edge pressures;

(4) using moderate fitting interferences in order to prevent the pinching of the rolling elements.

It is good practice to install bearings on spherical supports (the use of self-aligning spherical bearings is not recommended because the shape of their outer raceways is unfavourable for contact strength).

In twin radial and radial thrust bearing installations it is expedient to use a light spring preloading to take up the clearances and prevent the gyroscopic spinning of the balls of the unloaded bearing in the pair.

To decrease the peripheral velocity and the centrifugal forces of the rolling elements it is advisable to reduce the diameter of the journals to the limits permitted by the strength and rigidity of the shaft and the load-carrying capacity of the bearings.

(b) Design Features of Bearings

High-speed bearings are manufactured to the highest grades of accuracy. The accuracy of the shape of the rolling-contact surfaces and of the dimensions of the rolling elements is especially important. The rolling elements are grouped into sets having diametral deviations not exceeding 0.5 μm.

To account for heavier temperature conditions, the clearances between the rolling elements and raceways are made by 20-30 per cent larger than in bearings of ordinary speed capacity.

In ball bearings loaded with small forces the radius of the raceways is made equal to 1.05-1.1 of the ball radius in order to reduce friction.

The ball diameter and the mean bearing diameter are reduced to lessen the centrifugal forces, which in high-speed bearings may considerably exceed the working loads, and also to decrease the generation of heat, which is proportional to the fourth power of the peripheral velocity of the rolling elements.

Eq. (3.15) for the centrifugal force of the ball may be written as

$$P_{cf} = Ca^3 \frac{d_m^4}{\left(1 + \frac{1+a}{1-a}\right)^2}$$

where $d_m = \frac{d}{2}\left(\frac{D}{d} + 1\right)$ is the mean diameter of the bearing, $a = \frac{d_b}{d_m}$ is the ratio of the ball diameter to the mean bearing diameter, and C is a constant covering all constant factors.

In order to diminish the centrifugal force in high-speed bearings it is adopted that $a = 0.12$, $D/d = 1.6$, $d_m = 1.3d$ instead of $a = 0.18$, $D/d = 1.8$ and $d_m = 1.4d$ usual for bearings of the light series (Fig. 264a). Substituting these values into the above equation we get $P_{cf} = 0.00095d^4$ for the bearing with $a = 0.12$, and $P_{cf} = 0.0038d^4$ for the bearing of the light series. Hence, with the same d (Fig. 264b) the centrifugal force of the balls in the bearing with $a = 0.12$ is four times less than in the bearing of the light series.

The centrifugal forces can further be decreased by reducing d (Fig. 264c and d). When the diameter of the journal is equal to 0.8 and 0.6 of the initial diameter and $a = 0.12$, the centrifugal force is less than that in the light-series bearing by 10 and 30 times, respectively.
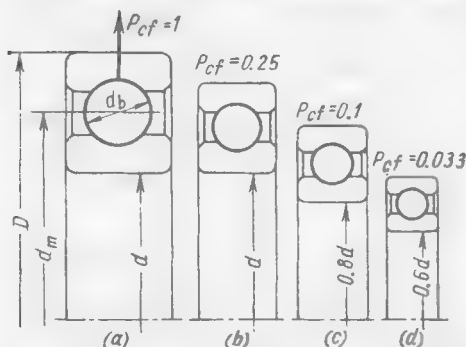
Fig. 264. Reducing the centrifugal force of balls

Roller bearings use hollow rollers with a ratio of their internal diameter to the external one of 0.4-0.5 (the gain as to the magnitude of the centrifugal forces is 30-40 per cent). The advantage of hollow rollers is that they can be cooled internally with oil.

(c) Cages

High-speed bearings are designed with rigid cages thoroughly balanced and centred on the inner (Fig. 265a, b) or outer (265c, d) bearing race.

The centring on the outer race facilitates the feed of oil into the bearing and improves the lubrication of the centring surface of the
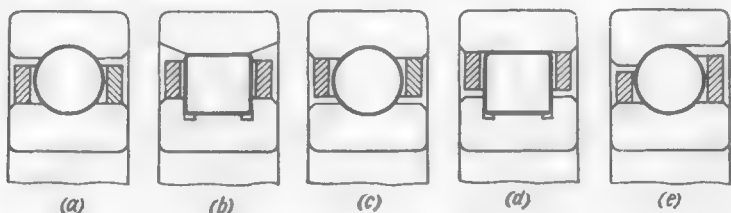
Fig. 265. Centring of cages

cage. The oil is withdrawn from the bearing by means of drainage grooves in the centring surface of the cage.

The centring on the inner race hampers the feed of oil into the bearing and impairs the lubrication of the centring surface. The outflow of oil from the bearing is free.

The peripheral velocities on the centring surfaces are the same when the centring is done on the outer and on the inner races. But the cages centred on the inner race wear out faster because in the process of wear the centre of gravity of the cage is displaced and the centrifugal forces are increased.

In the case of one-sided wear the centre of gravity of the cage shifts from the rotation axis to a distance a (Fig. 266a) equal to the sum of the wear depth and
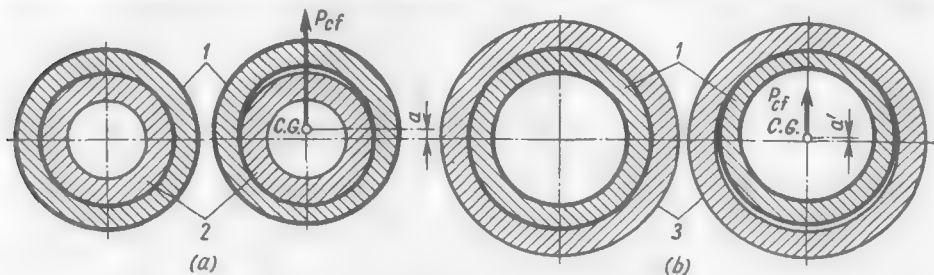
Fig. 266. Wear of cages with internal and external centring
1 — inner race; 2 — cage; 3 — outer race

the displacement of the centre of gravity of the cage due to the change in its shape caused by attrition. The centrifugal force P_{cf} produced due to the displace-

ment intensifies wear, which further increases the eccentricity and the cen-
trifugal force. In view of this the cage wear is intensified.

In cages centred on the other race (Fig. 266b) the displacement of the centre
of gravity of the cage due to its wear is directed oppositely to the geometrical
displacement of the cage. The total displacement a' is much less, the cage wear
takes a slower course and its centring is maintained for a longer time.

The cage centring in ball and roller bearings is mainly done on
the outer race. The inner race is used to centre cages made of a mate-
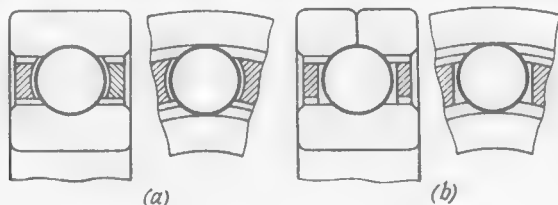
Fig. 267. Forms of ball seats

rial with a high coefficient of linear expansion (light alloys, plas-
tics), which may get pinched in the outer race when heated.

The cage centring on the inner race is also used in radial thrust
bearings (see Fig. 265e) where the shape of the raceways makes the
centring on the outer race difficult.
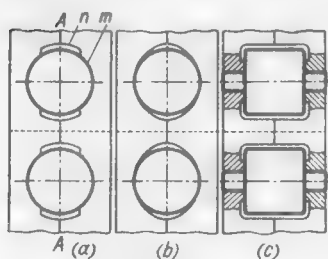
Fig. 268. Locking of rolling
elements in the cage seats

In radial ball bearings the cages are
split in the equatorial plane; the cage
halves are centred with respect to each
other and riveted together. The condi-
tions of assembly of roller radial thrust
and three-contact bearings permit the
use of solid cages which are more rigid
and easier to centre.

The walls of ball seats in split cages are
made spherical (Fig. 267a), this facilitat-
ing the formation of a hydrodynamic
film in the sections where the balls come
into contact with the cages. In solid
cages the ball seat walls are made cylindrical (Fig. 267b) to faci-
litate their machining and ease the assembly of the bearing.

The peripheral velocity of the ball rotation reaches its maximum
in the equatorial plane of symmetry AA of the bearing (Fig. 268a)
and may be very high (50-100 m/s) at high peripheral speeds of the
bearing. The peripheral velocity of the balls drops as the points on
their surface come closer to the rotation axis and becomes zero at
the poles of the balls. To reduce the losses due to friction it is advisa-
ble to locate the balls in their seats in sections m close to the poles,

and make relieving recesses in sections *n*. The same result can be obtained by making the seats elliptical (Fig. 268*b*).

In roller bearings it is advisable to locate the rollers in their cages by means of small diameter journals (Fig. 268*c*), the rollers being separated from the cage partitions by clearances.

Axial grooves provided on the internal and external surfaces of the cage are used to feed in and withdraw oil, the grooves being made in the partitions between the ball seats in a staggered order so as not to weaken the cage (Fig. 269*a*).

The inflow and outflow of the oil will be made easier if the noncentred surfaces of the cage are imparted a polyhedral (Fig. 269*b*, *c*),
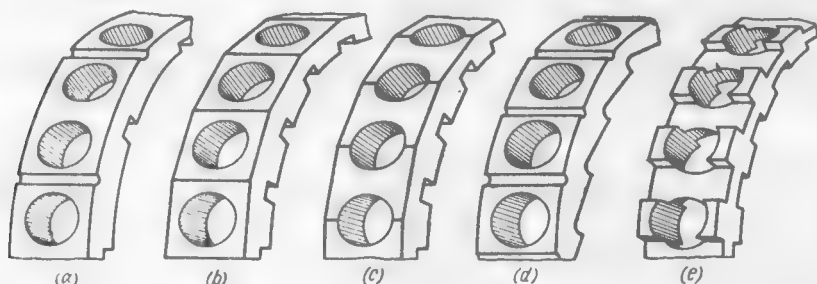
Fig. 269. Cages

saw-tooth (Fig. 269*d*) or shaped (Fig. 269*e*) form reinforced by local thickenings at places where the ball seats are arranged.

Cages intended to operate at temperatures less than 120°C are manufactured from heat-treated forged aluminium alloys, such as duralumin, and composite plastics (glass-fibre laminates, wood-resin laminates, teflon reinforced with fibre glass). To improve their antifriction properties, babbitt and bronze powders, graphite molybdenum disulphide and other hard lubricants are introduced into the compositions.

The cages of bearings operating at higher temperatures are made of lead or nickel brass, silicon bronze, antifriction cast iron, graphitized steel, copper-nickel alloys and heat-resistant plastics.

The best overall properties as to the wear and corrosion resistance are exhibited by the cages made of Monel metal (68% Ni, 28% Cu, 2.5% Fe and 1.5% Mn) and sintered porous bronze and copper-nickel alloys impregnated with teflon with additions of lead and MoS_2.

The active surfaces (centring portions, ball seat walls) of metal cages are machined to a finish not worse than that of the 12th class. In plastic cages the required smoothness is obtained by carefully machining and chrome-plating the surfaces of press moulds.

In cageless high-speed roller bearings the rollers are separated by stepped pins *1* (Fig. 270) rotated by two cup-shaped washers *2* rigidly connected to the inner race of the bearing. The pins are pressed by centrifugal forces against the raceways of the cup-shaped washers and are locked in the axial direction by the roller end faces.
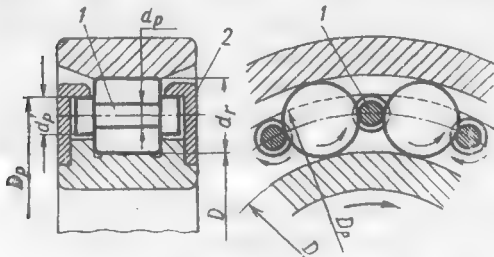
Fig. 270. Cageless roller bearing

The condition of pure rolling on the contact lines between the pins and rollers consists in the equality of the peripheral velocities of the pins and rollers

$$\omega_r \frac{d_r}{2} = \omega_p \frac{d_p}{2} \quad (3.29)$$

where d_r and d_p are the diameters of the rollers and pins, and ω_r and ω_p are the angular velocities of the rollers and pins, respectively, expressed as

$$\omega_r = \omega_0 \frac{D}{d_r} \quad (3.30)$$

and

$$\omega_p = \omega_0 \frac{D_p}{d'_p} \quad (3.31)$$

where ω_0 = angular velocity of the roller centres
D and D_p = raceway diameters of the inner race and cup-shaped washers
d'_p = diameter of the thickened portion of pins

Substituting the values of ω_r and ω_p from Eqs. (3.30) and (3.31) into Eq. (3.29), we obtain the condition of pure rolling

$$\frac{d'_p}{d_p} = \frac{D_p}{D}$$

The losses due to friction in cageless bearings are about two times smaller than in bearings with cages.

(d) Lubrication

The oil used to lubricate high-speed bearings must have a low viscosity, a gently sloping viscosity *versus* temperature characteristic, and the ability to form strong molecular films on metal surfaces.

The thermostability of the lubricant is of special importance. High-speed bearings are, as a rule, lubricated with finely sprayed oil which is rapidly oxidized because of the sharp increase of its surface of contact with air. Insoluble products of oxidation thicken the oil and form dense deposits on the metal surfaces of the bearings (coke-clogging of bearings).

Bearings operating at moderate temperatures ($<200°C$) are lubricated with refined mineral oils with antioxydant, anticorrosion and

wear-preventive additives [MoS$_2$, colloidal graphite, silicones, organic compounds of P (tricresylphosphate) and S (dibenzoyl-disulphide)].

At higher temperatures use is made of synthetic fluorocarbon, polyphenylether and paraffine lubricants (the maximum long-term temperature 300-350°C).

Finely dispersed oil is directly applied to the rolling-contact surfaces in strictly metered quantities. Surplus oil and also stagnation
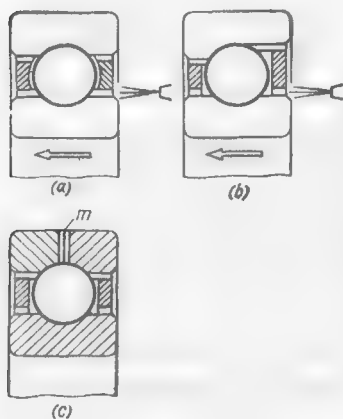
Fig. 271. Inflow and outflow of oil
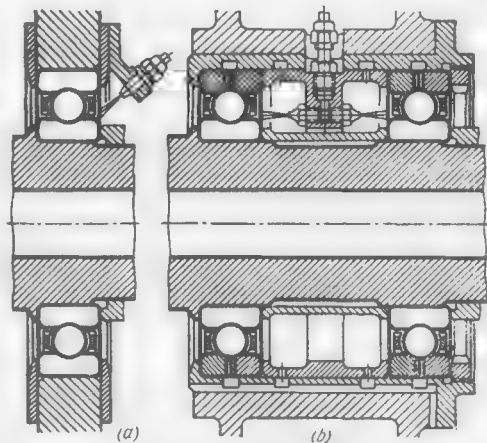
Fig. 272. Jet lubrication

phenomena (accumulation of the oil on the active surfaces, especially in the outer raceways) sharply increase the hydrodynamic losses, cause overheating and result in a rapid failure of the bearings (radial thrust ball bearings with open outer raceways have in this respect certain advantages over radial bearings).

Circulatory lubrication systems are used for the continuous withdrawal of heat from bearings.

In the case of jet lubrication the oil supplied by compressed air under a pressure of 5-10 kgf/cm^2 is applied onto the active surface of the inner race (Fig. 271a) so that the rotation of the rolling elements throws it to the periphery of the bearing. The used oil is removed through recesses in the external surface of the cage.

In bearings loaded with an axial force and in radial thrust bearings (Fig. 271b) oil should be supplied in the direction of the axial load (bright arrows). When the oil is fed in the opposite direction it is difficult for it to reach the contact points.

Oil is effectively withdrawn from the raceway in bearings with a split (in the equatorial plane) outer race. Oil flows outside through radial slots *m* provided at the joint of the half-races (Fig. 271c).

Figure 272 shows some examples of bearing units with jet lubrication.

The circulatory atomized lubrication system almost completely eliminates hydrodynamic losses, reduces the coefficient of friction and intensively withdraws heat from the bearing with moderate oil consumption.

In a special unit oil is atomized in a jet of dry air (moisture content not more than 1 g/m³). The particles of oil in the suspension are 0.01-0.1 μm in size. At increased temperatures some of the oil is present in the vapour phase.

The suspension is blown with the aid of a fan through the bearings. The content of oil in the suspension and the blowing rate must be kept strictly constant. The oil feed rate is usually 20-50 g/h.

In the case of nonrecovery lubrication fresh oil is continuously fed into the system while the used oil is drained into a sump.

In closed systems oil circulates along the following loop: atomizer → bearings → sump → filter → cooler → atomizer. Fresh oil should periodically be added to compensate for the losses. Sometimes an oil regenerating device is incorporated into the system (in series or in parallel).

Oil atomization in a jet of nitrogen completely eliminates oxidation and allows the working temperature to be increased by 50-80°C as compared with atomization in a jet of air. In practice, jet lubrication is usually used as it is simpler than atomized lubrication.

(e) Increasing the Cyclic Durability of Bearings

The durability of high-speed bearings is sharply reduced when their rotational speed is increased. A number of metallurgical and production measures are taken to prolong the service life of bearings.

Durability can be increased five or six times by vacuum pouring and repeated remelting of steel in vacuum. This produces a fine granular structure and frees the steel of hydrogen porosity and oxide and nitride inclusions which are the nuclei of fatigue cracks.

Steels having a stable austenitic-state interval within 500-550°C are subjected to a low-temperature thermomechanical treatment which additionally increases durability three or five times.

The elements of the bearings are thoroughly checked for defects (nonmetal inclusions, carbide segregation, carbide network, porous structure) by a number of methods of which the ultrasonic method is most sensitive.

Methods of forging the races have been developed, which ensure the arrangement of the metal fibres parallel to the active surfaces (Fig. 273a), thus appreciably increasing the cyclic strength as compared with that in the case of the fibre arrangements as in tubular (Fig. 273b) or upset (Fig. 273c) blanks.

Experiments show that the durability of bearings is significantly increased if the hardness of the rolling elements somewhat exceeds that of the races. For high-speed bearings the rolling elements are grouped so that the hardness variations of the elements in a set do

not exceed 0.5 Rockwell hardness C unit, their mean hardness being by 2-2.5 Rockwell hardness C units higher than that of the races.
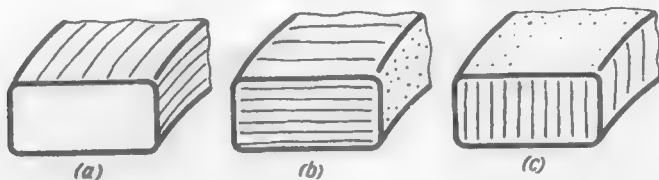
Fig. 273. Arrangement of fibres in bearing races

The active surfaces of bearings should be strengthened by building up residual compressive stresses in their surface layers.

The races can be strengthened by *roll-burnishing*, by lathe-turning their heat-treated surfaces with *cemented-carbide tools* under heavy machining conditions, etc.

The balls are subjected to a *thermal strengthening* based on the artificial retardation of the martensite transformation in the surface layer. The surface of the balls is saturated with nitrogen which sharply reduces the temperature of martensite formation. When hardening is done in oil at the usual cooling rates (100-150°C per second) the martensite first forms in the core. The external layer saturated with nitrogen maintains for some time its austenitic structure and plastically deforms under the effect of the volumetric expansion of the core. As the temperature drops further, martensitic transformation takes place in the surface layer, attended by an increase in its volume. As a result of the interaction with the previously solidified core, in the surface layer there develop high residual compressive stresses (80-100 kgf/mm^2) which noticeably increase the cyclic strength.

3.16. High-Temperature Bearings

Bearings manufactured from ordinary ball bearing steels satisfactorily operate at temperatures <200-220°C. At higher temperatures martensite is transformed into temper troostite. This is attended by a drop in hardness and a sharp reduction in the operating capacity of the bearings.

Figure 274 shows the change in the load-carrying capacity of bearings made of typical bearing steel grades depending on their hardness (the carrying capacity with the maximum attainable hardness for a given steel is taken as 100 per cent).

It can be seen that a decrease in hardness even by a few Rockwell hardness C units sharply diminishes the carrying capacity. When the hardness of steel *1* drops by four Rockwell hardness C units, the carrying capacity decreases to 50 per cent of the initial value. For steel grades *2* and *3* an identical reduction of the carrying capacity occurs when their hardness diminishes by six or seven Rockwell hardness C units.

A Rockwell hardness C of 58-60 may be considered the lower hardness limit at which a sufficiently high carrying capacity is maintained for the majority of steel grades.

Bearings operating at temperatures higher than 250°C are manufactured from heat-resistant alloys which retain their hardness within a wide temperature range (Fig. 275).
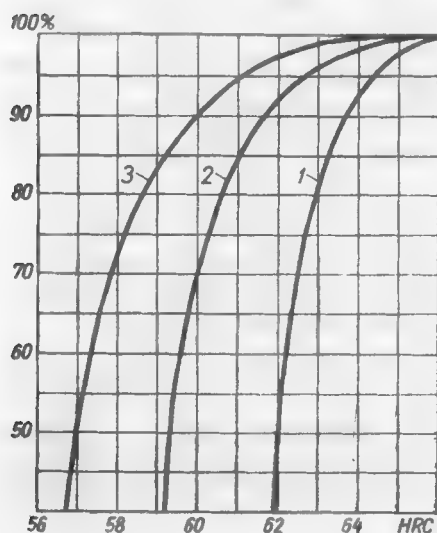
Fig. 274. Effect of hardness on the load-carrying capacity of bearings
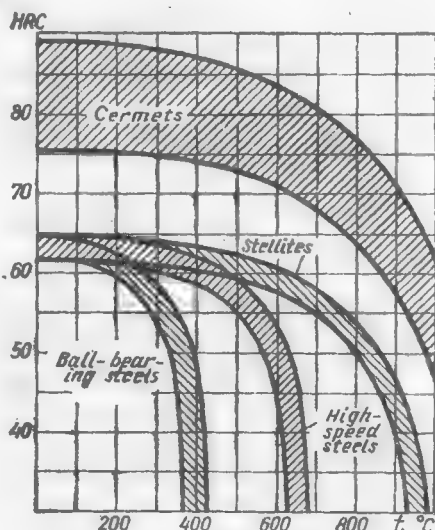
Fig. 275. Effect of temperature on the hardness of bearing materials

The alloys used to make high-temperature bearings are arranged in the order of their heat-resistance as follows:

(1) martensitic and ledeburitic steels alloyed with chromium, tungsten and silicon;

(2) high-tungsten tool steels (high-speed steels);

(3) Stellites;

(4) metal ceramic hard alloys.

The first group includes high-chromium steel grades X12M and X12Ф1, stainless chromium steel with additions of Mo, alloyed tool steel grades XBГ and XB5, and silchrome steels (Table 39).

The increased heat resistance of high-chromium steel is due to the presence of refractory chromium carbides. They maintain the hardness required for the bearings (>60 Rc) up to a temperature of 300-350°C.

Silchrome steels are martensitic steels (self-hardening in air).

For the manufacture of high-temperature bearings wide use is made of *high-speed tungsten steels* (0.6-1.5% C, 9-18% W, $\approx 4\%$ Cr and 1-2% V).

The alloying elements, being active carbide-forming agents, bind almost all carbon into refractory carbides. Carbides of W and Mo

Table 39

Steels of Increased Heat Resistance

Grade	Composition, %						
	C	Cr	Si	Mn	Mo	V	other elements
X12M	1.5	10	<0.4	<0.4	0.5	0.3	—
X12Ф1	1.3	11	<0.4	<0.4	—	1	—
XBГ	1	1	<0.4	1	—	—	1.5% W
XB5	1.5	0.5	<0.4	<0.4	—	0.2	5% W
Silchrome steels							
X7MC	0.15	7	1.5	<0.7	0.5	—	—
X10C2M	0.4	10	2	<0.7	0.5	—	—
X13H7C2	0.3	13	2	<0.7	0.8	—	7% Ni

are especially heat-resistant: they retain their hardness up to temperatures of 550-600°C (after which the carbides coagulate and the hardness drops).

The composition of high-speed steel grades of the Soviet and foreign make is given in Table 40.

Table 40

High-Speed Steels

Grade	Composition, %							Long-term working temperature, °C ($\approx$)
	C	W	Mo	Cr	V	Co	Other elements	
3X2B8	0.3	8	1	2.5	0.4	—	—	350
P9	0.9	9	—	4	2	—	—	380
P18	0.9	18	—	4	1-1.5	—	—	450
P9K10	0.9	9	—	4	2	10	—	500
P18K5Ф2	0.9	18	—	4	2	5	—	550
Halmo	0.6	—	5	4.5	0.5	—	1.2% Si	320
AISIM10	0.85	—	8	4	2	—	—	420
AISIM1	0.8	1.5	8	4	1	—	—	450
AISIM2	0.8	6	5	4	2	—	—	500
WB-49	1.0	7	4	4.5	1	6	—	550

To prevent the coagulation of carbides and increase impact strength it is advisable to reduce somewhat the content of C (to 0.6-0.8 per cent) and V (to 0.5-1 per cent) as compared with those in standard steel grades.

High-speed steel is hardened in oil from a temperature of 1270-1290°C and then subjected thrice to tempering at 550-570°C with a 1-hour holding time and also to treatment by cold (to reduce the amount of residual austenite).

Almost all grades of high-speed steel can be strengthened by the low-temperature thermomechanical treatment.

Depending on the content of W, the specific weight of high-speed steel varies within 9-12 gf/cm³.

Stellites (alloys of Cr, W and Mo with Co or Ni as the base) possess a high hardness (60-65 *Rc*) maintained up to temperatures of 550-600°C and effectively resist hot corrosion. They require no heat treatment.

The composition of Stellites of the Soviet and foreign make is given in Table 41.

Table 41

Stellites

Grade	Composition, %							
	C	Co	Ni	Cr	W	Fe	Mo	other elements
B2K	2-2.5	47-53	2	27-33	13-17	1	—	1.2% Si, 2% Mn
B3K	1-1.5	58-62	2	28-32	4-6	—	—	2.5% Si
Haynes Stellite Star	2.5	53-55	2.5	32	17	3	—	—
Hayness Stellite 98M2	2.0	42-43	3.5	30	18.5	2.5	—	—
Haynes 25	0.1	48-49	10	20	15	3	—	1% Si, 1.5% Mn
Rene 41	0.1	11	63-64	10	—	—	10	3% Ti, 1.5% Al
M252	0.15	10	59-60	20	—	—	10	3% Ti, 1% Al

Cobalt-base alloys are used in cast form. Nickel Stellites can easily be forged, this appreciably impoving their mechanical properties.

The specific weight of Stellites is 10-12 gf/cm³.

The use of Stellites is limited by their high cost.

Metal ceramic hard alloys are composed of 85-96 per cent of W and Ti carbides with a bond of metallic Co taken in the amount of 4-15 per cent.

The most popular are tungsten-carbide alloy grades BK4, BK6 and BK8 (the figures after the letter K indicate the per-cent content of Co, the balance being the carbides of W).

Alloys with a reduced content of Co are harder but more brittle than those with a high content of Co.

High hardness distinguishes the tungsten-titanium-carbide alloy grades T30K4, T15K6, T14K8 and T5K10 (the figures after the letters K and T indicate the per-cent content of Co and Ti, respectively, the balance being the carbides of W).

The highest heat resistance with a good hardness is possessed by tungsten-titanium-tantalum-carbide alloy grades TT7K12, TT7K15 (the figure after the letters TT indicates the total content of Ti and Ta carbides; usually the content of carbides of Ta is 3.5 per cent).

The specific weight of metal ceramic alloys is 11-14 gf/cm^3.

Despite their high hardness (75-85 *Rc*) and heat resistance, the load carrying capacity of bearings made of metal ceramic alloys is negligible because of the brittleness, low antifriction properties and low cyclic strength of metal ceramic.

The manufacture of bearings from *cermets* is in the experimental stage. These are sintered alloys of ceramic materials (carbides, oxides, borides and silicides of metals) with powders of Ni, Co, Cr and Mo (in a proportion of approximately 1 : 1).

Cermets combine the hardness and heat resistance of ceramic materials with the plasticity and heat conductivity of metals. As to hardness, they occupy an intermediate position between tool steel and metal ceramic alloys.

The essential advantage of cermets is their low specific weight coming to 6-7 gf/cm^3.

The cages for high-temperature bearings are made of Monel metal, beryllium bronze, sulphidized steel grade P9 and heat-resistant self-lubricating materials (cabron graphite, pressed compositions of MoS_2 with bronze and nickel powders, etc.).

Bearings operating at temperatures below 350°C are lubricated with liquid thermostable synthetic oil. Electrolytic deposition of gallium on the frictional surfaces to a depth of 25-30 μm ensures stable operation of bearings at temperatures up to 400°C. The shortcoming of this method is that the lubricant cannot be renewed. At still higher temperatures solid greases are used.

Self-lubricating properties are exhibited by the compounds of Mo, W, V. Ti and Ta of flaky microstructure: sulphides (MoS_2, WS_2, TiS_2, Ti_2S_3), selenides (WSe_2, $TaSe_2$, VSe_2) and tellurides ($MoTe_2$, $TiTe_2$). The heat resistance of such lubricants is 400-500°C.

A higher heat resistance is possessed by lubricants based on oxides of Pb and Cd (PbO, CdO) and fluorides of Ca, Ba, Be (CaF_2, BaF_2, BeF_2).

The lubricating properties, cohesion strength with metal surfaces and temperature stability can appreciably be increased if small quantities of Fe and Cu and, especially, Au, Pt and Pd are introduced.

The best properties are observed in lubricants based on MoS_2, Fe and Pt (80-90% MoS_2, 10-15% Fe and 2-4% Pt).

In the case of lubrication by *transfer*, solid grease is packed into recesses (pockets) made in the ball seats of the cage (Fig. 276a). The rotating balls entrain particles of grease and place it in a thin layer onto the rolling-contact surfaces.

It is good practice to increase the capacity of the grease pockets in order to enhance the bearing service life (Fig. 276b). In the design shown in Fig. 276c the ball seats have press-fitted cylinders of solid grease which simultaneously lubricate the balls and the centring surface of the race.

Sometimes the cage is made entirely of self-lubricating materials with a silicate bond (Fig. 276d) or metal reinforcement (Fig. 276e); the latter design is adapted to centring on the inner race.

In the case of *ventilation powder lubrication*, a suspension of highly dispersed particles of graphite, MoS_2, WS_2, PbO or CdO is blown
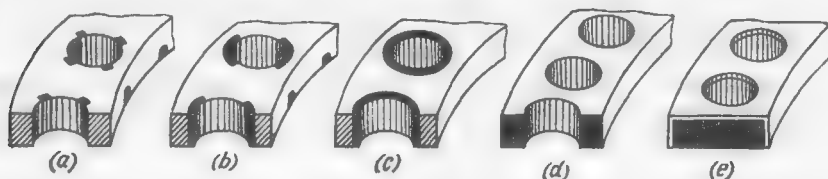
Fig. 276. Cages with solid lubricants

through the bearings with a jet of air or nitrogen. The concentration of the suspension and the velocity of the carrier gas must be kept within narrow limits so as to prevent the sticking of the lubricant to the metal surfaces.

In bearings operating at the highest temperatures the active surfaces are coated with a thin (15-20 μm) layer of sinterable solid grease.

Coatings of microfibrous colloidal hydrate of aluminium oxide AlO(OH) (20%) and MoS_2 (80%) are distinguished by their low coefficient of friction ($f = 0.02\text{-}0.03$ at 200-300°C) and good adhesion to metal. An aqueous solution of AlO(OH) with a suspension of MoS_2 (particle size ≈ 0.02 μm) is placed on the metal surface, dried and heated to 230-280°C, which results in the formation of a strong surface film that retains its lubricating properties up to 400°C.

Sinterable coatings based on lead oxide PbO can operate at 600-650°C. To reduce the melting point, the lead oxide is mixed in the eutectic proportion with fusible silicate of Pb (tetrasilicon lead). The aqueous suspension of the mixture is placed on the metal surface, dried and roasted at 750-800°C. This produces a strong glazed layer on the surface.

The temperature stability of glazes with CaF_2 and BaF_2 as their base reaches 750-800°C.

The service life of glazed coatings is limited due to the small store of the lubricant and the fact that it cannot be renewed. The durability of glazed bearings operating at 600-650°C (red heat region) does not exceed several dozens of hours.

Lubrication with powders is a new trend in the high-temperature bearing technology. These powders consist of regular microspheres (diameter 1-3 μm, deviations in the size of spheres in the powder < 10 per cent) made of very hard (800-1000 VPH) and heat-resistant

materials (tungsten alloys, carburized carbonyl iron). The carrying surfaces of bearings are made of materials of the same hardness (nitrided steel, steel coated with metal ceramics and Stellites). The diametral clearance in the bearings $\psi = 0.0002\text{-}0.0005$.

In such bearings the carrying surfaces partly roll over the microspheres and partly slip on the extremely mobile powder layer (pseudo-liquid layer). The coefficient of friction $f = 0.01\text{-}0.05$ (higher than in bearings of pure rolling, but much less than in bearings with dry-film lubricants). The coefficient of static friction is equal to the coefficient of friction in motion, in view of which the starting torque is insignificant.

The thermal stability of the bearings with a microspherical powder grease depends on the material of the spheres and the carrying surfaces. When the bearings are manufactured from tungsten alloys, their thermal stability is 450-500°C.

Lock (Snap) Rings

For the axial fixing of parts fitted on shafts or in holes wide use is made of *lock* (snap) *rings* which are split spring rings inserted with a radial interference into grooves cut in the shaft (or in the hole) and retained there by elastic forces.

Snap rings are convenient to install and occupy small space. Their use makes it unnecessary to design shafts (holes) with steps, shoulders or threads for lock nuts. Snap rings can endure rather significant axial loads.

Their shortcoming is that they weaken parts by the inevitable annular grooves, especially in shafts.

The fitting interference of the rings installed on shafts is weakened by centrifugal forces. For very high rotational speeds the rings must be safeguarded against leaving the grooves.

Ordinary-purpose snap rings are manufactured from manganese spring steel grade 65Γ or chrome-manganese steel grade 50ХГ and are subjected to hardening and medium tempering to 45-50 Rc, a heat treatment common for spring steel.

Rings which must be especially corrosion-resistant are made of stainless steel grade 3Х13 and beryllium bronze grade БрБ2. Chrome-silicon-vanadium and silicon-tungsten steels are used to make rings operating at elevated temperatures.

By the method of assembly snap rings are classified as rings of *axial* and *radial assembly*.

By the method of their manufacture snap rings are divided into lathe-turned, wire, and punched.

4.1. Lathe-Turned Rings

These rings are manufactured from sheet or tubular blanks. After heat treatment the end faces and cylindrical seating surfaces of the rings are ground.

This method is mainly used to make rings of large diameter (on the average >50 mm). The rings usually have a rectangular cross-section (Fig. 277) which is kept constant over the entire circumference (Fig. 278a). By using eccentrically bored tubular blanks the rings can be imparted a more rational shape that gives equal resistance to bending (Fig. 278b).

Structural proportions. Figure 279*a*, *b* illustrates the basic proportions of *internal snap rings*, i.e., the rings fitted into housings.

When inserting the ring into the groove, it is compressed so as to make it pass through the housing bore of diameter D. The stresses
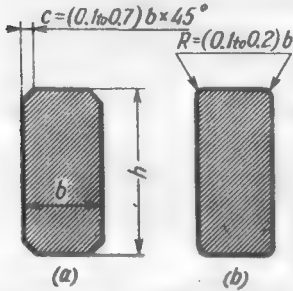
Fig. 277. Cross-sections of snap rings
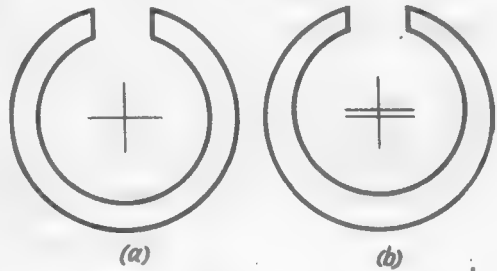
Fig. 278. Rings of constant (*a*) and variable (*b*) height

produced in the ring in this case reach their maximum in the section opposite to the cut. The magnitude of the stresses is determined by the ratio of the height h of the ring to its mean diameter ($\approx D$) and by the degree of compression of the ring during its installation,
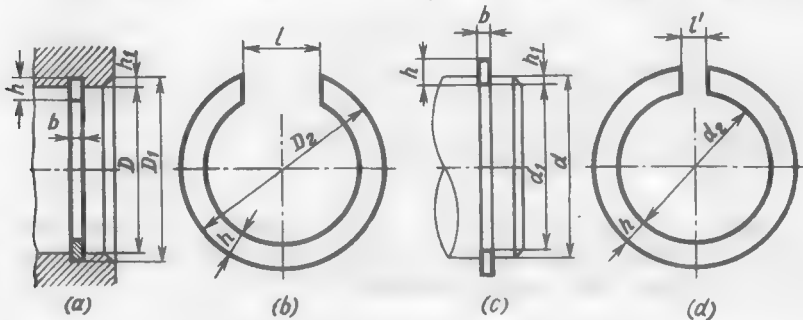
Fig. 279. Parameters of snap rings of rectangular cross-section

i.e., by the ratio of the external diameter D_2 of the ring in a free state to the diameter D of the housing bore. The stresses do not depend on the ring thickness b.

With the ordinary values of D_2/D the maximum height h of steel rings, conditioned on their bending strength, is equal to $0.15D$. In practice it is adopted that

$$h = (0.08 \text{ to } 0.15)\, D \qquad\qquad (4.1)$$

where the lower limit refers to large-diameter rings ($D > 50$ mm) and the upper limit, to small-diameter rings ($D < 50$ mm).

Satisfactory results within the range $D=10\text{-}200$ mm are given by the formula

$$h = 0.4\, D^{2/3}$$

The thickness b of the ring can vary within wide limits. Usually $b = 0.4\, h$. Substituting into this relation the value of h from Eq. (41), we get

$$b = (0.03 \text{ to } 0.06)\, D$$

where the lower limit refers to large-diameter rings and the upper limit, to small-diameter ones.

The depth h_1 of the groove in the housing is, on the average, equal to $(0.25 \text{ to } 0.3)\, h$. The external diameter of the groove is

$$D_1 = D + 2\,(0.25 \text{ to } 0.3)\, h$$

Substituting into this equation the value of h from Eq (4.1), we get

$$D_1 = (1.05 \text{ to } 1.09)\, D \tag{4.2}$$

where the lower limit refers to large-diameter rings and the upper limit, to small-diameter ones.

In order to obtain the required radial interference, the external diameter D_2 of the ring (Fig. 279b) is made slightly larger than the groove diameter D_1

$$D_2 = (1.03 \text{ to } 1.05)\, D_1$$

where the lower limit refers to rings of small diameter and the upper limit, to large-diameter rings. If the value of D_1 from Eq. (4.2) is substituted into this expression, we find that

$$D_2 \approx 1.1\, D \tag{4.3}$$

The width l of the cut in a free state is selected so that when the ring ends are closed the external diameter D_2 of the ring is reduced at least to the housing bore diameter D, i.e.,

$$l \geqslant \pi\,(D_2 - D) = 0.1\,\pi D \approx 0.3\, D$$

Since the closed ring has no correct cylindrical shape, we adopt with reserve that

$$l = (0.35 \text{ to } 0.4)\, D$$

To make the cut wider than $0.4\, D$ is not recommended. An unskilled worker may compress the ring until the ends are tightly closed and thus break it.

When the ring is fitted into the groove the cut width slightly diminishes (approximately in the ratio D_2/D_1, i.e., 1.03-1.05 times).

External snap rings (i.e., the rings mounted on shafts) are expanded during installation so that they can pass over the shaft diameter d (Fig. 279c, d). Assuming that $h = (0.08 \text{ to } 0.15)\, d$ and the

groove depth $h_1 = (0.25$ to $0.3)\,h$, we obtain the internal groove diameter

$$d_1 = d - 2\,(0.25 \text{ to } 0.3)\,h = (0.91 \text{ to } 0.95)\,d \qquad (4.4)$$

where the lower limit refers to rings of small diameter and the upper limit, to large-diameter rings.

To obtain the required radial interference, the internal diameter d_2 of the ring in a free state (Fig. 269d) is made to be

$$d_2 = (0.95 \text{ to } 0.97\,)\,d_1$$

where the lower limit refers to large-diameter rings and the upper limit, to small-diameter ones.

Substituting the value of d_1 from Eq. (4.4), we get

$$d_2 \approx 0.9d \qquad (4.5)$$

In this case the width l' of the cut is only conditioned on the convenience with which the ring can be removed. For rings of small
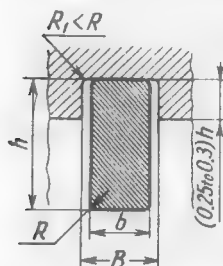
Fig. 280. Grooves for snap rings
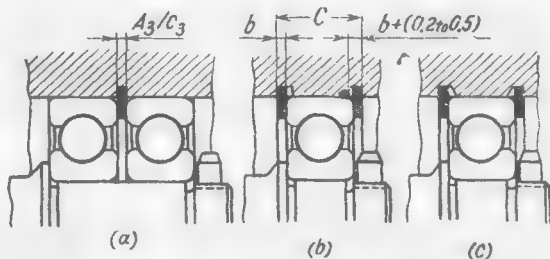
Fig. 281. Clearances in grooves

diameter $l' = 5$-10 mm and for those of large diameter $l' = 10$-20 mm. When the ring is fitted into the groove the cut width slightly increases (by 3-5 per cent).

The shape of grooves for internal and external snap rings is shown in Fig. 280. The radius R_1 at the root of the groove is made as large as possible, but less than the leg c of the chamfer or the radius R on the ring edges (see Fig. 277a, b) so that the ring tightly fits against the walls of the groove in extreme axial positions and has its cylindrical surface lying on the bottom of the groove.

The groove width B is selected depending on the operating conditions of the ring. When accurate axial locking in both directions is required (Fig. 281a) the ring is inserted in the groove by a slide fit (usually A_3/S_3). The groove width is immaterial in the case of rings loaded with unidirectional forces (Fig. 281b). The locking accuracy is determined here not by the ring clearance in the groove but by the distance C between the end faces of the grooves, which

take up axial loads. In this case the groove width is made by 0.2-0.5 mm larger than the ring thickness. The inactive groove edges are sometimes bevelled (Fig. 281c) to facilitate the groove cutting and control.

Carrying capacity. The carrying capacity of snap rings (their resistance to axial loads) is determined on the basis of an elementary scheme, assuming that the ring operates in shear (Fig. 282a).
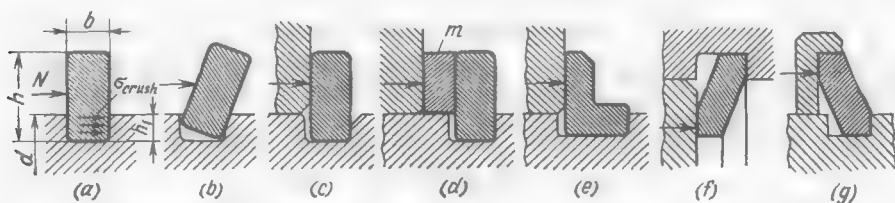
Fig. 282. Calculating snap rings for strength

The maximum axial force the ring can withstand is

$$N = \pi db\tau \tag{4.6}$$

where d = diameter of the shaft (or of the housing bore for internal rings), mm

b = ring width, mm

τ = shear strength of the ring material, kgf/mm² (for ordinary spring steel $\tau = 80\text{-}100$ kgf/mm²)

With the average value of $b = 0.03d$

$$N \approx 0.1D^2\tau \tag{4.7}$$

The limiting axial force conditioned on the crushing strength of the groove walls is

$$N \approx \pi \, dh_1\sigma_{crush} \tag{4.8}$$

where h_1 is the groove depth in mm and σ_{crush}, the crushing strength in kgf/mm² ($\sigma_{crush} \approx 100$ kgf/mm² for improved structural steel).

With the average values of $h_1 = 0.3h$ and $h = 0.1d$

$$h_1 = 0.03d$$

and

$$N \approx 0.1D^2\sigma_{crush} \tag{4.9}$$

It can be seen from the comparison of Eqs. (4.9) and (4.8) that when $\tau \approx \sigma_{crush}$ (steel rings in steel shafts) the calculations for shear and for crushing yield about the same values of N.

If the groove is made in a soft material, the most important factor are the crushing stresses on the groove walls.

Since the calculations for shear are arbitrary, Eqs. (4.6) and (4.8) give exaggerated values of N even if large factors of safety are introduced.

Experience shows that the skewing of the ring (at first within the axial clearance in the groove) which concentrates the load at the groove edge (Fig. 282b) is of decisive importance for strength. Since the resistance to crushing of the hardened ring is higher than that of the groove material, the groove edge is crushed and the ring twists out of it. Even if the ring remains in the groove, the joint fails because of the disturbed locking accuracy.

The defect rapidly progresses if the axial load is of dynamic nature.

The strength of lock joints can be improved by increasing the hardness of the groove walls (for example, by carburizing or nitriding the shaft), reducing the axial clearance in the groove and enlarging the ring thickness and the groove depth. However, a deeper groove will weaken the shaft and intensify the bending stresses in the ring during assembly.

Chamfers on the edges of the groove and of the part that transmits the axial force (Fig. 282c) impair the strength of the joint. The edges should be sharp. If the edge of the part is chamfered or filleted (races of rolling-contact bearings), an intermediate washer m (Fig. 282d) with sharp edges should be mounted between the part and the snap ring.

L-shaped snap rings (Fig. 282e), in which the bending moment of the axial force is taken up by the cylindrical portion of the ring resting against the groove bottom, have an increased load-carrying capacity.

The strength of lock joints with internal snap rings can be improved by tapering the ring (Fig. 282f). The axial force wedges the ring radially against the bottom and wall of the groove.

In the case of external snap rings this method can be used only if the ring is enclosed into a cup-shaped part (Fig. 282g).

It has been established experimentally that snap rings of rectangular cross-section reliably operate in steel shafts without being wrenched out (even with large clearances in the groove) if the nominal shear stress as illustrated in Fig. 282a does not exceed 2 kgf/mm².

Substituting this value in Eq. (4.6) we obtain the permissible load in kgf

$$N = 2\pi \, db$$

With the ordinary value of $b = 0.03d$

$$N = 0.2d^2$$

If the load is of dynamic nature, the value of N should be approximately halved. When snap rings are installed in light-alloy housings, account should be taken of the diminished crushing strength of these alloys and the value of N decreased 3-4 times.

Installation and removal. During assembly internal snap rings are compressed until their ends touch and inserted slantwise into the housing bore. If the groove is close to the end of the bore, the part of the ring opposite to the cut is seated in the groove (Fig. 283a) and the rest of the ring introduced by rotating it about this point as about an axis.

External snap rings are fitted on in a similar manner (Fig. 283c).

To facilitate assembly the edges of the housing bores and shafts are chamfered, usually at an angle $\alpha = 30°$ (Fig. 283a, c). Best of
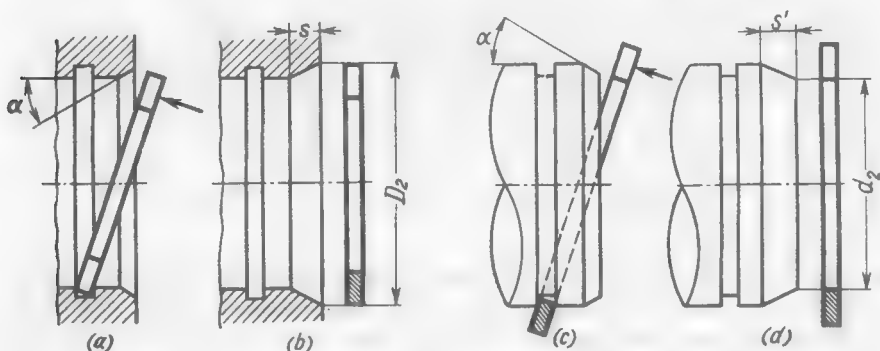
Fig. 283. Installation of snap rings

all, if the inlet diameter of the chamfer in the bores is equal to the external diameter D_2 of the ring (Fig. 283b), and on shafts, to the internal diameter d_2 of the ring in its free state (Fig. 283d).

The length of the chamfer is $s = \dfrac{D_2 - D}{2 \tan \alpha}$ for internal rings and $s' = \dfrac{d - d_2}{2 \tan \alpha}$ for external rings. Using Eqs. (4.3) and (4.5) and taking $\alpha = 30°$, we obtain, respectively, $s = 0.1D$ and $s' = 0.1d$. Sometimes, dimensions do not allow such large chamfers.

Some commonly used assembly fixtures are illustrated in Fig. 284. Internal snap rings 2 (Fig. 284a) are placed in bushing 1 which has a gently sloping tapered hole and a centring recess for the part and are pushed into the groove by means of rod 3. External snap rings 5 (Fig. 284b) are fitted onto tapered mandrel 4 which is centred from the shaft bore (or centre) and pushed into position by bushing 6.

These fixtures are rather cumbersome because the relation $l_1 \geqslant l$ has to be maintained, where l is the distance from the groove to the ring in initial position and l_1, the length of the entering portion of the rod or the bushing.

Internal snap rings can be removed easier if the parts are provided with radial holes m (Fig. 285a) or milled recesses n (Fig. 285b) or end

slots *q* (Fig. 285*c*) through which the ring is compressed before remov-
al. External snap rings are taken off with the aid of grooves *t*
(Fig. 285*d*) milled in the shaft, through which the ring is expanded
by means of a screw driver.

At least three holes or slots are required to remove the rings.
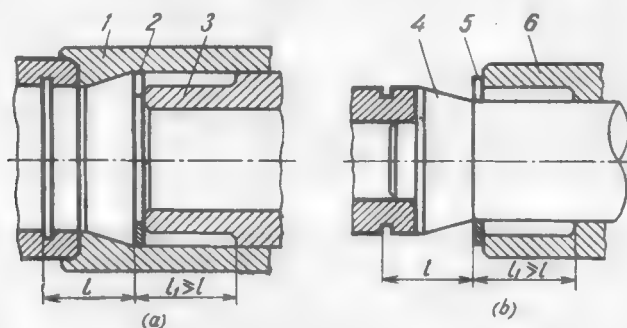
Fig. 284. Fixtures for installation of snap rings

All the above methods complicate the design and are not always
applicable because of the shape of parts.

Pulling elements provided on snap rings make special fixtures
unnecessary and ease the assembly in operational conditions and
during repairs.

Internal snap rings are provided with straight (Fig. 286*a*) or skew
(Fig. 286*b*) cuts. A screw driver is inserted into the space between
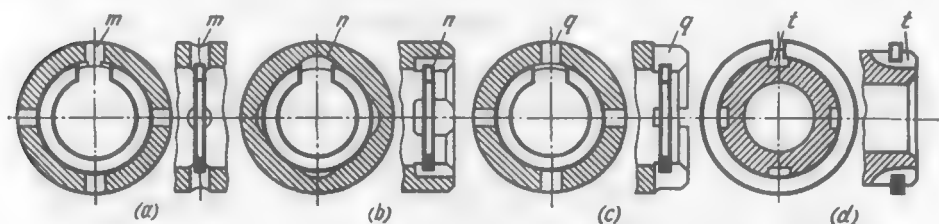
Fig. 285. Removal holes and slots

the cuts and the walls of the housing bore to bend the ring ends in-
wards, and is then turned in the axial direction to get the ring out
of the groove.

Better designs are those with cuts (Fig. 286*c*) or holes (Fig. 286*d*)
for the jaws of tongs, which make both the removal and installation
of the rings easier. The tongs draw the ends of the rings together,
after which the rings can easily be inserted into or withdrawn from
the groove.

The design with a wide cut (Fig. 286e) is used for very thick rings of small diameter, which are difficult to fit into a hole.

The external snap rings are provided with bevels for an expansion tool, made at an angle of 60° for the rings with a diameter less than
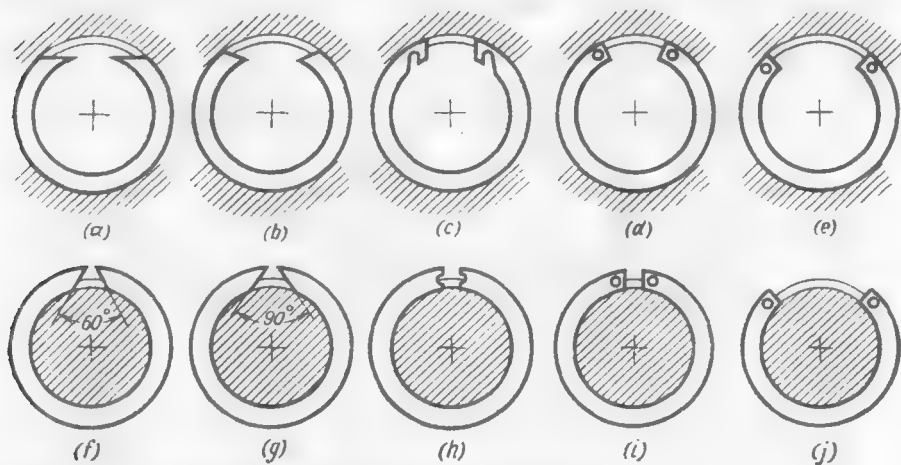
Fig. 286. Withdrawal devices of snap rings

40 mm (Fig. 286f) and 90° for those with a diameter larger than 40 mm (Fig. 286g). The best designs are the ones with semicircular recesses (Fig. 286h) or holes (Fig. 286j) for expanding tongs, which facilitate both the removal and installation of the rings.

4.2. Wire Rings

Snap rings of small diameter are frequently made of round (Fig. 287a), square (Fig. 287b) or rectangular (Fig. 287c) wire. A pro-
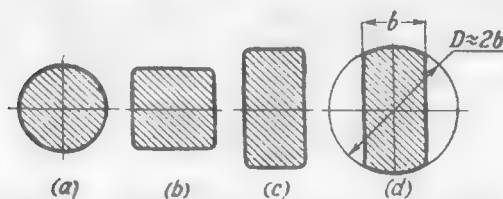
Fig. 287. Cross-sections of wire snap rings
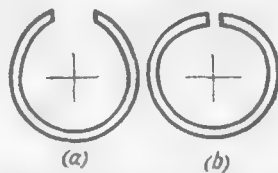
Fig. 288. Elliptic snap rings

file close to a rectangular one is obtained when rings made of round wire of increased diameter are ground on both sides (Fig. 287d).

Snap rings of round cross-section are more flexible than those of rectangular cross-section and can be installed easier. Semicircular

grooves for the rings lesser weaken the part, thanks to the lower stress concentration. Rings installed in tapered recesses in the shaft-fitted parts can carry appreciable axial loads.

Wire rings can be made elliptic (in plan) to ensure a more uniform circumferential interference, with the major axis of the ellipse being arranged along the cut (Fig. 288a) for internal rings and across the cut (Fig. 288b) for external rings.

The manufacture of wire snap rings is easy. Small-diameter rings are made by cutting off each coil of a spiral and flattening it afterwards, followed by hardening and tempering. The diameter of the spiral blank is established experimentally, account being taken of the deformation of the coils in cutting and heat treatment. Small errors are corrected by dressing in the hardened state.

The shortcoming of the round-section wire rings is that they lock parts poorly in the axial direction.
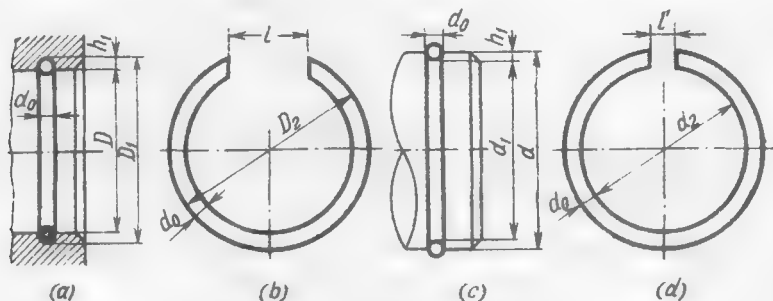
Fig. 289. Parameters of round-section snap rings

The dimensions for the rectangular-section wire rings are selected in the same manner as for lathe-turned ones.

The following relationships are used for the rings of round cross-section.

Wire diameter

$$d_0 = (0.03 \text{ to } 0.05) D \qquad (4.10)$$

where D is the mean diameter of the ring.

The lower limit refers to large-diameter rings (>30 mm) and the upper limit to small-diameter ones (<30 mm).

The groove depth is made equal to $0.55d_0$ so that the ring sinks in the groove slightly more than by half.

In the case of internal snap rings (Fig. 289a, b) the external groove diameter is

$$D_1 = D + 2 \cdot 0.55d_0 \approx (1.035 \text{ to } 1.06) D \qquad (4.11)$$

In order to obtain the required radial interference, the external diameter D_2 of the rings in its free state is made to be

$$D_2 = (1.05 \text{ to } 1.08) \, D_1$$

where the lower limit refers to rings of small diameter and the upper limit, to the large-diameter ones.

Substituting the value of D_1 from Eq. (4.11) into this expression, we get

$$D_2 \approx 1.1 D \tag{4.12}$$

For the ring to be easily fitted into the housing bore the width of the cut must be

$$l \gg \pi \, (D_2 - D) \geqslant 0.12 \, \pi D \geqslant 0.38 D$$

It is adopted in practice that

$$l = (0.42 \text{ to } 0.45) \, D$$

For external snap rings (Fig. 289c, d), when $d_0 = (0.03 \text{ to } 0.05) \, D$ and $h_1 = 0.55 d_0$, the internal diameter of the groove is

$$d_1 = d - 1.1 d_0 \approx (0.95 \text{ to } 0.97) \, d \tag{4.13}$$

where the lower limit refers to rings of small diameter and the upper limit, to the ones of large diameter.

The internal diameter of the ring in its free state is made to be

$$d_2 = (0.93 \text{ to } 0.96) \, d_1$$

where the lower limit refers to large-diameter rings and the upper limit, to small-diameter ones. Substituting the value of d_1 from Eq. (4.13) into this expression, we get

$$d_2 = (0.93 \text{ to } 0.96) \, (0.95 \text{ to } 0.97) \, d \approx 0.9 d \tag{4.14}$$

The width of the cut for small-diameter rings $l' = 5\text{-}10$ mm and for large-diameter ones, $l' = 10\text{-}20$ mm.

Formulas (4.3), (4.5), (4.12) and (4.14) may be used to formulate the following design rule common for rectangular- and round-section rings: the external diameter D_2 of internal snap rings in the free state must be approximately 10 per cent larger, and the internal diameter d_2 of external snap rings, 10 per cent smaller, than the diameter of the seating surfaces (D and d, respectively).

Grooves for rings are made semicircular (Fig. 290a), rectangular (Fig. 290b) with a width of (1.05 to 1.1) d_0, and trapezoidal (Fig. 290c-e) with an apex angle of 50-60°. The radius at the base of the rectangular grooves is made as large as possible, but not more than $0.4 d_0$.

The semicircular grooves weaken the part to a lesser degree. The rectangular and, especially, trapezoidal grooves lock the ring better.

If the conditions of assembly permit it, the edges of the shaft-fitted parts should be chamfered (Fig. 290e).

To make the installation and removal of the snap rings easier, the ends of the internal rings are bent to suit a screw driver (Fig. 291a),
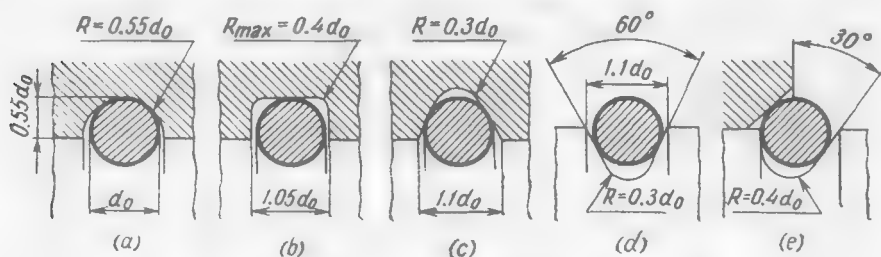
Fig. 290. Grooves for round-section snap rings

or tongs (Fig. 291b-d) or the rings are provided with extraction loops (Fig. 291e). The external snap rings are made smooth (Fig. 291f) or with nibs (Fig. 291g-i) or loops (Fig. 291j) for the withdrawal tools.
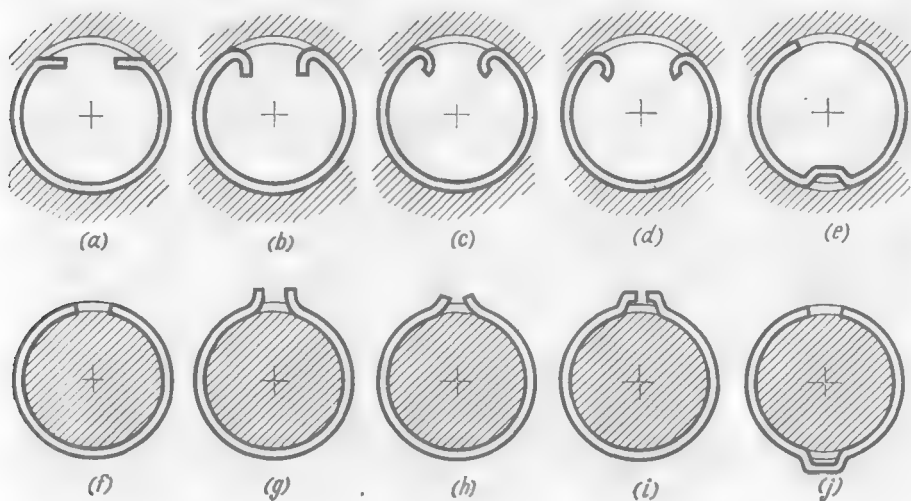
Fig. 291. Withdrawal devices of wire snap rings

Multi-coil snap rings (Fig. 292) comprise several (usually two) spiral coils of rectangular wire. They are preferred because of their increased radial elasticity, which allows deeper grooves to be used.

In internal snap rings (Fig. 292a) the distance l of the free ends of the coils from the point of bend must, because of assembly conditions, be

$$l > \pi (D_2 - D)$$

where D_2 is the diameter of the ring in its free state and D, the diameter of the housing bore.

In external snap rings (Fig. 292b) the value of l' is made equal to 6-10 mm.

Coiled rings can easily be installed in view of their increased elasticity. However, their removal (especially of the internal rings) is difficult because the coil ends are on different sides of the ring.
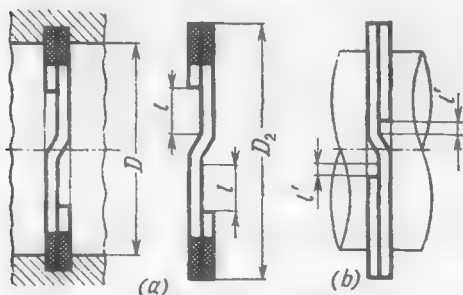
Fig. 292. Double-coil snap rings

4.3. Punched Rings

These rings are cold punched from sheet metal and subsequently hardened and tempered. The heat-treated end faces and seating surfaces are ground. The method imparts to the rings a most practicable crescent form which ensures equal bending resistance. Crescent-shaped rings have better elasticity than rings of constant cross-section.
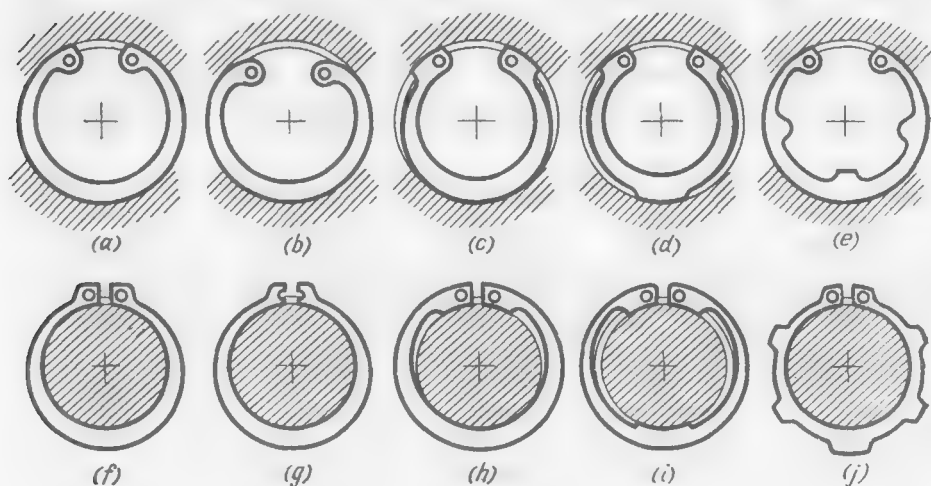
Fig. 293. Punched snap rings

The rings can easily be installed and their grooves can be made deeper. Besides, this form assures uniform interference along the circumference.

The most popular type of punched internal snap rings is shown in Fig. 293a. Pumpkin-shaped rings (Fig. 293b) are used where they

are difficult to insert into the housing bores (small-diameter bores, very thick rigid rings).

In *inverted-profile snap rings* (Fig. 293c, d) the internal surface is made in the form of a cylinder coaxial (in the working position) with the groove circumference. The shaped external surface imparts to the ring the form of equal bending resistance. While retaining the high elasticity inherent in crescent rings, the inverted rings ensure more reliable axial locking, and the load is taken up by three portions spaced approximately at 120°, whereas in the designs shown in Fig. 293a, b the load application centre is displaced from the axis of the bore.

Thick rings are provided with cuts (Fig. 293e) that ensure higher elasticity.

External punched rings (Fig. 293f, g) differ in the form of the pulling elements. Figure 293h, i shows external inverted rings, and Fig. 293j, a ring of increased elasticity.

4.4. Axial Locking in Stop Joints

In joints with snap rings of ordinary design there is always a small axial clearance which is inevitable in view of the installation conditions of the rings.

If clearance-free installation is required, the snap rings are used in combination with nuts (Fig. 294a). The nuts are tightened to a
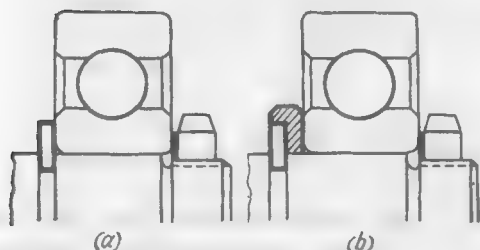
Fig. 294. Tightening of snap rings   Fig. 295. Elastic snap rings
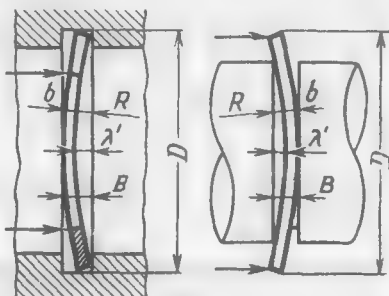
measured torque, since their tightening by hand may easily cause the deformation and even breakage of the rings. It is advisable to reinforce the rings with cups (Fig. 294b).

The clearance in the stop joints loaded with small forces is eliminated by means of elastic rings bent to a radius R (Fig. 295).

The groove width is $B = b + \lambda'$, where b is the ring thickness and λ', the elastic deflection of the ring, which ranges within (0.02

to 0.05) D depending on the operating conditions. The lower limit refers to rings of large diameter ($D > 50$ mm) and the upper one, to small-diameter rings ($D < 50$ mm).

The ring is inserted into the groove with an axial interference of $\lambda'' = a\lambda'$, where a is a proportionality factor (on the average $a = 1$). The total deflection of the ring in its free state is

$$\lambda = \lambda' \left(1 + a\right)$$

The required camber radius of the ring may be determined from the formula

$$R = \frac{D^2}{8\lambda} + \frac{\lambda}{2} \approx \frac{D^2}{8\lambda}$$

where D is the ring diameter.

Concave rings are sometimes used to preload rolling-contact bearings.

Rigid clearance-free locking is effected by means of *bevelled snap rings*, both internal (Fig. 296a) and external (Fig. 296b). When inserted into the groove the inherent elasticity causes the internal
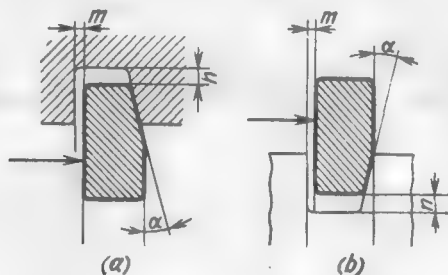
Fig. 296. Bevelled snap rings

rings to expand and the external ones, compress, and thus take up the axial clearance in the joint. The angle α is made less than the angle of friction ($\alpha = 12\text{-}15°$) to prevent the squeezing of the ring out of the groove.

When the ring is fitted into the groove to a depth l, the axial displacement of the ring $s = l/\tan \alpha$. To eliminate an axial clearance of 0.3 mm, for example, when $\alpha = 15°$, the ring should sink in the groove to a depth $l = 0.3/\tan 15° \approx 1$ mm.

The groove should be provided with an axial clearance m slightly exceeding the specified clearance s and a radial clearance $n = m/\tan \alpha$.

4.5. Reinforcing Stop Joints

The load-carrying capacity of snap rings can appreciably be increased if measures are taken which will not allow them to leave their grooves under the action of the axial load and centrifugal forces. For this purpose the rings are enclosed into intermediate cup-shaped washers (Fig. 297*a*, *b*). These methods can be applied to external
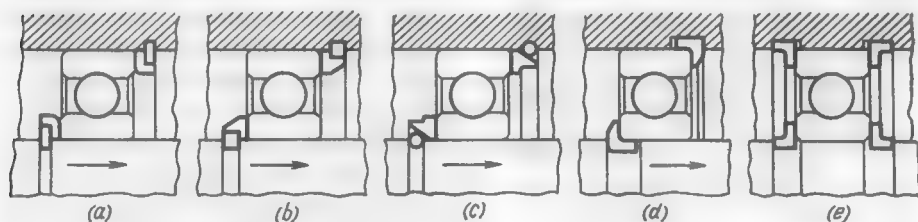
Fig. 297. Reinforcing of stop joints

snap rings with a cylindrical external surface and to internal snap rings with a cylindrical internal surface, i.e., to lathe-turned and wire rings and also to punched rings of inverted profile (see Fig. 293*d*, *i*).

A very strong joint can be obtained when round-section wire rings are fitted into tapered cups (Fig. 297*c*). In this case the ring operates in pure compression. The chamfer leg must be at least $0.5d_0$ (d_0 is the wire diameter). 30-degree chamfers are preferred.

In the reinforced design shown in Fig. 297*d* the ring is L-shaped. The cylindrical gland of the ring is brought under the shaft-fitted part.

Joints of this type can be applied if the design of the unit makes it possible for the part being locked to be shifted onto the ring previously inserted into the groove.

L-shaped rings with glands arranged on the outside (Fig. 297*e*) can be applied to any installation method.

4.6. Radial-Assembly Snap Rings

These rings are used to lock parts on shafts when the installation of an ordinary snap ring along the shaft axis is hampered by adjacent elements. Their simple and convenient installation also makes them suitable when axial assembly is possible.

Radial-assembly snap rings are split spring rings with a large cut that permits the ring to be fitted into the groove in the plane of its arrangement.

The internal diameter d_2 of the ring in the free state (Fig. 298a) is made equal to 0.95-0.97 of the groove diameter d_1 so that the ring fits into the groove with inter-ference. During insertion into the groove the ring ends open and then, after passing the diam-eter line, close, thus embracing the shaft (Fig. 298b). The snap ring will reliably lock if its embrace angle α is not less than 240°, which corresponds to the cut width $l \approx 0.85d_1$ in the closed state and $l' \approx 0.8d_1$ in the free state. Larger embrace angles $\alpha = 270\text{-}300°$ [$l' = (0.7$ to $0.5)d_1$] assure more reliable locking, but only with increased ring elasticity.

Fig. 298. Diagram of radial-assembly snap ring

The simplest radial-assembly snap ring (Fig. 299a) is a ring made of round wire or strip. Figure 299b, c shows punched crescent-shaped rings, and Fig. 299d, the most popular three-point ring.
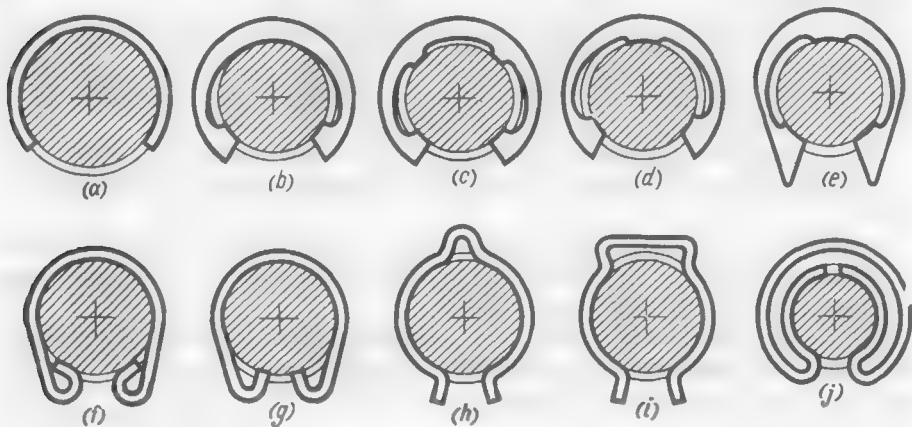
Fig. 299. Radial-assembly snap rings

The design with bevelled ends (Fig. 299d) allows the ring to be easily introduced into the groove.

The load-carrying capacity of radial-assembly snap rings and their resistance to centrifugal forces are lower than those of the axial-assembly snap rings. The axial load-carrying capacity can be increas-ed if the rings are made thicker and the grooves deeper. In contrast

to axial-assembly stop joints, the groove depth is not limited in this case by the condition of the snap ring strength required for installation.

Snap rings with a cylindrical external surface (Fig. 299*a-d*) can be reinforced by placing them into cup-shaped washers.

Figure 299*f-j* illustrates light wire rings used to lock small parts.

4.7. Grooveless Stops

These stops, used to lock parts on smooth shafts (or in smooth bores), are cone-shaped washers (Fig. 300*a*) with lugs having a taper angle α smaller than the friction angle ($\alpha < 12\text{-}15°$).

The stops are placed onto the shaft (or introduced into the housing bore) with the lugs facing the direction of motion (Fig. 300*b*) until they touch the end face of the part being locked. The working axial force (Fig. 300*c*) presses the lugs onto the seating surface and prevents the part from moving.
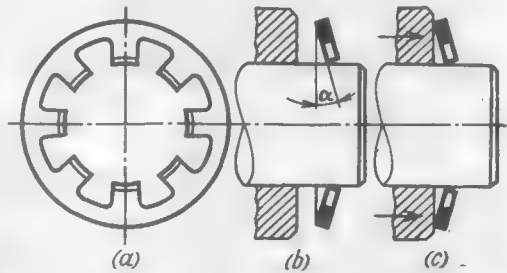
Fig. 300. Diagram of a grooveless stop

For reliable operation the lug ends must engage the seating surface with interference and, hence, must be made to a sufficient degree
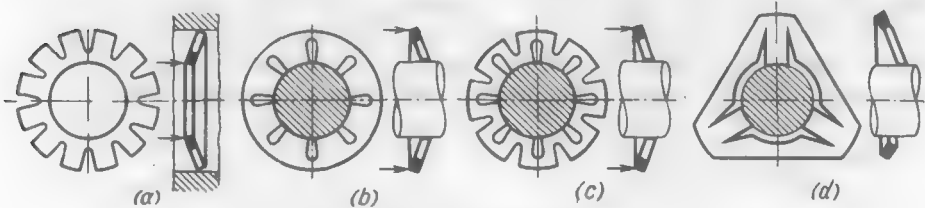
Fig. 301. Grooveless stops

of accuracy. Reliable locking depends to a large extent on the condition of the seating surface.

Sometimes the lugs are inserted into shallow annular grooves, but this does not allow the part to be locked in any arbitrary position.

Grooveless stops are difficult to remove.

Figure 301 illustrates some varieties of grooveless stops, internal (Fig. 301*a*) and external (Fig. 301*b* and *c*). The design shown in Fig. 301*d* has very high lugs, which lessens the required manufacturing accuracy.

4.8. Special Designs

Spring stops made of corrugated thin-walled pipe (Fig. 302a) can carry rather high axial loads. Their high elasticity makes them suitable for installation in deep grooves.

The spring stops displayed in Fig. 302b and c are installed in a semicircular-section groove in the shaft. The part to be locked must
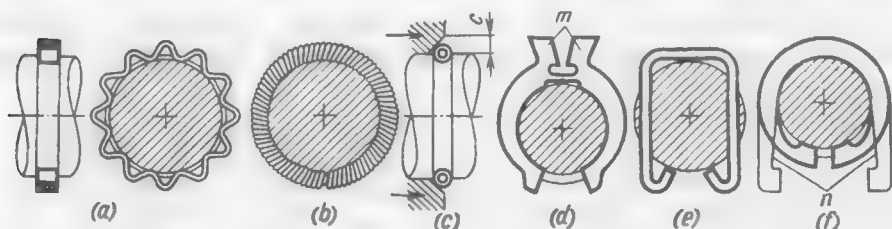
Fig. 302. Special designs of stops

have a chamfer with its leg c being slightly larger than the radius r of the spring. The ends of these springs are connected as usual by screwing one end of the spring on the other end which is wound to a smaller diameter.

Expandable spring stops (Fig. 302d) are installed in grooves by compressing the legs m with pliers. Both radial and axial assembly are possible.

A light wire stop intended to lock parts (Fig. 302e) is introduced into grooves milled diametrally opposite in the shaft.

Lock rings made of plastic metals and bent into annular grooves in the shaft (Fig. 302f) produce permanent joints. Shaped necks n are used to facilitate the bending of the lock ring ends.

Index

TO THE READER

Mir Publishers welcome your comments on the content, translation, and design of the book.

We would also be pleased to receive any suggestions you care to make about our future publications.

Our address is:

USSR, 129820, Moscow, I-110, GSP, Pervy Rizhsky Pereulok, 2, Mir Publishers

OTHER BOOKS FOR YOUR LIBRARY

MECHANISMS IN MODERN ENGINEERING DESIGN
BY I. ARTOBOLEVSKY

A handbook in six volumes for engineers, designers, and inventors on the mechanisms used in modern engineering design. Each mechanism is represented by a diagram of its working principle, with a concise description, and classified by a scheme proposed and developed by the author.

Vol. I. Lever Mechanisms

Illustrates and describes 912 lever mechanisms
Contents. Elements. Simple lever mechanisms. Jointed lever mechanisms.

Vol. II. Lever Mechanisms (in two parts)

Illustrates and describes 1376 lever mechanisms
Contents. Link-gear mechanisms. Slider-crank mechanisms. Lever-cam mechanisms. Gear-lever mechanisms. Lever-ratchet mechanisms. Flexible-link lever mechanisms. Elastic-link lever mechanisms. Wedge-lever mechanisms. Lever-screw mechanisms.

Vol. III. Gear Mechanisms

Illustrates and describes 689 toothed, friction and cam mechanisms.
Contents. Simple gear mechanisms. Lever-gear mechanisms. Pin-gear mechanisms. Cam-gear mechanisms. Ratchet-gear mechanisms. Worm-gear mechanisms. Complex gear mechanisms.

ENGINEERING TECHNIQUES FOR ANALYZING STRENGTH
AND RIGIDITY
BY G. GLUSHKOV

A monograph on the theory of moments developed by the author and its application to engineering design problems on the strength, rigidity, and stability of beams and columns. The approximate (and occasionally exact) solutions obtained can be employed to analyze loads of all kinds. The method is also applicable to various non-linear problems.

Contents. Fundamentals of the theory of moments. Application of the theory. Fundamentals of the moment-operational techniques.

Formulas for Designing Complex Frames
by G. Glushkov, I. Egorov, V. Ermolov
A collection of formulas for calculating the moments and reactions at supports and joints of complex frames and arches under various loads.

Contents. Frames with stepped supports (16 variants). Multispan and multistorey frames (49 variants). Arches (14 variants). Force diagrams and load factors (117 variants).

Appendices. Examples of analyses. Formulas for calculating shearing forces, bending moments, and the angles of rotation and sag of simple beams (117 variants).

MACHINE ELEMENTS
BY V. DOBROVOLSKY ET AL.

A textbook for university mechanical engineering faculties. Contains rules, methods and standards for designing the elements on the basis of their working conditions. Acquaints the reader with the design of individual elements, and the various forms of assembly and drive used in modern engineering.

Contents. Part I. Fundamentals of designing machine elements. Criteria of operating capacity and calculation of machine elements. Selection of material. Standardization. Production soundness.

Part II. Joints. Types of joint. Riveted joints. Welded joints. Joints formed by interference fits. Threaded joints. Cottered fastenings. Keyed, splined and keyless joints.

Part III. Power transmission. Types of drive. Friction drives. Belting. Gearing. Helical and hypoid gears. Worm gears. Globoidal gears. Reduction gears. Chain drives. Power screws.

Part IV. Shafts, bearings and couplings. Shafts and axles. Sliding-contact bearings. Rolling-contact bearings. Couplings and clutches.

Part V. Springs and frames. Springs. Machine frames.
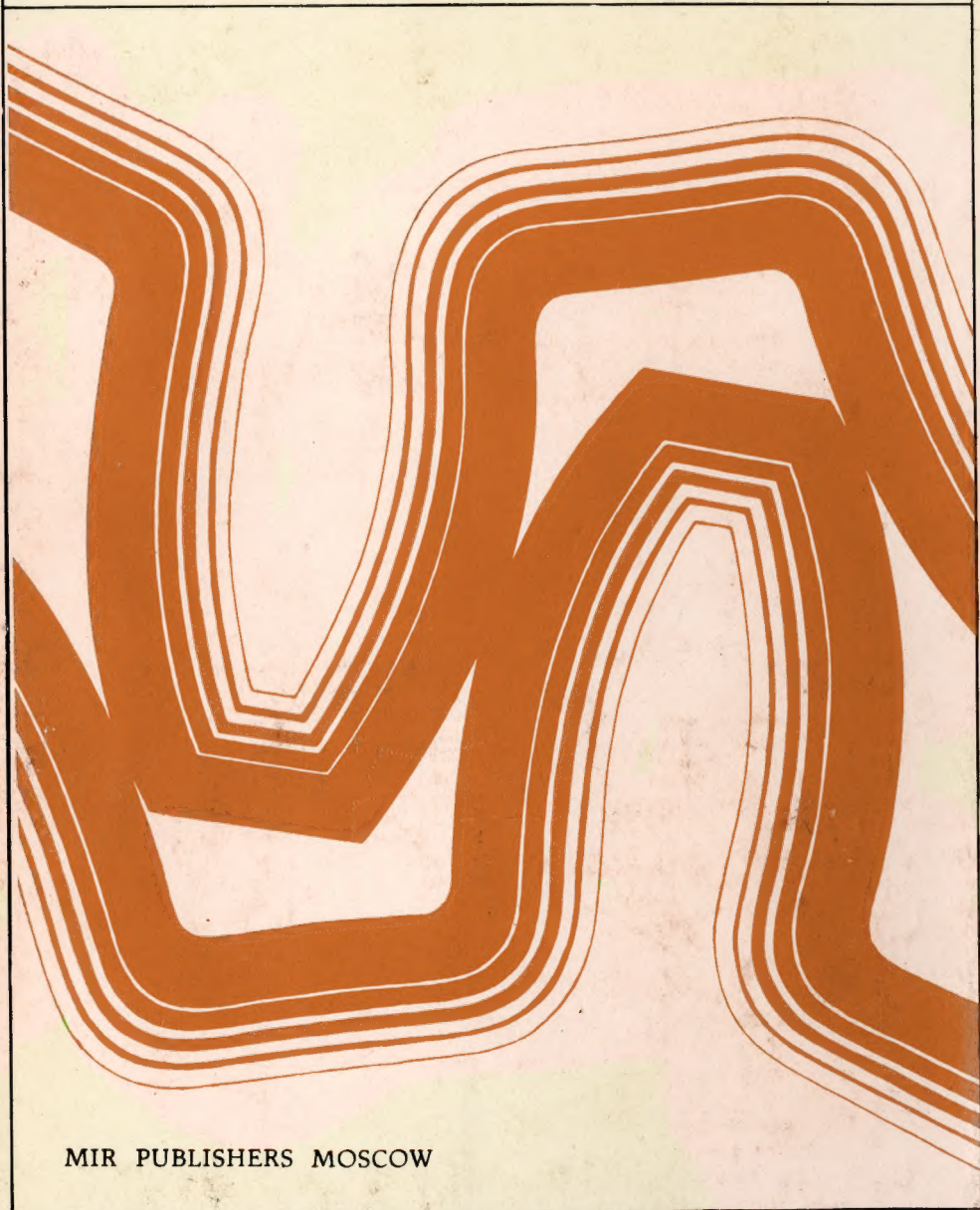
MACHINE TOOLS
BY N. CHERNOV

A textbook for technical colleges and apprentice engineers on the standard parts and mechanisms, electrical and hydraulic equipment of machine tools, the equipment of automatic transfer lines, and N/C machine tools.

Contents. Introduction to machine tools. Standard parts and mechanisms. Electrical equipment. Hydraulic equipment. Automatic (Numerical) control. Standard lathes. Turret lathes. Backing-off lathes. Multihead machines. Semiautomatic and automatic lathes. Drilling machines. Boring machines. Milling machines. Dividing heads. Principles of tracer milling machines. Thread-cutting machines. Shapers and planers. Broaching machines. Grinders. Lapping machines. Gear-cutting machines. Machine tools built from standard units. Automatic transfer lines. Electrosparking, ultrasonic and other machines. N/C machine tools. Modernization. Installation. Testing, maintenance and repairs of machine tools.